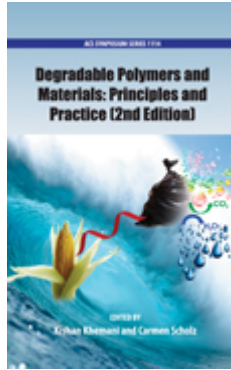
ACS SYMPOSIUM SERIES 1116
Degradable Polymers and Materials: Principles and Practice (2nd Edition)
CO2
EDITED BY
Kohan Khemani and Carmen Scholz

Degradable Polymers and Materials: Principles and Practice (2nd Edition)

In Degradable Polymers and Materials: Principles and Practice (2nd Edition); Khemani, K., et al.;
ACS Symposium Series; American Chemical Society: Washington, DC, 2012.

In Degradable Polymers and Materials: Principles and Practice (2nd Edition); Khemani, K., et al.;
ACS Symposium Series; American Chemical Society: Washington, DC, 2012.

ACS SYMPOSIUM SERIES **1114**

Degradable Polymers and Materials: Principles and Practice (2nd Edition)

Kishan Khemani, Editor
AJ Industries

Carmen Scholz, Editor
University of Alabama at Huntsville

Sponsored by the
ACS Division of Polymer Chemistry

American Chemical Society, Washington, DC

Distributed in print by Oxford University Press, Inc.

Library of Congress Cataloging-in-Publication Data

Degradable polymers and materials : principles and practice / Kishan Khemani, editor, AJ Industries, Carmen Scholz, editor, University of Alabama at Huntsville ; sponsored by the ACS Division of Polymer Chemistry. -- 2nd edition.
pages cm. -- (ACS symposium series ; 1114)
Includes bibliographical references and index.
ISBN 978-0-8412-2822-1 (alk. paper)
1. Polymers--Biodegradation--Congresses. I. Khemani, Kishan C., 1955- editor of compilation. II. Scholz, Carmen, 1963- editor of compilation. III. American Chemical Society. Division of Polymer Chemistry, sponsoring body.
QP801.P64A44 2012
572′.33--dc23

2012040630

The paper used in this publication meets the minimum requirements of American National Standard for Information Sciences—Permanence of Paper for Printed Library Materials, ANSI Z39.48n1984.

Distributed in print by Oxford University Press, Inc.

PRINTED IN THE UNITED STATES OF AMERICA

In Degradable Polymers and Materials: Principles and Practice (2nd Edition); Khemani, K., et al.; ACS Symposium Series; American Chemical Society: Washington, DC, 2012.

Foreword

The ACS Symposium Series was first published in 1974 to provide a mechanism for publishing symposia quickly in book form. The purpose of the series is to publish timely, comprehensive books developed from the ACS sponsored symposia based on current scientific research. Occasionally, books are developed from symposia sponsored by other organizations when the topic is of keen interest to the chemistry audience.

Before agreeing to publish a book, the proposed table of contents is reviewed for appropriate and comprehensive coverage and for interest to the audience. Some papers may be excluded to better focus the book; others may be added to provide comprehensiveness. When appropriate, overview or introductory chapters are added. Drafts of chapters are peer-reviewed prior to final acceptance or rejection, and manuscripts are prepared in camera-ready format.

As a rule, only original research papers and original review papers are included in the volumes. Verbatim reproductions of previous published papers are not accepted.

ACS Books Department

In Degradable Polymers and Materials: Principles and Practice (2nd Edition); Khemani, K., et al.;
ACS Symposium Series; American Chemical Society: Washington, DC, 2012.

Preface

Not too long ago, the world economy was mainly based on agricultural products and its trades and barters between various communities and countries. With the discovery of crude oil, petroleum based fuels, chemicals, polymers and all of their downstream products took a foothold and the world economy was changed forever. Although it is still a very important part of the world economy, agriculture has been second tier to the oil economy for over a hundred years now.

However, the sands of time are shifting once again. With peak oil behind us, rising prices of petroleum based chemicals and plastics, and more importantly the rude awakening and realization that the rising consumption of crude oil is putting the entire Earth's ecosystem and its living beings at grave risk of total annihilation *via* a man-made global warming phenomenon, the world is once again turning its attention to renewable and closed-loop bio-based (i.e. agriculture based) products to fulfill its non-food related needs including transportation fuels and the manufacture of chemicals and plastics.

In this revised edition book, renowned experts from the field of bio-based chemicals, plastics and materials present the most compelling case and a comprehensive overview of the paradigm shift that is taking place in the present day movement to replace crude oil with bio-based raw materials.

There are several new chapters in this edition that address new topics of: Biodegradation Testing Protocols, Life Cycle Assessment, Starch and other Natural Polymers, Bioplastics from Waste Materials, and Biodegradable Agricultural Mulches derived from Biopolymers.

In addition, all of the original chapters from the first edition that have been retained in this second edition have been revised and updated with current references and published literature. All of the chapters in this book have been peer reviewed by experts in their respective fields and have met stringent content and quality requirements of the editors and the publisher.

We sincerely hope that this book will be an asset to anyone who works in the field of degradable and renewable polymers and materials. It should be of interest not only to research scientists and product developers, but also to graduate and undergraduate students and perhaps even the general public and also the policy makers in local, state and federal governments of developed and developing nations around the Globe.

Dr. Kishan Khemani
Santa Barbara, CA, USA
kkhemani@gmail.com (e-mail), (805) 570-8134 (telephone)

Prof. Carmen Scholz
Huntsville, AL, USA
cscholz@chemistry.uah.edu (e-mail), (256) 617-1646 (telephone)

In Degradable Polymers and Materials: Principles and Practice (2nd Edition); Khemani, K., et al.;
ACS Symposium Series; American Chemical Society: Washington, DC, 2012.

In Degradable Polymers and Materials: Principles and Practice (2nd Edition); Khemani, K., et al.;
ACS Symposium Series; American Chemical Society: Washington, DC, 2012.

Editors' Biographies

Kishan Khemani

Dr. Kishan Khemani is a Director of development at A.J. Industries located in Santa Barbara, California. He received his Ph.D. in Organic Chemistry from the University of Western Ontario in London, Ontario, Canada in 1987. He has worked in the materials, polymers and biopolymers field for the past 23 years and holds 22 US patents, has published 31 scientific journal articles, edited three ACS Series Books, and has organized three international symposia at past ACS National Meetings. Dr. Khemani started his career in materials research at University of California, Santa Barbara in 1988, and in 1992 joined the Polymer Research Laboratory of Eastman Chemical Company where he worked on the development of the first synthetic biodegradable polyester, Eastar Bio. He left Eastman in 1999 to pursue full-time research in biodegradable and renewable polymers and has developed and commercialized several films, sheet and injection molding products. His work has been cited in C&E News, and in 2007 he was named as one of the 10 Most Influential Persons by the Australian Packaging magazine.

Carmen Scholz

Prof. Carmen Scholz is a Professor of Chemistry at the University of Alabama in Huntsville. She received a Diploma (MS) in Polymer Chemistry and a Doctorate degree in Chemistry from the University of Technology in Dresden, Germany. Dr. Scholz worked at the University of Massachusetts in Amherst and in Lowell and at Tokyo Science University prior to taking a faculty position in Alabama in 1998. Dr. Scholz's research concentrates on biocompatible and biodegradable polymers. She worked for several years with the Boston Retinal Implant Project and designed and synthesized block copolymers for the modification of biomedically relevant surfaces. Her group's research into bacterial polyesters developed the first gene delivery system based on medium-chain length polyhydroxyalkanoates. She has published more than 50 scientific articles, edited three ACS Series Books and organized several symposia at ACS National Meetings. She is an executive officer in the North Alabama local section of ACS.

In Degradable Polymers and Materials: Principles and Practice (2nd Edition); Khemani, K., et al.;
ACS Symposium Series; American Chemical Society: Washington, DC, 2012.

Chapter 1

Introduction and Overview of Degradable and Renewable Polymers and Materials

Kishan Khemani[1,*] and Carmen Scholz[2,*]

[1]AJ Industries, 4751 Amarosa Street, Santa Barbara, CA 93110
[2]Dept. of Chemistry, University of Alabama in Huntsville, 301 Sparkman Drive, Huntsville, AL 35899
[*]Corresponding authors: kkhemani@gmail.com, scholzc@uah.edu

This second edition adds new insights into the field of biodegradable and renewable plastics. It describes novel approaches in products as well as processes that have been developed over the past seven years since this book was first published. Following the trend of the industry, more emphasis has been placed upon plastics from renewable resources. As the biodegradable plastics industry establishes itself, questions of Standards and Regulations that govern biodegradable polymers become more essential and are addressed in the first two chapters. The biodegradable industry is not only focused on producing plastics that undergo degradation, but considers the responsible use of energy as well as the end-of-life disposability as paramount. Use of *Life Cycle Analysis* (LCA) to address this aspect of the industry has become a norm for all new product and process developments. The various chapters have been organized in the order such that they describe tools and regulations that address biodegradability, advances in natural polymers and plastics from alternative feedstock, synthetic polymers and updates on synthetic procedures. The twenty chapters presented in this book have been written by world's leading scientists in their respective fields.

In Degradable Polymers and Materials: Principles and Practice (2nd Edition); Khemani, K., et al.;
ACS Symposium Series; American Chemical Society: Washington, DC, 2012.

Introduction

Plastic materials are used worldwide for a multitude of applications, in fact it is very difficult, if not impossible, to imagine life without plastics today. The application range for plastics is extremely wide and includes such high-performance and high-tech applications as Kevlar in bulletproof vests and low-end applications such as garbage and shopping bags. Some of the manufacturing processes for common polymers that we use on a daily basis have been known for almost two centuries, for instance, the making of polystyrene and polyvinylchloride has been known since the 1830's. But it was only after World War II that plastics quickly conquered the materials market. Plastic materials were, and still are, appreciated for their durability, high moduli, impact and tensile strengths, reliability and the ability to tailor properties to match intended uses, and in addition, plastics show virtually no corrosion and age slowly. However, with a worldwide increase of plastic waste build-up, paired with a better understanding of the impact of human action on the environment and new and growing environmental awareness, new demands have been prescribed for plastic materials, specifically their ability to degrade according to a specific, pre-set timetable. Thus, there is a growing general concern among consumers and government agencies in most countries around the world that conventional plastic products, although useful, are causing tremendous damage to the environment, water supplies, sewer systems as well as to rivers and streams. While by no means all currently used plastics ought to be replaced by degradable materials, and certainly no plastics in high-performance applications should be degradable, it is paramount to take into account new procedures for plastics production that are based on raw materials derived from renewable resources, and/or lead to degradable products especially for materials used in single-use applications. This book reflects on the latest developments in the area of degradable materials by summarizing new trends in the synthesis, characterization, physical, chemical and degradation behavior as well as information on legislative regulations.

The biodegradable plastics industry in the United States has grown by nearly 20% annually over the past several years. In 2012, 720 million pounds of biodegradable plastics valued at $845 million, will be produced and sold in the United States. This is over an order of magnitude higher than the 52 million pounds sold in 2004! Even though the demand is growing, average prices will continue to fall as production becomes more efficient and production capacities expanded. The packaging industry continues to be a major area of interest when considering degradable plastic materials, primarily due to the package's limited span. High and low density polyethylene, polypropylene, polystyrene, polyethylene terephthalate, and polyvinyl chloride and polyvinylidene chlorides cover almost the entire packaging market. Almost 70% of all the plastic packaging material, which is roughly 11 million tons, is used for food packaging, thus intended explicitly for short term or single use application. However the packaging industry, while it could be the largest consumer of degradable materials, is rather conservative in adopting new technologies. This is partially, due to the fact that olefin-based polymeric materials have been well established in the industries, both from the manufacturing as well as engineering points of

In Degradable Polymers and Materials: Principles and Practice (2nd Edition); Khemani, K., et al.;
ACS Symposium Series; American Chemical Society: Washington, DC, 2012.

view. Due to the nearly one hundred years of process optimization experience, the production of polymers for packaging is highly efficient, stable and hence the resulting polymers are cost-effective and difficult to replace. In spite of these hurdles, natural and degradable polymers like poly(lactic acid) by NatureWorks, BASF's Ecoflex, Novamont's MaterBi, Mirel by Telles (a joint venture between Metabolix and Archer Daniels Midland, although the joint venture has terminated as of February 8, 2012) have become mainstream plastics for the packaging industry. Since biodegradable plastics became an established commodity that is produced from renewable resources like starch and soy and from petroleum as in biodegradable polyesters, scientist are now looking for renewable resources that have not yet been exploited, as for instance chicken feathers and plant fibers. Producing biodegradable plastics from renewable, domestic resources relieves the reliance on oil, 4.6% (331 million barrels) of which is currently used for plastics production (*1*). Four new chapters have been added to this book, which specifically address new and alternative feedstock for the plastics industry.

Natural Polymers

Nature provides a chemically diverse variety of degradable polymers. These polymers were the first materials used by humankind. Early men dressed themselves in hides (proteins, polysaccharides), later in cotton (polysaccharide), silk and wool (proteins). Early men used wood (polysaccharides, polyphenols) for tools and construction materials. Where available, natural rubber (polyisoprene) was used for a variety of daily-life functions, from construction to water-proofing storage containers.

Due to their natural origin, i.e. an enzyme catalyzed biosynthesis, all natural polymers are inherently biodegradable. For every polymerase enzyme whose action leads to a natural polymer there exists a depolymerase capable of catalyzing the degradation of that natural polymer. In other words, "if nature has a process to make it, nature also has a process to break it." Thereby, nature keeps a balance in the generation and degeneration of materials. Depolymerase enzymes for individual natural polymers are either present in the polymer-generating species itself, with poly(hydroxyalkanoate) being a prime example where the natural polymer actually serves as an internal carbon and energy source, or the depolymerase enzyme resides in other species, mainly bacteria and fungi, for which the respective natural polymer serves as food source.

We use natural polymers either directly or after physical and/or chemical conversions that aim at improving upon their physical and functional properties or adding to characteristics. Natural polymers are derived from plants, animals and microorganisms, and besides finding extensive use as food, many natural polymers are used in applications ranging from construction and clothing to biomedical materials.

Polysaccharides are available from plants, fruits, grains & vegetables (starch, cellulose, alginate), animals (chitin), fungi (pullulan) and bacteria (dextran, emulsan, pectin). For a summary on industrial polysaccharides see Stivala *et al*. (*2*) and Heinze (*3*). Proteins are produced by all living species in order to

In Degradable Polymers and Materials: Principles and Practice (2nd Edition); Khemani, K., et al.;
ACS Symposium Series; American Chemical Society: Washington, DC, 2012.

maintain their metabolic functions, but from a materials point of view it is the fibrous proteins from plants (soy) and animals (wool, silk) (*4*) and the polyamino acids from bacteria (polyglutamic acid) that are exploited. Lignin, a polyphenolic compound (*5*), and natural rubber, a polyisoprene (*6*), are synthesized by plants. Poly(hydroxylalkanoates) are synthesized naturally exclusively by bacteria (*7*), polymerase genes have been successfully transferred into other bacteria thus producing highly efficient engineered strains capable of sustaining an industrial exploitation (*8*) and into plants as well (*9*).

Polymers from Renewable Resources

Polymers from renewable resources are distinct from natural polymers by the fact that their synthesis is purposely initiated, triggered either by a microbial cascade or by chemical means. Renewable resources are of biological origin and are distinguished by their ability of seasonal (agricultural) or triggered (animal, microbial) renewal. When considering renewable resources for the manufacturing of plastic materials two distinctly different approaches can be taken: *(i) direct conversion of renewable resources into finished polymeric products, and (ii) renewable resources are first converted into small molecules, not unlike the processes performed in an oil refinery, and are subsequently converted by chemical means into plastic materials*. One of the prime examples of the first approach is the bacterial production of poly(hydroxyalkanoates) where a renewable resource, often a sugar is converted by enzymatic actions directly into the polymer. The physical properties of this polymer depend upon the polymerization characteristics of the bacterial strain. Every bacterial synthesis leads to one distinct polymer with a microbiologically pre-determined set of physical properties. Another example of this type for renewable resource raw material is the water dispersible and biodegradable packaging made from a hybrid specialty high amylose corn starch (containing 80% amylose). This starch naturally has better film forming properties than the regular commodity corn starch (which contains only 20% amylose), and is chemically modified further through a hydroxylpropylation step to prevent retrogradation of the finished products made from it. The second approach allows a large variety of polymeric materials with a broad spectrum of physical properties. As described below, given the versatility provided by the second approach, it is undoubtedly the more viable option for the future.

Sorona, a polyester marketed by DuPont (*10*) exploits a hybrid process that combines a building block produced by fermentation from starch (1,3-Propanediol) with the acid building block (Dimethyl terepthalate), which is produced by chemical synthesis from petroleum. Ingeo, a Poly(lactic acid) biopolymer, produced by NatureWorks LLC, is also the product of a hybrid process: the monomer, lactic acid, is produced by fermentation of corn starch using Lactobacilli. The subsequent polymerization is accomplished either by anionic ring-opening polymerization of the lactide dimer, or more recently by an azeotropic dehydration condensation, a chemical process (*11*). More recently, Dow Chemical has set up a 350,000 ton per year capacity LLDPE joint venture

In Degradable Polymers and Materials: Principles and Practice (2nd Edition); Khemani, K., et al.;
ACS Symposium Series; American Chemical Society: Washington, DC, 2012.

company in Brazil where sugar derived from sugarcane is first converted into the ethylene monomer (via fermentation to ethanol followed by dehydration) and subsequently into polyethylene with identical properties to that of the polymer derived from petroleum oil based polymer. This is the first example of a direct replacement of oil by a natural raw material to produce an identical commodity polymer. Dow has even established a 17,000 hectare sugarcane plantation in Brazil to supply the natural raw material to this project (*12*). Along the same lines, Braskem has also been manufacturing 200,000 metric tons per year of HDPE in Brazil based on the ethanol process (*12*).

Degradable Polymers from Petroleum

In addition to using natural polymers as degradable materials or making use of renewable resources, biodegradability can also be induced in chemically synthesized polymers. A large variety of polyesters have been designed where the ester linkage is accessible to undergo hydrolysis, by introducing aliphatic segments into the polymer (e.g. Ecoflex (*13*)) or using fully aliphatic polyesters (e.g. Starcla Bionolle, Kuredux (*14*, *15*)). This chemical approach to degradable materials allows for the largest variety in products and their properties, simply because of the rich diversity of chemical building blocks and the chemical means of their combination.

Degradable polymers were originally developed for biomedical applications. Copolymers of polylactic acid and polyglycolic acid were the first polymers considered for resorbable sutures and bone fixtures (*16*, *17*). Poly(beta-hydroxyalkanoates) were considered for bone related applications in the past (*18*) and are now studied for tissue engineering scaffolds (*19*). Other polyesters, such as polycaprolactone, have been used in long-term drug delivery devices and tissue engineering scaffolds (*20*). More recent work has shifted from polyesters to polycarbonates (*21*) and polyamino acids (*22*). Biodegradable polymers in biomedical applications are still a very active research area and several chapters are dedicated to this sub-section of degradable materials.

Legislature, Recycling and the Public

Unlike in the past, the public is now very interested in and strives to participate and implement sustainability programs. This shift has occurred mainly due to the extensive media coverage of the effects of pollution on global warming and the resulting potentially long term dire consequences on all life of this planet. According to a recent Scientific American article (January 2012 issue), global warming is already close to becoming an irreversible phenomenon! Current adverse and globally changing weather patterns only go to add fuel to this raging debate, and legislative actions to curb use of oil and to reduce pollution in general have become a welcome development amongst the general public. For instance, the states of California and Texas have passed state legislation banning the use of petroleum-based shopping bags. In addition, Montgomery County, MD, and Washington, D.C., have a 5-cent fee on plastic bags handed out at

In Degradable Polymers and Materials: Principles and Practice (2nd Edition); Khemani, K., et al.;
ACS Symposium Series; American Chemical Society: Washington, DC, 2012.

retail, and Basalt, CO has a 20-cent fee on plastic bags (*23*). More communities and even many other US states are now providing curb-side pick-up for plastics to be recycled. Food waste and yard trimmings made up a large percentage (27%) of the 250 million tons of trash Americans generated in 2010. Many biodegradable plastics manufacturers see a huge market potential in this by supplying compostable bags for collection of these wastes for direct shipment to a composting facility. Several environmentally conscious US towns (e.g. Ann Arbor, MI; Madison, WI) already have programs in place to collect food waste. Many countries including Canada, Italy, Belgium, Holland, Switzerland and Germany have had wide spread home food waste collection programs for years.

While manufacturers of biodegradable plastics have established themselves as a strong and growing industry, the problem now seems to be in customer education. It is a common misconception among the public that all problems can be solved by making plastics biodegradable and that they will somehow just disappear when their use has been exhausted. The biodegradable industry now also has a responsibility in consumer education: biodegradable plastics will "disappear" but only when placed in a commercial composting facility, where microbes are plentiful and use these plastics as Carbon source for their life cycle. Outside of the presence of this microbiological driving force, biodegradable plastics are just another plastic. The responsibility to guarantee sustainability does not end with the manufacturing of materials that have the potential to undergo biodegradation when placed in the right environment. We now have to assure that this potential is indeed utilized. The US Composting Council has made great strides over the past several years as the number of communities that participate in residential food waste collection has grown over 50% since 2009 (*24*). It might be the right time to start talks with the composting industries and their legislature to join forces in our efforts for a sustainable future. After all, in the biodegradable plastics we have the food, literally, for the microbes in the composting facilities.

Due to low volumes and curtailed process optimization, biodegradable materials are currently still comparatively expensive as compared to conventional plastics. Whilst consumers in most European countries seem to be more willing to pay extra for an environmentally friendly product, their counterparts in other parts of the world are less inclined to do so. Of course, the imposition of the green-dot disposal fees in several European countries has a lot to do with this trend. At present, use and disposal of non-degradable plastic products are either banned or discouraged through government laws and imposed fees in several countries, and in fact Germany, The Netherlands, Switzerland, Italy, Ireland etc. have all levied taxes on all non-degradable plastic goods. Similar laws are under consideration throughout other European countries. Canada, Japan, Taiwan and South Africa have banned the use of plastic bags. Other developed nations, such as USA, Singapore, Hong Kong, as well as developing nations such as India, China, and Mexico are all moving towards legislation discouraging the use of conventional plastic products by levying "disposal tax" for all non-degradable products. The State of Orissa in India banned the use and manufacture of non-biodegradable plastics that is less than 20 microns thick in 2004 and plans on strongly enforcing this law under the Environment Protection Act of 1986. Even in some parts of the US, the use of non-degradable plastic bags is either being banned or levied

a disposal fee, thereby discouraging their usage. The very high landfill tipping fees in Europe, Japan and other countries also have a positive impact on the development of the biodegradable products markets in these countries.

After its intended use, packaging materials and especially food packaging materials are discarded and end-up as municipal waste. In fact, the extent of plastics production is mirrored by waste generated. According to the EPA, in 2010, Americans generated 250 million tons of municipal waste and recycled and composted over 85 million tons of this material, equivalent to a 34.1 percent recycling rate. Of all the municipal solid waste, 12.4 percent or 31 million tons were plastics. The recycling rate for different types of plastic varies greatly, resulting in an overall plastics recycling rate of only 8 percent, or 2.4 million tons in 2010. However, the recycling rate for some plastics is much higher, for example in 2010, 28 percent of HDPE bottles and 29 percent of PET bottles and jars were recycled. In 2010, the United States generated almost 14 million tons of plastics as containers and packaging, almost 11 million tons as durable goods, such as appliances, and almost 7 million tons as nondurable goods, (e.g. plates and cups). In 2010, the category of plastics which includes bags, sacks, and wraps was recycled at almost 12 percent (*25*). All of the remaining plastic waste was disposed of by either combustion or landfill disposal. Despite many efforts made by communities, the recycling efficiency of plastics is still very low and ranges well below the average 30% recycling of the total municipal solid waste. Considering that almost half of the amount of plastics produced every year is discarded and is likely to be permanently deposited in a landfill, it becomes even more important to consider replacing current petroleum-based plastics with biodegradable materials. The situation is even more dire in developing countries, which often lack the means and technologies for an effective waste removal, thus leaving plastic waste to litter not only entire communities and industrial sites but also beaches and non-industrialized zones, a phenomenon that has become infamously known as the white litter. For instance in China, the "white line" along its railway lines could be seen from the outer space and has been attributed to the discarded foamed polystyrene lunch boxes thrown out of the moving trains.

References

1. How much oil is used to make plastic? http://www.eia.gov/tools/faqs/faq.cfm?id=34&t=6.
2. *Industrial Polysaccharides: The Impact of Biotechnology and Advanced Methodologies*; Stivala, S. S., Crescenti, V., Dea, I. C. M., Eds.; Gordon and Breach Science Publishers: 1987.
3. *Polysaccharides I : Structure, Characterisation and Use (Advances in Polymer Science)*; Heinze, T. T., Ed.; Springer Verlag: 2005.
4. *Silk Polymers Materials Science and Biotechnology*; Kaplan, D., Adams, W. W., Farmer, B., Viney, C., Eds.; ACS Symposium Series 544; American Chemical Society: Washington, DC, 1994.

In Degradable Polymers and Materials: Principles and Practice (2nd Edition); Khemani, K., et al.;
ACS Symposium Series; American Chemical Society: Washington, DC, 2012.

5. *Lignin: Properties and Materials*; Glaser, W., Sarkanen, S., Eds.; ACS Symposium Series 397; American Chemical Society: Washington, DC, 1989.
6. *Immobilized Biocatalysts to Isoprene*; Ullmann's Encyclopedia of Industrial Chemistry, 5th ed.; Arpe, H.-J., Ed.; Wiley-VCH: 1989; Vol. A14.
7. Doi, Y. *Microbial Polyesters*; VCH Publishers, Inc.: New York, Weinheim, Cambridge, 1990.
8. Peoples, O. P.; Sinskey, A. J. Polyhydroxybutyrate (PHB): a model system for biopolymer engineering. *Prog. Biotechnol.* **1987**, *3*, 51.
9. Bohmert-Tatarev, K.; McAvoy, S.; Daughtry, S.; Peoples, O. P.; Snell, K. D. High Levels of Bioplastic Are Produced in Fertile Transplastomic Tobacco Plants Engineered with a Synthetic Operon for the Production of Polyhydroxybutyrate. *Plant Physiol.* **2011**, *155*, 1690.
10. Sorona® renewably sourced fiber. http://www.Dupont.com/sorona.
11. The Ingeo Journey. http://www.natureworksllc.com/the-ingeo-journey.aspx.
12. Tullo, A. Notes On Dow's Brazilian Biopolymers Project. http://cenblog.org/the-chemical-notebook/2011/07/447/.
13. Ecoflex® Biodegradable Plastic Overview. http://www.bioplastics.basf.com/ecoflex.html.
14. Starcla - Bio-based Bionolle resin. http://www.showa-denko.com/index.php?id=6&tx_ttnews[tt_news]=181&tx_ttnews[backPid]=5&cHash=0496d5ccb0.
15. New-age materials that lessen the environmental load -PGA (poly glycolic acid) resin. http://www.kureha.co.jp/en/guidance/division/pga/index.html.
16. Nair, L. S.; Laurencin, C. T. Biodegradable polymers as biomaterials. *Prog. Polym. Sci.* **2007**, *32* (8−9), 762.
17. Middleton, J. C.; Tipton, A. J. Synthetic biodegradable polymers as orthopedic devices. *Biomaterials* **2000**, *21*, 2335.
18. Doyle, C.; Tanner, E. T.; Bonfield, W. In vitro and in vivo evaluation of polyhydroxybutyrate and of polyhydroxybutyrate reinforced with hydroxyapatite. *Biomaterials* **1991**, *12*, 841.
19. Chen, G. Q.; Wu, Q. The application of polyhydroxyalkanoates as tissue engineering materials. *Biomaterials* **2005**, *26*, 6565.
20. Martina, M.; Hutmacher, D. W. Biodegradable polymers applied in tissue engineering research: a review. *Polym. Int.* **2007**, *56*, 145.
21. Bourke, S. L.; Kohn, J. Polymers derived from the amino acid L-tyrosine: polycarbonates, polyarylates and copolymers with poly(ethylene glycol). *Adv. Drug Delivery Rev.* **2003**, *55*, 447.
22. Obeid, R.; Scholz, C. Synthesis and self-assembly of well-defined poly(amino acid) end capped poly(ethylene glycol) and poly(2-methyl-2-oxazoline). *Biomacromolecules* **2011**, *12* (10), 3797.
23. Verespej, M. Carpinteria, Calif., bans plastic and paper bags. http://www.plasticsnews.com/headlines2.html?id=24781&q=basalt.
24. Goldstein, N. Momentum to Build in 2012. *BioCycle* **2012**, *53* (1), 4.
25. U.S. Environmental Protection Agency. Municipal Solid Waste (MSW) in the United States: Facts and Figures. http://www.epa.gov/osw/nonhaz/municipal/msw99.htm.

Chapter 2

Biobased & Biodegradable Plastics: Rationale, Drivers, and Technology Exemplars

Ramani Narayan*

Department of Chemical Engineering & Materials Science, Michigan State University, East Lansing, MI 48824
***narayan@msu.edu**

Biobased and biodegradable plastics can form the basis for an environmentally responsible, sustainable alternative to current materials based exclusively on petroleum feedstocks. Biobased plastics offer value in the sustainability/life-cycle equation by offering a reduced carbon footprint in complete harmony with the rate and time scales of the biological carbon cycle and responsible end-of-life option through recycling and biodegradability in targeted disposal environments. Identification and quantification of biobased carbon content uses radioactive C-14 signature. The biobased carbon content provides the amount of CO_2 emissions reduction achievable for switching from the fossil to bio carbon – the material carbon footprint. Single use, short-life, disposable products can be engineered to be biboased and biodegradable. These products should be completely biodegradable in a defined time frame in the selected disposal environment as opposed to degradable or partially biodegradable. International standards from ASTM, ISO, EN on biobased content and biodegradability is presented. The manufacture of starch foam and starch bioplastics is discussed as technology exemplars for biobased and biodegradable products.

Why Biobased Plastics?

Sustainability, industrial ecology, ecoefficiency, and green chemistry are the new principles guiding the development of the next generation of products and

In Degradable Polymers and Materials: Principles and Practice (2nd Edition); Khemani, K., et al.; ACS Symposium Series; American Chemical Society: Washington, DC, 2012.

processes. New plastics or new manufacturing approaches to current conventional plastics have to be designed and engineered from "cradle to cradle" incorporating a holistic "life cycle thinking approach". The carbon and environmental footprint of the feedstock (fossil vs biological) used in the manufacture of a product and the ultimate fate (disposal) of the product when it enters the waste stream are important considerations.

Carbon is the major basic element that is the building block of plastics and most polymeric materials -- biobased products, petroleum based products, biotechnology products, fuels, even life itself. Therefore, discussions on sustainability, sustainable development, environmental responsibility centers on the issue of managing carbon (carbon based materials) in a sustainable and environmentally responsible manner. Today, the major concern is the increasing human-made CO_2 emissions with no offsetting sequestration and removal of the released CO_2. Reducing our carbon footprint and thereby minimizing the global warming-climate change problems is a major challenge

Biological Carbon Cycle – Biobased Plastics Rationale

Replacing the petro-fossil carbon with biobased carbon in plastics and other polymer materials intrinsically offers a zero material carbon footprint value proposition. This can be readily seen by reviewing the biological carbon cycle shown in Figure 1. Carbon is present in the atmosphere as CO_2. Photoautotrophs like plants, algae, and some bacteria fix this inorganic carbon to organic carbon (carbohydrates) using sunlight for energy as shown in equation 1.

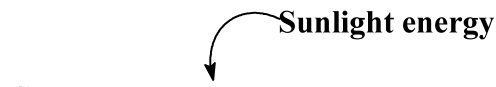

Equation 1

Over geological time frames (>10^6 years) the plant biomass is fossilized to provide petroleum, natural gas and coal. We utilize these fossil feedstocks to make polymers, chemicals & fuel and release the carbon back into the atmosphere as CO_2 in a short time frame of 1-10 years (see Figure 1). Clearly, the rate and time scales of carbon sequestration is not in balance with the use and release of carbon emissions back to the environment. Therefore, this is not sustainable, and we are not managing carbon in a sustainable and environmentally responsible manner.

By using plant biomass, agricultural and forestry crops and residues to manufacture carbon-based products so that the CO_2 released at the end-of-life of the product is captured by planting new biomass in the next season.Specifically, the rate of CO_2 release to the environment at end-of-life equals the rate of photosynthetic CO_2 fixation by the next generation of crops planted—a zero material carbon footprint. Furthermore, if we manage our biomass resources effectively by making sure that we plant more biomass (trees, crops) than we utilize, we can begin to start reversing the CO_2 rate equation and move towards a

In Degradable Polymers and Materials: Principles and Practice (2nd Edition); Khemani, K., et al.;
ACS Symposium Series; American Chemical Society: Washington, DC, 2012.

net balance between CO_2 fixation/sequestration and release due to consumption. Thus, using biomass carbon feedstocks allows for:

- Sustainable development of carbon based polymer materials
- Control and even reduce CO_2 emissions and help meet global CO_2 emissions standards
- Provide for an improved environmental profile

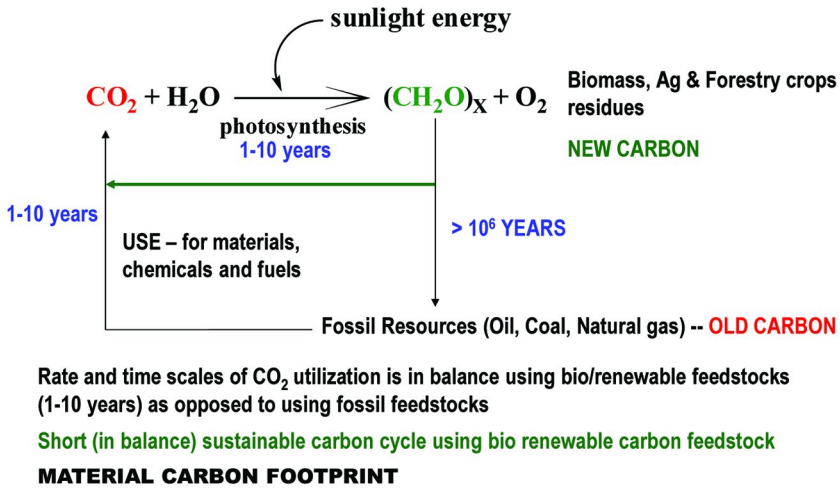

Figure 1. Biological carbon cycle – value proposition for using biobased feedstocks instead of petro-fossil carbon feedstock

Material Carbon vs Process Carbon Footprint

The fundamental intrinsic value proposition of a zero material carbon footprint arises from the origin of the carbon in the product as described in the earlier section – using biobased in place of petro-fossil feedstock. This does not address the carbon emissions and other environmental impact for the process of converting the feedstock to product, use and ultimate disposal – the process carbon footprint. LCA methodology and standards (ISO 14040 standards) are the accepted tools to compute the process environmental footprint. Unfortunately, LCA focuses almost exclusively on the process (carbon and environmental) footprint. The impact of the carbon present in the product, the material carbon footprint, is treated as feedstock energy or embodied carbon energy for potential use in the next product cycle.

It is important to calculate and report on the process carbon and environmental footprint using LCA tools and ensure that the process carbon and environmental footprint is equal or better than the process being replaced. However, the intrinsic fundamental value proposition for biobased plastics arises from the zero aterial carbon footprint in harmony with time scales of the natural biological carbon cycle.

In Degradable Polymers and Materials: Principles and Practice (2nd Edition); Khemani, K., et al.; ACS Symposium Series; American Chemical Society: Washington, DC, 2012.

Examples of Material Carbon Footprint – Bio Polyethylene (bio-PE) and Bio Polyethylene Terephthalate (bio-PET)

Basic stoichiometry teaches that for every 100 kg of polyolefin (polyethyl ene, PE; polypropylene, PP) manufactured, a net 314 kg CO_2 is released into the environment at its end-of-life (100 kg of PE contains 85.7% kg carbon and upon combustion will yield 314 kg of CO_2 (44/12) × 85.7). Similarly, PET (polyethylene terephthalate) contains 62.5% carbon and result in 229 kg of CO_2 released into the environment at end-of-life. However, if the carbon in the polyester or polyolefin comes from biomass feedstock, the net release of CO_2 into the environment is zero, because the CO_2 released is sequestered in a short time period by the next crop or biomass plantation (Figure 2). Thus, the fundamental value proposition for biobased plastics arises from this intrinsic **zero material carbon footprint** and not necessarily from the process carbon footprint which may be equal or slightly better than current processes.

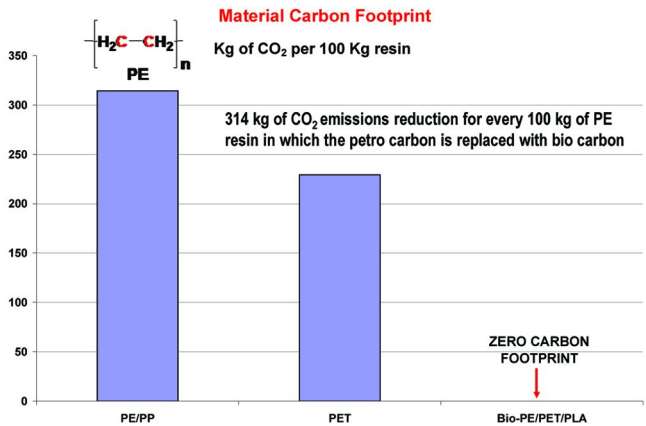

Figure 2. Material carbon footprint calculations.

This approach is illustrated by Braskem who have a 200 kton bio PE plant using sugarcane as the biobased feedstock in Brazil (*1*) Sugar from sugar cane is fermented to ethanol which is dehydrated to ethylene. In addition, the company has a plant manufacturing 30 ktons of bio PP as well.

Another example is the switch by Coca Cola to bio-PET with 20% biobased carbon content (31.25% by mass of plant material). PET (polyethylene terephthalate) bottle is extensively used for packaging beverages, water, and a number of other food and non-food items. It is manufactured by condensation polymerization of terephthalic acid and ethylene glycol. In the bio-PET the glycol component is biobased and there is efforts underway to manufacture the terephthalic acid from biobased feedstocks, but currently is made from fossil feedstock.

As shown in Figure 3, there are two biobased carbons and eight fossil carbons per PET molecule and therefore 20% biobased carbon content. On a mass basis, there is 31.25% biobased glycol component and 68.75% terephthalic

In Degradable Polymers and Materials: Principles and Practice (2nd Edition); Khemani, K., et al.;
ACS Symposium Series; American Chemical Society: Washington, DC, 2012.

acid component. From a material carbon footprint perspective the CO_2 arising from the glycol components two carbons would have a zero carbon emissions impact and only the eight fossil carbons from the terephtahlic acid component would contribute to the carbon emissions impact.

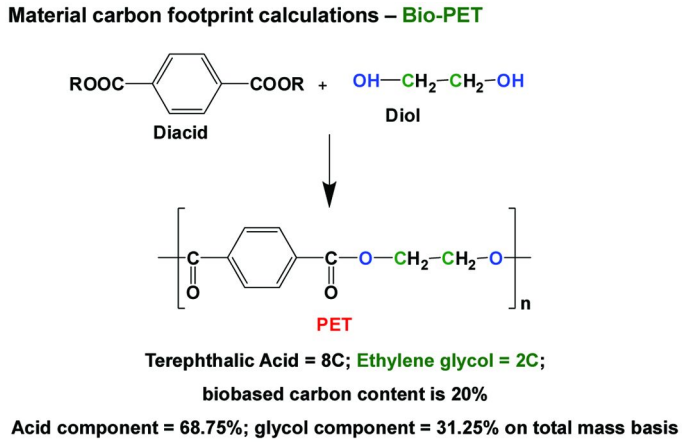

Figure 3. Biobased carbon content of bio-PET

Figure 4 schematically shows the manufacturing process to PET from biobased and fossil feedstocks. As shown in the figure, currently only the ethylene glycol component is made from bio feedstocks.

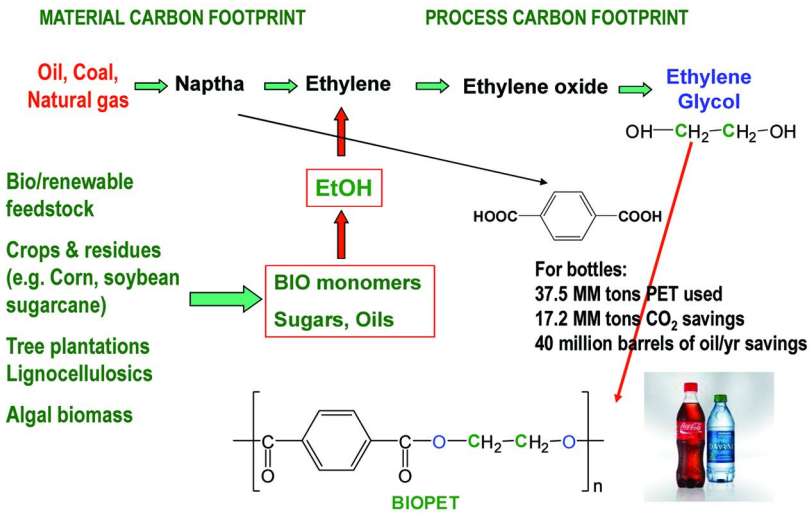

Figure 4. Manufacturing route to PET using fossil and bio feedstocks

In Degradable Polymers and Materials: Principles and Practice (2nd Edition); Khemani, K., et al.;
ACS Symposium Series; American Chemical Society: Washington, DC, 2012.

About 37.5 million metric tons of PET is used to make bottles. As discussed earlier two of the ten carbons in PET coming from the glycol component would have zero carbon emissions impact. So replacing just two of the PET carbons with bio carbons results in 17.2 million metric tons of CO_2 savings. This translates to saving 40 million barrels of oil use per year. Recently, major brand owners The Coca-Cola Company, Ford Motor Company, H.J. Heinz Company, NIKE, Inc. and Procter & Gamble today announced the formation of the Plant PET Technology Collaborative (PTC) (*2*), a strategic working group focused on accelerating the development and use of 100% plant-based PET materials and fiber in their products.

Experimental Method To Quantify Biobased Carbon Content

As shown in Figure 5, ^{14}C signature forms the basis for identifying and quantifying biboased content. The CO_2 in the atmosphere is in equilibrium with radioactive $^{14}CO_2$. Radioactive carbon is formed in the upper atmosphere through the effect of cosmic ray neutrons on ^{14}N. It is rapidly oxidized to radioactive $^{14}CO_2$, and enters the Earth's plant and animal lifeways through photosynthesis and the food chain. Plants and animals which utilise carbon in biological foodchains take up ^{14}C during their lifetimes. They exist in equilibrium with the ^{14}C concentration of the atmosphere, that is, the numbers of C-14 atoms and non-radioactive carbon atoms stays approximately the same over time. As soon as a plant or animal dies, they cease the metabolic function of carbon uptake; there is no replenishment of radioactive carbon, only decay. Since the half life of carbon is around 5730 years, the fossil feedstocks formed over millions of years will have no ^{14}C signature. Thus, by using this methodology one can identify and quantify biobased content. ASTM subcommittee D20.96 developed a test method (D 6866) to quantify biobased content using this approach (*3*).

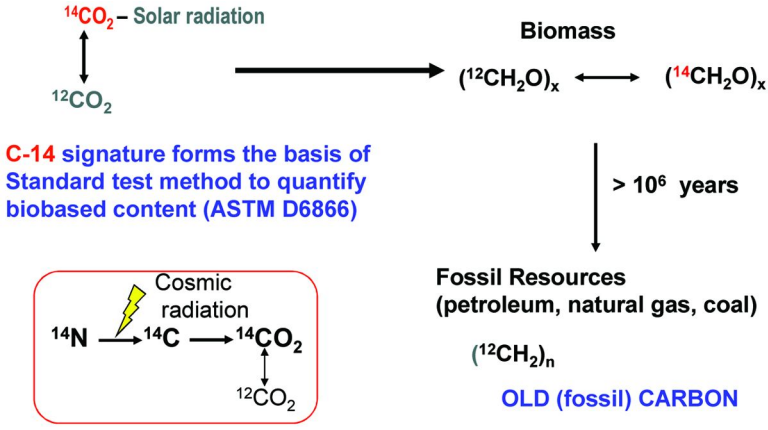

Figure 5. Carbon-14 method to identify and quantify biobased content

In Degradable Polymers and Materials: Principles and Practice (2nd Edition); Khemani, K., et al.;
ACS Symposium Series; American Chemical Society: Washington, DC, 2012.

D6866 test method involves combusting the test material in the presence of oxygen to produce carbon dioxide (CO_2) gas. The gas is analyzed to provide a measure of the products. $^{14}C/^{12}C$ content relative to the modern carbon-based oxalic acid radiocarbon Standard Reference Material (SRM) 4990c, (referred to as HOxII). Three different methods can be used for the analysis. The methods are:

Test Method A utilizes Liquid Scintillation Counting (LSC) radiocarbon (^{14}C) techniques by collecting the CO_2 in a suitable absorbing solution to quantify the biobased content. The method has an error from 5-10% depending on the LSC equipment used. This method is de-listed from the ASTM D6866 standard because of its high percent error

Test Method B utilizes Accelerator Mass Spectrometry (AMS) and Isotope Ratio Mass Spectrometry (IRMS) techniques to quantify the biobased content of a given product with possible uncertainties of 1 to 2 % and 0.1 to 0.5 %, respectively. Sample preparation methods are identical to Method A, except that in place of LSC analysis the sample CO_2 remains within the vacuum manifold and is distilled, quantified in a calibrated volume, transferred to a quartz tube, torch sealed. The stored CO_2 is then delivered to an AMS facility for final processing and analysis.

Test Method C uses LSC techniques to quantify the biobased content of a product. However, whereas Method A uses LSC analysis of CO_2 cocktails, Method C uses LSC analysis of sample carbon that has been converted to benzene. This method determines the biobased content of a sample with a maximum total error of ±2 % (absolute).

Method A has now been removed from the ASTM D6866 method because of the large errors (+/- 15%) in measurements. Method B using Accelerator Mass Spectrometry (AMS) is now the method of choice because the ^{14}C measurement precision is typically within 0.5 to 1%. AMS facilities can be found in most major Universities and commercial labs like Beta Analytic (www.betalabservices.com) which is one of the approved labs for measuring biboased carbon content for the USDA Biopreferred program (*4*).

The 1950's nuclear testing programs resulted in a considerable enrichment of ^{14}C in the atmosphere. Although it continues to decrease by a small amount each year, the current ^{14}C activity in the atmosphere has not reached the pre 1950 level. Because all ^{14}C sample activities are referenced to a "pre-bomb" standard, and because nearly all new biobased products are produced in a post-bomb environment, all values (after correction for isotopic fractionation) must be multiplied by 0.93 (as of the writing of this standard) to better reflect the true biobased content of the sample.

Terminology

Based on the discussions above, the following terminology apply:

Biobased Plastics/Materials – Organic polymers or material/s containing in whole or part biogenic carbon (carbon from biological sources)

Organic Polymers/Material/s -- material(s) containing carbon based compound(s) in which the carbon is attached to other carbon atom(s),

In Degradable Polymers and Materials: Principles and Practice (2nd Edition); Khemani, K., et al.;
ACS Symposium Series; American Chemical Society: Washington, DC, 2012.

hydrogen, oxygen, or other elements in a chain, ring, or three dimensional structures (IUPAC nomenclature)

Bio(carbon) Content -- The bio content is based on the amount of biogenic carbon present, and defined as the amount of bio *carbon* in the plastic as fraction weight (mass) or percent weight (mass) of the total organic carbon in the plastic. (ASTM D6866)

% bio or biobased content = Bio (organic) carbon/total (organic carbon) * 100

ASTM D6866 – Standard Test Methods for Determining the Biobased Content of Solid, Liquid, and Gaseous Samples Using Radiocarbon Analysis

Examples of Biobased Carbon Content Determination

The following examples illustrate biobased content determinations.

Product 'O' is a fiber reinforced composite with the composition 30% biofiber (cellulose fiber) + 70% PLA (biobased material). The biobased content of Product 'O' is 100% -- all the carbon in the product comes from bioresources.

Product 'P' is a fiber reinforced composite with the composition 30% glass fiber + 70% PLA (biobased material. The biobased content of Product 'P' is 100%, not 70%. This is because the biobased content is on the basis of carbon, and glass fiber has no carbon associated with it. However, in all cases, one must define biobased content and organic content. Thus, the biobased content of Product 'P' is 100% but organic content is 70%, implying that the balance 30% is inorganic material. In the earlier example of Product 'O' the biobased content is 100% and organic content is 100%. Thus this allows the end-user/customer to clearly differentiate between two 100% biobased products and make their choice on additional criteria – looking at the LCA profile of the two products (using ASTM D 7075).

Product 'N' is a fiber reinforced composite with the composition 30% biofiber (cellulose) + 70% polypropylene (petroleum based organic). Product 'N' biobased content = 18.17% and not 30%. Again, biobased content is not based on weight (mass), but on a carbon basis i.e. amount of biobased *carbon* as fraction weight (mass) or percent weight (mass) of the total organic carbon. Therefore, biobased content = 0.3*44.4 (percent biocarbon; cellulose)/0.7*85.7 (percent carbon in polypropylene)+ 0.3*44.4 (percent biocarbon) * 100 which computes to 18.17%.

The justification and rationale for using carbon and not the weight or moles or other elements like oxygen, or hydrogen as the basis for establishing biobased content of products should now be very self evident. As discussed in earlier sections, the rationale for using biobased products is to manage carbon in a sustainable and efficient manner as part of the natural carbon cycle, therefore it makes sense to use carbon as the basis for determining biobased content. It is also fortituous that an absolute method using ^{14}C is available to measure the biobased carbon present in a material. The theoretical calculations presented

In Degradable Polymers and Materials: Principles and Practice (2nd Edition); Khemani, K., et al.;
ACS Symposium Series; American Chemical Society: Washington, DC, 2012.

earlier have been validated in experimental observations using ASTM D6866 and are in agreement within +/- 2%.

The U.S. Congress passed the Farm Security and Rural Investment Act of 2002 (P.O. 107 – 171) requiring the purchase of biobased products by the Federal Government. The U.S. Department of Agriculture (USDA) was charged with developing guidelines for designating biobased products and publish a list of designated biobased product classes for mandated Federal purchase (*4*). In its rule-making the USDA adopted the methodology described above for identifying and quantifying biobased content and requires the use of ASTM D6866 to establish biobased content of products. More recently, a voluntary labeling program "USDA certified biobased product" has been launched and managed by ASTM. The basis for the certification is to have the product tested for biobased carbon content using ASTM D6866 and meeting several other requirements.

Material Design Principles for the Environment

The focus of any product design and engineering has typically been on performance and cost in the manufacturing stage. However, the impact of using a particular feedstock whether it be petroleum or biobased has not been factored into the equation except for cost. The question of what happens to a product after use when it enters the waste stream has, also, not been considered. Both these factors are beginning to play an increasingly important role in product design and engineering. Figure 6 schematically depicts these concepts.

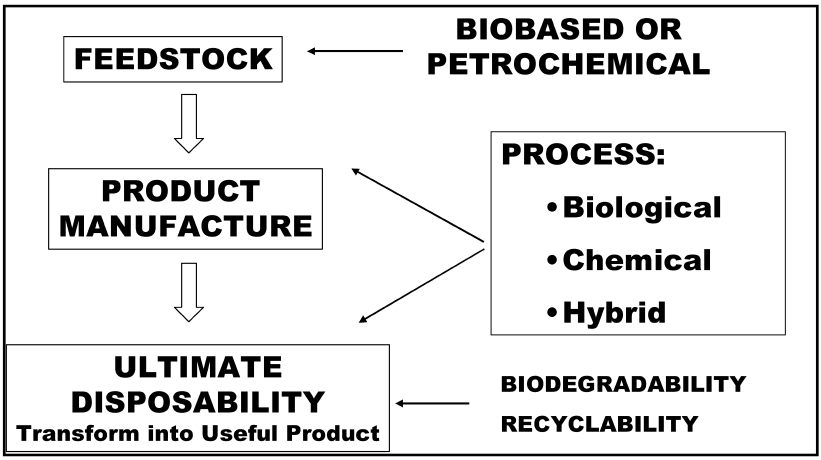

Figure 6. Material design principles for the environment; Life Cycle thinking

In Degradable Polymers and Materials: Principles and Practice (2nd Edition); Khemani, K., et al.;
ACS Symposium Series; American Chemical Society: Washington, DC, 2012.

In the earlier section, the use of biobased as opposed to petroleum feedstocks to manage our carbon based products in a sustainable and environmentally responsible manner has been discussed. The zero material carbon footprint value propostion for biobased plastics like bio-PE and bio-PET was demonstrated. However, that is onlypart of the equation, environmental responsibility requires us to look at the entire product cycle from feedstock to ultimate disposal from a holistic point of view and measure the process carbon and environmental footprint using LCA methodology. Towards meeting this goal, a new ASTM standard (D 7075) (*5*) has been published on evaluating and reporting on environmental performance of biobased products.

As shown in Figure 6, end-of-life of a product using biodegradability, recyclability or other recovery options, is an important element of sustainability and environmental responsibility.

Biobased polymers are synthesized by many types of living matter - plants, animals and bacteria - and are an integral part of ecosystem function. Because they are synthesized by living matter, biopolymers are generally capable of being utilized by living matter (biodegraded), and so can be disposed in safe and ecologically sound ways through disposal processes (waste management) like composting, soil application, and biological wastewater treatment. Therefore, for single use, short-life, disposable, materials applications like packaging, and consumer articles, biobased materials can and should be engineered to retain its biodegradability functionality. For durable, long life articles biboased materials needs to be engineered for long-life and performance, and biodegradability may not be an essential criteria.

Finally, it is important to note that not all biobased plastics are biodegradable-compostable and similarly biodegradable-compostable plastics are not necessarily biobased. For biobased plastics that are not biodegradable-compostable, the end-of-life option would be recycling.

Biodegradable-Compostable Plastics

Currently, most products are designed with limited consideration to its ecological footprint especially as it relates to its ultimate disposability. Of particular concern are plastics used in single-use, disposable packaging and consumer goods. Designing these materials to be biodegradable and ensuring that they end up in an appropriate disposal system is environmentally and ecologically sound. For example, by composting our biodegradable plastic and paper waste along with other "organic" compostable materials like yard, food, and agricultural wastes, we can generate much-needed carbon-rich compost (humic material). Compost amended soil has beneficial effects by increasing soil organic carbon, increasing water and nutrient retention, reducing chemical inputs, and suppressing plant disease. Composting is increasingly a critical element for maintaining the sustainability of our agriculture system. The food wastes along with other biowastes are separately collected and composted to generate a good, valuable soil amendment that goes back on the farmland to re-initiate the carbon cycle (*6*, *7*).

In Degradable Polymers and Materials: Principles and Practice (2nd Edition); Khemani, K., et al.;
ACS Symposium Series; American Chemical Society: Washington, DC, 2012.

Polymer materials have been designed in the past to resist degradation. The challenge is to design polymers that have the necessary functionality during use, but destruct under the stimulus of an environmental trigger after use. The trigger could be microbial, hydrolytically or oxidatively susceptible linkage built into the backbone of the polymer, or additives that catalyze breakdown of the polymer chains in specific environments. More importantly, the breakdown products should not be toxic or persist in the environment, and should be completely assimilated (as food) by soil microorganisms in a defined time frame. In order to ensure market acceptance of biodegradable products, the ultimate biodegradability of these materials in the appropriate waste management infrastructures (more correctly the assimilation/utilization of these materials by the microbial populations present in the disposal infrastructures) in short time frames (one or two growing seasons) needs to be demonstrated beyond doubt.

Polyethylene (PE) or PE-wax coated paper products are problematic in composting because the paper will fully biodegrade under composting conditions, but the PE or wax coating does not biodegrade and builds up in the compost. Paper products coated with fully biodegradable film can provide comparable water resistance, tear strength like the PE coating. However, it is completely biodegradable and non-interfering in recycling operations (unlike current polytheylene or PE-wax coated paper). These new packaging products along with other biowastes, including food wastes can be collected and composted to generate a good, valuable soil amendment that goes back on the farmland to re-initiate the carbon cycle.

Integration with Disposal Infrastructure

Making or calling a product biodegradable or recyclable has no meaning whatsoever if the product after use by the customer does not end up in a disposal infrastructure that utilizes the biodegradability or recyclability features. Recycling makes sense if the recyclable product can be easily collected and sent to a recycling facility to be transformed into the same or new product. Biodegradable products would make sense if the product after use ends up in a disposal infrastructure that utilizes biodegradation. Composting, waste water/sewage treatment facilities, and managed, biologically active landfills (methane/landfill gas for energy) are established biodegradation infrastructures Therefore, producing biodegradable plastics using annually renewable biomass feedstocks that generally end up in biodegradation infrastructures like composting is ecologically sound and promotes sustainability. Materials that cannot be recycled or biodegraded can be incinerated with recovery of energy (waste to energy). Landfills are a poor choice as a repository of plastic and organic waste. Today's sanitary landfills are plastic-lined tombs that retard biodegradation because of little or no moisture and negligible microbial activity. Organic waste such as lawn and yard waste, paper, food, biodegradable plastics, and other inert materials should not be entombed in such landfills. Figure 7 illustrates the integration of biodegradable plastics with disposal infrastructures that utilize the biodegradable function of the plastic product.

In Degradable Polymers and Materials: Principles and Practice (2nd Edition); Khemani, K., et al.;
ACS Symposium Series; American Chemical Society: Washington, DC, 2012.

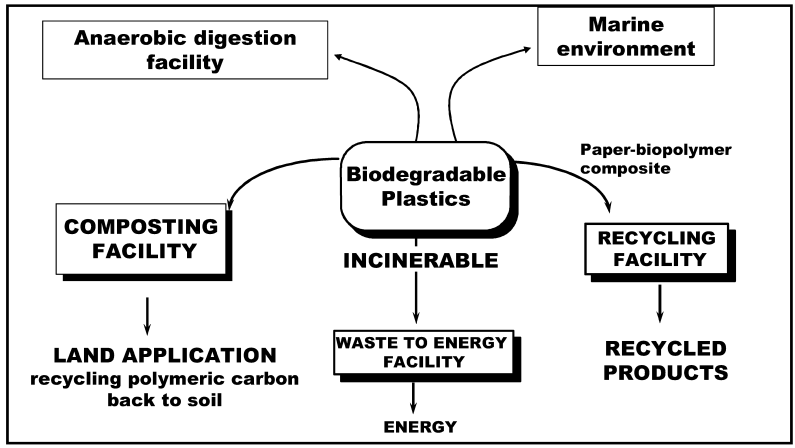

Figure 7. Integration of biodegradable plastics with disposal infrastructures.

Amongst disposal options, composting is an environmentally sound approach to transfer biodegradable waste, including the new biodegradable plastics, into useful soil amendment products. Composting is the accelerated degradation of heterogeneous organic matter by a mixed microbial population in a moist, warm, aerobic environment under controlled conditions. Biodegradation of such natural materials will produce valuable compost as the major product, along with water and carbon dioxide. The CO_2 produced does not contribute to an increase in greenhouse gases because it is already part of the biological carbon cycle. Composting our biowastes not only provides ecologically sound waste disposal but also provides much needed compost to maintain the productivity of our soil and sustainable agriculture. Figure 7 shows disposal infrastructures that can receive biodegradable plastics.

As discussed earlier, composting is an important disposal system because greater than 50% of the municipal soild waste (MSW) stream is biowastes like yard trimmings, food, non-recyclable paper products (see Figure 8).

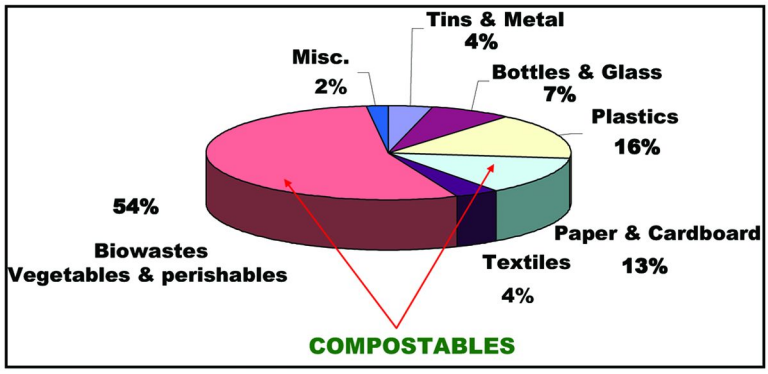

Figure 8. Typical MSW distribution by weight

In Degradable Polymers and Materials: Principles and Practice (2nd Edition); Khemani, K., et al.;
ACS Symposium Series; American Chemical Society: Washington, DC, 2012.

Degradable vs Biodegradable – An Issue

Designing products to be degradable or partially biodegradable causes irreparable harm to the environment. Degraded products may be invisible to the naked eye. However, out of sight does not make the problem go away. One must ensure complete biodegradability in a short defined time frame (determined by the disposal infrastructure). Typical time frames would be up to one growing season or one year. As discussed earlier the disposal environments are composting, anaerobic digestion, marine/ocean, and soil.

Unfortunately, there are products in the market place that are designed to be degradable, i.e they fragment into smaller pieces and may even degrade to residues invisible to the naked eye. However, there is no data presented to document complete biodegradability within the one growing season/one year time period. It is assumed that the breakdown products will eventually biodegrade. In the meanwhile, these degraded, hydrophobic, high surface area plastic residues migrate into the water table and other compartments of the ecosystem causing irreparable harm to the environment. In a Science article (*8*) researchers report that plastic debris around the globe can erode (degrade) away and end up as microscopic granular or fiber-like fragments, and that these fragments have been steadily accumulating in the oceans. Their experiments show that marine animals consume microscopic bits of plastic, as seen in the digestive tract of an amphipod. The Algalita Marine Research Foundation (*9*) report that degraded plastic residues can attract and hold hydrophobic elements like PCB and DDT up to one million times background levels. The PCB's and DDT's are at background levels in soil, and diluted out so as to not pose significant risk. However, degradable plastic residues with these high surface area concentrate these highly toxic chemicals, resulting in a toxic time bomb, a poison pill floating in the environment posing serious risks.

Recently, Japanese researchers (*10*) confirmed these findings. They reported that PCBs, DDE, and nonylphenols (NP) were detected in high concentrations in degraded polypropylene (PP) resin pellets collected from four Japanese coasts. The paper documents that plastic residues function as a transport medium for toxic chemicals in the marine environment.

The issue of degradable and partial biodegradable plastics released into the environment causing serious environmental and health impacts is documented in peer reviewed articles published in a special theme issue of the Philosophical Transactions of the Royal Society (Biological Sciences) journal (*11*) titled "Plastics, the environment, and human health".

Therefore, designing hydrophobic polyolefin plastics, like polyethylene (PE) to be degradable, without ensuing that the degraded fragments are completely assimilated by the microbial populations in the disposal environment in a very short time period poses more harm to the environment than if it was not made degradable. These concepts are illustrated in Figure 9. The Figure shows that heat, moisture, sunlight and/or enzymes shorten & weaken polymer chains, resulting in fragmentation of the plastic and some cross-linking creating more intractable persistent residues. It is possible to accelerate the breakdown of the plastics in a controlled fashion to generate these fragments, some of which could

In Degradable Polymers and Materials: Principles and Practice (2nd Edition); Khemani, K., et al.;
ACS Symposium Series; American Chemical Society: Washington, DC, 2012.

be microscopic and invisible to the naked eye, and some elegant chemistry has been done to make this happen as reported in some papers in this book.

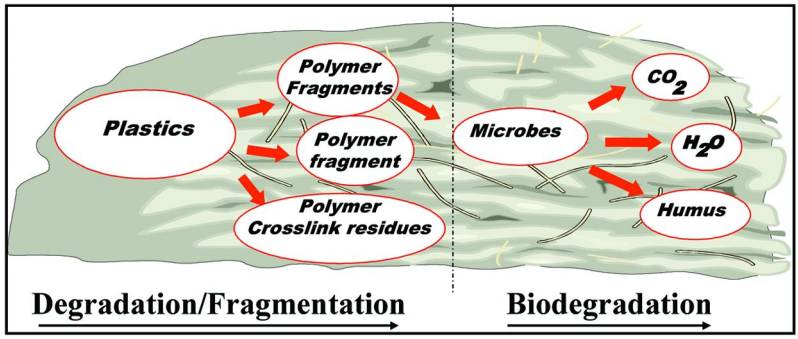

Figure 9. Degradation vs biodegradation

However, this constitutes only degradation/fragmentation, and not biodegradation. As discussed earlier hydrophobic polymer fragments pose risk to the environment, unless the degraded fragments are completely assimilated as food and energy source by the microbial populations present in the disposal system in a very short period (one year). Microorganisms use the carbon substrates to extract chemical energy for driving their life processes by aerobic oxidation of glucose and other readily utilizable C-substrates as shown by the Equation 2.

AEROBIC

$$\text{C-substrate} + 6\ O_2 \longrightarrow 6\ CO_2\uparrow + 6\ H_2O;\ \Delta G^{0'} = -686\ \text{kcal/mol} \quad \text{Equation 2}$$

$(CH_2O)_X$; x = 6

Thus, a measure of the rate and amount of CO_2 evolved in the process is a direct measure of the amount and rate of microbial utilization (biodegradation) of the C-polymer. This forms the basis for ASTM and International Standards for measuring biodegradability or microbial utilization of the test polymer/plastics. Thus, one can measure the rate and extent of biodegradation or microbial utilization of the test plastic material by using it as the sole carbon source in a test system containing a microbially rich matrix like compost in the presence of air and under optimal temperature conditions (preferably at 58° C – representing the thermophilic phase). Figure 10 shows a typical graphical output that would be obtained if one were to plot the percent carbon converted to CO_2 as a function of time in days.First, a lag phase during which the microbial population adapts to the available test C-substrate. Then, the biodegradation phase during which the adapted microbial population begins to utilize the carbon substrate for its cellular life processes, as measured by the conversion of the carbon in the test material to CO_2. Finally, the output reaches a plateau when all of the substrate is completely utilized.

In Degradable Polymers and Materials: Principles and Practice (2nd Edition); Khemani, K., et al.;
ACS Symposium Series; American Chemical Society: Washington, DC, 2012.

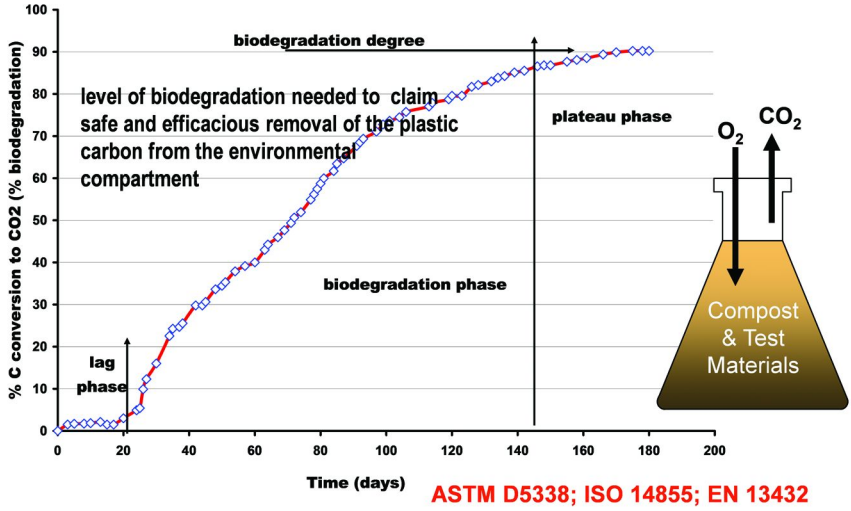

Figure 10. Test method to measure the rate and extent of microbial utilization (biodegradation) of biodegradable plastics

Based on the above concepts, ASTM committee D20.96 (*12*) has developed a Specification Standard for products claiming to be biodegradable under composting conditions or compostable plastic. The specification standard ASTM D6400 identifies 3 criteria

- **Complete biodegradation (using ASTM D5338 test method)**:
    - Conversion to CO_2, water & biomass via microbial assimilation of the test polymer material in powder, film, or granule form.
    - 60% carbon conversion of the test polymer to CO_2 for homopolymer & 90% carbon conversion to CO_2 for copolymers, polymer blends, and addition of low MW additives or plasticizers.
    - Same rate of biodegradation as natural materials -- leaves, paper, grass & food scraps
    - Time -- 180 days or less; if radiolabeled polymer is used 365 days or less.
- **Disintegration**
    - <10% of test material on 2mm sieve using the test polymer material in the shape and thickness identical to the product's final intended use – see ISO 16929 (*13*) and ISO 20200 (*14*).

In Degradable Polymers and Materials: Principles and Practice (2nd Edition); Khemani, K., et al.;
ACS Symposium Series; American Chemical Society: Washington, DC, 2012.

- **Safety**
    - The resultant compost should have no impacts on plants, using OECD Guide 208, Terrestrial Plants, Growth Test
    - Regulated (heavy) metals content in the polymer material should be less than 50% of EPA (USA, Canada) prescribed threshold.

The above specification standard is in harmony with standards in Europe, Japan, Korea, China, and Taiwan, for example EN13432 titled "Requirements for Packaging Recoverable through Composting and Biodegradation—Test Scheme and Evaluation Criteria for the Final Acceptance of Packaging" is the European standard (norm) and similar to D6400. At the International level, the International Standards Organization (ISO) has ISO 17088, "Specification for Compostable Plastics" which is in harmony with ASTM D 6400, and the European norms.

Figure 11 summarizes the current standards for the different disposal systems.

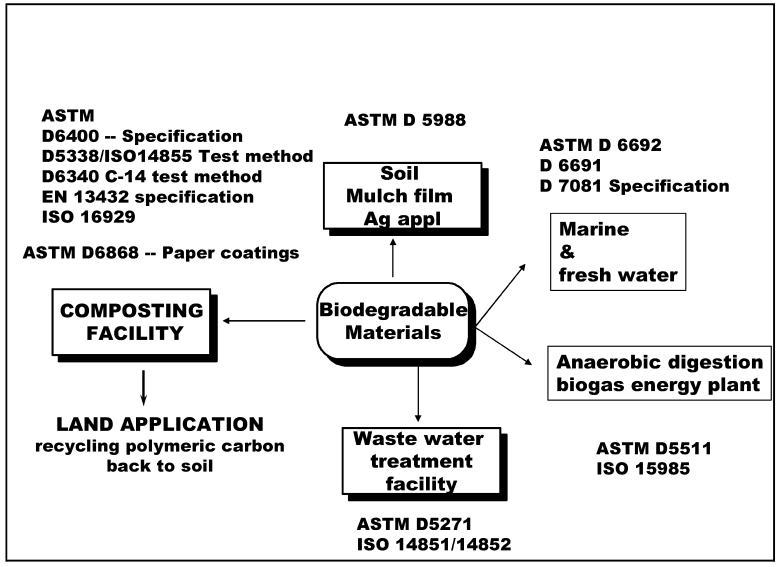

Figure 11. ASTM and European (EN) Standards for biodegradable plastics in different disposal systems.

Technology Exemplars

Biobased and Biodegradable Polymer Materials

Polymer materials based on annually renewable agricultural and biomass feedstocks can form the basis for a portfolio of sustainable, environmentally

In Degradable Polymers and Materials: Principles and Practice (2nd Edition); Khemani, K., et al.;
ACS Symposium Series; American Chemical Society: Washington, DC, 2012.

preferable alternatives to current materials based exclusively on petroleum feedstocks. Two basic routes are possible. Direct extraction from biomass yields a series of natural polymer materials (cellulose, starch, proteins), fibers, and vegetable oils that can form the platform on which polymer materials and products can be developed as shown in Figure 12 , the bolded items in the Figure represents our work in this area.

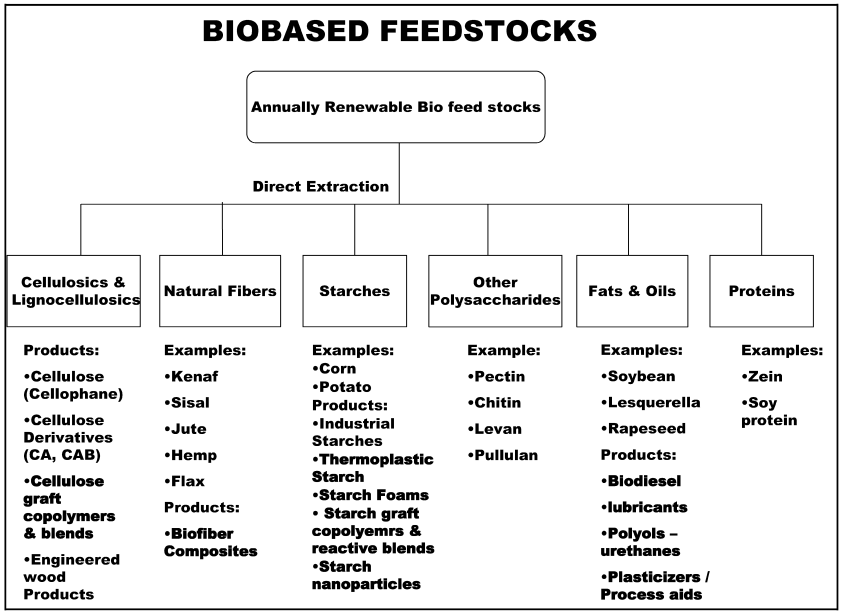

Figure 12. Direct extraction of biomass to provide biopolymers for use in manufacture of biobased products.

Alternatively, the biomass feedstock (annually renewable resources) can be converted to bio-monomers by fermentation or hydrolysis. The biomonomers can be further modified by a biological or chemical route. As shown in Figure 13, the biomonomers can be fermented to give succinic acid, adipic acid, 1,3-propane diol – precursor chemicals for the manufacture of polyesters – example is DuPont's Sorona polyestyer made from a bio 1,3-propanediol. Biomonomers can be fermented to lactic acid, which is then converted into poly(lactic acid) – currently being commercialized by NatureWorks LLC with a 300 MM lb manufacturing plant in Blair, Nebraska (*15*). Bio-monomers can also be microbially transformed to biopolymers like the polyhydroxyalkanoates (PHA's). Papers relating to PHA polymers can be found in other chapters in this book.

In Degradable Polymers and Materials: Principles and Practice (2nd Edition); Khemani, K., et al.;
ACS Symposium Series; American Chemical Society: Washington, DC, 2012.

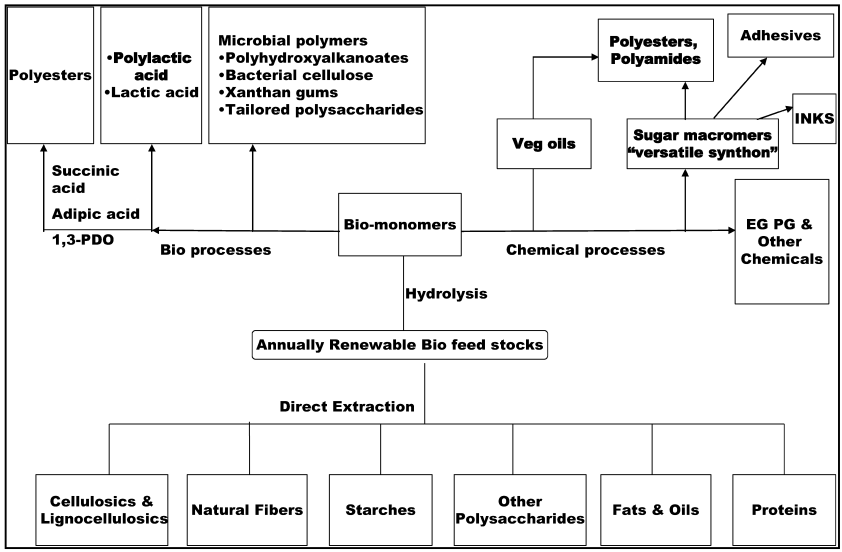

Figure 13. Conversion to biomonomer and otherchemicals and polymers.

Instead of microbial fermentative processes, chemical conversion of biomonomers yields intermediate chemicals like ethylene, and propylene glycols. Vegetable oils offer a platform to make a portfolio of polyols, lubricants, polyesters, polyamides. In another chapter in this book, we report on ozone mediated transformation of vegetable oils to polyols, urethane foams, polyesters, and polyamides.

Surfactants, detergents, adhesives, and water-soluble polymers can be engineered from biomass feedstocks. As discussed earlier, biobased materials targeted for short-life, single use, disposable packaging materials and consumer products can and should be engineered to retain inherent biodegradability properties, thereby offering an environmentally responsible disposal option for such products.

References

1. About Braskem. http://www.braskem.com.br/plasticoverde/eng/default.html.
2. About Coca Cola company. http://www.thecoca-colacompany.com/dynamic/press_center/2012/06/pet-collaborative.html (June 5, 2012).
3. *Annual Book of Standards*; Standard D 6866; ASTM International: Philadelphia, PA, 2012; Vol. 8.03.
4. About Federal Biopreferred Program. www.biopreferred.gov.
5. *Annual Book of Standards*; Standard D 7075; ASTM International: Philadelphia, PA, 2012; Vol 8.03.

In Degradable Polymers and Materials: Principles and Practice (2nd Edition); Khemani, K., et al.; ACS Symposium Series; American Chemical Society: Washington, DC, 2012.

6. Narayan, R. In *Science and Engineering of Composting: Design, Environmental, Microbiological and Utilization Aspects*; Hoitink, H. A. J., Keener, H. M. Renaissance Publications: OH, 1993; p 339.
7. Narayan, R. In *Biodegradable Plastics and Polymers*; Doi, Y., Fukuda, K.; Elsevier: New York, 1994; p 261.
8. Thompson, R. C.; Olsen, Y.; Mitchell, R. P.; Davis, A.; Rowland, S. J.; John, A. W. G.; McGonigle, D.; Russell, A. E. *Science* **2004**, *304*, 838.
9. From Algalita Marine Research Foundation. www.algalita.org/pelagic_plastic.html.
10. Mato, Y; Isobe, T; Takada, H; Kahnehiro, H; Ohtake, C; Kaminuma, T. *Environ. Sci. Technol.* **2001**, *35*, 318–324.
11. Thompson, R. C.; Olsen, Y.; Mitchell, R. P.; Davis, A.; Rowland, S. J.; John, A. W. G.; McGonigle, D.; Russell, A. E. *Philos. Trans. R. Soc. B* **2009**, *364* (July 27) (special issue).
12. ASTM International, Committee D20 on Plastics, Subcommittee D20.96 on Biobased and Environmentally Degradable Plastics. www.astm.org.
13. Internationa Standards Organization (ISO) Plastics ISO 16929 – Determination of the degree of disintegration of plastic materials under defined composting conditions in a pilot-scale test.
14. International Standards Organization (ISO) Plastics ISO 202004 – Determination of the degree of disintegration of plastic materials under simulated composting conditions in a laboratory-scale test.
15. About Nature works, PLA producer. www.natureworks.com.

Chapter 3

Biodegradation Testing Protocols

B. De Wilde*

Organic Waste Systems (OWS) nv, Dok Noord 5, B-9000 Gent, Belgium
***bruno.dewilde@ows.be**

Many methods have been described in literature how to test biodegradation. Several are measuring only indirect parameters or even incorrect parameters. Yet, the essence of biodegradation is well known and involves the measurement of carbon to CO2 conversion in case of aerobic conditions and carbon to CH4 and CO2 conversion in case of anaerobic conditions. An alternative in case of aerobic biodegradation is measurement of oxygen consumption. Optimum test conditions with regard to temperature, pH, nutrients, buffering capacity, oxygen supply, particle size, etc. are provided making the carbon source, which is the sample, the only limiting factor.

Since biodegradation is determined by environmental factors, the rate and extent of biodegradation can be different from one environment to the other. Therefore it is important to test biodegradation in an environment representative of real disposal conditions.

Finally, it must be noted that biodegradation alone if mostly not sufficient for acceptance in biological disposal but that also requirements with regard to disintegration and environmental safety are formulated.

Introduction

Several factors can lead to degradation of polymers including light, heat, biological activity, mechanical impact, etc. This chapter deals with biodegradation only, which is degradation caused by biological activity, more in particular enzymatic, microbial or fungal activity.

A major distinction is made whether biodegradation is taking place under conditions where oxygen is available, so-called aerobic biodegradation, and

In Degradable Polymers and Materials: Principles and Practice (2nd Edition); Khemani, K., et al.;
ACS Symposium Series; American Chemical Society: Washington, DC, 2012.

conditions where oxygen is not available, so-called anaerobic biodegradation. In the first case of aerobic biodegradation, the process is a basic biological process in which organic, carbon-based matter is oxidized leading to conversion of carbon to carbon dioxide. This is equivalent to respiration and can considered being the opposite of photosynthesis. The standard equation is represented in Figure 1. Oxygen is consumed through which carbon of the sample is converted into carbon dioxide and water. Some carbon can remain in residual original sample parent material or in metabolites; the total of this is the residual carbon. Some carbon is used to produce new biomass, multiplication of micro-organisms or longer, fatter micro-organisms, this is the biomass yield.

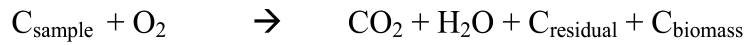

Figure 1. Standard aerobic biodegradation reaction

In anaerobic biodegradation, no oxygen is consumed. The sample is converted into methane and carbon dioxide, residual sample or metabolites and biomass, see equation in Figure 2. Anaerobic conditions are created when oxygen is not present or when oxygen is consumed or depleted more rapidly than it is replaced (mostly by diffusion). Natural examples are bottoms of rivers, swamps and lakes and the rumen of herbivores. Man-made examples are landfills, septic tanks, anaerobic digesters for treatment of wastewater, sludge or solid waste.

Figure 2. Standard anaerobic biodegradation reaction

From these basis equations it can be seen that true monitoring of biodegradation is based on CO_2 (and eventually CH_4) production or O_2 consumption. Other parameters such as visual disappearance, weight loss, decrease in molecular weight, disappearance of parent compound, decrease in mechanical characteristics such as tensile strength, tear resistance, etc. are only monitoring secondary effects and at best only demonstrate partial and incomplete biodegradation. They cannot be used to make claims on (full) biodegradability.

Another important aspect with regard to biodegradation is the importance of the environment in which it is supposed to take place. Rate and degree of biodegradation are determined by various factors which can be different from one environment to the other. These factors include moisture content (going from aquatic to dry), oxygen availability (aerobic or anaerobic), temperature (high in industrial composting, ambient to low in soil and water), type of microbiology (bacteria and/or fungi and/or actinomycetes), density of microbiology (high in composting and in wastewater treatment, low in soil and marine), salt concentration, etc. For polymers, mainly the temperature and the presence or absence of fungi can have a big impact on the degree of biodegradation. The other

In Degradable Polymers and Materials: Principles and Practice (2nd Edition); Khemani, K., et al.;
ACS Symposium Series; American Chemical Society: Washington, DC, 2012.

factors mainly have an influence on the rate of biodegradation. As a consequence, polymers can be biodegradable in one environment and not in the other. Also, a biodegradability claim without specifying an environment in which it is supposed to take place is an incomplete or even useless claim.

A ranking of major environmental niches with regard to aggressiveness of biodegradation is given in Figure 3.

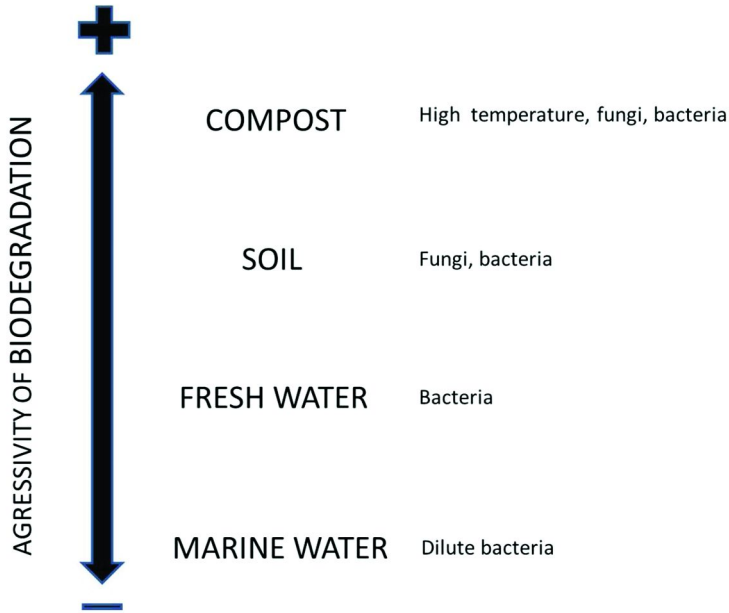

Figure 3. Relation between environment and aggressivity of biodegradation

A common characteristic of biodegradation testing protocols is that all test conditions are optimized except for the carbon source. This means for example that temperature is kept constant at an optimum level typical of the environment which is being tested (e.g. 21°C for soil and water, 58°C for industrial composting). Also pH and buffering capacity are optimal and constant. Macro- and micro-nutrients are sufficiently available, the only limiting "food source" is carbon. Biological life is present in high concentration and also ideally as diversified as possible. Because of the biology introduced in the reactors, some background activity is present –all biological life consumes oxygen and produces carbon dioxide under aerobic conditions; methane and carbon dioxide under anaerobic conditions-; yet, background activity is kept as low as possible in order to achieve a maximum signal to noise ratio which in turn increases the sensitivity and the reproducibility of the test. For that reason, the inoculum (which is the biological life introduced in the test reactors) is stabilized prior to use.

In order to shorten the test duration, the sample is introduced at a small particle size: liquid or powder. To that extent, it might be needed to mill the sample (cryogenically) prior to testing. As biodegradability is linked to the chemical

In Degradable Polymers and Materials: Principles and Practice (2nd Edition); Khemani, K., et al.;
ACS Symposium Series; American Chemical Society: Washington, DC, 2012.

structure of the sample, the physical form plays no role but will only have an effect on the duration of biodegradation.

Biodegradation testing protocols typically foresee at least 3 different, parallel test series. One is the blank which only contains the inoculum without any extra carbon source and which is needed to determine the background activity. Another test series is the positive control which includes an easily biodegradable reference material with a known biodegradation pattern, examples are glucose and cellulose. Often, minimum requirements are mentioned for the positive reference which must be met in order for the test to be valid. The third test series is the sample of which the net biodegradation is determined after subtraction of the background activity in the blank from the total activity in the test reactors. Sometimes also a negative control is included with a reference material which is not biodegradable and of which biodegradation measured must be zero. As biological tests inherently give some variation, each test series is run in several replicates, mostly 3 at minimum.

Historically, biodegradation test methods have first been developed for chemicals in wastewater with first protocols being published by OECD (the Organization for Economic Cooperation and Development) in 1981 (*1*). Later on, biodegradation methods were described for other environments and also for other, more complex samples such as polymers.

For clear and correct communication it is important to use correct terminology as recommended by IUPAC and described by Vert et al. (*2*)

In this chapter an overview of different testing protocols is given, organized per category of environment. Also other aspects with regard to compostability are discussed.

Aquatic, Aerobic Biodegradation Tests

Several aquatic biodegradation test methods have been published in the OECD Guidelines for the Testing of Chemicals (*1*). The basic concept is always more or less the same, the difference mainly being the parameter followed to monitor biodegradation. The 2 best known and most widely applied methods are the so-called “Sturm” test and the respirometric test.

Sturm Test

In the Sturm test the carbon dioxide production is precisely measured and biodegradation is determined as $C \rightarrow CO_2$ conversion. The test is named after the person who developed the procedure (*3*). Afterwards the test was published as OECD #301 B (*1*). A further step in standardization was the publication by ISO, the International Organization for Standardization, in 1990 of ISO 9439, *Water quality -- Evaluation in an aqueous medium of the "ultimate" aerobic biodegradability of organic compounds -- Method by analysis of released carbon dioxide*. This procedure was written for low-molecular-weight compounds to be tested pure and at low concentrations and was less suitable for biodegradable polymers with high molecular weight Therefore, the test procedure was slightly

In Degradable Polymers and Materials: Principles and Practice (2nd Edition); Khemani, K., et al.;
ACS Symposium Series; American Chemical Society: Washington, DC, 2012.

modified and published in 1999 as ISO 14852, *Determination of the ultimate aerobic biodegradability of plastic materials in an aqueous medium – Method by analysis of evolved carbon dioxide.*

The sample is brought in a mineral medium (this is a recipe of distilled water to which macro- and micro-nutrients have been added), spiked with inoculum and incubated under batch conditions. The latter means the sample is added in a single, "one-shot" feeding session and has to be distinguished from semi-continuous or continuous tests in which the sample is added at regular intervals or continuously. The inoculum is activated sewage sludge, surface water or soil or in the case of ISO 14852 also compost eluate. Mixtures of several sources can also be used. The duration of the test is typically 4 weeks but can also be longer. The test should be run until a 'plateau in activity' is reached. After several months however, reproducibility becomes smaller and ISO 14852 for example specifically mentions a maximum duration of 6 months.

In order to have a more complete equation of biodegradation, it would be useful if also the biomass production could be determined (see Figure 1). Although this is not precisely possible, ISO 14852 includes a procedure based on determination of protein and some assumptions regarding protein and carbon content of biomass.

Besides OECD and ISO, similar procedures have been published also by ASTM (the American standards organization, ASTM D.5209), EN (European, EN 14047), JIS (Japanese, JIS K 6951) and various other national standards organizations.

Respirometric Test

The respirometric test is an aquatic, aerobic biodegradation test based on oxygen consumption. The procedure is very similar or identical to that of the Sturm test, the main difference being that instead of CO_2 production, O_2 consumption is measured. This is the so-called biological oxygen demand (BOD) which is compared to the theoretical oxygen demand (ThOD, based on calculation of oxygen required to fully oxidize each element in the stoichiometric formula of the sample) or chemical oxygen demand (COD or oxygen required to chemically fully oxidize the sample) to calculate the percentage of biodegradation. Mineral medium, inoculum, conditions of incubation and batch feeding are same as for Sturm test.

The test has first been published as OECD 301C and ISO 9408 and afterwards also as ISO 14851, ASTM D.5271, EN 14048 and JIS K 6950.

Other Aquatic Aerobic Biodegradation Tests

Other aquatic biodegradation tests can be distinguished in batch tests and in semi-continuous or continuous tests. Batch tests have been developed for simple, pure chemical substances and monitor parameters such as DOC (dissolved organic carbon), DO (dissolved oxygen), parent compound or specific metabolites. Except for soluble samples these tests are limited in application possibilities.

In Degradable Polymers and Materials: Principles and Practice (2nd Edition); Khemani, K., et al.;
ACS Symposium Series; American Chemical Society: Washington, DC, 2012.

In semi-continuous or continuous tests the sample is fed at regular intervals or continuously and reactors are operated for a much longer time, typically several months. These tests have been developed for simulation of wastewater treatment plants and evaluation of long-term effects. They can also be used for adaptation of inoculum. Examples are the semi-continuous activated sludge (SCAS) test (ISO 9887) and the continuous activated sludge (CAS) or coupled-units test (ISO 11733).

Some chemical substances require adaptation of micro-organisms before they can be degraded. This means the extra-cellular enzymes need to be modified in order to be able to degrade the substance. If such a substance enters a wastewater treatment plant by accident just once, the micro-organisms in the wastewater sludge have no time to adapt and the sample will leave the wastewater treatment plant again before it has been biodegraded. Yet, if such a substance is continuously present in the wastewater, the micro-organisms can adapt and will degrade the chemical substance. PVOH, poly (vinyl alcohol), is an example of such a substance which needs adaptation.

Marine Biodegradation

Marine conditions in seas and oceans form a special case of aquatic environment. Specific biodegradation methods have been published which are comparable to the other, freshwater biodegradation tests. Main differences are the mineral medium, modified to be more representative of seawater, and also the inoculum, containing marine micro-organisms. The most relevant standard was published in 2009 as *ASTM D6691 – 09- Standard Test Method for Determining Aerobic Biodegradation of Plastic Materials in the Marine Environment by a Defined Microbial Consortium or Natural Sea Water Inoculum.* Biodegradation is measured via CO_2 production.

Composting Biodegradation Tests

Standard Controlled Composting Biodegradation Test

After the introduction of biodegradable polymers in the late 80's and the early 90's, it quickly became clear that other biodegradation tests were needed besides aquatic and soil biodegradation. Especially for (industrial) composting as this is the preferred route for organic solid waste. Conditions in industrial composting are very different from aquatic conditions. First of all, temperature is much higher with typical temperatures of 60-65°C in composting compared to ambient temperature in water. Moisture and aeration obviously also are very different. A very important difference is the activity of fungi and actinomycetes. Whereas in water these organisms can be detected but are not really active, in compost they are dominantly present and very active. Several polymers or chemicals are much better and faster degraded by fungi than by bacteria. A well-known and very common example is lignin, and its biodegradation by white-rot fungi (*4*, *5*). For these reasons, a new test method was developed for determination of

In Degradable Polymers and Materials: Principles and Practice (2nd Edition); Khemani, K., et al.;
ACS Symposium Series; American Chemical Society: Washington, DC, 2012.

biodegradation in composting conditions at high temperature based on carbon to carbon dioxide conversion (*6*, *7*).

The sample is added to stable, mature compost and incubated under batch conditions at 58°C under optimum oxygen and moisture conditions. The stable compost at the same time functions as carrier matrix, source of microorganisms (bacteria and fungi) and source of nutrients. Oxygen (air) is continuously supplied by forced aeration. The exhaust air is analyzed for CO_2, either by on-line measurement or by absorption and titration. In principle, the maximum test duration is 6 months while a typical minimum duration is 45 days. Strict requirements are imposed on the results for the positive reference, cellulose, in order to validate the test. Preferably, the sample is added under the form of fine powder in order to keep the test duration as short as possible.

The first international standard published on this procedure is ASTM D.5338-92. Afterwards ISO 14855 was published in 1999 as ISO 14855 - *Determination of the ultimate aerobic biodegradability and disintegration of plastic materials under controlled composting conditions - Method by analysis of evolved carbon dioxide*. Later on also EN 14046 in Europe and JIS K 6953 in Japan was published.

Mineral Bed Composting Test

With regard to biodegradation of polymers, both the aquatic and composting test have some particular advantages and disadvantages. Because of the very standardized test conditions, the aquatic tests permit not only the determination of biodegradation through CO_2 production or O_2 consumption but also of metabolites and biomass. Yet, water is of course a very poor simulation of a composting environment and biodegradation is (much) weaker. On the other hand, the controlled composting test is a much better simulation of composting in reality, with high fungal activity and aggressive conditions. Yet, compost is a complex matrix making a precise measurement of biomass and metabolites much more difficult.

In an attempt to combine the benefits of both tests, a new method was developed in which the compost matrix is replaced by a mineral, inert medium (*8*, *9*). More in particular this medium is vermiculite which is a type of expanded clay mineral with an overall physical structure and water holding capacity behavior very similar to compost. This medium or matrix is inoculated with a compost extract and mineral medium is added. The inert matrix should lead to more standardized and reproducible test conditions and enable the extraction and determination of metabolites and biomass. This new method was introduced in international standards in 2005 with a new edition of ISO 14855.

Afterwards, another modification was published in 2007 as ISO 14855-2 in which the quantification of CO2 is done by absorption on soda lime and soda talc and weight determination.

Other Composting Biodegradation Test Procedures

In order to overcome the difficulty of distinguishing CO_2 coming from the sample or from the inoculum, another approach is to use radio-labeled samples. In

In Degradable Polymers and Materials: Principles and Practice (2nd Edition); Khemani, K., et al.;
ACS Symposium Series; American Chemical Society: Washington, DC, 2012.

conventional biodegradation testing net CO_2 production is obtained by subtraction where it cannot be ascertained that net CO_2 is actually indeed coming from the sample. By using radio-labeled ^{14}C-atoms in the sample and subsequently determining $^{14}CO_2$ there is no doubt about biodegradation of the sample itself. A method has been developed in which biodegradation is measured by determining ^{14}C to $^{14}CO_2$ conversion in respectively an aquatic and a composting environment. $^{14}CO_2$ is measured by absorption and liquid scintillation counting. The method has been published by ASTM as *ASTM D.6340-98(2007) - Standard Test Methods for Determining Aerobic Biodegradation of Radiolabelled Plastic Materials in an Aqueous or Compost Environment*. Nevertheless, this procedure still shows 2 disadvantages. One is the cost and difficulty (or even feasibility) to radiolabel each and every carbon atom of the sample. On top of that, this method does also not allow a precise determination of biomass produced from the sample.

Soil Biodegradation Tests

Several types of chemicals and polymers are directly applied in or on soil and need to biodegrade in situ. Examples are pesticides, agricultural aid items (e.g. mulching film, clips, planting pots), road construction aids, funeral items (body bag), etc. Soil is a different environment compared to composting as it only has ambient temperature. Some polymers do need a thermal trigger and will only see a first hydrolysis at high temperate after which biodegradation goes on. Consequently, biodegradability in such case is different from compost to soil. Soil is also different to water as there is also fungal activity. All this results in the need for also a soil biodegradation test.

The principle again is a batch test in which a sample is added once at start of the test to a soil matrix which is at the same time acting as a carrier matrix, a source of micro-organisms (the inoculum) and a source of nutrients. The reactors are incubated at optimum conditions of (ambient) temperature, oxygen supply and moisture. CO_2 production is monitored by absorption and titration or by on-line measurement combined with active aeration. A typical minimum duration is 3-4 months whereas standards prescribe a maximum of 6 months. Yet, experiments have demonstrated that reliable and reproducible results can also be obtained after even much longer periods.

In order to improve the reproducibility of the test it is better to use a blend of different soils obtained from different sources. Differences are caused by different biology included (e.g. forest soil typically has more fungi than pasture or field soil) and by different texture (e.g. clay versus loamy sand, etc.). By using different soils in which these variances are covered, the variations they cause can be reduced.

Standard norms on soil biodegradation of pure chemicals have first been published as OECD 301 and ISO 11266. Later, ASTM D.5988-96 was written for plastics and in 2003 an ISO norm was published, entitled ISO 17556 – *Plastics - Determination of the ultimate aerobic biodegradability in soil by measuring the oxygen demand in a respirometer or the amount of carbon dioxide evolved.*

In Degradable Polymers and Materials: Principles and Practice (2nd Edition); Khemani, K., et al.;
ACS Symposium Series; American Chemical Society: Washington, DC, 2012.

Anaerobic Biodegradation Tests

Aquatic Anaerobic Biodegradation Test Procedures

The European Centre for Ecotoxicology and Toxicology of Chemicals was the first to publish an official standard as ECETOC Technical Report N° 28 (*10*) in 1988. The sample is introduced into an aqueous mineral medium, spiked with inoculum (anaerobic sludge) and incubated under batch conditions at mesophilic temperature (35°C). The duration of incubation is 60 days. Biodegradation is measured by following the biogas production (measured by volume displacement or pressure build-up) and the increase of DIC (Dissolved Inorganic Carbon) in the medium. Depending on the frequency of biogas determinations also the kinetics of biodegradation can be established.

Later, the same protocol was accepted as ISO 11734 in 1995 and ASTM D.5210 in 1992. In 2005 a new version with some minor modifications was published, relevant for polymers: *ISO 14853– Plastics - Determination of the ultimate anaerobic biodegradability in an aqueous system – Method by measurement of biogas production*.

High-Solids Anaerobic Biodegradation

Also in anaerobic digestion a distinction can be made between aquatic conditions and "dry" or better high-solids conditions. The first are operated at high moisture content (>95%) and at mesophilic temperature. The latter are run at (much) drier conditions, with moisture content going down as low as 60%. They can be run at both mesophilic (30-35°C) and thermophilic temperature (50-55°C), which are 2 optimum temperature zones for anaerobic digestion. Because of these different operational conditions biodegradation pattern can be different with regard to rate and level of biodegradation.

A new biodegradation test method was first developed at ASTM level in 1994 and later adopted in 2004 as *ISO 15985– Plastics – Evaluation of the ultimate anaerobic biodegradability and disintegration under high-solids anaerobic-digestion conditions– Method by analysis of released biogas*.

The procedure is again a batch test in which a small amount of sample is added to a large amount of highly active inoculum that has been stabilized prior to the start of the biodegradation test. The inoculum consists of residue obtained directly from a high-solids biogasification unit or obtained after dewatering of anaerobic sludge. Optimal conditions are provided and the mixture is left to ferment batch wise. The volume of biogas produced is measured and used to calculate the percentage of biodegradation based on carbon conversion.

Landfill Biodegradation

A particular form of anaerobic biodegradation is landfill biodegradation. Upon disposal oxygen is quickly consumed and not replaced at the same rate, turning the conditions into anaerobic. In USA biologically active landfills remain a viable waste management option for the future. On the contrary, in Europe, interest is much less, especially after the adoption in 1999 of the EU landfill

In Degradable Polymers and Materials: Principles and Practice (2nd Edition); Khemani, K., et al.;
ACS Symposium Series; American Chemical Society: Washington, DC, 2012.

directive, which is phasing out the disposal of biodegradable materials in landfills. Because of unfavorable conditions with regard to temperature, moisture content and concentration of micro-organisms, biodegradation in a landfill is much slower. Biodegradation methods have been published measuring biodegradation through loss of properties after exposure (ASTM D.5525-94a) or through biogas production (ASTM D.5526-94).

Compostability vs Biodegradation

Often biodegradation under composting conditions and compostability are confused or terms are used interchangeably. Yet, compostability encompasses more than just biodegradation. First of all, it also includes aspects of disintegration. This is the degradation on a macro physical level or the degradation or fragmentation of a product in small, often invisible particles. Biodegradation, on the contrary, as seen above, is a degradation process on a micro molecular level and involves the conversion of organic carbon to CO2 (and CH4 if anaerobic). Consequently, disintegration is linked to the physical dimensions of the sample, such as thickness or density, whereas biodegradation is linked to the chemical composition of the sample. Disintegration is determined at the end of a composting test by sieving, retrieving and mass determination of the remaining sample.

Besides requirements related to degradation, covering biodegradation and disintegration, international compostability standards such as ASTM D.6400, EN 13432 and ISO 17088, also define specifications with regard to environmental safety. These include heavy metal analyses and plant toxicity tests. Compostable polymers are therefore not only degradable under composting conditions but also environmentally safe (*11*).

It must be noted that the above-mentioned standards are related to industrial composting, which is always operated at high temperature (60°C or more) and cannot be used for home composting, operated at ambient temperature or slightly above. For home composting a voluntary program has been developed by Vincotte in Belgium (OK Compost Home) while a national standard was published in Australia in 2010 as AS 5810 – *Biodegradable plastics – Biodegradable plastics suitable for home composting.*

Conclusion

In biodegradation testing 2 aspects are of key importance. The first is that biodegradation should primarily be determined by measuring carbon to carbon dioxide conversion (and methane in case of anaerobic conditions). For aerobic conditions oxygen consumption is a good alternative. Other parameters such as weight loss, decrease of molecular weight, deterioration of mechanical characteristics, etc. are only secondary parameters and are not a proof of biodegradation but only, at best, of partial degradation.

In Degradable Polymers and Materials: Principles and Practice (2nd Edition); Khemani, K., et al.;
ACS Symposium Series; American Chemical Society: Washington, DC, 2012.

A second important aspect is the necessity to specify the environment when talking about biodegradation as both level and rate of biodegradation can be different from one environment to the other.

Several biodegradation testing protocols have been developed and many of these have been standardized. What is however still missing for several environments is specifications. When is biodegradation good enough? In what time frame? For industrial compostability this has been well established but for several other environments this is still missing.

References

1. OECD. *Guidelines for the Testing of Chemicals*; OECD: Paris, 1981.
2. Vert, M.; Doi, Y.; Hellwich, K.-H.; Hess, M.; Hodge, Ph.; Kubisa, P.; Rinaudo, M.; Schué, F. Terminology for biQorelated polymers and applications (IUPAC Recommendations 2012). *Pure Appl. Chem.* **2012**, *84* (2), 377–410.
3. Sturm, R. N. Biodegradability of Nonionic Surfactants : Screening Test for Predicting Rate and Ultimate Biodegradation. *J. Am. Oil Chem. Soc.* **1973**, *50* (May), 159.
4. Zimmermann, W. Minireview – Degradation of Lignin by Bacteria. *J. Biotechnol.* **1990**, *13*, 119.
5. Kirk, T. K. Degradation of Lignin. In *Microbial Degradation of Organic Compounds*; Gibson, D. T., Ed.; Marcel Dekker, Inc.: New York, Basel, 1984; p 399.
6. De Wilde, B., De Baere, L., Tillinger, R. *Test Methods for Biodegradability and Compostability*; Mededelingen Faculteit Landbouw, University of Gent: Gent, Belgium, 1993; Vol. 58/4a, p 1621.
7. Pagga, U.; Beimborn, D. B.; Boelens, J.; De Wilde, B. Determination of the Aerobic Biodegradability of Polymeric Material in a Laboratory Controlled Composting Test. *Chemosphere* **1995**, *31* (11/12), 4475.
8. Bellia, G.; Tosin, M.; Floridi, G.; Degli Innocenti, F. Activated Vermiculite, a Solid Bed for Testing Biodegradability under Composting Conditions. *Polym. Degrad. Stab.* **1999**, *66*, 65.
9. Spitzer, B., Menner, M. Simulation of a Compost Environment in a Mono-Substrate Fixed-Bed System. *Dechema Monographs*; VCH Verlagsgesellschaft: 1996; Vol. 133, p 681.
10. ECETOC. *Evaluation of Anaerobic Biodegradation*; Technical Report No. 28; Brussels, 1988 (ISSN-07773-8072-28).
11. De Wilde, B. Compostable Packaging – A Potential or a Threat for Compost? *Proceedings of Workshop 'Biological Treatment of Biodegradable Waste – Technical Aspects'*, Brussels, Belgium, April 8−10 2002; Workshop jointly co-organised by EU Commission DG Environment and JRC; Langenkamp, H., Marmo, L.; Publication EUR 20517 EN; 2003; pp 330−338.

In Degradable Polymers and Materials: Principles and Practice (2nd Edition); Khemani, K., et al.;
ACS Symposium Series; American Chemical Society: Washington, DC, 2012.

Chapter 4

Life Cycle Assessment (LCA) and Degradable Polymers

Tim Grant*

Director, Life Cycle Strategies Pty Ltd., Melbourne VIC 3000, Australia
***tim@lifecycles.com.au**

Life Cycle Assessment (LCA) is an internationally standardized method for analysing the environmental impacts of materials, products and services. LCA analyses the impacts of products from cradle to grave taking into account life cycle stages beginning with raw materials extraction, manufacturing, use and end of life stage with transport and distribution stages occurring in between many of these steps. LCA has been used extensively in the area of packaging and product design and there are substantial numbers of LCA applied to degradable polymers. These are in two forms – life cycle inventories of specific polymers that are available for product developers and decision makers to use in life cycle studies, and comparative LCA studies usually of conventional and degradable polymers. The results from these studies show some established trends such as lower use of fossil resources for the biologically derived polymers but higher land use and water use. Greenhouse emissions production impacts are often lower for biopolymers, however the impacts of degradable polymers at landfill are highly dependent on the technology and assumptions around landfill performance. Life cycle assessment has already played an essential role in the understanding and consideration of degradable polymers. The use of comparative studies of degradable polymers need to be explicit regarding the assumptions at end of life and in the future need to expand to take better account of land and water impacts.

In Degradable Polymers and Materials: Principles and Practice (2nd Edition); Khemani, K., et al.;
ACS Symposium Series; American Chemical Society: Washington, DC, 2012.

Introduction

Life Cycle Assessment (LCA) is an internationally standardized method for analysing the environmental impacts of materials, products and services. Its origins come from energy and environmental impact analysis which developed in the 1970 and 80's where competing environmental priorities were often involved in product decisions with one problem being solved at the expense of another. Electric cars reduce urban air pollution from direct combustion of liquid fossil fuels but increased impacts from power stations and electric storage devices. One of the earliest developments of LCA was in the assessment of degradable polymers in a Swiss study in the early 1970's (*1*). After the initial focus of comparing degradable and non-degradable polymers the study broadens its focus to the function and packaging and the alternative ways of providing this. This became a central pillar in LCA – the comparison of alternative ways of delivering equivalent functionality – referred to in LCA as the functional unit.

Humans and the Environment

LCA fundamentally is an analysis of the movement of substances and energy on the planet, the impacts of these as well as the ability of the earth to sustain human populations both now and into the future.

LCA also aims to protect selected environments - or aspects of the environment - which we believe have intrinsic value beyond our needs from them. The underlying motivation is to keep this environment which has been producing resources and has been sustaining us over thousands of years, as stable and as original as possible. By avoiding drastic changes in the state of the natural environment, we are willing to prevent any unforseen impacts on our sustainability.

Regarding substance flows, LCA differentiates between substances which are controlled or managed by people and those which are not managed but exist in our environment.

Those which are managed by humans are deemed to be part of the techno sphere. We normally refer to these substances as materials and products, but in essence they are substances in different configurations. Examples include mined coal, water in pipes and flat screen TV's. Their direct effects here are generally deliberate and beneficial – the coal provides heat, the water grows crops and the TV entertains the masses.

Unmanaged substances are deemed to be part of the ecosphere or the environment. This consists of resources, minerals, the air and water in rivers, lakes and oceans. It also includes pollutants and emissions released from the techno sphere into the environment.

The inventory part of LCA is concerned with interactions between the techno sphere and the environment. These are referred to as elementary flows: the flow of coal – from the ground – into the mine management is an elementary flow. More specifically it is an input from nature to the techno sphere. The emission of carbon

In Degradable Polymers and Materials: Principles and Practice (2nd Edition); Khemani, K., et al.;
ACS Symposium Series; American Chemical Society: Washington, DC, 2012.

dioxide from coal combusted in a steam boiler represents an elementary flow as well, and more specifically a flow from the techno sphere to nature.

Flows within the techno sphere are of interest only to the extent that we need to calculate them to determine the total elementary flows occurring within each techno-process (process occurring in the techno sphere).

Flows within the ecosphere which are not induced by human activity are of no interest to the LCA. Emissions from volcanoes for example are not related to products systems and therefore would never appear in an LCA. Flows in the ecosphere that are initiated by an elementary flow, such as the movement of a toxic emission through air, into water, then into fish and consequently into the food chain, are of interest to LCA. These flows form part of the calculations required in the environmental impact indicator models in order to predict damages to the environment.

These distinctions are useful as they allow a more objective view of the net impact of the environment from elementary flows without getting distracted by the pathway taken within the techno-sphere. To borrow from the regulatory domain, LCA is more like a performance-based approach than prescriptive one.

Structure of LCA

The structure of LCA is described in the international standard ISO 14040 (*2*) as a four step process consisting of:

- Goal and scope definition
- Inventory analysis
- Impact Assessment; and
- Interpretation

Figure 1 shows how the four stages of LCA interrelate with each other and the final step of interpretation, which checks all stages of LCA prior to application of the LCA.

Goal and Scope

Goal and scope definition frame the LCA question in terms of the function being studied, alternative options for fulfilling that function, processes required for each option and the criteria for environmental evaluation. For example, alternative options for the function of "transport and preservation of mixed lettuce leaves" could be polyethylene films, a degradable film, and a rigid PET tray. Production pathways are identified based on the relevant production steps for each of these products in the region where the study in being undertaken.

In Degradable Polymers and Materials: Principles and Practice (2nd Edition); Khemani, K., et al.;
ACS Symposium Series; American Chemical Society: Washington, DC, 2012.

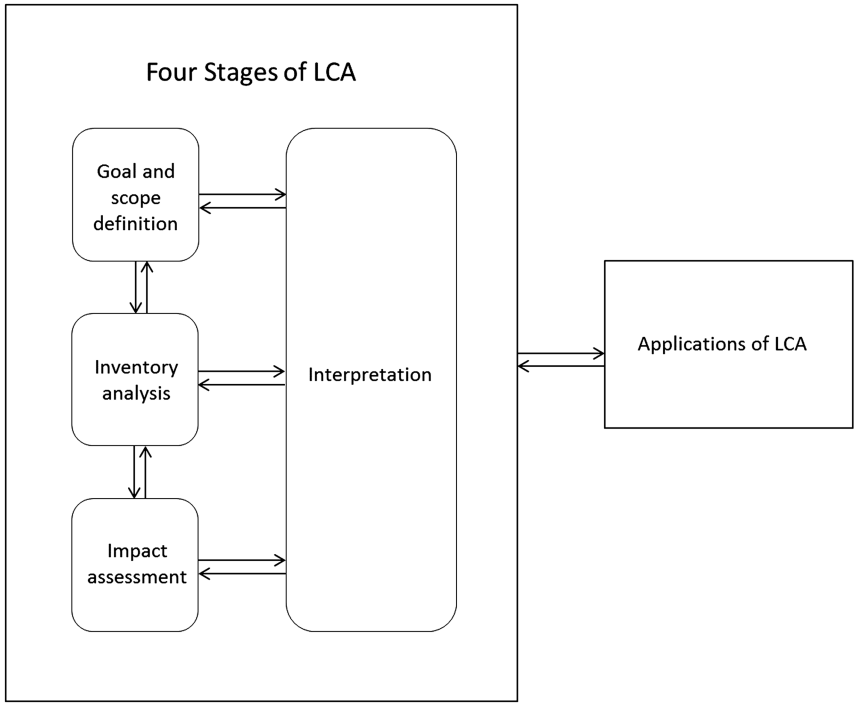

Figure 1. Structure of Life Cycle Assessment ISO 14040

The inventory involves the collection of data which originates from measurements, expert judgment, calculations, literature and the calculation of production processes along the supply chain for each option being assessed. For each of these processes the interactions with the environment are collated. These interactions include the extraction of resources, occupation of land and emissions of substances into the environment. As explained above, these interactions are referred to as elementary flows in LCA. The culmination of the inventory analysis stage is a collation of the total elementary flows. In the case of the option "polyethylene films", these flows would be the extraction natural gas for use in ethylene production and the emission of vented carbon dioxide, methane and other hydrocarbon from gas well head and refinery processes. For a maize starch based polymer, elementary flows include the land occupations for crop production and emission of nitrous oxide from fertilizer application. Typical LCAs involve hundreds of unit processes and potentially over a thousand elementary flows. Typically the important processes and elementary flows are many fewer than this, however this is only apparent and provable once the full collection of processes and elementary flows have been collated. Simplified LCA approaches may shortcut this processes by only focusing on those processes and flows identified by other studies as the ones dominating the environmental impacts over the product life cycle.

In Degradable Polymers and Materials: Principles and Practice (2nd Edition); Khemani, K., et al.;
ACS Symposium Series; American Chemical Society: Washington, DC, 2012.

Impact Assessment

Inventory data represent what has changed about the environmental due to the production of a given product, however the data is nearly impossible to interpret unless it is related the specific environmental objects of LCA. These objectives are referred to in the ISO standards as category endpoints – the environmental issues which we are concerned about. Figure 2 shows how inventory flows undergo a series of chemical, physical and biological processes which link the original emission or resource use to the ultimate environmental damage to a category endpoint such as human health. This series of processes is referred to as the environmental mechanism. Indictors in LCA can be defined at the category endpoint, however more often than not indicators are defined at a midpoint somewhere along this environmental mechanism.

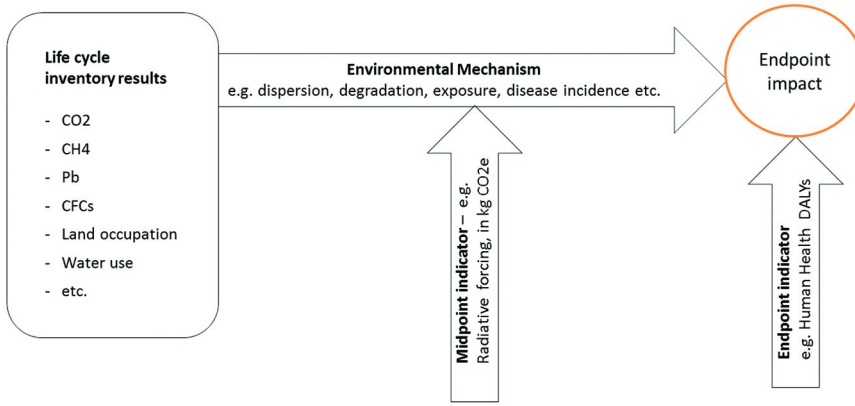

Figure 2. Relationship of life cycle inventory to midpoint and endpoint indicators

For example ozone depleting gases move through the air to the upper troposphere where they react with stratospheric ozone, lowering the radiation shield effect provided by these chemicals, increasing ground level UV and over time increasing skin cancer rates in humans. While the ultimate endpoint is human health, it has been more common to measure ozone depletion impact based on the potential for emission to destroy stratospheric ozone. The reason for this is the uncertainty introduced when modelling through to the category endpoint, however the benefit of modelling to category endpoints is the increase in the relevance of the indicator, and the comparability with other indicators modelled to the same endpoint.

Impact Assessment involves selecting and then evaluating environmental impacts indicators, such as climate change, photo-chemical oxidation, resource depletion and human toxicity. The selection of these indicators is not arbitrary and is required, by the LCA standards, to be based on the main environmental impacts of the product system being studied. This selection has also to take into account the goal and scope of the study (*3*). Having chosen these indicators, characterisation models are required to identify which elementary flows contribute

In Degradable Polymers and Materials: Principles and Practice (2nd Edition); Khemani, K., et al.;
ACS Symposium Series; American Chemical Society: Washington, DC, 2012.

to each indicator, as well as the extent to which these flow effects that indicator. For example carbon dioxide emission and nitrous oxide both contribute to the climate change indictor, with the latter being 296 times more potent a contributor on a mass basis. Such equivalencies are required for all elementary flows and for each indicator which they contribute to.

This information is typically contained in impact methods which have been developed by research bodies and are provided in most LCA calculation tools. The indicator results can be compared to total national or international impacts for each indicator to normalize the results. If a product contributes 2 kg of CO_2 eq. and depletes 50 MJ of fossil fuel oil equivalents, and the total global impacts of greenhouse gases are $2x10^9$ and oil depletion in $1x10^{10}$ then the normalised results would be $1X10^{-9}$ for climate change and $5x10^{-9}$ for fossil fuel depletion. What can be drawn from ignoring the absolute values is that the fossil impact is 5 times higher than the climate change impact in terms of contribution to the current level of global damage. This says nothing about the sustainability of such damage or about the importance of each issue, but does provide a relevance test for each product. The final step in the impact assessment, which is optional, consists in weighting these indicators against each other. In the ISO standards weighting is forbidden for comparisons. When weighting is used the standards require the results prior to weighting to also be presented. The standards also suggest it may be desirable to use several different weighting factors and weighting methods. There are many approaches to weighting which range from natural science approaches, monetisation and social preference methods. These will not be examined here.

Interpretation

The interpretation of the LCA provides an opportunity to take the results from inventory and impact assessment and test the robustness of the results by a series of check and sensitivities. Important flows are prioritised for data quality checks sensitivities and uncertainty analysis. Critical pinch points are identified where the answer of the LCA will flip depending of assumptions around important input data. In a world where there is absolute certainty in production and more behavioural data, these pinch points and sensitivities can represent much more useful information than any particular result based on a single set of assumptions. For example the end of life fate of the lettuce packaging mentioned above is unknowable in absolute terms, and then the impacts of the most likely disposal methods is a valuable result from the LCA.

Life Cycle Stages

Figure 3 shows the life cycle stages beginning with raw materials extraction, manufacturing, use and end of life stage with transport and distribution stages occurring in between many of these steps. There is also the potential for materials and products at the end of life to return to the raw materials production or the manufacturing phase.

In Degradable Polymers and Materials: Principles and Practice (2nd Edition); Khemani, K., et al.;
ACS Symposium Series; American Chemical Society: Washington, DC, 2012.

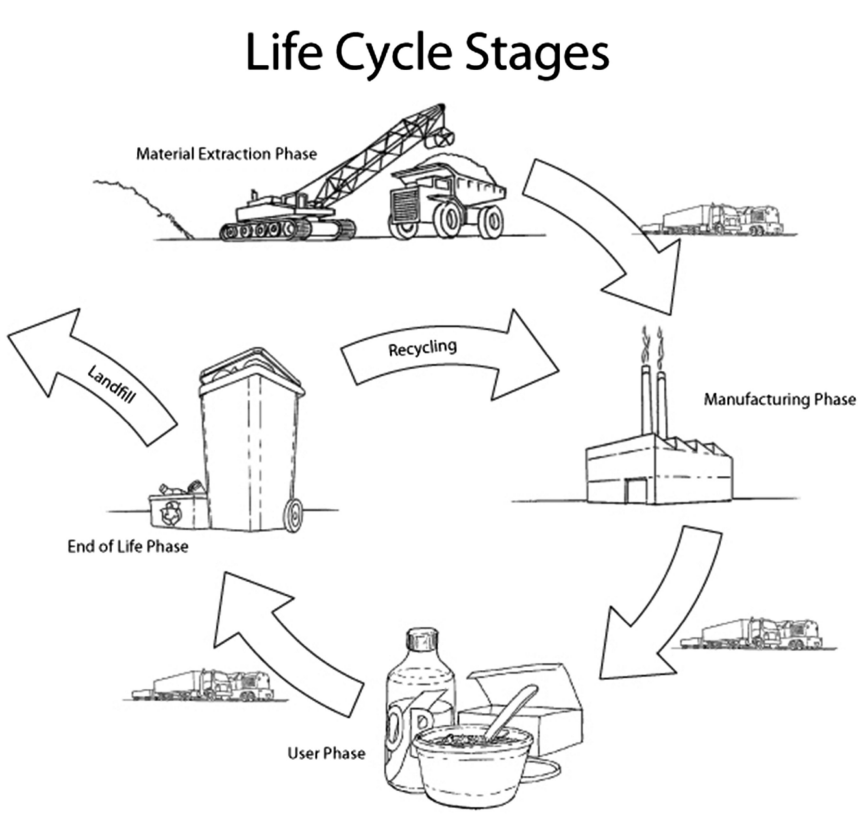

Figure 3. Product Life Cycle Stages

Raw Material Extraction and Production

The world is made up of the elements of the earth configured in different ways by the use of energy. The raw material production step has two major pathways – to process existing material reserves through the application of mechanical chemical transformations. Minerals need to be found, dug, ground, dissolved, reduced, oxidized and combined until they have the desired properties to be used in manufacturing of products. In this process, molecules will be broken down while other will be built up – or synthesized – and hence we often refer to these materials as synthetic.

The second option is to use a living system and the sun to synthesize compounds usually with additions of some synthetic materials such as phosphorus and nitrogen fertilizers. There is invariably a gap here between what is possible in an agricultural production system and what is normal, in terms of inputs and farming practices. While it is possible to grow crops without external synthetic fertilisers, it is normal, with the demands for yields and the range of areas used for agriculture, for synthetic fertilisers to be added.

Any LCA involving materials from agricultural or forest systems needs to properly account carbon emissions over the life cycle. If carbon absorption by

In Degradable Polymers and Materials: Principles and Practice (2nd Edition); Khemani, K., et al.;
ACS Symposium Series; American Chemical Society: Washington, DC, 2012.

plants or trees is included at the production stage this will show a major greenhouse gas emission benefit until the carbon is reemitted when they are eaten, burnt or biodegraded.. If carbon absorption is not included, the release of carbon dioxide emission from material breakdown or combustion at end of life needs not to be counted as a contributing greenhouse gas.

The modelling of agricultural production represents a significant challenge compared with modelling conventional hydrocarbon based polymers. Crude oil and gas are part of a global production system managed by a relatively small group of companies and technologies. Refining and petrochemical production similarly are part of a mature industry and the impacts of product in each region is based on similar approaches. This variability in production impacts from region to region are relatively small, and the shipping and trading across the world mean that many users would struggle to guarantee the location of all of their production in any case. This contrasts to agricultural production, which is a part of a living system, and varies according to climate, soil and water, and where local conditions such as competing pests lead to vastly different management practices.

The impact of raw material production can be reduced with the recycling of materials from further up the life cycle, back into the raw material supply. This can include minerals such as aggregates, metals and polymers and also the elemental inputs to agriculture – nitrogen, phosphorous, potassium and so on. It's also important that the use of raw materials in material production are used efficiently to maximise the usable products from the raw materials extracted or produced.

Material and Product Manufacture

The manufacture stage is where the largest value added will be made to the product, with the possible exception of distribution and retailing, but is generally not the most important in terms of environmental impacts. Electronics and complex manufactured products are and exception to this rule, although they also have very intensive and environmentally valuable material inputs.

The most important information from manufacturing will be the efficiency of material use to provide the level of functionality desired. An efficient use of materials will reduce the upstream impacts of material production which are allocated to the product.

Transport and Distribution

Transport and distribution are an economically important part of the life cycle, but from an environmental point of view, transport is not traditionally as important as most people believe. Long haul transport by ship or road freight tends to be relatively efficient with large loads making the final allocation to each individual product being relatively low. Collection by the consumer in their private vehicle can have much more significant impacts than the trucks on the way to the retail outlet. Special situations here are air freighting of products – due the high impacts of aviation, and the long haul of very low value products such as agricultural waste

In Degradable Polymers and Materials: Principles and Practice (2nd Edition); Khemani, K., et al.;
ACS Symposium Series; American Chemical Society: Washington, DC, 2012.

and raw materials, and because of the relativity between the impacts of what is being transported compared with the transport impacts themselves. Therefore, food miles as a concept is a poor indicator of environmental impacts of a product due to the large variation in the environmental impacts of different transport modes and the fact food transport impacts have a small to moderate contribution to the overall impacts. Fridge storage duration or waste factors would be more interesting metrics when looking at environmental impacts in the food supply chain.

Use Phase

The use of products is, from a life cycle perspective the most poorly understood. This is because it is the first stage not in direct control of the product manufacturer which undertakes the study. At the use phase, the number of actors moves from a few – to many. Data collection is not about measurement processes, but about statistical analysis of behaviour. In addition, the imperative to quantify the impacts of the product now that it has been sold to the consumer is significantly less for the study commissioner. Despite this, the way materials are used can have major impacts on their impacts on the environment.

The use phase is also the stage where products interact with each other. Packaging interacts with product, toaster interact with bread, coffee with its cup, food with the fridge and so on.

End of Life

End of life management of waste in most instances is driven less by the management impacts of waste and more by beneficial outcomes of waste management. It is not rare for the waste management stage of the life cycle to contribute positively to the environmental credentials of a product system. This is because the waste management stage is first about safe disposal of used products but secondly the recovery of environmental and economic value from the material resources. Mathematically in the LCA it is common, especially in LCA of waste management, to credit the product system with the avoidance of the production impacts of the materials and/or energy processes which are produced as part of that waste management system.

For example, if rigid PET containers are recycled and produced a recycled polymer flake which is used for the production of polyester fleece, then the PET container production is credited with a negative production amount of polyester fibre. In the context of the PET container system the subtraction of polyester fibre will be negated by initial production of PET.

LCA of Degradable Polymers

The value of LCA of degradable polymers is the fact that degradability is not credited or valued in an intrinsic way within an LCA study. Potential degradation of the polymer at some point in its life cycle is just another process to be modelled – either as a "part of the techno sphere" if the degradation is in a managed technology

In Degradable Polymers and Materials: Principles and Practice (2nd Edition); Khemani, K., et al.;
ACS Symposium Series; American Chemical Society: Washington, DC, 2012.

– be that a landfill, compost, or waste to energy facility or as part of a nature with fate modelling of the molecular components of the polymer in the environment. This means that within the scope of our indicator models we can assess two or more polymers which have different production systems and end of life behaviour.

Renewable similarly has no intrinsic value in LCA. Any renewable material will usually involve the use of non-renewable resources and will have emissions and impacts on the environment. Anything which grows requires sunlight and therefore is based on the use of land (or aquatic area) which is constrained on the planet. This is not to say that non-renewable resource depletion is not included in LCA – it is an important indicator – and a "renewable" material is likely to use less non-renewable resources than a material made from non-renewable resources.

Results from LCA Studies of Degradable Polymers

Rudnik (*4*) provides an overview of LCA studies on compostable polymers and concludes that the availability of LCA studies is still limited. A reasons for this may be the immaturity of the market, with very few full scale plants in operation, and as a developing technology, producers may be reluctant to release information of what are still evolving processes.

However LCA occurs at many levels and while large comparative studies are few, there is substantial amount of activity going on at the company level with internal assessment of polymers being undertaken by product manufacturers looking for alternative to conventional plastics.

Two types of studies should be differentiated here. One is the provision of life cycle inventory (LCI) data by manufacturers to enable users to undertake LCA, and the second is comparative LCA studies themselves.

LCIs

There are public LCI data available for Mater-Bi® starch-based polymer produced by Novamont (*5*) which provides an overview of the impacts from the cradle up to, but not including, the use phase. The greenhouse gas emissions amount to 2kg CO_2eq. which is very similar to conventional polymers such as polypropylene resin (*6*).

Natureworks has produced LCI data and ecoprofiles for PLA initially in 2002 (*7*) and more recently in 2007 (*8*). For PLA, advancements in its production have been reflected in the updated LCI data with a mix of process improvements and purchase, and an integration of renewable electricity sources used to reduce the energy and greenhouse gas emission from its production. Nature works have purchased green electricity certificate so that the total of 3.82kg CO_2eq. emitted from the production life cycle is reduced, with electricity credits of 1.75 kg CO_2eq. The emissions are further reduced when the 1.82 kg CO_2eq. being absorbed in the growing stage of the maize used in the production process is accounted for, giving a net value of 0.25 CO_2e.

It is important to note that theses LCI datasets are only partial as they do not include the end of life management where the fate of the carbon absorbed into the

In Degradable Polymers and Materials: Principles and Practice (2nd Edition); Khemani, K., et al.;
ACS Symposium Series; American Chemical Society: Washington, DC, 2012.

polymer will be a key determinate of the overall performance over the life cycle of the degradable polymer-based product.

LCAs

Comparative LCA studies of degradable polymers are nearly always compared with conventional polymers. There are general themes that can be drawn from the results from comparisons of degradable and conventional (*9–11*). These are discussed based on key indicators, namely fossil fuel resources, greenhouse gas emissions, land use and litter.

Fossil Fuel Depletion

Biopolymers reduce the demand for fossil fuel resources. While all products use some fossil fuel inputs through the supply chain, this is substantially higher for polymers which are made from liquid and gaseous fossil fuels. Mater-Bi® has a gross energy requirement of 41.7MJ/kg (*5*) while the best performing PLA is 27.2MJ/kg (*8*). These values compare with conventional polymers like polypropylene, which has fossil fuel feedstock as well as fossil fuel used in processing and has gross energy requirement of 73MJ/kg.

Land Use and Water Use

Counter to this the biopolymers will have increased demand on land use. This will vary depending on how the organic material is sourced, either as a dedicated crop or by-product of a cropping or other biomass system. Many studies do not include land use because methodologies for reporting on land use impacts are not as well formulated as the chemical based indicators such global warming, acidification and so on. Defining the impacts of specific type of land use is also difficult with the productivity and biodiversity value of land being highly variable for different areas of the world and even within regions. PLA reports a land use of 1.7 m^2/kg which is ambiguous as land use requires a time dimension. For Mater-Bi®, no land use data is presented in its EPD but other data (*12*) suggests the land use is 0.6m^2a/kg of polymer which compares with polypropylene at 0.03m^2a/kg. Here lies a key trade-off between using oil and gas which represent many millennia of land use in production of these reserves, or the synthesis of new material based on today's agricultural system.

Water use is in many ways another side of the land use debate. With the addition of irrigation, the land productivity can be vastly improved. Dryland production systems are limited to fewer areas and generally have lower yields. Water use data can also be very specific to each area, with high water uses in areas of water abundance being of less concern than moderate water uses in areas of high water stress. There is a developing approach (*13*) for water footprinting of products, using a water stress approach but this is yet to make its way to biopolymer assessments.

In Degradable Polymers and Materials: Principles and Practice (2nd Edition); Khemani, K., et al.;
ACS Symposium Series; American Chemical Society: Washington, DC, 2012.

Greenhouse Gas Impacts

For biopolymers, the greenhouse gas impacts are generally lower than conventional polymers. This can be due to lower processing inputs, in manufacture and or the use of bioenergy (energy from biomass) supplied in the production stage of the polymer. The greenhouse impacts at the end of life are highly dependent on the waste management practices in place in the location where the polymer is being used. It is also sensitive to some methodological decisions in carbon accounting, especially in landfilling of waste – a major fate to used polymers.

If polymers are composted a majority of the carbon in the polymer is released to the atmosphere as carbon dioxide. If it was a biopolymer then this carbon dioxide is not counted as it just completing a short term carbon cycle from the biomass involved in its production. If it's a fossil derived degradable polymer, and the plastic is degraded to carbon dioxide and water then this emission is an emission of fossil based carbon dioxide.

If polymers are landfilled there are complex series of assumptions coming into play as shown in Figure 4.

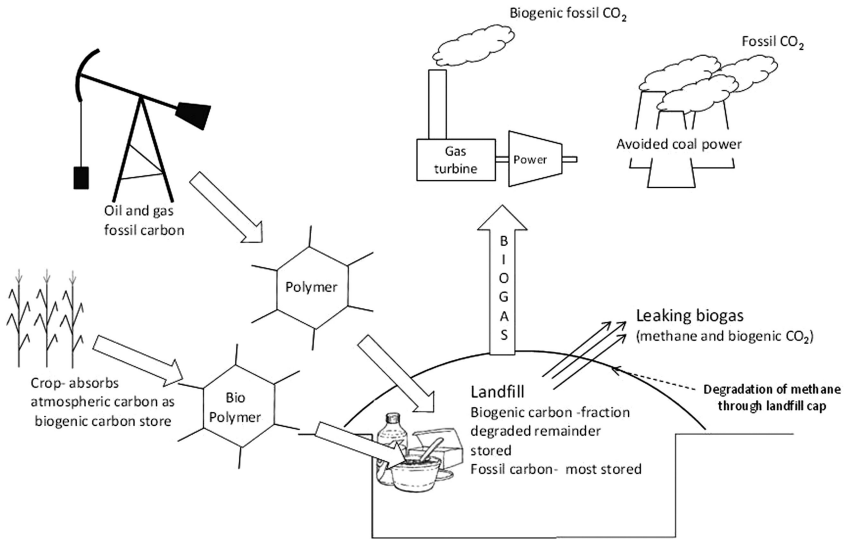

Figure 4. Greenhouse gas emissions from polymers sent to landfill

Firstly, for conventional polymers, there is minimal degradation, so the landfill represents a re-storing of the carbon from oil and gas used to make the polymer in the residual material in the landfill. If the carbon dioxide is from biomass, and a portion of the polymer is assumed not to degrade in the landfill, it may be counted as a new storage of atmospheric carbon being beneficial from a climate change point of view. Having said this, under the IPCC guideline, such storage of carbon is not counted as a carbon sink. If there is degradation of the polymer in landfill, then a substantial portion of released gases will be methane,

In Degradable Polymers and Materials: Principles and Practice (2nd Edition); Khemani, K., et al.;
ACS Symposium Series; American Chemical Society: Washington, DC, 2012.

whereas if this material can be captured and flared, its emission will be as carbon dioxide, similar to a compost situation, or, if its combusted for energy generation, these benefits from offsetting other fossil energy supply can be positive from a climate change point of view. If methane generated in landfill is emitted to the environment, its contribution to climate change is very substantial, being between 21-25 times more potent a contributor of greenhouse gas emissions on a mass basis. The performance of the landfill itself is subject to design factors – does it have gas collection, how is it filled, what other materials are present, is moisture being minimized in the landfill, is it well capped preventing infiltration and potentially oxidising methane as it pass through the organic layer in the cap.

If polymers are combusted in waste to energy, the outcome is similar to that when methane from landfill is captured and used for energy, potentially providing benefit from offsetting other, usually fossil energy supplies.

If the polymers are littered to the environment, the biopolymers could mostly decompose aerobically, being something like that of composting, so the greenhouse gas impacts, at least, would be minimal.

Litter Impacts

Despite being one of the major drivers for the development of degradable polymers, few LCA studies have included litter as an impact category, principally because there is no agreed or even established characterisation model for litter in LCA. An Australian study in 2004 (*11*) added such indicators to the list of midpoint indicators assessed by an LCA undertaken on shopping bags in Australia in 2005. One waste based indicator dealt with the aesthetic impact of litter and the other with the potential impacts of litter to marine mammals. Rather predictable persistent polymers scored higher than degradable polymers; however there was no comparison of the seriousness of this damage to other impact categories in the LCA.

Conclusions

Life cycle assessment has already played an essential role in the understanding and consideration of degradable polymers. Improvements in the performance of degradable polymers has been demonstrated and partly driven by LCA results.

The use of comparative studies of degradable polymers has some challenges in relation to the modelling of end of life fate, as simple assumptions have potentially large impacts on the results. Also the indicators typically used in LCA need to expand to take better account of land and water impacts in conjunction with the traditional impacts categories of greenhouse gases and energy.

References

1. Bonifaz, O.; Nikodem, H.; Klopffer, W. LCA - How it Came About - An Early Systems Analysis of Packaging for Liquids. *Int. J. Life Cycle Assess.* **1996**, *1* (2), 62–65.

In Degradable Polymers and Materials: Principles and Practice (2nd Edition); Khemani, K., et al.; ACS Symposium Series; American Chemical Society: Washington, DC, 2012.

2. International Organization for Standardization. *International Standard, ISO/ DIS14040, Environmental Management Standard- Life Cycle Assessment, Principles and Framework*; Swizerland, 2006.
3. International Organization for Standardization. *International Standard, ISO/ DIS14044, Environmental Management Standard- Life Cycle Assessment, Requirements and Guidelines*; Switzerland, 2006.
4. Rudnik, E. Environmental impact of compostable polymer materials. *Compostable Polymer Materials*; Elsevier: Amsterdam, 2008; Chapter 8, pp 182−199.
5. Novamont. *Environmental Product Declaration MATER-BI® CF05S*; Novara, Italy, 2010.
6. PlasticsEurope. *Environmental Product Declarations of the European Plastics Manufacturers Polypropylene (PP)*; Brussels, Belgium, 2008.
7. Vink, E. T. H.; et al. Applications of life cycle assessment to NatureWorks™ polylactide (PLA) production. *Polym. Degrad. Stab.* **2003**, *80* (3), 403–419.
8. Vink, E. T. H.; et al. The eco-profiles for current and near-future NatureWorks® polylactide (PLA) production. *Ind. Biotechnol.* **2007**, *3* (1), 58–81.
9. Patel, M.; et al. Life-cycle Assessment of Bio-based Polymers and Natural Fiber Composites. *Biopolymers Online*; Wiley-VCH Verlag GmbH & Co. KGaA: 2005.
10. Bohlmann, G. M. Biodegradable packaging life-cycle assessment. *Environ. Prog.* **2004**, *23* (4), 342–346.
11. ExcelPlas Australia, Centre for Design at RMIT, and Nolan-ITU. *The impacts of degradable plastic bags in Australia: Final Report to Department of the Environment and Heritage*; Centre for Design at RMIT: Melbourne, Victoria, 2004.
12. ecoinvent Centre. ecoinvent data version 2.2, reports Nos. 1-25, as implemented in *SimaPro 7.2*; Swiss Centre for Life Cycle Inventories: Dübendorf, 2010.
13. Ridoutt, B.; et al. Water footprinting at the product brand level: case study and future challenges. *J. Cleaner Prod.* **2009**, *17*, 1228–1235.

In Degradable Polymers and Materials: Principles and Practice (2nd Edition); Khemani, K., et al.;
ACS Symposium Series; American Chemical Society: Washington, DC, 2012.

Chapter 5

Polymer Degradation as a Tool To Study Polyelectrolyte Complex Formation and Stability

L. Leclercq,* M. Boustta, and M. Vert

Max Mousseron Institute for Biomolecules - UMR CNRS 5247, University of Montpellier 1 - Faculty of Pharmacy, 15 Avenue Charles Flahault - BP 14491, 34093 Montpellier Cedex 5, France
***leclercq@univ-montp1.fr**

As part of our investigations of the interest in degradable artificial biopolymers, attention was recently paid to other applications such as analysis of polyelectrolyte complexes or release of one of their polyelectrolyte component. The present work is aimed at comparing the enzymatic degradation of polyelectrolyte complexes formed when polyanions made of similar building blocks but having different chemical structures and charge densities are mixed with an enzyme sensitive polycation, namely poly(L-lysine). The two selected polyanions were poly(L-lysine citramide) and poly(L-lysine citramide imide) and the selected enzyme was trypsin. Fractions were prepared at different values of the degree of neutralization by adding the polycation in solution to a polyanion solution and vice-versa, according to a titration protocol. Dynamic light scattering was used to assess the size and stability of the complexes in the presence of salt at various concentrations. The molecular dimensions of the fractionated polyanions recovered after the degradation of the associated polycation molecules were determined by size exclusion chromatography. Nuclear Magnetic Resonance spectroscopy was used in complement to determine the molar charge ratio within the complexes and the nature of the degradation products was determined by capillary zone electrophoresis. Data are used to discuss the influence of the chemical structure, the charge density and the order of

In Degradable Polymers and Materials: Principles and Practice (2nd Edition); Khemani, K., et al.;
ACS Symposium Series; American Chemical Society: Washington, DC, 2012.

addition of the oppositely charged polyelectrolyte precursors on the complexation.

Introduction

The interest of polymers for therapeutic applications is well known in surgery, pharmacology, dentistry, tissue engineering and even gene transfection. To overcome the risks of diseases raised by virus-based gene transfection, non-viral cationic species such as liposomes and synthetic polycations are presently investigated to condense DNA fragments and genes. Such condensation is based on electrostatic interactions between oppositely charged polyelectrolytic species that form polyelectrolytic-type complexes or PECs (*1*, *2*). Regardless of whether it is a polynucleotide polyanion or a non-biological one, the formation and stability of PECs are affected by similar factors including acid or base strengths, charge density and concentration, proportion of opposite charges, polymer molar mass, pH and ionic strength of the medium, and even the way the oppositely charged polymers are mixed (*3–5*). At low polymer concentrations and far from charge stoichiometry, PECs are nanodispersed in solution, whereas they precipitate at high polymer concentrations, especially at charge stoichiometry. PECs can be re-dissolved at high salt concentrations, or in acid or basic medium, depending on the nature of the polyions (*3–5*).

When one deals with polyelectrolyte complexes, one of the major problems is the determination of the composition of the formed PEC because they are generally very stable due to the cooperativity between interchain electrostatic interaction and occasionally the synergistic contribution of hydrophobic interactions. Two methods using mild conditions were recently developed in our laboratory to analyze PECs. Both are based on the initial destabilization of the PEC using a suitable salted medium to bring the components back to solution independently (*6*, *7*). The first method is based on affinity chromatography. In practice, the resulting solution is percolated through an ion exchange column that retains either the polyanion or the polycation selectively, depending on the nature of the charged gel. Later on, the retained component is recovered using a more concentrated salted mobile phase (*6*). The second method is based on the degradation of one of the polyelectrolyte that results in the release of the non-degradable partner. The non-degradable polymer partner can then be easily analyzed using classical techniques or made available for further uses (*7*).

In the present article, we wish to complement our investigation by comparing the enzymatic degradation of polyelectrolyte complexes formed when polyanions made of similar building blocks but having different chemical structures and charge densities are mixed with a enzyme sensitive polycation, namely poly(L-lysine) (PLL). The two selected polyanions were polydisperse poly(L-lysine citramide) (PLCA) and poly(L-lysine citramide imide) (PLCAI) (*8*) and the selected enzyme was trypsin. Fractions were prepared at different values of the degree of neutralization by adding the polycation in solution to a polyanion solution or vice-versa, according to a titration protocol. The chemical formulae of PLCA, PLCAI and PLL are presented in Scheme 1. Dynamic light scattering

In Degradable Polymers and Materials: Principles and Practice (2nd Edition); Khemani, K., et al.;
ACS Symposium Series; American Chemical Society: Washington, DC, 2012.

was used to assess the size and stability of the complexes in the presence of salt at various concentrations. The molecular dimensions of the fractionated polyions recovered after the degradation of the associated polycation molecules were determined by size exclusion chromatography. The nature of the degradation products was determined by capillary zone electrophoresis and the composition was deduced from ^{1}H NMR data. The influences of chemical structures and of charge densities on complex formation during progressive blending of the oppositely charged complex precursors were discussed and the influence of the order of addition as well.

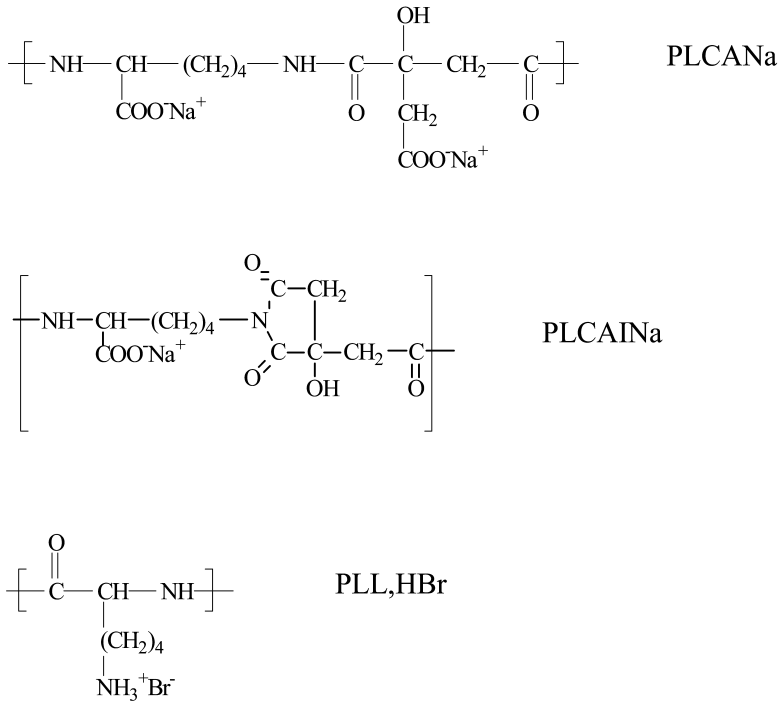

Scheme 1. Chemical formulae of PLCA, PLCAI and PLL.

Materials and Methods

Chemicals

Poly(L-lysine),HBr with different molar mass and polydispersity (PLL: $\overline{Mw}$ = 46,000 g/mol, I = 1.3; LMW-PLL: $\overline{Mw}$ = 10,700 g/mol, I = 1.5) were purchased from Sigma (France).

Poly(L-lysine citramide),Na and poly(L-lysine citramide imide),Na, respectively PLCA ($\overline{Mw}$ = 21,000 g/mol) and PLCAI ($\overline{Mw}$ = 24,000 g/mol), were synthesized as previously described (*8*).

Trypsin (EC 3.4.21.4; from hog pancreas) and 2,4,6-trinitrobenzene-1-sulfonic acid (TNBS) were purchased from Fluka (France).

In Degradable Polymers and Materials: Principles and Practice (2nd Edition); Khemani, K., et al.;
ACS Symposium Series; American Chemical Society: Washington, DC, 2012.

Methods

Fractions of PEC According to the Titration Method

Typically, four fractions were prepared by stepwise addition of a 1 M polycation solution to a vigourously stirred polyanion solution (20 mg in 1 cm^3 0.15 M phosphate buffer saline at pH=7.4 (PBS)) in a plastic vial at room temperature. The first stage corresponded to a cation–to-anion charge ratio N_{PC}/N_{PA} = 0.3. A coacervate formed that was collected by centrifugation (F1 fraction). The second stage corresponded to N_{PC}/N_{PA} = 0.6 (F2). The third stage corresponded to a N_{PC}/N_{PA} = 1 (F3). Coacervates were washed with de-ionized water. The stage 3 supernatant was also dialyzed against de-ionized water using a Spectra/por membrane with a cut-off of 1,000 Da and freeze-dried. The recovered solid was referred to as F4.

PEC fractions were also prepared similarly but the addition order was inversed, i.e. the polyanion solution was added to the polycation one.

Centrifugation was carried out using a Sigma 112 centrifuge at 6000 rpm for 5 min. A Christ LDC-1 apparatus was used for freeze-drying.

Size Exclusion Chromatography (SEC)

SEC experiments were carried out using an equipment composed of a P500 pump and a LCC501 Plus controller (LCC501 from Pharmacia, and a Model 486 UV-Visible detector from Waters working at 214 nm for all the experiments. The column was loaded with a anionic CM Sepharose CL-6B gel purchased from Amersham Pharmacia Biotech.. The mobile phase was a solution of 0.15 M phosphate buffer and 1 M NaCl at pH=7.4 delivered at 0.25 mL/min.

Capillary Zone Electrophoresis (CZE)

Capillary zone electrophoresis was carried out using a Beckman P/ACE system 5000 equipped with a UV-Visible detector set at 214 nm. The capillary was coated with poly(diallyl dimethyl ammonium chloride) to make the surface cationic. Samples were injected at the cathode using a 25kV tension. Under these conditions, anionic species eluted faster than cationic ones. The elution medium was pH=6.8 0.05 M phosphate buffer. Benzylic alcohol was used as internal tracer to reflect electro-osmose.

NMR Spectroscopy

^{1}H NMR spectra were recorded using a Brücker 400 MHz spectrometer operated by the Laboratory of Physical Measurements of the Montpellier 1 University. ^{1}H NMR spectra were performed in solution after decomplexation of the solid PECs in 2 M NaCl/D_2O.

In Degradable Polymers and Materials: Principles and Practice (2nd Edition); Khemani, K., et al.;
ACS Symposium Series; American Chemical Society: Washington, DC, 2012.

Dynamic Light Scattering (DLS)

Vertically polarized DLS measurements (λ_0= 514.5 nm) were performed at 25°C using a commercial Brookhaven Instrument Corporation BI-200SM instrument equipped with a BI-9000AT correlator. Hydrodynamic radius R_H data were determined in NaCl solutions using the Stokes-Einstein equation. The viscosity of polymer solutions was determined using a Rheometer Rheostress RS 100 (from Haake) at 25°C.

Typically, a PEC fraction was first dissolved in 2.5 M NaCl at a concentration of 0.4 mg/cm^3. 0.065 cm^3 of the resulting solution in a Pyrex® tube was then mixed with a vigorously stirred NaCl solution whose concentration was calculated to be at the desired final concentration in NaCl, the final concentration in precipitates and the total volume being 13 µg/mL and 2 mL, respectively. DLS measurements were performed 24 hours after obtention of the fraction.

Enzymatic Degradation

Enzymatic degradation was carried out in a 0.1 M NaH_2PO_4 and 1.9 M NaCl solution at pH = 7.9 and 25 °C. Prior to introduction into a Spectra/por dialysis tube (cut-off = 3,500 Da), a 10 mg/mL test sample was dissolved in the buffer solution. 0.1 cm^3 of a 1 mg/mL trypsin solution was then added. Dialysis was carried out against 15 mL of the buffer solution. At various time intervals, the content in amine groups of the outer phase was determined by the TNBS assay (*9*). Dialysis against fresh buffer solution was performed as long as no more amine was detected in the outer phase. The inner phase was then dialysed against de-ionized water to remove the salts, degradation of PLL being considered as total. The content of the dialysis tube was finally freeze-dried.

TNBS Assay (10)

0.1 mL of the solution to be analyzed was introduced into a 1 cm Hellma quartz cell containing 0.875 mL of a 0.1 M borate buffer at pH = 9.3 and 0.025 mL of a 0.03 M TNBS solution. After 120 min incubation, absorbance at λ = 420 nm using a Perkin Elmer Lambda 15 spectrophotometer was measured. A quartz cell containing 0.975 mL borate buffer and 0.025 mL TNBS solution was used as reference.

Results and Discussion

Because one of the major interests of the study of the formation and the stability of polyeletrolyte complexes is related to therapeutic potential applications, the present work was performed at rather low polyion concentrations comparable with those generally used in the case of the administration of

In Degradable Polymers and Materials: Principles and Practice (2nd Edition); Khemani, K., et al.;
ACS Symposium Series; American Chemical Society: Washington, DC, 2012.

macromolecular prodrugs for drug delivery or of PECs for gene transfection (*11–13*).

Behavior of the Various PEC Fractions in the Presence of NaCl

Four PLL/PLCA and PLL/PLCAI PEC fractions were collected as described in the experimental section. The ^{1}H NMR spectrum of one of the PLL/PLCA complex is presented in Figure 1a as example. The comparison of PLL-CH_2-N^+ and PLCA-CH_2-N resonances at 3.05 and 3.2 ppm corresponded to a 1.0 ± 0.1 positive to negative charge ratio, i.e. to stoichiometry in charges as previously observed (*6*, *14*). The same feature was found for all PLCA fractions and for PLL/PLCAI ones as well.

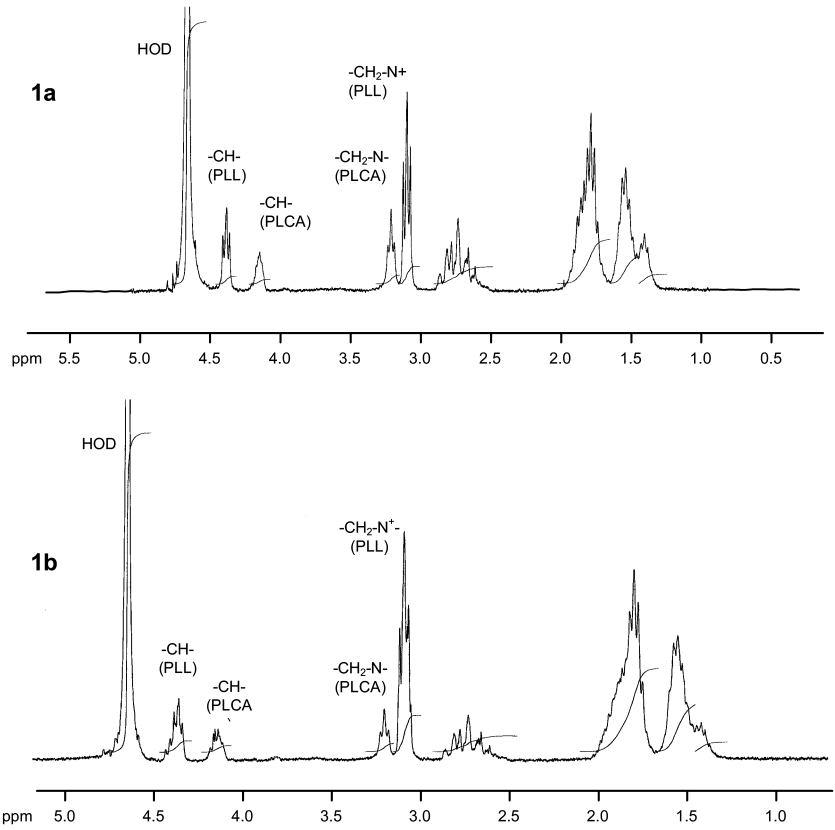

Figure 1. Typical ^{1}H NMR spectrum of PLL/PLCA complex when PLL was added to PLCA (Figure 1a) and when PLCA was added to PLL (Figure 1b)

In Degradable Polymers and Materials: Principles and Practice (2nd Edition); Khemani, K., et al.;
ACS Symposium Series; American Chemical Society: Washington, DC, 2012.

The influence of the concentration in NaCl on the interactions between the polyanions and PLL was investigated by dilution starting from a NaCl concentration high enough to initially separate the polyelectrolytes, namely 2.5 M NaCl. Under these conditions, it was not possible to decrease the salt concentration below 0.1 M NaCl. DLS was used to monitor the presence of complex in the media of various salt concentrations keeping the final polymer concentration constant at 13 µg/mL. At 2.5 M in NaCl, the measured sizes of scattering species were around 10 nm in agreement with dimensions of separated polyions. Decreasing the salt concentration led to the appearance of scattering species with sizes larger than 100 nm. The salt concentration at which the formation of these rather large scattering species became detectable was named C_{recomp}, with "recomp" standing for recomplexation. The study was carried out using PEC dispersions in comparison with non-fractionated PECs. All the PEC fractions led to similar features with onsets and plateaux (Figure 2). In the case of the PEC fractions obtained from the mixtures of PLL and PLCA, recomplexation was detected for C_{recomp} values decreasing from 0.99 M for fraction 1 to 0.53 M for fraction 4. In the case of the PEC fractions obtained from the mixtures of PLL and PLCAI, the C_{recomp} values decreased from 0.76 M for fraction 1 to 0.38 M for fraction 4. It is interesting to note that no macroscopic flocculation was observed up to the salt limit of 0.1 M, as it was previously shown in literature for other systems (*15*, *16*). This particular behavior can be assigned to the low charge density of the polyanions and to the presence of hydroxyl groups which compensated the effects of the increase in hydrophobicity generally associated with charge neutralization and ion dehydration. For the PLL/PLCA couple and the PLL/PLCAI one, the curve corresponding to F1, F2 and F3 levelled off at almost the same R_H value, namely 780 nm and 650 nm, respectively. The plateau R_H values obtained for fractions 4 were much lower (325 nm in the case of PLL/PLCA and 310 nm in the case of PLL/PLCAI). It is worth noting that the C_{recomp} values for the non-fractionated systems decreased as compared to fractions 1. It is worthwhile to note that PEC nanoparticles had similar sizes and were stable in a broad range of ionic strength.

Separation of the Two Components from the PEC Fractions by Selective Degradation of the Polycation

An endopeptidase, namely trypsin, known as capable to degrade preferentially PLL while keeping intact the PLCA and PLCAI nylon-type polyamides was selected (*7*). All the PEC fractions were destabilized in a 0.1 M NaH_2PO_4 and 1.9 M NaCl solution at pH = 7.9 and at 25°C, before introduction into a 1,000 Da cut-off dialysis tube together with trypsin. The same procedure was applied to PLL alone for comparison. The degradation of PLL led to the formation of lysine or small lysine oligomers which could diffuse through the dialysis membrane. The degradation process was stopped and considered as complete when no more amine was released during two days. The absence of amine in the dialysis tube was checked at the end.

In Degradable Polymers and Materials: Principles and Practice (2nd Edition); Khemani, K., et al.;
ACS Symposium Series; American Chemical Society: Washington, DC, 2012.

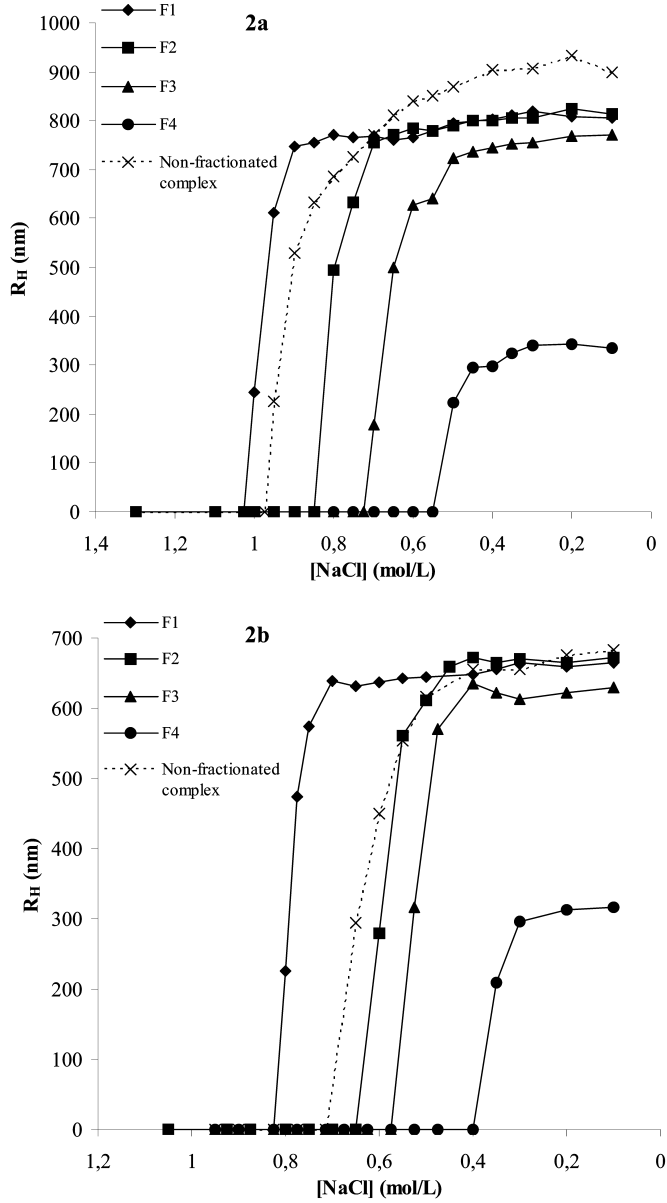

Figure 2. R_H dependence of the four PLL/PLCA (Figure 2a) and PLL/PLCAI (Figure 2b) PEC fractions and of the non-fractionated complexes on NaCl concentration. [PEC] = 13 µg/mL.

In Degradable Polymers and Materials: Principles and Practice (2nd Edition); Khemani, K., et al.;
ACS Symposium Series; American Chemical Society: Washington, DC, 2012.

Figure 3 shows degradation data obtained from PLL/PLCA and PLL/PLCAI PEC fractions after initial separation of the polyanion and polycation using concentrated salt. The degradation profiles of PLL alone and of PLL in the polyanion-polycation mixtures were similar and showed that degradation was completed in less than 24 hours as born out by the absence of amine in the dialysis tube. There was no significant difference in the degradation rate of PLL in the PLL-PLCAI and the PLL-PLCA mixtures in agreement with the salt-promoted decomplexation. The presence in the medium of a polyanion even of high charge density did not perturb the enzymatic degradation of the PLL. The final absorbance obtained by adding intermediate absorbance values observed at the various steps of the degradation process was compared to the absorbance value of an equivalent amount of lysine in the presence of TNBS. It was found that the ratio between the two values was almost 0.55 for each system, suggesting that degradation of the PLL by the trypsin endopeptidase led to dialyzable lysine oligomers and not monomers. This finding fully agrees with the mechanism of action of this enzyme (*10*). On another hand, the degradation of PLL issued from destabilized PEC and that of the same quantity of free PLL gave the same final absorbance value, implying that oligolysine of similar length were formed and diffused through the dialysis membrane.

Molecular Weights Determination

After the degradation of the polycation, the recovered polyanion component of each PEC fraction was analyzed by SEC and data were compared with the chromatogram of the corresponding parent (Figure 4a and 4b). For both PLCA and PLCAI polyanions, the molar mass decreased from fraction 1 to fraction 4 and chromatograms were part of the chromatogram of the initial polyanion, in agreement with fractionation according to molar masses. The molar mass of the polyanions present in the fractions 4 could not be determined precisely because the retention times at the top of the corresponding SEC peaks were out of the calibration curves (Figure 4).

Identification of the Nature of the Degradation Products

The amine-bearing degradation by-products issued from the PLL degradation by trypsin and diffusing through the dialysis membrane were characterized by capillary zone electrophoresis. Figure 5 shows the electrophoregram of the low molar mass PLL (LMW-PLL) and that of a mixture of LMW-PLL and a tetralysin oligomer for peak identification. Oligomers containing from three to ten units appeared in the LMW-PLL CZE electrophoregram whereas only trilysin and tetralysin were found in the degradation products generated by the action of trypsin (Figure 6) in agreement with previous observation (*17*).

In Degradable Polymers and Materials: Principles and Practice (2nd Edition); Khemani, K., et al.;
ACS Symposium Series; American Chemical Society: Washington, DC, 2012.

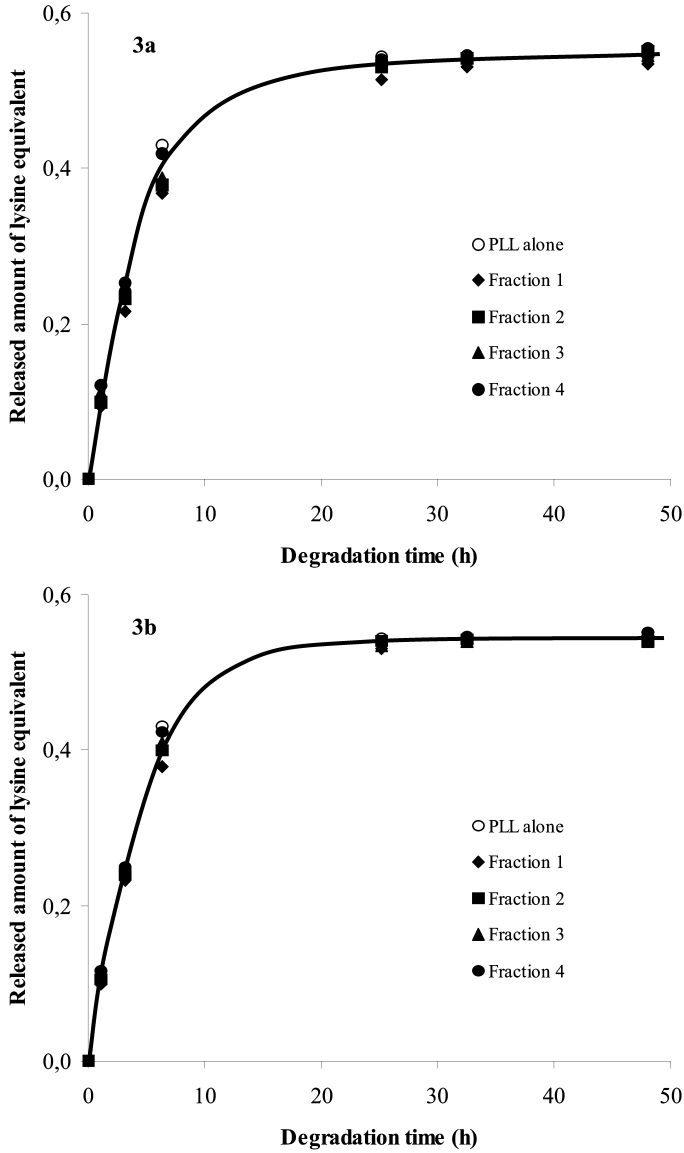

Figure 3. Released amount of aminated compounds in terms of lysine equivalent during the enzymatic degradation by trypsin of the PLL alone and of the PLL component in the four PLL / PLCA (Figure 3a) and PLL / PLCAI (Figure 3b) PEC fractions. [Trypsin] = 0.1 mg/mL; [PEC] = 10 mg/mL; degradation medium: 0.1 M phosphate buffer and 1.9 M of NaCl at pH = 7.9 and 25 °C.

In Degradable Polymers and Materials: Principles and Practice (2nd Edition); Khemani, K., et al.;
ACS Symposium Series; American Chemical Society: Washington, DC, 2012.

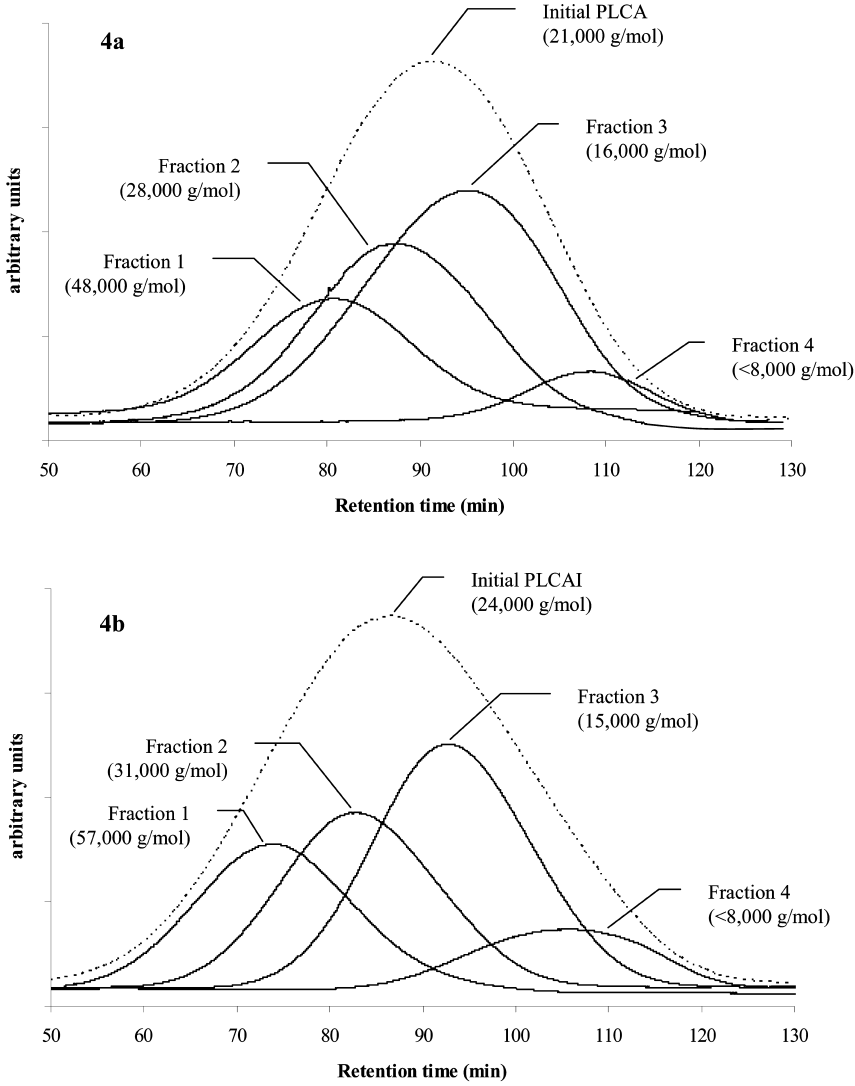

Figure 4. SEC chromatograms of the four PLCA (Figure 4a) and PLCAI (Figure 4b) components obtained from the four corresponding PLL/PLCA and PLL/PLCAI PEC fractions. Gel and elution conditions: anionic cellulose-based gel as the stationary phase and a 1 M NaCl and 0.15 M phosphate buffer solution at pH = 7.4 as the mobile phase.

In Degradable Polymers and Materials: Principles and Practice (2nd Edition); Khemani, K., et al.;
ACS Symposium Series; American Chemical Society: Washington, DC, 2012.

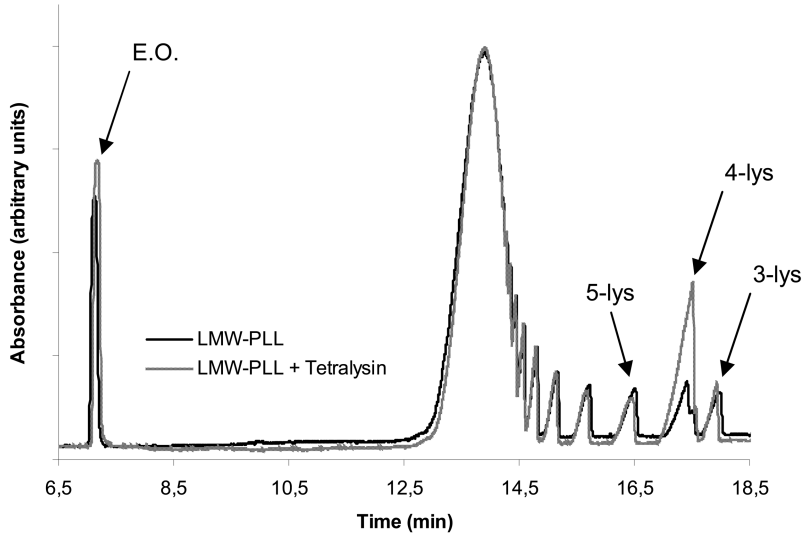

Figure 5. Electrophoregram of LMW- PLL and of a mixture of LMW-PLL and tetralysin (4-lys); E.O. = Electro-osmose peak.

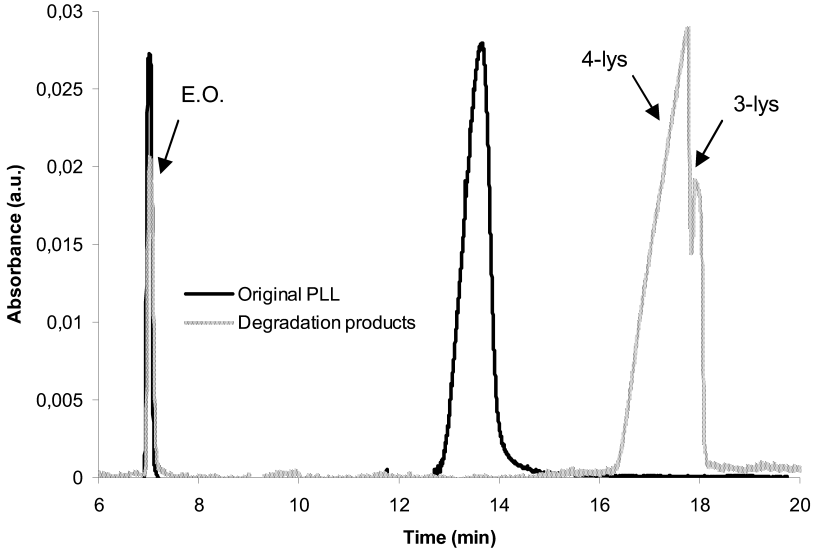

Figure 6. Electrophoregram of PLL and of the degradation products issued from the enzymatic degradation by trypsin of the complexed PLL with PLCA; E.O. = Electro-osmose peak.

In Degradable Polymers and Materials: Principles and Practice (2nd Edition); Khemani, K., et al.; ACS Symposium Series; American Chemical Society: Washington, DC, 2012.

Influence of the Addition Order

The influence of the addition order was considered in the case of the PLL/PLCA system. When PLCA was added to PLL, the behavior of the resulting PECs in the presence of NaCl did not change significantly. The R_H plateau and C_{recomp} values were found close to those observed when adding PLL to PLCA. The molar masses of PLCA recovered from the four PEC fractions showed no significant selectivity among the PLCA molecules. In contrast, considering the ^1H NMR spectrum of the complexes (see one example displayed in Figure 1b) and the ratio of PLL-CH_2-N^+/PLCA-CH_2-N resonances, it was deduced that complex fractions were formed according to a positive to negative charge ratio of 2.0 ± 0.2 instead of 1.0 ± 0.1 found above for the inverse order of mixing. The occasional need for more positive charges that negative ones to form a PEC was previously discussed in terms of charge parameter ξ = Bjerrum length/distance between two neighboring charges within the oppositely charged macromolecules (*18*).

Conclusion

Enzymatic degradation of PLL was observed for all PLL/PLCA and PLL/PLCAI nanosized complexes that were formed under titration conditions. The nanodispersed particles remained stable in aqueous media, even in the presence of rather high salt concentrations provided the polyion concentration was kept very low. This finding could be explained by the presence of hydrophilic groups along the chains and the low charge density of the PLCA and PLCAI polyanions. The critical salt concentration C_{recomp} at which nanosized particles were formed was previously shown depending on the molecular weight. Herein it was shown that complex formation depended on the precipitated fraction and on the structure of the polyanion too. The higher the molar mass, the higher the C_{recomp}.

The degradation of PLL macromolecules engaged within the complex fractions showed that the method can be a powerful tool to isolate and analyze the non-degraded partner. Using this method, we were able to confirm that fractionation occurs in molar mass during progressive complex formation. We also showed that the order of addition did not affect C_{recomp} but changed dramatically the charge stoichiometry. The method can also give access to the degradation products issued from the degradation of the polycation as exemplified in the case of the enzymatic degradation of PLL using capillary zone electrophoresis. In this particular case, the enzymatic degradation generated exclusively trilysin and tetralysin. The method can also be applied if the polycation is hydrolytically degradable.

References

1. Kossel, A. *J. Physiol. Chem.* **1896**, *22*, 178–183.
2. Fuoss, R. M.; Sadek, H. *Science* **1949**, *110*, 552–573.
3. Tsuchida, E.; Abe, K. *Adv. Polym. Sci.* **1982**, *45*, 1–119.
4. Bekturov, E. A.; Bimendina, L. A. *Adv. Polym. Sci.* **1981**, *41*, 99–147.

In Degradable Polymers and Materials: Principles and Practice (2nd Edition); Khemani, K., et al.;
ACS Symposium Series; American Chemical Society: Washington, DC, 2012.

5. Philipp, B.; Dautzenberg, H.; Linow, K. J.; Koetz, J.; Dawydoff, W. *Prog. Polym. Sci.* **1989**, *14*, 91–172.
6. Boustta, M.; Leclercq, L.; Vert, M. *J. Bioact. Compat. Polym.* **2004**, *19*, 155–171.
7. Etrych, T.; Boustta, M.; Leclercq, L.; Vert, M. *J. Bioact. Compat. Polym.* **2006**, *21*, 89–105.
8. Boustta, M.; Huguet, J.; Vert, M. *Makromol. Chem. Macromol. Symp.* **1991**, *47*, 345–355.
9. Huber, R.; Bode, W. *Acc. Chem. Res.* **1978**, *11*, 114–122.
10. Snyder, S. L.; Sobocinski, P. Z. *Anal. Biochem.* **1975**, *64*, 284–288.
11. Behr, J. P. *Bioconjugate Chem.* **1994**, *5*, 382–389.
12. Howard, K. A.; Dash, P. R.; Read, M. L.; Ward, K.; Tomkins, L. M.; Nazarova, O.; Ulbrich, K.; Seymour, L. W. *Biochim. Biophys. Acta* **2000**, *1475*, 245–255.
13. Abdellaoui, K.; Boustta, M.; Morjani, H.; Manfait, M.; Vert, M. *J. Drug Targeting* **1997**, *5*, 193–206.
14. Leclercq, L.; Boustta, M.; Vert, M. *J. Bioact. Compat. Polym.* **2011**, *26*, 3–19.
15. Dautzenberg, H.; Kötz, J.; Linow, K. J.; Philipp, B.; Rother, G. *Macromolecular complexes in chemistry and biology*; Springer-Verlag: Berlin, Germany, 1994; p 119.
16. Etrych, T.; Leclercq, L.; Boustta, M.; Vert, M. *Eur. J. Pharm. Sci.* **2005**, *25*, 281–288.
17. Leclercq, L.; Boustta, M.; Rixte, J.; Vert, M. *J. Colloid Interface Sci.* **2010**, *350*, 459–464.
18. Leclercq, L.; Boustta, M.; Vert, M. *J. Bioact. Compat. Polym.* **2011**, *26*, 301–316.

Chapter 6

Factors Controlling the Rate of Photodegradation in Polymers

Bevin C. Daglen and David R. Tyler*

Department of Chemistry, University of Oregon, Eugene, Oregon 97403
***dtyler@uoregon.edu**

The onset of degradation in a photochemically degradable polymer should be reliably predictable. However, it is difficult to predict polymer lifetimes in practice because there is limited understanding of the parameters, both molecular and environmental, that control degradation rates and degradation onsets. In this study, the effect of temperature on the degradation quantum yield of a poly(vinyl chloride) polymer with $Cp_2Mo_2(CO)_6$ units incorporated into its chains was investigated (Cp = cyclopentadienyl). The polymer is photochemically reactive in the absence of oxygen because the $CpMo(CO)_3$ radicals formed by photolysis of the Mo-Mo bonds react with C-Cl bonds to form $CpMo(CO)_3Cl$ units. Quantum yields as a function of temperature were obtained for this polymer and for two control systems, $Cp'_2Mo_2(CO)_6$ dispersed in PVC and $Cp'_2Mo_2(CO)_6$ in hexane/CCl_4 solution ($Cp' = \eta^5\text{-}C_5H_4CH_3$). The quantum yields of the two control systems showed only slight increases with an increase in temperature. For the control reaction in hexane/CCl_4, the slight temperature dependence is attributed to the decrease in viscosity of the solution and the subsequent decrease in the radical-radical recombination efficiency. For the $Cp'_2Mo_2(CO)_6$ dispersed in PVC, the small temperature dependence is attributed to an increase in free volume as the temperature increases. In contrast to these results, the temperature dependence of the quantum yield of the PVC polymer with $Cp_2Mo_2(CO)_6$ units along its chains is relatively large. It is proposed that an increase in temperature facilitates the polymer chain relaxation processes (involving recoil and rotation) following photolysis of the Mo-Mo bond.

In Degradable Polymers and Materials: Principles and Practice (2nd Edition); Khemani, K., et al.;
ACS Symposium Series; American Chemical Society: Washington, DC, 2012.

The radical-radical recombination efficiency is subsequently decreased, which leads to a net increase in chain cleavage and degradation efficiency. In support of this proposal, the apparent activation energy obtained from the temperature dependence of the quantum yield of the metal-metal bond containing PVC polymer (14.1 ± 0.3 kcal mol^{-1}) is consistent with secondary relaxation chain movements in polymers.

Introduction

Considerable research is being devoted to devising new photodegradable polymers with improved performance because there are compelling economic and social reasons for using degradable plastics in certain applications (*1–4*). The biggest use for photodegradable plastics is in agriculture, specifically in the burgeoning technique called plasticulture. In plasticulture, the ground is covered with plastic sheeting (typically a polyolefin), which acts as a mulch to prevent the growth of weeds (thus requiring the use of fewer herbicides), to decrease water demand, and to extend the growing season by keeping the ground warmer. By making these agricultural films out of degradable plastics, considerable labor and money can be saved in the plastics recovery phase of the technique. In the environmental area, photodegradable plastics are finding increased use as packaging materials in items that have a high probability of becoming litter. The idea is that if such materials should end up as litter they will degrade rather quickly and not be an eyesore.

There are two basic methods for making polymer materials photochemically degradable (*2*, *3*). One method is to chemically incorporate a chromophore into the polymer chains. Although numerous chromophores have been evaluated, the most commercially successful chromophore is the carbonyl group (*2*, *3*, *5*). Absorption of UV radiation leads to degradation by the Norrish Type I and II processes or by an atom abstraction process (Scheme 1), all of which are typical photoreactions of the carbonyl chromophore. Note that once radicals are introduced into the system, chain degradation can occur by the autooxidation mechanism (Scheme 2).

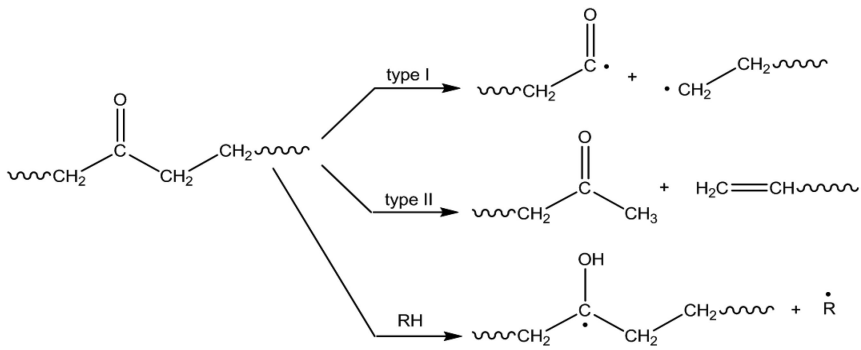

Scheme 1. Photochemical degradation pathways for polymers containing carbonyl groups

In Degradable Polymers and Materials: Principles and Practice (2nd Edition); Khemani, K., et al.;
ACS Symposium Series; American Chemical Society: Washington, DC, 2012.

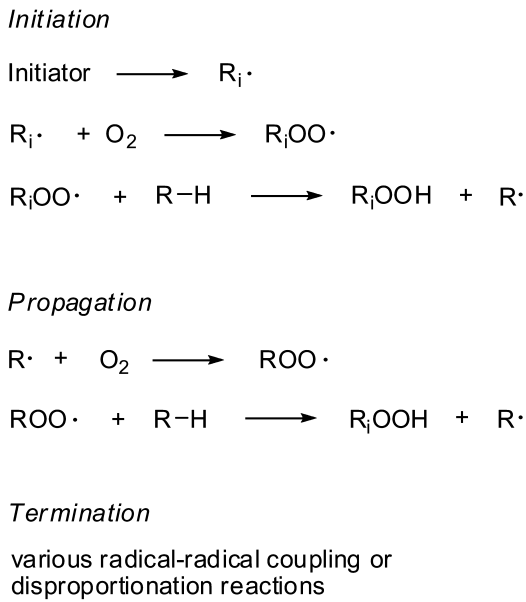

Scheme 2. The autooxidation mechanism for hydrocarbon materials

The second general method for making polymer materials photochemically degradable is to mix a radical initiator into the polymer. Once carbon-based radicals have formed, the chains degrade by the autooxidation cycle (Scheme 2). Numerous radical initiators have been investigated, and a partial list includes metal oxides (e.g., TiO_2, ZnO, CuO), metal chlorides (e.g., LiCl, $FeCl_3$), $M(acac)_n$ complexes, $M(stearate)_n$ complexes, benzophenone, quinones, and peroxides (*2*, *3*).

The ideal photodegradable polymer has (at least) three ideal properties. First, the onset of degradation should be reliably predictable. Although it is obvious why this property is desirable for practical applications, it is noted that it is difficult to predict polymer lifetimes in practice because light intensities vary, as do temperatures and a host of other mechanistic variables that control degradation rates and degradation onsets. Second, the onset of degradation should be tunable. Photodegradable polymers have different applications and each application will generally require different polymer lifetimes. Methods must be found for manipulating polymer lifetimes. Third, the polymer should degrade completely and quickly once degradation starts. This characteristic is important for practical reasons because most polymer mechanical properties are related to molecular weight (*6*). Small amounts of degradation can drastically decrease the molecular weight (and thus mechanical properties) of a plastic, yet to all appearances the plastic piece is visually unchanged. In essence, the plastic is still present but it is not structurally sound – and hence useless and perhaps dangerous. Under such circumstances, it may as well be completely degraded.

In Degradable Polymers and Materials: Principles and Practice (2nd Edition); Khemani, K., et al.;
ACS Symposium Series; American Chemical Society: Washington, DC, 2012.

In order to predict polymer lifetimes, to control when a polymer starts to degrade, and to control the rate of degradation, it is necessary to identify the experimental parameters that affect polymer degradation rates and to understand how these parameters affect degradation. Among the parameters that have been identified as affecting polymer lifetime are the glass transition temperature, radical trap concentration, exposure to ultraviolet radiation, light intensity and wavelength, oxygen diffusion rates in the polymer, tensile stress, compressive stress, chromophore concentration, molecular weight, humidity, and polymer morphology (*2–4*, *7*). In this chapter, we add to this list by reporting how the temperature affects polymer photodegradation rates.

Results and Discussion

Experimental Approach to the Problem

Several challenging experimental problems hinder the rigorous experimental mechanistic exploration of polymer photodegradation. One of the difficulties is that polymer degradations are mechanistically complicated (*8*). This is not to say that the mechanisms are not understood; in fact, they are understood in detail (*8*). Rather, the mechanisms are intricate, often involving multiple steps, cross-linking, and side-reactions; this makes pinpointing the effects of various molecular and environmental parameters difficult. Another complication is that oxygen diffusion is the rate-limiting step in photooxidative degradations, the primary degradation mechanism in most polymers (*9*, *10*). This can add to the intricacy of the kinetics analysis because cracks and fissures develop in the polymer as degradation proceeds; these fractures provide pathways for direct contact of the polymers with oxygen, which will then no longer degrade at a rate controlled by oxygen diffusion. To circumvent these experimental and mechanistic complexities and therefore make it less difficult to interpret data and obtain fundamental insights, we use three key experimental strategies in our investigations. First, we study the problem using special photodegradable polymers of our own design that contain metal-metal bonds along the backbone (*11–16*). These polymers are photodegradable because the metal-metal bonds can be cleaved with visible light (eq 1) and the resulting metal radicals captured with an appropriate radical trap, typically an organic halide or molecular oxygen; Scheme 3 (*17*, *18*).

$$L_nM{-}ML_n \xrightarrow{h\nu} L_nM\cdot + \cdot ML_n \qquad (1)$$

$$\cdot ML_n = CpMo(CO)_3,\ (Cp = \eta^5\text{-}C_5H_5),\ CpW(CO)_3,\ Mn(CO)_5,\ Re(CO)_5,\ CpFe(CO)_2$$

In Degradable Polymers and Materials: Principles and Practice (2nd Edition); Khemani, K., et al.;
ACS Symposium Series; American Chemical Society: Washington, DC, 2012.

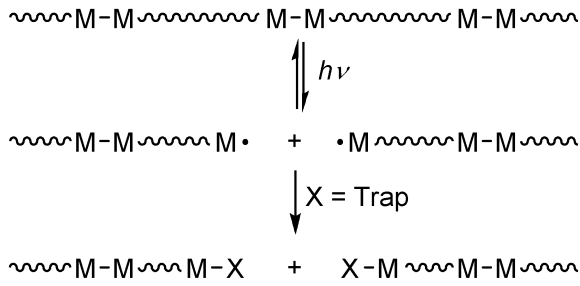

Scheme 3. Photochemical reaction of a polymer with metal-metal bonds along its backbone.

By studying these "model" systems, we are able to extract information without the mechanistic complications inherent in the degradation mechanisms of organic radicals. (For example, metal radicals do not lead to crosslinking, so we can avoid this complicating feature found with organic radicals.) The second key experimental strategy is to use polymers that have built-in radical traps, namely C-Cl bonds (*19*, *20*). By eliminating the need for external oxygen to act as a trap, we excluded the complicating kinetic features of rate limiting oxygen diffusion. The third experimental strategy is to use the distinctive M-M bond chromophore to spectroscopically monitor the photodegradation reactions of the polymers. This allows us to compare the efficiencies of the photodegradations by measuring the quantum yields of the reactions. (The quantum yield, Φ, is defined as the rate of a photoreaction divided by the absorbed light intensity; i.e., Φ = rate/absorbed intensity.) The use of quantum yields to quantify and compare the various degradation rates is a crucial advance because polymer degradation reactions have typically been monitored by stress testing, molecular weight measurements, or attenuated total reflection (ATR) spectroscopy (*21*), all of which can be laborious and time consuming. Relative to these techniques, quantum yield measurements are straightforward. (Note that quantum yields in regular carbon-chain polymers cannot be measured conveniently by UV-vis spectroscopy because there are generally no suitable chromophores.) To further expedite our quantum yield measurements, we use a computerized apparatus that automatically measures the quantum yields on thin film polymer samples (*22*).

Polymer Synthesis Strategy

Metal-metal bonds can be incorporated into polymers using standard polymer synthetic methods, including step reaction methods, chain reaction methods, ROMP, ADMET, ROP, and click chemistry (*23*). Examples of functionalized metal-metal bonded dimers that can be used in these polymerization reactions are shown in Figure 1. Polymerization reactions that use these molecules have been reviewed (*23*). As one example, it is noted that step polymers containing metal-metal bonds can be synthesized using difunctional, cyclopentadienyl-substituted metal dimers. A sample polymerization reaction

In Degradable Polymers and Materials: Principles and Practice (2nd Edition); Khemani, K., et al.;
ACS Symposium Series; American Chemical Society: Washington, DC, 2012.

using a functionalized cyclopentadienyl-containing metal-metal bonded dimer is shown in eq 2, which illustrates the reaction of a metal-metal bonded "diol" with hexamethylene diisocyanate (HMDI) to form a polyurethane (*13*). This step polymerization strategy is quite general, and a number of metal-metal bond-containing polymers have been made from monomers containing functionalized Cp ligands (*11*, *23*). Another synthetic strategy (and one that frequently leads to higher molecular weights) is to react metal-metal dimer species with functionalized prepolymers. In an example of this method, the polymer used in this study (**1**) was synthesized by the route in Scheme 4 (*20*). M_n for polymer **1** was > 500,000. Note that it is not necessary to have a metal-metal bond in every repeat unit in order for the polymer to be degradable. Thus, copolymers containing only several percent of the metal-metal bonded monomer are still readily degradable.

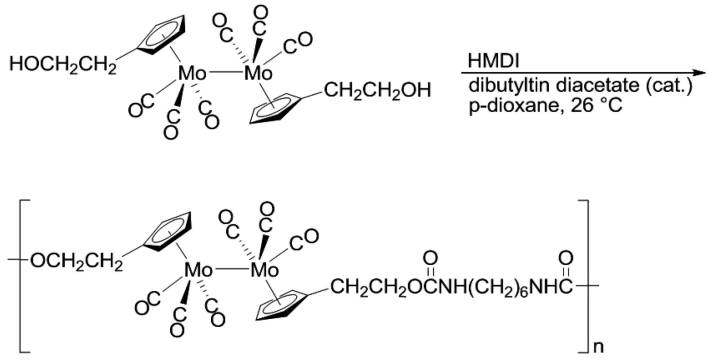

(2)

Photodegradation Occurs in the Absence of O_2.

Metal radicals will typically abstract the chlorine atom from a C-Cl bond, and thus C-Cl bonds make excellent traps for metal radicals. Consequently, polymers containing C-Cl bonds photochemically degrade in the absence of oxygen according to the pathway in Scheme 3 (*20*). Spectroscopic monitoring of the reactions shows the disappearance of the $Cp_2Mo_2(CO)_6$ chromophore (λ_{max} = 390 and 510 nm; ν(C≡O) 2009, 1952, and 1913 cm^{-1}) and the appearance of the $CpMo(CO)_3Cl$ unit (ν(C≡O) = 1967 and 2048 cm^{-1}). In addition, the number average molecular weight decreases steadily during the course of the reaction. In the case of polymer **1**, the reaction is shown in Scheme 5.

In Degradable Polymers and Materials: Principles and Practice (2nd Edition); Khemani, K., et al.;
ACS Symposium Series; American Chemical Society: Washington, DC, 2012.

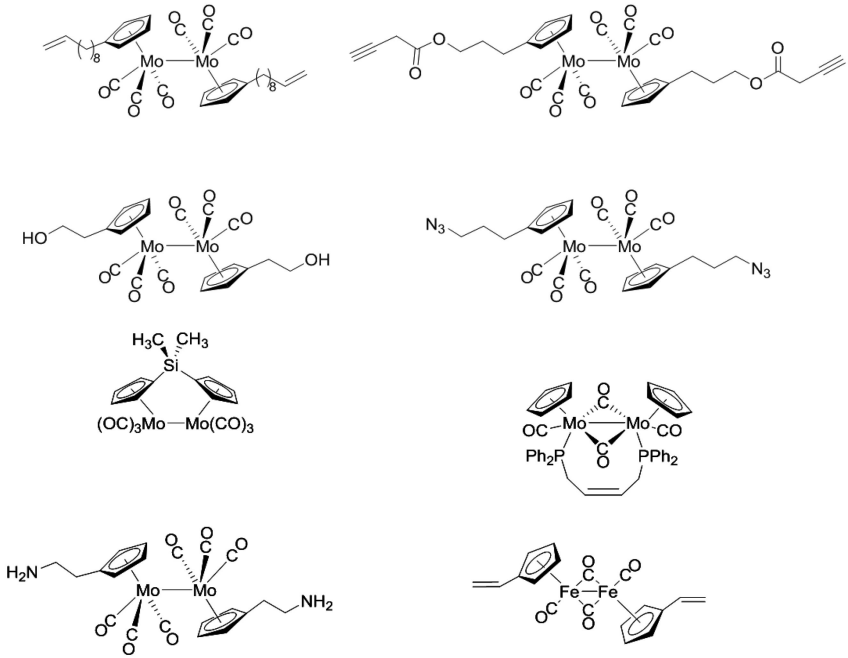

Figure 1. Functionalized metal-metal dimers for use in various polymerization reactions.

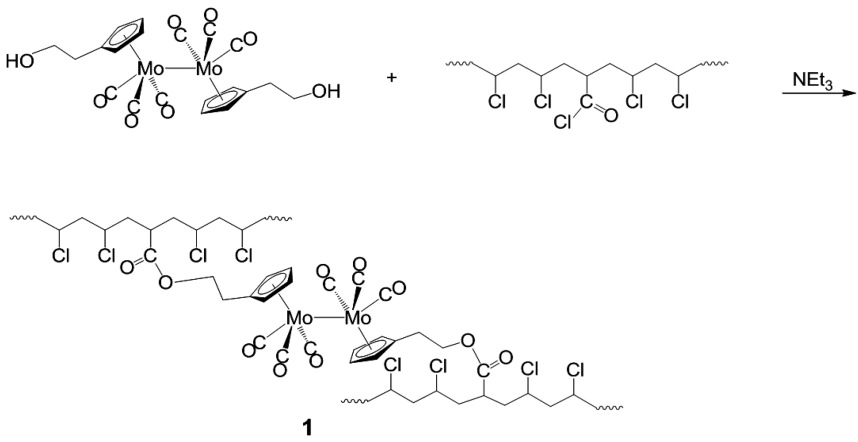

*Scheme 4. Synthesis of a poly(vinyl chloride) polymer with $Cp_2Mo_2(CO)_6$ units incorporated into its chains. The polymer is denoted as **1** in this chapter.*

In Degradable Polymers and Materials: Principles and Practice (2nd Edition); Khemani, K., et al.;
ACS Symposium Series; American Chemical Society: Washington, DC, 2012.

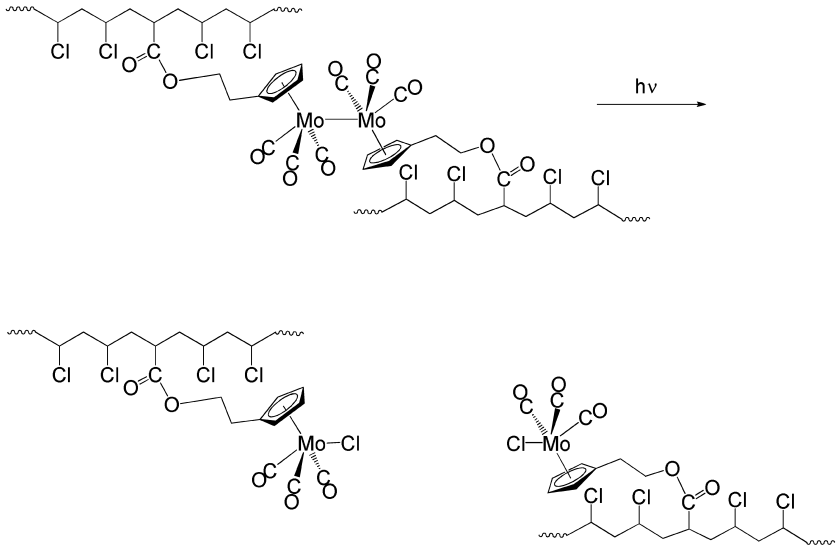

*Scheme 5. Photochemical reaction of polymer **1** in the absence of an external radical trap.*

Effect of Temperature (T) on the Efficiency of Photodegradation

The temperature dependence of the quantum yields for the degradation of polymer **1** could depend on: 1) the inherent temperature dependence of the $Cp_2Mo_2(CO)_6$ photolysis and the subsequent trapping reaction of the $CpMo(CO)_3$ radicals; 2) the temperature dependent behavior of the polymer morphology, or 3) a temperature-dependent dynamical property of the photogenerated radicals in the polymer. To differentiate between these possibilities, two control experiments were carried out, namely the photolysis of $Cp'_2Mo_2(CO)_6$ dispersed in a PVC polymer matrix and the photolysis of $Cp'_2Mo_2(CO)_6$ in hexane/CCl_4 solution (*24*). (The molecule with Cp′ ligands (Cp′ = η^5-$C_5H_4CH_3$) was used in these experiments because it is more soluble than the molecule with η^5-C_5H_5 ligands.) The quantum yields for the disappearance of the $Cp'_2Mo_2(CO)_6$ unit in polymer **1**, for $Cp'_2Mo_2(CO)_6$ dispersed in PVC, and for $Cp'_2Mo_2(CO)_6$ in hexane/CCl_4 solution are plotted versus temperature in Figure 2. Note that all of the solid-state data were collected below the glass transition temperatures of the polymer films (T_g = 65-72 °C). The plots show there is a significant increase in the quantum yields for polymer **1** with increasing temperature. In contrast, for $Cp'_2Mo_2(CO)_6$ dispersed in PVC and for $Cp'_2Mo_2(CO)_6$ in hexane/CCl_4 solution (in which the Mo-Mo chromophores are unattached to polymer chains) there are only slight increases in the quantum yields over this temperature range. An immediate conclusion is that the large increase in the quantum yield with temperature for polymer **1** is not attributable to an inherent temperature dependence of the photolysis and subsequent radical trapping reaction of the $Cp'_2Mo_2(CO)_6$ unit. (Otherwise, the quantum yields for $Cp'_2Mo_2(CO)_6$ in the hexane/CCl_4 solution

In Degradable Polymers and Materials: Principles and Practice (2nd Edition); Khemani, K., et al.;
ACS Symposium Series; American Chemical Society: Washington, DC, 2012.

would also show a sizeable temperature dependence.) Also, because the quantum yields for $Cp'_2Mo_2(CO)_6$ dispersed in PVC show only a slight temperature dependence, the temperature dependence observed for polymer **1** cannot be ascribed solely to changes in PVC morphology. (Otherwise, the $Cp'_2Mo_2(CO)_6$ dispersed in PVC and polymer **1** would show a similar temperature dependence because the morphologies of PVC and polymer **1** are similar in regard to crystallinity, modulus (1300 ± 100 vs. 1200 ± 50 MPa), and glass transition temperature (65 ± 4 vs. 72 ± 3 °C).)

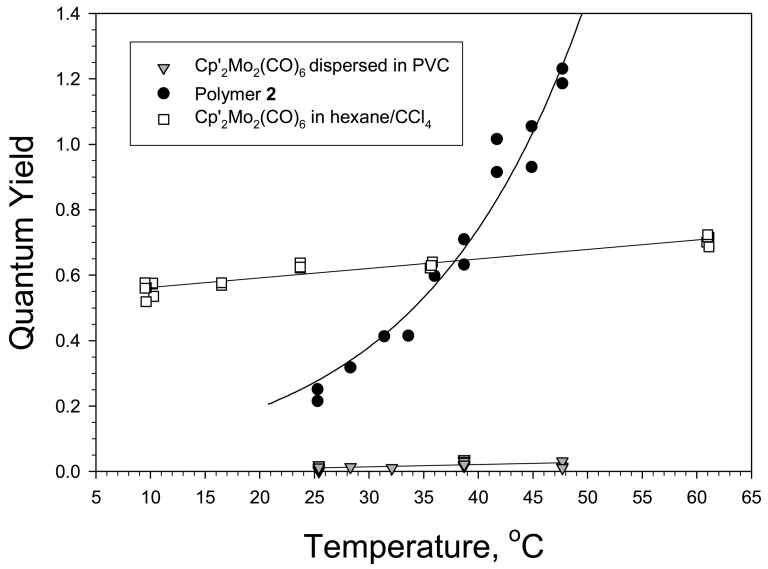

*Figure 2. Plots of the quantum yields for disappearance of the $Cp'_2Mo_2(CO)_6$ unit in polymer **1**, $Cp'_2Mo_2(CO)_6$ dispersed in PVC, and $Cp'_2Mo_2(CO)_6$ in hexane/CCl_4.*

The quantum yield data for polymer **1** in Figure 2 has an exponential dependence on the inverse temperature, and it is tempting therefore to extract activation parameters from the natural log plots of quantum yield vs. inverse temperature. Balzani, however, has cautioned that the relationship between the temperature and activation parameters in a photochemical reaction is a complex one, and the "apparent activation energies" thus obtained must be interpreted with care (*25*). With that disclaimer in mind, the activation energy obtained from the lnΦ vs. T^{-1} plot is 14.1 ± 0.3 kcal mol^{-1} (Figure 3). This value is typical for secondary relaxation chain movements in polymers (which generally fall in the range 10 – 20 kcal mol^{-1} (*26–28*) and is consistent with the proposal that the temperature dependence of Φ results from chain movements involved in recoil and rotation processes. Scheme 6 shows a suggested rotation process (i.e., a secondary relaxation process) that could give rise to the temperature dependence of the quantum yield. To be specific, it is suggested that the temperature dependence of the quantum yields arises from the temperature dependence of the k_s rate constant.

In Degradable Polymers and Materials: Principles and Practice (2nd Edition); Khemani, K., et al.;
ACS Symposium Series; American Chemical Society: Washington, DC, 2012.

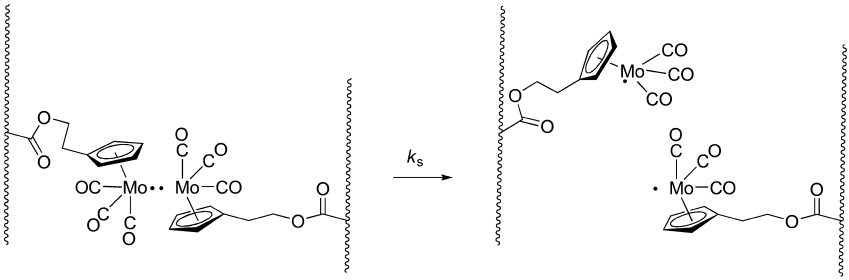

*Scheme 6. The temperature dependence of the polymer degradation quantum yield for polymer **1** arises from the temperature dependence of the secondary relaxation chain movements. A rotation process is shown but radical recoil will also lead to increased radical-radical separation.*

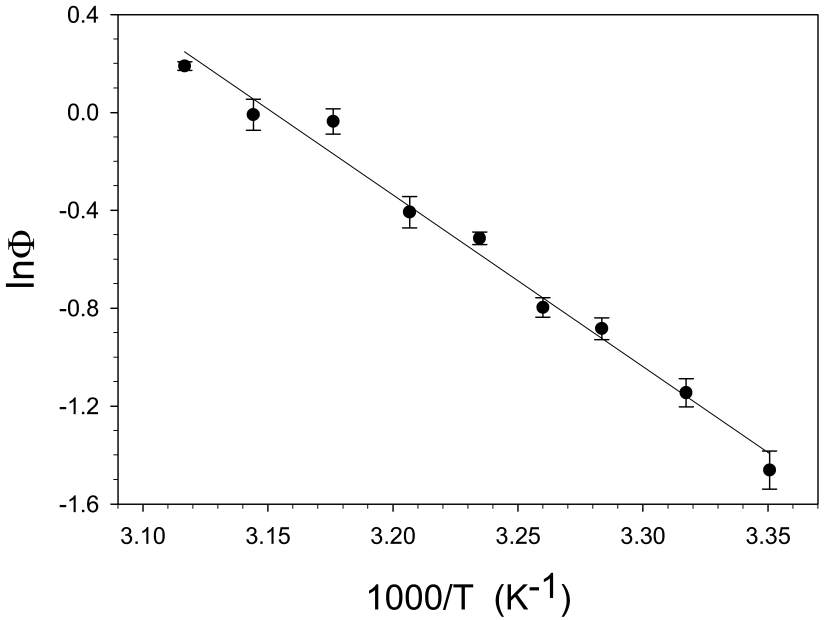

*Figure 3. Plot of ln Φ vs. T^{-1} for polymer **1**.*

Summary and Conclusions

The photochemical reactivity of polymers is of considerable interest because photodegradable plastics have a number of applications. Additional interest in polymer photoreactivity stems from the need to limit and control "weathering" in polymer materials. Photodegradation is an important component of polymer weathering, and a proper understanding of degradation processes and of the experimental factors that affect degradation is necessary for the accurate estimation of polymer lifetime and for the development of stabilizing systems.

In Degradable Polymers and Materials: Principles and Practice (2nd Edition); Khemani, K., et al.;
ACS Symposium Series; American Chemical Society: Washington, DC, 2012.

Among the experimental parameters that have been shown to affect polymer degradation rates are light intensity, glass transition temperature, oxygen diffusion, chromophore concentration, radical-trap concentration, polymer morphology and stress. This study added one more experimental parameter to this list, namely temperature. To investigate the effect of temperature on degradation efficiencies, specially designed polymers with metal-metal bonds along their backbones were synthesized. These polymers degrade by a straightforward mechanism that makes it possible to extract meaningful information. Using these polymers, it was shown that when the $Cp_2Mo_2(CO)_6$ unit is incorporated into a polymer chain, the quantum yields of degradation are strongly temperature dependent. It is proposed that when a polymer chain is cleaved, the chains relax by secondary chain movements. Furthermore, it is proposed that increased thermal energy facilitates the rotation and recoil relaxation processes, which effectively increases the rate constant for diffusion of the radicals out of the cage, k_s. In effect, the cage recombination efficiency is decreased and this leads to an increase in the efficiency of degradation. In support of this proposal, the apparent activation energy obtained from the temperature dependence of the quantum yield of polymer **1** (14.1 ± 0.3 kcal mol^{-1}) is consistent with secondary relaxation chain movements in polymers.

Acknowledgments

Acknowledgment is made to the National Science Foundation (DMR-0096606), to the NSF GK-12 grant to the University of Oregon, and to the Petroleum Research Fund, administered by the American Chemical Society, for the support of this research.

References

1. Guillet, J. E. In *Degradable Materials*; Barenberg, S. A., Brash, J. G., Narayan, R., Redpath, A. E., Eds.; CRC Press: Boston, 1990, pp 55−97.
2. Grassie, N.; Scott, G. *Polymer Degradation and Stabilization*; Cambridge University Press: New York, 1985.
3. Guillet, J. *Polymer Photophysics and Photochemistry: An Introduction to the Study of Photoprocesses in Macromolecules*; Cambridge University Press: New York, 1985.
4. Hamid, S. H., Ed. *Handbook of Polymer Degradation: Second Edition, Revised and Expanded*; Environmental Science and Pollution Control Series 21; Marcel Dekker: New York, 2000.
5. Hocking, P. J. *J. Macromol. Sci., Rev. Macromol. Chem. Phys.* **1992**, *C32*, 35–54.
6. Pittman, C. U., Jr.; Rausch, M. D. *Pure Appl. Chem.* **1986**, *58*, 617–22.
7. Rabek, J. F. *Mechanisms of Photophysical Processes and Photochemical Reactions in Polymers*; Wiley: New York, 1987.
8. Geuskens, G. *Compr. Chem. Kinet.* **1975**, *14*, 333–424.
9. Huvet, A.; Philippe, J.; Verdu, J. *Eur. Polym. J.* **1978**, *14*, 709–13.

In Degradable Polymers and Materials: Principles and Practice (2nd Edition); Khemani, K., et al.;
ACS Symposium Series; American Chemical Society: Washington, DC, 2012.

10. Cunliffe, A. V.; Davis, A. *Polym. Degrad. Stab.* **1982**, *4*, 17–37.
11. Tyler, D. R. *Coord. Chem. Rev.* **2003**, *246*, 291–303.
12. Tenhaeff, S. C.; Tyler, D. R. *Organometallics* **1991**, *10*, 1116–23.
13. Tenhaeff, S. C.; Tyler, D. R. *Organometallics* **1991**, *10*, 473–82.
14. Tenhaeff, S. C.; Tyler, D. R. *Organometallics* **1992**, *11*, 1466–73.
15. Nieckarz, G. F.; Tyler, D. R. *Inorg. Chim. Acta* **1996**, *242*, 303–10.
16. Nieckarz, G. F.; Litty, J. J.; Tyler, D. R. *J. Organomet. Chem.* **1998**, *554*, 19–28.
17. Meyer, T. J.; Caspar, J. V. *Chem. Rev. (Wash., D. C.)* **1985**, *85*, 187–218.
18. Geoffroy, G. L.; Wrighton, M. S. *Organometallic Photochemistry*; Academic Press: New York, 1979.
19. Chen, R.; Yoon, M.; Smalley, A.; Johnson, D. C.; Tyler, D. R. *J. Am. Chem. Soc.* **2004**, *126*, 3054–3055.
20. Chen, R.; Tyler, D. R. *Macromolecules* **2004**, *37*, 5430–5436.
21. Krisyuk, B. E.; Popov, A. A.; Zaikov, G. E. *Vysokomol. Soedin., Ser. A* **1980**, *22*, 329–34.
22. Male, J. L.; Lindfors, B. E.; Covert, K. J.; Tyler, D. R. *J. Am. Chem. Soc.* **1998**, *120*, 13176–13186.
23. Shultz, G. V.; Tyler, D. R. *J. Inorg. Organomet. Polym. Mater.* **2009**, *19*, 423–435.
24. Daglen, B. C.; Harris, J. D.; Tyler, D. R. *J. Inorg. Organomet. Polym. Mater.* **2007**, *17*, 267–274.
25. Balzani, V.; Carassiti, V. *Photochemistry of Coordination Compounds*; Academic Press: New York, 1970, p 12.
26. Fried, J. R. *Polymer Science and Technology*, 1st ed.; Prentice Hall PTR: Upper Saddle River, NJ, 1995; p 195.
27. Elicegui, A.; Del Val, J. J.; Millan, J. L.; Mijangos, C. *J. Non-Cryst. Solids* **1998**, *235−237*, 623–627.
28. David, L.; Girard, C.; Dolmazon, R.; Albrand, M.; Etienne, S. *Macromolecules* **1996**, *29*, 8343–8348.

Chapter 7

Starch in Polymers Technology

C. Bastioli,* P. Magistrali, and S. Gesti Garcia

Novamont, Via G. Fauser 8, 28100 Novara, Italy
***Email: catia.bastioli@novamont.com**

This chapter reviews the main topics related to starch in polymers technology taking into account all the different forms in which starch can appear (native, gelatinized, retrograded, destructurized, complexed) giving more details for those which are related to starch-based polymers.

Without intention of a whole starch treaty, authors' desire was to disclose the large variety of starch forms and their use in polymers technology in order to give a wide basic knowledge of this topic, giving an instrument for further in-depth studies to the reader.

Introduction

Starch is a natural product coming from renewable resources, which is produced during photosynthesis as food reserve for plants and vegetables. It is the second most abundant biomass material in nature. It is found in plant roots, stalks, crop seeds, and staple crops such as rice, corn, wheat, tapioca and potato.

The most important industrial starch sources are crops such as corn, wheat, potato, tapioca and rice. By refining these crops several by-products can be obtained such as oil, bran, gluten, dextrin, sugar (glucose, fructose, HFCS), ethanol (for beverages and bio-fuels) and starch.

Starch is in general a low cost and highly available product but in recent years it has been subjected to financial speculation as have several natural and fossil raw materials, so its price can highly fluctuate from one year to the following one. This fact arises from the changing in feed habits of emerging countries and from the use of crops by-products as fuel source. Regarding this aspect it has to be noted that the percentage of starch and of ethanol for fuels based on the overall corn production in the USA, was 16% and 25% respectively in 1990 and has moved to 4% and 77% in 2009 (*1*).

In Degradable Polymers and Materials: Principles and Practice (2nd Edition); Khemani, K., et al.;
ACS Symposium Series; American Chemical Society: Washington, DC, 2012.

Worldwide, the main sources of starch are corn (82%), wheat (8%), potatoes (5%) and cassava (5%) from which tapioca starch is derived. Worldwide production of corn in 2010 was approximately 800 millions of tons. The main corn producer in 2010 were USA (331 millions of tons, 12.1 billion bushels), China (158 millions of tons), Brazil and EU-27 (57 millions tons each) (*1*).

Referring to USA, 39.40% of the corn production in 2010 (331 millions of tons) was used as livestock feed, 10.5% was processed into food, seed and industrial products (excluding ethanol) and the 34.9% was converted to ethanol. The remaining 15.2% was exported (*2*).

Besides the food, pharmaceutical and paper industry, the availability of starch associated to its renewability, aroused, in the last 25 years, to an increasing interest in the sector of polymers either as an alternative to polymers based on petrochemicals due to its intrinsic polymeric structure, or as a source of glucose syrup for production of renewable monomers through fermentation processes.

The first alternative, because of the use of the natural polymeric structure of starch as such, permits to minimize the environmental impact of resulting renewable products, preserving at the same time the property of starch to be easily biodegraded in almost all the different environments: soil, composting, water. Starch based products are therefore particularly suitable for those applications where the risk of dispersion in the environment is high or the risk of polluting biodegradable streams, such as the food and yard waste, is significant.

In starch-based bioplastics starch is fully utilized with a yield very close to 100% whereas in starch-derived bioplastics, synthesized from monomers resulting from fermentation of glucose syrup, the yield is generally less than 45%, and involve more complex processes and a less efficient use of resources.

Starch based polymers have a wide range of final properties. They can be as flexible as polyethylene or as rigid as polystyrene. They can also be soluble or insoluble in water and sensitive or mostly insensitive to humidity. Such properties explain the interest in this kind of product.

Polymeric materials are performance products which cover an impressively wide range of applications. This is the reason why many different polymers have been developed in the last 70 years and combined in an infinite number of alloys. Moreover the total amount of petrol used for the production of polymers is about 5% of total consumption, whereas 90% is going in energy and fuels.

This simple consideration and the fact that the annual fuel consumption worldwide is of 1.5 Bl ton and that the worldwide production of corn is only of 0.8Bl ton can easily permit to understand the risks connected to an extensive production of ethanol from starch. In other terms the use of renewable resources becomes beneficial as much as it is oriented to performance products, with the aim to maximize efficiency of resources, instead of mass products in a replacement logic.

The peculiar properties of starch limit the number of applications where starch-based bioplastics are highly advisable in terms of in-use performances and end of life behaviour. It means that with starch-based bioplastics it is not possible to just think in terms of replacement of traditional plastics and they represent a perfect opportunity to redesign systems with attention to the efficient use of resources.

In Degradable Polymers and Materials: Principles and Practice (2nd Edition); Khemani, K., et al.;
ACS Symposium Series; American Chemical Society: Washington, DC, 2012.

This chapter reviews the main topics related to starch in polymers technology taking into account all the different forms in which starch can appear (native, gelatinized, retrograded, destructurized, complexed) giving more details for those which are related to starch-based polymers.

Starch

Starch is obtained from crops refining by several steps depending on the crop source. For instance, corn starch is extracted from kernel by wet milling in order to split the kernel and remove the oil-containing germ. Finer milling separates the fiber from the endosperm which is then centrifuged to separate the less dense protein from the most dense starch.

The starch slurry is then washed in a centrifuge, dewatered and dried. Either prior or subsequent to the drying step, the starch may be processed in a number of ways to improve its properties.

Starch is constituted by two major components: amylose, a mostly linear α-d-(1,4)-glucan (Figure 1a); and amylopectin, an α-d-(1,4) glucan (Figure 1b) that has α-d-(1,6) linkages at the branch point. The linear amylose molecules of starch have a molecular weight of 0.2–2 million, while the branched amylopectin molecules have molecular weights as high as 100–400 million (*3*, *4*).

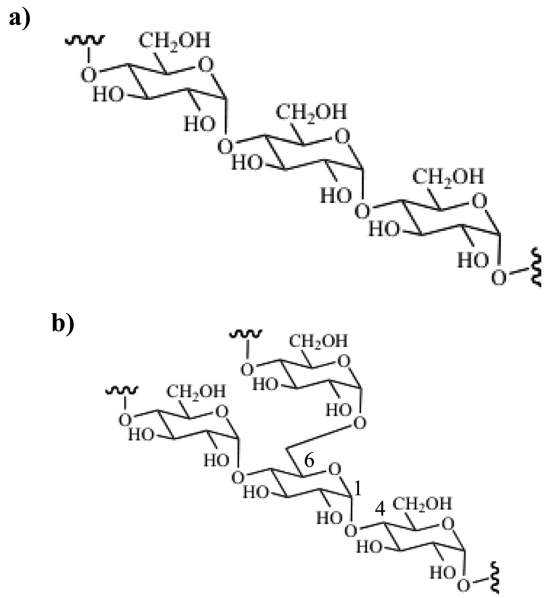

Figure 1. Molecular structure of amylose (a) and amylopectin (b).

These two macromolecules are arranged in granules having a size ranging from 2 to 100 μm depending on the source (corn, potato, etc.) and genotype. These grains have a kernel (hilum) from which start an alternate lamellar structure of crystalline and amorphous shells. The shells are constituted of blocklets having

In Degradable Polymers and Materials: Principles and Practice (2nd Edition); Khemani, K., et al.;
ACS Symposium Series; American Chemical Society: Washington, DC, 2012.

a size from 20 to 500 nm formed of amylopectin clusters and amylose. Blocklets are alternated lamellar structures of crystalline and amorphous amylopectin arrangements.

The ratio of the two polysaccharides varies according to the botanical origin of the starch. The 'waxy' starches contain less than 15% amylose, 'normal' 20–35% and 'high' amylose starches greater than about 40%. The moisture content of air-equilibrated starches ranges from about 10–12% (cereal) to about 14–18% (some roots and tubers).

Native granules, yield X-ray diffraction patterns, which although they are generally of low quality, can be used to identify the several allomorphs (*5*). In native form, both amylopectin and amylose have a double helix structure with hydrogen bonds between these helices, either direct or through the water molecules in the unit cell.

Such an ordered structure is able to deviate polarized light, so if native starch granules are observed by means of polarized optical microscopy Maltese crosses will be detected.

This structure is an almost perfectly left-handed six-fold double helix. Depending on the starch genotype three different crystal native forms can be detected: A (cereal starches), B (tuber starches and cereal starches rich in amylose), and C (smooth pea and various beans) (*6*). The difference between A and B type is due to how the double helices are packed and how many water molecules are incorporated in the crystal cell.

In A type structure, double helices give rise to a monoclinic lattice with space group B_2 (a = 2.083 nm, b = 1.145 nm, c = 1.058 nm, γ = 122.0°), that contains four maltotriosyl units per unit cell and two water molecules per maltotriosyl unit (*7*). Besides, B type structure has a hexagonal lattice with space group $P6_1$-C_6^2 (a = b = 1.852 nm, c = 1.057 nm, γ = 120°) that contains four maltotriosyl units (12 glucose residues) and 36 water molecules (*8*).

C type structure or so called C polymorph is a combination of A and B crystalline form (*9*). A allomorph (60% of the total polymorph) is mainly located in the outer part of the granules whereas B allomorph (40% of the total polymorph) is mainly located in the inner part of it (*10*).

Native starch cannot be treated as a traditional polymer as the arrangement of amylose and amylopectin lead to the already explained grain structure. As observed by Donovan (*11*) this grain structure has a melting process related to the amount of water contained in it.

The melting mechanism of such systems is described by the Flory-Huggins theory of polymer-diluent interaction, which correlates the melting temperature of the dilute polymer T_m to that one of the undiluted polymer T_m^0 as a function of the volume fraction of the diluent:

$$\frac{1}{T_m} - \frac{1}{T_m^0} = \frac{R}{\Delta H_u} \cdot \frac{V_u}{V_1} \cdot (V_1 - \chi \cdot V_1^2) \qquad (1)$$

Equation 0 Flory-Huggins equation

In Degradable Polymers and Materials: Principles and Practice (2nd Edition); Khemani, K., et al.;
ACS Symposium Series; American Chemical Society: Washington, DC, 2012.

Where:

- ✓ T_m: melting point of the crystalline polymer plus diluent (water) (K);
- ✓ T_m^0: melting point of undilute polymer crystallites (K);
- ✓ R: gas constant;
- ✓ ΔH_u: fusion enthalpy per anhydroglucose repeating unit;
- ✓ V_u: volume fraction of anhydroglucose repeating unit;
- ✓ V_1: volume fraction of diluent (water);
- ✓ χ: Flory-Huggins interaction parameter;

T_m^0 for starch crystallites is approximately 257°C which is above the degradation temperature of amylose and amylopectin macromolecules.

For this reason starch, unless used as a polymer filler (see § Starch-Filled Plastics), has to be transformed in order to change its original structure (see § Structural Starch-Modifications) allowing its macromolecules to be treated as those of a thermoplastic polymer.

Besides structural modification, starch can even undergo chemical modification which can confer to it different hydrophilic, swelling, rheological, physical and chemical properties. Examples of chemical modification of starch are esterification, etherification or crosslinking of hydroxyl groups or oxidation of anhydroglucose repeating unit.

Both native and chemically modified starches can be structurally modified in order to be used like polymers either alone or in combination with specific synthetic polymers.

In conclusion, a starchy material is converted into thermoplastic starch (often referred as TPS) by melting in closed devices such as heated extruders or other closed devices capable of securing temperature, pressure and shear conditions. Starch which has undergone a thermoplastic transformation does not show anymore the typical melting peaks of native starch at specific water content under DSC analysis in sealed vials and can be defined as thermoplastic starch. In case of starch blends with synthetic polymers the presence of starch in form of submicronic particles dispersed into the matrix is a clear demonstration that a thermoplastic transformation occurred on starch itself.

Starch-Filled Plastics

The use of native starch in traditional plastics such as polyolefins is nowadays (*12–15*) less popular than in the past.

Nevertheless in this paragraph a short review of such kind of products will be disclosed.

When blended with starch beads, PE films (*16*) deteriorate on exposure to a soil environment. The microbial consumption of the starch component, in fact, leads to increased porosity, void formation, and the loss of integrity of the plastic matrix.

Generally (*17*) starch is added at fairly low concentrations (6-15%); the overall disintegration of these materials is achieved by the use of transition metal

In Degradable Polymers and Materials: Principles and Practice (2nd Edition); Khemani, K., et al.;
ACS Symposium Series; American Chemical Society: Washington, DC, 2012.

compounds, soluble in the thermoplastic matrix, as pro-oxidant additives which catalyze the photo and thermo-oxidative process (*18–21*).

Starch-filled polyethylenes containing pro-oxidants have been used in the past in agricultural mulch film, in bags, and in sixpack yoke package. Commercial products based on this technology were first sold by Ecostar and Archer Daniels Midland Companies (*22*). According to St. Lawrence Starch technology, regular cornstarch was treated with a silane coupling agent to make it compatible with hydrophobic polymers, and dried to less than 1% of water content. It was then mixed with the other additives such as an unsaturated fat or fatty-acid autoxidant to form a masterbatch that is added to a commodity polymer. The polymer could then be processed by convenient methods, including film blowing, injection molding, and blow molding.

When processing this sort of materials, temperature has to be kept below 230°C to prevent decomposition of the starch and exposure of the masterbatch to air had to be minimized to avoid water absorption.

Direct addition of starch and pro-oxidant without the masterbatch step can also be used: as this requires some specific equipment, it is only practical for large volumes (*20*).

It has been claimed that under appropriate condition the disintegration time of a buried carrier bag, containing an Ecostar of up to 6% starch, will be reduced from hundreds of years to three to six years (*17*).

The non compliance of these materials with the international standards of biodegradability in different environments, the high concern for the increasing presence of plastic debris in the marine environment, even favoured by their tendency to fragment, and their potential negative impact on recyclability of traditional plastics, should not permit to consider this technology as a real industrial and environmentally preferable option.

Other attempts of fully or partially biodegradable starch-filled plastics were studied such as starch/poly(ε-caprolactone) (PCL) (*23*), others which are partially biodegradable, starch/polyvinylchloride/poly(ε-caprolactone) (PCL) (*24*) or starch/modified polyesters (*25*). In all these cases, starch granules are used to increase the surface area available for attack by microorganisms.

Today, PSM (HK) Co. Ltd. (a subsidiary of Engrowth Investments Limited incorporated in BVI) is one of the few companies which still use starch-filled plastics producing raw materials for injection moulded products usually for catering purposes (*26*).

Structural Starch Modifications

Modifications of the native starch form can be made by means of thermal and mechanical treatments where the amount of water has an essential role. Referring to Equation 0, when starch is heated at a water volume fraction above 0.9 a pure gelatinization phenomenon (and afterwards gelation and retrogradation) or jet-cooking occurs. On the contrary, when the water volume fraction is low (e.g.below 0.45), a real melting of starch crystallites occurs (*27*, *28*) and thermoplastic starch can be obtained (*28*).

In Degradable Polymers and Materials: Principles and Practice (2nd Edition); Khemani, K., et al.;
ACS Symposium Series; American Chemical Society: Washington, DC, 2012.

Starch Gelatinization and Retrogradation

Starch gelatinization occurs when aqueous suspensions of native starch granules are heated above a characteristic temperature (gelatinization temperature) (*29*). It is an irreversible process in which granules swell leading to loss of molecular order and crystallinity (*9*, *30*) which brings about a loss of birefringence. Moreover, swelling of starch granules is also accompanied by leaching of starch molecules (mainly amylose).

The gelatinization process can be observed by DSC techniques. Depending on the amount of water present in the system several endotherm peaks can be detected. If the water volume fraction is significantly above 0.45 (conditions that lead to gelatinization) a single endotherm peak, pointed as G is observed (*27*).

On the contrary, if the water volume fraction is below 0.45 more than one endotherm peak is observed. The first two peaks (M_1 and M_2) are the most relevant ones. The first peak, assigned as M_1 (which becomes less intense when water volume fraction decreases) occurs at the same temperature of the single endotherm G and is due to crystallite destabilization occurring when amorphous zones swell. The second peak, assigned as M_2 is related to the crystallites melting, and (as shown by Flory-Huggins theory – eq 1) the higher the water volume fraction (V_1) is, the lower the melting temperature of the polymer . For instance: for rice starch if V_1 is approximately 0.5 M_2 occurs at ca. 90°C, if V_1 is approximately 0.2 M_2 occurs at ca. 160°C (*27*).

When a gelatinized starch system is cooled, an increase in viscosity is observed due to re-association of starch molecules. This phenomenon, called retrogradation, is characterized by gradual increase in rigidity and a phase separation between solvent and polymer chains. The re-association of starch molecules (both amylose and amylopectin) give rise to short-range molecular order and crystallization of double helical aggregates in the B lattice form (*9*). Starch retrogradation depends on a large variety of factors such as the source of starch, its concentration, cooking and cooling temperature speeds, pH and the presence of solutes (lipids, electrolytes, sugars).

Both amylose and amylopectin take part in the retrogradation process and network structure formation and up to four different steps of ordering have been postulated (*31*). The first one which take place in few hours has been ascribed to gelation of the solubilized amylose in the intergranular space forming double helices structures. The second and the third one, for which days are needed, has been ascribed to chain reordering and crystallization of amylopectin. The fourth step involves phase separation of water (syneresis) due to excessive retrogradation of starch chains (*31–34*).

As gelatinization, retrogradation phenomenon can be studied by DSC technique.

For instance, if gelatinized corn starch is stored in conditions suitable for retrogradation (i.e. 5°C for several hours or days) and a DSC scan is performed, two endotherms peaks will be detected. These two peaks are pointed as Gr and M_1r and are correlated to G and M_1 peak of gelatinization phenomenon. Gr and M_1r are mainly due to amylopectin which, after the gelatinization process, can rebuild its structure under appropriate time-temperature conditions giving rise to

In Degradable Polymers and Materials: Principles and Practice (2nd Edition); Khemani, K., et al.;
ACS Symposium Series; American Chemical Society: Washington, DC, 2012.

new thermal transitions close to the original ones (*35*). Gr and M_1r are detectable both in normal starches and in waxy (high amylopectin content) starches (in this case Gr and M_1r are more pronounced) (*35*, *36*).

One practical effect of starch retrogradation is on bakery products: recrystallization of amylopectin has a great role in staling of baked products during storage. As amylopectin crystallization depends on T_g (the lower, the easier crystallization), that is related to the water content in the baked products, staling can be reduced by rising the T_g of the baked system. Also amylose crystallization has an important role as the more it is crystallized the less it is digestible by enzymes (*30*).

Starch Jet-Cooking

Jet-cooking of starch is another method used to destroy the crystallinity of starch in excess of water (*9*). By injecting steam into a slurry of starch while it passes through a mixing device such as a Venturi-nozzle, against a back pressure, the stream of high-velocity steam mixes the slurry intimately and smoothly and raises its temperature quickly. This system provides the shear and temperature needed to swell and destroy starch granules to a certain extent. Usually, temperatures of 120C or higher are reaches and starch concentrations of up to 30% are used for the slurry dispersion. The final concentration is in the range of 2-14% and is obtained by adding preheated water in the desired amount in order to achieve a proper starch dilution. Subsequently, the slurry is cooled to 60-70C.

One of the main industrial uses of jet-cooked starch is in the paper industry where it is used as sizing (*37*).

Starch Extrusion Cooking

A different form of starch gelatinization is extrusion cooking technology (*38*). As described by Conway in 1971 (*39*), extrusion cooking and forming is characterized by sufficient work and heat being applied to a cereal-based product to cook all the ingredients to obtain a crunchy foam though a die. The effects of processing conditions on the starch and on the texture of the extruded products have been studied by several researchers (*40–46*). Cooked foamed materials with different starch viscosity, water solubility and water absorption have been prepared by altering the moisture content of the raw product and the temperature or the pressure in short extruders specifically designed for this purpose.

It has been demonstrated that an extrusion-cooked starch can be solubilized without forming maltodextrins and that the extent of solubilization depends on extrusion temperature, moisture content of the starch before extrusion and amylose/amylopectin ratio. For instance, Mercier et al. (*40*) determined the properties of different types of starch and considered the influence of the moisture content (10.5 and 28%), barrel temperature (65 and 250C), and residence time (20 seconds and 2 min), in a short twin-screw extruder. After extrusion cooking, corn starch gave a solubility lower than 35%, while potato starch solubility was up to 80%.

In Degradable Polymers and Materials: Principles and Practice (2nd Edition); Khemani, K., et al.;
ACS Symposium Series; American Chemical Society: Washington, DC, 2012.

Hanna et al. (*43*) observed that the degree of gelatinization of ordinary corn (30% amylose) and waxy corn (1% amylose) decreased with increasing moisture content but increased with increasing temperature. Corn starches were extruded between 17.8 and 42.2% moisture contents and extruder barrel temperatures of 116°, 120°, 140°, 160° and 164°C. Screw speeds of 93.5, 100, 130, 160 and 166.5 rpm were used to generate different residence times.

Starch Destructurization in Absence of Synthetic Polymers

In the patent literature, the terminology "destructurized starch" (*47–66*) refers to a form of thermoplastic starch described as molecularly dispersed (*57*). Destructurization of starch is defined as melting and disordering of the molecular structure of the starch granules as a molecular dispersion (*56*, *57*). It means that at the same time the native crystallinity of starch and its granular structure disappear.

This is achieved by heating the starch above the glass transition temperature (T_g) and the melting temperatures (T_m) of its components, until they undergo endothermic transitions under shear, temperature and pressure for a time sufficient to also destroy the granular structure. As already stated before, the water volume fraction required has to be below 0.45 and preferably below 0.28 (*28*).

Starch can be destructurized using extrusion technologies in specific conditions. Sufficient work, heat and time have to be applied to a cereal-based product in the presence of plasticizers to destructurize it. The best plasticizer for starch is water in quantities lower than 45%. Other plasticizers are glycols such as glycerol, sorbitol, etc. Whereas thermoplastic starch can contain a certain amount of granular residues and few maltese crosses could be detected in polarized light microscopy, destructurized starch is substantially free from those feartures .

After undergoing destructurization, starch no longer shows its native crystallinity and loses its characteristic left handed double helices as previously reported.

Neverthless other forms of crystallinity, different from the native form is induced by the interaction of the amylose component with specific molecules. These forms of crystallinity are characterized by single helical structures and are known as V complexes (*67*).

The disappearance of the crystalline structure of the starch granule may be determined using conventional light microscopy techniques (*68*).

When native starch is observed using phase contrast microscopy, starch granules ranging from 2 to 100 μm (depending on starch source) in size are detected (Figure 2a). If the same sample is observed using polarized light microscopy, Maltese crosses due to starch birefringence will be detected (Figure 2b).

When gelatinized starch is observed using phase contrast microscopy, swollen starch granules are detected (Figure 2c). The swelling factor (SF) which is the ratio between the volume of the swollen and native starch granule can vary from 10 to 50 and depends on the starch source, native granule size, and the final temperature reached during the gelatinization process (*9*). As already mentioned before, the gelatinization process gives rise to disordered structures but swollen granules or ghosts of swollen granules are still visible. Nevertheless, swollen granules are no

In Degradable Polymers and Materials: Principles and Practice (2nd Edition); Khemani, K., et al.;
ACS Symposium Series; American Chemical Society: Washington, DC, 2012.

longer able to deviate polarized light. Consequently, a dark area will be seen if the same sample is observed using polarized light microscopy (Figure 2d).

When destructurized starch is observed using phase contrast microscopy, a continuous surface is detected that is void of starch granules (Figure 2e). Amylopectin and amylose macromolecules which behave like polymer macromolecules in the bulk, are arranged in a disordered way (just local point of V lattice structure could eventually be formed). This sort of amorphous structure is not able to deviate polarized light, so, if the same sample is observed using polarized light microscopy, a dark area will be seen (Figure 2f).

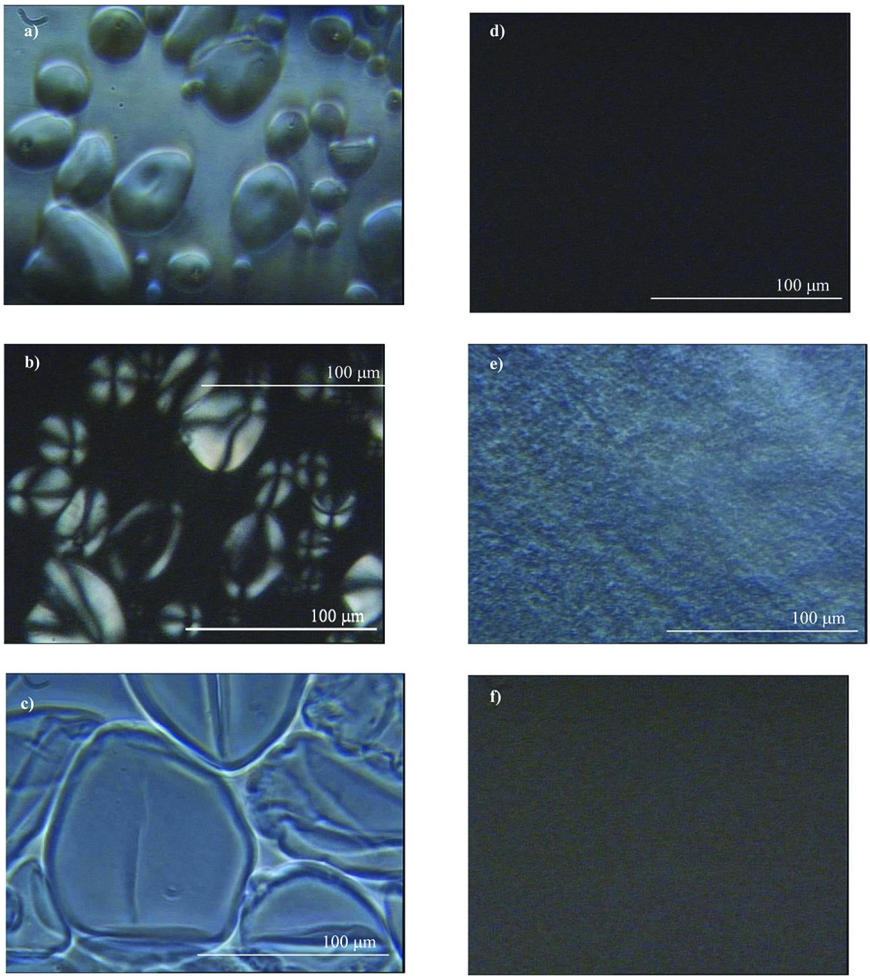

Figure 2. Phase Contrast Microscopy of native (a), gelatinized (c) and destructurized potato starch (e), respectively. Polarized Optical Microscopy of native (b), gelatinized (d) and destructurized (f) potato starch, respectively.

In Degradable Polymers and Materials: Principles and Practice (2nd Edition); Khemani, K., et al.;
ACS Symposium Series; American Chemical Society: Washington, DC, 2012.

Another term that can be found in the literature is "thermoplastically processable starch" (TPPS), defined as a thermoplastic starch that is substantially water free. TPPS is a form of destructurized starch that is obtained using high boiling point plasticizers or additives rather than water (*69–74*).

If plasticizers are not removed from TPS (or TPPS) in order to avoid that the glass transition temperature of these systems becomes too high, they can be processed as a traditional plastic (*28*, *57*, *75*) as their melt viscosity is comparable with those of traditional polymers (*76*).

This aspect makes possible the transformation of destructurized starch in absence of water in finished products through traditional manufacturing technologies for plastics.

Their sensitivity to humidity, however, makes TPS or TPPS alone unsuitable for most applications (*77*).

Starch Destructurization in the Presence of Synthetic Polymers

Starch can undergo a thermoplastic transformation up to destructurization in presence of different synthetic polymers to satisfy a broad spectrum of market needs. Destructurized starch composites can reach starch contents higher than 50%.

With some of these polymers a real complexation of single helical amylose with the polymer backbone can happen, which gives rise to supramolecular structures characterized by V type crystallinity. This sort of modified amylose crystallinity is the same mentioned in § Starch Destructurization in Absence of Synthetic Polymers and has been widely studied with small molecules such as alcohols, glycerol, dimethylsulphoxide, fatty acids, iodine (*67*).

Complexation of starch by macromolecules, can give rise to even more stable complexes playing an important role on the final properties of the starch-based polymer.

Unlike amylose, amylopectin interacts less with complexing agents and remains in its amorphous state.

In the following paragraphs, a summary of the state of the art related to starch destructurization with synthetic polymers will be made.

Ethylene-Acrylic Acid Copolymer (EAA)

Otey reported the interactions between ethylene-acrylic acid copolymer (EAA) and gelatinized starch beginning in 1977 (*78–84*).

In these formulations, a further compatibilization of EAA with starch was made by using ammonium hydroxide. In fact, it has been demonstrated that a fraction of starch interacts (*85*, *86*) with EAA after neutralization with ammonium hydroxide or other bases during gelatinization and extrusion, providing not only partial miscibility between the two polymers, but also enhancing the formation of molecular complexes.

Formulations based on thermoplastic starch-EAA-PE in different ratios, are suitable for film production. In Table I a few examples of such compositions (some of them containing also PVOH) with their related tensile strength properties are

In Degradable Polymers and Materials: Principles and Practice (2nd Edition); Khemani, K., et al.;
ACS Symposium Series; American Chemical Society: Washington, DC, 2012.

reported. As can be seen, the film obtained with a gelatinized starch level of about 50% shows good tensile properties.

Table I. Influence of starch/EAA ratio and of partial replacement of EAA with PE or PVOH on the tensile strength and elongation of starch/EAA films (*84*, *88*).

Starch (phr)	*EAA (phr)*	*PE (phr)*	*PVOH[a] (phr)*	*Elongation (%)*	*UTS (MPa)[b]*
10	90	-	-	260	23.9
30	70	-	-	150	22.2
40	60	-	-	92	26.7
40	40	20	-	66	23.9
40	25	25	-	85	21.7
40	20	40	-	34	20.1
40	55	-	5	97	32.0
40	40	-	20	59	39.7

[a] PVOH: polyvinyl alcohol [b] UTS: ultimate tensile strength

In 1989, studies on EAA-thermoplastic starch films containing 40% by weight of EAA (acrylic acid content 20% by weight), processed at water content lower than 2%, led to destructurization of starch, improved processability and film properties with elongation at break up to 200% without the need for ammonia or sodium hydroxide (*87*). Observing these materials by means of microscopic analysis at least three different phases were observed. One phase consisted of destructurized starch, one consisted of synthetic polymer alone and a third one described as 'interpenetrated' was characterized by a strong interaction between the two components.

It has been also seen that the use of urea in EAA- starch films, enhances the tear propagation resistance and reduces ageing phenomena due to segmental motion in amorphous starch (*88*, *89*).

Unfortunately, due to the lack of biodegradability of EAA, films based on such formulations do not comply the international biodegradation standards precluding their use in most of the packaging applications.

Ethylene-Vinyl Alcohol Copolymers (EVOH)

Thermoplastic starch and EVOH copolymer systems, depending on the processing conditions, starch type, and copolymer composition, can generate a wide variety of morphologies and properties (*90–99*). Different microstructures have been observed: from a droplet-like to a layered one (*93*), as a function of

In Degradable Polymers and Materials: Principles and Practice (2nd Edition); Khemani, K., et al.;
ACS Symposium Series; American Chemical Society: Washington, DC, 2012.

different hydrophylicity of the synthetic copolymer. An in-depth description of this aspect will be treated in § Additional Information on Starch Complexation.

The products based on thermoplastic starch and EVOH show mechanical properties suitable to meet the needs of specific industrial applications (*100*) Their mouldability in traditional processing technologies is comparable with that of traditional plastics such as PS, ABS, and LDPE (*96*). The main limits of these materials are in the high sensitivity to low humidities, with consequent embrittlement.

To improve their characteristics, such as migration phenomena and physical ageing specific types of plasticizers were selected (*100*). Boric acid, borax or other saline compounds were used to improve film transparency (*99*). With these materials, it is possible to obtain final products by film blowing, injection molding, blow-molding thermoforming and it is also possible to foam these compositions giving rise to products having cushioning characteristics close to expanded polystyrene (EPS-55) (*101*).

Biodegradation of these products has been tested in different environments (*91*). Ten months of aerobic biological treatment performed by an high sensitivity respirometric Sturm test, brought to the degradation of more than 90% w/w of a product consisting of 60% of maize starch and natural additives and by 40% of EVOH copolymer (ethylene content 40% by mole) (*91*, *92*). Replacing EVOH, 40% ethylene content by mole, with EVOH,29% ethylene content by mole in such a product, a reduced ability of starch to generate interpenetrated structures has been observed as well as a significantly higher initial biodegradation rate under Sturm test (*91*). Furthermore, the semi continuous activated sludge test (SCAS) and biodegradation in lake water of a product consisting of 70% maize starch plus natural additives and 30% EVOH, supported the hypothesis of a substantially different biodegradation mechanism for the two components (*92*):

- Starch, even though significantly shielded by the interpenetrated structure, seems to undergo to hydrolysis by extracellular enzymes.
- EVOH appears biodegraded through a superficial adsorption of microorganisms, made easier by the increase of available surface that occurred during the hydrolysis of starch.

The presence of starch improves the biodegradation rates of these synthetic polymers, where a fundamental role is also played by size and distribution of ethylene blocks.

Attempts of speeding up the biodegradation rate by modification of EVOH copolymers with carboxyl groups have been pursued but the degradation rate of thermoplastic starch and EVOH composition is too slow to consider them compostable.

Polyvinyl Alcohol (PVOH)

The combination of starch with a water soluble polymer such as PVOH (or polyalkylene glycols) has been widely considered since 1970 (*102*). In the last 20 years these compositions have been mainly studied for starch-based loose fillers

In Degradable Polymers and Materials: Principles and Practice (2nd Edition); Khemani, K., et al.;
ACS Symposium Series; American Chemical Society: Washington, DC, 2012.

production as a substitute for expanded PS (*103–109*) using compositional water as expanding gas. In these blends native as well as chemically modified starch such as hydroxy propylated high amylose starch can be used, especially to improve foam resilience and density (*103*, *107*).

Optimization of compositions and foaming process have been pursued during the years in order to improve finals foams properties, leading, for example to foam densities of 8-6 kg/m^3 (*110–112*).

Aliphatic Polyesters (APE)

Starch can also be destructurized in presence of more hydrophobic polymers, totally incompatible with starch, such as aliphatic polyesters (*113*).

Aliphatic polyesters having low melting point are difficult to be processed by conventional techniques for thermoplastic materials, such as film blowing and blow molding. It has been found that the blending of starch with aliphatic polyesters allows the improvement of their processability and biodegradability.

Particularly suitable polyesters considered in the past have been poly-ε-caprolactone (PCL) and its copolymers Nevertheless, films made of thermoplastic starch and PCL are tacky as extruded, rigid, and have low melt strength at temperatures over 130°C. Moreover, due to the slow crystallization rate of such polymers, the complete cooling process needs a long time after production of the finished articles, giving an undesirable change of properties with time.

Other APE having a higher melting point that can be used in presence of destructurized starch, are those formed by the reaction of glycols such as 1,4-butandiol with: succinic acid, sebacic acid, adipic acid, azelaic acid, dodecanoic acid, or brassilic acid.

The presence of compatibilizers between starch and aliphatic polyesters is preferred. Some examples are amylose/EVOH V-type complexes (*93*), starch grafted polyesters, and chain extenders such as diisocyanates, and epoxydes is preferred. Such materials are characterized by excellent compostability, excellent mechanical properties, and reduced sensitivity to water.

Aliphatic-Aromatic Polyesters (AAPE)

The most important achievement of the last years in the sector of starch technology is related to the creation of nanostructured composites where thermoplastic starch is the dispersed phase and aliphatic-aromatic polyesters of different type are the continuous phase. .

This technology has been developed and patented by Novamont (*114*, *115*). In these families of products starch gives a technical contribution to the mechanical performance of the finished products in terms of high toughness and excellent performance and stability at different humidities and temperatures. Such products can cover a wide range of demanding applications in the film sector and meet the different needs in terms of end of life conditions such as home compostability and soil biodegradation.

In Degradable Polymers and Materials: Principles and Practice (2nd Edition); Khemani, K., et al.;
ACS Symposium Series; American Chemical Society: Washington, DC, 2012.

The development of new aliphatic and aliphatic-aromatic copolyesters containing monomers from vegetable oils, covered by a range of Novamont's patents, have further improved and widened the performance of these products from an environmental and technical point of view.

One of the main applications of these products is related to shopping bags: the substitution of traditional plastics with biodegradable ones in this field can greatly reduce the impact on the environment of this sort of product. Moreover their re-use for the separate collection of organic waste can help to enhance organic wastes value converting them into high quality compost. Again referring to 'cradle-to-cradle' applications, these products can advantageously replace traditional plastic used for agricultural films.

Such development has justified the significant industrial investment made by Novamont to build the first local biorefinery of this type in Europe, which comprises plants for the production of nanostructured starch and polyesters from vegetable oils. Moreover new investments on monomers from vegetable oils from local crops will permit a further up-stream integration of the biorefinery.

This family of tailor made products has permitted Novamont to work on many case studies aimed to demonstrate the opportunity given by biodegradable and bio-based plastics to rethink entire application sectors. This affects not only the manner in which raw materials are produced, but also enables a 'cradle-to-cradle' of entire agro-industrial non-food chains, or chains that are synergistic with food. This also affects the way products are used and disposed of, expanding the scope of experimentation to the local areas.

Other Polymers

Thermoplastic starch can also be blended with other polymers such as polyolefins (*116*). In this sort of blends, a compatibilizer such as ethylene maleic anhydride copolymer can be used in order to make hydroxyl starch groups and anhydride copolymer groups to react and obtain ester bonds. This sort of esterification helps to compatibilize the starch (hydrophile) with polyolefins (lipophile).

Other studies have been performed on polyamide/high amylase (*56*, *117*, *118*) and acrylic copolymers/high amylose starch systems (*56*, *118*, *119*).

The non compliance of these products with the international norms of biodegradability and compostability, however, did not permit a significant market growth in western countries.

Thermoplastic starch and cellulose derivative systems have been also reported (*99*, *113*, *120*, *121*) particularly with cellulose acetate and butyrate in presence of glycerine and epoxidized soybean oil (*120*).

These materials are especially suitable for injection moulding technology and have been industrially used for compostable cutleries.

Additional Information on Starch Complexation

Novamont's Mater-Bi starch-based technology utilizes processing conditions that destroy the crystallinity of amylose and amylopectin, in the presence of

In Degradable Polymers and Materials: Principles and Practice (2nd Edition); Khemani, K., et al.;
ACS Symposium Series; American Chemical Society: Washington, DC, 2012.

macromolecules which are able to form a complex with amylose such as specific polyesters. They can be of natural or synthetic origin. The specification of the starch, i.e., the ratio between amylose and amylopectin, the nature of the additives, the processing conditions and the nature of the complexing agents allows engineering of various supramolecular structures with very different properties.

For example, destructurized starch and vinyl alcohol copolymer composites, materials containing starch with an amylose/amylopectin ratio above 20/80 w/w do not dissolve even under stirring in boiling water. Under these conditions a microdispersion, constituted by microsphere aggregates, is produced, whose individual particle diameter is lower than 1 μm (Figure 3).

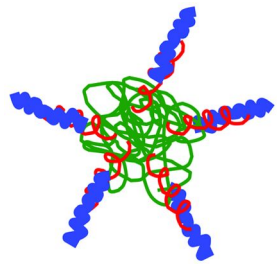

Figure 3. Mater-Bi technology: Droplet-like structure.

A droplet-like structure, where a core of an almost amorphous amylopectin molecule is surrounnded by complexed amylose molecules, has been confirmed by transmission electron microscopy (TEM) analysis of film slices (*91*). The droplet size is comparable with that of the microdispersion obtained by boiling.

On the other hand, the morphology of materials in film form, containing starch with an amylose/amylopectin ratio below 20/80 w/w, gradually looses the droplet-like form, generating layered structures (Figure 4). In this case the starch component becomes partially soluble. The layered structure consists of sub-micron layers of amylopectin molecules intercalated by layers of complexing agent, such layers being compatibilised by complexed amylose. The two structures and the many others derived from them explain the wide range of mechanical, physical-chemical, rheological properties and the different biodegradation rates of Mater-Bi products.

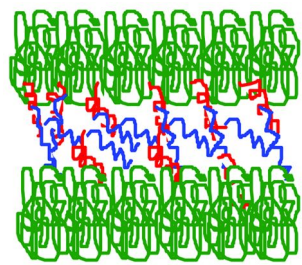

Figure 4. Mater-Bi technology: Layered structure.

In Degradable Polymers and Materials: Principles and Practice (2nd Edition); Khemani, K., et al.;
ACS Symposium Series; American Chemical Society: Washington, DC, 2012.

Fourier transform infrared (FTIR) second-derivative spectra of thermoplastic starch and vinyl alcohol copolymer systems with droplet-like structure, in the range of starch ring vibrations between 960 and 920 cm^{-1}, provides for an absorption peak at about 947 cm^{-1} (Figure 5), as observed for amylose when complexed (V-type complex) by low-molecular-weight molecules such as butanol and fatty acids.

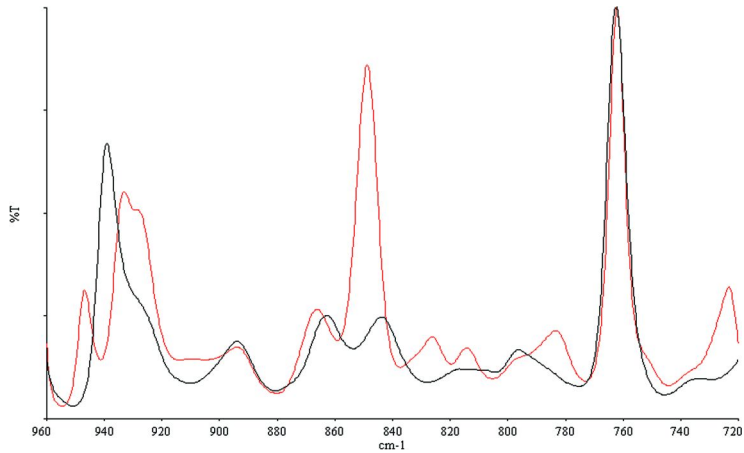

Figure 5. FTIR second derivative spectrum of corn starch (red spectrum), and destructurized with EVOH (black spectrum).

This peak is attributed to starch ring vibrations (*93*, *122*), and does not correspond to crystalline or gelatinized amylose but to a complexed one, which results when amylose assumes V-type structures conformations after destructurization. Comparable starch-based materials with an amylose content close to zero, even in presence of complexing agents, do not show any peak at 947 cm^{-1}.

V-type structure formation can be also detected, by X-Ray diffraction analysis and ^{13}CP-MAS solid state NMR (*123–126*).

As far as X-Ray diffraction analysis is concerned (WAXD), characteristic peaks of different V-type structures can be detected on destructurized starch in presence of complexing agents either molecular or macromolecular ones.

As already stated, V lattices form of complexed amylose is mainly characterized by a single left-handed helical forms, which surround the complexing agent. With certain complexing agents, it can be possible that the left-handed structure is stabilized by the formation of supramolecular structures where the complexing agent is on the outer side of the amylose single left-handed helical (*127*).

V-type amylose structures nomenclature is still not univocal. Moreover, these forms have different stabilities and transitions to a less stable form to a more stable one can be achieved by changing the environmental storage conditions (such as temperature and humidity) (*128–130*). Depending on the numbers of anhydroglucose repeating unit present in the helical pitch, which are correlated

In Degradable Polymers and Materials: Principles and Practice (2nd Edition); Khemani, K., et al.;
ACS Symposium Series; American Chemical Society: Washington, DC, 2012.

to the complexing agent used, slightly different V-type amylose structure can be obtained.

Usually, starch destructurization in presence of specific synthetic polymers, give rise to V_H and E_H structures (always a V-type one). The latter is especially obtained with high mechanical stress and low moisture content (*131*).

Referring to starch destructurized in presence of EVOH copolymer, this sort of composition leads to the V_{6I} structure (WAXD patterns are reported in Figure 6).

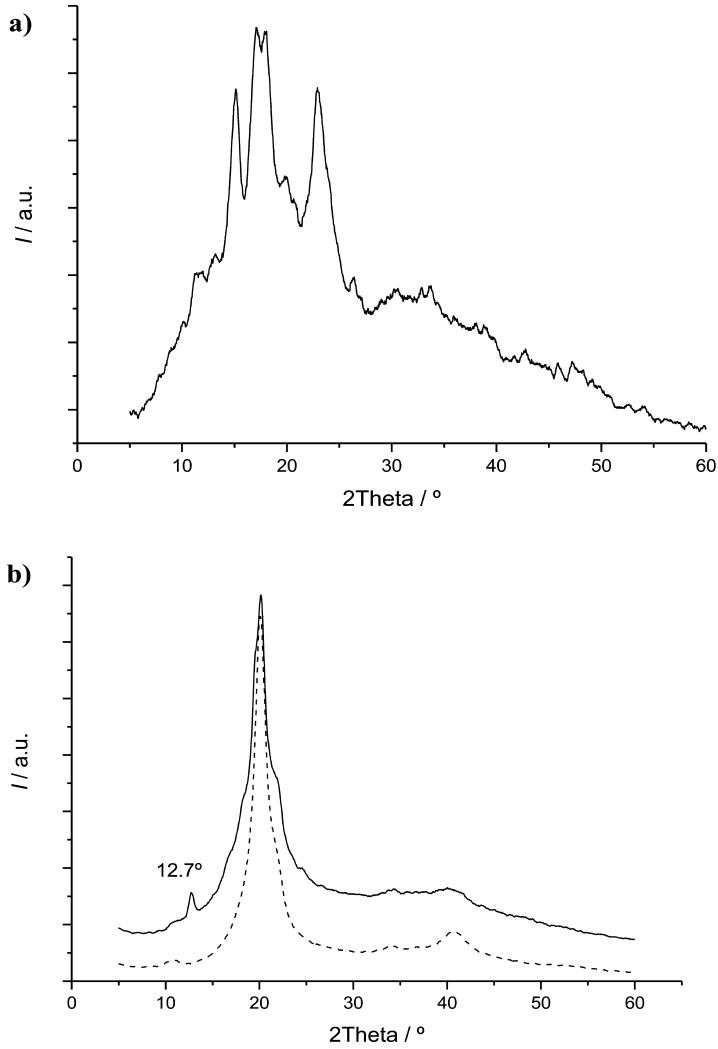

Figure 6. WAXD patterns of corn starch: Native (a), destructurized with EVOH (b). The black pattern corresponds to the starch destructurized with EVOH, while the red pattern corresponds to the EVOH pattern.

In Degradable Polymers and Materials: Principles and Practice (2nd Edition); Khemani, K., et al.;
ACS Symposium Series; American Chemical Society: Washington, DC, 2012.

Vinyl alcohol copolymers, as well as butanol, leave the amylopectine conformation unchanged. A model has been proposed considering large individual amylopectin molecules interconnected at several points per molecule as a result of hydrogen bonds and entanglements by chains of amylose/vinyl alcohol copolymer V complexes. This structure has been defined in the literature as "interpenetrated" (*93*).

The amount of V-type structure present in the final formulation affects the biodegradation rate of starch. is the more amylose complexed with other molecules, the lower becomes its rate of biodegradation. This aspect is confirmed by second derivative FTIR spectra which shows the 947 cm^{-1} peak increasing with biodegradation, due to a delayed microbial attack of complexed amylose relative to amylopectin (*93*). Furthermore, the degree of complexation affects the water vapor permeability (WVTR) of thermoplastic starch and EVOH blends ranging from 820 to 334 g 30μm/m^2/24h (according to Lissy method) (*95*).

The droplet-like structure of destructurized starch having an amylose/ amylopectin ratio above 20/80 w/w in presence of EVOH copolymer, is responsible for the peculiar melt rheology of these compositions, ,characterized by strong pseudoplasticity at high shear stresses as well as by yield stress at lower shear stress and by an high levels of melt elasticity (*132*). Notwithstanding, the peculiar rheological behavior shown by these systems, traditional processing techniques such as film blowing can be easily applied.

This sort of droplet-like structure developed by Novamont is easily dispersible in rubbers and allows a decrease of hysteresis in the final rubber compositions that are useful for lowering the roll resistance in tire tread. The first industrial application in this field was made by Goodyear in 2001, when the tyre Biotread GT3 was launched in Europe (*133–135*).

The last Novamont's developments in this sector have been achieved inside the EU project Biotyre (LIFE06 ENV/L/000118) which have brought Goodyear to produce for BMW a new tyre with a "BioTRED" compound and a tyre structure optimized that achieves a reduction in rolling resistance of 34% (higher than original target of 30%) that corresponds to a 5%-6% decrease in fuel consumption. This tyre is used in the BMW 1-Series model and partner BMW foresees using BioTyres in other car models (e.g. for the 2012 BMW 3-Series).

Starch-Based Materials on the Market

Europe is the largest biodegradable polymers-consuming region, with about half of the global total. In 2009, despite the economic crisis, growth was in the range of 5% to 10%, depending on products and applications, compared with 2008. The following factors have contributed to and will continue to contribute to growth:

- Improvement of the properties and processing of biodegradable polymers
- Growing consumer interest in sustainable plastic solutions (e.g. eco-friendly packaging) and the reduction of greenhouse gas emissions

In Degradable Polymers and Materials: Principles and Practice (2nd Edition); Khemani, K., et al.;
ACS Symposium Series; American Chemical Society: Washington, DC, 2012.

- Increasing support at the local and state levels for these kind of products and for addressing needs about solid waste disposal
- Existence of large-scale composting facilities

The largest share in terms of volume corresponds to the starch-based plastic market. The main applications are compost bags, shopping bags, loose-fill packaging and mulch films.

Novamont, following the recent start-up of its seventh line dedicated to the production of Mater-Bi film grades in Terni, claims an internal production capacity of 120000 tons/year. Established in 1990, its expertise grew out of the Fertec research facility set up by Montedison, the chemical unit of Ferruzzi agro-industrial group in 1989, expanded through the acquisition of the bioplastics IP of Warner-Lambert in 1997 (Warner-Lambert suspended the manufacture of starch-based materials in 1993) (*136*) and the Eastar Bio patents of Eastman in 2004. Nowadays, the company holds a patent portfolio that includes more 90 patent families and 800 internationally registered patents.

German company Biotec has been jointly owned by Sphere and Stanelco of the UK since 2005, creating Biosphere. The Sphere Group compound starch, copolyesters and other materials into a variety of grades of bioplastic resin under the Bioplast trademark. Its factories, settled in France, the UK and Spain, manufacture biodegradable carrier bags, bin liners, catering objects and refuse bags. Its claimed production capacity is of 20000 tons/year.

Plantic Technologies Ltd is an Australian research company which offers products for thermoforming based on hydroxypropylated non-genetically modified high amylose corn starch. Its production capacity is of 7500 tons/year (*137*).

BIOP Biopolymer Technologies Ag entered the market with a starch-based material containing an additive consisting of a vinyl-alcohol/vinyl-acetate copolymer (*138*). The material is sold under the Biopar trademark.

Cardia Bioplastics Ltd (Australia) acquired in 2008 the resins business established in 2002 as Biograde Limited. Their Product Development Centre and manufacturing plant is in Nanjing, China. Cardia Bioplastics Ltd commercializes a biomaterial obtained mixing starch and biodegradable polyesters in the presence of a transesterification catalyst (*139*).

In the Netherlands, Rodenburg built up a plant for the transformation of potato wastes generated by the fried potatoes industry. The waste is fermented and it can be used to combine with natural fibres as well as being blended with other biopolymers. The resulting granulate was mainly used for the injection moulding of slow release devices. Notwithstanding the claimed capacity of 40000 tons/year the products sold under the Solanyl trademark did not get significant market share (*140*).

Conclusions

After more than 20 years of research and development starch-based materials have achieved specific in-use performances and can replace traditional plastics in

In Degradable Polymers and Materials: Principles and Practice (2nd Edition); Khemani, K., et al.;
ACS Symposium Series; American Chemical Society: Washington, DC, 2012.

different application sectors. They are able to offer original solutions both from the technical and the environmental point of view

Starch-based bioplastics constitute a class of materials able to significantly reduce the environmental impact in terms of energy consumption and greenhouse effect in specific applications. If they are engineered to be compostable through the action of living organisms, these sort of materials can also permit 'cradle-to-cradle' solutions through the entire agro-industrial non food chains.

They even offer a possible alternative to traditional materials when recycling is unpractical or uneconomical or when environmental impact has to be minimized.

Today, some of the bioplastics available in the market are used in specific applications where biodegradability is required such as the sector of composting (bags and sacks), fast food tableware (cutleries, cups, plates, straws, etc.), packaging (soluble foams for industrial packaging, film wrapping, laminated paper, food containers), agriculture (mulch film, nursery pots, plant labels), hygiene (nappies back sheet, cotton swabs), slow release of active molecules in the agricultural and pharmaceutical sectors.

The world market for biodegradable plastics started as a niche one, has grown significantly in the last few years, reaching a total capacity of 664000 tons/year production in 2010 where a significant amount is represented by products coming partially or totally from renewable resources. The global biodegradables' market in terms of volume is expected to grow to 2330 thousand metric tons in 2016 at an estimated compound average annual growth rate (CAGR) of 20.24% from 2011 to 2016 (*141*).

Without intention of a whole starch treaty, authors' desire was to disclose the large variety of starch forms and their use in polymers technology in order to give a wide basic knowledge of this topic, giving an instrument for further in-depth studies to the reader.

References

1. US Department of Agriculture (USDA). *Grains:World markets and trade*; Corn Refiners Association 2010 Annual Report.
2. US Department of Agriculture (USDA). *WASDE*; Corn Refiners Association 2010 Annual Report.
3. Otey, F. H.; Doane, W. M. In *Starch Chemistry and Technology*; Whistler, R. L., BeMiller, J. N., Paschall, E. F., Eds.; Academic Press: Orlando, FL, USA, 1984; p 154 and p 667.
4. Otey, F. H.; Doane, W. M. In *Starch Chemistry and Technology*; Whistler, R. L., BeMiller, J. N., Paschall, E. F., Eds.; Academic Press: Orlando, FL, USA, 1984; p 397.
5. Kavesh, S.; Schultz, J. M. Meaning and measurement of crystallinity in polymers: A review. *Polym. Eng. Sci.* **1969**, *5*, 331–338.
6. Zobel, H. F. Starch crystal transformations and their industrial importance. *Starch/Staerke* **1988**, *40*, 1–7.
7. Popov, D.; Buléon, A.; Burghammer, M.; Chanzy, H.; Montesanti, N.; Putaux, J.-L.; Potocki-Véronèse, G.; Riekel, C. Crystal structure of

A-amylose: A revisit from synchrotron microdiffraction analysis of single crystals. *Macromolecules* **2009**, *42*, 1167–1174.
8. Takahashi, Y.; Kumano, T.; Nishikawa, S. Crystal structure of B-amylose. *Macromolecules* **2004**, *37*, 6827–6832.
9. BeMiller, J.; Whistler, R. *Starch Chemistry and Technology*, 3rd ed.; Academic Press: USA, 2009.
10. Buléon, A.; Gerard, C.; Riekel, C.; Vuong, R.; Chanzy, H. Details of the crystalline ultrastructure of C-starch granules revealed by synchrotron microfocus mapping. *Macromolecules* **1998**, *31*, 6605–6610.
11. Donovan, J. W. Phase transitions of the starch–water system. *Biopolymers* **1979**, *18*, 263.
12. Griffin, G. J. L U.S. Patent 4,016,117, 1977.
13. Griffin, G. J. L. U.S. Patent 4,324,709, 1982.
14. Griffin, G. J. L. EP 363,383B1, 1995.
15. Griffin, G. J. L. WO 9201741A2, 1992.
16. Griffin, G. J. L. *Biodegradable Fillers in Thermoplastics*; Advances in Chemistry Series 134; American Chemical Society: Washington, DC, USA, 1974; p 159.
17. Maddever, W. J.; Chapamn G. M. In *Proceedings of Symposium on Degradable Plastics*; Washington, DC, USA, 1987; p 41.
18. Gilead D.; Scott, G. U.S. Patent 4,519,161, 1985.
19. Sipinen, A. J.; Jaeger, J. T.; Rutherford D. R.; Edblom, E. C. U.S. Patent 5,216,043, 1993.
20. Hocking, P. J. The classification, preparation, and utility of degradable polymers. *J. Macromol. Sci., Part C* **1992**, *32*, 35–54.
21. Andrady, A. L.; Pegram, J. E.; Nakatsuka, S. J. Studies on enhanced degradable plastics. 1. The geographic variability in outdoor lifetimes on enhanced photodegradable polyethelenes. *J. Environ. Polym. Degrad.* **1993**, *1*, 31–43.
22. Wilder, R. Degradability I: Disappearing package: pipe dream or savior? *Mod. Plast. Int.* **1989**, *19*, 74.
23. JP 146953, 1992.
24. Aime, J.-M.; Mention, G.; Thouzeau, A. U.S. Patent 4,873,270, 1989.
25. Gallagher, F. G.; Shin, H.; Tietz, R. F. U.S. Patent 5,219,646, 1993.
26. Wang, S.; Zhang, X. AU2002366251A1, 2002.
27. Donovan, J. W. Phase Transitions of the Starch-Water System. *Biopolymers* **1979**, *18*, 263–275.
28. Colonna, P.; Mercier, C. Pisum sativum and Vicia faba carbohydrates. Part 6. Gelatinization and melting of maize and pea starches with normal and high-amylose genotypes. *Phytochemistry* **1985**, *24*, 1667–1674.
29. Blanshard, J. M. V. *Starch, Properties and Potential*; John Wiley & Sons: 1987.
30. Morris, V. J. Starch gelation and retrogradation. *Trends Food Sci. Technol.* **1990**, 2–6.
31. Roulet, P.; MacInnes, W. M.; Gumy, D.; Wuersch, P. Retrogradation kinetics of eight starches. *Starch/Staerke* **1990**, *42*, 99–101.

32. Biliaderis, C. G.; Juliano, B. O. Thermal and mechanical properties of concentrated rice starch gels of varying composition. *Food Chem.* **1993**, *48*, 243–250.
33. Leloup, V. M.; Colonna, P.; Ring, S. G. Physico-chemical aspects of resistant starch. *J. Cereal Sci.* **1992**, *16*, 253–266.
34. Van Soest, J. J. G.; De Wit, D.; Tournois, H.; Vliegenthart, J. F. G. Retrogradaton of potato starch as studied by Fourier transform infrared spectroscopy. *Starch/Staerke* **1994**, *46*, 453–457.
35. Liu, H.; Yu, L.; Tong, Z.; Chen, L. Retrogradation of cornstarch studied by DSC. *Starch/Staerke* **2010**, *62*, 524–529.
36. Liu, H.; Yu, L.; Chen, L.; Li, L. Retrogradation of waxy corn starch after thermal treatment at different temperatures. *Carbohydr. Polym.* **2007**, *69*, 756–762.
37. Klem, R. E.; Brogly, D. A. Methods for selecting the optimum starch binder preparation system. *Pulp Paper* **1981**, *55*, 98–103.
38. Bastioli, C. *Handbook of Biodegradable Polymers*; Rapra Technology Ltd.: UK, 2005.
39. Conway, H. F. Extrusion cooking of cereals and soybeans. *Food Prod. Dev.* **1971**, *5* (3), 14–17.
40. Mercier, C.; Feillet, P. Modification of carbohydrate components by extrusion-cooking of cereal products. *Cereal Chem.* **1975**, *52* (3), 283–297.
41. Chiang, B. Y.; Johnson, A. J. Gelatinization of starch in extruded products. *Cereal Chem.* **1997**, *54*, 436–443.
42. Huber, D.; Escher, F. Structural changes of starch and starch-like products during extrusion cooking. *Mitt. Geb. Lebensmittelunters. Hyg.* **1986**, *77*, 73–84.
43. Bhattacharya, M.; Hanna, M. A. Kinetics of starch gelatinization during extrusion cooking. *J. Food Sci.* **1987**, *52*, 764–766.
44. Chinnaswamy, R.; Hanna, M. A.; Zobel, H. F. Microstructural, physiochemical, and macromolecular changes in extrusion-cooked and retrograded corn starch. *Cereal Foods World* **1989**, *34*, 417–422.
45. Lai, L. S.; Kokini, J. L. Physicochemical changes and rheological properties of starch during extrusion (A Review). *Biotechnol. Prog.* **1991**, *7*, 251–266.
46. Orford, P. D.; Parker, R.; Ring, S. G. The functional properties of extrusion-cooked waxy-maize starch. *J. Cereal Sci.* **1993**, *18*, 277–286.
47. Sacchetto, J.-P.; Stepto, R. F. T.; Zeller, H. U.S. Patent 4,900,361, 1990.
48. Stepto, R. F. T.; Dobler, B. EP 0,326,517B1, 1994.
49. Sacchetto, J.-P.; Lentz, D. J.; Silbiger, J. EP 0,404,723B1, 1994.
50. Silbiger, J.; Lentz, D. J.; Sacchetto, J.-P. EP 0,408,503B1, 1994.
51. Sacchetto, J.-P.; Silbiger, J.; Lentz, D. J. EP 0,409,781B1, 1994.
52. Lentz, D. J.; Sacchetto, J.-P.; Silbiger, J. EP 0,409,782B1, 1994.
53. Sacchetto, J.-P.; Silbiger, J.; Lentz, D. J. EP 0,409,783B1, 1994.
54. Lentz, D. J.; Sacchetto, J.-P.; Silbiger, J. EP 0,409,788B1, 1994.
55. Egli, M.; Cole, E. T. EP 0,500,885B1, 1997.
56. Lay, G.; Rehm, J.; Stepto, R. F. T.; Thoma, M. EP 0,327,505B1, 1997.
57. Wittwer, F.; Tomka, I. EP 0,118,240A2, 1984.
58. Silbiger, J.; Sacchetto, J.-P.; Lentz, D. J. EP 0,404,728A3, 1990.

59. Sacchetto, J.-P.; Rehm, J. EP 0,407,350A3, 1991.
60. Silbiger, J.; Sacchetto, J.-P.; Lentz, D. J. EP 0,408,501A3, 1991.
61. Sacchetto, J.-P.; Silbiger, J.; Lentz, D. J. EP 0,408,502A3, 1991.
62. Sacchetto, J.-P.; Egil, M.; Stepto, R. F. T.; Zeller, H. EP 0,391,853A3, 1992.
63. Loomis, G. L.; Izbicki, M. J.; Flammino, A. EP 0,679,172A3, 1995.
64. Fischer, H. R.; Fischer, S. EP 1,134,258A1, 2001.
65. Bastioli, C.; Bellotti, V.; Del Tredici, G.; Guanella, I.; Lombi, R. EP 0,965,615B1, 2002.
66. Bastioli, C.; Lombi, R.; Nicolini, M.; Tosin, M.; Degli Innocenti, F. EP 1,109,858B1, 2003.
67. Le Bail, P.; Rondeau, C.; Buléon, A. Structural investigation of amylose complexes with small ligands: helical conformation, crystalline structure and thermostability. *Int. J. Biol. Macromol.* **2005**, *35*, 1–7.
68. Wigman, H. B.; Leathen, W. W.; Brackenbeyer, M. J. Phase contrast microscopy in the examination of starch granules. *Food Technology* **1956**, *10*, 179–184.
69. Tomka, I. EP 0,397,819B1, 1995.
70. Tomka, I. EP 0,539,544B1, 1994.
71. Tomka, I.; Meissner, J.; Menard, R. EP 0,537,657B1, 1997.
72. Tomka, I. EP 0,542,155B1, 1998.
73. Tomka, I. US 6,242102, 2001.
74. Tomka, I. EP 0,596,437B1, 1997.
75. Mellies, R. L.; Wolff, I. A. U.S. Patent 2,788,546, 1957.
76. Willett, J. L.; Jasberg, B. K.; Swanson, C. L. Rheology of thermoplastic starch: effects of temperature, moisture content, and additives on melt viscosity. *Polym. Eng. Sci.* **1995**, *35*, 202–210.
77. Van den Berg, C. *Vapour Sorption Equilibria and other Water-Starch Interactions; a Physico-Chemical Approach*. PhD thesis. Agricultural University Wageningen, The Netherlands, 1981, p 49.
78. Otey, F. H.; Westhoff, R. P. U.S. Patent 4,133,784, 1979.
79. Otey, F. H.; Westhoff, R. P. U.S. Patent 4,337,181, 1982.
80. Otey, F. H.; Westhoff, R. P. U.S. Patent 4,454,268, 1984.
81. Otey, F. H.; Westhoff, R. P. EP 0,132,299B1, 1989.
82. Fanta, G. F.; Otey, F. H. U.S. Patent 4,839,450, 1989.
83. Otey, F. H.; Westhoff, R. P.; Doane, W. M. Starch-based blown films. 2. *Ind. Eng. Chem. Res.* **1987**, *26*, 1659–1663.
84. Otey, F. H.; Westhoff, R. P.; Doane, W. M. Starch-based blown films. *Ind. Eng. Chem. Prod. Res. Dev.* **1980**, *19*, 592–595.
85. Fanta, G. F.; Swanson, C. L.; Doane, W. M. Complexing between starch and poly (ethylene-co-acrylic acid) a comparison of starch varieties and complexing conditions. *Carbohydr. Polym.* **1992**, *17*, 51–58.
86. Fanta, G. F.; Swanson, C. L.; Shogren, R. L. Starch–poly(ethylene-co-acrylic acid) composite films. Effect of processing conditions on morphology and properties. *J. Appl. Polym. Sci.* **1992**, *44*, 2037–2042.
87. Bastioli, C.; Bellotti, V.; Del Giudice, L.; Del Tredici, G. F.; Lombi, R.; Rallis, A. U.S. Patent 5,262,458, 1993.

88. Swanson, C. L.; Shogren, R. L.; Fanta, G. F.; Imam, S. H. Starch-plastic materials: Preparation, physical properties, and biodegradability (a review of recent USDA research). *J. Environ. Polym. Degrad.* **1993**, *1*, 155–166.
89. Shogren, R. L. Effect of moisture content on the melting and subsequent physical aging of cornstarch. *Carbohydr. Polym.* **1992**, *19*, 83–90.
90. Bastioli, C.; Bellotti, V.; Del Giudice, L.; Lombi, R. EP 0,400,532B1, 1994.
91. Bastioli, C.; Bellotti, V.; Del Giudice, L.; Gilli, G. Mater-Bi: properties and biodegradability. *J. Environ. Polym. Degrad.* **1993**, *1*, 181–191.
92. Bastioli, C.; Bellotti, V.; Del Giudice, L.; Gilli, G. *Biodegradable Polymers and Plastics*; Vert, M.; Feijem, J.; Albertsson, A.; Scott, G.; Chiellini E., Eds.; The Royal Society of Chemistry: Cambridge, UK; 1992.
93. Bastioli, C.; Bellotti, V.; Camia, M.; Del Giudice, L.; Rallis, A. *Biodegradable Plastics and Polymers*; Doi, Y., Fukuda, K., Eds.; Elsevier: Amsterdam, The Netherlands; 1994.
94. Halley, P.; McGlashan, S.; Gralton, J. WO 02083784, 2002.
95. Bastioli, C.; Bellotti, V.; Del Tredici, G. F.; Montino, A.; Ponti, R. IT T092 A000199, 1992.
96. Bastioli, C.; Bellotti, V.; Rallis, A. Microstructure and melt flow behavior of a starch-based polymer. *Rheol. Acta* **1994**, *33*, 307–316.
97. Bastioli, C.; Bellotti, V.; Del Giudice, L.; Lombi, R. EP 0,437,561B1, 1994.
98. Bastioli, C.; Bellotti, V.; Del Tredici, G. F. EP 0,437,589B1, 1996.
99. Bastioli, C.; Bellotti, V.; Montino, A.; Del Tredici, G. F.; Lombi, R. EP 0,494,287B1, 1995.
100. Bastioli, C.; Bellotti, V.; Montino, A. WO 9214782, 1992.
101. Yoshida, Y.; Uemura, T. *Biodegradable Plastics and Polymers*; Doi, Y.; Fukuda, K., Eds.; Elsevier: Amsterdam, The Netherlands; 1994.
102. Maxwell, C. S. *Tappi J.* **1970**, *53*, 1464.
103. Lacourse, N. L.; Altieri, R. A. U.S. Patent 4,863,655, 1989.
104. Lacourse, N. L.; Altieri, R. A. EP 0,375,831, 1990.
105. Lacourse, N. L.; Altieri, R. A. EP 0,376,201A1, 1990.
106. Lacourse, N. L.; Altieri, R. A. U.S. Patent 5,035,930, 1991.
107. Lacourse, N. L.; Altieri, R. A. U.S. Patent 5,043,196, 1991.
108. Neumann, P. E.; Seib, P. A. U.S. Patent 5,185,382, 1993.
109. Anfinsen, J. R.; Garrison, R. R. WO 9208759, 1992.
110. Bastioli, C.; Bellotti, V.; Del Tredici, G. F.; Rallis, A. EP 0,667,369A1, 1995.
111. Bastioli, C.; Bellotti, V.; Del Tredici, G. F.; Montino, A.; Ponti, R. EP 0,696,611A3, 1996.
112. Bastioli, C.; Bellotti, V.; Del Tredici, G.; Rallis, A. EP 0,696,612A2, 1996.
113. Bastioli, C.; Bellotti, V.; Del Tredici, G. F.; Lombi, R.; Montino, A.; Ponti, R. WO 9219680, 1992.
114. Bastioli, C.; Floridi, G.; Del Tredici, G. WO 2008037749A2, 2008.
115. Bastioli, C.; Floridi, G.; Del Tredici, G. WO 2008037744A2, 2008.
116. Tomka, I. EP 0,539,544B1, 1994.
117. Buehler, F. S.; Baron, V.; Schmid, E.; Meier, P.; Schultze, H. J. EP 0,541,050A3, 1993.
118. Schmid, E.; Buehler, F. S.; Schultze, H. J. EP 0,522,358A3, 1993.
119. Bastioli, C.; Bellotti, V.; Del Tredici, G. EP 0,437,589A1, 1991.

120. Tomka, I. EP 0,542,155, 1994.
121. Schröter, J. EP 0,551,125A1, 1993.
122. Cael, J. J.; Koenig, J. L.; Blackwell, J. Infrared and raman spectroscopy of carbohydrates. Part VI: Normal coordinate analysis of V-amylose. *Biopolymers* **1975**, *14*, 1885–1903.
123. Shogren, R. L.; Thompson, A. R.; Greene, R. V.; Gordon, S. H.; Cote, G. Complexes of starch polysaccarides and poly(ethylene co-acrylic acid): Structural characterization in the solid state. *J. Appl. Polym. Sci.* **1991**, *47*, 2279–2286.
124. Fanta, G. F.; Shogren, R. L.; Salch, J. H. Steam jet-cooking of high-amylose starch-fatty acid mixtures, an investigation of complex formation. *Carbohydr. Polym.* **1999**, *38*, 1–6.
125. Veregin, R. P.; Fyfe, C. A.; Marchessault, R. H. Investigation of the crystalline "V" amylose complexes by high-resolution 13C CP/MAS NMR Spectroscopy. *Macromolecules* **1987**, *20*, 3007–3012.
126. Gidley, M. J.; Bociek, S. M. 13C CP/MAS NMR Studies of amylose inclusion complexes, cyclodextrins, and the amorphous phase of starch granules: Relationships between glycosidic linkage conformation and solid-state 13C chemical shifts. *J. Am. Chem. Soc.* **1988**, *110*, 3820–3829.
127. Bias, B.; Le Bail, P.; Robert, P.; Pontoire, B.; Buleon, A. Structural and stoichiometric studies of complexes between aroma compound and amylose. Polymorphic transitions and quantification in amorphous and crystalline areas. *Carbohydr. Polym.* **2006**, *66*, 306–315.
128. Shogren, R. L.; Fanta, G. F.; Felker, F. C. X-Ray Diffraction study of crystal transformations in spherulitic amylose/lipid complexes from jet-cooked starch. *Carbohydr. Polym.* **2006**, *64*, 444–451.
129. van Soest, J. J. G.; Hulleman, S. H. D.; de Wit, D.; Vliegenthart, J. F. G. Changes in the mechanical properties of thermoplastic potato starch in relation with changes in B-type crystallinity. *Carbohydr. Polym.* **1999**, *29*, 225–232.
130. van Soest, J. J. G.; Knooren, N. Influence of glycerol and water content on the structure and properties of extruded starch plastic sheets during aging. *J. Appl. Polym. Sci.* **1997**, *64*, 1411–1422.
131. van Soest, J. J. G.; Hulleman, S. H. D.; de Wit, D.; Vliegenthart, J. F. G. Crystallinity in starch bioplastics. *Ind. Crops Prod.* **1996**, *5*, 11–22.
132. Herschel, W. H.; Bulkley, R. *Proc. ASTM* **1926**, *26*, 621.
133. Corvasce, F. G.; Linster, T. D. U.S. Patent 5,545,680, 1996.
134. Corvasce, F. G.; Linster, T. D. U.S. Patent 5,374,671, 1994.
135. Bastioli, C.; Bellotti, V.; Montino, A. EP 1,127,089B1, 2001.
136. Tollefson, C. *Chem. Mark. Rep.* **1993**, *224*, 9.
137. Yu, L.; Christie, G. B. Y.; Coombs, S. WO 0036006, 2000.
138. Berger, W.; Jeromin, L.; Mierau, U.; Opitz, G. WO 9925756, 1999.
139. Changping, C. WO 2007012142, 2007.
140. Jongboom, R. O. J.; Stuut, P. I.; Rodenburg, J. A. U.S. Patent 6,482,341B1, 2002.
141. *Biodegradable Plastics markets: by type, applications, regulations, prices, trends & forecast (2011-2016)*; Research and Markets, USA, 2011.

In Degradable Polymers and Materials: Principles and Practice (2nd Edition); Khemani, K., et al.;
ACS Symposium Series; American Chemical Society: Washington, DC, 2012.

Chapter 8

Bioplastics from Waste Materials and Low-Value Byproducts

Helan Xu[a] and Yiqi Yang[a,b,c,*]

[a]Department of Textiles, Merchandising and Fashion Design, University of Nebraska-Lincoln, Lincoln, NE 68583-0802, United States
[b]Department of Biological Systems Engineering, University of Nebraska-Lincoln, Lincoln, NE 68583-0802, United States
[c]Department of Nebraska Center for Materials and Nanoscience, 234, HECO Building, University of Nebraska-Lincoln, Lincoln, NE 68583-0802, United States
[*]E-mail: yyang2@unl.edu

Various bioplastics produced from waste materials and byproducts from agricultural, agro-food and biofuel industries are introduced in this chapter. As renewable and low carbon-emission substitutes for conventional petroleum-based plastics, bioplastics suffer from high cost since current feedstocks are relatively expensive agricultural raw materials. Using inexpensive wastes and byproducts as feedstocks would be a promising alternative to reduce the cost of production of bioplastics. Two types of bioplastics, thermoplastics from natural macromolecules via chemical modifications or graft polymerizations and bioplastics produced by fermentation of lignocellulose, molasses, whey, oils and other wastes and low-value byproducts from agricultural, agro-food and biofuel industries, are discussed in details. The advantages and drawbacks of using low-value waste materials and byproducts for bioplastics will be summarized based on cost efficiency of production and performance properties of final thermoplastics.

In Degradable Polymers and Materials: Principles and Practice (2nd Edition); Khemani, K., et al.;
ACS Symposium Series; American Chemical Society: Washington, DC, 2012.

Introduction

The indispensable plastic materials in various forms have contributed greatly to quality and comfort for everyday life. By 2010, over 300 million tons of plastic materials have been utilized worldwide (*1*). Rapid growth in plastic consumption during last few decades will continue in the future. Polyethylene (PE), polypropylene (PP), polystyrene (PS) and polyvinyl chloride (PVC) represent the big four commodity plastics, which are all derived from petroleum resources. As demand of plastic products increases, the rate of discovery of fossil oil reserves declines continuously since it has been acknowledged that 95% of all recoverable oil has now been found. The discrepancy between oil consumption and oil discovered will undoubtedly lead to future oil crisis. In addition, plastic products derived from petroleum presents a major disposal problem due to its non-biodegradability. Once the plastic materials have been discarded, they persist in the environment and cannot be degraded by ecosystem, thus give rise to a multitude of environmental and ecological issues. The common approaches to dispose plastics are all problematic. The landfill method leads to extremely slow rates in degradation and decomposition of plastics as well as discharge of toxic agents into the soil (*2*). The incineration method, which generates toxic degradation products, is energy-consuming and costly (*3*). The recycling method suffers from difficulties in categorizing different plastics and therefore is restricted in certain types of plastic products, such as food packaging materials and water bottles (*4*, *5*). High carbon emission during production, usage and disposal of petroleum-based polymers leads to global warming and climate change issues (*6*).

To reduce economical and ecological impacts induced by manufacture, utilization and disposal of conventional petrochemical plastics, it is a prospective alternative to use bioplastics as substitutes. Bioplastics or bio-based plastics are defined as man-made or man-processed organic macromolecules derived from renewable biological resources, such as cellulose, starch, protein, vegetable oil and microbes, and used for conventional plastic applications (*7*, *8*). Though generated from biodegradable resources, bioplastics could be either biodegradable or non-biodegradable depending on different fabrication methods and application purposes (*8*). Albertsson and Karlsson defined biodegradation as an event which occurs through the action of enzymes and/or chemical decomposition associated with living organisms (bacteria, fungi, etc.) and their secretion products (*9*). In this review, only biodegradable bioplastics will be discussed. Utilization of biodegradable plastics could significantly reduce economical and environmental issues associated with non-degradability of conventional plastic products.

Common agricultural feedstocks, which are rich in ingredients such as starch, protein and cellulose, have been made into bioplastics through chemical and biological technologies for various applications. Starch is a biodegradable, renewable and low cost carbohydrate, which could be extracted from various types of plants and is widely used in food, paper-making and many other industries. By addition of plasticizers, such as glycerol and sorbitol, starch can be thermo-processed. Thermoplastic starch, constitutes almost half of the bioplastics markets, is the most widely used bioplastics currently (*10*, *11*). Thermoplastic starch originated from agricultural crops such as potato and corn is mainly utilized

In Degradable Polymers and Materials: Principles and Practice (2nd Edition); Khemani, K., et al.;
ACS Symposium Series; American Chemical Society: Washington, DC, 2012.

for applications such as packaging materials, utensils and cutlery. The major drawback of using starch as bio-thermoplastics is the potential adverse impact on food prices owing to increasing demand for starch. Starch is the most common resource of carbohydrate in human diet and is contained in many staple foods globally, and therefore it is of importance to maintain current low price and sufficient supply of starch as a food resource. As the world population grows continuously, increasing consumption of dietary starch as well as thermoplastic starch could lead to soaring prices of starch-rich agricultural products and possible shortage in starch for food industry. In addition, the production cost of bioplastics comparing that of petrochemical synthetic polymers is also much higher because the feedstocks which are agricultural commodities are relatively expensive.

Identification of inexpensive carbon sources has become an important research aim in order to produce low-cost bioplastics. Currently, thermoplastics from agricultural commodities have much higher selling prices than any petroleum-based plastics. However, the possibility to lower the selling price by reducing the prices of raw materials is relatively low. In addition, to avoid potential impact on global food safety and to reduce carbon emission in growing crops, much attention has been switched from using agricultural commodities to waste materials and byproducts from agricultural, agro-food and biofuel industries to produce bioplastics.

Waste materials and byproducts are generated in large quantity from agricultural, agro-food and biofuel industries, and usually contain proteins, carbohydrates (hemicellulose, lignocellulose or polysaccharides) and oils. These ingredients could be transformed into thermoplastics after chemical treatments or be fermented to small molecules that can be used for polymer synthesis. For example, more than 10 million tons of Distillers Dried Grains (DDG) are produced from corn ethanol industry in the USA and the selling price is approximately $150 per ton (*12*). DDG contains oil (8-10%), proteins (25-30%) and carbohydrates (35-50%) (*13*). About 54 million tons of sugarcane bagasse is generated annually worldwide from sugar industry and bioethanol industry (*14*). Sugarcane bagasse contains 50% cellulose, 25% hemicellulose and 25% lignin (*15*). Ethanol from corn starch and sugarcane sugar is currently predominant and economically favorable at the industrial level in biofuel fields. As a result, the production of byproducts and waste stream, such as DDG and sugarcane bagasse, from bioethanol will increase accordingly, though only a small portion of them could be sold at low price as animal feedstocks. Dairy industry is a major contributor to generate waste water in food industry regarding both amount and characteristics. About 2.5 gallon wastewater is generated per gallon of processed milk (*16*). With approximate 700 million tons of milk produced worldwide, more than 1750 million tons of wastewater has been generated. The major compositions in dairy waste water stream are proteins (whey and casein), carbohydrates (lactose), lipids, detergents and sanitizers (*17*).

To avoid adverse environmental impacts that could be aroused by direct discharge or discard of the waste materials, certain treatments with extra cost are often required for these waste materials. Most wastewater effluent from agro-food industries, such as whey containing wastewater from dairy plants, suffers from the problem of high chemical oxygen demand (COD) and biochemical oxygen

In Degradable Polymers and Materials: Principles and Practice (2nd Edition); Khemani, K., et al.;
ACS Symposium Series; American Chemical Society: Washington, DC, 2012.

demand (BOD) values, which will degrade surface water and ground water and should be treated chemically or biologically (*18*). Solid wastes, such as feather from the poultry industry and DDG from bioethanol industry, are usually disposed in landfill or incineration (*19*). The former method occupies land and could potentially transmit diseases, and the latter one generates waste gas, heat and ash, which are sources of air pollution. Therefore, to effectively utilize waste materials could partially solve related environmental issues as well as reduce cost for waste treatments.

Due to limited industrial applications, economical utilization of waste materials and byproducts from agricultural, agro-food and biofuel industries will not lead to competition with the raw materials of major industries. In addition, turning these waste materials into profitable industrial products, such as bioplastics, will reduce cost for pollution-free treatments, save resources, energy and land, and increase value-added to the related industries.

In this review, bioplastics from naturally occurring macromolecules from agricultural, agro-food and biofuel industries wastes and byproducts through chemical modifications and grafting will be summarized. The second category of bioplastics to be discussed is polylactic acid (PLA) based on lactic acid fermented from waste materials. The third type of bioplastics is polyhydroxyalkanoates (PHAs) fermented from waste materials.

Bioplastics from Naturally Occurring Macromolecules in Waste Materials

Waste materials from agricultural, agro-food and biofuel industries generally exist as mixtures of various types of macromolecules, such as carbohydrates (cellulose, hemicellulose, lignin), proteins and oil. Use the waste materials in their natural forms, namely directly use these macromolecules for bioplastics applications afford multiple advantages. First, complicated and costly procedures to separate and purify different macromolecules will not be necessary. Secondly, elimination of discomposition of macromolecules into small molecules and subsequent re-assembly of the small molecules into certain macromolecules can significantly reduce energy consumption and is considered as with high energy efficiency and high energy returned on energy invested (EROEI). In addition, the intrinsic properties of naturally occurring macromolecules could also be beneficial for bioplastics. For example, the cellulose in bamboo fibers could offer cyanoethylated cellulosic plastics with good mechanical properties.

However, there have not been many studies done on fabrication of bioplastics from naturally occurring macromolecules so far, due to existence of many obstacles to be overcome. First, since transformation of hydrophilic macromolecules in waste materials from agricultural, biofuel and food-processing industries into thermoplastics requires significant enhancement in hydrophobicity and decrease in hydrophilicity, a high degree of modification or grafting is necessary. However, most macromolecules are basically hydrophilic due to the existence of various hydrophilic functional groups, for example, hydroxyl group (-OH), carboxylic group (-COOH) amine group ($-NH_3$) and amide group

In Degradable Polymers and Materials: Principles and Practice (2nd Edition); Khemani, K., et al.;
ACS Symposium Series; American Chemical Society: Washington, DC, 2012.

(-CONH-). To obtain bioplastics with good thermoplasticity from natural polymers, high degree of substitution should be achieved through chemical modifications. In addition, since many waste materials are mixtures of proteins, cellulose and hemicellulose, conventional reaction conditions for modifications of individual type of substrate are not suitable. Compromise reaction conditions may be used to obtain acceptable thermoplasticity of the mixture as well as to preserve the properties of each type of components in the mixture. For example, to acetylate DDG which contains proteins and cellulose, the optimal alkaline condition for acetylation of cellulose should not be used since proteins could be hydrolyzed. Instead, an acidic condition is employed to obtain higher degree of acetylation and better thermoplasticity (*20*).

Chemical Modifications

Multiple chemical modifications and grafting methods have been used to endow waste materials and byproducts with thermoplasticity.

Acetylation

Acetylation, esterification using acetyl anhydride, is one of the most common modification methods to develop thermoplastics from biopolymers (*21*). As compared to many other chemical modifications, acetylation is a relatively inexpensive process that is simple, uses green chemicals, produces products with good performing properties and good biodegradability and is generally environmental friendly. Cellulose and starch acetates are the two most widely used biopolymers to develop fibers, films composites and many other products (*22–24*). Proteins are also used to develop thermoplastics (*25*, *26*). Efficiency of acetylation (% acetylation) and properties of the product depend largely on the conditions of acetylation, such as concentration of chemicals, pH and temperature. For different substrates, different pHs are used to obtain high degree of modification and reduce damage to the substrates. For example, acidic condition is used for cellulose acetylation, alkaline condition is used for starch and mild alkaline condition is used for proteins.

Different types of waste materials and byproducts have been acetylated to fabricate thermoplastics. Acetylation of DDGS under acidic conditions showed considerably higher % acetyl content, intrinsic viscosity and thermoplasticity than that under alkaline conditions at even lower ratios of acetic anhydride and catalyst concentrations (*20*). Feather acetylated under acidic conditions and optimized reaction conditions could obtain 7.2% acetyl content, which was sufficient to endow transparency to the compression molded acetylated feather (*27*). However, for later industrial applications, mechanical properties of the acetylated products should be studied in details.

There are also some problems associated with acetylation of macromolecules from waste materials and byproducts. First, the reaction conditions may be too harsh for some susceptible substrates, such as proteins, in the raw materials. In addition, acetylation may lead to low flexibility of final products, since small

In Degradable Polymers and Materials: Principles and Practice (2nd Edition); Khemani, K., et al.;
ACS Symposium Series; American Chemical Society: Washington, DC, 2012.

acetyl groups attached onto the substrate molecules could not contribute much to decrease intermolecular friction. Many waste materials and byproducts from agricultural, agro-food and biofuel industries are mixtures of bio-macromolecules with diverse properties, and therefore the reaction conditions of modifications should be optimized to obtain end products with satisfactory thermoplasticity and performing properties.

Esterification using succinic anhydride and many other chemicals has also been reported. Bagasse has been converted into a thermomoldable material through esterification using succinic anhydride (*28*). The mechanical properties were reported to increase with increasing of the monoester contents. Corn DDG, corncob and hardwood sawdust have been acylated using glutaric anhydride, maleic anhydride, phthalic anhydride and succinic anhydride (*28–31*). However, thermoplastic properties and mechanical properties of these modified materials were not sufficiently evaluated. Table I shows the bio-thermoplastics through esterification on various biomass substrates.

Table I. Bioplastics from macromolecules from biomass via esterification

Substrate	*Monomer*	*pH*	*Ref*
DDG	Acetic anhydride	Acidic Alkaline	(*20*)
Feather	Acetic anhydride	Acidic	(*27*)
Bagasse	Succinic anhydride	NA[a]	(*28*, *32*)
Corn distillers dried grains	Glutaric anhydride, Maleic anhydride, Phthalic anhydride, Succinic anhydride	Alkaline	(*31*)
Corncob	Glutaric anhydride, Maleic anhydride, Phthalic anhydride, Succinic anhydride	Alkaline	(*29*)
Sawdust	Glutaric anhydride, Maleic anhydride, Phthalic anhydride, Succinic anhydride	Alkaline	(*30*)

[a] NA: Not available

Cyanoethylation

Cyanoethylation is a widely adapted etherification using acrylonitrile due to its simplicity, low cost, and acrylonitrile could provide modified products with desired properties, such as flexibility. The ether linkage with three carbons and the bulky side groups -C≡N could reduce entanglement of macromolecular chains and allow them to slide easily under strain. Even low percentage of reaction or percent

In Degradable Polymers and Materials: Principles and Practice (2nd Edition); Khemani, K., et al.;
ACS Symposium Series; American Chemical Society: Washington, DC, 2012.

weight gain could enable cyanoethylated products to have good thermoplasticity. In addition, etherification uses relatively mild reaction conditions (lower temperatures and neutral pH) comparing to acetylation, and therefore leads to less damage to susceptible polymers, such as proteins. Feather and DDG have been cyanoethylated by Reddy and by Hu (*33*, *34*). The cyanoethylated bioplastics have obvious melting points, and both were compression molded into films with considerable transparency and flexibility. Wood meal has been cyanoethylated to obtain thermoplasticity (*35*). Cellulose from bamboo and sugarcane bagasse was cyanoethylated and was used to develop thermoplastic films (*36–38*). However, the strength under high degree of cyanoethylation was not very satisfactory, since the adjacent molecules could slide from each other so easily that they cannot share load efficiently. To produce final products with reasonable elongation and tensile properties, the degree of cyanoethylation should be well controlled.

Graft Polymerization

Graft polymerization is an efficient and versatile chemical modification to impart a variety of functional groups onto molecular chains of a polymer. Graft polymerization is also an attractive method to make thermoplastics from natural polymers, and the products all showed better thermoplasticity than the unmodified ones (*39–41*).

To reduce the cost of bioplastics from waste materials and byproducts from agricultural, agro-food and biofuel industries via graft polymerization, reaction conditions should be well adjusted to obtain high grafting percentage (% grafting), high conversion of monomer to polymers (% monomer conversion) and high grafting efficiency (% grafting efficiency). Grafting percentage (% grafting) is the weight ratio of grafted branches to the substrate. Conversion of monomer to polymers (% monomer conversion) indicates the amount of monomer converted into polymers, which include homopolymers and branches grafted onto the substrates. Grafting efficiency represents the weight ratio of the sum of grafted branches and ungrafted homopolymers. In many papers, only % grafting and improved thermoplasticity were demonstrated. However, considering future industrial scale production of bioplastics, more attention should be paid on the efficiency and cost of the processes.

Owing to the high efficiency of generation of free radicals under mild conditions, using a redox system becomes the most common method to initiate graft copolymerization. In addition, temperature does not change drastically during graft polymerization in the redox system. Thus, polymerization process can be easily controlled. Free radicals are produced from the initiators and transferred to the substrate to react with monomer to form graft co-polymers. Inexpensive and nontoxic persulfates are commonly used as oxidant, which exhibits high initiation efficiency and reproducibility. Sodium bisulfite and ferrous ammonium sulfate are generally reductant for the redox system of persulfate, which can substantially decrease activation energy of decomposition of persulfate.

Grafting polymerization process is influenced by physical structures and chemical compositions of substrates. Graft polymerization involves formation

In Degradable Polymers and Materials: Principles and Practice (2nd Edition); Khemani, K., et al.;
ACS Symposium Series; American Chemical Society: Washington, DC, 2012.

of covalent bonds between a monomer and pre-formed polymeric backbones. To achieve high degree of grafting, functional groups on the backbones should be physically accessible. Cellulose is resistant to the grafting in aqueous environment due to its insolubility. Decrease in crystallinity and regular structures in backbones could facilitate graft polymerization. Chemical composition also plays an important role on grafting. The presence of lignin (phenolic -OH) in biomass could adversely affect grafting effect since lignin is a good radical scavenger (*42*). For proteins with cystine residues, the mercapto groups on cystine which were preferred as grafting sites could facilitate grafting polymerization (*43*). Quantities and positions of functional groups, such as -OH, -SH, -COOH and $-NH_3$ in the backbones will have significant influence on the grafting results.

So far, only a few waste materials and byproducts from agricultural, agro-food and biofuel industries have been grafted to make thermoplastics. Bioplastics via graft polymerization from feather have been done by Jin et al. (*44*). In this work, instead of using extracted keratin, feathers in their native forms have been used for grafting. It could not only reduce the cost, but also retain the special structures of feather for further applications. Konjac glucomannan is a water soluble polysaccharide that is considered as a dietary fiber. Vinyl acetate and methyl acrylate have been grafted onto Konjac glucomannan to obtain bioplastics with acceptable thermoplasticity and thermal processing properties (*45*). Graft polymerization of acrylonitrile onto cellulose from bamboo has been conducted in non-aqueous medium (toluene), and the % grafting for optimized samples was 210% and grafting efficiency was 97%. Soyprotein isolate has also been methyl acrylated into thermoplastics (*46*). Table II summarized fabrication of bioplastics from waste materials via graft polymerizations.

Table II. Bioplastics from waste materials via graft polymerizations

Substrate	*Monomer*	*pH*	*Ref*
Feather	Methyl acrylate	Acidic	(*44*)
Feather keratin	Methyl methacrylate	Acidic	(*47*)
Konjac glucomannan	Vinyl acetate, Methyl acrylate	NA[a]	(*45*)
Soyprotein isolate	Methyl acrylate	NA	(*46*)
Cellulose from bamboo	Acrylonitrile	NA	(*48*)

[a] Not available

Shortcomings of Using Natural Macromolecules

There are several major obstacles that need to be overcome before large amounts of bioplastics with satisfiactory qualities and economical efficiency could be produced from natural macromolecules in waste materials and byproducts from agricultural, agro-food and biofuel industries. So far, the thermoplasticity of bioplastics from natural macromolecules is still not sufficient. Performing properties of these bioplastics, such as mechanical properties and cost assessment

In Degradable Polymers and Materials: Principles and Practice (2nd Edition); Khemani, K., et al.;
ACS Symposium Series; American Chemical Society: Washington, DC, 2012.

of production, are critical to determine feasibility of large-scale production, and therefore should be carefully considered in the future work. The compactness of naturally molecular structures hindered thorough reaction of monomers and substrates, and thus swelling agents may be used to create more accessible reaction sites on the macromolecules. The inconsistent quality and complicated compositions of waste materials and byproducts could lead to variation in qualities of bioplastics.

Bioplastics from Waste Materials via Fermentation

Currently, polylactic acid (PLA) and polyhydroxyalkanoate (PHA) are two mostly studied degradable aliphatic polyesters. Both PLA and PHA have mechanical properties that are comparable to commercial plastics, such as polyethylene (PE), polypropylene (PP) and polystyrene (PS). PLA and PHA can be produced from renewable bio-based sources such as starch and sugars and are completely compostable in industrial composting facilities. However, these fully biodegradable plastics are more expensive than petrochemical based plastics. One of the major reasons is high cost of raw materials. Using waste materials and byproducts from agricultural, agro-food and biofuel industries to replace currently used feedstock could effectively reduce the cost of production of bioplastics.

Polylactic Acid (PLA)

Polylactic acid (PLA) is a thermoplastic polyester synthesized from lactic acid (2-hydroxypropionic acid, $CH_3CHOHCOOH$), which is the most widely occurring hydroxycarboxylic acid and have a prime position due to its versatile applications in food, pharmaceutical, textile, leather, and chemical industries (*49*). Capable of being either chemically synthesized or fermented, about 90% lactic acid is now commercially produced by fermentation of sugars present in biomass. Fermentation has the advantage to produce one of the lactic acid isomers, whereas synthetic production results in a racemic mixture of lactic acid. The economics of lactic acid production by fermentation is dependent on many factors, of which the cost of the raw materials is very significant. It is very expensive when sugars, such as glucose, sucrose, starch are used as the feedstocks for lactic acid production. Cheap raw materials, such as whey, molasses, starch, beet and sugarcane and many other carbohydrate-rich materials can be used for fermentation of lactic acid. As will be described later in details, these waste materials and byproducts contain essential substrates that are beneficial to lactic acid production.

Most PLA produced currently is via ring-opening polymerization from lactide formed by esterification of two lactic acids. Poly L-lactic acid (PLLA) which is synthesized from L-lactic acid, has crystallinity of about 37%, glass transition temperature around 60 °C, melting temperature around 175 °C and a tensile modulus between 2.7-16 GPa (*50*, *51*). PLLA has been widely adapted in textile, packaging and medical applications. D-lactic acid is used for the production of poly D-lactic acid (PDLA). Poly-D-L-lactide (PDLLA) is polymerized from a racemic mixture of L- and D- lactides. The ratio of L- and D- lactic acids could

In Degradable Polymers and Materials: Principles and Practice (2nd Edition); Khemani, K., et al.;
ACS Symposium Series; American Chemical Society: Washington, DC, 2012.

greatly affect mechanical properties and degradability of PDLLA (*52*). PDLLA is more biodegradable and has higher melting temperatures than polymers synthesized from one isomer.

The conventional method to produce lactic acid is saccharification fermentation (SF) or separate hydrolysis and fermentation (SHF), which means hydrolysis of raw materials is conducted before fermentation. Another method is simultaneous saccharification and fermentation (SSF), which defines a process that combines enzymatic hydrolysis of cellulose and fermentation of its derived sugar to ethanol simultaneously (*53*). Using SSF, hydrolysate inhibition of enzymes in the enzymatic hydrolysis could be avoided, and therefore the risk of contamination is reduced. Capital investments for SSF are decreased since the total reactor volume is decreased due to higher productivity. However, the different optimal temperatures for yeast for fermentation and enzymes for hydrolysis could be a disadvantage for SSF.

Polyhydroxyalkanoate Acid (PHAs)

Polyhydroxyalkanoates (PHAs) are linear aliphatic polyesters composed of various hydroxyalkanoates, which are accumulated intracellularly as granule inclusions as carbon and energy storage in prokaryotic microorganisms. They are synthesized in presence of excess carbon, especially when another essential nutrient, such as nitrogen, sulfur or phosphorous is limited. Most PHAs are thermoplastics and can be thermally processed using existing technologies in plastics industry. PHAs can be easily completely biodegraded and are more readily biodegradable under various natural environments as compared to PLA (*54*). So far, approximately 150 different constituents of PHAs as homopolymers or as copolymers have been identified (*55*). Several widely studied types of PHAs are introduced as below.

Poly-3-hydroxybutyrate (PHB) is the most extensively studied PHA with high brittleness and high crystallinity (*56*). Polymerization of 3-hydroxyhexanoic acid (3HV) and 3-hydroxybutyric acid (3HB) produces copolymer poly-3-hydroxybutyrate-co-3-hydroxyvalerate (PHBV), which processes less stiffness and better ductility (*56*). PHBV shows higher elongation at break and lower melting temperatures ranging from 100 to 160 °C, depending on the mol % of 3HB in PHBV. Poly-3-hydroxybutyrate-3-hydroxyhexanoate (PHBHHx) is a copolymer of 3-hydroxybutyrate (3-HB) and 3-hydroxyhexanoate (3-HHx) (*57*). By varying monomer percentage, PHBHHx could have superior mechanical properties similar to low density polyethylene (LDPE). Diverse PHAs could be fermented due to the remarkably broad range of substrates for PHA producing microorganisms as well as the effects of numerous types of carbon sources that could be fed.

Submerged fermentation (SF) and solid state fermentation (SSF) are the two approaches to produce PHAs from microorganisms. Submerged fermentation (SF) is the most popular liquid fermentation for many products. SF process occurred in aqueous medium which contains microorganisms, nutrients and substrates. The productivity of SF is high because the microorganisms could grow, reproduce and function in high efficiencies using SF approaches. However, SF process generates

In Degradable Polymers and Materials: Principles and Practice (2nd Edition); Khemani, K., et al.;
ACS Symposium Series; American Chemical Society: Washington, DC, 2012.

a large amount of wastewater, and could be easily interfered by contamination. Solid state fermentation (SSF) attracted researchers' attentions for its applications in producing PHAs recently. In SSF approach, the microorganisms are cultured on moist solid raw materials. SSF approach has lower energy consumption, lower wastewater discharge, and therefore are considered as more environmental friendly than SF. SSF can be easily carried out aerobically. However, SSF substrate should have relatively high surface-to-volume ratio to gain high productivity. For both SF and SSF methods, pretreatment of raw materials may be required to obtain high efficiency of bioconversion. Using polysaccharides such as cellulose or hemicellulose as substrates requires fractionation to produce sugar rich hydrolysates that are fermentable by microorganisms. For example, bagasse is first hydrolyzed and the hydrolysate is used as the substrate for fermentation.

Waste Materials for Fermentation of PLA and PHAs

The demand for PLA and PHAs is increasing considerably due to wide range of industrial applications. The high cost of raw materials remains one of the major obstacles for fermentative production of bioplastics to compete with petrochemical polymers (*49*, *58*). Currently, the feedstocks for fermentation of PLA are refined sugars and polysaccharides, and that for PHAs are mainly refined sugars, polysaccharides and lipids. Seeking cheap raw materials is essential for the feasibility of biotechnological production of PLA and PHAs. Nowadays, lignocellulose, polysaccharides and oils from agricultural, agro-industrial, and biofuel sources represent potentially inexpensive and renewable feedstocks for large-scale fermentation of PLA and PHAs due to their abundance, low price, renewability and high content of fermentative materials.

Lignocellulose

Lignocellulosic biomass is organic material derived from a biological origin, and is mainly composed of cellulose, hemicellulose (noncellulosic polysaccharides including xylans, mannans and glucans) and lignin (polyphenolic structure). Since cellulose and hemicellulose can be used as carbon sources for sugar production, lignocellulose could be a suitable substrate to produce useful chemicals for lactic acid production via fermentation of polysaccharides. Annual global production of lignocellulosic biomass amounts to approximate 200 billion tons, most of which has not been utilized (*59*). Lignocellulosic biomass could come from forest and crop residues, municipal solid waste and waste paper, and are therefore regarded as abundant, renewable and inexpensive.

Several lignocellulosic waste materials and byproducts from agricultural, forestry and paper making industries have been studied for their potentials to produce lactic acid or PHAs via fermentation. As considered as abundant agricultural waste which contains about 45% cellulose, 35% hemicellulose and 15% lignin, corncobs have a great potential to produce various value-added chemicals (*60*). Straws, the agricultural by-products, which account for half of the yield of cereal crops, is composed of approximate 40% cellulose, 30%

In Degradable Polymers and Materials: Principles and Practice (2nd Edition); Khemani, K., et al.;
ACS Symposium Series; American Chemical Society: Washington, DC, 2012.

hemicellulose and 15% lignin. Soy straw, rice straw and wheat straw have been studied to be fermented to produce bioplastics (*61–63*). Paper sludge discharged from paper-making mills has high cellulosic and hemicellulosic fractions. These fractions could be completely converted into glucose and xylose, which could be used as fermentation medium for lactic acid (*64*). Sugarcane bagasse is the fibrous matter that remains after extraction of the juice by crushing sugarcane, and is composed of 40-50% cellulose, 25% hemicellulose and 25% lignin (*15*). The percentage of ash in sugarcane bagasse is much lower as compared to other crop residues, such as rice straw and wheat straw, which have approximate 15% of ash.

As shown in Table III, lignocellulosic waste materials from various origins, such as paper sludge, corncob, bagasse, straws, have been fermented into lactic acid, mostly by *Lactobacillus* under anaerobic environments. *Lactobacillus* comprises a major part of the lactic acid bacteria group that converts lactose and other sugars to lactic acid. However, even though the raw materials are very low in cost, the whole process to produce lactic acid from lignocellulose is not feasible and potentially high in cost. First, to produce bioplastics through fermentation using lignocellulosic substrates, specific pretreatment should be conducted. The cellulose and hemicellulose in lignocellulose are not directly available for bioconversion because of their intimate association with lignin. The purpose of pretreatment is to enlarge accessible surface area of substrate and to partial solubilize and/or degrade hemicellulose and lignin in order to improve digestibility and easy access for microbial attack. Steam explosion, alkali treatment, hydrogen peroxide treatment and radiation are the usual pretreatment methods. After that, expensive enzymatic hydrolysis of cellulose into sugars should be conducted since cellulose cannot be directly fermented into lactic acid. In some research, certain type of pure material, such as cellulose from raw materials was purified before fermentation to facilitate enzymatic hydrolysis (*65*). However, addition of purification steps may potentially increase the assumed low cost to use waste materials.

Whey

Whey is defined as the liquid or watery remaining of milk after coagulation and separation of milk casein in cheese-making process (*81*). Whey contains approximate 70-72% lactose, 8-10% protein, 12-15% minerals and fat (*82*). Whey effluent arising from cheese and casein manufacture has high biochemical oxygen demand (BOD: 30000-50000 ppm) and high chemical oxygen demand (COD: 60000-80000 ppm), which are mainly attributed to high percentage of lactose, and must be processed prior to disposal (*83*). Currently, production of dairy whey effluent exceeds 150 million tons annually worldwide, and still has an annual growth rate of 1 to 2% (*84*). The large amount of lactose in the whey effluent could be substrate for fermentation to produce lactic acid and PHAs. Therefore, to solve water-pollution problem, bioconversion of whey effluent into useful chemicals for bioplastics production via fermentation could be a simple and economical approach.

In Degradable Polymers and Materials: Principles and Practice (2nd Edition); Khemani, K., et al.;
ACS Symposium Series; American Chemical Society: Washington, DC, 2012.

Table III. Fermentation of lactic acid from lignocellulosic waste materials and byproducts

Substrate	*Organism*	*Lactic acid*			*Ref*
		Conc (g/L)	*Yield (g of Lactic acid/ g of substrate)*	*Productivity (g/L/h)*	
Paper sludge	*Bacillus coagulan strains* 36D1 and P4-102B	92.0	0.77	NA[a]	(*66*)
Recycled paper sludge	*Lactobacillus rhamnosus* ATCC 7469	73	0.97	2.90	(*64*)
Agro-industrial wastes (corncobs, Trimming vine shoots, barley bran husks)	*Lactobacillus pentosus*	33	0.76	NA	(*67*)
Cellubiose and cellutriose	*Lactobacillus delbrueckii Mutant* Uc-3	90	0.9	2.25	(*68*)
Lignocellulosic hydrolysates	*Lactobacillus sp.* RKY2	42	0.9	6.70	(*69*)
Sugarcane bagasse	*Penicillium janthinellum mutant* EU1 *Lactobacillus delbrueckii mutant* Uc-3	67	0.84	0.93	(*65*)
Sugarcane bagasse hydrolysates	*Lactococcus lactis* IO-1	10.9	NA	NA	(*70*)
Lime-treated wheat straw	*Bacillus coagulans* DSM 2314	40.7	0.43	0.74	(*63*)
Cellulosic biosludge	*Lactobacillus rhamnosus* CECT-288	42	0.38	0.88	(*71*)
Waste paper	*Lactobacillus delbrueckii* B445		0.84	1.00	(*72*)
Agricultural residues (alfalfa fiber, soya fiber, corncob, wheat straw)	*Lactobacillus delbrueckii* and *Lactobacillus plantarum*	42.8	0.68	0.46	(*73*)
Corncob	*Lactobacillus rhamnosus* CECT-288	50	NA	NA	(*74*)

Continued on next page.

Table III. (Continued). Fermentation of lactic acid from lignocellulosic waste materials and byproducts

Substrate	*Organism*	*Lactic acid*			*Ref*
		Conc (g/L)	*Yield (g of Lactic acid/ g of substrate)*	*Productivity (g/L/h)*	
Rice straw	*L. brevis* IFO 3960	34.2	0.96	0.55	(*62*)
Steam-exploded wood hydrolysate	*Rhizopus oryzae*	16.6	NA	NA	(*75*)
Xylan	*Lactobacillus brevis* ATCC367 transformed with a xylanase gene	7.1	NA	NA	(*76*)
Cassava pulp	*Rhizopus oryzae* NRRL395	23.8	0.85	0.42	(*77*)
Corncob hydrolysate	*Lactobacillus casei* and *L. lactis*	NA	NA	30	(*78*)
Soybean stalk hydrolysate	*Lactobacillus sake* and *Lactobacillus casei*	11	0.24	0.46	(*79*)
Corncob	*Trichocherium reesei* and *Aspergillus niger*	33.97	0.79	NA	(*80*)
Wheat straw	*Lactobacillus pentosus* and *Lactobacillus brevis*	NA	0.88	NA	(*61*)

[a] Not available

Conversion of whey into lactic acid by *Lactobacillus* has been reported by several groups as shown in Table IV. Due to high content of lactose in whey, high concentration of lactic acid could be fermented without extensive pretreatment. Protein in whey could also function as nitrogen source for lactic acid microorganism fermentation. Productivity of lactic acid from whey is much higher than that from lignocellulosic resources.

Table IV. Fermentation of lactic acid from whey

Substrate	***Organism***	***Lactic acid***			***Ref***
		Conc (g/L)	***Yield (g of Lactic acid/ g of substrate)***	***Productivity*** *(g/L/h)*	
Whey	*Lactobacillus bulgaricus*	40	0.89	22.5	(*85*)
Whey	*Lactobacillus casei*	77	NA[a]	2.5	(*86*)
Whey	*Lactobacillus casei* NRRL B-441	102.9	0.93	3.97	(*87*)
Whey permeate	*Lactobacillus helveticus*	NA	NA	22	(*88*)

[a] Not available

More studies have been done to use whey as resources to produce PHAs as shown in Table V. The lactose content in whey is optimal carbon source for PHA fermentation. However, the protein content in whey was considered to be too high for PHA fermentation. Therefore, to obtain high productivity of PHAs, pretreatment to whey to achieve optimal C/N ratio should be conducted or carbon resource may be added (*89*). From most of the examples of PHA production from whey resources, aseptic conditions are required. PHA fermented from non-sterile fermentation process without pH control was reported by Bosco (*89*). Elimination of sterilization step in fermentation could effectively reduce the cost. However, low yield and productivity from this method restricted its applications.

Molasses

Molasses is a by-product with 50% or higher percentage of sugar, generated from the final step of sugar crystallization step in the sugar refinery industry with various crude materials, such as sugarcane, sugar beet and grapes (*97*). Molasses is a convenient raw material for lactic acid and PHA fermentation since it contains a high concentration of sucrose, is cheap and abundant, and requires

In Degradable Polymers and Materials: Principles and Practice (2nd Edition); Khemani, K., et al.;
ACS Symposium Series; American Chemical Society: Washington, DC, 2012.

only a little handling before fermentation. The BOD and COD, the indexes of polluting characters of molasses, typically range between 35,000–50,000 and 100,000–150,000 ppm, respectively (*98*). The much lower price of molasses comparing to pure polysaccharide and many other industrial raw materials makes it competitive as a substrate for fermentation of lactic acid and PHAs.

Fermentation of lactic acid using molasses is shown in Table VI. Sugarcane molasses has been widely studied for fermentation of lactic acid by *Lactobacillus*, due to large availability of sugarcane molasses from sugar refinery industry. Beet molasses, corncob molasses also have been utilized. Yield and productivity of lactic acid per unit weight of molasses are generally high for all of them owing to high content of sucrose, which are readily to be utilized by microorganisms as carbon sources. However, significant amount of salt existed in molasses may affect growth of microorganisms during bioconversion, and therefore, removal of salts or screening of halophilic bacteria may be necessary for molasses from different origins.

Fermentation of PHAs from molasses is shown in Table VII. As mixtures, using molasses as feedstocks facilitates production of a variety of monomers which offers possibility of producing PHAs with a wide range of thermal and mechanical properties without need of addition of co-substrates. A previous acidogenic fermentation step is required for PHA production from carbohydrate-rich raw materials in order to transform high portion of carbohydrate in molasses into organic acids, such as volatile fatty acid (VFA), which can be effectively stored as PHA by microbial cultures. It is assumed that extra acidogenic step may potentially increase the cost. Further research to simplify the whole process is required considering the economic impact.

Oils, Fatty Acids and Glycerol

Oils and fatty acids from oil refinery industries could be good candidates as carbon sources for PHA fermentation. As reported, per weight of oil contains higher carbon content and could potentially generate more PHAs than polysaccharides, which are commonly used as feedstocks for PHA accumulation (*106*). The oils are assumed to yield high amount of PHAs and subsequently reduce the cost (*107*). Various palm oil byproducts, such as palm olein (PO), palm stearin (PS), refined, bleached and deodorized (RBD) palm oil, kernel olein, kernel stearin, palm kernel acid oil (PKAO), palm acid oil (PAO), and palm fatty acid distillate (PFAD) are generated from refining processes during removal of free fatty acids from CPO which are detrimental to oil properties (*108*). First, the oil is hydrolyzed by enzymes and the resultant free fatty acids are taken up by cells for PHA synthesis. Byproduct from fishing industry is rich in oil contents that could also be carbon source for PHA fermentation (*109*).

In Degradable Polymers and Materials: Principles and Practice (2nd Edition); Khemani, K., et al.;
ACS Symposium Series; American Chemical Society: Washington, DC, 2012.

Table V. Fermentation of PHAs from whey

Substrate	*Organism*	*Polyhydroxyalkanoate (PHA)*					*Ref*
		Monomer	*Conc (g/L)*	*Cell Dry Weight (CDW, g/L)*	*PHA content (% of CDW)*	*Productivity (g/L/h)*	
Cheese whey	*Methylobacterium* sp. ZP24	3HB	3	5.25	59	0.02	(*90*)
Cheese whey	*Escherichia coli*	3HB	20.1	51	1.01	1.35	(*91*)
Lactose and cheese whey permeate	*Hydrogenophaga pseudoflava* DSM 1034 and *Sinorhizobium meliloti* 41	3HB	NA[a]	NA	5.04	NA	(*92*)
Whey	*Escherichia coli* CGSC 4401	3HB	168	194	87	NA	(*93*)
Whey	*Escherichia coli* CGSC 4401 harboring pJC4	3HB	96.2	119.5	81	0.34	(*94*)
Milk whey	Dairy wastewater activated sludge		0.28	NA	12.82	NA	(*89*)
Whey lactose	*Haloferax mediterranei* *Pseudomonas hydrogenovora* and *Hydrogenophaga pseudoflava*	3HB 3HV	5.5	11	50	NA	(*95*)
Lactose	Recombinant *Cupriavidus necator* DSM 545	3HB		8.5	30	NA	(*96*)

[a] Not available

Table VI. Fermentation of lactic acid from molasses

Substrate	*Organism*	*Lactic acid*			*Ref*
		Conc (g/L)	*Yield (g of Lactic acid/ g of substrate)*	*Productivity (g/L/h)*	
Sugarcane Molasses	*Lactobacillus delbrueckii mutant Uc-3*	166	0.87	4.15	(*99*)
Sugarcane bagasse	*Penicillium janthinellum mutant EU1* *Lactobacillus delbrueckii mutant* Uc-3	67	0.84	0.93	(*65*)
Sugarcane bagasse hydrolysates	*Lactococcus lactis* IO-1	10.9	NA[a]	NA	(*70*)
Corncob molasses	*Bacillus* sp. strain XZL9	74.7	0.82	1.15	(*100*)
Sugarcane molasses, sugarcane juice and sugar beet	*Lactobacillus delbrueckii* JCM 1148	120	0.8	1.67	(*101*)
Beet molasses	*Lactobacillus delbrueckii* IFO 3202	60.3	0.95	11.2	(*102*)

[a] Not available

Table VII. Fermentation of PHAs from molasses

Substrate	*Organism*	*Polyhydroxyalkanoate (PHA)*					*Ref*
		Monomer	*Conc (g/L)*	*Cell Dry Weight (CDW, g/L)*	*PHA content (% of CDW)*	*Productivity (g/L/h)*	
Soy molasses	Pseudomonas corrugata	3HDD[a] 3HO[b] 3HTD[c]	0.58	3.4	17	3.6	(*103*)
Fermented sugarcane molasses	An open mixed culture enriched in glycogen accumulating organisms (GAOs)	3HB 3HV 3HHx 3H2MB[d] 3H2MV[e]	NA[f]	NA	66	NA	(*104*)
Sugarcane molasses		3HB 3HV	NA	NA	61	NA	(*105*)

[a] 3-hydroxyoctadecanoic acid [b] 3-hydroxyoctanoic acid [c] 3- Hydroxytetradecenoate [d] 3-Hydroxy-2-methyl- butyrate [e] 3-Hydroxy-2-methylvaleric acid [f] Not available

In Degradable Polymers and Materials: Principles and Practice (2nd Edition); Khemani, K., et al.;
ACS Symposium Series; American Chemical Society: Washington, DC, 2012.

Waste glycerol from biodiesel is another carbon source for PHA fermentation. Glycerol is accumulated during methanolic cleavages of fats in the biofuel production (*110*). Biodiesel fuel is produced through a methyl esterification process using oil and fat. Waste glycerol at about 10 wt% from raw material is generated as a byproduct. As the biodiesel fuel is becoming popular as a carbon-neutral fuel, more waste glycerol will be produced accordingly (*111*).

Multiple oils, fatty acids and glycerol from a wide range of waste materials and byproducts from food-processing and biofuel industries have been studied for PHA fermentation as shown in Table VIII. PHAs with various monomer contents could be produced from one type of waste material, since the raw material itself could become a mixture of a wide range of fatty acids after pretreatment. The variation in monomer types and portions could potentially lead to inconsistence in quality and productivity of PHA fermentation. In addition, though the theoretical yield and productivity of PHAs from oil-based substrates should be high, some PHA-producing bacteria have relatively low growth rate and may result in low PHA content in cell content (*112*).

Pomace

Pomace is the solid waste of apples, grapes, olives, or other fruits after pressing for juice or oil. Pomace contains skins, pulp, seeds and stems of the fruits and accounts for 25-35 wt % of the processed raw material. Several million tons of pomace are produced annually globally from juice making and oil refinery industries (*120–122*). Pomace could be good candidate for fermentation of lactic acid, because compositions of pomace are suitable for lactic acid fermentation. There are high contents of glucose and fructose, which are excellent carbon sources for lactic acid production, and high contents of polysaccharides (cellulose, starch, and hemicelluloses) which can be hydrolyzed to obtain monosaccharides by enzymes. Fermentation of lactic acid from apple pomace is shown in Table IX. Polysaccharides in pomace were enzymatically saccharified to achieve a high final monosaccharide concentration. The presence of organic acids, such as malic acid and citric acid and metal ions in small amounts could be nutrient supplementation for bacteria growth.

In Degradable Polymers and Materials: Principles and Practice (2nd Edition); Khemani, K., et al.;
ACS Symposium Series; American Chemical Society: Washington, DC, 2012.

Table VIII. Fermentation of PHAs from oils, fatty acids and glycerol

Substrate	*Organism*	*Polyhydroxyalkanoate (PHA)*				*Ref*
		Monomer	*Conc (g/L)*	*Cell Dry Weight (CDW, g/L)*	*PHA content (% of CDW)*	
Whey, vegetable oils, rice and wheat bran, mustard oil cake, palm oil cake	*Pseudomonas aeruginosa* MTCC 7925	3HB 3HV 3HHD[b] 3HOD[c]	5	NA[a]	60	(*113*)
Biodiesel co-product stream (glycerol, fatty acid soaps, residual fatty acid methyl esters)	*Pseudomonas oleovorans* NRRL B-14682 and *P. corrugata* 388	3HB 3HO 3HD[d] 3-Hydroxytetradeca-dienoic acid	NA	NA	21	(*114*)
Tallow free fatty acids and triglyceride	*Pseudomonas resinovorans, P. resinovorans, P. putida, P. citronellolis*	C8 C10	NA	NA	19	(*115*)
Oil from rhamnose production	*Pseudomonas oleovorans* and *Ralstonia eutropha*	3HHD 3HO 3HD 3HDD[e]	NA	16.4	41.3	(*116*)
Palm olein	*FLP1* and *FLP2*	3HB	NA	5.1	57.4	(*117*)
Waste glycerol	*Halomonas* sp. KM-1	3HB	1.9	NA	41	(*111*)
Olive oil	*Aeromonas caviae* 440	3HB 3HHx	NA	NA	NA	(*118*)

Continued on next page.

In Degradable Polymers and Materials: Principles and Practice (2nd Edition); Khemani, K., et al.;
ACS Symposium Series; American Chemical Society: Washington, DC, 2012.

Table VIII. (Continued). Fermentation of PHAs from oils, fatty acids and glycerol

Substrate	*Organism*	*Polyhydroxyalkanoate (PHA)*				*Ref*
		Monomer	*Conc (g/L)*	*Cell Dry Weight (CDW, g/L)*	*PHA content (% of CDW)*	
Alaskan Pollock oil	*P. oleovorans* NRRL B-778 and *P. oleovorans* NRRL B-14682	3HB 3HO 3HD	2.5	4.7	27	(*109*)
Volatile fatty oil from activated sludge	Activated sludge	3HB 3HV	NA	NA	56.5	(*119*)

[a] Not available [b] a 3-hydroxyhexadecanoic acid [c] 3-hydroxyoctadecanoic acid [d] 3-hydroxydecanoic acid [e] 3-hydroxydodecanoic acid

In Degradable Polymers and Materials: Principles and Practice (2nd Edition); Khemani, K., et al.;
ACS Symposium Series; American Chemical Society: Washington, DC, 2012.

Table IX. Fermentation of lactic acid from apple pomace

Substrate	*Organism*	*Lactic acid*			*Ref*
		Conc (g/L)	*Yield (g of Lactic acid/ g of substrate)*	*Productivity (g/L/h)*	
Apple pomace	*Lactobacillus rhamnosus* CECT-288	29.5	0.36	1.23	(*123*)
Apple pomace	*Lactobacillus rhamnosus* CECT-288	32.5	0.88	5.41	(*124*)
Apple pomace	*Lactobacillus rhamnosus* CECT-288	27.8	0.37	2.78	(*125*)

Concluding Remarks

Bioplastics from waste materials will play an increasingly important role in the global plastic markets due to their biodegradability and use of low-price renewable waste materials for their productions. The unavoidable increasing trend of prices of petrochemical-based plastics and increasing awareness of environmental issues induced by conventional plastics will promote broad applications of bioplastics from waste materials. Currently, the manufacturing prices are still too high to compete with conventional petrochemical-derived plastics due to the relatively small scale of production and expensive feedstocks, advances in fermentation technologies and the utilization of the inexpensive waste resources will certainly reduce the manufacturing cost.

So far, a variety of waste materials and byproducts from agricultural, agro-food and biofuel industries have been utilized to produce bioplastics through chemical or biological approaches, and promising results in productivity and cost have been achieved. Products showed certain performance properties that are comparable to conventional synthetic polymers. However, there are still several obstacles to be overcome in future studies. For instance, inconsistence in the compositions and qualities of waste materials may lead to variations in quality and productivity of final products. Low cost of bioplastics productions could not be achieved if expensive co-substrates or nutrients should be added into the fermentation media with waste materials. Pretreatments for some ingredients that cannot be readily fermented into bioplastics in waste materials as well as removal of detrimental ingredients in waste materials will also increase the cost. The bacteria widely used currently for fermentation from commercial refined feedstocks are not optimal for substrates from waste materials, which are usually mixtures of multiple components. Therefore, there is still much work remaining to be done for the ultimate goals of decrease in production cost and achievement of sufficient performance properties of bioplastics.

In Degradable Polymers and Materials: Principles and Practice (2nd Edition); Khemani, K., et al.;
ACS Symposium Series; American Chemical Society: Washington, DC, 2012.

References

1. Halden, R. U. *Annu. Rev. Public Health* **2010**, *31*, 179–194.
2. Yamamoto, T\.; Yasuhara, A.; Shiraishi, H.; Nakasugi, O. *Chemosphere* **2001**, *42*, 415–418.
3. Simoneit, B. R. T.; Medeiros, P. M.; Didyk, B. M. *Environ. Sci. Technol.* **2005**, *39*, 6961–6970.
4. Subramanian, P. M. *Resour., Conserv. Recycl.* **2000**, *28*, 253–263.
5. Al-Salem, S. M.; Lettieri, P.; Baeyens *J. Waste Manage.* **2009**, *29*, 2625–2643.
6. Lal, R. *Science* **2004**, *304*, 1623–1627.
7. Bastioli, C. *Starch/Staerke* **2001**, *53*, 351–355.
8. Carole, T.; Pellegrino, J.; Paster, M. *Appl. Biochem. Biotechnol.* **2004**, *115*, 871–885.
9. Albertsson, A.-C.; Andersson, S. O.; Karlsson, S. *Polym. Degrad. Stab.* **1987**, *18*, 73–87.
10. Averous, L. *J. Macromol. Sci., Part C: Phys. Polym. Rev.* **2004**, *44*, 231–274.
11. Swanson, C. L.; Shogren, R. L.; Fanta, G. F.; Imam, S. H. *J. Polym. Environ.* **1993**, *1*, 155–166.
12. Xu, W.; Reddy, N.; Yang, Y. *J. Agric. Food Chem.* **2007**, *55*, 6279–6284.
13. Xu, W.; Reddy, N.; Yang, Y. *Carbohydr. Polym.* **2009**, *76*, 521–527.
14. Sun, J. X.; Sun, X. F.; Sun, R. C.; Su, Y. Q. *Carbohydr. Polym.* **2004**, *56*, 195–204.
15. Pandey, A.; Soccol, C. R.; Nigam, P.; Soccol, V. T. *Bioresour. Technol.* **2000**, *74*, 69–80.
16. Ramasamy, E. V.; Gajalakshmi, S.; Sanjeevi, R.; Jithesh, M. N.; Abbasi, S. A. *Bioresour. Technol.* **2004**, *93*, 209–212.
17. Venkata Mohan, S.; Lalit Babu, V.; Sarma, P. N. *Enzyme Microb. Technol.* **2007**, *41*, 506–515.
18. Fang, H. H. P. *J. Dairy Sci.* **1991**, *74*, 2015–2019.
19. Salminen, E.; Rintala *J. Bioresour. Technol.* **2002**, *83*, 13–26.
20. Reddy, N.; Hu, C.; Yan, K.; Yang, Y. *Appl. Energy* **2011**, *88*, 1664–1670.
21. Edgar, K. J.; Buchanan, C. M.; Debenham, J. S.; Rundquist, P. A.; Seiler, B. D.; Shelton, M. C.; Tindall, D. *Prog. Polym. Sci.* **2001**, *26*, 1605–1688.
22. Reddy, N.; Yang, Y. *Biotechnol. Bioeng.* **2009**, *103*, 1016–1022.
23. Xu, W.; Yang, W.; Yang, Y. *Biotechnol. Prog.* **2009**, *25*, 1788–1795.
24. Shogren, R. L. *Carbohydr. Polym.* **1996**, *29*, 57–62.
25. El-Adawy, T. A. *Food Chem.* **2000**, *70*, 83–91.
26. Kabirullah, M.; Wills, R. B. H. *Int. J. Food Sci. Technol.* **1982**, *17*, 235–249.
27. Hu, C.; Reddy, N.; Yan, K.; Yang, Y. *J. Agric. Food Chem.* **2011**, *59*, 10517–10523.
28. Hassan, M. L.; Rowell, R. M.; Fadl, N. A.; Yacoub, S. F.; Christainsen, A. W. *J. Appl. Polym. Sci.* **2000**, *76*, 575–586.
29. Schilling, C. H.; Tomasik, P.; Karpovich, D. S.; Hart, B.; Garcha, J.; Boettcher, P. T. *J. Polym. Environ.* **2005**, *13*, 57–63.

In Degradable Polymers and Materials: Principles and Practice (2nd Edition); Khemani, K., et al.;
ACS Symposium Series; American Chemical Society: Washington, DC, 2012.

30. Schilling, C. H.; Tomasik, P.; Karpovich, D. S.; Hart, B.; Garcha, J.; Boettcher, P. T. *J. Polym. Environ.* **2005**, *13*, 177–183.
31. Schilling, C. H.; Tomasik, P.; Karpovich, D. S.; Hart, B.; Shepardson, S.; Garcha, J.; Boettcher, P. T. *J. Polym. Environ.* **2004**, *12*, 257–264.
32. Hassan, M. L.; Rowell, R. M.; Fadl, N. A.; Yacoub, S. F.; Christainsen, A. W. *J. Appl. Polym. Sci.* **2000**, *76*, 561–574.
33. Hu, C.; Reddy, N.; Yan, K.; Yang, Y. *J. Agric. Food Chem.* **2011**, *59*, 1723–1728.
34. Reddy, N.; Hu, C.; Yan, K.; Yang, Y. *Mater. Sci. Eng. C* **2011**, *31*, 1706–1710.
35. Hon, D. N. S.; San Luis, J. M. *J. Polym. Sci., Part A: Polym. Chem.* **1989**, *27*, 4143–4160.
36. Hassan, M. L.; El-Wakil, N. A.; Sefain, M. Z. *J. Appl. Polym. Sci.* **2001**, *79*, 1965–1978.
37. Kalan, E. B.; Neistadt, A.; Well, L.; Gordon, W. G. *Anal. Biochem.* **1965**, *12*, 488–496.
38. Khullar, R.; Varshney, V. K.; Naithani, S.; Soni, P. L. *J. Nat. Fibers* **2008**, *5*, 138–147.
39. Yoshioka, M.; Hagiwara, N.; Shiraishi, N. *Cellulose* **1999**, *6*, 193–212.
40. Senna, M. M.; Salmieri, S.; El-naggar, A.-W.; Safrany, A.; Lacroix, M. *J. Agric. Food Chem.* **2010**, *58*, 4470–4476.
41. Lanthong, P.; Nuisin, R.; Kiatkamjornwong, S. *Carbohydr. Polym.* **2006**, *66*, 229–245.
42. Lu, F. J.; Chu, L. H.; Gau, R. J. *Nutr. Cancer* **1998**, *30*, 31–38.
43. Tsukada, M.; Shiozaki, H.; Freddi, G.; Crighton, J. S. *J. Appl. Polym. Sci.* **1997**, *64*, 343–350.
44. Jin, E.; Reddy, N.; Zhu, Z.; Yang, Y. *J. Agric. Food Chem.* **2011**, *59*, 1729–1738.
45. Xu, C.; Luo, X.; Lin, X.; Zhuo, X.; Liang, L. *Polymer* **2009**, *50*, 3698–3705.
46. Lu, Y.; Luo, X.; Lin, X.; Zhang, C. *Adv. Mater. Res.* **2011**, *221*, 644–648.
47. Martinez-Hernandez, A. L.; Velasco-Santos, C.; de-Icaza, M.; Castano, V. M. *Composites, Part B* **2007**, *38*, 405–410.
48. Khullar, R.; Varshney, V. K.; Naithani, S.; Soni, P. L. *eXPRESS Polym. Lett.* **2008**, *2*, 12–18.
49. Datta, R.; Henry, M. *J. Chem. Technol. Biotechnol.* **2006**, *81*, 1119–1129.
50. Sodergard, A.; Stolt, M. *Prog. Polym. Sci.* **2002**, *27*, 1123–1163.
51. Middleton, J. C.; Tipton, A. J. *Biomaterials* **2000**, *21*, 2335–2346.
52. Garlotta, D. *J. Polym. Environ.* **2001**, *9*, 63–84.
53. Wyman, C. E.; Spindler, D. D.; Grohmann, K. *Biomass Bioenerg.* **1992**, *3*, 301–307.
54. Tokiwa, Y.; Calabia, B. P. *Biotechnol. Lett.* **2004**, *26*, 1181–1189.
55. Steinbuchel, A.; Lutke-Eversloh, T. *Biochem. Eng. J.* **2003**, *16*, 81–96.
56. Reddy, C. S. K.; Ghai, R.; Rashmi; Kalia, V. C. *Bioresour. Technol.* **2003**, *87*, 137–146.
57. Qu, X.-H.; Wu, Q.; Liang, J.; Qu, X.; Wang, S.-G.; Chen, G.-Q. *Biomaterials* **2005**, *26*, 6991–7001.

58. Mumtaz, T.; Yahaya, N. A.; Abd-Aziz, S.; Abdul Rahman, N.; Yee, P. L.; Shirai, Y.; Hassan, M. A. *J. Clean Prod.* **2010**, *18*, 1393–1402.
59. Lin, Y.; Tanaka, S. *Appl. Microbiol. Biotechnol.* **2006**, *69*, 627–642.
60. Abdel-Rahman, M. A.; Tashiro, Y.; Sonomoto, K. *J. Biotechnol.* **2011**, *156*, 286–301.
61. Garde, A.; Jonsson, G.; Schmidt, A. S.; Ahring, B. K. *Bioresour. Technol.* **2002**, *81*, 217–223.
62. Kim, J.-H.; Block, D.; Shoemaker, S.; Mills, D. *Appl. Microbiol. Biotechnol.* **2010**, *86*, 1375–1385.
63. Maas, R.; Bakker, R.; Jansen, M.; Visser, D.; de Jong, E.; Eggink, G.; Weusthuis, R. *Appl. Microbiol. Biotechnol.* **2008**, *78*, 751–758.
64. Marques, S.; Santos, J. A. L.; Girio, F. M.; Roseiro, J. C. *Biochem. Eng. J.* **2008**, *41*, 210–216.
65. Adsul, M. G.; Varma, A. J.; Gokhale, D. V. *Green Chem.* **2007**, *9*, 58–62.
66. Budhavaram, N. K.; Fan, Z. *Bioresour. Technol.* **2009**, *100*, 5966–5972.
67. Moldes, A.; Torrado, A.; Converti, A.; Domínguez, J. *Appl. Biochem. Biotechnol.* **2006**, *135*, 219–227.
68. Adsul, M.; Khire, J.; Bastawde, K.; Gokhale, D. *Appl. Environ. Microbiol.* **2007**, *73*, 5055–5057.
69. Wee, Y.-J.; Ryu, H.-W. *Bioresour. Technol.* **2009**, *100*, 4262–4270.
70. Laopaiboon, P.; Thani, A.; Leelavatcharamas, V.; Laopaiboon, L. *Bioresour. Technol.* **2010**, *101*, 1036–1043.
71. Romani, A.; Yanez, R.; Garrote, G.; Alonso, J. L. *Bioresour. Technol.* **2008**, *99*, 4247–4254.
72. Schmidt, S.; Padukone, N. *J. Ind. Microbiol. Biotechnol.* **1997**, *18*, 10–14.
73. Sreenath, H. K.; Moldes, A. B.; Koegel, R. G.; Straub, R. J. *Biotechnol. Lett.* **2001**, *23*, 179–184.
74. Rivas, B.; Moldes, A. B.; Dominguez, J. M.; Parajo, J. C. *Enzyme Microb. Technol.* **2004**, *34*, 627–634.
75. Woiciechowski, A. L.; Soccol, C. R.; Ramos, L. P.; Pandey, A. *Process Biochem.* **1999**, *34*, 949–955.
76. Hu, C.-Y.; Chi, D.-J.; Chen, S.-S.; Chen, Y.-C. *Green Chem.* **2011**, *13*, 1729–1734.
77. Thongchul, N.; Navankasattusas, S.; Yang, S.-T. *Bioprocess. Biosyst. Eng.* **2010**, *33*, 407–416.
78. Melzoch, K.; Votruba, J.; Habova, V.; Rychtera, M. *J. Biotechnol.* **1997**, *56*, 25–31.
79. Xu, Z.; Wang, Q.; Wang, P.; Cheng, G.; Ji, Y.; Jiang, Z. *Process Biochem.* **2007**, *42*, 89–92.
80. Luo, J.; Xia, L.; Lin, J.; Cen, P. *Biotechnol. Prog.* **1997**, *13*, 762–767.
81. Siso, M. I. G. *Bioresour. Technol.* **1996**, *57*, 1–11.
82. Panesar, P. S.; Kennedy, J. F.; Gandhi, D. N.; Bunko, K. *Food Chem.* **2007**, *105*, 1–14.
83. Mawson, A. J. *Bioresour. Technol.* **1994**, *47*, 195–203.
84. Smithers, G. W. *Int. Dairy J.* **2008**, *18*, 695–704.
85. Tejayadi, S.; Cheryan, M. *Appl. Microbiol. Biotechnol.* **1995**, *43*, 242–248.

86. Altıok, D.; Tokatlı, F.; Harsa, Ş. *J. Chem. Technol. Biotechnol.* **2006**, *81*, 1190–1197.
87. Büyükkileci, A. O.; Harsa, S. *J. Chem. Technol. Biotechnol.* **2004**, *79*, 1036–1040.
88. Schepers, A. W.; Thibault, J.; Lacroix, C. *Enzyme Microb. Technol.* **2006**, *38*, 324–337.
89. Bosco, F.; Chiampo, F. J. *Biosci. Bioeng.* **2010**, *109*, 418–421.
90. Yellore, V.; Desai, A. *Lett. Appl. Microbiol.* **1998**, *26*, 391–394.
91. Park, S. J.; Park, J. P.; Lee, S. Y. *Biotechnol. Lett.* **2002**, *24*, 185–189.
92. Povolo, S.; Casella, S. *Macromol. Symp.* **2003**, *197*, 1–10.
93. Ahn, W. S.; Park, S. J.; Lee, S. Y. *Biotechnol. Lett.* **2001**, *23*, 235–240.
94. Ahn, W. S.; Park, S. J.; Lee, S. Y. *Appl. Environ. Microbiol.* **2000**, *66*, 3624–3627.
95. Koller, M.; Hesse, P.; Bona, R.; Kutschera, C.; Atlić, A.; Braunegg, G. *Macromol. Biosci.* **2007**, *7*, 218–226.
96. Povolo, S.; Toffano, P.; Basaglia, M.; Casella, S. *Bioresour. Technol.* **2010**, *101*, 7902–7907.
97. Satyawali, Y.; Balakrishnan, M. *J. Environ. Manage.* **2008**, *86*, 481–497.
98. Nandy, T.; Shastry, S.; Kaul, S. N. *J. Environ. Manage.* **2002**, *65*, 25–38.
99. Dumbrepatil, A.; Adsul, M.; Chaudhari, S.; Khire, J.; Gokhale, D. *Appl. Environ. Microbiol.* **2008**, *74*, 333–335.
100. Wang, L.; Zhao, B.; Liu, B.; Yu, B.; Ma, C.; Su, F.; Hua, D.; Li, Q.; Ma, Y.; Xu, P. *Bioresour. Technol.* **2010**, *101*, 7908–7915.
101. Calabia, B.; Tokiwa, Y. *Biotechnol. Lett.* **2007**, *29*, 1329–1332.
102. Göksungur, Y.; Güvenç, U. *J. Chem. Technol. Biotechnol.* **1997**, *69*, 399–404.
103. Solaiman, D.; Ashby, R.; Hotchkiss, A.; Foglia, T. *Biotechnol. Lett.* **2006**, *28*, 157–162.
104. Bengtsson, S.; Pisco, A. R.; Reis, M. A. M.; Lemos, P. C. *J. Biotechnol.* **2010**, *145*, 253–263.
105. Albuquerque, M. G. E.; Concas, S.; Bengtsson, S.; Reis, M. A. M. *Bioresour. Technol.* **2010**, *101*, 7112–7122.
106. Akiyama, M.; Tsuge, T.; Doi, Y. *Polym. Degrad. Stab.* **2003**, *80*, 183–194.
107. Loo, C.-Y.; Lee, W.-H.; Tsuge, T.; Doi, Y.; Sudesh, K. *Biotechnol. Lett.* **2005**, *27*, 1405–1410.
108. Sudesh, K.; Bhubalan, K.; Chuah, J.-A.; Kek, Y.-K.; Kamilah, H.; Sridewi, N.; Lee, Y.-F. *Appl. Microbiol. Biotechnol.* **2011**, *89*, 1373–1386.
109. Ashby, R.; Solaiman, D. *J. Polym. Environ.* **2008**, *16*, 221–229.
110. Chi, Z.; Pyle, D.; Wen, Z.; Frear, C.; Chen, S. *Process Biochem.* **2007**, *42*, 1537–1545.
111. Kawata, Y.; Aiba, S. *Biosci., Biotechnol., Biochem.* **2010**, *74*, 175–177.
112. Tsuge, T. J. *Biosci. Bioeng.* **2002**, *94*, 579–584.
113. Singh, A.; Mallick, N. *J. Ind. Microbiol. Biotechnol.* **2009**, *36*, 347–354.
114. Ashby, R. D.; Solaiman, D. K. Y.; Foglia, T. A. *J. Polym. Environ.* **2004**, *12*, 105–112.
115. Cromwick, A. M.; Foglia, T.; Lenz, R. W. *Appl. Microbiol. Biotechnol.* **1996**, *46*, 464–469.

116. Füchtenbusch, B.; Wullbrandt, D.; Steinbüchel, A. *Appl. Microbiol. Biotechnol.* **2000**, *53*, 167–172.
117. Alias, Z.; Tan, I. K. P. *Bioresour. Technol.* **2005**, *96*, 1229–1234.
118. Shimamura, E.; Kasuya, K.; Kobayashi, G.; Shiotani, T.; Shima, Y.; Doi, Y. *Macromolecules* **1994**, *27*, 878–880.
119. Mengmeng, C.; Hong, C.; Qingliang, Z.; Shirley, S. N.; Jie, R. *Bioresour. Technol.* **2009**, *100*, 1399–1405.
120. Hang, Y. D.; Woodams, E. E. *Biotechnol. Lett.* **1984**, *6*, 763–764.
121. Hang, Y. D.; Woodams, E. E. *Biotechnol. Lett.* **1985**, *7*, 253–254.
122. Tekin, A. R.; Dalgic, A. C. *Resour., Conserv. Recycl.* **2000**, *30*, 301–313.
123. Gullón, B.; Alonso, J. L.; Parajó, J. C. *J. Chem. Technol. Biotechnol.* **2008**, *83*, 609–617.
124. Gullon, B.; Yanez, R.; Alonso, J. L.; Parajo, J. C. *Bioresour. Technol.* **2008**, *99*, 308–319.
125. Gullon, B.; Garrote, G.; Alonso, J. L.; Parajo, J. C. *J. Agric. Food Chem.* **2007**, *55*, 5580–5587.

Chapter 9

Recent Advances in Polyhydroxyalkanoate Biosynthesis in *Escherichia coli*

Ryan C. Tappel and Christopher T. Nomura*

Department of Chemistry, College of Environmental Science and Forestry, State University of New York, 1 Forestry Drive, Syracuse, NY 13210, USA
***email: ctnomura@esf.edu**

Polyhydroxyalkanoates (PHAs) are biodegradable polyesters that can be produced by a wide variety of microorganisms as a carbon storage material. PHAs have a large range of physical properties that are influenced by the side chain length of the repeating units and the variety of those repeating units in a given polymer. The physical properties can range from strong and stiff to elastomeric in nature, making PHAs desirable materials for numerous applications including use as thermoplastics and in medical applications. Our focus here is on the recent advances in PHA biosynthesis in recombinant *Escherichia coli*. Since *E. coli* does not natively produce PHAs, it is incapable of degrading the PHAs once they are synthesized, and it lacks transcriptional and translational regulatory factors that are present in native PHA producers, making it an ideal strain for PHA production. Numerous factors are of crucial consideration in PHA production in *E. coli*, and we have demonstrated improvements in multiple areas via enzyme and metabolic pathway engineering.

Introduction

Most plastics are synthesized from petroleum, and the majority of these polymers are not biodegradable in the environment. Petroleum-based plastics are resource intensive, and in 2006, nearly 331 million barrels of petroleum and natural gas were used to make plastics in the United States (*1*). The United States produced just over 31 million tons of plastic in 2010 (*2*), which made up 12.4%

In Degradable Polymers and Materials: Principles and Practice (2nd Edition); Khemani, K., et al.; ACS Symposium Series; American Chemical Society: Washington, DC, 2012.

of the total municipal solid waste that year. Only 8.2% of those plastic materials generated were recovered for recycling, leaving the majority to accumulate as non-biodegradable waste. An attractive alternative to petroleum-based plastics is the use of biodegradable plastics generated from renewable substrates and synthesized biologically. These biobased and biodegradable plastics may aid in reducing dependence on and use of non-renewable fossil fuels for plastic production. Polyhydroxyalkanoates, or PHAs, are a class of biopolymers that can potentially replace some fossil fuel-derived plastics.

PHAs are polyesters that are produced by numerous microorganisms as a carbon and energy sink when grown under nutrient stress in the presence of excess carbon (*3*, *4*). These polyesters can be readily synthesized by enzymatic machinery in the cells from simple, renewable starting materials such as sugars and plant oils. Poly(3-hydroxyalkanoates) are the most commonly produced and well studied PHAs, and their physical properties are largely dependent on the repeating unit composition of the polymers (unless otherwise noted, PHAs refer to poly(3-hydroxyalkanotes) in this article). Short-chain-length (SCL) PHAs consist of repeating units that are 3-5 carbon atoms in length. The most common and well characterized SCL PHA, poly(3-hydroxybutyrate) (PHB), consists of 4-carbon repeating units and is strong but has a low elongation to break (*3*). Medium-chain-length (MCL) PHAs consist of repeating units that are 6-14 carbon atoms in length. MCL PHAs are most commonly random assortments of different repeating unit lengths, and polymers consisting of these repeating units are less crystalline and more tacky and elastomeric in nature compared to SCL PHAs (*5*). SCL-MCL PHA copolymers consist of repeating units that are 3-14 carbon atoms in length and have a wide range of physical properties that are largely dependent on the mol ratio of SCL to MCL monomer units. SCL-MCL PHAs with a relatively high mole percent of SCL repeating units to MCL repeating units have properties similar to the bulk commodity plastics polypropylene and polyethylene (*3*, *5*, *6*). Although PHA polymers can be produced by native microorganisms, recombinant bacteria offer distinct advantages for the production of these polymers.

Despite the fact that *Escherichia coli* is not a native producer of PHAs, this bacterium has proven to be a useful host for the generation of new pathways and pathway modification for PHA synthesis. It readily expresses genes from a variety of other native PHA-producing organisms that are involved in PHA synthesis. It grows quickly, its genomic sequence is known, and it can easily be genetically modified (*21*) *E. coli*, like any non-native PHA production host, also does not have any PHA regulatory systems in place or enzymes that degrade PHAs. There are numerous examples of *E. coli* producing SCL PHAs (Table I) and PHAs containing MCL repeating units (Table II). This article serves as a review of our own recent contributions to PHA production in *E. coli*.

In Degradable Polymers and Materials: Principles and Practice (2nd Edition); Khemani, K., et al.;
ACS Symposium Series; American Chemical Society: Washington, DC, 2012.

Table I. SCL PHA production examples in recombinant *E. coli*[a]

Strain	*Introduced genes*	*Carbon source*	*PHA content (wt%)*	*Repeat unit composition (mol%)*			*Ref.*
				3HB	*4HB*	*3HV*	
DH5α	*phaCAB*$_{Re}$	gluconate (LB)	54	100	ND	ND	(*7*)
K12	*phaCAB*$_{Re}$	glucose (LB)	30	100	ND	ND	(*8*)
JM109	*phaCAB*$_{Re}$	glucose (LB)	85	100	ND	ND	(*9*)
MC4100	*phaCAB*$_{Re}$	glucose/	95	100	ND	ND	(*10*)
GCSC6576	*phaCAB*$_{Re}$	lactose/ whey	80	100	ND	ND	(*11*)
S17-1	*phaE*$_{Syn}$, *phaC*$_{Syn}$	glucose (LB)	13	100	ND	ND	(*12*)
BL21	*phaCAB*$_{Al}$	glucose	52	100	ND	ND	(*13*)
XL1-Blue	*phaCAB*$_{Pd}$, *phaP*$_{Pd}$, *phaR*$_{Pd}$	lactate (LB)	44	100	ND	ND	(*14*)
XL1-Blue	*phaCAB*$_{Al}$	glucose/	77	100	ND	ND	(*15*)
CGSC4401	*phaCAB*$_{Al}$	lactose/ whey	76	100	ND	ND	(*16*)
HB101	*fabD*$_{Ec}$, *phaC*$_{Ac}$	glucose (LB)	4.6	100	ND	ND	(*17*)
HB101	*fabH*$_{Ec}$, *phaC*$_{Ac}$	glucose (LB)	6.5	100	ND	ND	(*17*)
JM109	*fabH*$_{Ec}$, *phaC*$_{Ac}$	glucose (LB)	9.8	100	ND	ND	(*18*)
DH5α	*phaCAB*$_{Re}$, *sucD*$_{Ck}$, *4hbD*$_{Ck}$, *orfZ*$_{Ck}$	Glucose (LB)	46	98.5	1.5	ND	(*19*)
GJT001	*phaCAB*$_{Re}$, *prpE*$_{St}$	Glucose/ propionate	22	82.3	ND	17.7	(*20*)

[a] Re, *Ralstonia eutropha*; Al, *Alcaligenes latus*; Pd, *Paracoccus denitrificans*; Syn, *Synecocystis* sp. PCC 6803; Ec, *Escherichia coli*; Ac, *Aeromonas caviae*; Ck, *Clostridium kluyveri*; St, *Salmonella typhimurium* LT2; LB, Luria-Bertani medium; 3HB, 3-hydroxybutyrate; 4HB, 4-hydroxybutyrate; 3HV, 3-hydroxyvalerate. ND, not determined.

In Degradable Polymers and Materials: Principles and Practice (2nd Edition); Khemani, K., et al.;
ACS Symposium Series; American Chemical Society: Washington, DC, 2012.

Table II. Examples of MCL-containing PHAs synthesized in recombinant *E. coli*[a]

Strain	*Introduced genes*	*Carbon source*	*Repeat unit composition (mol%)*					*Ref.*
			3HB	*3HHx*	*3HO*	*3HD*	*3HDD*	
JMU193	*tesA*$_{Ec}$, *phaC*$_{Pp}$	Gluconate (LB)	ND	27	67	6	ND	(*28*)
LS1298	*tesA*$_{Ec}$, *phaC*$_{Pa}$	Gluconate (LB)	ND	ND	ND	100	ND	(*29*)
JM109	*fabH(F87T)*$_{Ec}$, *phaC*$_{Ac}$	Glucose (LB)	97	3	ND	ND	ND	(*18*)
JM109	*fabH(F87T)*$_{Ec}$, *phaAB*$_{Re}$, *phaC1(STQK)*$_{Ps}$	Glucose (LB)	99	1	ND	ND	ND	(*30*)
JM109	*fabH(F87T)*$_{Ec}$, *phaC1(STQK)*$_{Ps}$	Glucose (LB)	91	6	2	1	ND	(*31*)
JM109	*fabH(F87T)*$_{Ec}$, *fabG*$_{Ec}$, *phaC1(STQK)*$_{Ps}$	Glucose (LB)	94	5	1	ND	ND	(*31*)
LS5218	*fabG*$_{Ec}$, *fabH(F87T)*$_{Ec}$, *phaC1(STQK)*$_{Ps}$	Glucose	96.1	3.9	0	ND	ND	(*32*)
MG1655	*fabH(H244A/F87C)*$_{Ec}$, *phaC1(STQK)*$_{Ps}$	Glucose (LB)	93.5	6.3	0.2	0	0	(*27*)
LS5218	*phaJ*$_{Ac}$, *PhaC*$_{Ac}$	Dodecanoate	83	16	ND	ND	ND	(*22*)
LS5218	*phaJ1*$_{Pa}$, *phaC1*$_{Ps}$	Dodecanoate	12	73	8	4	3	(*24*)
LS5218	*phaJ4*$_{Pp}$, *phaC1*$_{Ps}$	Dodecanoate	10	31	32	18	10	(*25*)
BL21	*phaJ*$_{Ah}$, *phaC*$_{Ah}$	Dodecanoate	75.2	24.8	ND	ND	ND	(*33*)
CAG18496	*phaJ4*$_{Pa}$, *acs*$_{Pp}$, *phaC1*$_{Pp}$	Dodecenoate	ND	0	0	4.2	95.8	(*34*)
LSBJ	*phaJ4*$_{Pp}$, *phaC1(STQK)*$_{Ps}$	Dodecanoate (LB)	0	0	0	Trace	≤100	(*26*)

Strain	*Introduced genes*	*Carbon source*	*Repeat unit composition (mol%)*					*Ref.*
			3HB	*3HHx*	*3HO*	*3HD*	*3HDD*	
S17-1	*phaG*$_{Pp}$, *phaC*$_{Pa}$	Gluconate (LB)/ triclosan	0	ND	0	100	0	(*35*)
LS5218	*phaG*$_{Pp}$, *PP0763*$_{Pp}$, *phaC1(STQK)*$_{Ps}$	Glucose (LB)	0	1.3	39.2	56.9	2.6	(*36*)

[a] Ec, *Escherichia coli*; Pp, *Pseudomonas putida*; Pa, *Pseudomonas aeruginosa*; Ac, *Aeromonas caviae*; Ps, *Pseudomonas* sp. 61-3; Re, *Ralstonia eutropha*; Ah, *Aeromonas hydrophila*; LB, Luria-Bertani medium; 3HB, 3-hydroxybutyrate; 3HHx, 3-hydroxyhexanoate; 3HO, 3-hydroxyoctanoate; 3HD, 3-hydroxydecanoate; 3HDD, 3-hydroxydodecanoate. ND, not determined.

In Degradable Polymers and Materials: Principles and Practice (2nd Edition); Khemani, K., et al.;
ACS Symposium Series; American Chemical Society: Washington, DC, 2012.

PHA Monomer-Supplying Enzyme Engineering

There are numerous vital considerations in synthesizing PHAs in *E. coli*. One of these is determining which monomer-supplying enzymes should be used to generate substrates for PHA synthases to polymerize. Typically, for PHA production in non-native PHA-producing strains like *E. coli*, genes from native PHA producers are expressed to generate PHA precursors. Examples include beta-ketothiolase (*phaA*) and acetoacetyl-Coenzyme A (CoA) reductase (*phaB*) from *Ralstonia eutropha* for SCL PHA production (*7–11*) (more in Table I) and (*R*)-specific enoyl-CoA hydratase (*phaJ*) from various *Pseudomonas* species (*22–26*) (more in Table II) for MCL PHA synthesis. However, enzymes native to *E. coli* can also be modified and/or overexpressed to produce substrates for PHA production. FabH, the 3-ketoacyl-acyl carrier protein (ACP) synthase III that catalyzes the condensation of malonyl-ACP and acetyl-CoA to produce acetoacetyl-ACP in dissociated fatty acid biosynthesis, can act as a transacylase by converting β-ketoacyl-ACP to β-ketoacyl-CoA (*27*) (Figure 1). The 3-ketoacyl-ACP reductase, FabG, from fatty acid biosynthesis can then reduce the β-ketoacyl-CoA to the PHA synthase substrate, (*R*)-3-hydroxyacyl-CoA.

Numerous studies have shown that FabH can be used to generate precursors for PHA synthesis in *E. coli* (Tables I & II). When the native FabH enzyme is used, only the SCL PHA, PHB is produced (*17*). However, mutations to the phenylalanine 87 (F87) residue located in the binding pocket of FabH, led to the production of MCL repeating units that were incorporated into the PHA polymer produced in the presence of a PHA synthase (*18*). These SCL-MCL copolymers, as stated previously, can have more desirable physical properties compared to the PHB homopolymer (i.e. less crystalline and more flexible). Unfortunately, mutations to FabH almost always resulted in an overall decrease in total PHA production as a percent of cell mass. This decrease was something we hoped to overcome in our most recent work with FabH production of SCL-MCL PHA copolymers (*27*).

The transacylase activity of FabH is not the primary function of the enzyme in fatty acid biosynthesis, but it is critical for generating the β-ketoacyl-CoA PHA precursors (Figure 1). Davies *et al.*, after solving the crystal structure for FabH, showed that altering the histidine 244 (H244) and asparagine 274 (N274) residues to alanine in the active site of FabH increased the transacylase activity 6-fold compared to the wild type enzyme (*37*). These mutations were examined *in vitro* but had not been examined in terms of effect on PHA production and composition. Therefore, we sought out any possible benefits these active site mutations could have in combination with the F87 substituted mutants generated in previous studies (*18*).

In Degradable Polymers and Materials: Principles and Practice (2nd Edition); Khemani, K., et al.;
ACS Symposium Series; American Chemical Society: Washington, DC, 2012.

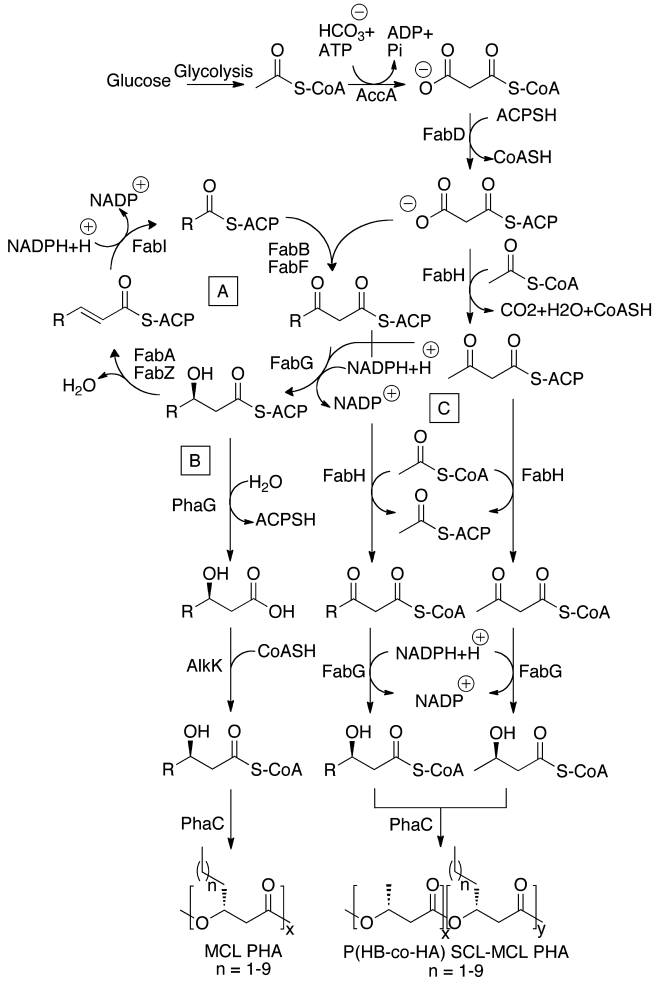

Figure 1. Examples of PHA production from the fatty acid biosynthesis pathway in recombinant E. coli strains. A. The fatty acid biosynthesis pathway. B. MCL PHA production utilizing a 3-hydroxyacyl-ACP thioesterase (PhaG), an acyl-CoA synthetase (AlkK), and a PHA synthase (PhaC). C. SCL-MCL PHA production utilizing the 3-ketoacyl-ACP synthase III (FabH) and 3-ketoacyl-ACP reductase (FabG) from the fatty acid biosynthesis pathway along with a PHA synthase.

In Degradable Polymers and Materials: Principles and Practice (2nd Edition); Khemani, K., et al.;
ACS Symposium Series; American Chemical Society: Washington, DC, 2012.

The N274A and H244A FabH derivatives were compared individually to wild type FabH in terms of generating substrates for PHA production and combined with various F87 mutations to evaluate if these mutations would have a synergistic effect on PHA production in recombinant *E. coli* (*27*). The H244A mutation resulted in a 679% increase in PHA production over the wild type enzyme, and the MCL portion of the SCL-MCL PHA copolymer was approximately 3 mol%. Combining the H244A mutation with an F87T increased the MCL portion to about 5 mol%. If the F87 was mutated to a serine or cysteine, the MCL PHA mol% increased to 6-7 mol%. The MCL repeating units were composed of 3-hydroxyhexanoate and 3-hydroxyoctanoate. All mutations examined either matched or surpassed the ability of wild type FabH to enhance PHA production in recombinant *E. coli*.

Both the histidine and asparagine residues in the active site of the FabH enzyme are thought to stabilize an oxyanion generated during the native condensation reaction (*37*). The increased transacylation arising from mutations of these amino acids may be due to loss of the native activity. The phenylalanine mutation aids in expanding the binding pocket, allowing for larger, MCL-sized substrates to be converted to β-ketoacyl-CoAs. This work shows the benefits of exploring multiple point mutations in monomer-supplying enzymes for PHA synthesis. Although experiments for the histidine and asparagine mutations suggested that they may be able to improve PHA production via FabH, there was no previous *in vivo* evidence to confirm this prior to our study (*27*, *36*, *37*).

This work may have implications beyond *E. coli* for PHA production. The FabH pathway for generating PHA precursors is part of the ubiquitous fatty acid biosynthesis pathway. Because of its universal presence, these modifications could be transferred to other organisms so that only a PHA synthase would be required for PHA synthesis. Plants are a very attractive option for PHA synthesis as their feedstock for conversion to PHA polymers would be carbon dioxide. There is already a great amount of focus on PHA production in plants, and FabH had been shown to be an option for PHA generation in plants (*38*). Continued exploration of engineered monomer-supplying enzymes like FabH should continue to improve biodegradable plastic production in bacteria and plants.

Confirming PHA Biosynthesis Pathways and Improving MCL PHA Production

Another consideration for PHA production in *E. coli* is the carbon source selected for growth and/or PHA production and how that carbon source is metabolized within the cell. For PHA synthesis, carbon sources can be classified as structurally "related" (e.g. fatty acids and oils) or "non-related" (e.g. sugars) to the polymer's repeating units. For producing PHAs, non-related carbon sources have some advantages over related carbon sources in *E. coli*. With current concerns over the use of biomass and biobased resources to produce value-added products, the main benefit of using non-related carbon sources such as sugars is that they can be derived from cellulosic and hemicellulosic materials. Also, non-related carbon sources can be readily metabolized anaerobically. This

In Degradable Polymers and Materials: Principles and Practice (2nd Edition); Khemani, K., et al.;
ACS Symposium Series; American Chemical Society: Washington, DC, 2012.

becomes advantageous compared to production from related carbon sources like fatty acids that typically require an intact β-oxidation pathway, which can be highly dependent on oxygen availability during growth. Production of MCL PHAs in *E. coli* from non-related carbon sources results in lower yields of cell mass and polymer as compared to the production SCL PHAs like PHB when using a non-related carbon source (Tables I & II). PHB can be synthesized up to 95% weight of *E. coli* from glucose (Table I). MCL-containing PHAs typically are not synthesized above 25% weight in *E. coli* from non-related carbon sources, and often times the polymers consist mostly of SCL repeating units (see references in Table II). One of our areas of focus is to improve MCL PHA yield from non-related carbon sources in *E. coli*.

The majority of MCL-containing PHAs produced from non-related carbon sources in *E. coli* have been synthesized via FabH-mediated pathways. However, another metabolic pathway option utilizes the enzyme PhaG (Figure 1). PhaG was identified as a key link between the fatty acid biosynthesis pathway and PHA production in *Pseudomonas putida* KT2440 (*39*). It was first reported to be a 3-hydroxyacyl-ACP-CoA transferase, and thought to catalyze the transfer of an ACP moiety for a CoA moiety that can be recognized for the polymerization reaction by a PHA synthase. However, expression of the PhaG enzyme and a PHA synthase in *E. coli* only produced very low amounts of PHA from gluconate when the bacteria were grown with triclosan, a fatty acid biosynthesis inhibitor (*35*). Furthermore, expression of PhaG alone in *E. coli* readily produces 3-hydroxy fatty acids excreted from the cells into the media (*36*, *40*, *41*). These results suggested that another enzyme might play a role with PhaG in generating MCL substrates for PHA production from fatty acid biosynthesis.

We investigated the possibility that various AlkK homologues were involved in PHA synthesis in *P. putida* KT2440 (*36*). AlkK, an acyl-CoA synthetase from *Pseudomonas oleovorans*, was shown to catalyze the attachment of free CoA to 3-hydroxy fatty acids *in vitro* (*42*). Since the PHA synthase can only recognize substrates with CoA carrier molecules, we hypothesized that an AlkK-like protein or CoA-ligase enzyme would be essential for producing PHA substrates from fatty acid biosynthesis. Because of this, we analyzed ten open reading frames in *P. putida* KT2440 with homology to AlkK by quantitative real-time PCR (q-PCR) (*36*). The experiments analyzed transcription levels of the AlkK homologues under growth conditions known to produce PHAs and growth conditions that did not produce PHAs, and the induction of the various open reading frames were determined by the ratio of transcription levels in PHA producing vs. non-PHA producing conditions. The gene coding for PhaG showed a very large increase in transcription when cells were grown under PHA producing conditions, as did one of the ten AlkK homologues. This AlkK homologue was selected to assess it's ability to provide PHA precursors from unrelated carbon sources in *E. coli* (*36*).

When *E. coli* was grown with transgenic expression of PhaG and a PHA synthase, only 0.2% of the total cell mass was PHAs. When the AlkK homologue was coexpressed along with PhaG and the PHA synthase, the PHA yield increased to 11.6% of the total cell mass and 400 mg L^{-1} of cell culture, all of which were MCL PHAs. We confirmed that the PHAs were coming from fatty acid biosynthesis by repeating the experiments in β-oxidation depleted strains of *E.*

In Degradable Polymers and Materials: Principles and Practice (2nd Edition); Khemani, K., et al.;
ACS Symposium Series; American Chemical Society: Washington, DC, 2012.

coli which showed similar levels of MCL PHA production despite the absence of a functioning β-oxidation pathway. This marked the highest level of production of MCL PHAs in *E. coli* from glucose (*36*).

When PhaG was expressed alone in *E. coli*, the cells produced 3-hydroxy fatty acids that were secreted out of the cell into the media, a result that was also observed in previous studies (Table III). These results, along with the data collected on the AlkK homologues suggest that PhaG was acting as a thioesterase, not a transferase, in *E. coli*. These conflicting reports stress the importance of being able to extract, purify, and characterize PHAs by NMR in addition to gas chromatography. We were able to confirm the composition of our PHAs produced via PhaG, the AlkK homologue, and a PHA synthase by NMR (*36*).

Table III. Production of 3-hydroxy fatty acids in *E. coli* using the PhaG enzyme[a]

E. coli strain	*Introduced Genes*	*Growth medium*	*3-hydroxy fatty acid (mg L^{-1})*	*3-hydroxy fatty acid composition (mole %)*		*Ref.*
				3HO	*3HD*	
HB101	*$phaG_{Pp}$*	LB/fructose/ triclosan	722	0	100	(*40*)
JM105	*$phaG_{Pp}$, $tesB_{Ec}$*	LB/fructose/ triclosan	1021	ND	100	(*41*)
CH01	*$phaG_{Pp}$, $tesB_{Ec}$*	LB/fructose/ triclosan	956	ND	100	(*41*)
LS5218	*$phaG_{Pp}$*	LB/glucose	1600	45	55	(*36*)

[a] Pp, *Pseudomonas putida*; Ec, *Escherichia coli*; LB, Luria-Bertani; 3HO, 3-hydroxyoctanoate; 3HD, 3-hydroxydecanoate; ND, not determined

Repeating Unit Control in PHAs Produced by Recombinant *E. coli*

Not all common metabolic pathways that lead to PHA production have been fully elucidated (*36*). An ever increasing number of enzymes involved in native PHA biosynthesis have been discovered and analyzed over the past decade. PhaG was established to be a critical link for fatty acid biosynthesis but may not work the way it was initially thought to (*36*, *39*, *40*). The ways in which native MCL PHA-producing bacteria can make MCL PHAs seems to be more complex than the pathways to produce SCL PHA in native PHA producing organisms. In addition to the PhaG and AlkK-like enzymes that may be involved in MCL PHA production from fatty acid biosynthesis, MCL PHAs can also be derived from the β-oxidation pathway when related carbon sources like fatty acids are utilized as a carbon feedstock by native PHA producers. There are a number of (*R*)-specific

In Degradable Polymers and Materials: Principles and Practice (2nd Edition); Khemani, K., et al.;
ACS Symposium Series; American Chemical Society: Washington, DC, 2012.

enoyl-CoA hydratases (PhaJ) that can convert the β-oxidation intermediate enoyl-CoA to the PHA monomer (*R*)-3-hydroxyacyl-CoA (Figure 2) (*23–25*, *43*).

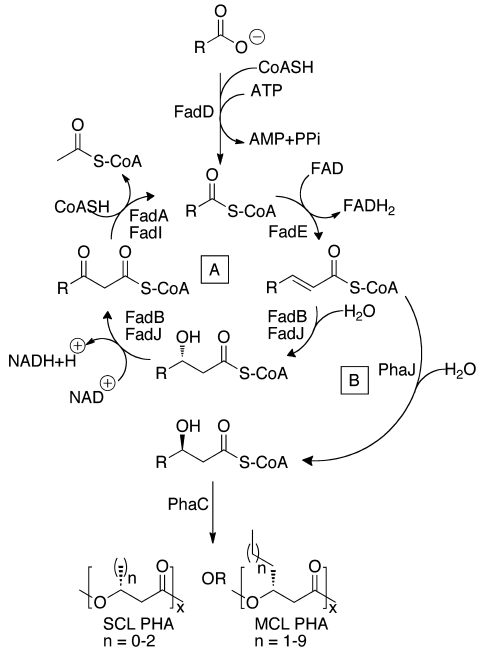

Figure 2. An example of SCL and MCL PHA production from the β-oxidation pathway in recombinant E. coli as discussed in this article. A. The fatty acid β-oxidation pathway. B. Multiple examples are given in the text that utilize an (R)-specific enoyl-CoA hydratase (PhaJ) and a PHA synthase (PhaC) to generate SCL and/or MCL PHAs.

The fatty acid biosynthesis and β-oxidation pathways in bacteria either add or remove two carbon units from the substrate per cycle, respectively. A result of the cyclic nature of these pathways is that the PHA substrates derived from them are almost always random assortments of 3-hydoxy fatty acid derivatives that differ by two carbons per repeating unit. These substrates are then incorporated into PHAs which then have different repeating unit sizes in native PHA producing bacteria (*5*) with rare exceptions (*44*). Given the variability of physical properties with different repeating unit compositions (*3*, *5*, *6*), it is important to develop systems through which the repeating unit composition of PHA polymers can be controlled. These facts have led to increased efforts to expand repeating unit control often found in SCL PHA synthesis (i.e. PHB) to MCL PHAs.

This leads to another vital consideration in PHA production in *E. coli* that must be taken into account to achieve repeating unit control of MCL PHAs: strain selection/development. We selected an *E. coli* strain that proved advantageous in developing a system capable of MCL repeating unit control (*26*). Alternatively,

In Degradable Polymers and Materials: Principles and Practice (2nd Edition); Khemani, K., et al.;
ACS Symposium Series; American Chemical Society: Washington, DC, 2012.

work has also been completed toward establishing MCL PHA repeating unit control in native PHA producers (*45–47*). These strains are successful in generating MCL PHA homopolymers, but the range of repeating unit sizes is mostly limited to only a couple repeating units per strain or the repeating unit control is lost once the repeating unit size is more than seven carbons. The *E. coli* strain we developed outperformed the modified native PHA-producing strains in MCL PHA repeating unit control. *E. coli* in general may be preferred as a host for PHA synthesis since it does not have regulatory factors in place to alter PHA synthesis gene expression or a PHA depolymerase that can degrade the polymer once it is created. Also, *E. coli* can be easily altered via chromosomal gene knockouts (*21*), which we utilized in development of our new strain (*26*).

Towards the goal of gaining control over repeating unit composition of MCL PHAs, we selected *E. coli* LS5218 as a parent bacterium and used fatty acids as substrates for the PHAs. *E. coli* LS5218 has mutations that enhance its abilities to uptake and degrade fatty acids relative to wild type *E. coli* (*48–51*). We engineered a roadblock into the β-oxidation pathway of this strain by eliminating genes encoding the (*S*)-specific enoyl-CoA hydratase, *fadB*, and its homologue, *fadJ* from the chromosome of *E. coli* LS5218. Eliminating both these genes prevents *E. coli* from growing on fatty acids (*52*). This new strain, *E. coli* LSBJ, readily takes up fatty acids and converts them to enoyl-CoA products but cannot complete β-oxidation. Fatty acid substrates are not degraded in this strain.

Subsequently, an (*R*)-specific enoyl-CoA hydratase (PhaJ4 from *P. putida* KT2440) and PHA synthase (PhaC1(STQK) from *P.* sp. 61-3) with broad substrate specificities were expressed from a plasmid to complete conversion of fatty acids to PHAs (Figure 2) (*26*). The repeating unit composition of the PHAs were then chosen simply by using a fatty acid substrate equal in carbon length. For example, sodium octanoate was converted to poly(3-hydroxyoctanoate). Because of the broad substrate specificities of the PHA synthase and enoyl-CoA hydratase (*25*, *53*), PHA repeating unit control was achieved for 4, 8, 10, 11, and 12 carbon repeating units from fatty acids equal in length (*26*).

This *E. coli* LSBJ system is the first bacterial system to exhibit control over such a large range of PHA repeating units. The system is actually more versatile than what has been published thus far, which consisted of 4, 8, 10, 11, and 12-carbon repeating units. Unpublished data from our lab has demonstrated that 7 and 14 carbon fatty acids can also be converted to PHAs with repeating units equal in length. This spans 3-hydroxyacyl SCL and all 3-hydroxyacyl MCL sized PHA repeating units. An added advantage may be that since the strain is not relying on the fatty acids for growth, the production of PHAs in this organism may not be oxygen dependent and may continue even under anaerobic conditions.

The system we have developed offers enormous potential for expanding the types of PHA polymers that can be synthesized in *E. coli* with control over polymer composition. Copolymers could theoretically be reproducibly synthesized with control over the mole ratio of more than one type or class of repeating units based on the mole ratio of the pertinent substrates. This may open the door for increased control over post-polymerization modifications by controlling the amount of functional groups present in the polymer. There is already work published (*54*) and underway for creating new polymers with

In Degradable Polymers and Materials: Principles and Practice (2nd Edition); Khemani, K., et al.;
ACS Symposium Series; American Chemical Society: Washington, DC, 2012.

biodegradable properties via chemical modification after extraction of PHAs from cells. If a certain PHA polymer composition is desired, this system may be able to synthesize it easily if the equivalent sized fatty acid exists.

Conclusions and Outlook

There are four major factors that must be considered for improving PHA biosynthesis in *E. coli*: selection/development of a strain of *E. coli* for PHA production, the carbon source and how the carbon source is metabolized, the monomer-supplying enzymes used for generating (*R*)-3-hydroxyacyl CoA, and the PHA synthase. We demonstrated the importance of *E. coli* strain selection by using *E. coli* LS5218 for producing a system that can precisely control PHA repeating unit composition from four to twelve carbons (*26*). We improved yield of MCL PHA synthesis from non-related carbon sources to the highest reported for *E. coli* (*36*). We showed that another enzyme (an AlkK homologue) must play a role in production of PHAs using PhaG to produce such a high yield (*36*). We also engineered another monomer-supplying enzyme (FabH) to improve upon its abilities to generate PHA monomers (*27*).

The factor we did not delve into here is in the area of PHA synthases. Although we produced the PHAs in our various studies with an engineered PHA synthase capable of incorporating a very broad range of repeating units into the polymer (*53*), there is still a great deal of other work that can be done in improving PHA synthases and tailoring them to achieve desired results. The same synthase we used here has been further engineered to increase 3HB incorporation into SCL-MCL copolymers without a loss of overall yield (*55*, *56*). Other work has been published that has created PHA synthase chimeras (*57*). These chimeric synthases take advantage of two separate synthases' desirable qualities to generate new, more robust synthases capable of incorporating both SCL and MCL repeating units into PHAs. These engineered PHA synthases with broad substrate specificities are integral to improving PHA production in *E. coli*.

Our work has demonstrated that *E. coli* is an exceptionally useful strain for PHA production. In addition to our work reviewed here, numerous other recent studies have shown the versatility and usefulness of *E. coli* for producing PHA polymers. One of the highlights of using *E. coli* to synthesize PHA polymers is the ability to produce polymers comprised of repeating units that cannot be achieved in native organisms. For the first time, PHA copolymers containing stereospecific repeating units of polylactic acid were synthesized in *E. coli* (*58*, *59*). These polymers have the potential to expand the number of applications for PHAs. Recombinant *E. coli* has also been used as a host strain for the production of poly(2-hydroxypropionate) (P2HP), which was successfully synthesized as a homopolymer for the first time in any biological system without a related precursor (*60*). In addition, *E. coli* can be utilized as a host strain to control the molecular weight of the PHA polymers produced. A recent study by Hiroe, et al, demonstrated that molecular weight and yield of PHA synthesized in *E. coli* can be controlled by specific arrangement of the gene order of PHA synthesis genes in an operon (*61*). These studies demonstrate the power of using recombinant *E. coli*

In Degradable Polymers and Materials: Principles and Practice (2nd Edition); Khemani, K., et al.;
ACS Symposium Series; American Chemical Society: Washington, DC, 2012.

to synthesize PHA polymers. Based on these works, the biological production of plastics continues to expand, and the limits of biodegradable plastic production and application have yet to be reached. Further studies are sure to result in the production of new classes of PHA polymers and copolymers with unique and novel properties.

References

1. How much oil is used to make plastic? - FAQ - U.S. Energy Information Administration (EIA), 2011. http://www.eia.gov/tools/faqs/faq.cfm?id=34&t=6 (accessed Mar. 2, 2012).
2. U.S. Environmental Protection Agency. *MSW Fact Sheet 2010*; 2012; pp 1–12.
3. Lu, J.; Tappel, R. C.; Nomura, C. T. *Polym. Rev.* **2009**, *49*, 226–248.
4. Sudesh, K.; Abe, H.; Doi, Y. *Prog. Polym. Sci.* **2000**, *25*, 1503–1555.
5. Rai, R.; Keshavarz, T.; Roether, J. A.; Boccaccini, A. R.; Roy, I. *Mater. Sci. Eng., R* **2011**, *72*, 29–47.
6. Matsusaki, H.; Abe, H.; Doi, Y. *Biomacromolecules* **2000**, *1*, 17–22.
7. Slater, S. C.; Voige, W. H.; Dennis, D. E. *J. Bacteriol.* **1988**, *170*, 4431–4436.
8. Schubert, P.; Steinbüchel, A.; Schlegel, H. G. *J. Bacteriol.* **1988**, *170*, 5837–5847.
9. Lee, S. Y.; Chang, H. N. *Can. J. Microbiol.* **1995**, *41*, 207–215.
10. Kalousek, S.; Lubitz, W. *Can. J. Microbiol.* **1995**, *41*, 216–221.
11. Wong, H. H.; Lee, S. Y. *Appl. Microbiol. Biotechnol.* **1998**, *50*, 30–33.
12. Hein, S.; Tran, H.; Steinbüchel, A. *Arch. Microbiol.* **1998**, *170*, 162–170.
13. Choi, J. I.; Lee, S. Y.; Han, K. *Appl. Environ. Microbiol.* **1998**, *64*, 4897–4903.
14. Maehara, A.; Ueda, S.; Nakano, H.; Yamane, T. *J. Bacteriol.* **1999**, *181*, 2914–2921.
15. Lee, S. Y.; Choi, J. I.; Han, K.; Song, J. Y. *Appl. Environ. Microbiol.* **1999**, *65*, 2762–2764.
16. Ahn, W. S.; Park, S. J.; Lee, S. Y. *Appl. Environ. Microbiol.* **2000**, *66*, 3624–3627.
17. Taguchi, K.; Aoyagi, Y.; Matsusaki, H.; Fukui, T.; Doi, Y. *Biotechnol. Lett.* **1999**, *21*, 579–584.
18. Nomura, C. T.; Taguchi, K.; Taguchi, S.; Doi, Y. *Appl. Environ. Microbiol.* **2004**, *70*, 999–1007.
19. Valentin, H. E.; Dennis, D. *J. Biotechnol.* **1997**, *58*, 33–38.
20. Wong, M. S.; Causey, T. B.; Mantzaris, N.; Bennett, G. N.; San, K.-Y. *Biotechnol. Bioeng.* **2008**, *99*, 919–928.
21. Datsenko, K. A.; Wanner, B. L. *Proc. Natl. Acad. Sci. U.S.A.* **2000**, *97*, 6640–6645.
22. Fukui, T.; Yokomizo, S.; Kobayashi, G.; Doi, Y. *FEMS Microbiol. Lett.* **1999**, *170*, 69–75.
23. Fiedler, S.; Steinbüchel, A.; Rehm, B. *Arch. Microbiol.* **2002**, *178*, 149–160.

24. Tsuge, T.; Taguchi, K.; Taguchi, S.; Doi, Y. *Int. J. Biol. Macromol.* **2003**, *31*, 195–205.
25. Sato, S.; Kanazawa, H.; Tsuge, T. *Appl. Microbiol. Biotechnol.* **2011**, *90*, 951–959.
26. Tappel, R. C.; Wang, Q.; Nomura, C. T. *J. Biosci. Bioeng.* **2012**, *113*, 480–486.
27. Mueller, A. P.; Nomura, C. T. *J. Biosci. Bioeng.* **2012**, *113*, 300–306.
28. Klinke, S.; Ren, Q.; Witholt, B.; Kessler, B. *Appl. Environ. Microbiol.* **1999**, *65*, 540–548.
29. Rehm, B. H.; Steinbüchel, A. *Appl. Microbiol. Biotechnol.* **2001**, *55*, 205–209.
30. Nomura, C. T.; Tanaka, T.; Gan, Z.; Kuwabara, K.; Abe, H.; Takase, K.; Taguchi, K.; Doi, Y. *Biomacromolecules* **2004**, *5*, 1457–1464.
31. Nomura, C. T.; Taguchi, K.; Gan, Z.; Kuwabara, K.; Tanaka, T.; Takase, K.; Doi, Y. *Appl. Environ. Microbiol.* **2005**, *71*, 4297–4306.
32. Nomura, C. T.; Tanaka, T.; Eguen, T. E.; Appah, A. S.; Matsumoto, K.; Taguchi, S.; Ortiz, C. L.; Doi, Y. *Biotechnol. Prog.* **2008**, *24*, 342–351.
33. Hu, F.; Cao, Y.; Xiao, F.; Zhang, J.; Li, H. *Curr. Microbiol.* **2007**, *55*, 20–24.
34. Sato, S.; Ishii, N.; Hamada, Y.; Abe, H.; Tsuge, T. *Polym. Degrad. Stab.* **2012**, *97*, 329–336.
35. Rehm, B. H. A.; Mitsky, T. A.; Steinbüchel, A. *Appl. Environ. Microbiol.* **2001**, *67*, 3102–3109.
36. Wang, Q.; Tappel, R. C.; Zhu, C.; Nomura, C. T. *Appl. Environ. Microbiol.* **2012**, *78*, 519–527.
37. Davies, C.; Heath, R. J.; White, S. W.; Rock, C. O. *Structure* **2000**, *8*, 185–195.
38. Matsumoto, K.; Murata, T.; Nagao, R.; Nomura, C. T.; Arai, S.; Arai, Y.; Takase, K.; Nakashita, H.; Taguchi, S.; Shimada, H. *Biomacromolecules* **2009**, *10*, 686–690.
39. Rehm, B. H.; Krüger, N.; Steinbüchel, A. *J. Biol. Chem.* **1998**, *273*, 24044–24051.
40. Zheng, Z.; Zhang, M.; Zhang, G.; Chen, G. *Anton. Leeuw. Int. JG* **2004**, *85*, 93–101.
41. Zheng, Z.; Gong, Q.; Liu, T.; Deng, Y.; Chen, J. C.; Chen, G. Q. *Appl. Environ. Microbiol.* **2004**, *70*, 3807–3813.
42. Satoh, Y.; Murakami, F.; Tajima, K.; Munekata, M. *J. Biosci. Bioeng.* **2005**, *99*, 508–511.
43. Fukui, T.; Shiomi, N.; Doi, Y. *J. Bacteriol.* **1998**, *180*, 667.
44. Rai, R.; Yunos, D. M.; Boccaccini, A. R.; Knowles, J. C.; Barker, I. A.; Howdle, S. M.; Tredwell, G. D.; Keshavarz, T.; Roy, I. *Biomacromolecules* **2011**, *12*, 2126–2136.
45. Wang, H.-H.; Li, X.-T.; Chen, G.-Q. *Process Biochem.* **2009**, *44*, 106–111.
46. Liu, Q.; Luo, G.; Zhou, X. R.; Chen, G.-Q. *Metab. Eng.* **2010**, 1–7.
47. Wang, H.-H.; Zhou, X. R.; Liu, Q.; Chen, G.-Q. *Appl. Microbiol. Biotechnol.* **2010**, *89*, 1497–1507.
48. Rhie, H. G.; Dennis, D. *Appl. Environ. Microbiol.* **1995**, *61*, 2487.

49. DiRusso, C. C.; Heimert, T. L.; Metzger, A. K. *J. Biol. Chem.* **1992**, *267*, 8685–8691.
50. Spratt, S. K.; Ginsburgh, C. L.; Nunn, W. D. *J. Bacteriol.* **1981**, *146*, 1166.
51. Jenkins, L. S.; Nunn, W. D. *J. Bacteriol.* **1987**, *169*, 42.
52. Campbell, J. W.; Morgan-Kiss, R. M.; Cronan, J. E., Jr. *Mol. Microbiol.* **2003**.
53. Takase, K.; Taguchi, S.; Doi, Y. *J. Biochem.* **2003**, *133*, 139–145.
54. Scholz, C. *Appl. Microbiol. Biotechnol.* **2010**, *88*, 829–837.
55. Shozui, F.; Matsumoto, K.; Sasaki, T.; Taguchi, S. *Appl. Microbiol. Biotechnol.* **2009**, *84*, 1117–1124.
56. Shozui, F.; Sun, J.; Song, Y.; Yamada, M.; Sakai, K.; Matsumoto, K.; Takase, K.; Taguchi, S. *Biosci. Biotechnol. Biochem.* **2010**, *74*, 1710–1712.
57. Matsumoto, K.; Takase, K.; Yamamoto, Y.; Doi, Y.; Taguchi, S. *Biomacromolecules* **2009**, *10*, 682–685.
58. Taguchi, S.; Yamada, M.; Matsumoto, K.; Tajima, K.; Satoh, Y.; Munekata, M.; Ohno, K.; Kohda, K.; Shimamura, T.; Kambe, H.; Obata, S. *Proc. Natl. Acad. Sci. U.S.A.* **2008**, *105*, 17323–17327.
59. Yang, T. H.; Kim, T. W.; Kang, H. O.; Lee, S.-H.; Lee, E. J.; Lim, S.-C.; Oh, S. O.; Song, A.-J.; Park, S. J.; Lee, S. Y. *Biotechnol. Bioeng.* **2010**, *105*, 150–160.
60. Andreessen, B.; Lange, A. B.; Robenek, H.; Steinbüchel, A. *Appl. Environ. Microbiol.* **2010**, *76*, 622–626.
61. Hiroe, A.; Tsuge, K.; Nomura, C. T.; Itaya, M.; Tsuge, T. *Appl. Environ. Microbiol.* **2012**.

Chapter 10

Bacterial Poly(β-hydroxybutyrate): Hydrophilized and Colored

K. Busse,[1] H. Budde,[1] C. Scholz,[2] and J. Kressler[1,*]

[1]Department of Engineering Science, Martin-Luther-University Halle-Wittenberg, D-06099 Halle (Saale), Germany
[2]Department of Chemistry, University of Alabama in Huntsville, Huntsville, AL 35899, USA
[*]joerg.kressler@chemie.uni-halle.de

This study describes the synthesis and investigation of the physical properties of hydrophilized and colored poly(β-hydroxybutyrate) (PHB) copolymers obtained by modulated fermentation of *Azotobacter vinelandii UWD* and *Wautersia eutropha*. During fermentation, poly(ethylene glycol) (PEG), di(ethylene glycol) (DEG), pentaerythritol ethoxylate (PEE) and ethoxylated anthraquinone dye were used to modulate the bacterial synthesis of PHB. Small-angle X-ray scattering (SAXS) showed that lamellar distances decreased for modulated PHB when compared to neat PHB. Furthermore, the contact angle of water on the PHB/PEG or PHB/DEG polymer surfaces decreased when compared to that of PHB, which corresponds to an increase in surface tension, and therefore to hydrophilization. The ethoxylated anthraquinone dye (alizarin) was chemically linked to the PHB chain and led to a change of the color from white to yellow or orange, depending on the pH-value of the environment.

Poly(β-hydroxyalkanoate)s, PHAs, the term is generally reserved for microbial polyesters, are a family of biopolyesters with varying side-chain lengths. PHAs were shown to be biocompatible, in particular in the realm of treatment of bone related deseases. Poly(β-hydroxybutyrate), PHB, is the most widely investigated PHA and has been studied for a variety of bone-replacement

In Degradable Polymers and Materials: Principles and Practice (2nd Edition); Khemani, K., et al.;
ACS Symposium Series; American Chemical Society: Washington, DC, 2012.

applications (*1–5*). However, due to its hydrophobicity, PHB is not blood compatible and the exposure of blood to PHB-surfaces leads to platelet adhesion and subsequent thrombi formation (*6*). It has been shown, that end-capping a growing PHB-chain with PEG will increase the surface tension of bulk samples (*7*). These PEGylated PHAs are potential candidates for many medical applications (*8*). PEG is able to penetrate the cell walls of polyester-producing microorganisms and in small concentration (below 10%) does not deter their growth. PEG-modulated fermentation has been shown in the past to produce natural-synthetic hybrid block copolymers (*9–12*). The microorganisms carry out the PEG-ylation of nascent PHB chains via a competition reaction at the active site of the polymerase enzyme, thus guaranteeing the formation of PHB and its subsequent end-capping with PEG (*13*). PHB is isotactic and the *R*-configuration is known to be responsible for the bone-compatibility (*14*, *15*). Pentaerythritol ethoxylate (PEE) is structurally rather similar to PEG, and can be regarded as a starlike PEG oligomer (Fig. 1), it can also be used for modified fermentation (*16*).

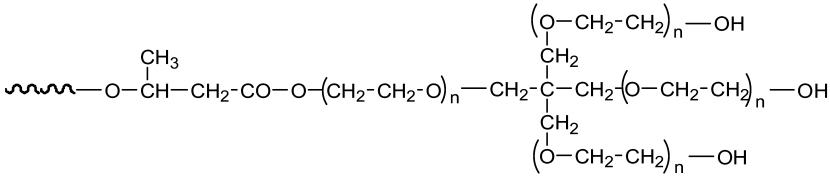

Figure 1. Pentaerythritol ethoxylate, a starlike PEG oligomer linked to PHB via ester bond

The present study focuses on elucidating and quantifying the physical changes in the polymers that were induced by the PEG-modulation of the PHB-synthesis. Several microbes are known to form PEGylated PHAs (*17*). PEG is a polyether that is known for its exceptional blood and tissue compatibility, it is used extensively as stealth material in a variety of drug delivery vehicles and is also under investigation as surface coating for biomedical implants. PEG, when dissolved in water, has a low interfacial free energy, exhibits rapid chain motion, and its large excluded volume leads to steric repulsion of approaching molecules (*18*, *19*). These properties are responsible for the superb biocompatibility of PEG. However, PEG is not a thermoplastic material and therefore not moldable. A PEG-modified alizarin dye is used for modulated fermentation in order to synthesize colored bacterial PHB. Colored PHB might replace normal PHB in fields where pH sensitivity is required or when absorption in the range of visible light is preferred. Furthermore, it should be mentioned that modeling approaches

In Degradable Polymers and Materials: Principles and Practice (2nd Edition); Khemani, K., et al.;
ACS Symposium Series; American Chemical Society: Washington, DC, 2012.

are increasingly important for the microbial production of tailor-made PHBs, and PHB's carrying a color tag could be of significance for these studies (*20*).

In previous works, PEG-modified fermentations of *Wautersia eutropha* (syn. *Alcaligenes eutrophus,* ATCC 17697) and *Azotobacter vinelandii UWD* (ATCC 53799) were conducted and PHB was end-capped with diethyleneglycol (DEG), pentaerythritol ethoxylate (PEE, molecular weigth 270 and 800 g/mol), and PEG's of varying molecular weight (400, 2000 and 3400 g/mol PEG) (*7*, *13*, *15*). These polymers were characterized for their molecular weight by GPC, static light scattering, and viscometry. In addition, the chemical structure of the polymer was characterized by ^{1}H-NMR and heteronuclear multiple bond correlation (HMBC) spectroscopy. The results verified a covalent bond for the PHB/DEG copolymers. In subsequent cell adhesion experiments, it was shown that the naturally hydrophobic PHB-surface could be modified to a more cell-deterring surface by modification with PEG of varying molecular weights. Contact angles of PHB, PHB/DEG, and PHB/PEG block copolymers with water were compared. Wide angle X-ray scattering (WAXS) studies of PHB have shown the chains to be in a helical conformation (whether right or left-handed is still debatable) (*21–23*). PHB has lath-shaped lamellar crystals, meaning they are folded chain crystals in which the fiber axis is normal to the lamellar surface (*24*). This is a common feature of crystalline morphology, especially when the polymer is precipitated from dilute solution (*25*). PHB has a great propensity for assuming this lamellar morphology and is therefore a prime candidate for identification studies (*26*, *27*). It is this definitive nature of PHB that allowed for X-ray comparison studies using small angle X-ray scattering (SAXS) to determine the interplane or lamellar distance. The dye modified PHB was analyzed by UV-Vis spectroscopy and colored bulk samples were produced.

Experimental Section

Materials

PEGs of different molecular weight (400, 2000 and 3400 g/mol) were used as received. PEEs of different molecular weight (270 and 800 g/mol) were purchased from Sigma Aldrich and used as received.

The ethoxylated dye was synthesized anionically from alizarin dye according to the following reaction scheme (Figure 2) in a pressurized steel reactor. After chromatographic purification from side products using a silica gel column, the structure of the dye was confirmed by NMR spectroscopy (500 MHz Varian Unity Inova, using $CDCl_3$ as solvent at 25°C). and the molecular weights were measured by GPC. α-hydroxy-β-hydroxy-oligoethoxy anthraquinone (eth. dye; Fig. 2 b) is formed as the main product, since the OH group at β-position is most acidic and can readily be transformed to the alcoholate. As a side product, α,β-hydroxy-oligoethoxy anthraquinone (Fig. 2 c) can be observed, whereas α-hydroxy-oligoethoxy,β-hydroxy anthraquinone (Fig. 2 d) is not formed.

In Degradable Polymers and Materials: Principles and Practice (2nd Edition); Khemani, K., et al.;
ACS Symposium Series; American Chemical Society: Washington, DC, 2012.

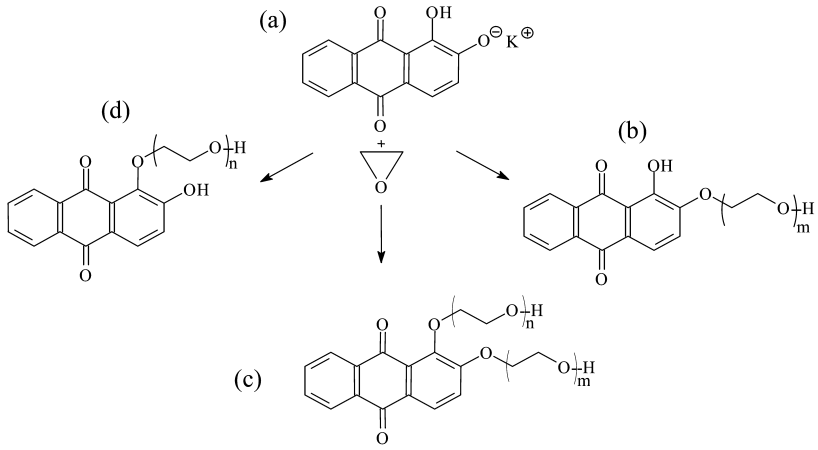

Figure 2. Formation of various ω-hydroxy-oligoethoxy-9,10-anthraquinones (b-d) from 1,2-dihydroxy-9,10-anthraquinone potassium salt(a)

Synthesis of Block Copolymers

A. vinelandii UWD and *W. eutropha* were grown in a two-step process, employing a pre-culture and a polymer-producing medium. For PEG and DEG modulated fermentations, *A. vinelandii UWD* was used. Fermentation experiments were conducted in a shaker-incubator (New Brunswick Scientific) at 30 °C and 180 rpm. After 48 h of growth, 10 vol.% of a pre-culture were used as inoculum for the polymer medium (*35*), and cells were harvested after 24 h by centrigugation (*13*). Both media were amended with 2.0 wt % of the respective PEGs. It is noteworthy that *A. vinelandii UWD* must be grown in the presence of 20 mg/L rifampicin, in order to prevent the back mutation of the engineered strain to the *A. vinelandii UW* parental strain genotype, which does not produce polymer and is not resistant to the antibiotic (*13*). The polymer was extracted from the dry cell mass by refluxing for 8 h with methylene chloride, concentrating the solution in a rotary evaporator, and precipitating the polymer into chilled methanol. After collecting by filtration and drying under vacuum, the polymer was purified by recrystallization, i.e. redissolving in methylene chloride, concentrating, and precipitating into chilled methanol (*15*). The hydrophilic PEG and DEG are expected to wash out of the polymer if they were not covalently linked.

For PEE and dye modulated fermentation, *W. eutropha* was used. Five cultures of 50 mL were prepared in 200 mL shake flasks for the inoculation. The cultures grew for 5 h. These pre-cultures were used as inoculum for batch fermentation with an initial volume of 4 L. A specific culture broth formulation was used: 20 g/L fructose, 6.7 g/L $Na_2HPO4 \cdot 7H_2O$, 2 g/L $(NH_4)_2SO_4$, 1.5 g/L $MgSO_4 \cdot 7H_2O$, 6 mg/L KH_2PO_4, 7.5 mg/L Fe(NH_4)citrate, 7.5 mg/L $CaCl_2$. All broth formulations were prepared in deionized water. The pH was kept constant at 7.0 by continuously adding aqueous ammonia (20 wt %) solution and 1 M H_3PO_4 at a temperature of 30 °C. The growth of *W. eutropha* was initiated in a fermenter Biostat C in nutrient-rich broth under aerobic conditions for 24 h. The cells were

In Degradable Polymers and Materials: Principles and Practice (2nd Edition); Khemani, K., et al.;
ACS Symposium Series; American Chemical Society: Washington, DC, 2012.

then harvested aseptically by centrifugation (5900g, 10 min). Typically, the cell dry mass (CDM) of the first-stage *W. eutropha* cultivations was approximately 9 g/L. The cells were aseptically transferred into four fermenters (Sixfors) containing 400 mL of nitrogen-free broth and 30 g/L sterile fructose as the polymer-producing substrate with different amounts of PEE and of ethoxylated anthraquinone dye. The organisms were cultivated at 30 °C and a pH value of 7.0. At the end of the fermentations, the cells were separated, washed with deionized water, and freeze dried. The CDM (approximately 8 g) was then extracted with 250 mL of methylene chloride, and the polymers were recovered by precipitation in an excess of cooled methanol, filtration, and drying.

The characteristics of the samples investigated are given in Table I.

Table I. Description of Investigated Samples.

Sample (abbrev)	*Sample*	*M_w by GPC [kg/mol]*
PHB-1	PHB (*A. vinelandii UWD*)	630
DEG	PHB-1 + DEG	650
PEG4	PHB-1 + PEG 400	140
PEG20	PHB-1 + PEG 2000	n.d.[a]
PEG34	PHB-1 + PEG 3400	500
PHB-2	PHB (*W. eutropha*)	1220
PEE-270	PHB-2 + 2 vol% PEE (270 g/mol)	500
PEE-270b	PHB-2 + 5 vol% PEE (270 g/mol)	260
PEE-800	PHB-2 + 2 vol% PEE (800 g/mol)	890
eth. dye	α-hydroxy-β-hydroxyethyl-oligoethoxy anthraquinone	0.8
Col.-PHB	PHB-2 + ethoxylated anthraquinone dye	100

[a] n.d.: not determined

Polymer Analyses

The chemical structure of the biopolymers was determined by nuclear magnetic resonance spectrometry. Molecular weights of the polymers were determined by gel permeation chromatography (GPC) in chloroform using a Biorad system equipped with a Styragel HR4E column (Waters). The molecular weight data obtained by GPC were verified by static light scattering using a He-Ne laser with a wavelength of 632.8 nm and by viscometry using a Cannon-Ubbelohde viscometer. Samples were dissolved in chloroform with concentrations ranging between 0.1 and 2.5 mg/mL and solution flow times were

In Degradable Polymers and Materials: Principles and Practice (2nd Edition); Khemani, K., et al.;
ACS Symposium Series; American Chemical Society: Washington, DC, 2012.

recorded to the nearest 0.01 s. Molecular weights were determined using the Kuhn-Mark-Houwink formula with K = 7.7 x 10^{-3} mL/g and α = 0.82 (*28*).

SAXS data for PEG and DEG modified PHBs were obtained in the θ range of 0.2-5° from measurements with a two-dimensional (2D) detector (SIEMENS HI star) installed on a rotating anode (Rigaku) X-ray instrument with fine focus source. SAXS measurements for PEE modified PHB were performed in a Kratky camera (Anton Paar). The PEE modified samples were isothermally crystallized at 140 °C for 1 week. The SAXS data are background corrected and Fourier transformed to obtain the one dimensional correlation function. The PHB crystallinity was determined by wide-angle X-ray scattering (WAXS) using a Rigaku RU-200 (50kV/180mA) in the θ range of 5-50°.

The AFM experiments were carried out using a Nanoscope IIIa (Digital Instruments). The dried material was pressed between cover glasses on a hot stage, annealed at 180 °C for several minutes and rapidly quenched to the crystallization temperature of 140 °C. After the crystallization was completed, the samples were placed in distilled water in order to remove the cover glass from the film surface.

The light microscope was equipped with a hot stage for isothermal annealing experiments. Photographs of spherulites were taken after isothermal crystallization at 130 °C.

The contact angles were measured using the sessile drop method on a polymer film. The films were obtained by dissolving the polymers in methylene chloride (~ 2 wt.% solution), putting drops of the solution on a glass slide, and then spinning the slide using a Micro-Bit (Model PWM32) for 30 sec at 2000 rpm. This provided a uniform and thin polymer surface suited for contact angle analysis. A drop of 30 µl of freshly bidistilled water was placed on each sample. The sessile drop analyses were performed with an OCA 20 (DataPhysics Instruments GmbH) contact angle instrument, employing both digital imaging and drop-shape analysis. The advancing contact angle was measured for 8 drops on both sides at a temperature of 20°C and the average was calculated from the data. In this study, the surface tension or free energy (γ) is calculated from the contact angle (θ) using an iterative method due to Li and Neumann (*29*, *30*), based on results of Good and Girifalco (*31*).

UV-Vis spectra were obtained using a Cary 5000 spectrometer (Varian). The samples were dissolved in chloroform.

Results and Discussion

The modification of PHB during fermentation is frequently carried out using PEG-like oligomers, since OH containing molecules terminate the polymerization reaction and the terminating reagent can be covalently incorporated into the polymer chain. Thus, it seems reasonable, that an ethoxylated dye will lead to colored PHB when used as terminating reagent during fermentation.

Figure 3 shows the ^{1}H-NMR spectra of initial alizarin and its oligoethoxylated product, eth. dye. From the broadening and appearance of additional peaks, it can be concluded, that the ethoxylation was successful.

In Degradable Polymers and Materials: Principles and Practice (2nd Edition); Khemani, K., et al.;
ACS Symposium Series; American Chemical Society: Washington, DC, 2012.

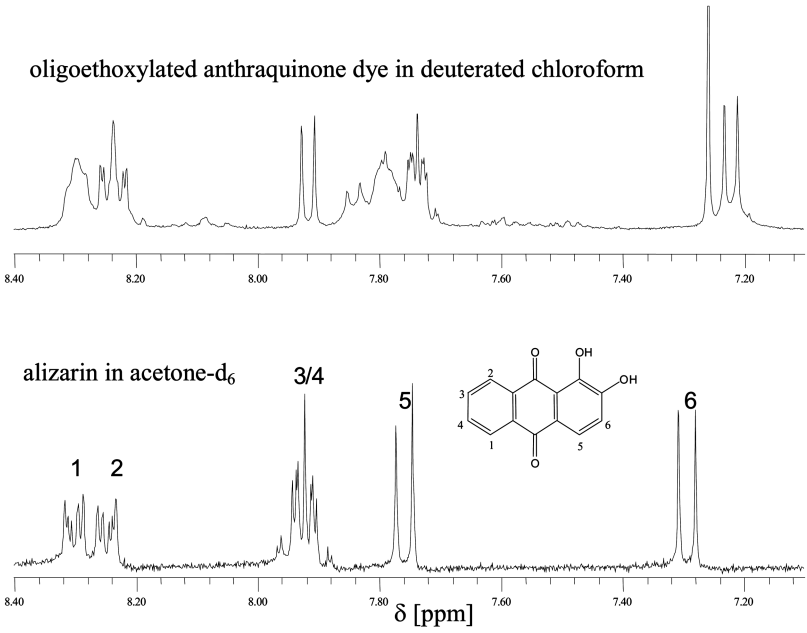

Figure 3. [1]H-NMR-spectroscopy of eth.-dye in deuterated chloroform (top) and original alizarin dye in deuterated acetone (bottom)

A characteristic [1]H NMR spectrum of the PEE-modified PHBs is shown in Figure 4. The sample PEE-270b showed the characteristic peaks of PHB, and additionally signals indicating the presence of covalently bound PEE were observed. Signals in the range of 3.6 ppm (inset a) were caused by the methylene protons of PEE, and the signal at 4.25 ppm (inset b) can unambiguously assigned to the methylene protons adjacent to the ester group that linked the PHB terminal carboxyl group to the PEE moiety (*11*). Similar NMR spectra were observed for the other modified PHB samples. Additional information on the spectroscopic analysis of these copolymers, especially two-dimensional HMBC spectra has been provided previously (*13*).

As described in the experimental part, one fermentation of PHB in the presence of eth. dye was carried out. After extensive purification of the polymer, by dissolution and precipitation processes, it can be assumed, that the original eth. dye was completely removed. Nevertheless, the polymer remained yellow in color after precipitation. This is also demonstrated in the UV-Vis spectrum, depicted in Figure 5.

When the pH value of the environment is changed to larger than 7, the polymer changes its color to red. This is the typical behavior of alizarin obviously maintained when the dye is covalently attached to PHB via the oligoethylene oxide spacer.

In Degradable Polymers and Materials: Principles and Practice (2nd Edition); Khemani, K., et al.;
ACS Symposium Series; American Chemical Society: Washington, DC, 2012.

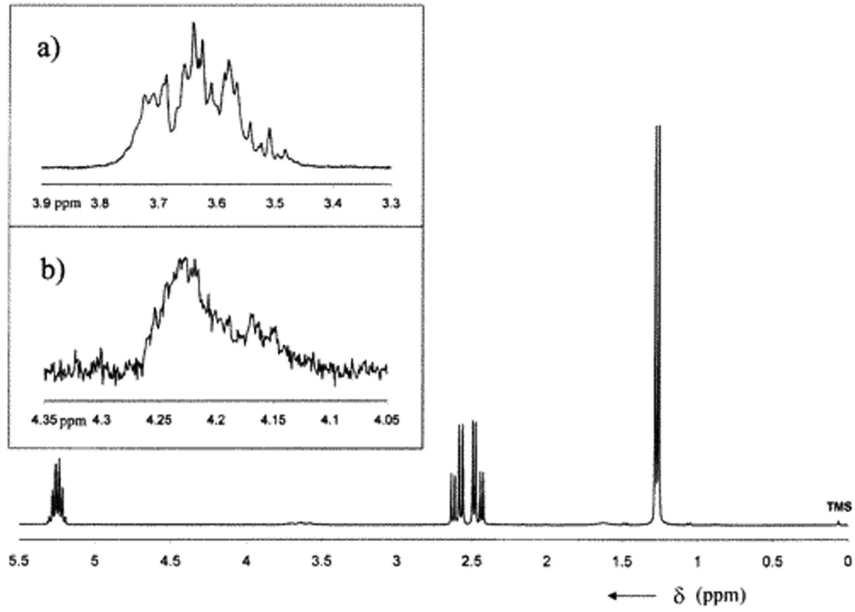

Figure 4. [1]H NMR spectrum of PEE-modified PHB. The insets show the region of the methylene protons of PEE (a) and the methylene protons indicating the ester linkage between PEE and PHB (b). (Reproduced from reference (16)).

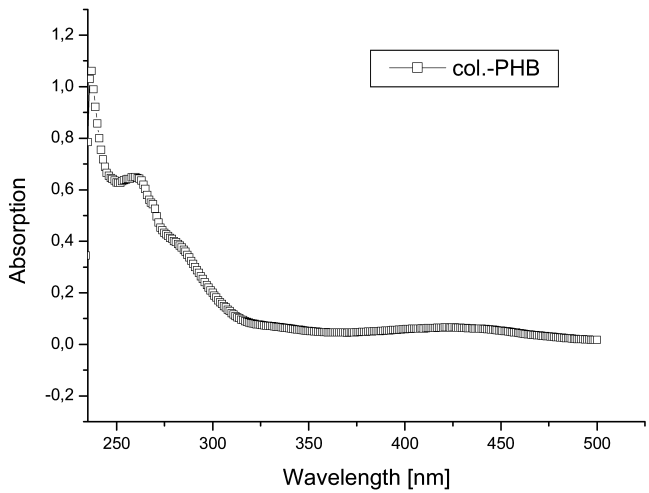

Figure 5. UV-Vis spectrum of colored PHB dissolved in chloroform

In Degradable Polymers and Materials: Principles and Practice (2nd Edition); Khemani, K., et al.;
ACS Symposium Series; American Chemical Society: Washington, DC, 2012.

During PHB crystallization, the attached end units cannot be included into the crystal lattice of PHB. Thus, PEG, DEG or PEE moieties are enriched in the amorphous phase of the lamella staples. Observing the initiation and growth of PHB-2 and PEE modified PHB spherulites, differences in the crystallization behaviour were detected. Whilst the spherulite growth rate *R* was comparable for all samples, i.e. the expelling of PEE from the crystalline phase did not hinder the spherulite growth, the sphrulite initiation time was different. Spherulites of PEE-270, PEE-270b, and PEE-797 were observed immediately after starting the measurement, i.e. immediately after reaching the crystallization temperature between 120 and 140 °C. Initial spherulites in neat PHB-2 appeared later, in case of a crystallization temperature of 130 °C, a delay of 800 sec was observed. This effect can be explained by a nucleating effect of the incorporated PEE.

These results were supported by the fact that after isothermal crystallization at 120 °C PEE-270b had clearly the highest degree of crystallinity for PEE modified PHB (58%) and even higher than the crystallinity of neat PHB-2, crystallized at this temperature. Again, this indicated the nucleating effect of the PEE units incorporated into the polyester. On the other hand, after crystallization from solution of PHB-1 and PEG and DEG modified samples, the neat PHB-1 samples have shown the highest crystallinity (~80%) and the modified ones are slightly lower in crystallinity. The reason can be found in the higher amount of amorphous matter in the modified samples due to their PEG and DEG parts.

The desmeared SAXS data of PEE modified PHB are depicted in Figure 6. Generally, the scattering trace can be assigned to a lamellar system with first and higher order reflections. The first maximum at q^* can be used for the calculation of the long period L_p using the Bragg relation ($L_p = 2\pi/q^*$) where q^* is the scattering vector at the first maximum. According to the measurements, L_p decreased with the amount of PEE incorporated into the polymer. PHB-2 had a long period of 11.6 nm, PEE-270 and PEE-797 had a value of 11.2 nm, and the long period of PEE-270b was 10.8 nm.

Observing the crystallization process in a polarized light microscope, in neat PHB samples only unstructured spherulites can be seen, whereas the copolymers show the occurrence of banded spherulites as a microstructure (Figure 7a) (*15*). The twist-banding of lamellar ribbon crystals caused by chainfolding in different directions on opposite faces of the lamellae (*32*) typically leads to band spacings of 10 μm or more in the temperature range under investigation. Therefore, the neat PHB sample seems to be unstructured as the band spacing is larger than the observed spherulite radius. The occurrence of banded spherulites with a typical band spacing of 3 μm in the case of the copolymers is therefore caused by the non-crystallizable PEE polymer units that force the lamellae to bend (*33*). The periodicity of the rings in the banded spherulites can be related to the amount of impurities of excluded polymer units. In AFM measurements after isothermal crystallization at 140 °C (Figure 7b) staples of lamellae can be observed. Obviously, the growth of lamellae is stopped by visible spherical entities. This might be the reason for the initiation of the bending process.

In Degradable Polymers and Materials: Principles and Practice (2nd Edition); Khemani, K., et al.;
ACS Symposium Series; American Chemical Society: Washington, DC, 2012.

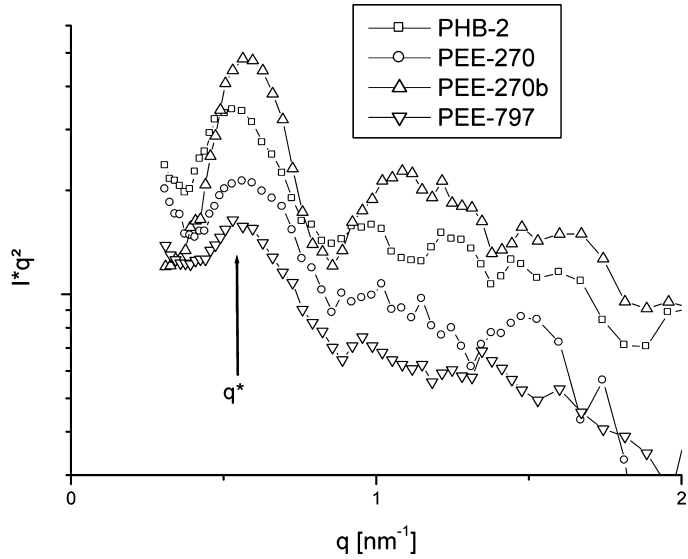

Figure 6. SAXS measurements of PHB-2 and PEE modified samples iso-thermally crystallized at 140 °C for 8 days.

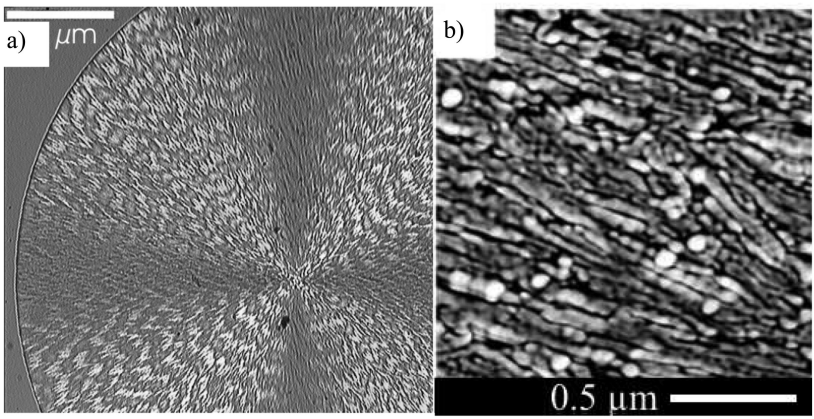

Figure 7. PEE-270b isothermally crystallized at 130 °C observed by polarized light microscopy (a) and crystallized at 140 °C observed by AFM (b) (15)

In surface tension studies the contact angles for sessile drops of water on the PHB, PHB/DEG, and PHB/PEG surfaces were determined (Table II). As expected, the contact angle for the hydrophobic PHB was with 89° the highest. Contact angles for the PHB/DEG and PHB/PEG were expected to be decreased due to the hydrophilic modification with PEG and DEG, respectively. The modified samples with higher masses, DEG and PEG 3400, show a significantly stronger decrease

In Degradable Polymers and Materials: Principles and Practice (2nd Edition); Khemani, K., et al.;
ACS Symposium Series; American Chemical Society: Washington, DC, 2012.

in contact angle (~76°), compared to the lower mass sample, PEG 400 with 83.4°. The surface tension γ_{sv} was calculated via Neumann iteration (*26*) from the contact angles. PHB has the lowest surface tension with a 29.8 mN/m value and the PHB/DEG and PHB/PEG samples ranged from 33 – 38 mN/m.

Table II. Water contact angle and surface tension of some samples. Data are taken from Ref. (*7*).

Sample	*Contact angle* θ *[°]*	*error*	*Surface tension* γ_{sv} *[mN/m]*
PHB-1	89.0	± 0.9	29.8
DEG	75.7	± 0.8	38.2
PEG4	83.4	± 0.7	33.4
PEG34	76.0	± 1.1	38.0

Summary

The reaction between the alizarin mono potassium salt and ethylene oxide gave α-hydroxy-β-hydroxy-oligoethoxy anthraquinone as main product and α,β-hydroxy-oligoethoxy anthraquinone as side product. The content of PEG with anthraquinone end groups as segment in poly(β-hydroxybutyrate) was qualitatively confirmed by UV-Vis spectroscopy. Thus it is possible to synthesize colored PHB during the fermentation process, without the need for a polymer-analogous reaction. It is suggested that colored PHB could also be applied where photodegration is important (*34*). Using PEG-like oligomers in modulated fermentation leads to PHBs with improved wettability and thus better properties for many biomedical applications, especially in the field of bone replacement.

Acknowledgments

We gratefully acknowledge the German Academic Exchange Service (DAAD), Deutsche Forschungsgemeinschaft (DFG, SFB 418), and VolkswagenStiftung (AZ: 77742) for financial support.

References

1. Gogolewski, S.; Jovanovich, M.; Perren, S. M.; Dillon, J. G.; Hughes, M. K. *J. Biomed. Mater. Res.* **1993**, *27*, 1135–1148.
2. Doyle, C.; Tanner, E. T.; Bonfield, W. *Biomaterials* **1991**, *12*, 841–847.
3. Yagmurlu, M. F.; Korkusuz, F.; Gürsel, I.; Korkusuz, P.; Örs, Ü.; Hasirci, V. *J. Biomed. Mater. Res.* **1999**, *46*, 494–503.
4. Sendil, D.; Gursel, I.; Wise, D. L.; Hasirci, V. *J. Controlled Release* **1999**, *59*, 207–217.

5. Scholz, C. In *Polymers from Renewable Resources - Biopolyesters and Biocatalysis*; Scholz, C., Gross, R. A., Eds.; ACS Symposium Series 764; American Chemical Society: Washington, DC, 2000; 328−334.
6. van der Giessen, W. J.; Lincoff, A. M.; Schwartz, R . S.; van Beusekom, H. M.; Serruys, P. W.; Holmes, D. R., Jr.; Ellis, S. G.; Topol, E. J. *Circulation* **1996**, *94*, 1690–1697.
7. Townsend, K. J.; Busse, K.; Kressler, J.; Scholz, C. *Biotechnol. Prog.* **2005**, *21*, 959–964.
8. Hazer, B. *Int. J. Polym. Sci.* **2010**, Article ID 423460.
9. Ashby, R. D.; Shi, F.; Gross, R. A. *Biotechnol. Bioeng.* **1999**, *62*, 106–113.
10. Shi, F.; Ashby, R.; Gross, R. A. *Macromolecules* **1996**, *29*, 7753–7758.
11. Shi, F.; Gross, R. A.; Rutherford, D. R. *Macromolecules* **1996**, *29*, 10–17.
12. Shi, F.; Scholz, C.; Deng, F.; Gross, R. A. *Polym. Prepr.* **1998**, *39* (2), 102–103.
13. Zanzig, J.; Scholz, C. *J. Polym. Environ.* **2003**, *11*, 145–154.
14. Doyle, C.; Tanner, E. T.; Bonfield, W. *Biomaterials* **1991**, *12*, 841–847.
15. Holland, S. J.; Yasin, M.; Tighe, B. J. *Biomaterials* **1990**, *11*, 206–215.
16. Jenzsch, M.; Volk, N.; Kressler, J.; Scholz, C. *Biomacromolecules* **2001**, *2*, 1055–1060.
17. Foster, L. J. R. *Appl. Microbiol. Biotechnol.* **2007**, *75*, 1241–1247.
18. Lee, J. H.; Andrade, J. D. In *Polymer Surface Dynamics*; Andrade, J. D., Ed.; Plenum Publishing Press: New York, NY, 1988; pp 119−136.
19. Lee, J. H.; Kopecek, J.; Andrade, J. D. *J. Biomed. Mater. Res.* **1989**, *23*, 351–368.
20. Penloglou, G.; Chatzidoukas, C.; Kiparissides, C. *Biotechnol. Adv.* **2012**, *30*, 329–337.
21. Okamura, K.; Marchesaault, R. H. In *Conformation of Biopolymers*; Ramachandran, G. M., Ed.; Academic Press: New York, NY, 1967; Vol. 2; pp 709−720.
22. Cornibert, J.; Marchessault, R. H. *J. Mol. Biol.* **1972**, *71*, 735.
23. Yokouchi, M.; Chatani, Y.; Tadokoro, H.; Teranishi, K.; Tani, H. *Polymer* **1973**, *14*, 267.
24. Alper, R.; Lundgren, D. G.; Marchessault, R. H.; Cote, W. A. *Biopolymers* **1963**, *1*, 545.
25. Geil, P. H. *Polymer Single Crystals*; Wiley: New York, NY, 1963.
26. Lundgren, D. G.; Alper, R.; Schnaitman, C.; Marchessault, R. H. *J. Bacteriol.* **1965**, *89*, 245.
27. Barham, P. J.; Selwood, A. U.S. Patent 4,391,766, 1983.
28. *Polymer Handbook*; Mark, J. E., Ed.; Oxford University Press: New York, NY, 1999.
29. Li, D.; Neumann, A. W. *J. Colloid Interface Sci.* **1990**, *137*, 304.
30. Grundke, K.; Bogumil, T.; Gietzelt, T.; Jacobasch, H.-J.; Kwok, D. Y.; Neumann, A. W. *Prog. Colloid Polym. Sci.* **1996**, *101*, 58–68.
31. Girifalco, L. A.; Good, R. J. *J. Phys. Chem.* **1957**, *61*, 904–909.
32. Owen, A. J. *Polymer* **1997**, *38*, 3705–3708.
33. Wang, C.; Thomann, R.; Kressler, J.; Craemer, K.; Stuehn, B.; Svoboda, P.; Inoue, T. *Acta Polym.* **1997**, *48*, 354–362.

34. Sadi, R. K.; Fechine, G. J. M.; Demarquette, N. R. *Polym. Degrad. Stab.* **2010**, *95*, 2318–2327.
35. Chen, G.; Page, WJ *Biotechnol. Tech.* **1997**, *11*, 347.

Chapter 11

Physical Properties, Structure Analysis, and Enzymatic Degradation of Poly[(*R*)-3-hydroxybutyrate-*co*-(*R*)-3-hydroxyvalerate] Films and Fibers

Toshihisa Tanaka[1] and Tadahisa Iwata[2,*]

[1]Faculty of Textile Science and Technology, Shinshu University, 3-15-1 Tokida, Ueda-shi, Nagano 386-8567, Japan
[2]Graduate School of Agricultural and Life Sciences, The University of Tokyo, 1-1-1 Yayoi, Bunkyo-ku, Tokyo 113-8657, Japan
[*]atiwata@mail.ecc.u-tokyo.ac.jp

High tensile strength films and fibers of poly[(*R*)-3-hydroxybutyrate-*co*-8mol%-(*R*)-3-hydroxyvalerate] were prepared by cold-drawing from amorphous preforms at a temperature near the glass transition temperature (T_g). High tensile strength fibers of over 1 GPa were processed by one-step-drawing with small crystal nuclei grown near T_g. Melt-quenched films in a rubber state could be stretched reproducibly to a draw ratio of 16, and subsequent annealing under tension led to the improvement of the tensile strength and Young's modulus. The highly-ordered structure of films and fibers was investigated by wide- and small-angle X-ray diffractions, and X-ray tomography in synchrotron radiation of SPring-8. The mechanical properties remained unchanged after storing for 6 months at room temperature, suggesting that a high crystallnity of the stretched-annealed films avoids a process of secondary crystallization. Cold-drawn films were enzymatically degraded with an extracellular PHB depolymerase purified from *Ralstonia pickettii* T1, and it was revealed that the stretched films had the shish-kebab structure.

In Degradable Polymers and Materials: Principles and Practice (2nd Edition); Khemani, K., et al.;
ACS Symposium Series; American Chemical Society: Washington, DC, 2012.

Poly[(*R*)-3-hydroxybutyrate-*co*-(*R*)-3-hydroxyvalerate] (P(3HB-*co*-3HV)) is accumulated by a wide variety of microorganisms as intracellular carbon and energy storage material, and has been extensively studied as a biodegradable and biocompatible thermoplastics (*1*, *2*). P(3HB-*co*-3HV) is successful copolyester, which has been produced commercially under the trade name of Biopol™. While P(3HB-*co*-3HV) has attracted much attention as textile products such as fishing line or surgical suture, etc., it has not been recognized as practical because of its stiffness and brittleness (*3*). Furthermore, P(3HB-*co*-3HV) is a relatively unusual copolymer because 3HB and 3HV units are isodimorphous, that is, due to their similarity in shape and size, the 3HV units are incorporated into poly[(*R*)-3-hydroxybutyrate] (P(3HB)) crystal lattice (*4*).

Recently, we succeeded in obtaining strong fibers and films from P(3HB) and its copolymers by hot-drawing and cold-drawing techniques (*5*–*15*). The structure of P(3HB) fibers with high tensile strength of 1.32 GPa was analyzed by micro-beam X-ray diffraction with synchrotron radiation, and it was revealed that the P(3HB) fiber has a new core-sheath structure consistent with two types of molecular conformations: a 2_1 helix conformation (α-form) in the sheath region and a planar zigzag conformation (β-form) in the core region (*10*, *14*).

In this paper, we describe the processing of P(3HB-*co*-3HV) films and fibers with high tensile strength by cold-drawing from amorphous preform. The highly-ordered structures were investigated by X-ray diffraction, and the fiber structure of mono-filament was revealed by micro-beam X-ray diffraction with synchrotron radiation at SPring-8, Japan (*15*). Furthermore, the enzymatic degradability of P(3HB-*co*-3HV) films by using an extracellular PHB depolymerase purified from *Ralstonia pickettii* T1 is also addressed.

Experimental

Materials

Bacterial poly[(*R*)-3-hydroxybutyrate-*co*-8mol%-(*R*)-3-hydroxyvalerate] (P(3HB-*co*-8%-3HV)) was supplied by Monsanto Japan Co. M_w and polydispersity of P(3HB-*co*-8%-3HV) are 1.0×10^6 and 2.8, respectively. Samples after dissolution in chloroform at 100 °C were purified by precipitation in *n*-hexane and dried in vacuum. Melting temperature (T_m) and glass transition temperature (T_g) of the P(3HB-*co*-8%-3HV) powder are 143 °C and –4 °C, respectively, as measured by differential scanning calorimetry (DSC). The composition of 3HV unit determined by ^{1}H nuclear magnetic resonance (^{1}H-NMR) in $CDCl_3$ was 7.7 mol%.

Processing of Films with High Tensile Strength

The films of P(3HB-*co*-8%-3HV) were prepared by a conventional solvent-casting technique from chloroform solution using glass petri dishes as casting surface. The amorphous preforms of films were prepared by melting of solvent-cast films in a hot press at 180 °C for 30 s and subsequently quenching into ice water. These amorphous preforms were oriented by cold-drawing 200% - 1600%

In Degradable Polymers and Materials: Principles and Practice (2nd Edition); Khemani, K., et al.;
ACS Symposium Series; American Chemical Society: Washington, DC, 2012.

of their initial length in ice water and annealed in an autoclave at 50 °C - 125 °C with weak tension to increase the crystallinity. All samples were used after aging for at least 3 days at room temperature.

Processing of Fibers with High Tensile Strength

Melt-spinning of P(3HB-*co*-8%-3HV) was carried out using a laboratory-size extruder equipped with a single nozzle with an inner diameter of 1 mm. P(3HB-*co*-8%-3HV) was extruded at 170 °C, which was 10 - 20 °C higher than T_m. The extruder was taken up at 50 - 60 mm/s by roll and directly quenched into ice water placed 15 cm below the nozzle to obtain the amorphous fibers. The extrusion rate was 0.1 - 0.2 mm/s. One-step-drawing was performed against the quenched amorphous fibers by using a stretching machine at room temperature after isothermal crystallization for 24 h in ice water of near the T_g. Drawing rate by stretching machine was 4.5 - 5.0 mm/s. All drawn fibers to increase the crystallinity were annealed at 60 °C in an autoclave under constant tension for 30 min. All samples after aging for at least one week at room temperature were used to analyze.

Stress-Strain Test

Mechanical properties of films and fibers were evaluated by using a tensile testing machine (SHIMADZU EZTest). An initial specimen length of 10 mm was used. Tests were carried out a cross-head speed of 20 mm/min at room temperature. These results obtained were averaged over five samples for each condition.

Wide- and Small-Angle X-ray Diffraction

The two dimensional wide-angle X-ray diffraction (WAXD) and small-angle X-ray scattering (SAXS) were carried out at beam line BL45XU with wavelength of 0.09 nm in synchrotron radiation at SPring-8, Harima, Japan. The diffraction patterns were recorded with a CCD camera (C7330-12-NR, Hamamatsu Photonics, Japan) with exposure time of 76 - 1058 ms. The pixel size of CCD camera was 125 μm × 125 μm. The camera length for WAXD and SAXS were 110 and 2337 mm, respectively.

Micro-Beam X-ray Diffraction

The micro-beam wide-angle X-ray diffraction was carried out at beam line BL47XU with wavelength of 0.15497 nm at 8 keV of synchrotron radiation at SPring-8, Harima, Japan. The experimental focus beam size was obtained as 0.5 μm by using Fresnel Zone Plate technique. Measurement for highly-ordered structure of strong P(3HB-*co*-8%-3HV) fiber with isothermal crystallization was linearly scanned perpendicular to the fiber axis with a step width of 4 μm between the individual frames. The diffraction patterns were recorded with a CCD camera (C4880-10-14A, Hamamatsu Photonics, Japan) with exposure time of 10 s. The camera length was 110 mm.

In Degradable Polymers and Materials: Principles and Practice (2nd Edition); Khemani, K., et al.;
ACS Symposium Series; American Chemical Society: Washington, DC, 2012.

X-Ray Microtomography

The high resolution X-ray microtomography system was developed using beamline BL47XU with a wavelength of 0.15497 nm at 8 keV in the SPring-8 synchrotron radiation facility in Japan. The system consists of high precision stages using a light source, a double crystal monochromator, and a high spatial resolution X-ray image detector (CCD-based image detector (Hamamatsu Photonics, Japan K. K., C4880-41S)) with exposure times of 300 ms. Samples were fixed on a rotation rod in steps of 0.2° angles. The effective pixel size was 0.2 μm. Three-dimensional reconstruction software (Studio PON, Forge version 2.0) was used to superimpose the X-ray tomography cross-sectional images, and image analysis software (Media Cybernetics, Inc., Image Pro Plus version 4.0) was used to calculate cross-sectional areas and sizes of voids.

Enzymatic Degradation

Polyhydroxybutyrate (PHB) depolymerase purified from *Ralstonia pickettii* T1 (200 μg/ml in phosphate buffer) was used for enzymatic degradation of P(3HB-*co*-8%-3HV) films. For enzymatic degradation tests of films, samples of 1 cm^2 film and 5 μl of *R. pickettii* T1 PHB depolymerase in 1 ml of potassium phosphate-buffer (pH 7.4) were incubated at 37 °C. Onset of degradation was measured as weight-loss over time. For weight-loss measurement, films were periodically removed, washed twice with distilled water, and dried to constant weight before analysis. Weight measurements of solvent-cast and stretched P(3HB-*co*-8%-3HV) films were performed every 1 h over a period of 6 h. Samples incubated without enzyme showed no weight loss even after 4 days.

Scanning Electron Microscopy

Scanning electron micrographs (SEM) for the surface on samples were taken by using a JEOL JSM-6330F microscope, operated at an acceleration voltage of 5 kV, after samples were coated with gold using a SANYU DENSHI SC-701 quick coater.

Results and Discussion

Structure and Mechanical Properties of Films

The cold-drawing of melt-quenched films (amorphous preform) of P(3HB-*co*-8%-3HV) succeeded easily and reproducibly at a temperature below, but near to, the glass transition temperature of 4 °C in ice water. The films were easily drawn at very low stress by 16 times against their initial length, but elastic recovery occurred on release from stretching machine. Accordingly, the annealing procedure is required for fixing the extended polymer chains. The maximum values of tensile strength were obtained at annealing temperature of 75 °C. Figure 1 shows the tensile strength and crystal orientation of P(3HB-*co*-8%-3HV) cold-drawn and annealed film. The tensile strength of P(3HB-*co*-8%-3HV) films

In Degradable Polymers and Materials: Principles and Practice (2nd Edition); Khemani, K., et al.;
ACS Symposium Series; American Chemical Society: Washington, DC, 2012.

was drastically increased up to 117 MPa, when the film was stretched at the draw ratio of 10. At the draw ratio of over 12, the tensile strength was almost identical as near 170 MPa, suggesting that the chain orientation parallel to the stretching direction is a limit at the draw ratio of over 12. This phenomenon can be explained by the fact that crystal orientation has already reached ca. 0.95, when the film was stretched at the draw ratio of over 10, as shown in Figure 1. Mechanical properties of cold-drawn and annealed films of P(3HB-*co*-8%-3HV) are summarized in Table I, together with crystal orientation and X-ray crystallinity (Xc).

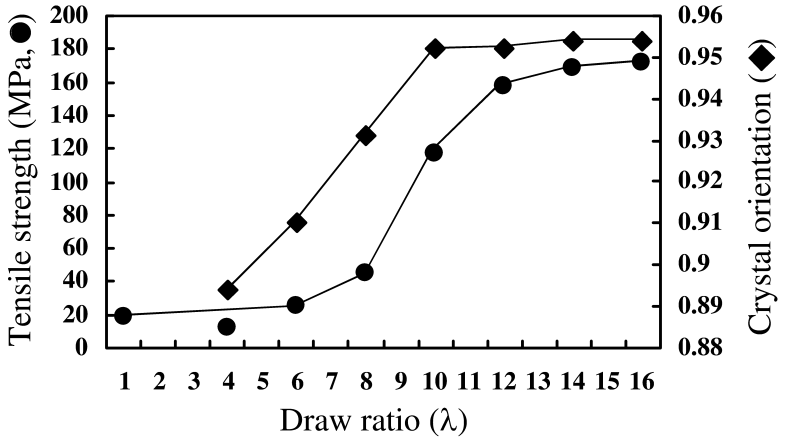

Figure 1. Tensile strength (•) and crystal orientation (▪) of P(3HB-co-8%-3HV) cold-drawn and annealed films, as functions of draw ratio. The crystal orientation was obtained from azimuthal scans of the (020) reflection in 2D WAXD pattern.

Table I. Mechanical properties, crystal orientation, and crystallinity of cold-drawn and annealed P(3HB-*co*-8%-3HV) films, stored for 10 days or 6 months.

Draw ratio (λ)	*Aging time (days)*	*Tensile strength (MPa)*	*Elongation to break (%)*	*Young's modulus (GPa)*	*Crystal orientation*	*Xc (%)*
1	10	19±1.3	35±2	0.3±0.0	-	53
10	10	117±17	109±31	0.5±0.1	0.950	77
16	10	172±24	74±13	1.1±0.2	0.954	78
10	180	109±14	101±20	1.9±0.1	0.951	80

All reflections of wide-angle X-ray fiber diagram (WAXD) of 10 times cold-drawn film as shown in Figure 2A were indexed with orthorhombic unit cell parameters of P(3HB) homopolymer (α-form: a = 0.576 nm, b = 1.320 nm and c(fiber axis) = 0.596 nm, $P2_12_12_1$ space group) as reported by Yokouchi

In Degradable Polymers and Materials: Principles and Practice (2nd Edition); Khemani, K., et al.;
ACS Symposium Series; American Chemical Society: Washington, DC, 2012.

et al. (*16*) and by Okamura and Marchessault (*17*). However, one sees a new reflection on the equatorial line in X-ray fiber diagram (Figure 2B) obtained from 16 times cold-drawn film, derived from the planar zigzag conformation (*β*-form), together with *α*-form reflections. Two kinds of molecular structures of P(3HB) were presented in Figure 2E. This *β*-form has been already confirmed in P(3HB-*co*-3HV) film by Orts *et al.* (*18*) and in P(3HB) fibers and films by Iwata *et al*. (*8–10*, *12–15*). Until now, it was considered that *β*-form is generated from the molecular chains in amorphous region between lamellar crystals by two-step-drawing (*8–10*, *12*, *15*, *18*). However, it is of interest that the *β*-form is clearly observed in X-ray fiber diagram of 16 times one-step cold-drawn film. This result indicates that the high orientation leads directly to the *β*-form from amorphous state of molecular chains. Thus, the generation of *β*-form supports the increase in tensile strength of cold-drawn films with the draw ratio of over 10, in spite of the crystal orientation being limited.

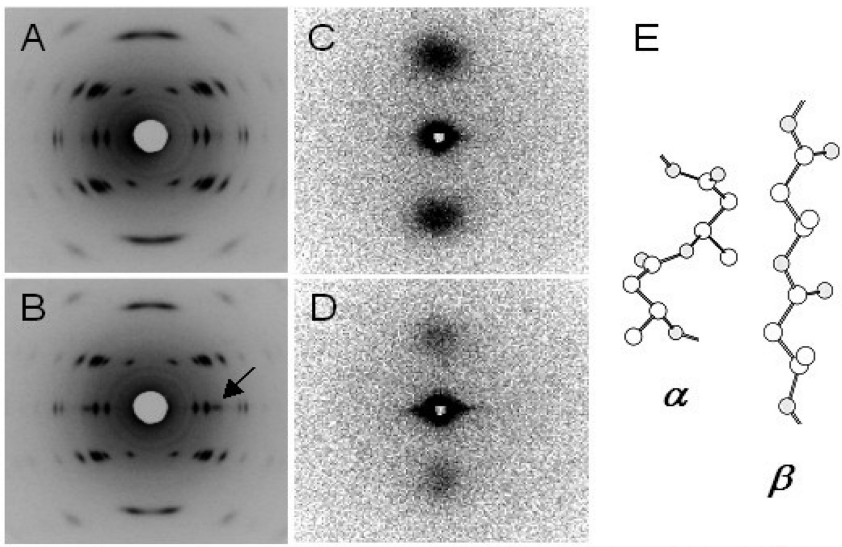

Figure 2. WAXD and SAXS patterns of P(3HB-co-8%-3HV) cold-drawn and annealed films: (A and C) 10 times drawn film, and (B and D) 16 times drawn film. (E) Two kinds of molecular conformations (2_1 helix (α-form) and planar zigzag (β-form) conformations) of P(3HB) built by using the atomic coordinates reported in ref. (16) and ref. (18), respectively. Arrow indicates a reflection derived from β-form.

The small-angle X-ray scatterings (SAXS) of 10 times and 16 times cold-drawn films are shown in Figure 2C and 2D, respectively. The long periods of 10 times and 16 times cold-drawn films are 6.7 nm and 7.8 nm, respectively. Two spots along the meridian were clearly observed in SAXS pattern of 10 times cold-drawn film (Figure 2C), suggesting that this film consists of two regions of lamellar crystal (*α*-form crystal) and amorphous between lamellar crystals.

However, in the case of 16 times cold-drawn film, the intensities of two reflections decreased, indicating that whole regions have almost same densities along the stretching direction. Based on the results that 16 times cold-drawn film has two kinds of crystalline domains (α-form and β-form) as shown in Figure 2B, it is concluded that the crystal densities of both crystalline domains are almost the same.

Structure and Mechanical Properties of Fibers

P(3HB-*co*-8%-3HV) fiber was prepared by one-step-drawing procedure of amorphous fiber with small crystal nuclei at room temperature (*15*). Amorphous fibers were obtained by quenching the melt-spun fibers of P(3HB-*co*-8%-3HV) into ice water. Isothermal crystallization of amorphous P(3HB-*co*-8%-3HV) fibers was achieved by holding the fibers in ice water for a certain period to prevent rapid crystallization and to grow small crystal nuclei. One-step-drawing after isothermal crystallization was performed by the stretching machine at room temperature, and then annealed at 60 °C for 30 min in an autoclave for fixing the extended polymer chains. One-step-drawn fibers with isothermal crystallization for 24 h were opaque and maximum total draw ratio was *ca.* 10 times.

The mechanical properties of one-step-drawn fibers of P(3HB-*co*-8%-3HV) are summarized in Table II (*15*). While the tensile strength of non-drawn fibers was ca. 30 MPa, the tensile strength of 5 times one-step-drawn fiber with isothermal crystallization increased to 710 MPa. Moreover, the tensile strength of 10 times one-step-drawn fiber increased to 1,065 MPa. The isothermal crystallization near the glass transition temperature induces the growth of many small crystal nuclei. Drawing with isothermal crystallization leads to the high orientation of molecular chains in the amorphous region between small crystal nuclei.

Table II. Mechanical properties of cold-drawn and annealed P(3HB-*co*-8%-3HV) fibers (*15*).

Draw ratio (λ)	*Tensile strength (MPa)*	*Elongation to break (%)*	*Young's modulus (GPa)*
1 (as-spun)	27±3	15±5	1.2±0.2
5	710±126	50±6	6.8±1.4
10	1065±187	40±12	8.0±1.1

Figure 3 shows the WAXD and SAXS patterns of one-step-drawn P(3HB-*co*-8%-3HV) fibers without and with isothermal crystallization. The WAXD and SAXS patterns of as-spun fiber without isothermal crystallization showed the ring and four-point patterns, respectively, indicating that α-form crystals are not oriented and inclined (Figures 3A and 3B). On the other hand, the WAXD pattern of 10 times one-step-drawn fiber without isothermal crystallization showed the arc reflections of α-form and a weak reflection of β-form (Figure 3C),

In Degradable Polymers and Materials: Principles and Practice (2nd Edition); Khemani, K., et al.;
ACS Symposium Series; American Chemical Society: Washington, DC, 2012.

indicating the low orientation of α-form crystals along the drawing direction. The SAXS pattern of 10 times one-step-drawn fiber showed clear two-spot reflections corresponding to oriented lamellae along the meridian (Figure 3D).

The WAXD pattern of non-drawn fiber with isothermal crystallization showed only ring pattern contributed to unoriented α-form crystal (Figure 3E) as the case of as-spun fiber without isothermal crystallization. On the other hand, the WAXD patterns of 10 times one-step-drawn fibers with isothermal crystallization showed the sharp reflections of α-form and a strong reflection of β-form (Figure 3G). The orientation of α-form crystals and the intensity of β-form reflection increased with increasing draw ratio for one-step-drawn fiber with isothermal crystallization. The (020) and (110) reflections are observed on the ring patterns in the WAXD patterns of one-step-drawn fibers as shown in Figure 3G. These ring patterns are considered to be derived from pseudo-hexagonal crystals oriented perpendicular to the fiber axis, as reported by Furuhashi *et al*. (*19*).

The SAXS patterns of 10 times one-step-drawn fibers with isothermal crystallization (Figure 3H) showed clear streak scatterings along the equator and weak reflections along the meridian, while the SAXS pattern of non-drawn fiber showed only ring pattern by unoriented lamellae (Figure 3F). The clear streak scatterings along the equator suggest that many voids seem to exist in one-step-drawn fibers. The weak reflection along the meridian is considered to indicate that one-step-drawn fibers with isothermal crystallization have highly-oriented structure with almost same crystal densities of lamellar crystals (α-form) and planar zigzag chains (β-form).

Micro-diffraction techniques have been developed mainly at the ID13 beamline of the European Synchrotron Radiation Facility (ERSF) with a beam size of 3 - 10 μm for viscose rayon fibers (*20*), spider silk (*21*), spherulites of P(3HB) (*22*), and a poly(lactic acid)/atactic-P(3HB) blend (*23*). Recently, we developed the micro-diffraction techniques with 0.5 μm beam size for analysis ultra-high-molecular-weight-P(3HB) mono-filament (*10*) and P(3HB) copolymer spherulites (*24*). To reveal the detail fiber structure and the distribution of two types of molecular conformations in drawn P(3HB-*co*-8%-3HV) mono-filament, a micro-beam X-ray diffraction experiment was performed with synchrotron radiation at SPring-8, Japan. The beam size was focused to 0.5 μm with the Fresnel Zone Plate technique and the P(3HB-*co*-8%-3HV) mono-filament was scanned linearly perpendicular to the fiber axis with a step of 4 μm.

Figure 4 shows a series of micro-beam X-ray diffraction patterns of one-step-drawn P(3HB-*co*-8%-3HV) fiber with isothermal crystallization scanned perpendicular to the fiber axis. All micro-beam X-ray diffraction patterns of one-step-drawn fiber showed the reflections of both α- and β-forms. These reflections were not changed throughout fiber except for intensities. This result indicates that one-step-drawn P(3HB-*co*-8%-3HV) fiber with isothermal crystallization has not a core-sheath structure such as cold-drawn and two-step-drawn UHMW-P(3HB) fiber (*10*). In the other word, one-step-drawn P(3HB-*co*-8%-3HV) fibers with isothermal crystallization is an uniform structure throughout fiber consistent with both α- and β-form crystals. This structure supports the result that one-step-drawn fiber with isothermal crystallization has a high tensile strength in spite of low draw ratio.

In Degradable Polymers and Materials: Principles and Practice (2nd Edition); Khemani, K., et al.;
ACS Symposium Series; American Chemical Society: Washington, DC, 2012.

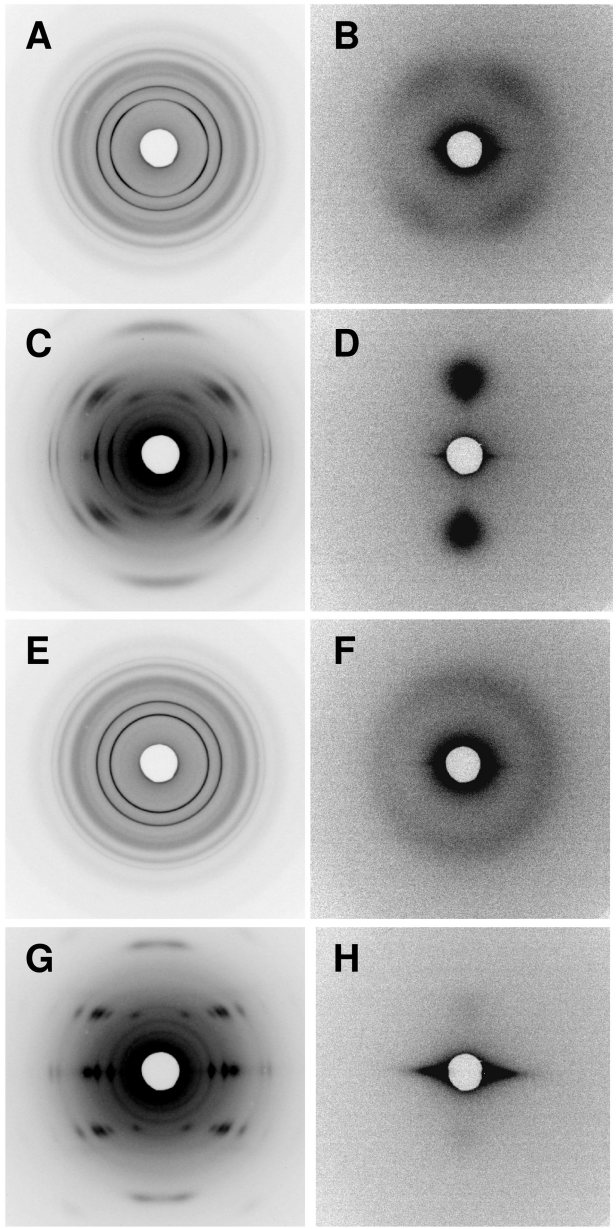

Figure 3. WAXD and SAXS patterns of P(3HB-co-8%-3HV) fibers: (A and B) non-drawn fibers without isothermal crystallization, (C and D) 10 times one-step-drawn fibers without isothermal crystallization, (E and F) non-drawn fibers with isothermal crystallization, (G and H) 10 times one-step-drawn fibers with isothermal crystallization (15).

In Degradable Polymers and Materials: Principles and Practice (2nd Edition); Khemani, K., et al.;
ACS Symposium Series; American Chemical Society: Washington, DC, 2012.

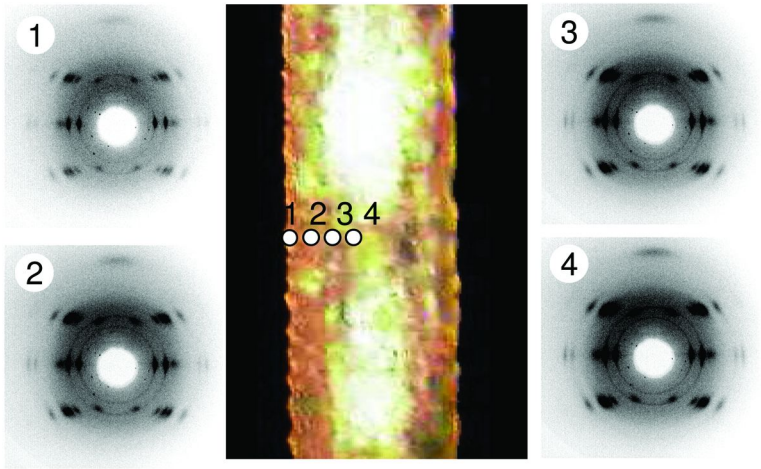

Figure 4. Micro-beam X-ray fiber diagrams of 10 times one-step-drawn P(3HB-co-8%-3HV) mono-filament with isothermal crystallization, recorded from the point in the microscope image (15).

Figure 5 shows the X-ray microtomography reconstructed stereoscopic model for one-step-drawn P(3HB-*co*-8%-3HV) fibers (100 - 120 μm diameter) without and with isothermal crystallization. The one-step-drawn fiber without isothermal crystallization is uniform throughout the fiber (Figure 5A). However, after isothermal crystallization, the one-step-drawn fiber has many fine voids of cohesive elliptic shape in the drawing direction (Figure 5B). The results show that the streak scattering in the SAXS pattern shown in Figure 3H is due to the presence of many fine voids throughout the fiber.

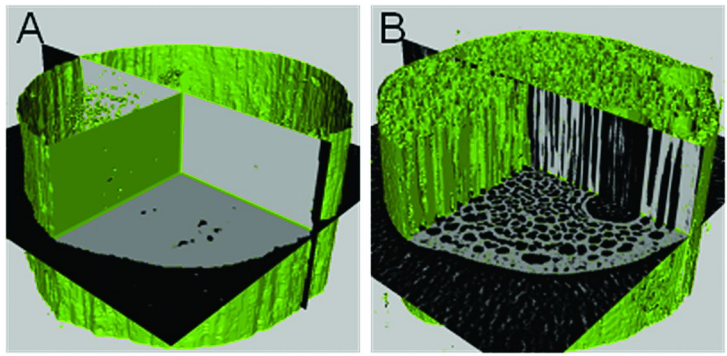

Figure 5. Reconstructed stereoscopic model of 10 times one-step-drawn P(3HB-co-8%-3HV) fibers: (A) without isothermal crystallization (B) with isothermal crystallization. (Reproduced with permission from Ref. (25). Copyright 2007 Elsevier.)

In Degradable Polymers and Materials: Principles and Practice (2nd Edition); Khemani, K., et al.; ACS Symposium Series; American Chemical Society: Washington, DC, 2012.

Most void diameters in the one-step-drawn P(3HB-*co*-8%-3HV) fibers after isothermal crystallization were 1.0 - 1.6 μm and the average was 2.3±1.5 μm. Cross-sectional area versus load stress is an important parameter for evaluating the tensile strength of materials. To assess the mechanical properties of a uniaxial structure with many fine voids such as the one-step-drawn P(3HB-*co*-8%-3HV) fiber with isothermal crystallization (Figure 5B) one needs to know its true cross-sectional area. The calculated tensile strengths derived from the recalculated cross-sections for one-step-drawn P(3HB-*co*-8%-3HV) fibers without and with isothermal crystallization are summarized in Table III. The recalculated cross-sectional area was the same as the apparent cross-sectional area for the one-step-drawn fiber without isothermal crystallization (*15*). However, the recalculated cross-sectional area of the one-step-drawn fiber after isothermal crystallization was 52.7% of the apparent cross-sectional area. Therefore, the tensile strength determined by recalculation of the cross-sectional area for the latter fiber is considered to be 2,020 MPa. This calculated value indicates that the physical properties of P(3HB-*co*-8%-3HV) fibers are highly suitable for use as biodegradable materials.

Table III. Apparent and calculated cross-sectional areas, and tensile strengths of 10 times one-step-drawn P(3HB-*co*-8%-3HV) fibers without and with isothermal crystallization near T_g. (Reproduced with permission from Ref. (*25*). Copyright 2007 Elsevier.)

Isothermal crystallization time (h)	*Apparent cross-section*		*Tensile strength (MPa)*[a]	*Calculated cross-section*		*Calculated tensile strength (MPa)*[b]
	area (μm^2)	*ratio (%)*		*area (μm^2)*	*ratio (%)*	
0	1.21×10^4	100	90	1.21×10^4	99.9	90
24	1.29×10^4	100	1065	0.68×10^4	52.7	2020

[a] Obtained from the apparent cross-sectional areas in reference (*15*) and Table II.
[b] Recalculated from measured cross-sectional areas (1,065/0.527=2,020 MPa).

Effect of Storage Time on Mechanical Properties

It is well known that the mechanical properties of P(3HB-*co*-8%-3HV) films markedly deteriorate to stiffness and brittleness by a process of secondary crystallization. The cold-drawn and annealed films of P(3HB-*co*-8%-3HV) were stored for 6 months at room temperature to study the time dependent change of the mechanical properties, and the stress-strain test was performed. The tensile strength and elongation to break of cold-drawn and annealed films remained unchanged for 6 months as summarized in Table I. It is of importance to note that the mechanical properties of the cold-drawn and annealed film did not deteriorate during 6 months. It is concluded that a highly oriented and crystallized P(3HB-*co*-3HV) film keeps superior mechanical properties for long periods.

In Degradable Polymers and Materials: Principles and Practice (2nd Edition); Khemani, K., et al.;
ACS Symposium Series; American Chemical Society: Washington, DC, 2012.

It is interesting to note that Young's modulus increased after the storage for 6 months. This result relates to the glass transition temperature (T_g) of P(3HB-*co*-8%-3HV). P(3HB-*co*-8%-3HV) molecules can move at room temperature during the storage because T_g of P(3HB-*co*-8%-3HV) is below room temperature. This molecular mobility causes the secondary crystallization and deterioration. However, in the case of cold-drawn and annealed film, since the entanglements of molecular chains are considered as less in amorphous region, the scission of molecular chains caused by the incorporation of molecular chains from amorphous region to crystal domain does not occur. Furthermore, the crystallinity measured by X-ray diffraction remained unchanged during the storage. Based on these results, the increase of Young's modulus of P(3HB-*co*-8%-3HV) cold-drawn and annealed film after the storage is due to the improvement of the stability for the chain-packing state of P(3HB-*co*-8%-3HV) molecules in crystal region.

Enzymatic Degradation

The enzymatic degradation of three kinds of P(3HB-*co*-8%-3HV) films, solvent-cast, 10 times cold-drawn film, and 16 times cold-drawn film, were performed in 0.1 M phosphate buffer (pH 7.4) using an extracellular PHB depolymerase from *Ralstonia pickettii* T1 at 37°C. Figure 6 shows the rate of erosion profiles of P(3HB-*co*-8%-3HV) films as a function of time.

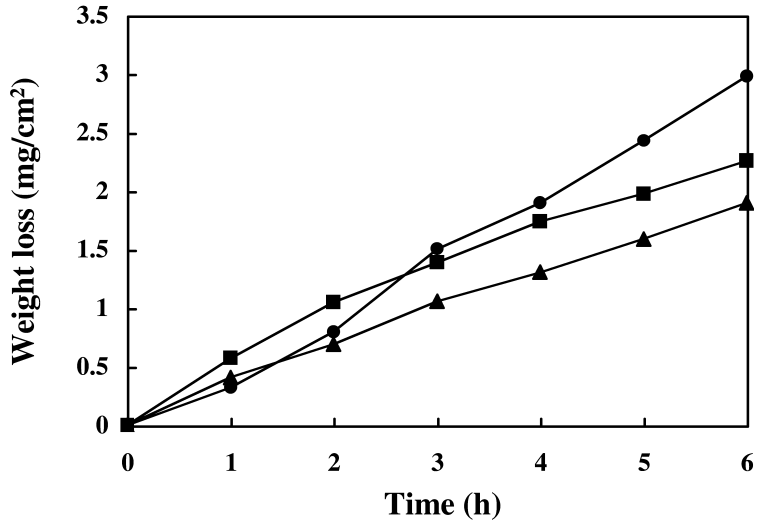

Figure 6. Enzymatic degradation of P(3HB-co-8%-3HV) films in an aqueous solution of extracellular PHB depolymerase from Ralstonia pickettii T1 at 37 °C; (•) solvent-cast film, (▪) 10 times cold-drawn and annealed film, and (▲) 16 times cold-drawn and annealed film.

The amount of film erosion increased proportionally with time for all the samples. The rate of erosion of solvent-cast film of P(3HB-*co*-8%-3HV) was 0.50

In Degradable Polymers and Materials: Principles and Practice (2nd Edition); Khemani, K., et al.;
ACS Symposium Series; American Chemical Society: Washington, DC, 2012.

mg/h/cm^2, and this value is five times faster than that of P(3HB) homopolymer solvent-cast film (0.10 mg/h/cm^2) (*6*). On the other hand, the rates of erosion of the 10 times and 16 times cold-drawn films were 0.38 and 0.32 mg/h/cm^2, respectively, suggesting the effect of the crystallinity and long period on the rate of erosion. We reported the effect of crystallinity and solid state structure on enzymatic erosion of P(3HB) stretched films (*6*). In the case of P(3HB-*co*-8%-3HV), the enzymatic erosion rate seems to be strongly affected by the level of crystallinity and long period, as the case of P(3HB).

Figure 7 shows a scanning electron micrograph of 10 times cold-drawn film of P(3HB-*co*-8%-3HV) after partial enzymatic degradation using an extracellular PHB depolymerase from *R. pickettii* T1 at 37 °C for 3 h. It is well known that the amorphous region is etched faster than the crystal one. Accordingly, this micrograph shows the unetched core along the draw direction and lamellar crystals perpendicular to the core. The P(3HB-*co*-8%-3HV) at the surface of the film seems to have a shish-kebab morphology similar as found P(3HB) stretched films. The high tensile strength of both films might be due to a stretched chain core in the shish-kebab morphology, together with the generation of planar zigzag conformation.

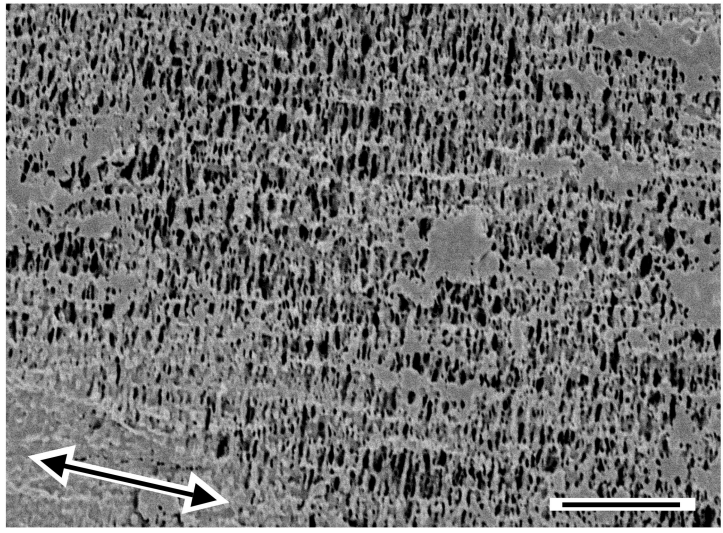

Figure 7. Scanning electron micrograph of the cold-drawn and annealed P(3HB-co-8%-3HV) film after partial enzymatic degradation in an aqueous solution of extracellular PHB depolymerase from Ralstonia pickettii T1 at 37 °C. The scale bar represents 10 μm and the arrow indicates the stretching direction.

Conclusions

Uniaxially oriented films of P(3HB-*co*-8%-3HV) were prepared by cold-drawing from amorphous preform at a temperature near to the glass transition

In Degradable Polymers and Materials: Principles and Practice (2nd Edition); Khemani, K., et al.;
ACS Symposium Series; American Chemical Society: Washington, DC, 2012.

temperature (T_g). High tensile strength fibers of P(3HB-*co*-8%-3HV) were produced from amorphous states by one-step-drawing at room temperature after isothermal crystallization at T_g to grow small crystal nuclei. The cold-drawn films had acceptable mechanical properties with high tensile strength and elongation to break, and showed hardly any variation after storing for 6 months at room temperature. It has been suggested that the embrittlement of P(3HB-*co*-8%-3HV) films due to secondary crystallization is avoided by its high crystallinity and high degree of orientation. The rate of enzymatic degradation of cold-drawn films by using an extracellular PHB depolymerase purified from *Ralstonia pickettii* T1 decreased with increasing in draw ratio, and it was revealed that the cold-drawn films had the shish-kebab structure.

The tensile strength of 10 times one-step-drawn fiber with isothermal crystallization was over 1.0 GPa, which corresponded to those of common plastics such as polyethylene and poly(ethylene terephthalate). The molecular and highly ordered structure of mono-filament was analyzed by micro-beam, wide- and small-angle X-ray diffraction, and X-ray microtomography with synchrotron radiation at SPring-8, Japan.

Both stretched films and fibers had two kinds of molecular conformations, 2_1 helix (α-form) and planar zigzag (β-form) conformations. The improvement of mechanical properties is due to the generation of β-form that exists between α-form lamellar crystals. In SAXS patterns of highly stretched films and fibers, the intensities of reflections along the stretching direction, which indicate the long period of lamellar crystals, remarkably decreased, suggesting that two crystalline forms have almost same crystal densities. The one-step-drawn fiber after isothermal crystallization has many fine voids of cohesive elliptic shape in the drawing direction.

Acknowledgments

This work has been supported by a Grant-in-Aid for Young Scientists (A) (No. 15685009) and Scientific Research (B) (No. 19350075) (to T. Iwata) from the Ministry of Education, Culture, Sports, Science and Technology (MEXT) of Japan and by a grant for Ecomolecular Science Research provided by RIKEN Institute. The authors are grateful to Y. Doi of the RIKEN Institute, and N. Adachi, M. Hasegawa, S. Teramachi of the Kogakuin University. The synchrotron radiation experiments were performed at the SPring-8 with the approval of the Japan Synchrotron Radiation Research Institute (JASRI) (Proposal No. 2003B0054, No. 2004B0016, No. 2005A0307, and No. 2005B0039).

References

1. Doi, Y. In *Microbial Polyesters*; VCH Publishers: Weinheim, 1990.
2. Yoshie, N.; Inoue, Y. In *Biopolymers, Vol. 3b, Polyesters II*; Doi, Y., Steinbüchel, A., Eds.; Wiley-VCH: Weinheim, 2002; pp 133−156.
3. Holmes, P. A. In *Developments in Crystalline Polymers Vol. 2*; Bassett, D. C., Ed.; Elsevier Applied Science: London, 1988; pp 1−65.

4. Yoshie, N.; Saito, M.; Inoue, Y. *Macromolecules* **2001**, *34*, 8953.
5. Kusaka, S.; Iwata, T.; Doi, Y. *J. Macromol. Sci. - Pure Appl. Chem.* **1998**, *35*, 319.
6. Kusaka, S.; Iwata, T.; Doi, Y. *Int. J. Biol. Macromol.* **1999**, *25*, 87.
7. Iwata, T.; Kusaka, S.; Doi, Y. In *Polymer from Renewable Resources: Biopolyesters and Biocatalysis*; Scholz, C., Gross, R. A., Eds.; ACS Symposium Series 76; American Chemical Society: Washington, DC, 2000; pp 67−76.
8. Aoyagi, Y.; Doi, Y.; Iwata, T. *Polym. Degrad. Stab.* **2003**, *79*, 209.
9. Iwata, T.; Tsunoda, K.; Aoyagi, Y.; Kusaka, S.; Yonezawa, N.; Doi, Y. *Polym. Degrad. Stab.* **2003**, *79*, 217.
10. Iwata, T.; Aoyagi, Y.; Fujita, M.; Yamane, H.; Doi, Y.; Suzuki, Y.; Takeuchi, A.; Uesugi, K. *Macromol. Rapid Commun.* **2004**, *25*, 1100.
11. Fischer, J. J.; Aoyagi, Y.; Enoki, M.; Doi, Y.; Iwata, T. *Polym. Degrad. Stab.* **2004**, *83*, 453.
12. Iwata, T.; Fujita, M.; Aoyagi, Y.; Doi, Y.; Fujisawa, T. *Biomacromolecules* **2005**, *6*, 1803.
13. Iwata, T.; Doi, Y. *Macromol. Symp.* **2005**, *224*, 11.
14. Iwata, T. *Macromol. Biosci.* **2005**, *5*, 689.
15. Tanaka, T.; Fujita, M.; Suzuki, Y.; Takeuchi, A.; Uesugi, K.; Ito, K; Fujisawa, T.; Doi, Y.; Iwata, T. *Macromolecules* **2006**, *39*, 2940.
16. Yokouchi, M.; Chatani, Y.; Tadokoro, H.; Teranishi, K.; Tani, K. *Polymer* **1973**, *14*, 267.
17. Okamura, K.; Marchessault, R. H. In *Conformation of Biopolymers, Vol. 2*; Ramachandra, G. N., Ed.; Academic Press: New York, 1967; pp 709−720.
18. Orts, W. J.; Marchessault, R. H.; Bluhm, T. L.; Hamer, G. K. *Macromolecules* **1990**, *23*, 5368.
19. Furuhashi, Y.; Ito, H.; Kikutani, T.; Yamamoto, T.; Kimizu, M.; Cakmak, M. *J. Polym. Sci., Part B: Polym. Phys.* **1998**, *36*, 2471.
20. Muller, M.; Riekel, C.; Vuong, R.; Chanzy, H. *Polymer* **2000**, *41*, 2627.
21. Riekel, C.; Madsen, B.; Knight, D.; Vollrath, F. *Biomacromolecules* **2000**, *1*, 622.
22. Gazzano, M.; Focarete, M. L.; Riekel, C.; Scandola, M. *Biomacromolecules* **2000**, *1*, 604.
23. Gazzano, M.; Focarete, M. L.; Riekel, C.; Scandola, M. *Biomacromolecules* **2004**, *5*, 553.
24. Tanaka, T.; Fujita, M.; Takeuchi, A.; Suzuki, Y.; Uesugi, K.; Doi, Y.; Iwata, T. *Polymer* **2005**, *46*, 5673.
25. Tanaka, T.; Uesugi, K.; Takeuchi, A.; Suzuki, Y.; Iwata, T. *Polymer* **2007**, *48*, 6145.

Chapter 12

Harnessing Biopolyesters in the Design of Functional and Nanostructured Architectures

Daniel Grande,* Estelle Renard, Julien Babinot, Julien Ramier, and Valérie Langlois*

Institut de Chimie et des Matériaux Paris-Est, UMR 7182 CNRS – Université Paris-Est Créteil, 2, rue Henri Dunant, 94320 Thiais, France
***E-mail : grande@icmpe.cnrs.fr, langlois@icmpe.cnrs.fr**

This contribution critically reviews some recent developments on the chemical modification and macromolecular engineering of poly(3-hydroxyalkanoate)s (PHAs) with a specific focus on typical examples from our group. Unsaturated PHAs were chemically modified *via* the transformation of pendant double bonds into carboxylic acid, hydroxyl or alkyne groups. Moreover, these reactive side functions could be used for further grafting biocompatible oligomers based on hydrolyzable polylactide (PLA) or poly(ε-caprolactone) (PCL) and hydrophilic poly(ethylene glycol) (PEG). Additionally, PHA-based block copolymers with a PLA, PCL or PEG segment were synthesized by ring-opening polymerization or "click" chemistry using a suitably functionalized PHA building block.

Introduction

Poly(3-hydroxyalkanoate)s (PHAs) constitute an enlarged family of aliphatic polyesters that can be considered as promising biopolymers for biomedical and environmental applications, due to their renewability, biodegradability, and biocompatibility (*1–4*). PHAs represent a class of natural polyesters accumulated by many bacteria as intracellular energy and carbon storage materials when they are subjected to stress conditions (limiting oxygen, nitrogen, or other essential nutrient) (*5*, *6*). Using various substrates, a large variety of PHAs can be synthesized, differing notably by the length of their side chains (*7*). Two

In Degradable Polymers and Materials: Principles and Practice (2nd Edition); Khemani, K., et al.;
ACS Symposium Series; American Chemical Society: Washington, DC, 2012.

main types are generally distinguished, *i.e.* one type with short-chain length (*scl*-PHAs) that possess alkyl side chains having up to two carbon atoms, and a second type with medium-chain length (*mcl*-PHAs) that display between three and eleven carbon atoms on their side chains. The side-chain length strongly affects the physical properties of PHAs: indeed, *scl*-PHAs are rigid and brittle like semi-crystalline thermoplastics, while *mcl*-PHAs behave as thermoplastic elastomers. Accordingly, to target high added-value applications, especially controlled drug delivery or tissue engineering, PHA-based frameworks need to be diversified so that the mechanical properties of native PHAs might be improved.

In this contribution, the versatility of PHAs in the design of a wide array of biodegradable and/or biocompatible macromolecular architectures with controlled degradability will be illustrated through different systems investigated in our group (Figure 1).

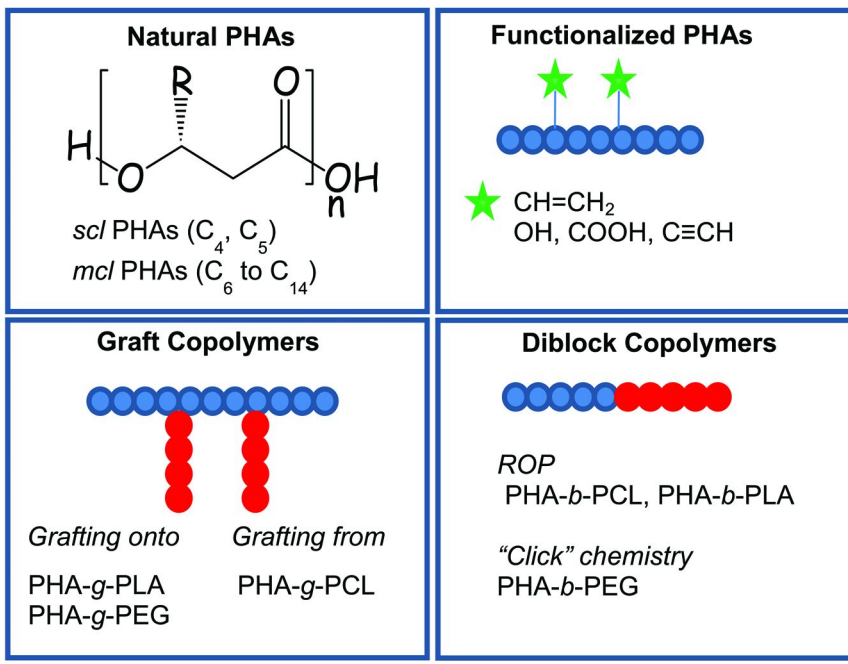

Figure 1. Well-defined macromolecular architectures based on PHAs.

Experimental Section

Materials

Poly(3-hydroxybutyrate-*co*-3-hydroxyvalerate) PHBHV (12 mol % HV units, M_n = 84 000 g.mol^{-1}, PDI = 2.4) was purchased from Goodfellow and purified from his plasticizer by precipitation in ethanol. Poly(3-hydroxybutyrate-*co*-3-hydroxyhexanoate) PHBHHx (9 mol % HHx units, M_n = 206 000 g.mol^{-1}, PDI = 1.6) was generously supplied by Procter and Gamble, under the trade name NODAX®. Poly(3-hydroxyoctanoate-*co*-3-hydroxyhexanoate)

In Degradable Polymers and Materials: Principles and Practice (2nd Edition); Khemani, K., et al.;
ACS Symposium Series; American Chemical Society: Washington, DC, 2012.

(PHOHHx, 15 mol % HHx units, M_n = 130 000 g.mol^{-1}, PDI = 1.5) and poly(3-hydroxyoctanoate-*co*-3-hydroxyundecenoate) (PHOU, 25 mol % U units, M_n = 80 000 g.mol^{-1}, PDI = 2.0) were obtained from EMPA (Swiss Federal Laboratories for Materials Testing & Research, Laboratory for Biomaterials, St Gallen, Switzerland), and were biosynthesized according to procedures previously reported (*8*, *9*). 3,6-dimethyl-1,4-dioxane-2,5-dione (D,L-Lactide, LA), and tin (II) 2-ethylhexanoate (95 %, $SnOct_2$) were purchased from Sigma-Aldrich. ε-caprolactone (CL, Aldrich) was dried over CaH_2, and distilled under vacuum prior to use. Triethylaluminum ($AlEt_3$, Fluka) was used as received.

Preparation of PHA Oligomers

Ester-terminated monohydroxylated PHA oligomers were prepared by acid-catalyzed methanolysis of corresponding native PHAs following a procedure established by Timbart *et al.* (*10*) (Figure 2).

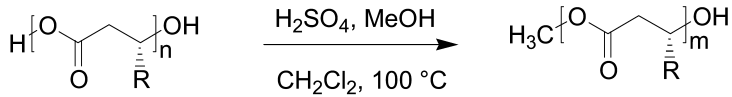

R=CH_3 (0.88), C_2H_5 (0.12): PHBHV
R=CH_3 (0.91), C_3H_7 (0.09): PHBHHx
R=C_5H_{11} (0.85), C_3H_7 (0.15): PHOHHx

Figure 2. Acid-catalyzed methanolysis of PHAs.

PHA oligomers with a terminal carboxyl group were prepared by thermal degradation of corresponding native PHAs at 190 °C for a determined time (*11*). Oligomers were purified by precipitation in cold ethanol.

Instrumentation

^{1}H and ^{13}C NMR spectra were run at room temperature using a Bruker AC 200 spectrometer at resonance frequencies of 200 and 50 MHz, respectively. Solid-state ^{13}C NMR spectra were recorded at a resonance frequency of 75 MHz on a Bruker Avance 300 spectrometer. The Size Exclusion Chromatography (SEC) equipment comprised a Spectra Physics P100 pump, two PLgel 5 µm mixed-C columns (Polymer Laboratories), and a Shodex RI 71 refractive index (RI) detector. The eluent was tetrahydrofuran (THF) at a flow rate of 1 mL min^{-1}; the calibration was effected with polystyrene (PS) standards from Polymer Laboratories. FTIR spectra were recorded between 4000 and 450 cm^{-1} on a Bruker Tensor 27 DTGS spectrometer in Attenuated Total Reflection (ATR) mode. Glass transition temperature (T_g) analyses were performed by Differential Scanning Calorimetry (DSC) with a Perkin Elmer Diamond calorimeter under nitrogen atmosphere. The following protocol was generally used for each sample:

In Degradable Polymers and Materials: Principles and Practice (2nd Edition); Khemani, K., et al.;
ACS Symposium Series; American Chemical Society: Washington, DC, 2012.

first heating from -70 °C to 200 °C at 10 °C.min-1, fast cooling to -70 °C at 200 °C.min^{-1}, and then second heating to 200 °C at 20 °C.min^{-1}.

Design of PHA-Based Graft Copolymers

Side-Functionalized PHAs

Among bacteria able to produce *mcl*-PHAs, *Pseudomonas sp* Gpo 1 has the particularity to create functional PHAs with side-chain double bonds (*12*). Hence, PHOU, namely a bacterial copolyester containing repeating units with terminal alkene substituents at the 3-position, was produced using sodium octanoate and 10-undecenoic acid as carbon sources. The polymer composition was fine-tuned by the initial substrate composition. By taking advantage of the reactivity of pendant double bonds, miscellaneous functionalized PHAs were prepared *via* the chemical transformation of (C=C) into different functional groups. Chemical modifications were successfully completed under conditions in which negligible chain scission reactions were noticed, thus affording novel functional biopolyesters (*13*, *14*). Unsaturated groups were transformed into carboxylic acid groups by oxidation using $KMnO_4$ to generate poly(3-hydroxyoctanoate-*co*-9-carboxy-3-hydroxydecanoate) (PHOD) (*15*). Alcohol functions were also introduced by hydroboration-oxidation of PHOU (*16*) (Figure 3). Through such side-chain functionalizations, it was possible to control the hydrophilic/hydrophobic balance, and to improve the water solubility so as to enhance significantly the hydrolytic degradability of PHAs. For instance, at 37 °C and pH = 10, a PHOU sample did not undergo any degradation in a buffered aquous solution, whereas the corresponding PHOD sample was totally hydrolyzed within 2 h (*17*). The latter sample was even substantially degraded at pH = 7.

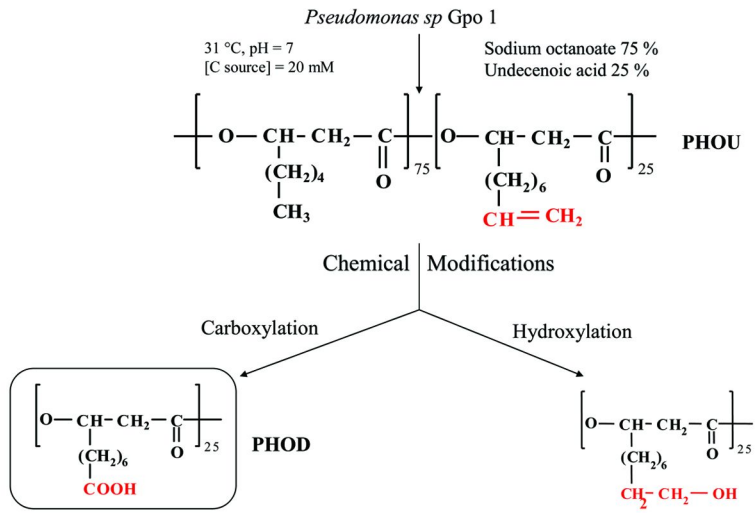

Figure 3. Design of functionalized PHAs by chemical modifications of PHOU.

In Degradable Polymers and Materials: Principles and Practice (2nd Edition); Khemani, K., et al.; ACS Symposium Series; American Chemical Society: Washington, DC, 2012.

Synthesis of PHA-Based Graft Copolymers

The resulting copolyesters with pendant carboxylic acid functionality (PHOD) can be used to further conjugate bioactive or targeting molecules, as well as reactive oligomers. Thus, graft copolymers constituted of a PHO main chain and either poly(D,L-lactide) (PLA) or poly(ethylene glycol) (PEG) short grafts were respectively synthesized by direct esterification of PHOD using monohydroxylated PLA or PEG oligomers (M_n = 350 g.mol^{-1}) (*18*). Graft copolymers contained around 10-15 mol % of residual unmodified carboxylic acid groups (Figure 4). Nanoparticles were derived from these copolymers by solvent displacement (*i.e.* nanoprecipitation of acetone solution in water, followed by evaporation of acetone) without any stabilizer. They were obtained quantitatively as indicated by the absence of precipitation. Stable nanoparticles were formed in water, and the suspensions remained stable for several weeks without visible aggregation. Potential applications as drug delivery carriers may be envisioned for such PHA-based nanoparticles.

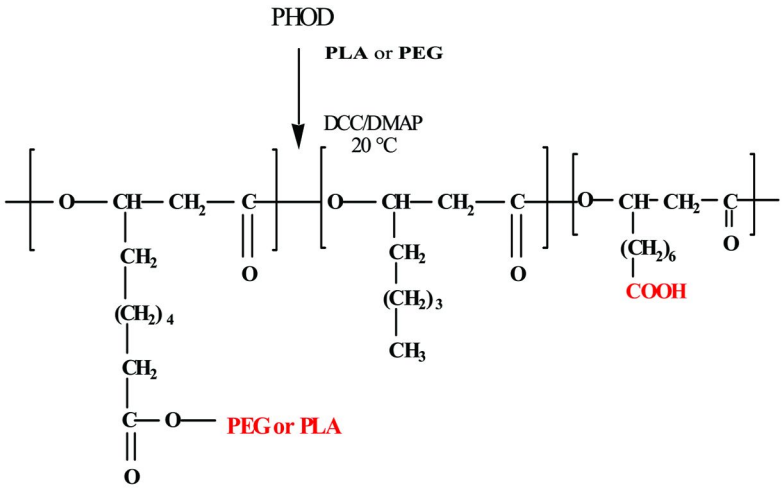

Figure 4. Synthesis of graft copolymers by direct esterification of PHOD.

Alternatively, two amphiphilic PHA-*g*-PEG copolymers with controlled block lengths and narrow molar mass distributions were synthesized *via* "click" chemistry (Figure 5) (*19*). To investigate the influence of PEG length on the reaction efficiency, PEG550 and PEG5000 were considered, where 550 and 5000 correspond to their theoretical number-average molar mass (M_n). First, well-defined PHOU oligomers were prepared by acid-catalyzed methanolysis of native PHOU. By adjusting the reaction time, oligomers with M_n of around 5000 g.mol^{-1} were obtained in 93 % mass yield. PHOU oligomers were converted into PHOD analogues according to our aforementioned procedure. The side terminal carboxylic acid functions of the oligomers were used to acetylene-functionalize PHOD by esterification with propargyl alcohol using EDC hydrochloride as a coupling agent. This reaction occurred at room temperature in dichloromethane

In Degradable Polymers and Materials: Principles and Practice (2nd Edition); Khemani, K., et al.;
ACS Symposium Series; American Chemical Society: Washington, DC, 2012.

to give alkyne-functionalized PHOD with a 71 % conversion. The optimization of reaction conditions did not permit to increase the conversion rate; it could be assigned to the fact that COOH side groups did not fully react because of the formation of *N*-acylurea as a by-product. This compound is unreactive toward alcohol and does not form ester bonds. ^{1}H NMR and SEC analyses of molar masses did not show any significant change compared to those of PHOD precursor, thus indicating that the esterification conditions did not cause a degradation of the polyester chains. It is noteworthy that the T_g of alkyne-derivatized PHOD (-42 °C) was lower than that of corresponding PHOD (-32 °C), which could be attributed to the absence of hydrogen bonding in the esterified product.

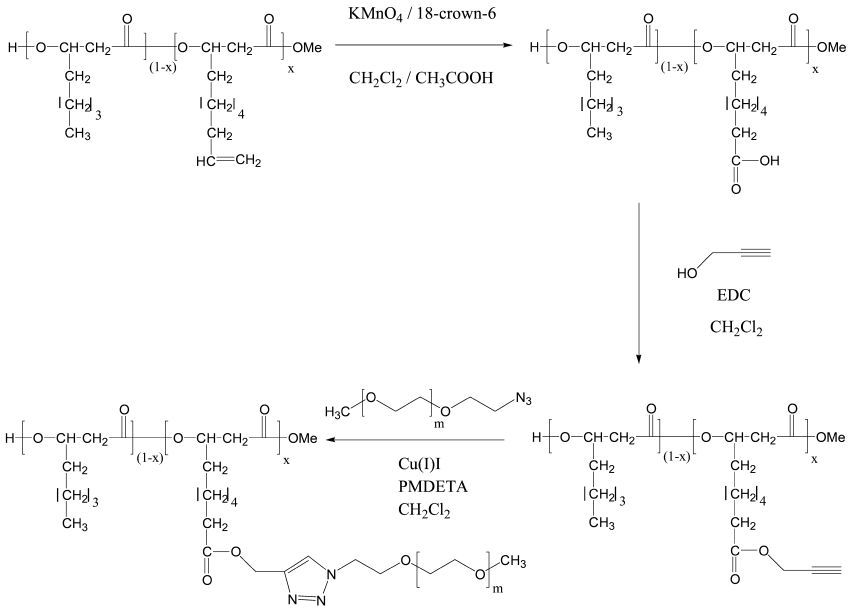

Figure 5. Synthetic route to PHA-g-PEG via "click" chemistry.

α−monomethyl ether ω−azide PEG was synthesized by nucleophilic substitution of monomethyl ether mesylate PEG5000 using sodium azide. For PEG550, a tosylated PEG derivative was used. "Click" chemistry through the copper (I)-catalyzed azide-alkyne cycloaddition (CuAAC) between alkyne-containing PHOD and azide-terminated PEG was performed in dichloromethane at 50 °C, using CuI and PMDETA as a catalyst and a base, respectively (Figure 5). After evaporation of dichloromethane and dissolution in DMSO, the resulting copolymers were purified by dialysis against water in order to remove free unreacted PEG, and they were recovered by freeze-drying. The success of the reaction was confirmed by ^{1}H NMR and FTIR with the disappearance of the azide strectching band at 2105 cm^{-1}. SEC analyses revealed a substantial increase in molar masses compared to the PHOD precursor in the expected orders of magnitude. Indeed, with a PHA oligomer of 5000 g.mol^{-1}, one can foresee about 3.3 PEG grafted chains. For PHA-*g*-PEG550, the conversion

In Degradable Polymers and Materials: Principles and Practice (2nd Edition); Khemani, K., et al.;
ACS Symposium Series; American Chemical Society: Washington, DC, 2012.

rate was 94 %, which resulted in the grafting of 3.1 PEG chains, while 2.8 PEG chains were grafted in the case of PHA-*g*-PEG5000 (conversion rate of 84 %).

DSC analyses of graft copolymers were also performed. In the case of PHA-*g*-PEG550, the incorporation of short and soft grafts did not notably modify the amorphous character of the PHOD backbone. In contrast, the PHA-*g*-PEG5000 copolymer exhibited a semi-crystalline behavior with a melting temperature (54 °C) close to that of PEG segments (60 °C).

A more straightforward "click" methodology for the preparation of PHA-*g*-PEG graft copolymers has recently been developed. Starting from PHOU oligomers and thiol-appended monomethyl ether PEG, graft copolymers based on a poly(3-hydroxyoctanoate-*co*-3-hydroxyundecanoate) backbone and short PEG grafts were quantitatively obtained by the well-known thiol-ene addition (*20*). It is also noteworthy that thiol-ene addition is better suited for biomedical applications than the CuAAC process, as no toxic catalyst that could be detrimental for further *in vitro* or *in vivo* studies is employed. Nanoscale vesicles with narrow particle size and high stability were prepared by the aforementioned solvent displacement technique. Such biocompatible polymer vesicles may find interesting applications as drug delivery carriers in the biomedical area.

The latter syntheses proceeded through a "grafting onto" approach. Interestingly, a "grafting from" methodology was also implemented by using a side-functionalized PHOU with pendant hydroxyl groups as macronitiators for the ring-opening polymerization (ROP) of CL in conjunction with $SnOct_2$. PHA-*g*-poly(ε-caprolactone) (PCL) graft copolyesters with varying graft lengths were thus generated (*16*). Such copolymers were recovered as powders and were semi-crystalline, in contrast to their hydroxy-functionalized PHOU precursor which was sticky and amorphous.

Design of PHA-Based Block Copolymers

Synthesis of PHA-Based Diblock Copolymers by ROP

The amorphous character of several graft copolyesters has limited their potential applications. We then turned our attention on the design and synthesis of block copolyesters constituted of a soft PHOHHx block and a more crystalline PCL block (*10*). For this purpose, a two-step process was designed: the first step consisted in the preparation of hydroxy-terminated PHOHHx oligomers, and in the second step, these oligomers were used as macroinitiators for the ROP of CL to generate the desired diblock copolymers.

The effective one-step synthesis of PHOHHx oligomers containing a hydroxyl end group on one side and an ester end group on the other side was achieved by exposing native PHOHHx of high molar mass to an acid-catalyzed methanolysis. Such a reaction led to the control over the molar masses of the samples. Thus, the methanolysis reaction was allowed to proceed for a period of time ranging from 10 to 60 min to produce well-defined oligomers with a M_n value varying from 20,000 to 800 $g.mol^{-1}$, respectively. The hydroxy-functionalized PHOHHx oligomers with different molar masses were used to trigger the controlled polymerization of CL with $AlEt_3$ as a catalyst to generate PHA-*b*-PCL diblock copolymers with

In Degradable Polymers and Materials: Principles and Practice (2nd Edition); Khemani, K., et al.;
ACS Symposium Series; American Chemical Society: Washington, DC, 2012.

tunable compositions. The degree of cristallinity associated with the resulting copolymers could be tuned by varying the lengths of both blocks.

The same procedure could be applied to PHOU-*b*-PCL copolyesters (*21*). The unsaturations in the side chains of the PHOU block could then be oxidized in carboxylic acid functions to give rise to novel amphiphilic PHOD-*b*-PCL diblock copolyesters. All these biodegradable PHO-based copolymers may represent useful model systems to investigate the encapsulation of doxorubicin inside nanoparticles and the drug delivery thereby. This bioactive molecule is an important agent involved in bladder cancer treatment. In this context, nanoparticles based on PHOHHx, PHOD, PHOHHx-*b*-PCL and PHOD-*b*-PCL were prepared using the aforementioned nanoprecipitation/evaporation technique. The encapsulation efficiency of doxorubicin was larger than 50 % due to the hydrophobicity of both doxorubicin and polyesters. The *in vitro* release behavior of doxorubicin-loaded particles at pH 6 (bladder pH) was investigated (*22*). A typical two-phase release profile was observed (case of matricial type particles). These results were consistent with the method of particle preparation: doxorubicin was co-precipitated with the polymer. The burst effect was inferior to 10 %. It is noteworthy that these nanoparticles were also mucodhesive (Figure 6).

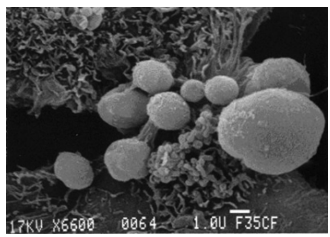

Figure 6. SEM image showing the mucoadhesivity of PHO-b-PCL nanoparticles containing 24 mol % of PHO (x 6600).

As a process with a weak environmental impact and many advantages, including higher yields, shorter reaction times, and ease of conducting solvent-free reactions, microwave (MW) activation is a highly efficient and versatile heating technique. The MW process comprises an electromagnetic radiation which leads to a dielectric heating mechanism, thus resulting in the elimination of the wall effects. Therefore, the heating homogeneity is higher than that encountered in a conventional conduction/convection heating (*23*). The first MW-assisted synthesis has been reported in the 1980s in the field of organic chemistry (*24*), but over the last decade, MW procedures have largely been extended to polymer synthesis (*25*). Among the homopolymers synthesized by MW-assisted ROP, PCL, poly(ε-caprolactam), PLA, and poly(2-oxazoline) have been obtained in significantly shorter times than those needed in conventional conduction/convection thermal processes. Besides, graft copolymers and several random, statistical or block copolymers can be prepared by MW-assisted ROP. Zhang *et al.* have synthesized PLA-based diblock (*26*) and triblock (*27*) copolymers through the use of various short PEG macroinitiators with $SnOct_2$ as a catalyst to produce amphiphilic architectures. Such a ROP process has also

In Degradable Polymers and Materials: Principles and Practice (2nd Edition); Khemani, K., et al.;
ACS Symposium Series; American Chemical Society: Washington, DC, 2012.

been performed with a PEG/PCL system (*28*) and small peptide sequences with PEG (*29*). In this context, our group first reported on the formation of PHA-based copolymers under MW irradiation (*30*).

PHA-*b*-PLA diblock copolymers were prepared by MW-assisted bulk ROP of LA initiated by the corresponding hydroxy-terminated PHA macroinitiators, previously produced *via* acid-catalyzed methanolysis of native PHAs (Figure 7).

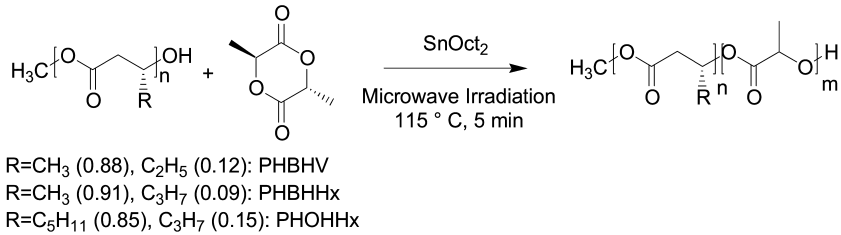

R=CH_3 (0.88), C_2H_5 (0.12): PHBHV
R=CH_3 (0.91), C_3H_7 (0.09): PHBHHx
R=C_5H_{11} (0.85), C_3H_7 (0.15): PHOHHx

Figure 7. MW-assisted synthesis of PHA-b-PLA diblock copolyeters.

Miscellaneous copolymers with tunable compositions were efficiently synthesized with a reaction time of 5 min and a set temperature of 115 °C. Under the experimental conditions investigated, diblock copolymers with M_n values ranging from 13,750 to 45,400 g.mol^{-1} and polydispersity indices (PDIs) varying from 1.5 to 1.9 were obtained. It should be stressed that these PDI values were lower than those associated with the initial macroinitiators (1.9-2.2). The M_n values determined by ^{1}H NMR increased almost linearly with increasing the $[LA]_0/[PHA]_0$ molar ratio (from 60/1 to 250/1). Furthermore, a very important parameter was the initiator efficiency (*f*) whose values were very close to 1 (between 0.91 and 0.99). Such high values corroborated the true blockiness associated with the copolyesters, regardless of the molar mass and the chemical structure of the PHA-based macroinitiator. The conversion values ranged from 52 % to 86 %: the lower the $[LA]_0/[PHA]_0$ molar ratio, the lower the conversion. The moderate conversion values obtained for the lowest $[LA]_0/[PHA]_0$ molar ratios could be attributed to a difficult melting of the bulk, due to the high concentration of PHA associated with a high viscosity. Consequently, the LA polymerization slowed down, so in turn the conversion was relatively low. Higher conversions were reached when the PHA-based macroinititator concentration was lower, due to the easier melting of the bulk constituted of a large fraction of LA (T_m = 119°C). As a conclusion, the high initiator efficiency values conjugated with the decrease of the PDI values confirmed the "living"/controlled character of the MW-assisted LA polymerization initiated by PHA macroinitiators.

Synthesis of PHA-Based Diblock Copolymers *via* "Click" Chemistry

Alternatively, "click" chemistry was implemented to generate well-defined amphiphilic block copolymers based on PHAs and PEG. A series of PHBHV, PHBHHx, and PHOHHx oligomers was first synthesized by thermal treatment at 190 °C of corresponding native PHAs (*11*) (Figure 8). Different reaction times ranging from 60 to 420 min were used to obtain a range of molar masses varying

In Degradable Polymers and Materials: Principles and Practice (2nd Edition); Khemani, K., et al.;
ACS Symposium Series; American Chemical Society: Washington, DC, 2012.

from 15,000 to 4,000 g.mol^{-1}, respectively. By resulting from a β-elimination reaction, this method has the major advantage to produce well-defined oligomers with an unsaturated end group on one side and a carboxylic acid group on the other side. It is noteworthy that thermal stability of PHOHHx is higher than that of PHBHV or PHBHHx, probably due to the longer pendant side chain lowering the β-elimination speed (*31*).

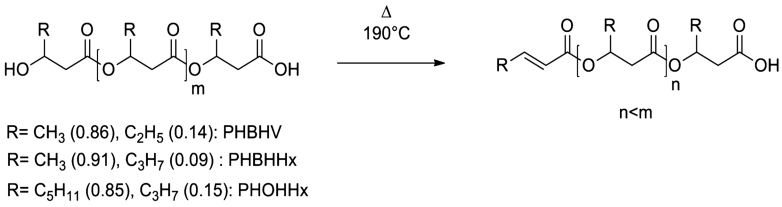

Figure 8. Preparation of PHA-based oligomers by thermal degradation of corresponding native PHAs.

To achieve CuAAC "click" coupling of PHAs and PEG building blocks, it was necessary to introduce azide and alkyne end groups within the oligomer structures (*31*). A α−monomethyl ether ω−azide PEG with a M_n of 5,000 g.mol^{-1} was prepared by nucleophilic substitution of monomethyl ether mesylate PEG5000 using sodium azide. For PHA oligomers, the carboxylic acid chain-end groups were used to bind propargylamine using EDC and NHS as coupling agents (Figure 9). The reaction occurred quantitatively at room temperature in dichloromethane with good yields ranging from 83 % to 95 %. ^{1}H NMR and SEC analyses of the molar masses did not show any significant change compared to those of the precursors, thus indicating that amidification conditions did not cause side reactions or degradation of the polyester chains.

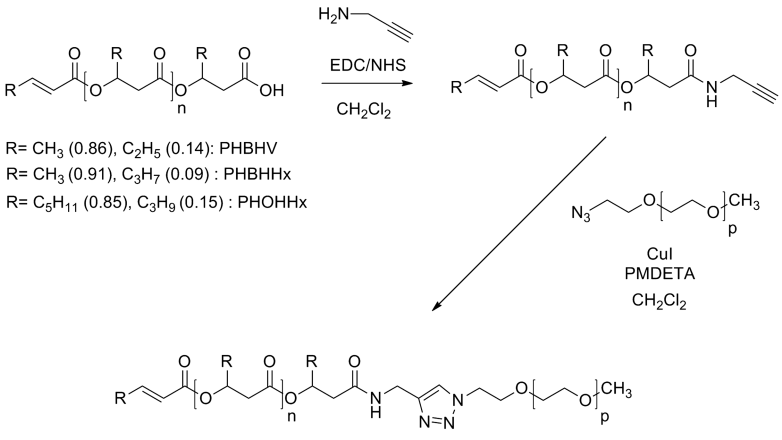

Figure 9. Synthetic route to PHA-b-PEG amphiphilic diblock copolymers.

In Degradable Polymers and Materials: Principles and Practice (2nd Edition); Khemani, K., et al.;
ACS Symposium Series; American Chemical Society: Washington, DC, 2012.

The ligation of constitutive blocks was accomplished by resorting to CuAAC in dichloromethane at 50 °C with CuI as a catalyst and PMDETA as a base (Figure 9). All resulting block copolymers self-assembled into colloidal suspensions in water. They were subsequently poured into an ultrafiltration cell to remove unreacted PEG using a 30000 Da cut-off membrane. This membrane appeared to be suitable for all copolymers, since the solution in the cell remained turbid, and only clear solution was salted out in the trash. After purification, both PHBHV- and PHBHHx-based copolymers formed unstable colloidal suspensions, whereas PHOHHx-based copolymers resulted in very stable colloidal suspensions (*32*). Our preliminary studies showed that they formed stable micelles in aqueous media with low critical micelle concentrations (Figure 10). Again, such biocompatible colloidal systems may be envisioned for biomedical applications as drug delivery nanocarriers able to transport bioactive hydrophobic molecules.

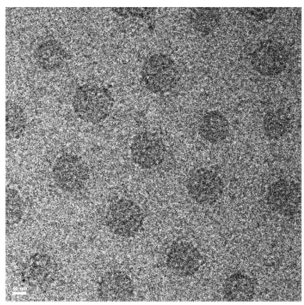

Figure 10. Cryo-TEM of micelles formed in water by PHOHHx-b-PEG copolymers (scale bar represents 10 nm)

SEC analyses were performed to determine the molar masses and polydispersity indices of diblock copolymers. All SEC chromatograms exhibited monomodal distributions along with a shift of the copolymer peaks toward lower retention times, thus attesting for a quantitative "click" coupling.

The thermal stability of PHA-*b*-PEG diblock copolymers was evaluated using TGA under dynamic argon atmosphere. Typically, the copolymers exhibited a two-step degradation behavior, with a first step occurring from 225 to 310 °C, due to the degradation of the PHA block, followed by a second stage from 310 to 425 °C arising from the PEG block destruction. Since the degradation temperatures were sufficiently far-off, we were able to determine the copolymer compositions. They were in good agreement with those obtained from ^{1}H NMR analyses.

DSC analyses were also carried out to get an insight into the thermal characteristics of the diblock copolymers. PHBHV and PHBHHX oligomers exhibited semi-crystalline behaviors, whereas PHOHHx oligomers were totally amorphous. In PHBHV-*b*-PEG copolymers, separate crystalline phases of both PHBHV and PEG domains were present. It is noticeable that the melting temperature and corresponding enthalpy of PEG decreased with increasing the PHBHV content. Obviously, the presence of the hard PHBHV block restricted the crystallization of the PEG block. For PHBHHx-*b*-PEG copolymers, the lower crystallinity of the PHBHHx segment hindered the crystallization of PEG

In Degradable Polymers and Materials: Principles and Practice (2nd Edition); Khemani, K., et al.;
ACS Symposium Series; American Chemical Society: Washington, DC, 2012.

to a lower extent, thus resulting in a higher melting enthalpy compared to that of PHBHV-*b*-PEG analogues. Finally, PHOHHx-*b*-PEG copolymers displayed a PEG melting enthalpy of 149 $J.mol^{-1}$, close to that of PEG5000 (166 $J.g^{-1}$), indicating that the amorphous PHOHHx segments induced limited hindrance of the PEG crystallization.

Conclusions

Bacterial polyesters are of great interest for biomedical permanent or non-permanent applications, due to their excellent biocompatibility and non-toxicity. Nevertheless, due to their limited mechanical properties, PHA-based frameworks have been diversified in order to attain specific high added-value devices, including drug delivery carriers and tissue engineering scaffolds. This contribution has demonstrated the potentialities offered by the chemical modification and macromolecular engineering of PHAs as effective and versatile approaches to a large variety of functional and nanostructured architectures. Specifically, we have been interested in the design and synthesis of side-functionalized PHAs, graft copolymers derived therefrom, and block copolymers. PHA-based frameworks can be tailor-made by fine-tuning topology, functionality, and composition to fit the requirements for a targeted application.

The development of novel multifunctional polymeric materials with controlled (bio)degradability will require diversification of the polyester systems, either by using novel precursors, catalysts, and/or building blocks, or by varying the connectivity, functionality, and/or the processing of macromolecular architectures. The aim of our investigations is to broaden the application portfolio, *e.g.* therapeutics, diagnostics, and tissue engineering.

Acknowledgments

The authors thank the CNRS and the "Université Paris-Est Créteil" for financial support. They are also indebted to the French Ministry of Research for providing J. R. with a Ph.D. grant.

References

1. Lenz, R. W.; Marchessault, R. H. *Biomacromolecules* **2005**, *6*, 1.
2. Sparks, J.; Scholz, C. *Biomacromolecules* **2009**, *10*, 1715.
3. Chen, G. Q. *Chem. Soc. Rev.* **2009**, *38*, 2434.
4. Hazer, D. B.; Kiliçay, E.; Hazer, B. *Mater. Sci. Eng. C* **2012**, *32*, 637.
5. Zinn, M.; Witholt, B.; Egli, T. *Adv. Drug Delivery Rev.* **2001**, *53*, 5.
6. Vert, M. *Biomacromolecules* **2005**, *6*, 538.
7. Lee, S. Y. *Biotechnol. Bioeng.* **1996**, *49*, 1.
8. Hartmann, R.; Hany, R.; Geiger, T.; Egli, T.; Witholt, B.; Zinn, M. *Macromolecules* **2004**, *37*, 6780.
9. Hany, R.; Bohlen, T.; Geiger, T.; Hartmann, R.; Kawada, J.; Schmidt, M.; Zinn, M.; Marchessault, R. H. *Macromolecules* **2004**, *37*, 385.

10. Timbart, L.; Renard, E.; Langlois, V.; Guérin, Ph. *Macromol. Biosci.* **2004**, *4*, 1014.
11. Nguyen, S.; Yu, G. E.; Marchessault, R. H. *Biomacromolecules* **2002**, *3*, 219.
12. Bear, M. M.; Leboucher-Durand, M. A.; Langlois, V.; Lenz, R. W.; Goodwin, S.; Guérin, Ph. *React. Funct. Polym.* **1997**, *34*, 65.
13. Grande, D.; Renard, E.; Langlois, V.; Rohman, G.; Timbart, L.; Guérin, P. In *Degradable Polymers and Materials - Principles and Practice*; Khemani, K., Scholz, C., Eds.; ACS Symposium Series 939; American Chemical Society: Washington, DC, 2006; Chapter 9, pp 140−155.
14. Renard, E.; Langlois, V.; Guérin, P. *Corros. Eng. Sci. Technol.* **2007**, *42*, 300.
15. Kurth, N.; Renard, E.; Brachet, F.; Robic, D.; Guérin, Ph.; Bourbouze, R. *Polymer* **2002**, *43*, 1095.
16. Renard, E.; Poux, A.; Timbart, L; Langlois, V.; Guérin, Ph. *Biomacromolecules* **2005**, *6*, 891.
17. Renard, E.; Walls, M.; Guérin, Ph.; Langlois, V. *Polym. Degrad. Stab.* **2004**, *85*, 779.
18. Renard, E.; Ternat, C.; Langlois, V.; Guérin, Ph. *Macromol. Biosci.* **2003**, *3*, 248.
19. Babinot, J.; Renard, E.; Langlois, V. *Macromol. Rapid Commun.* **2010**, *31*, 619.
20. Babinot, J.; Guigner, J. M.; Renard, E.; Langlois, V. *Chem. Commun.* **2012**, *48*, 5364.
21. Timbart, L.; Renard, E.; Tessier, M.; Langlois, V. *Biomacromolecules* **2007**, *8*, 1255.
22. Renard, E.; Vergnol, G.; Langlois, V. *IRBM* **2011**, *31*, 619.
23. Sosnik, A.; Gotelli, G.; Abraham, G. A. *Prog. Polym. Sci.* **2011**, *36*, 1050.
24. Gedye, R.; Smith, F.; Westaway, K.; Ali, H.; Baldisera, L.; Laberge, L.; Rousell, J. *Tetrahedron Lett.* **1986**, *27*, 279.
25. Kempe, K.; Becer, C. R; Schubert, U. S. *Macromolecules* **2011**, *44*, 5825.
26. Zhang, C.; Liao, L.; Gong, S. *Macromol. Chem. Phys.* **2007**, *208*, 1122.
27. Zhang, C.; Liao, L.; Gong, S. *Macromol. Rapid Commun.* **2007**, *28*, 422.
28. Yu, Z. J.; Liu, L. J. *J. Biomater. Sci., Polym. Ed.* **2005**, *16*, 957.
29. Anzovino, M. B.; Rutledge, K. E.; Baron, M. A.; Goh, S. L. *Polym. Prepr. (Am. Chem. Soc., Div. Polym. Chem.)* **2006**, *47* (1), 587.
30. Ramier, J.; Renard, E.; Grande, D. *J. Polym. Sci., Part A: Polym. Chem.* **2012**, *50*, 1445.
31. Babinot, J.; Renard, E.; Langlois, V. *Macromol. Chem. Phys.* **2011**, *212*, 278.
32. Babinot, J.; Guigner, J. M.; Renard, E.; Langlois, V. *J. Colloid Interface Sci.* **2012**, *375*, 88.

Chapter 13

Biodegradable Agricultural Mulches Derived from Biopolymers

Douglas G. Hayes,[1,*] Sathiskumar Dharmalingam,[1] Larry C. Wadsworth,[1] Karen K. Leonas,[2] Carol Miles,[3] and Debra A. Inglis[4]

[1]Department of Biosystems Engineering, University of Tennessee, 2506 E. J. Chapman Drive, Knoxville, TN 37996-4531, USA
[2]Department of Apparel, Merchandising, Design & Textiles, Washington State University, 51 Kruegel Hall, Pullman, WA 99164-2020
[3]Department of Horticulture and Landscape Architecture, [4]Department of Plant Pathology, Washington State University, Mount Vernon NWREC, 16650 State Route 536, Mount Vernon, WA 98273
[*]dhayes1@utk.edu

Plastic agricultural mulches provide many benefits to the cultivation of specialty crops such as vegetables, including weed prevention and increased soil temperature, leading to increased crop yield, hence to their expanded use worldwide. Most mulches are prepared from polyethylene (PE), a polymer that poorly biodegrades. The fate of PE mulches after their use is a major environmental concern. The ideal plastic mulch would be plowed into the soil at the end of the growing season, and undergo full mineralization within a few months. This chapter reviews biodegradable agricultural mulches: desirable traits, currently-available mulches that undergo biodegradation, the process of biodegradation for mulches, and the development of standards for the biodegradability of mulches in soil. Preliminary results on the performance of polylactic acid-based mulches prepared using nonwovens textile technology are presented.

In Degradable Polymers and Materials: Principles and Practice (2nd Edition); Khemani, K., et al.; ACS Symposium Series; American Chemical Society: Washington, DC, 2012.

Introduction: The Need for Biodegradable Mulches

Plastic mulching was introduced to agriculture in the 1950's and since then has successfully been used throughout the world to increase vegetable and fruit crop productivity. Mulches reduce weeds and prevent soil erosion. In addition, they lead to establishment of a "microclimate," which can enhance control of water levels, temperature, nutrients, and physical structure of the soil. All of these benefits can more than offset the expense of their use: 1400 USD hectare^{-1} (*1*, *2*). Since agricultural land is declining while the demand for food is increasing, there is a need for more intensive agricultural production, including season extension, soil protection, and the need to utilize marginal land or inhospital environments (e.g., drought prone regions), or make use of minimally available agricultural land in urban and suburban areas (*3–5*). In 1999, approximately 10 million hectares of land employed plastic mulches in China (which comprises 80% of the world's mulched surface) , and by 2006, an estimated 162,000 hectares were covered with plastic mulch in the USA (*1*, *6*). The use of plastics in mulching has also been reported to be 2.6 million metric tonnes (M) per year worldwide in 2003-2005, with usage in the USA and Europe being 130,000 tonnes each (*7*, *8*). In addition to mulches, polymers are employed for several other applications in agriculture (referred to collectively as "plasticulture"), including coverings for greenhouses and high and low tunnels, films for soil disinfestation and sterilization, drip tubes for irrigation, and as packaging and storage materials (*9*). Expanding further outward in scope, consumption of plastics annually was approximately 300 MMT in 2010; therefore, agricultural usage amounts to approximately 1 % of the plastics market (*10*, *11*).

Traditionally, mulches consist of films containing non-renewable petroleum-based plastics, particularly polyethylene (PE), with the latter's thickness falling between 0.5 and 1.25 mil. Concerns have been raised regarding the economic and environmental sustainability of PE mulches, including product cost, disposal concerns and the labor for removal from the field (*2*). Annual waste generation of agricultural plastics was reported to be 615,000 tonnes in Europe in 2007 (*12*). As reviewed in 2004, the disposal of PE mulches is expensive: 250 USD ha^{-1} (*7*, *13*), due in part to costs associated with its removal from soil and transportation to the disposal site. Traditional disposal methods are problematic. The burning of mulches, a common disposal method for agricultural plastics worldwide, can release airborne pollutants such as dioxane, and is illegal in the USA (*14*, *15*). Incineration is an expensive approach. Disposal in landfills can lead to increased levels of pesticides in the landfill due to adsorbed agents that accompany the mulches. The decreasing availability of landfill space as well as increased potential exposure of the plastics and chemical intermediates resulting from their partial breakdown or open air burning to the environment, exasperated by the ~9% increased annual production of plastics, reflects a societal concern that is growing in significance (*10*, *11*).

Degradation of PE mulches typically occurs during their long-term use, leading to embrittlement and subsequently fragmentation of the mulches (encountered by us in open field studies), which can further hinder the retrieval and recycling of the mulches (*7*). The presence of residual black PE in harvested

In Degradable Polymers and Materials: Principles and Practice (2nd Edition); Khemani, K., et al.;
ACS Symposium Series; American Chemical Society: Washington, DC, 2012.

crops can hinder their value in the marketplace (*7*). In addition, as noted recently by Thompson *et al.*, materials that do not fully biodegrade, but rather persist in the environment as debris, will significantly impact wildlife, plant life, and microbiota (*10*). PE is known to undergo biodegradation slowly, with abiotic thermal and photo-oxidation being important components of the process, yielding several possible degradation products, including environmentally harmful chemicals such as aldehydes and ketones (*16*). Furthermore, residual PE debris may adsorb pesticides due to the hydrophobic nature of adsorbent and adsorbate, hence increasing localized pesticide concentrations. For example, a recent report demonstrates that several pesticides such as DDT and PCB accumulate within the plastic debris fragments found throughout the world's oceans (*17*). In addition, PE film debris that persists in soils can cause soil drainage problems.

Another concern with PE mulches is their derivation from petroleum leading to poor sustainability. (However, it is noted that biobased PE (*18*), derived from bioethanol, may serve as a future source of plastic mulches.) Plastics consume approximately 8% of the world's petroleum production (*11*); therefore, the employment of biobased sources for plastics will significantly reduce petroleum demand. Ultimately, as petroleum prices continue to soar, biobased feedstocks for plastics will become increasingly attractive and cost-competitive (*11*). The market size for biopolymers in the USA in 2010 was estimated to be 191,000 tonnes, based on a 20% growth occurring since 2005 (*19*, *20*). Important drivers for the further growth of biopolymers were identified as the cost for landfill usage and changes in cultural values (e.g., growth of recycling programs and back-yard composting) (*11*, *20*).

As stated in a recent review on biopolymers employed in agriculture, ".. the best choice appears to be a mulch material with an outdoor service life which matches the crop duration, and which would later be incorporated by the agricultural system" (*9*). Moreover, after the growing season has ended, the mulch material would be plowed into the soil. The desired goal is the ultimate complete biodegradation of the mulch by soil microorganisms (with the term "biodegradable" defined in Table I), leading to 100% conversion of the mulches into carbon dioxide and water within a reasonable period of time, from several months to one year. This goal has not yet been achieved.

The primary constraint to adoption of biodegradable mulches is their high cost compared to conventional PE mulches, 2.54 times higher on average (*20*). The current market for biodegradable mulches focuses upon "sustainable agriculture," which maximizes natural resource utilization and emphasizes environmental stewardship while maintaining economic viability. A more challenging market for employment of biodegradable mulches is "organic agriculture," which entails more stringent and standardized requirements compared to sustainable agriculture. Full definitions of organic and sustainable agriculture are given in Table I. (Of note these two terms are defined differently between countries, even between states of the USA (*21*), and organizations.) As described below, many of the commercial biodegradable mulches are categorized as "synthetic" materials (definition given in Table I) according to USDA's National Organic Program (NOP), the national organization which sets the guidelines for organic certification in the USA, and therefore are not allowed in certified organic production. The

In Degradable Polymers and Materials: Principles and Practice (2nd Edition); Khemani, K., et al.;
ACS Symposium Series; American Chemical Society: Washington, DC, 2012.

use of the label "synthetics" for those polymers that fully biodegrade under compositing conditions (according to standard tests), including the potentially valuable biobased mulch feedstock polylactic acid (PLA), has been controversial (*21*), as discussed below.

In the remainder of this chapter, commercially available biodegradable mulches will be discussed first, with an emphasis placed on PLA and polyhydroxyalkanoate (PHA) as potentially valuable starting materials for biodegradable mulches. The assessment and standardization of biodegradability for agricultural mulches will be discussed thereafter. Criteria for biodegradation of plastics in soils have not been standardized (although a standard is currently being developed (ASTM WK 29802, 2012), and may vary between crop type, geographical region, and country (discussed below). Finally, initial results by the authors on the testing and evaluation of PLA-based mulch prototypes prepared using nonwovens textile technology will be provided.

Table I. Important definitions relating to biodegradable agricultural mulches

Term	***Definition***
Biobased	Commercial or industrial products (other than food or feed) that are composed in whole or in significant part of biological products or renewable domestic agricultural materials (including plant, animal, and marine materials) or forestry materials (*23*)
Biodegradable plastic	Degradable plastic in which the degradation results from the action of naturally occurring microorganisms such as bacteria, fungi, and algae (*24*, *25*)
Composting	A managed process that controls the biological decomposition and transforma-tion of biodegradable materials into a humus-like substance called compost (*24*, *25*)
Compostable plastic	A plastic that undergoes degradation by biological processes during composting to yield carbon dioxide, water, inorganic compounds, and biomass at a rate consistent with other known compostable materials, and leaves no visible, distinguishable, or toxic residue (*24*, *25*)
Degradable plastic	Plastic designed to undergo a significant change in its chemical structure under specific environmental conditions, resulting in a loss of some properties that may be measured by standard test methods (*24*, *25*)
Degradation	A deleterious change in the chemical structure, physical properties, or appearance of a plastic (*25*)
Mineralization	Microbial conversion of organic matter into inorganic substances, such as water and carbon dioxide (*26*)

Continued on next page.

In Degradable Polymers and Materials: Principles and Practice (2nd Edition); Khemani, K., et al.;
ACS Symposium Series; American Chemical Society: Washington, DC, 2012.

Table I. (Continued). Important definitions relating to biodegradable agricultural mulches

Term	*Definition*
Organic agriculture	An ecological production management system that promotes and enhances biodiversity, biological cycles, and soil biological activity. It is based on minimal use of off-farm inputs and on management practices that restore, maintain, or enhance ecological harmony (USDA-NOSB [a])
	Integration of cultural, biological, and mechanical practices that foster cycling of resources, promote ecological balance, and conserve biodiversity. Synthetic fertilizers, sewage sludge, ir-radiation, and genetic engineering may not be used (USDA-NOP [b])
Sustainable agriculture	Integrated system of plant and animal production practices having a site-specific application that will, over the long term: satisfy human food and fiber needs; enhance environmental quality and the natural resource base upon which the agricultural economy depends; make the most efficient use of nonrenewable resources and on-farm resources and integrate, where appropriate, natural biological cycles and controls; sustain the economic viability of farm operations; and enhance the quality of life for farmers and society as a whole. (1990 USA Farm Bill [c])
Synthetic material [d]	A substance that is formulated or manufactured by a chemical process or by a process that chemically changes a substance extracted from a naturally occurring plant, animal, or mineral sources, except that such term shall not apply to sub-stances created by naturally occurring biological processes (USDA-NOSB [a]) (*21*)

[a] US Dept. Agriculture (USDA), National Organic Standards Board; [b] USDANational Organic Program; [c] Food, Agriculture, Conservation, and Trade Act of 1990 (FACTA), Public Law 101-624; [d] As specified by the USDA-National Organic Program

Conceptual Model for the Biodegradability Process

A recent review lists and describes the main underlying factors that promote biodegradation of plastics (*19*). The factors were divided into three categories: abiotic (environmental) conditions, microbial requirements, and properties of the mulch material. Abiotic factors include temperature, pH, and moisture of soil, and ultraviolet radiation. Characteristics of microorganisms capable of biodegradation include the presence of extracellular enzymes, the ability to bind with hydrophobic surfaces, and the presence of biosurfactants. Abiotic and biotic factors are interrelated; to accelerate mineralization (i.e., full biodegradation), not only must fragmentation occur (typically by abiotic means); but also, the soil environment must be enriched in nutrients, particularly nitrogen (*22*), and additional carbon-energy sources. Important properties of the mulch material include its morphology (such as its low crystallinity), its tensile strength and flexibility, its chemical composition (i.e., the chemistry and relative amounts of its monomeric units and additives), and other chemical properties, including its

In Degradable Polymers and Materials: Principles and Practice (2nd Edition); Khemani, K., et al.;
ACS Symposium Series; American Chemical Society: Washington, DC, 2012.

molecular weight, the extent of cross-linking, the nature of its functional groups, and the supramolecular arrangement of polymer molecules. A recent article emphasized the importance of biodegradable plastics possessing a high aliphatic nature to improve flexibility, which in turn will enable attack by hydrolases (*20*). The importance of these properties will be demonstrated below.

The process of biodegradation is generally divided into two time stages (*27*). During the first stage, "fragmentation" occurs, whereby the mulch is divided into small fragments, leading to a large increase of surface area. Driving forces identified for the first stage include mechanical forces (e.g., wind, plant roots, and abrasion by sand or soil particulates), solar photodegradation, and hydrolysis or other chemical events promoted by moisture and inorganic soil constituents (including osmotic pressure). Insects and earthworms and rodents can also serve as agents (i.e., "biofragmentation"). A concern for the first stage is the occurrence of photo-induced cross-linking, which can reduce the extent of microbial catabolism (*8*). In the second stage, the partially fragmented mulch can be utilized by microorganism as a carbon-energy source (i.e., "mineralization," as defined in Table I). Concerning degradation of PLA materials, the first stage includes the abiotic chain scission of the polymer, resulting in a decrease of molecular weight, followed by mineralization as the second stage (*19*). The authors of this chapter believe that for PLA, chain scission occurs during the latter end of the first stage. Both stages are accelerated as temperature is increased (*19*, *27*).

Based on the literature, the authors propose a mechanistic model for the biodegradation of agricultural mulches prepared by us from PLA, or PLA- PHA blends, using nonwovens textile technology that is shown in Figure 1. The first phase of the process involves the partial fragmentation, or "opening up," of the plastic's supramolecular structure (analogous to the process that occurs during pretreatment of lignocellulosic biomass) to enable mineralization, that is, the complete conversion into CO_2, water, and inorganics (formal definition given in Table I). Common promoters of this first phase include moisture and sunlight, and other environmental factors. The first phase is observed by a significant weakening of tensile strength and a slight reduction of molecular weight. During the second phase, microbial activity initiates, leading to embrittlement and fragmentation, resulting ultimately in the disappearance of macroscopic fragments and production of small amounts of CO_2 and water. In the third stage, microorganisms completely mineralize oligomers produced during the second stage.

Commercially Available Biodegradable Mulches

Several commercial products that are deemed as "biodegradable plastics" have been introduced to the agricultural market in recent years. The term refers to polymeric materials that undergo significant change in their chemical structure due to microorganisms, leading to a loss of a measurable physical or chemical properties. An official definition is given in Table I.

In Degradable Polymers and Materials: Principles and Practice (2nd Edition); Khemani, K., et al.;
ACS Symposium Series; American Chemical Society: Washington, DC, 2012.

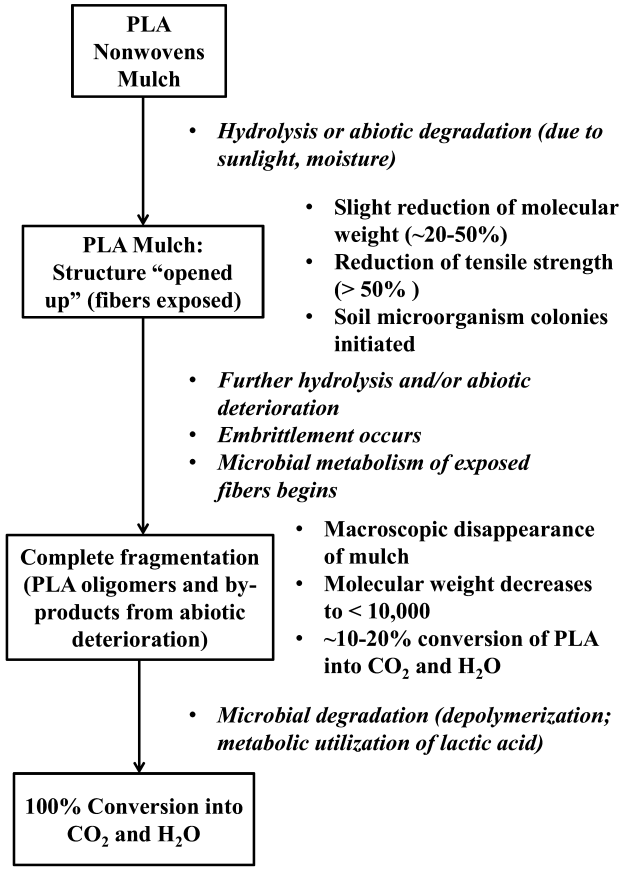

Figure 1. Proposed mechanistic model for the complete degradation of PLA nonwovens-based mulches

Recent reviews divide biodegradable polymers used to manufacture agricultural mulches into three different categories: biobased polymers (including starch, cellulose, chitin, chitosan, other polysaccharides, alginates, bacterial polyesters, and polypeptides), synthetic polymers (including polyesters such as PLA, polycaprolactone, polyamides, polyurethanes, and polyanhydrides), and poorly degradable polymers that contain oxidizable moieties and/or oxidation agents as additives or as monomeric constituents (*28*, *29*). The term "synthetic" is defined in Table I. Concern has been raised that plastics belonging to the latter category are not truly biodegradable, that their partial degradation yields oligomers and other by-products that are poorly biodegradable (*30*). Most agricultural mulches consist of thin films; therefore, biodegradable polymer feedstocks may require additives for their proper manufacturing due to deficiencies in their mechanical processing-related properties, such as nucleating agents, plasticizers, performance additives, and lubricants (reviewed in (*18*, *28*)). The environmental impact of these additives are a major concern (*21*, *27*).

In Degradable Polymers and Materials: Principles and Practice (2nd Edition); Khemani, K., et al.;
ACS Symposium Series; American Chemical Society: Washington, DC, 2012.

Table II lists commercially available biodegradable agricultural mulches and their major polymeric constituents. A more expansive list is given elsewhere (*9*, *31*). A recent review states that commercial mulches labeled as "biodegradable" perform similarly to PE mulches in terms of weed prevention, enhancement of crop yield, ease of laying at the beginning of the growing season, and mechanical strength (*9*). Also similar to PE, several of the black mulches of Table II underwent a significant decrease of mechanical strength during the first 1-5 weeks due to exposure to the sun's ultraviolet radiation and to water to a lesser extent (*9*). Several of the commercial biodegradable mulches disappeared visually when buried in soil for several months (*9*).

A popular polymer for biodegradable agricultural mulches is Ecoflex®, manufactured by BASF, consisting partially of the synthetic copolymer polybutylene adipate therephthalate, or PBAT. DuPont has also developed a PBAT-related copolymeric product referred to as Biomax®, with its designed application being as a biodegradable toughener for PLA. The molecular structure of PBAT is given in Figure 2. PBAT is reported to possess mechanical properties similar to low-density PE (*32*). Its possesses high flexibility, good impact strength, and good melt processability. PBAT is biodegradable under composting enviroments, possessing a low environmental impact (*22*, *33*, *34*). PBAT readily forms composites with several natural biobased polymers, including starch, cellulose, other polysaccharides, PLA, and PHA, and imparts desirable properties to the blend, such as increased flexibility and hydrophobicity (*28*). For the PBAT-based products listed in Table II, starch is a major component of the blend, with its presence greatly enhancing biodegradability (*35*).

A few studies have been published recently which assess the biodegradability and performance of commercially available biodegradable mulches, demonstrating the loss of mechanical strength and partial conversion into CO_2 when buried under soil or placed at the water-air surface (*36–41*). Ecoflex® is readily biodegradable under composting conditions (55-58°C), with only monomers (e.g., 1,4-butanediol, terephthalate, and adipate) detected at the end of the process (*22*, *34*). Biodegradation occurs more readily in amorphous morphological regions of PBAT, and near butanediol monomeric units, which are less rigid than terephthalate units (*22*). Auras and co-worker have thoroughly investigated the performance and biodegradation of Ecoflex® (PBAT) in field studies operated under ambient conditions (0-30°C soil temperatures). Their results demonstrate a loss of over 50% of tensile strength (breaking load) and over 90% loss for elongation, moreover, a significant loss of mechanical strength, during a 16 week period (*41*). The loss was attributed to photodegradation, which led to chain scission and to cross-link formation, the later promoting gel formation and enbrittlement (*40–42*). The cross-linkage formation reduced the extent of mineralization for PBAT (*40–42*). Black dyes such as carbon black reduced cross-link formation; but, titanium dioxide, an agent for forming white color, enhanced the formation of cross links (*41*, *43*). In field trials assessing its performance for mulching of tomato plants, PBAT was found to favorably increase soil temperature relative to PE mulches initially; however, this trend reversed in subsequent weeks, particularly for PBAT mulches possessing white compared to black color (*44*). In the same study, the white PBAT mulch

In Degradable Polymers and Materials: Principles and Practice (2nd Edition); Khemani, K., et al.;
ACS Symposium Series; American Chemical Society: Washington, DC, 2012.

performed poorly relative to black PBAT and PE mulches in regards to weed control, leading to lower yield of tomatoes. Both black PBAT and PE mulches performed similarly for weed control and crop yield (*44*).

Table II. Commercially available polymers and polymer blends employed in biodegradable agricultural mulches [a,b]

Product Name	***Polymer*** [c,d]	***Manufacturer***
Biocycle®	*Sucrose / PHA blend*	*PHB Industrial (Brazil)*
Bio-Flex	PLA / copolyester blend	FKUR, Willich (Germany)
Biomax TPS	*Starch + thermoplastic starch*	*DuPont (USA)*
Biomer L	*PHA*	*Biomer (Germany)*
Bionolle	PBS	Showa High Polymer (Japan)
Biopar	*Starch co-polyester*	*Biop (Germany)*
Biosafe™	PBAT / starch blend; PBS; PBSA	Xinfu Pharmaceutical Co (China)
Eastar Bio™	PBAT / starch blend	Novamont (Italy)
Eco-Flex®	PBAT / starch blend	BASF (Germany)
Ecovio	Ecoflex® + PLA	BASF (Germany)
EnPol	PBS	IRE Chemical (Korea)
Envio	Ecoflex (PBAT) +PLA+starch blend	BASF (Germany)
GreenBio	*PHA*	*Tianjin GreenBio Materials (China)*
Ingeo®	Starch + PLA; PBS + PLA	NatureWorks (USA)
Mater-Bi®	PCL + starch blend	Novamont (Italy)
Mirel®	*(PHA)*	*Metabolix (USA)*
Paragon	*Starch + thermoplastic starch*	*Avebe, (Netherlands)*
ReNew	*Polyhydroxy alkanoate (PHA)*	*Danimer Scientific (USA)*
Skygreen®	Terephthalic acid co-polyester [e]	SK Chemicals (Korea)

[a] Information taken from (*9*, *20*, *31*); [b] italicized entries are products that are almost entirely biobased; [c] abbreviations: PBAT: polybytylene adipate terephthalate; PHA: polyhydroxyalkanoate; PLA: polylactic acid; PCL: polycaprolactone; PBS: polybutylene succinate; PBSA: PBS-co-adipic acid; [d] the molecular structure for several of the polymers is given in Figure 2; [e] also contains ethylene glycol, and [4-(hydroxymethyl) cyclohexyl] methanol

In Degradable Polymers and Materials: Principles and Practice (2nd Edition); Khemani, K., et al.;
ACS Symposium Series; American Chemical Society: Washington, DC, 2012.

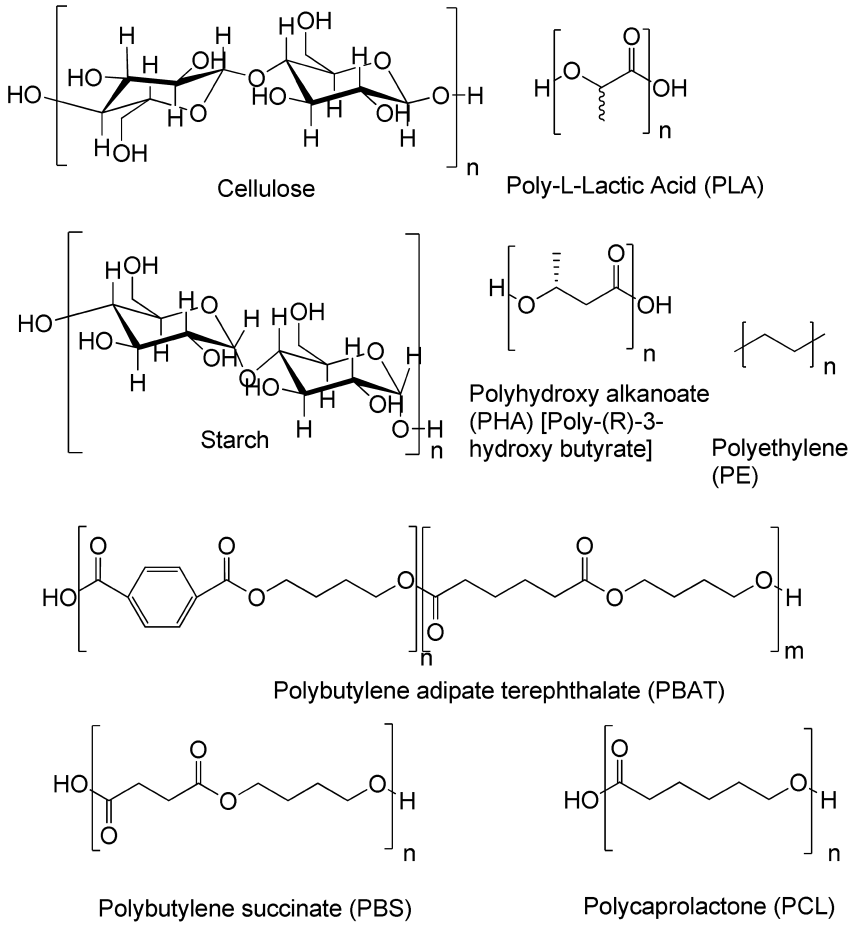

Figure 2. Molecular structures of polymers and biopolymers employed in agricultural mulches

Mater-Bi®, a film prepared from a polycaprolactone (PCL)-based co-polyester / starch blend by Novamont, "..is nowadays amongst the best developed products" according to a recent review (*9*). PCL, due in part to its low glass transition temperature (-60°C), is known to be readily biodegradable (*35*). (In a recent test in soil at 26°C, 70% of Mater-Bi®'s carbon atoms were mineralized into CO_2 (*8*).) Mater-Bi® readily undergoes loss of mechanical strength exposure (tensile strength and elongation) after > 3 months, to a greater extent than Ecoflex® and Bio-Flex®, a PLA-based copolyester blend. However, one publication raised concern that thin Mater-Bi films possesses great weakness, hence susceptibility to tearing, in the transverse direction (*37*). Several new commercial mulches have reached the market in recent years that contain polybutylene succinate (PBS), a co-polymer of 1,4-butanediol and succinic acid, as listed in Table I (with its molecular structure given in

In Degradable Polymers and Materials: Principles and Practice (2nd Edition); Khemani, K., et al.;
ACS Symposium Series; American Chemical Society: Washington, DC, 2012.

Figure 2), or other diacid-diol polyesters [e.g., polyethylene succinate (PES), PBS-co-adipate (PBSA), and a copolymer of terephthalic acid, ethylene glycol, and 4-(hydroxymethyl) cyclohexyl methanol]. Similar to PCL, PBS possesses a low glass transition temperature (< -10°C) and is reported to undergo mineralization, but to a lesser extent than PCL (*35*).

A problem with most of the biodegradable mulch products listed above is their inclusion of petroleum-derived polymers ("synthetics," as per the definition given in Table I), which prohibits their use in certified organic production in the USA. However, several petroleum-derived monomers can be produced from renewable resources, e.g., succinic acid via fermentation and adipic acid via the oxidation of ricinoleic acid, the major component of castor oil, using nitric acid. There is a great need to develop biodegradable mulches that are completely biobased.

Commercially-available biodegradable mulches can also be prepared from paper and other lignocellulosic biomass-derived sources (e.g., Weed Guard Plus®, described in Table III). Paper mulches were used extensively prior to 1950 (*45*). Paper mulches readily undergo complete biodegradation, and may possess greater puncture resistance than plastic mulches (*9*, *45*). However, paper mulches possess several inherent disadvantages (*9*, *45*). First, due to their high weight and tendency toward embrittlement, they are difficult to lay down in the field (*9*, *45*). In addition, they are susceptible to tearing from the wind, and rapidly lose mechanical strength when wetted (*9*, *45*). These trends were observed by us for paper mulches employed in specialty crops trials conducted in high tunnels and open field (discussed below). However, a recent study demonstrates that the incorporation of a polymerized vegetable oil increases the performance of paper mulches in the presence of water (*7*).

Polylactic Acid- and Polyhydroxyalkanoate-Based Mulches

Our focus has been on the use of PLA and PLA/PHA blends as feedstocks to prepare mulches. PLA (molecular structure given in Figure 2) has many desirable properties for biodegradable mulch employment. First, is it biobased, formed from lactic acid, derived from the fermentation of maize. Lactic acid is, typically polymerized using ring-opening polymerization of lactide, a cyclic dimer of lactic acid (using stannous octoate or other catalysts). Lactic acid exists in the L-optical form in nature, but can be racemized synthetically to form D-isomer. L- and D-, and DL- mixed lactides (i.e., dimeric ring structures) can be formed, producing optically pure homopolymers or those possessing both D- and L-momeric groups. PLA can also be oligomerized using lipases. Although it is biobased, when evaluated for organic certification PLA is considered to be a synthetic material due to the need to form it chemically (*8*). Synthesis of PLA is reviewed elsewhere (*46–48*). Second, PLA possesses good mechanical strength (e.g., tensile strength of 30-70 MPa). Third, compared to other biopolymers, PLA is less expensive and produced in large quantities (e.g., capacity of 140,000 metric tonnes at the Blair, NE USA facility operated by NatureWorks, LLC), with its worldwide production projected to reach 800,000 metric tonnes in 2020 (*18*). The relatively high capacity for PLA reflects its numerous uses in packaging

In Degradable Polymers and Materials: Principles and Practice (2nd Edition); Khemani, K., et al.;
ACS Symposium Series; American Chemical Society: Washington, DC, 2012.

(e.g., compostable cups, bottles, and wrappers) and for its fibers in textiles (e.g., apparel and heat-resistent automobile textiles), and nonwovens (e.g., wipes and diapers) (*47*, *49*). PHA is significantly less expensive than most other polymers, with its listed price being 2.1 USD kg^{-1} (*50*). In comparison, the prices for PHA, PCL, and starch blends are listed (on a per kg basis) as 7.2 USD (but as high as 19.6 USD), 6.9 USD, and 5.2 USD, respectively (*50*).

However, PLA also possesses significant disadvantages for use in agricultural mulches. First, it possesses a high glass transition temperature (~60°C), so that under most environmental conditions (except for industrial composting), PLA does not provide a large amount of amorphous morphology needed for access by microorganisms. Second, PLA is quite hard, leading to its embrittlement and poor thermostability. However, through blending with other polymers or plasticizers, increasing the extent of D-lactic acid monomeric units, or inducing branching *via* use of an organic peroxide, these properties can be reduced in prominence (*28*, *51*, *52*). (Also, impurities present in PLA resulting from the starting materials can strongly influence the physical properties (*53*).) PLA-starch blends, enabled by the use of plasticizers and/or grafting onto PLA (e.g., using maleic anhydride) to increase miscibility, are one common blend. Two starch-based blends employable for preparing biodegradable mulches are listed in Table II. Other polymers employed in blends with PLA include PBAT, polyethylene oxide, chitosan, epoxidized soybean oil, PCL, and polyvinyl alcohol, with common plasticizers such as lactic acid, glycerol, and citrate esters. Recent studies have shown that the employment of lactic acid derivatives (*54*), or linear or cyclic lactic acid oligomers (*55*), acting as plasticizers, can greatly accelerate biodegradation at temperatures of 30-40°C. The former enhanced accumulation of fungi and bacteria on the material's surface (*54*). The latter allowed for greater uptake of water, resulting in the desorption of plasticizer and subsequently the increased porosity of the PLA material, leading to a 80% decrease in molecular weight over a 15 week period at 37°C (*55*). Third, although readily compostable, PLA often slowly biodegrades under ambient conditions, including in soil (*35*). (In contrast, a recent report suggests that an enriched microbial community, e.g., a mixed culture of compost microorganisms, can lead to nearly complete disintegration of PLA in soil at 30°C (*56*).) Similarly, its crystallinity does not change appreciably when buried in soil for 7 months (*39*). An underlying cause may be its relatively high hydrophobicity, which makes it less assessable to microbial enzyme systems (*36*). Moreover, a recent study suggests that 30°C is a minimum temperature to obtain any occurrence for biodegradation (~10% in 20 d), with industrial composting temperatures (58°C) needed for biodegradation to occur at a reasonably fast rate (*39*). However, ultraviolet radiation, combined with the presence of moisture, has been reported to decrease the average molecular weight (*57–59*).

PHA, typically possessing 3-hydroxy butyrate (PHB; molecular structure given in Figure 2) as its major monomeric unit, is a natural polymer produced by many bacteria to serve as a means of storage for carbon and energy. Its current production is near 60,000 tonnes per year (*60*). It has several applications in biomedicine, injection molding and packaging. A major hindrance for its further utilization is its relatively high production cost (*60*), evidenced by the recent closing of the Clinton, IA USA facility that produced

In Degradable Polymers and Materials: Principles and Practice (2nd Edition); Khemani, K., et al.;
ACS Symposium Series; American Chemical Society: Washington, DC, 2012.

Mirel® PHA, and accompanying dissolution of Telles, a joint venture between Archer-Daniels-Midland and Metabolix to produce Mirel. PHA is readily biodegradable, including in soil (*29*, *35*, *39*, *61*). PHA is a highly crystalline thermoplastic polymer that is susceptible to embrittlement and to thermal degradation near its melting temperature. Furthermore, it is known to undergo secondary crystallization for its amorphous phase under storage, leading to a further increase in crystallinity and embrittlement and to a large decrease of elongation at break (*28*). A major problem is its incompatibility with several other polymers (*28*). PHA is susceptible to loss of elongation at break due to ultraviolet radiation produced by the sun, but with the tensile strength remaining constant over a 3 month exposure period (*39*). Therefore, similar to PLA, the blending of PHA with other polymers (e.g., polyvinyl acetate) or plasticizers is necessary to improve its physical properties. PHA / PLA blends are being evaluated as feedstock for the preparation of agricultural mulches prepared using nonwovens textile processing by the authors. The blending of PLA and PHA enhanced the biodegradation rate for the latter, but did not induce mineralization of the former (*62*, *63*).

On the Measurement of Biodegradability for Mulches

As stated in a recent review of biodegradation in soil, "[m]ost of the available international standards for biodegradable materials are designed for testing biodegradation under various conditions in a variety of media .. but not for testing specifically biodegradation in soil, especially in agricultural soils which [are] used for the production of food" (*8*). Therefore, there is a great need to develop new standard methods that can simulate actual environmental conditions of agricultural settings (e.g., in open fields, high tunnels, and greenhouses) and be assessed in a shorter time frame than those involved with the typical lifetime of agricultural mulches (several months to over a year).

Currently, one of the most commonly used tests for biodegradability is ASTM D5988 (*64*) (or similarly D5338 (*65*)), which involves measuring the release of CO_2 from a plastic placed in soil augmented with industrial compost (that meets specified requirements for pH and other soil properties), with biodegradation operated under a specified temperature (21°C and 58°C for D5398 and D5338, respectively) and aerobic conditions. ISO and other organizations that specify standards suggest similar tests (reviewed in (*8*)).

The ASTM tests described above are used in assessing compostability, the ability of plastics to be mineralized under industrial composting conditions. Since the ASTM D5338 and D5398 tests are associated with specified standards for composting (ASTM D6400 (*24*)), and therefore designed to evaluate compostability, a brief description of the conditions for composting is warranted. Also, because the PLA mulches prepared by us are most probably compostable, interest in this topic is relevant. As defined in ASTM D6400 (*24*), composting refers to a managed biodegradation process that, through microbial activity, yields CO_2, water, minerals, and a humus-like substance (complete definition

In Degradable Polymers and Materials: Principles and Practice (2nd Edition); Khemani, K., et al.;
ACS Symposium Series; American Chemical Society: Washington, DC, 2012.

given in Table I). "Industrial" or "commercial" composting refers to large-scale operations in which manure, yard waste, and food waste are combined and then subjected to aerobic microbial activity, which is enhanced by shredding and mixing via heavy machinery plus elevated temperatures and moisture levels in a multistage process (*31*). "Back-yard," "home", and/or "farm" compost is performed at a much smaller scale, and typically involves lower temperatures (10-40°C), and consequently is slower. The latter usually involves different components, sources, and compositions of medium. ASTM D6400 (*24*) specifies compostability is met through achievement of three criteria: disintegration (90% disappearance as assessed through sieving at 2 mm nominal size); absence of ecotoxicity (low heavy metals and no inhibition of germination and plant growth); and, "inherent biodegradability:" at least 60% conversion of the plastic's carbon atoms into CO_2 within 180 d, as measured using ASTM D5338 (*65*). Other organizations have developed standards that are similar in criteria to those of ASTM D6400 (reviewed in (*31*, *66*)). The cited critical reviews state that current standards such as ASTM D6400 and the testing methods associated with them such as D5338 need to be revised in order to better represent both non-thin forms of bioplastics (e.g., packaging materials), "farm" or "back-yard" composting conditions and variability in the procedure, as well as to be less time-consuming and labor-intensive (reviewed in (*20*, *31*, *66*)). Moreover, a "one size fits all" approach may not be appropriate for standardizing biodegradability under diverse composting conditions.

As a result, standardized tests for measuring biodegradation, such as ASTM D5338 are not necessarily representative of biodegradability in soil due to differences in time scale and environmental conditions (e.g., absence of appropriate abiotic factors). A recent critical review suggests possible specified standards for soil biodegradation, such as 70% biodegradation in 6 months and 90% in 2 years under soil conditions (ASTM D5988) at 28°C, and differing standardization for different categories of soil type (*66*).

Preliminary Studies

We have assessed the potential utility of several PLA-based mulches formed using nonwovens textile technology as agricultural mulches through several different experimental platforms. The mulches employed in our studies and their physical properties are given in Table III. As reviewed elsewhere (*67*), nonwovens are manufactured sheets, webs or bats of directionally or randomly oriented fibers, bonded by friction, and/or cohesion and/or adhesion. Specifically, the nonwoven processing employed for the PLA mulches consists of spunbond and meltblown processes. For the former, the polymer batch is first melted, then extruded through spinnerets, producing filaments. The resultant fibers are cooled and laid down on a conveyer belt to form a web. A thermal embossed calendering follows with 10-20% of the web surface area being fused into separated and discrete areas, usually forming a diamond pattern. For the latter, hot air flowing in the transverse direction is applied to the melted polymer exiting a die or spinneret,

In Degradable Polymers and Materials: Principles and Practice (2nd Edition); Khemani, K., et al.;
ACS Symposium Series; American Chemical Society: Washington, DC, 2012.

to stretch, disperse, and mechanically entangle the filaments, which are cooled by ambient entrained air and ultimately collected on a roll without the need for a thermal calendering step. Generally, meltblown nonwovens possess smaller fiber sizes and are weaker in mechanical strength than spunbond nonwovens.

The results in Table III are consistent with the abovementioned trends, showing higher tensile strength (breaking load in the machine direction) for the spunbond (SB) compared to the meltblown (MB) mulches. All nonwovens possess greater tensile strength than the PE or biodegradable black plastic mulches employed in our studies. Also consistent with this trend is the smaller fiber diameter size for MB-PLA-2010 (6.3 ± 0.2 μm) compared to SB-PLA-2010 (14.8 ± 0.1 μm), measured via scanning electron microscopy (SEM) (*68*). Therefore, the hypothesis being tested is that the employment of PLA-based nonwovens as agricultural mulches will accelerate biodegradation due to their relatively large surface area (which will more than overcome the increased crystallinity of PLA fibers (*39*)) relative to PLA film-based mulches.

The following experiments were conducted to assess the performance of the mulches listed in Table III. First, to evaluate the impact of the mulches on crop production as well as their biodegradability, mulches were investigated in the cultivation of specialty crops (tomatoes) grown in high tunnels and open fields. The plots were established in three regions of the USA possessing diversity in climate and soil types (eastern Tennessee, northwestern Texas, and northwestern Washington). The performance of PLA was compared to that for a set of commercial mulches that included three black films (BioAgri, BioTelo, and a PE mulch), a paper mulch (WeedGuardPlus), and the absence of mulch. Black PE and WeedGuardPlus served as negative and positive controls, respectively. BioAgri and BioTelo are advertised as "biodegradable," both consisting of Mater-Bi® as their major chemical component (described above and in Table II). Second, soil burial studies have been conducted under controlled conditions in a greenhouse, examining the effect of mulch type, soil amendment, and soil moisture among other variables of the biodegradation of the mulches (as per Figure 1). Third, weatherometry is currently being employed to understand the effects of abiotic events on the biodegradability and stability of the mulches. Fourth, biodegradability of PLA mulches using ASTM D5338 (*65*) is ongoing.

For the first three experiments described above, several physical and chemical tests are being employed. The main physical testing is tensile strength (breaking load in the machine direction), and percent elongation at breakage, which provide the most useful information on physical strength, and SEM, which provided average fiber thickness and evidence of breakage for the PLA fibers. Other physical tests have been employed less frequently, due to their inability to provide directly useful information (particularly for the nonwovens-based PLA mulches), such as weight (g m^{-2}), thickness, air permeability, and tear strength. For example, the former three tests more strongly reflected the adsorption of soil particles onto the nonwovens mulches, despite the employment of a thorough and elaborate cleaning procedure. Chemical testing consists of molecular weight determination via gel permeation chromatography and employment of FTIR spectroscopy and differential scanning calorimetry to analyze bond formation and breakage and morphological changes, respectively.

In Degradable Polymers and Materials: Principles and Practice (2nd Edition); Khemani, K., et al.;
ACS Symposium Series; American Chemical Society: Washington, DC, 2012.

Table III. Agricultural mulches investigated by authors in a 3-year study in high tunnels and open field conditions in the USA (Tennessee, Texas, and Washington), and/or in a greenhouse study in Tennessee

Commercial or Given Name	*Manufacturer*	*Polymer Type*	*Load (N)* [a]	*M_n, kDa* [b]	*Weight, g m^{-2}*	*Thickness, mm*
BioAgri	BIOgroup USA	Mater-Bi®-based	9.0	96.2 [c]	20	0.015
Bio Telo	Dubois Agro-inovation (Canada)	Mater-Bi®-based	8.0	73.1 [c]	19	0.015
Black Plastic	Berry Plastics Corp (USA)	PE	12.0	ND [d]	24	1 mil
WeedGuardPlus	SunShine Paper Co (USA)	Cellulosic	81.3	ND [d]	104	0.255 [e]
SB[f]-PLA 2010 White [e]	Prepared by authors	PLA	48.1	132 l	90 [l]	0.657
SB[f]-PLA 2011 Black or White	Prepared by authors	PLA	45.2	101.1	80	ND [d]
SB[f]-PLA+PHA 2012 Black and White	Prepared by authors	PLA / PHA 80 / 20 w/w	42.1	99.5	80	ND [d]
MB[g] -PLA 2010 White [e]	Prepared by authors [e]	PLA	26.2	115 l	75	0.459
MB[g]-PLA + PHA - 2011 White	Prepared by authors	PLA / PHA 85 / 15 w/w	ND [d]	89.9	75	ND [d]
MB[g]-PLA + PHA - 2011 White	Prepared by authors	PLA / PHA 75 / 25 w/w	ND [d]	75.8	75	ND [d]

[a] Breaking load in the machine direction; [b] Number-averaged molecular weight; [c] reflects chloroform-solubilized portion; [d] Not determined; [e] further information given, and values taken, from (*68*); [f] spunbond; [g] meltblown

Analysis of results from high tunnel and open field experiments in 2010 and 2011 at the three locations listed above are ongoing. Each experiment has consisted of carefully planned randomized experimental designs (Figure 3) that have spanned the 5-6 month-long summer growing season at each site. Data collected has included plant growth, vegetable yield, diseases, insects, and environmental measurements. From preliminary results obtained thus far, BioAgri and BioTelo mulches exhibited the greatest amount of deterioration as measured visually in the high tunnels in Tennessee, while BioAgri, Bio Telo and WeedGuardPlus all exhibited high levels of deterioration in the open field. In Texas, WeedGuardPlus exhibited the greatest amount of deterioration in both the high tunnel and open field; but, deterioration was statistically equivalent to BioAgri and BioTelo in the high tunnels. In Washington WeedGuardPlus exhibited the greatest amount of deterioration in both the high tunnel and open field. Laboratory analyses of physical and chemical properties revealed that WeedGuardPlus (cellulosic) mulch underwent the greatest extent of deterioration, particularly in the open field environment, as observed by an approximately 10-fold loss of break load and a 4-fold loss of percent elongation, respectively. BioAgri and Bio Telo also lost mechanical strength: approximately a 40% and 85% loss of break load and elongation, respectively, with the extent of mechanical strength loss varying between location and setting (high tunnel versus open field). A decrease of molecular weight occurred for the latter two mulches approximately 20% during a 3-4 month period (for their chloroform-soluble components). In contrast, the SB-PLA-2010 underwent minimal change of breaking load and elongation, as well as molecular weight. The SB-PLA-2011 mulch, composed of a lower molecular weight PLA feedstock than the 2010 mulch, underwent a slightly higher decrease of molecular weight, approximately 10%. The high tensile strength and low extent of deterioration experienced for the SB-PLA mulches suggests their possible use in long-term applications in sustainable agriculture, for mulching of perennial and ornamental crops, for instance (*9*), or as row covers. At the end of their long-term use, the SB-PLA mulches can be composted. This goal will enhance process sustainability, but would not reduce labor costs (e.g., for mulch retrieval). Moreover, for many growers, a composting facility may not be located in the vicinity of their operations.

Results from our initial soil burial study, conducted in a greenhouse, were recently described in a manuscript submitted for publication (*68*). In this 30 week study, SB-PLA-2010, MB-PLA-2010, and WeedGuardPlus were investigated for possible deterioration as a function of two soil amendments: compost and lime. The latter mulch served as a control. (The MB-PLA mulches were prepared at a small scale, thereby preventing their use in the large-scale high tunnel and open field studies.) From visual observations, MB-PLA underwent significant deterioration (Figure 4). In contrast, SB-PLA underwent minimal deterioration; and, WeedGuarPlus fragments were not visible after 10 wk. Consistent with the visual observations, the break load and elongation for MB-PLA decreased by 70% and 45%, respectively. However, the molecular weight of the PLA nonwovens-based mulches did not decrease appreciably over the 30 week period. In addition, SEM analysis demonstrated fibers in the MB mulches underwent breakage; and, several soil particles adsorbed strongly to the fibers (Figure

In Degradable Polymers and Materials: Principles and Practice (2nd Edition); Khemani, K., et al.;
ACS Symposium Series; American Chemical Society: Washington, DC, 2012.

5). Regarding the soil amendments, the addition of lime and compost both significantly increased the deterioration of the mulches (observed through the loss of tensile strength, for example), and led to a statistically significantly higher soil pH.

Figure 3. High tunnel study at the University of Tennessee, Knoxville, TN USA depicting the utilization of five different mulch treatments for the growth of tomatoes in an carefully planned randomized experimental design.

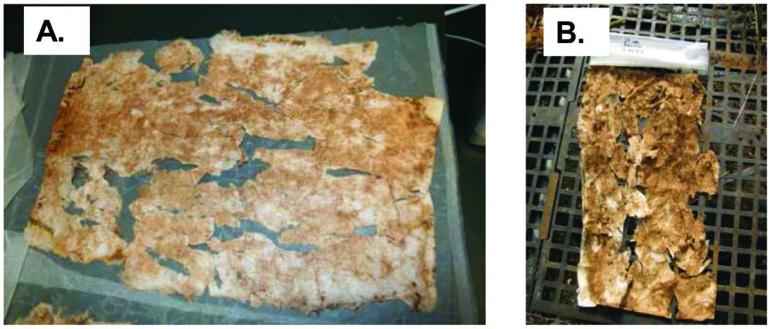

Figure 4. Photographs of Meltblown (MB) –PLA-2010 mulches after burial in lime-amended soil for (A) 10 wk and (B) 29 wk in a greenhouse study at the University of Tennessee, Knoxville, TN USA.

In Degradable Polymers and Materials: Principles and Practice (2nd Edition); Khemani, K., et al.; ACS Symposium Series; American Chemical Society: Washington, DC, 2012.

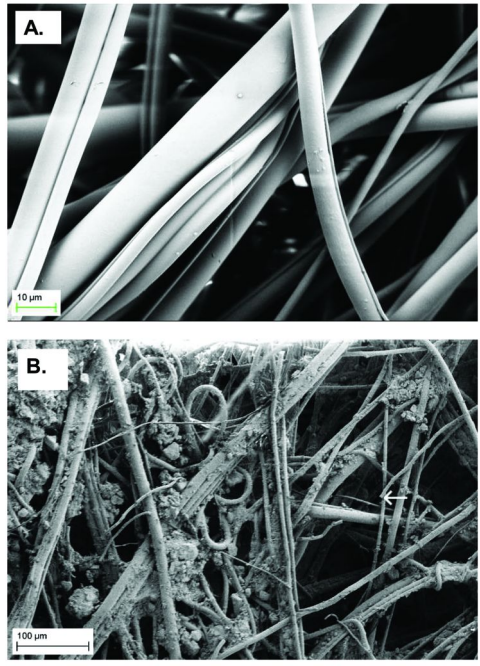

Figure 5. Scanning electron microscopy photomicrographs of Meltblown (MB) –PLA-2010 mulches (A) in its original state (1000 x); (B) after 29 wk of burial in lime-amended soil (500 x) in a greenhouse study at the University of Tennessee, Knoxville, TN USA. Arrow in Fig B depicts fiber breakage. Taken from (68). Reproduced courtesy of Journal of Engineered Fibers and Fabrics, P.O. Box 1288, Cary, North Carolina 27512-1288, USA. Tel: (919) 233-1210 Fax: (919) 233-1282 Internet: www.jeffjournal.org.

Conclusions

There is a compelling need to develop new biodegradable agricultural mulches that are completely biodegradable and biobased, which can be employed in sustainable, and also perhaps organic, agriculture. Initial tests of commercially available biodegradable mulches in laboratory and field studies demonstrate their potential utility; for instance, 70% mineralization within 30 weeks was reported for Mater-Bi® in soil at 26°C (*8*). However, long-term and large scale field studies are needed to determine the effects of environmental parameters (e.g., photo-induced cross-linking reaction that occurs for PBAT, a major component of Ecoflex® (*40–42*)). PLA is a potentially valuable material for biodegradable mulches due to its abundance and low cost relative to other biopolymers. However, its low biodegradation rate under typical soil conditions needs to be increased, perhaps through decreasing its crystallinity (via inclusion of plasticizers or hydrophilic polymers), increasing its surface area (e.g., via employment of nonwovens textile technology, as being investigated by the authors), and/or

In Degradable Polymers and Materials: Principles and Practice (2nd Edition); Khemani, K., et al.;
ACS Symposium Series; American Chemical Society: Washington, DC, 2012.

introducing an active microbial community near the PLA material. Development of standards for biodegradable mulch performance is a challenging, but worthy, task due in part to the heterogeneity of environmental conditions encountered in agricultural systems. The authors' nonwovens-based PLA prototypes undergo biodegradation too slowly for practical usage as short-term mulches although other longer-term agricultural purposes may prove quite appropriate. And as shown,, the use of proper selection of parameters for nonwovens preparation (e.g., a reduced molecular weight for PLA and employment of meltblown processing) can significantly improve the deterioration of the mulch. Recent greenhouse experiments demonstrate that PLA/PHA meltblown nonwovens (listed in Table III) demonstrate further improvement in loss of molecular weight and mechanical strength (unpublished results). Further research is ongoing.

Acknowledgments

The preliminary research reported upon herein was funded in part through a grant from the NIFA Specialty Crops Research Initiative, USDA SCRI-SREP Grant Award No. 2009-02484.

References

1. Espi, E.; Salmeron, A.; Fontecha, A.; Garcia, Y.; Real, A. I. *J. Plast. Film Sheeting* **2006**, *22*, 85–102.
2. Lamont, W. J., Jr. *HortTechnol* **2005**, *15*, 477–481.
3. Midmore, D. J.; Jansen, H. G. P. *Food Policy* **2003**, *28*, 13–27.
4. Khan, S.; Hanjra, M. A. *Food Policy* **2009**, *34*, 130–140.
5. Wallace, J. S. *Agric. Ecosystems Environ.* **2000**, *82*, 105–119.
6. Miles, C.; Klinglerk, E.; Nelson, L.; Smith, T.; Cross, C. Alternatives to plastic mulch in vegetable production systems. Washington State University, Vancouver Research and Extension Unit Report. June 19, 2008 [Online], 2007. http://vegetables.wsu.edu/MulchReport07.pdf.
7. Shogren, R. L.; Hochmuth, R. C. *HortScience* **2004**, *39*, 1588–1591.
8. Briassoulis, D.; Dejean, C. *J. Polym. Environ.* **2010**, *18*, 384–400.
9. Martin-Closas, L.; Pelacho, A. M. *Biopolymers* **2011**, 277–299.
10. Thompson, R. C.; Moore, C. J.; vom Saal, F. S.; Swan, S. H. *Philos. Trans. R. Soc., B* **2009**, *364*, 2153–2166.
11. Thompsond, R. C.; Swan, S. H.; Moore, C. J.; vom Saal, F. S. *Philos. Trans. R. Soc. London, Ser. B* **2009**, *364*, 1973–1976.
12. Bos, U.; Makishi, C.; Fischer, M. *Acta Hortic.* **2008**, *801*, 341–350.
13. Olsen, J. K.; Gounder, R. K. *Aust. J. Exp. Agric.* **2001**, *41*, 93–103.
14. Levitan, L. Reducing dioxin emissions by recycling agricultural plastics: Creating a viable alternative to open burning. Presented at Great Lakes Regional Pollution Prevention Roundtable, New York, 2005.
15. Lemieux, P. M. *Evaluation of emissions from the open burning of household waste in barrels*; U.S. Environmental Protection Agency Report 600/R-97-134a; Washington, DC, 1997; p 70.

16. Hakkarainen, M.; Albertsson, A.-C. *Adv. Polym. Sci.* **2004**, *169*, 177–199.
17. Takada, S. *Global distribution of organic micropollutants in marine plastics*; Report to Algalita Marine Research Foundation; April 20, 2010.
18. Shen, L.; Worrell, E.; Patel, M. *Biofuels, Bioprod. Biorefin.* **2010**, *4*, 25–40.
19. Kijchavengkul, T.; Kale, G.; Auras, R. *ACS Symp. Ser.* **2009**, *1004*, 31–40.
20. Tullo, A. H. *Chem. Eng. News* **2012**, *90* (12).
21. Sullivan, D. *BioCycle* **2011**, 36–41.
22. Kijchavengkul, T.; Auras, R.; Rubino, M.; Selke, S.; Ngouajio, M.; Fernandez, R. T. *Polym. Degrad. Stab.* **2010**, *95*, 2641–2647.
23. Biobased US. What are Bio-Based Products? 2007. http://www.biobased.us/biobased.html.
24. ASTM International. *Standard specification for compostable plastics (ASTM D6400)*; West Conshohocken, PA, USA, 2004.
25. ASTM International. *Standard terminology relating to plastics (ASTM D883)*; West Conshohocken, PA, USA, 2011.
26. Guggenberger, G. Microorganisms and soil genesis. In *Microorganisms in soils: roles in genesis and functions*; Buscot, F., Varma, A., Eds.; Springer-Verlag: Berlin, 2005; pp 85−106.
27. Kyrikou, I.; Briassoulis, D. *J. Polym. Environ.* **2007**, *15*, 125–150.
28. Briassoulis, D. *J. Polym. Environ.* **2004**, *12*, 65–81.
29. Vroman, I.; Tighzert, L. *Materials* **2009**, *2*, 307–344.
30. Society of the Plastics Industry Bioplastics Council. *Position paper on oxo-biodegradables and other degradable additives*; 2010.
31. Kijchavengkul, T.; Auras, R. *Polym. Int.* **2008**, *57*, 793–804.
32. Fomin, V. A.; Guzeev, V. V. *Prog. Rubber Plast. Technol.* **2001**, *17*, 186–204.
33. Muller, R. J.; Kleeberg, I.; Deckwer, W. D. *J. Biotechnol.* **2001**, *86*, 87–95.
34. Witt, U.; Einig, T.; Yamamoto, M.; Kleeberg, I.; Deckwer, W. D.; Muller, R. J. *Chemosphere* **2001**, *44*, 289–299.
35. Tokiwa, Y.; Calabia, B. P.; Ugwu, C. U.; Aiba, S. *Int. J. Mol. Sci.* **2009**, *10*, 3722–3742.
36. Mostafa, H. M.; Sourell, H.; Bockisch, F. J. *CIGR J.* **2010**, *12*, 1–16.
37. Briassoulis, D. *Polym. Degrad. Stab.* **2006**, *91*, 1256–1272.
38. Briassoulis, D. *Polym. Degrad. Stab.* **2007**, *92*, 1115–1132.
39. Rudnik, E.; Briassoulis, D. *J. Polym. Environ.* **2011**, *19*, 18–39.
40. Kijchavengkul, T.; Auras, R.; Rubino, M.; Ngouajio, M.; Fernandez, R. T. *Chemosphere* **2008**, *71*, 1607–1616.
41. Kijchavengkul, T.; Auras, R.; Rubino, M.; Ngouajio, M.; Fernandez, R. T. *Chemosphere* **2008**, *71*, 942–953.
42. Kijchavengkul, T.; Auras, R.; Rubino, M.; Alvarado, E.; Camacho Montero, J. R.; Rosales, J. M. *Polym. Degrad. Stab.* **2010**, *95*, 99–107.
43. Kijchavengkul, T.; Auras, R.; Rubino, M.; Selke, S.; Ngouajio, M.; Fernandez, R. T. *Polym. Degrad. Stab.* **2011**, *96*, 1919–1926.
44. Ngouajio, M.; Auras, R.; Fernandez, R. T.; Rubino, M.; Counts, J. W., Jr.; Kijchavengkul, T. *HortTechnology* **2008**, *18*, 605–610.
45. Shogren, R. L. *J. Sustain. Agric.* **2000**, *16*, 33–47.

In Degradable Polymers and Materials: Principles and Practice (2nd Edition); Khemani, K., et al.;
ACS Symposium Series; American Chemical Society: Washington, DC, 2012.

46. Lim, L.-T.; Cink, K.; Vanyo, T. Processing of poly(lactic acid). In *Poly(Lactic Acid): Synthesis, Structures, Properties, Processing, and Applications*; Auras, R., Lim, L. T., Selke, S. E. M., Tsuji, H., Eds.; John Wiley and Sons: Hoboken, NJ, USA, 2010; pp 191−215.
47. Sodergard, A.; Stolt, M. Industrial production of high molecular weight poly(lactic acid). In *Poly(Lactic Acid): Synthesis, Structures, Properties, Processing, and Applications*; Auras, R., Lim, L. T., Selke, S. E. M., Tsuji, H., Eds.; John Wiley and Sons: Hoboken, NJ, USA, 2010; pp 27−41.
48. Mehta, R.; Kumar, V.; Bhunia, H.; Upadhyay, S. N. *J. Macromol. Sci., Polym. Rev.* **2005**, *C45*, 325–349.
49. Mochizuki, M. Textile applications. In *Poly(Lactic Acid): Synthesis, Structures, Properties, Processing, and Applications*; Auras, R., Lim, L. T., Selke, S. E. M., Tsuji, H., Eds.; John Wiley and Sons: Hoboken, NJ, USA, 2010; pp 469−476.
50. Endres, H.-J.; Siebert-Raths, A. *Engineering Biopolymers - Markets, Manufacturing, Properties and Applications*; Hsanser Publishers: Munich, 2011.
51. Detyothin, S.; Kathuria, A.; Jaruwattanayon, W.; Selke, S. E. M.; Auras, R. *Poly(Lactic Acid)* **2010**, 227–271.
52. Sungsanit, K.; Kao, N.; Bhattacharya, S. N.; Pivsaart, S. *Korea-Aust. Rheol. J.* **2010**, *22*, 187–195.
53. Inkinen, S.; Hakkarainen, M.; Albertsson, A.-C.; Sodergard, A. *Biomacromolecules* **2011**, *12*, 523–532.
54. Hakkarainen, M.; Karlsson, S.; Albertsson, A.-C. *J. Appl. Polym. Sci.* **2000**, *76*, 228–239.
55. Andersson, S. R.; Hakkarainen, M.; Albertsson, A.-C. *Biomacromolecules* **2010**, *11*, 3617–3623.
56. Hakkarainen, M.; Karlsson, S.; Albertsson, A. C. *Polymer* **1999**, *41*, 2331–2338.
57. Belbachir, S.; Zairi, F.; Ayoub, G.; Maschke, U.; Nait-Abdelaziz, M.; Gloaguen, J. M.; Benguediab, M.; Lefebvre, J. M. *J. Mech. Phys. Solids* **2010**, *58*, 241–255.
58. Tsuji, H.; Echizen, Y.; Nishimura, Y. *J. Polym. Environ.* **2006**, *14*, 239–248.
59. Zhang, C.; Man, C.; Wang, W.; Jiang, L.; Dan, Y. *Polym.-Plast. Technol. Eng.* **2011**, *50*, 810–817.
60. Posada, J. A.; Naranjo, J. M.; Lopez, J. A.; Higuita, J. C.; Cardona, C. A. *Process Biochem. (Amsterdam, Neth.)* **2011**, *46*, 310–317.
61. Artsis, M. I.; Bonartsev, A. P.; Iordanskii, A. L.; Bonartseva, G. A.; Zaikov, G. E. *Mol. Cryst. Liq. Cryst.* **2010**, *523*, 21–49.
62. Focarete, M. L.; Ceccorulli, G.; Scandola, M.; Kowalczuk, M. *Macromolecules* **1998**, *31*, 8485–8492.
63. Koyama, N.; Doi, Y. *Can. J. Microbiol.* **1995**, *41*, 316–22.
64. ASTM International. *Standard test method for determining aerobic biodegradation in soil of plastic materials or residual plastic materials after composting*; ASTM D5988; West Conshohocken, PA, USA, 2003.

65. ASTM International. *Standard test method for determining aerobic biodegradation of plastic materials under controlled composting conditions*; ASTM D5338; West Conshohocken, PA, USA, 1998.
66. Briassoulis, D.; Dejean, C.; Picuno, P. *J. Polym. Environ.* **2010**, *18*, 364–383.
67. Khan, A. Y. A.; Wadsworth, L. C.; Ryan, C. M. *Int. Nonwovens J.* **1995**, *7*, 69–73.
68. Wadsworth, L. C.; Hayes, D. G.; Wszelaki, A. L.; Washington, T. L.; Martin, J.; Lee, J.; Raley, R.; Pannell, C. T.; Dharmalingam, S.; Miles, C.; Inglis, D. A.; Saxton, A. M. *J. Eng. Fibers Fabr.* **2012**, submitted.

In Degradable Polymers and Materials: Principles and Practice (2nd Edition); Khemani, K., et al.;
ACS Symposium Series; American Chemical Society: Washington, DC, 2012.

Chapter 14

Plant Oil-Based Curing Agents for Epoxies

Kun Huang,[1] Mei Li,[1] Shouhai Li,[1] Jianling Xia,[1,*] and Jinwen Zhang[2,*]

[1]Institute of Chemical Industry of Forest Products, Chinese Academy of Forestry, Nanjing, Jiangsu, China
[2]Composite Materials and Engineering Center, Washington State University, Pullman WA 99164,USA
[*]jwzhang@wsu.edu; xiajianling@126.com

Use of fatty acids and their derivatives in preparing amine type curing agents for epoxies was explored in this study. Dicarboxylic (C21) acids were prepared through addition reaction of esters of tung oil fatty aids and acrylic acid. The C21 acids were then reacted with polyamines to yield polyamidoamine type curing agents. The flexible hydrocarbon chains of fatty acids were also introduced to the Mannich base type curing agents for improved impact strength. Derivatives of fatty alcohols were used to prepare curing agents for waterborne epoxies. Furthermore, polyamidoamines based on rosin modified dimer fatty acids were also prepared. The properties of epoxies cured with these curing agents were evaluated.

Introduction

Plant oils are important renewable feedstocks for many industrial products. Traditionally, derivatives of plant oils or fatty acids are used in soaps, cosmetics, drying oils, inks, lubricants, plasticizers, etc. In recent years, plant oils, especially soybean oil, have seen high demend for the production of biodiesels. As public concerns of environmental impact of and sustainable development of petroleum-based polymer materials grow, use of plant oil feedstock for polymers has received extensive research. Castor oil-based polyamide 11 [-$(CH_2)_{10}$-CONH-] has become commercially available from Arkema, and polyurethanes based on soybean oil-derived polyols are also emerging in some niche applications. On the other hand, use of epoxidized plant oils for epoxy

In Degradable Polymers and Materials: Principles and Practice (2nd Edition); Khemani, K., et al.;
ACS Symposium Series; American Chemical Society: Washington, DC, 2012.

application has not been successful since the softness of long fatty acid chains makes this plant oil derivatives of little practical value for engineering epoxy resins (*1*). An attempt to reinforce the cured epoxidized soybean oil with nanoclay failed to increase the glass transition temperature (T_g) of the rsin (*2*). The high performance of epoxies relies on a high content of rigid molecular segments (aromatic or cycloaliphatic) originated from either epoxy, curing agent molecules or both. This generally limits the choice of epoxy precursors predominantly to the type of epoxies based on glycidyl ethers of bisphenol A (ca. 90% market share). Nevertheless, most epoxy resins do not have good impact strength and require toughening in certain applications. Fatty acids have flexible long hydrocarbon chains, and if incorporated into the structures of curing agents, can significantly flexibilize and/or toughen the cured epoxies. In fact, fatty acids and dimer acids have found use in the preparation of polyamidoamine type curing agents for epoxies. Polyamidoamines are the condensation products of fatty acid or dimeric fatty acids with polyamines. For the past years, we have also studied the use of different fatty acid derivatives for the preparation of epoxy curing agents. In this chapter, we summarize part of the results in this effort.

Rosin Modified Polyamidomine Curing Agents

Low molecular weight aliphatic polyamines can cure epoxy resins at ambient temperature, but have the disadvantages of high volatility and toxicity. The epoxy resins cured with simple aliphatic polyamines tend to be brittle. Polyamidoamines are condensation products of polyamines with monomeric, dimeric or trimeric fatty acids. Polyamidoamines are known to be low toxic and almost non-volatile. When used as curing agents for epoxies, polyamidoamines are found to have good adhesion on damp metalic and cementious surfaces. Polyamidoamine containing a long aliphatic hydrocarbon moiety renders the cured epoxy higher flexibility and impact strength but also lower thermal stability than its polyamine counterpart. Our recent investigations using rosin acid as a building block in the synthesis of curing agents for epoxies strongly suggest that the rigid hydrogenated phenanthrene ring structure of rosin acids makes rosin derivatives adequate alternatives to petroleum-based aromatic or cycloaliphatic compounds (*3*, *4*). To regulate the molecular chain stiffness of dimer acid-derived curing agents, we aslo introduced rosin to the fatty acid dimerization process to achieve modified dimer acids (*5*). The product was a mixture of dimeric fatty acids (C36 dicarboxylic acids or C36 DCA) and adducts of rosin and fatty acids, hereby denoted as R-DCA. The dimerization reaction was performed at 240 °C with 1% catalyst. With the incorporation of 5% rosin, the resulting mixture product contained ~51% diacids, having an acid value of 193.9 mg-KOH/g and a viscosity of 320 mPa·s at 40 °C. This mixture product was reacted with excess diethylenetriamine (DETA), triethylenetetramine (TETA) and tetraethylenepentamine (TEPA), respectively, yielding three polyamidoamines of different amine values (*6*). After completion of the condensation reaction, the unreacted amines and water produced were removed by vacuum distillation. For comparison, the condensation product of the unmodified dimer acid with DETA

In Degradable Polymers and Materials: Principles and Practice (2nd Edition); Khemani, K., et al.;
ACS Symposium Series; American Chemical Society: Washington, DC, 2012.

was also prepared. These four polyamidoamines were then used to cure the same epoxy under the same curing conditions. The epoxy used was a commercial product of glycidyl ether of bisphenol A type epoxy containing 0.51 moles of epoxide per 100 g resin. Table 1 gives the mechanical properties of epoxies cured with these four polyamidoamines. Apparently, the polyamidoamines prepared from rosin modified dimer acids resulted in general superior mechanical properties than the polyamidoamine from the unmodified dimer acids.

Table 1. Mechanical and thermal properties of rosin modified polyamidoamine cured epoxies.

Polyamidoamine curing agent	*Tensile strength (MPa)*	*Strain at break (%)*	*Modulus (MPa)*	*Flexural strength (MPa)*	*Shear strength (MPa)*	*T_g (°C)*
R-DCA-DETA	53.51	3.03	2311.1	79.93	17.69	73.46
R-DCA-TETA	54.94	2.44	2343.6	100.92	19.37	87.36
R-DCA-TEPA	55.60	1.04	2381.2	101.56	18.30	88.40
C36 DCA-TEPA	35.97	3.26	1913.2	73.62	15.83	53.00

Tung Oil-Based Polyamidoamine Type Curing Agents

In recent years, dicarboxylic acids having 21 carbon atoms (C21 dicarboxylic acids or C21 DCA) with structure as shown in Figure 1 have received growing applications in plasticizing alkyd resins and curing epoxies. The synthesis of C21 DCAs is based on the Diels-Alder reaction of conjugated C18 fatty acids and acrylic acid. Conventional industrial preparation of C21 DCA manufacturing uses tall oil containing a certain level of linoleic acid as raw feedstock (*7*). Because the two carbon-carbon double bonds (*cis,cis*-9,12) of linoleic acid are not conjugated, this reaction process requires a relatively high temperature (200 to 270 °C) and iodine catalyst under which the non-conjugated double bonds of linoleic acid is first converted to a conjugated structure (US Pat. 3,753,968). Still, because the linoleic acid content in the tall oil is relatively low, the yield of the dimer acid in final product is not high.

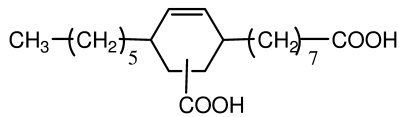

Figure 1. Structure of a commercial C21 dicarboxylic acid.

Tung oil is characteristic of rapid drying because of its conjugated double bonds, and therefore it has long been used for paints and waterproof coatings. Eleostearic acid (octadeca-9,11,13-trienoic acid) comprises ~80% of the total

In Degradable Polymers and Materials: Principles and Practice (2nd Edition); Khemani, K., et al.;
ACS Symposium Series; American Chemical Society: Washington, DC, 2012.

fatty acids in tung oil. Eleostearic acid exists in two isomers, i.e., α-eleostearic (9*Z*,11*E*,13*E*) acid and β-eleostearic ((9*E*,11*E*,13*E*), or all-trans) acid, of which the α-isomer is dominant. In the presence of catalysts, tung oil reacts with excess methanol, yielding a mixture of methyl esters of various fatty acids. The conjugated double bonds in the methyl eleostearate can react with various dienophiles through the Diels-Alder reaction, resulting in different derivatives (*8*).

Huang et al. recently studied the synthesis of new C21 dicarboxylic acids via the Diels-Alder reaction of methyl eleostearates and acrylic acid (*8*). Figure 2 gives the schematic synthesis routes of tung oil-based C21 diacids. Methyl eleostearate and acrylic acid in a weight ratio of 1:0.247 (w/w) were reacted at 180 °C for 3 h. This reaction condition was much milder than that of the addition reaction between linoleic and dienophiles. Hydroquinone was added as a polymerization inhibitor at 1% on the weight of acrylic acid. The reaction gave a yield of 85% for the total adducts. The chemical structures of the received C21 DCAs were very similar to that of the above commercial C21 DCAs except the former having a double bond in the aliphatic chains. For methyl α-eleostearate, the addition reaction occurred on the double bonds at C11 and C14, while for methyl β-eleostearate the addition occurred either on the double bonds at C9 and C12 or C11 and C14 (*9*). GC and GC-MS analyses revealed there were total six isomeric methyl esters of C21 DCAs.

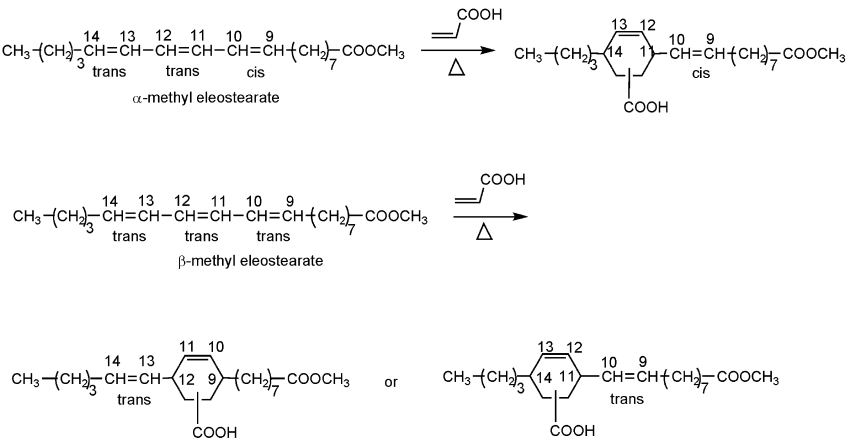

Figure 2. Tung oil-based methyl esters of C21 dicarboxylic acids through Diels-Alder addition of methyl eleostearates and acrylic acid.

The received adduct was then reacted with excess DETA, TETA and TEPA (Figure 3), respectively, to yield three polyamidoamines of different amine values (*10*, *11*). For comparison, a commercial dimeric fatty acid (C36 DCA) was also reacted with TETA and the resulting product was used as a control. These four polyamidoamines were used to cure a commercial epoxy resin in the same epoxide/amine stoichiometry. Table 2 gives the properties of the cured epoxy resins. The epoxy used is a commercial product of glycidyl ether of bisphenol A type epoxy

In Degradable Polymers and Materials: Principles and Practice (2nd Edition); Khemani, K., et al.;
ACS Symposium Series; American Chemical Society: Washington, DC, 2012.

containing 0.51 moles of epoxide per 100 g resin. In curing the same epoxy, the polyamidoamine derived from the C21 DCA resulted in the cured epoxy resin with higher tensile and flexural strengths and higher glass transition temperature (T_g) but lower shear strengths than the polyamidoamine derived from the C36 DCA. This result suggests that the reduction in chain length decreased the toughness but increased the stiffness and heat resistance of the cured resins.

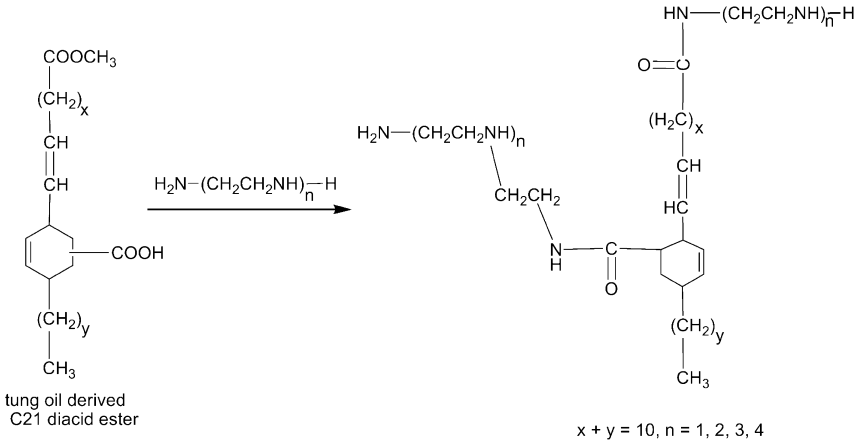

Figure 3. Synthesis of polyamidoamines using tung oil-derived C21 dicarboxylic acids

Table 2. Mechanical properties and glass transition temperatures of various polyamidoamine cured epoxy resins.

Polyamidoamine curing agent	*Tensile strength (MPa)*	*Elongation (%)*	*Modulus (MPa)*	*Flexural Strength (MPa)*	*Shear strength (MPa)*	*T_g (°C)*
C21 DCA-DETA	29.88	1.36	2395.64	85.43	10.62	108
C21 DCA-TETA	45.35	2.11	2634.53	98.42	9.04	109
C21 DCA-TEPA	58.63	3.27	2635.84	99.90	9.49	116
C36 DCA-TETA	35.97	3.26	1913.23	73.62	15.83	53

Fatty Acid Modified Mannich Bases as Curing Agents

Many amine or polyamine compounds are effective curing agents for epoxies. The Mannich base, which is the reaction product of phenol (or cresol), formaldehyde and amine through Mannich reaction, is one type of amines that can be used as curing agents. Curing of epoxy using Mannich base is fast because the phenolic hydroxyl has a catalytic effect on the cure reactions. The presence

In Degradable Polymers and Materials: Principles and Practice (2nd Edition); Khemani, K., et al.;
ACS Symposium Series; American Chemical Society: Washington, DC, 2012.

of the benzene ring structure of Mannich base also renders the cured resin better thermal stability compared with that of aliphatic amine cured epoxies. On the other hand, epoxies cured with simple Mannich bases are quite brittle. In order to improve the toughness of Mannich base cured epoxies, Xia et al. introduced a long hydrocarbon chain to the structure of phenol (or cresol) and prepared Mannich base curing agents using the modified phenol (or cresol) (*12*, *13*). As shown in Figure 4, methyl eleostearate was first reacted with phenol (or cresol) through the Friedel-Crafts alkylation. The reaction between phenol and methyl eleostearate was an addition reaction. The reaction was conducted with a molar stoichiometric ratio of phenol to methyl eleostearate in 7:3 and 0.2% p-toluene sulfonic acid, and the yield of the addition product was 83.7%. The alkylated phenol was then used to react with formaldehyde and amine at 60 – 70 °C to receive the modified Mannich bases, as shown in Figure 4.

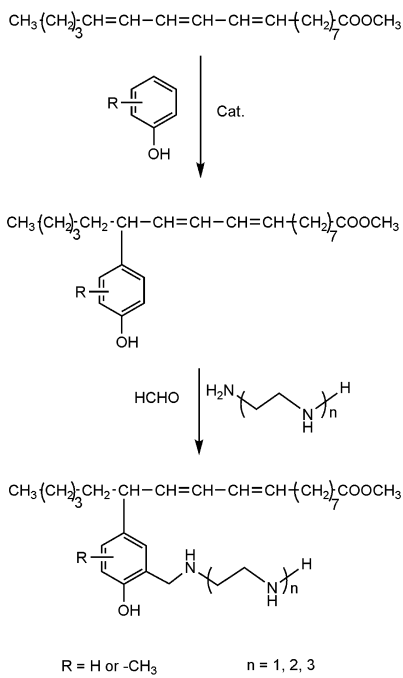

Figure 4. Synthesis of methyl eleostearate modified Mannich base curing agents.

Table 3 gives the tensile and physical properties of the epoxies cured using the modified Mannich bases. Modified Mannich base cured epoxy coatings exhibited superior toughness and adhesion than unmodified Mannich base (Cr-DETA) cured and C36 DCA-TETA cured epoxy coatings. Water and acid resistances of the epoxy coatings cured with modified Mannich bases were also higher but the solvent resistance was lower. In addition, modified Mannich base cured epoxies

In Degradable Polymers and Materials: Principles and Practice (2nd Edition); Khemani, K., et al.;
ACS Symposium Series; American Chemical Society: Washington, DC, 2012.

displayed higher tensile strength than their unmodified counterpart cured epoxy. Nevertheless, the former exhibited an inferior thermal stability, as noted in the clear weight loss in the TGA test (data not shown), probably due to the presence of the unreacted methyl eleostearate.

Table 3. Mechanical and physical properties of fatty acid modified Mannich base cured epoxies.

Sample[a]	*Flexibility Grade*[b]	*Adhesion Grade*[c]	*Tensile shear strength*[d] *(MP)*	*30-days' immersion*[e]		
				78% H_2SO_4	*xylene*	*H_2O*
mPh-EDA	1	2	14.5	E	E	A
mPh-DETA	1	1	16.9	C	E	A
mPh-TETA	1	1	15.8	B	B	A
mCr-DETA	2	1	16.3	C	D	A
Cr-DETA	2	2	12.7	E	B	E
C36 DCA-DETA	2	3	13.6	E	E	A

[a] mPh-DETA : adduct of alkylated (methyl eleostearate modified) phenol, formaldehyde and DETA; mPh-TETA : adduct of alkylated phenol, formaldehyde and TETA; mCr-DETA : adduct of alkylated cresol, formaldehyde and DETA; mPh-DETA : adduct of alkylated phenol, formaldehyde and ethylene diamine (EDA); Cr-DETA : adduct of cresol, formaldehyde and DETA; C36 DCA-TETA: polyamidoamine derived from condensation of C36 diacid and DETA. [b] Flexibility (mm) was tested according to GB 1731-93, evaluated by the diameter of the mandrels; grade 1 is the highest, and grade 7 is the lowest. [c] Adhesion (grade) was tested according to GB 1702-93; grade 1 is the highest, grade 7 is the lowest. [d] : Tensile shear strength was measured according to GB 7124-86, the material of the lapped plate was ABS. [e] A, no change; B, wrinkling or bubbling; C, wrinkling and bubbling; D, peeling; E, cracking

Curing Agents for Waterborne Epoxy Coatings

Waterborne epoxy coating is highly desired by resin manufacturers and end-users due to its low VOC benefits. The curing agent used in waterborne epoxy system also plays a role of emulsifying agent for the epoxy. This requires the curing agent is either water-soluble or water dispersible. Most curing agents for waterborne epoxies are polyamines and polyamidoamines. For coating applications, especially metal surface coating, fast lacquer dry of the coating is preferable. Therefore, now most epoxies used in waterborne coatings are solid epoxy resins which are dispersed in water with or without co-solvent. Since waterborne epoxy resins are supplied as dispersions, the curing agents do not have to function as the sole emulsifying agents for the epoxy resins, and that allows the use of less hydrophilic curing agents.

In Degradable Polymers and Materials: Principles and Practice (2nd Edition); Khemani, K., et al.;
ACS Symposium Series; American Chemical Society: Washington, DC, 2012.

Li et al. reported a water dispersible curing agent with a structure shown in Figure 5 (*14*, *15*). It was prepared by first reacting toluene diisocyanate with polyethylene glycol monooctadecyl ether, followed with DETA. The polyethylene glycol monooctadecyl ether moiety in the structure provided the emulsifying activity for the curing agent. Because the primary amine end group had high reactivity toward reacting with the epoxide, the curing reactions were prone to occur before the water was completely evaporated, resulting in formation of film with poor quality. Capping the primary amine with acrylonitrile was able to slow down the premature curing. However, the water resistance of epoxies cured with this curing agent was not very satisfactory.

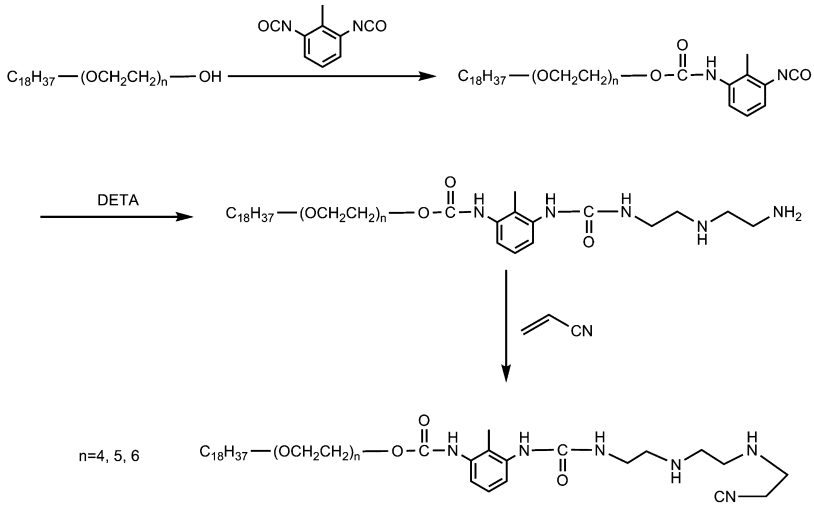

Figure 5. Synthesis of amphiphilic polyamine curing agents.

To improve water-resistance of waterborne epoxy coatings, Li et al. further modified the chemical structure of the above curing agent as shown in Figure 6 (*16*). Unlike the curing agent in Figure 5, in this structure, tetrahydromethylterephthalic anhydride was used in the condensation reaction instead of TDI to link the emulsifying block and the functional curing moiety. The introduction of the bisphenol A block and benzyl end capping group greatly improved the water resistance of the cured epoxy resins. Excellent water resistance, film hardness and impact resistance were achieved when the curing agent was in slight excess, i.e., the equivalent stoichiometric ratio of curing agent to epoxy was at 1.1:1 (Table 4).

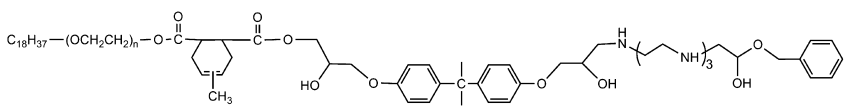

Figure 6. Structure of GLEBA modified amphiphilic polyamines.

In Degradable Polymers and Materials: Principles and Practice (2nd Edition); Khemani, K., et al.;
ACS Symposium Series; American Chemical Society: Washington, DC, 2012.

Table 4. Properties of waterborne epoxy coating cured using GLEBA modified amphiphilic polyamine

Properties[a]	*Equivalent oxide/amine ratio*	
	1:1	*1:1.1*
Pencil hardness	2H	3H
Flexibility (mm)	1	1
Adhesion (grade)	1	1
Impact resistance (kg·cm^{-1})	30	50
Water resistance (96 h immersion)	blushing	no blushing, no bubbling

[a] Pencil hardness was determined according to GB 6739-69, measured by the symbols used to describe a pencil's hardness. Flexibility (mm) was determined according to GB 1731-93, measured by the diameter of the mandrels; 0.5 mm is the highest, 15 mm is the lowest. Adhesion (grade) was measured according to GB 1702-93; grade 1 is the highest, grade 7 the lowest. Impact resistance (kg·cm^{-1}) was measured according to GB 1732-93; 50 kg·cm^{-1} means the coatings will not crack after the impact of a hammer (1 kg) falling freely from a height of 50 cm.

Conclusions

Fatty acids from plant oils are valuable feedstocks for the preparation of curing agents for epoxies. The flexible hydrocarbon chain of fatty acid, when incorporated to the structure of curing agent, is complementary to the rigid building block of epoxies and likely improves the flexibility and toughness of the cured epoxy resins. Tung oil fatty acids are more advantageous in the synthesis of C21 diacids through the Diels-Alder reaction because of the high eleostearic acid content in tung oil. The structure of fatty acid-derived curing agents can be further manipulated by introducing cyclic (aliphatic or aromatic) moiety to fine-tune the stiffness of the curing agent molecules and subsequently the properties of the cured epoxies.

References

1. Liu, Z; Erhan, S. Z.; Xu, J. Y. Preparation, Characterization and Mechanical Properties of Epoxidized Soybean Oil/clay Nanocomposites. *Polymer* **2005**, *46*, 10119–10127.
2. Park, S. J.; Jin, F. L.; Lee, J. R. Synthesis and thermal properties of epoxidized vegetable oil. *Macromol. Rapid Commun.* **2004**, *25*, 724–727.
3. Liu, X.; Xin, W.; Zhang, J. Rosin-based acid anhydrides as alternatives to petrochemical curing agents. *Green Chem.* **2009**, *11*, 1018–1025.
4. Liu, X.; Xin, W.; Zhang, J. Synthesis of Rosin-derived Imide-diacids as Epoxy Curing Agents and Properties of the Cured Epoxies. *Bioresour. Technol.* **2010**, *101*, 2520–2524.

5. Yang, X.; Xia, J.; Huang, K.; Zhang, Y. Synthesis of a complex dimeric acid by diels-alder reaction between industrial fatty acid and rosin. *Chem. Ind. Forest Prod.* **2010**, *30* (5), 31–34.
6. Yang, X.; Xia, J.; Huang, K.; Zhang, Y. Synthesis and properties of oil/rosin-based polyamide curing agents. *Thermosetting Resin* **2010**, *25* (6), 6–9.
7. Bufkin, B. G.; Thames, S. F.; Jen, S. J. Derivatives of eleostearic acid. *J. Am. Oil Chem. Soc.* **1976**, *53*, 677–679.
8. Huang, K.; Xia, J. Preparation and Characterization of Monomethyl Ester of C21 Dicarboxylic Acid derived from Methyl eleostearate. *Chemical Reagents* **2008**, *30*, 725–728.
9. Bickford, W. G.; Dupré, E. F.; Mack, C. H.; O'connor, R. T. The infrared spectra and the structural relationships between alpha- and beta-eleostearic acids and their maleic anhydride adducts. *J. Am. Oil Chem. Soc.* **1953**, *30*, 376–381.
10. Huang, K.; Xia, J.; Yang, X.; Li, M.; Ding, H. Properties and Curing Kinetics of C21-based Reactive Polyamides as Epoxy Curing Agents derived from Tung oil. *Polym. J.* **2010**, *42*, 51–57.
11. Huang, K.; Xia, J.; LI, M.; Ding, H. Properties and cure kinetics of c21 polyamides as epoxy curing agents derived from tung oil. *Fine Chemicals* **2009**, *26*, 79–84.
12. Xia, J.; Huang, H.; Li, J.; Wang, D. Synthesis and characterization of the adducts of methyl eleostearate with phenols. *Zhanjie* **2000**, *21* (6), 1–3, 13.
13. Xia, J.; Huang, H.; Wei, B.; Wang, D. Study on properties and synthesis of Mannich base modified with eleostearat. *Zhanjie* **2001**, *22* (4), 1–3.
14. Li, M.; Xia, J.; Ding, H.; Huang, K. Preparation and properties of urethane-modified fatty amine used as waterborne epoxy curing agents based on oil and fat. *Chem. Ind. Eng. Prog.* **2009**, *28* (7), 1226–1230.
15. Li, M.; Xia, J.; Huang, K.; Ding, H. Structure and properties of urethane modified fatty amine used as waterborne epoxy curing agents based on oil and fat. *Polym. Mater. Sci. Eng.* **2011**, *27*, 59–62.
16. Mei, L.; Xia, J.; Ding, H.; Huang, K. Research on preparation and properties of polyether alcohols waterborne amine epoxy curing agents. *Thermosetting Resin* **2009**, *24*, 21–25.

In Degradable Polymers and Materials: Principles and Practice (2nd Edition); Khemani, K., et al.;
ACS Symposium Series; American Chemical Society: Washington, DC, 2012.

Chapter 15

Strategies in Aliphatic Polyester Synthesis for Biomaterial and Drug Delivery Applications

Angela L. Silvers, Chia-Chih Chang, Bryan Parrish, and Todd Emrick*

Polymer Science & Engineering Department, University of Massachusetts Amherst, Conte Center for Polymer Research, Amherst, MA 01003
***tsemrick@mail.pse.umass.edu**

Aliphatic polyesters are among the most important class of synthetic polymers for biomedical applications due to their biodegradability and generally high biocompatibility. However, conventional aliphatic polyesters are semi-crystalline, hydrophobic solids lacking in functionality, such that strategic tailoring of their structure and functionality could expand their application base considerably. Numeorus synthetic methods have been examined for introducing functionality to aliphatic polyesters. This chapter will describe a number of reported methods, focusing on examples of ring-opening polymerization (ROP) of functionalized lactones, and post-polymerization functionalization that affords well-defined materials with high degrees of functionality and narrow polydispersities. In addition, new developments in biocompatible ROP catalysts as well as novel polyester architectures, such as cyclic polymers, will be discussed.

Introduction

Early efforts to use synthetic polymers as biomaterials were based on high volume commodity polymers such as polyurethanes, polyacrylates, nylon, and poly(tetrafluoroethylene), each designed initially for conventional materials purposes. Nevertheless, the wide availability and favorable physical properties of these polymers led to their use by surgeons in medical procedures that require durable and generally inert materials (*1*, *2*). However, the use of such polymer

In Degradable Polymers and Materials: Principles and Practice (2nd Edition); Khemani, K., et al.;
ACS Symposium Series; American Chemical Society: Washington, DC, 2012.

materials in surgical and other biological applications has been problematic, leading in some cases to inflammation, due to the immune response of the body to the presence of foreign materials. Notable pioneering examples of polymer materials in biological applications include efforts of DeBakey and coworkers, who as early as the 1950's used Dacron™ (polyethylene terepthalate) for cardiovascular prostheses (*3*). These procedures were found to be successful in the repair of large arteries, but unfortunately failed in cases where the internal diameter was less than 5 mm. The breadth of expertise needed to solve such challenging problems in biomaterials, and effectively introduce synthetic materials to the body, includes chemistry, biology, engineering, and medicine, thus generating a challenging interdisciplinary topic that requires collaborative activity among these disciplines.

While many different types of polymers are of interest in biomaterial applications, aliphatic polyesters are particularly relevant to consider due to their degradable nature under physiological conditions, thus making them desirable as resorbable materials. Aliphatic polyesters were initially used to fabricate degradable sutures in the 1960's (*4*), and have since found use in a wide range of biomaterial applications including drug-delivery systems (*5*), tissue-engineering scaffolds (*6*), and temporary tissue/bone replacement (*7*) as depicted in Figure 1.

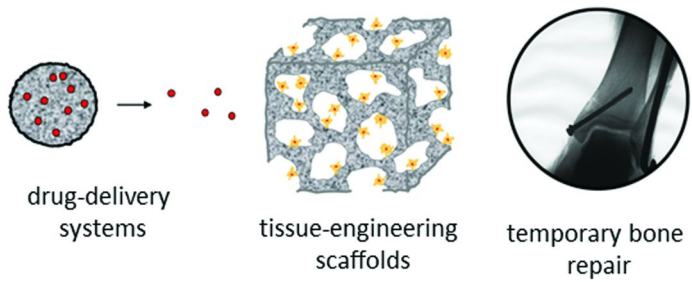

Figure 1. Examples of biomaterial applications using aliphatic polyesters

More recent advances include the work of Langer on aliphatic polyesters for tissue-engineering and drug-delivery (*8*), Fréchet and Grinstaff on drug-delivery (*9*) and surgical (*10–12*) applications of dendrimers, and Duncan in the area of drug-delivery systems and polymer therapeutics (*13*).

An effective approach to synthesizing aliphatic polyesters of controlled molecular weight and potential medical importance involves a ring-opening polymerization of monomers shown in Figure 2, such as lactide, glycolide, ε-caprolactone (ε-CL), and δ-valerolactone (δ-VL). The ring-opening homo- and copolymerization of lactones and lactides can be performed in the bulk or in solution using organometallic catalysts such as aluminum *iso*-propoxide ($Al(O^iPr)_3$), tin(II) 2-ethylhexanoate, ($Sn(Oct)_2$), tin(II) trifluoromethane sulfonate

In Degradable Polymers and Materials: Principles and Practice (2nd Edition); Khemani, K., et al.;
ACS Symposium Series; American Chemical Society: Washington, DC, 2012.

($Sn(OTf)_2$), as well as organic catalysts based on *N*-heterocyclic carbenes (*14*, *15*). Primary and secondary alcohols and amines effectively initiate polymerization, and give aliphatic polyesters with control over end-group functionality, overall molecular weight, and polydispersity (PDI, defined as M_w/M_n).

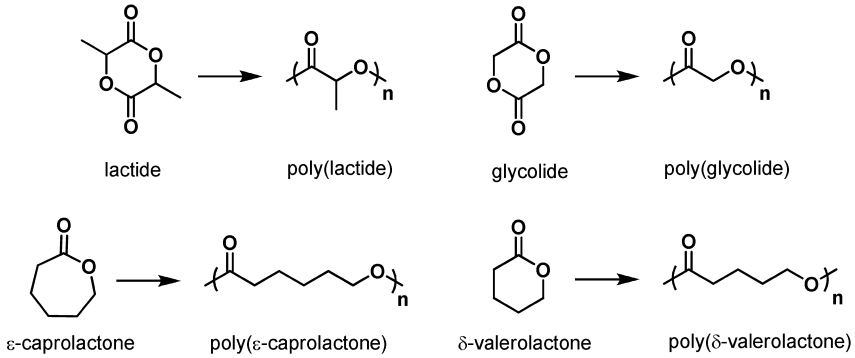

Figure 2. Aliphatic polyesters prepared by ring-opening polymerization

A range of mechanical properties and degradation rates can be achieved by copolymerization (*2*) of the monomers shown in Figure 2. However, many of these aliphatic polyesters are semi-crystalline, hydrophobic solids, and all lack access to functional groups that could otherwise be used to tailor their properties. Thus, methods to integrate functionality into aliphatic polyesters for fine-tuning their physical and biological properties have been sought. Obtaining water soluble polyesters is of particular interest for injectable applications, as are polyesters functionalized with drug moieties, cell-adhesion promoters, and targeting groups for drug-delivery and tissue-engineering applications.

A recent development in the utility of aliphatic polysters includes the formation of cyclic polymers, which are anticipated to exhibit numerous distinct properties that contrast linear polymers due the absence of end groups and topological constraints. Two common strategies for the formation of such polymers are cyclization of reactive chain ends (Figure 3a,b) and ring-expansion polymerization (Figure 3c). Cyclization of linear polymers typically requires high dilution in order to favor unimolecular chain-end coupling over intermolecular reactions. Covalent bond formation between chain ends of a single chain is accomplished by introducing catalysts/reagents to heterotelechelic polymers (such as the azide-alkyne click example of Figure 3a) or by adding a difunctional coupling agent to homotelechelic polymers (such as the thiol-maleimide example of Figure 3b). The cyclic topology offers slower hydrolytic degradation because chain scission into linear fragments must occur before further mass loss can take place.

In Degradable Polymers and Materials: Principles and Practice (2nd Edition); Khemani, K., et al.;
ACS Symposium Series; American Chemical Society: Washington, DC, 2012.

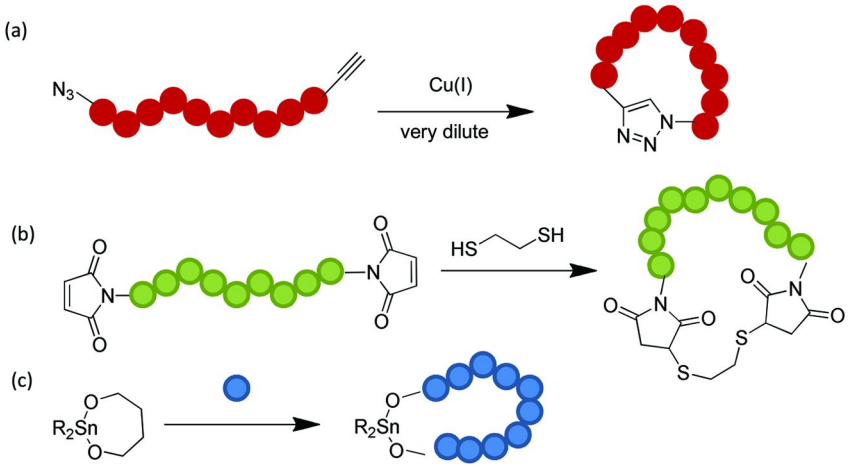

Figure 3. Schematic representation of strategies for forming cyclic polyesters by (a) ring-closing of a heterotelechelic polymer using CuAAC; (b) ring-closing of homotelechelic polymer using thiol-ene chemistry; (c) ring expansion polymerization with a cyclic tin alkoxide catalyst

Strategies for Functionalization of Aliphatic Polyesters

Functionalization of aliphatic polyesters is a delicate challenge from the perspective of organic and polymer synthesis, as their degradable nature that renders them desirable as biomaterials also limits the scope of chemical reactions available for successful modification. Consequently, mild synthetic strategies must be employed for controlled functionalization that can proceed in the absence of substantial ester bond degradation. Methods for functionalizing aliphatic polyesters include end-group functionalization of linear polyesters and non-linear polyesters such as dendritic and hyperbranched polymers that contain multiple functional groups as chain-ends. In addition, the introduction of pendent functionality distributed as grafts along a linear polyester backbone affords functional comb-type structures.

End-Group Functionalization

The simplest functionalization strategy of aliphatic polyesters is achieved at the chain-ends (Figure 4). This can be accomplished using functional initiators for ring-opening polymerization, and/or through end-capping reactions. For example, initiation of lactone polymerization from the chain-end hydroxyl groups of poly(ethylene glycol) (PEG) -diols and -monomethyl ethers produces tri- and di-block copolymers, respectively, that can assemble into micellar structures in water with a polyester core and a PEG corona (*16*, *17*). Other examples of end-capping include esterification of the polyester hydroxyl chain-end with 4-azidobenzoyl chloride to give UV-photocurable polyesters (*18*), and

In Degradable Polymers and Materials: Principles and Practice (2nd Edition); Khemani, K., et al.;
ACS Symposium Series; American Chemical Society: Washington, DC, 2012.

end-capping with phosphorylcholine residues to give polyesters with phospholipid like moieties that reduce protein adsorption relative to non-functionalized polyesters (*19*).

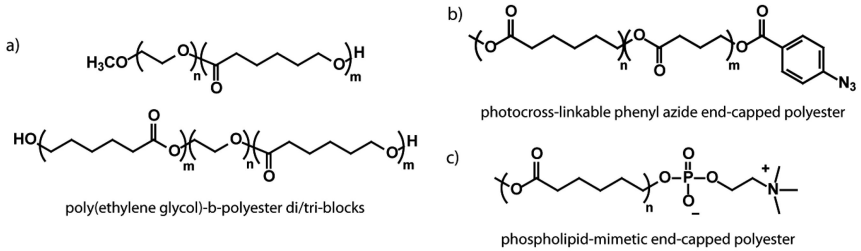

Figure 4. End-functionalized polyesters: a) poly(ethylene glycol)-b-polyester, b) phenyl azide terminated polyester, and c) phosphorylcholine terminated polyester

Chain-end functionalization limits functional group incorporation to one or two groups per polyester molecule. Thus, during polyester degradation, very little of the degraded material remains bound to the functional group of interest. Methods that increase the level of functionality on polyesters have been pursued by several groups, for example by the synthesis of dendritic, hyperbranched and comb-like polyester architectures.

Highly Functionalized Dendritic and Hyperbranched Aliphatic Polyesters

Non-linear polymer architectures including dendritic, hyperbranched, and linear-dendritic hybrid materials have been prepared as a means of altering polyester properties and introducing high levels of functionality (Figure 5). In addition to the effect of branching on solid-state and solution properties, the large number of end-groups that result from this branching offer the opportunity to obtain very high levels of functional group loading through end-capping reactions. Dendrimers are especially attractive for polymer-based drug delivery, where high drug loading per delivery vehicle is particularly beneficial. Fréchet, Szoka, and coworkers implemented this concept through the synthesis of aliphatic polyester dendrimers with covalently attached drugs such as the chemotherapy drug doxorubicin (Figure 5a) (*6*, *20*). *In vivo* evaluation of such conjugates demonstrated the improved effectiveness of the dendritic drug carrier relative to the free small molecule drugs. Hyperbranched polymers also provide considerable branching and chain-end functionality, but can be prepared by conventional polymerization chemistry rather than the step-wise coupling approach to dendrimers. Hyperbranched aliphatic polyesters have been prepared by ring-opening polymerization of lactones bearing hydroxyl groups, as seen for example in reports by Hedrick and coworkers on bis(hydroxymethyl)-substituted ε-CL (Figure 5b) (*21*), as well as by Fréchet and coworkers on ring-opening polymerization of hydroxyethyl-substituted ε-CL (*22*). Hybrid copolymers consisting of linear and dendritic segments have also been prepared and evaluated

In Degradable Polymers and Materials: Principles and Practice (2nd Edition); Khemani, K., et al.;
ACS Symposium Series; American Chemical Society: Washington, DC, 2012.

as biomaterials, for example by Grinstaff and coworkers on photocross-linkable dendritic-linear-dendritic triblocks (Figure 5c) prepared for opthalmic tissue repair applications (*10–12*). After methacrylate end-capping, the hybrid copolymers were cross-linked to seal corneal lacerations and were found to perform better than nylon sutures.

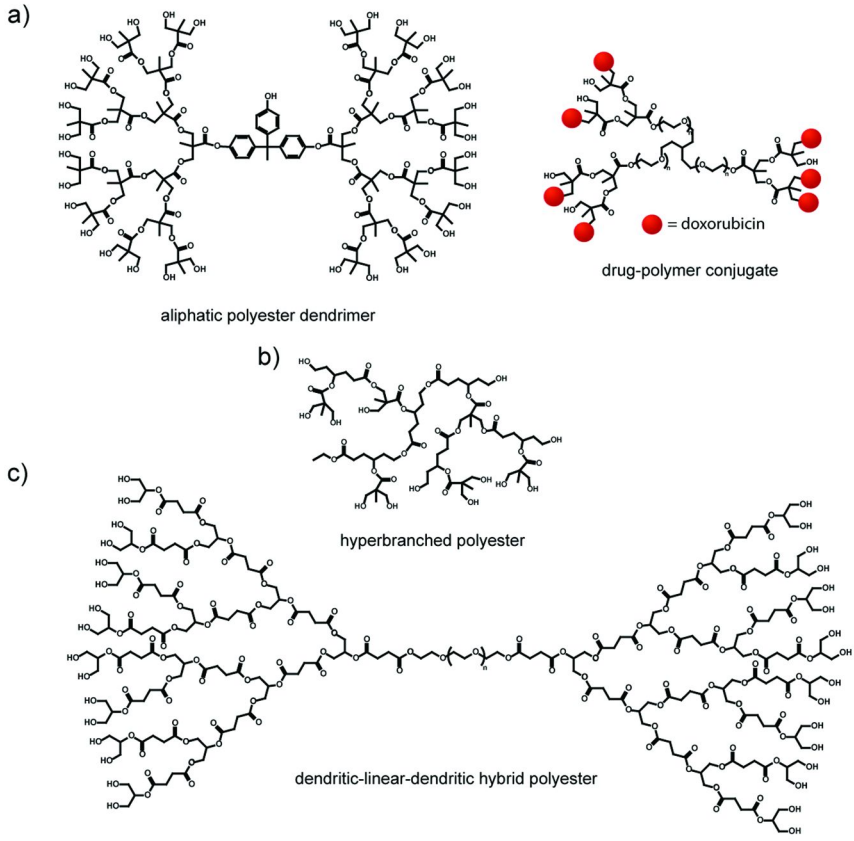

Figure 5. a) Polyester dendrimer and drug conjugate; b) hyperbranched aliphatic polyester; and c) dendritic-linear-dendritic triblock copolymer

Aliphatic Polyesters with Pendent Functionality

Functionalization of linear aliphatic polyesters with grafted moieties placed pendent to the polymer backbone has also been explored for integrating the desired functionality into the polymer material. As the introduction of pendent functionality to commercially available aliphatic polyesters presents few synthetic options and carries the risk of polymer degradation, recent work has focused on ring-opening polymerization (ROP) of functionalized lactones. Many substituents present slow lactone ROP, indicated for example by Jérôme and coworkers, where polymerization of a PEG-1,000-substituted ε-CL proved difficult (*23*).

In Degradable Polymers and Materials: Principles and Practice (2nd Edition); Khemani, K., et al.;
ACS Symposium Series; American Chemical Society: Washington, DC, 2012.

Consequently, a stepwise approach may be preferred, starting with the synthesis of lactones possessing small substituents that are compatible with ROP, followed by post-polymerization modification of the functionalized polyester products. By copolymerizing functionalized lactones with unsubstituted lactone monomers, the functional group density can be tailored over a wide range. However, conditions chosen for these post-polymerization reactions must be compatible with the polyester backbone to avoid degradation or cross-linking, while successful modification presents many options for polymer tailoring that are not possible in the case of unsubstituted polyesters. Indeed, several examples have been reported, including polyesters with pendent alkyl bromides (*24*, *25*), ketones (*26*), alcohols (*27–29*), alkenes (*25*, *28*, *29*), alkynes (*30*), carboxylic acids (*27*), acrylates (*31*), 2-bromo-2-methylpropionates (*32*), PEG (*23*, *30*, *33*), dendrons (*34*), and oligopeptides (*30*, *35*). The remainder of this chapter provides a brief description of a few such synthetic accomplishments, and potential applications for these pendent functionalized aliphatic polyesters, while also examining new catalytic methods for performing ROP of conventional and functional lactones.

Pendent Functionalization of Aliphatic Polyesters as Degradable Synthetic Polymers for Biology

The most commonly employed methods for producing functionalized lactones that are amenable to ring-opening polymerization (ROP) include: 1) Baeyer-Villiger ring-expansion of α-substituted cyclohexanones; 2) mono-substitution of 1,6-cyclohexane diol followed by oxidation with pyridinium chlorochromate (PCC), and subsequent ring-expansion using Baeyer-Villiger chemistry; and 3) substitution α to the carbonyl group of lactones, using for example lithium diisopropylamide (LDA) as a non-nucleophilic base, followed by addition of an appropriate electrophile. Taken together, these routes produce variously substituted ε-CL and δ-VL monomers, each having its own attractive features in terms of synthetic ease and versatility for polymerization and subsequent substitution.

Hedrick, Jérôme, and coworkers provided early examples of pendent functionalized poly(ε-CL) by polymerization of allyl-functionalized ε-CL monomer **1** (*25*), prepared from 2-allyl cyclohexanone by Baeyer-Villiger oxidation using *meta*-chloroperoxybenzoic acid (*m*-CPBA), (noting olefin epoxidation as an undesired side-product (Figure 6)).

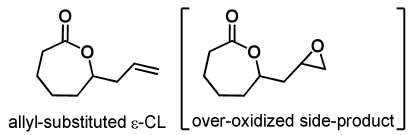

*Figure 6. Allyl-functionalized ε-CL (**1**) prepared from Baeyer-Villiger oxidation of 2-allylcyclohexanone*

In Degradable Polymers and Materials: Principles and Practice (2nd Edition); Khemani, K., et al.;
ACS Symposium Series; American Chemical Society: Washington, DC, 2012.

Lactone **1** was homopolymerized successfully and copolymerized with both ε-CL and L,L-lactide, using $Sn(Oct)_2$ as the catalyst, to give allyl functionalized polyesters shown as **2** in Figure 6, with good agreement of theoretical and experimental molecular weights (3,000-12,000 g/mol) and narrow polydispersities (1.1-1.4). Chemical transformations performed on the pendent allyl groups of polymer **2** included bromination, epoxidation, and hydrosilation reactions to give polyesters **3-5** in Figure 7. In all cases the transformations were achieved in the absence of degradation or cross-linking, demonstrating the compatibility of alkenes with controlled ROP, and the synthetic diversity of aliphatic polyesters upon post-polymerization modification.

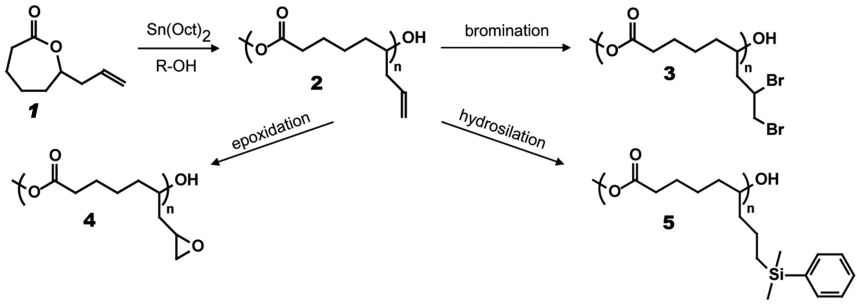

*Figure 7. Polymerization of lactone **1** and subsequent functional group transformations: bromination (**3**), epoxidation (**4**), and hydrosilation (**5**)*

Hedrick and coworkers further expanded the diversity of pendent polyester functionalization by the synthesis of hydroxyl and carboxyl containing polymers (**8**, **9** in Figure 8) from novel lactones, such as protected hydroxyl and acid ε-CL derivatives **6** and **7**, respectively, using $Sn(Oct)_2$ catalysis for ROP, and catalytic hydrogenolysis for removal of the benzylidene groups post polymerization (*27*). Importantly, this deprotection strategy proved compatible with the aliphatic polyester backbone, such that the functionalized polymers could be prepared and isolated efficiently.

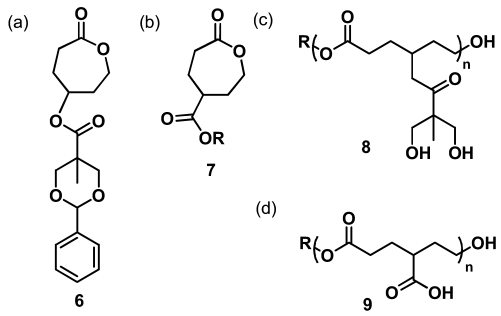

*Figure 8. Protected hydroxyl (**6**) and carboxyl (**7**) monomers and corresponding deprotected polyesters (**8**,**9**)*

In Degradable Polymers and Materials: Principles and Practice (2nd Edition); Khemani, K., et al.;
ACS Symposium Series; American Chemical Society: Washington, DC, 2012.

Emrick and coworkers synthesized and polymerized novel lactone monomers substituted α- to the carbonyl group by treatment of δ-VL and ε-CL with non-nucleophilic bases such as LDA (*36*) and subsequent addition of an electrophile. This strategy led to novel aliphatic polyesters substituted with allyl (*28*), cyclopentene (*29*), alkyne (*30*, *37*), and TMS-protected alkyne groups (*38*) (Figure 9). Lactone monomers **10** and **11** were prepared by deprotonation of δ-VL with LDA, followed by quenching with allyl bromide or propargyl bromide to give the allyl and alkyne derivatives, respectively. Cyclopentene derivative **13** was prepared by ring-closing metathesis of diallyl lactone **12**.

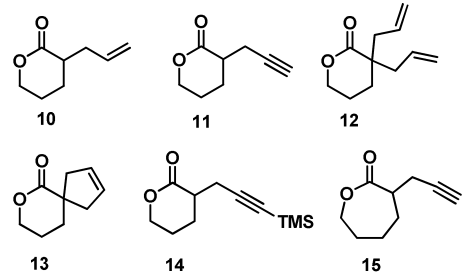

*Figure 9. Allyl (**10**), alkyne (**11**), diallyl (**12**), cyclopentene (**13**), TMS-protected alkyne (**14**) derivatives of δ-valerolactone, and alkyne-substituted ε-caprolactone (**15**)*

Lactones **10** and **13** were homo- and copolymerized using $Sn(OTf)_2$ (*14*) in conjunction with ε-CL or δ-VL as comonomers to give aliphatic polyesters with a controlled density of pendent allyl groups based on comonomer ratio (*28*, *29*). The cyclopentene-susbstituted structures proved uniquely suitable for oxidation (1,2-diol formation) and subsequent esterification, giving the first reported example of aliphatic polyester-*graft*-PEG copolymers with substantial PEG-grafting densities (greater than 20 mol % for PEG-1100) and narrow polydispersities (*29*).

Emrick and coworkers also demonstrated aliphatic polyester functionalization by "click" chemistry using Cu(I)-catalyzed cycloaddition of azides to alkynes (CuAAC), and thiol-ene addition. CuAAC has proven extremely useful in recent years for connecting small molecules, synthetic polymers, and biologically relevant materials (*39–41*). $Sn(OTf)_2$-catalyzed homopolymerization and copolymerization of alkyne-functionalized lactone **11** (Figure 9) with ε-CL led to novel aliphatic polyesters with tunable degrees of alkyne substitution along the polyester backbone. These polymers proved to be useful precurors for subsequent "click" coupling of azide-containing compounds (*30*, *42*). Key to the success of this concept is stability of the polyester to the click conditions; the polyesters proved amenable to a variety of click type reactions with organic azides. For example, water-soluble polyester-*graft*-PEG copolymers and polyester-*graft*-phosphorylcholine (PC) (**16** in Figure 10) could be prepared by reaction with azide-functionalized PEG-1100 monomethyl ether and PC-azide, respectively, to give grafting densities ranging from 10 to 100 mole percent for PEG (*30*) and 20-100 mole percent for PC (*42*).

In Degradable Polymers and Materials: Principles and Practice (2nd Edition); Khemani, K., et al.;
ACS Symposium Series; American Chemical Society: Washington, DC, 2012.

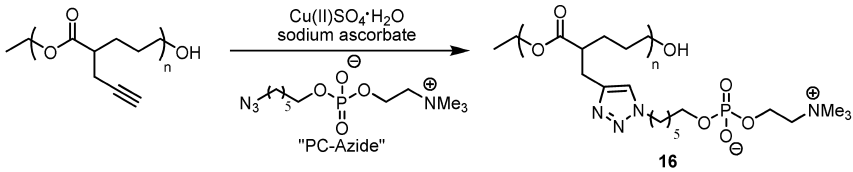

*Figure 10. Phosphorylcholine-grafted polyesters (**16**) by post-polymerization click chemistry of alkyne-substituted polyesters*

Click coupling also proved useful on alkyne-functionalized aliphatic polyesters for grafting oligopeptide sequences (*30*), and in the preparation of a polyester-drug conjugate with the cancer drug camptothecin (CPT). In the latter case, the polyester "prodrugs" were rendered water soluble with grafted PEG units (*43*). This methodology carries a number of benefits relative to other methods discussed thus far, including the relatively easy (one-step) monomer synthesis, the ability to homopolymerize or copolymerize the alkyne-functionalized lactone, and the single post-polymerization step that enables coupling of a very diverse range of azide-functionalized moieties with little-to-no polymer degredation imparted by the mild click conditions.

Emrick and coworkers extended this click cycloaddition concept on alkyne-functionalized aliphatic polyesters by exploring orthogonal click reactions for sequential functionalization of a diblock polyester (**17** in Figure 11) possessing blocks differentiated by a trimethylsilyl (TMS) protecting group on the alkynes of one block, free alkynes on the other block (*38*). TMS-propargyl valerolactone was synthesized following the same sequence performed for lactones **10** and **11**, by LDA deprotonation and alkylation with TMS-propargyl bromide. $Sn(Oct)_2$-mediated ring opening polymerization of the TMS-propargyl lactone afforded homopolymers with molecular weights ranging from 5,000 to 15,000 g/mol and low polydispersities (<1.2). Using this homopolymer (2,000 g/mol) as a macroinitiator, diblock copolymer **17** was prepared by $Sn(Oct)_2$ catalysis with propargyl valerolactone **11** at 100 °C, to afford a copolymer with molecular weight ~10,000 g/mol and narrow PDI (1.15). Diblock **17** proved useful for orthogonal click cycloaddition by sequential CuAAC, deprotection, and CuAAC reactions. For example, diblock copolymer **17** was sequentially functionalized by a click cycloaddition with phenyl azide, followed by deprotection of the TMS group with tetra-*n*-butylammonium fluoride (TBAF), and a second click cycloaddition with *m*-PEG-azide (550 to 5,000 g/mol) to yield amphiphilic diblock polyester **18** (Figure 11). ^{1}H-NMR spectroscopy indicated no loss of the TMS-progargyl group during the first click reaction, essential to the success of this orthogonal approach. To avoid polyester degredation, the TBAF deprotection was carried out at -78 °C, which afforded clean and complete alkyne deprotection without polyester chain scission. Amphiphilic diblock copolymer **18** was obtained with mole fractions of PEG ranging from 20 to 80 percent, molecular weights of 20,000 to 130,000 g/mol and narrow polydispersities (1.14-1.28). Amphiphilic diblock polyester **18**, with 15 to 80 wt % PEG, was shown to self assemble in solution into micellar

structures of envisioned utility for oncology drug delivery applications using biocompatible and degradable drug carriers.

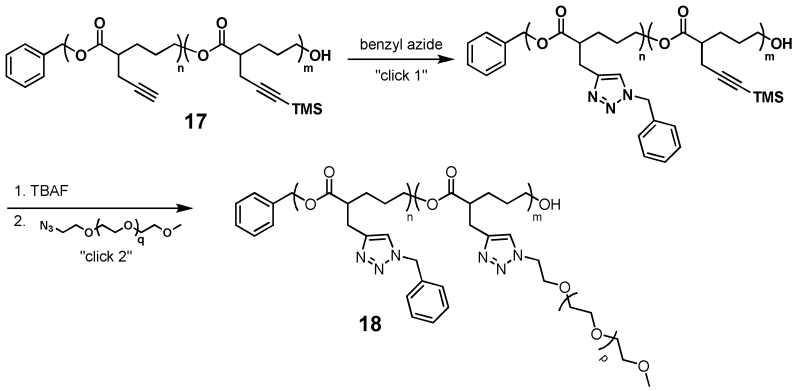

Figure 11. Click/deprotection/click sequence for orthogonal functionalization of aliphatic diblock polyesters

The concept of orthogonal click chemistry for post-polymerization modification was extended to a novel scaffold possessing both alkene and alkyne functionality (shown as **19** and **20** in Figure 12), which is amenable to orthogonal CuAAC and thiol-ene chemistries, without the need for protection/deprotection steps (*44*). Hawker and coworkers recognized the utility of thiol-ene reactions for post-polymerization reactions on alkene-functionalized polyesters (*45*), while Harth and coworkers recently described the conversion of functionalized aliphatic polyesters into cross-linked polyester nanoparticles (*46*). Though prior work explored end-group orthogonality of azide-alkyne and thiol-ene click reactions (*45*), and orthogonal surface-modification of SiO_2 nanospheres (*47*), diblocks **19** and **20** were the first examples of diblock polyesters possessing differentiated blocks by exploiting the distinct azide-alkyne and thiol-ene reactions. This work was also the first to employ the organic catalyst 1,5,7-triazabicyclo[4.4.0]dec-5-ene (TBD) for the ROP of functional lactones. Diblocks **19** and **20** were prepared in one-pot by sequential addition of monomers using TBD catalysis in toluene at room temperature. For diblock **19**, propargyl-functionalized caprolactone (**15** in Figure 9) was homopolymerized over 90 minutes, then allyl-functionalized valerolactone **10** was added and the reaction mixture stirred for 45 minutes. Polymer **19** was isolated by precipitation into cold methanol, and contained 50% AVL, which correlated closely to the feed ratio, and had a molecular weight of 14,800 g/mol, closely matching the theoretical (14,900 g/mol) molecular weight calculated from monomer to initiator ratio. For diblock **20**, allyl-functionalized valerolactone **10** was homopolymerized over 40 minutes, then propargyl valerolactone **11** was added and allowed to react for 20 minutes. Diblock polymer **20** with molecular weight ~30,000 and narrow PDI (<1.1) was isolated by precipitation. ^{1}H-NMR indicated a good agreement between feed ratio of monomers and observed polymer composition, as well as

In Degradable Polymers and Materials: Principles and Practice (2nd Edition); Khemani, K., et al.;
ACS Symposium Series; American Chemical Society: Washington, DC, 2012.

between theoretical and observed molecular weights. The carbonyl resonances of the ^{13}C-NMR spectra showed evidence of a diblock architecture for **19** and **20**. Orthogonal post-polymerization modification was performed using CuAAC followed by thiol-ene click on diblock **19** (Figure 12a). In this way, *m*-PEG azide was grafted onto the alkyne-functionalized block using copper(I)-catalyzed cycloaddition. The resulting polymer was isolated by dialysis, then subjected to thiol-ene addition of dodecane thiol onto the allyl-functionalized block, using AIBN as a thermal initiator. To further emphasize the utility of this novel scaffold, diblock **20** was subjected to a simultaneous thiol-ene/thiol-yne addition of dodecane thiol with AIBN to afford structures with twice the grafting density on the alkyne block (introducing 2 thiols per alkyne) relative to the alkene block (Figure 12b).

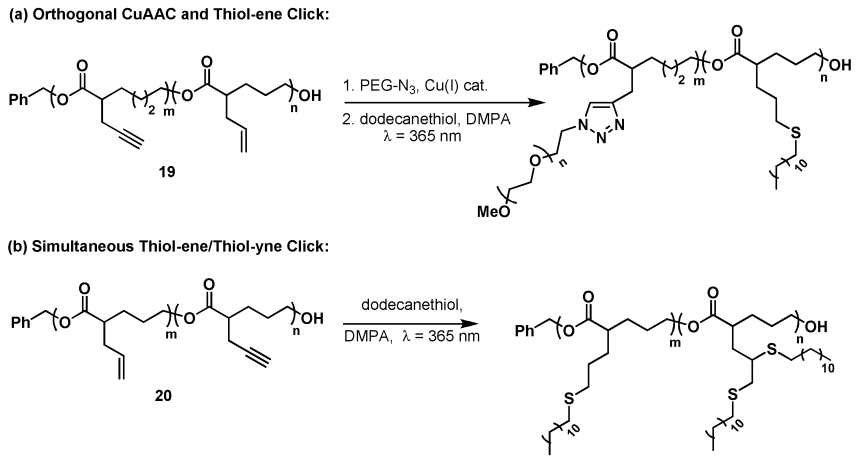

Figure 12. Synthesis of diblock polyesters differentiated using (a) sequential azide/alkyne and thiol-ene click chemistries orthogonally and (b) simultaneous thiol-ene/thiol-yne reactions, to yield a distinct diblock copolymer in both cases

As further evidence of the value of this approach, fully degradable polyester nanoparticles were obtained and subsequently modified using orthogonal CuAAC and thiol-ene click reactions. First, the alkyne-functionalized block of diblock **20** was cross-linked the using CuAAC with an α,ω-diazide, to give nanoparticles. DLS measurements indicated that the size of the nanoparticles formed could be controlled by varying the polymer concentration prior to cross-linking. ^{1}H-NMR spectroscopy showed evidence that the CuAAC reaction left the allyl-functionalized block unreacted and therefore amenable to subsequent functionalization using thiol-ene chemistry. The nanoparticles were further modified using a variety of thiols including dodecanethiol, phosphorylcholine (PC) thiol and rhodamine thiol, to show the modularity of this strategy for incorporating functionality important to biomedical applications such as solubilizing and/or targeting groups. Such degradable nanoparticulate structures

In Degradable Polymers and Materials: Principles and Practice (2nd Edition); Khemani, K., et al.;
ACS Symposium Series; American Chemical Society: Washington, DC, 2012.

are important as water-soluble drug delivery vehicles for the targeted delivery of oncology drugs.

Organocatalysts for ROP

Traditionally, ROP for the preparation of aliphatic polyesters has employed metal catalysts, such as tin and aluminum salts. However, recent success in catalyst development has revealed small organic molecules as appealing alternatives to metal catalysts, including for example 4-(dimethylamino)pyridine (DMAP), N-heterocyclic carbenes (NHCs), and 1,5,7-triazabicyclo[4.4.0]dec-5-ene (TBD) (Figure 13). These compounds function as ROP catalysts for lactones and lactides, offering fast polymerization kinetics and low polydispersity index (PDI) products in a metal-free environment at ambient temperature. Such catalysts could further improve the prospect of aliphatic polyesters in medicine by precluding potential contamination by trace metal in the finished product, device, or delivery system. For comprehensive reviews of the evolution of such organic initiators, see Platel, R.H. *et al.* (*48*). and Kamber, N.E. *et al.* (*49*). A brief synopsis is provided here.

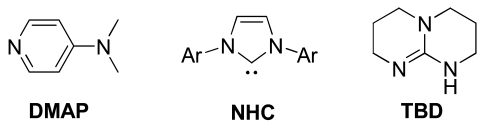

Figure 13. Organocatalysts for the ROP of lactones and lactides: 4-(dimethylamino)pyridine (DMAP), N-heterocyclic carbenes (NHC's), and 1,5,7-triazabicyclo[4.4.0]dec-5-ene (TBD); Ar = aromatic group.

Hedrick and Waymouth have pioneered organocatalysis for the controlled ROP of lactides, using for example 4-(dimethylamino)pyridine (DMAP) and 4-pyrrolidinopyridine (PPY). Organocatalyzed ROP of lactide using DMAP and PPY was performed in solution and in the bulk, with bulk polymerizations occurring faster than those in solution (minutes versus days), to yield PLAs with narrow polydispersity and molecular weights ranging from 4,000 to 17,000 g/mol. However, a limitation to this method was the requirement of high catalyst loadings to acheive reasonable conversion (*50*). Tertiary phosphines, N-heterocyclic carbenes (NHCs), thioureas and, more recently, amidine and guanidine analogues have proven to be effective catalysts for ROP of lactones and lactides. In most cases, polyesters were obtained with narrow PDI (1.1-1.4) and good agreement between theoretical and observed molecular weights (DPs ranging from 30-120 over the series of catalysts employed). Tertiary phosphines were reactive only at higher temperatures (>90 °C) and high catalyst loading (*51*), while NHCs afforded fast monomer conversion (within seconds for LA) at room temperature with low catalyst loading (0.5 mol %) (*52*). Co-catalyst systems of thiourea/amines required longer reaction times (48-72 h) compared to NHC-catalyzed ROP, but, notably, negligible broadening of the PDI was observed at long reaction times (up to 4 days), indicating minimal impact from transesterification (*53*). Most recently, Hedrick and co-workers reported amidine and guanidine analogues such

In Degradable Polymers and Materials: Principles and Practice (2nd Edition); Khemani, K., et al.;
ACS Symposium Series; American Chemical Society: Washington, DC, 2012.

as 1,4,7-triazabicyclodecene (TBD), 1,8-diazabicycloundec-7-ene (DBU), and *N*-methyl TBD (MTBD) to be highly reactive organocatalysts for ROP, affording complete monomer conversion in seconds to minutes (*54–56*). TBD was used alone as a catalyst for the ROP of δ-valerolactone (VL) and ε-caprolactone (CL), while DBU and MTBD required a thiourea cocatalyst for polymerization (*57*). TBD is the most reactive of the catalysts, presumably due to its basicity (*58*). Until recently, TBD had not been explored in the polymerization of functional lactones, though it had been shown to capably handle functional functional lactides (*59–61*). This work demonstrated the utility of TBD for the controlled, pseudo-living polymerization of functional lactones **10**, **11**, **14** and **15** (Figure 9), giving homopolymers, as well as random and diblock copolymers, with low PDI (1.1-1.2) (*44*).

Functional Cyclic Polyesters

Grayson described a simple preparation of cyclic poly(ε-caprolactone) from α-alkyne-ω-azido poly(ε-caprolactone) utilizing copper catalyzed alkyne-azide "click" cycloaddition (CuAAC) (Figure 14) (*62*). Using 3-azidopropanol as the functional initiator, ε-caprolactone was polymerized in bulk using $Sn(Oct)_2$ catalysis to prepare azido-terminated poly(ε-caprolactone) with absolute molecular weights ranging from 4000 to 15000 g/mol as characterized by matrix-assisted laser desorption ionization time-of-flight (MALDI-TOF) mass spectrometery. The hydroxyl chain-end was transformed to an alkyne by esterification with 4-pentynoic anhydride. Quantitative end-to-end coupling was then accomplished by slow addition of polymer with its click-ready end groups to the copper catalyst solution, which limits the concentration of telechelic polymer at any given time, thus promoting intramolecular cyclization. The cyclic topology was confirmed by a characteristic increase in the SEC retention time of the cyclic polyester relative to its linear precursor, as the reduced size in solution of the constrained cyclic structure results in slower elution. The $[M + Na]^+$ distribution observed by MALDI-TOF mass spectrometry for the linear precursor is retained after cyclization since there is no mass change associated with the click reaction, while ^{1}H-NMR spectroscopy indicates the appearance of the triazole proton and disappearance of the terminal alkyne proton after cyclization.

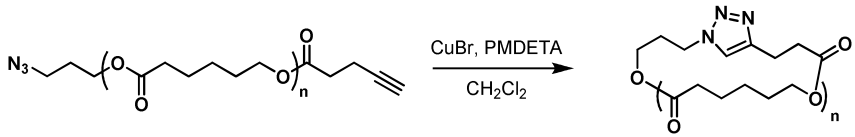

Figure 14. Synthesis of cyclic PCL by cyclization of an α,ω-heterodifunctional precursor with complimentary functionality at the chain ends for azide-alkyne click chemistry

Dove and coworkers developed a related cyclization method using thiol-ene click chemistry. Using aluminum catalysts, several stereoregular

α,ω-maleimido polylactides with tunable tacticities were prepared and cyclized by thiol-maleimide Michael addition in the presence of 1,2-ethanedithiol (*63*). In this work, functionality was also embedded into the initiator. For example, cyclization of polymer initiated by a disulfide containing diol gave degradable polylactide with a redox-responsive linkage within the polymer backbone, potentially providing additional functionality and control over degradation.

Another approach towards the synthesis of cyclic polyesters is ring-expansion polymerization. A cyclic initiator forces close proximity of the chain-ends, thus improving chain-end coupling efficiency. Several pathways enable permanent fixation of the cyclic architecture, including condensation with a bifunctional coupling agent (*64*, *65*), chain transfer to the polymer itself, and crossliking.

Jerome and Lecomte prepared cyclic poly(ε-caprolactone) by means of active endocyclic tin alkoxide, where both ends were connected to the catalyst during polymerization (*66*). A small amount of α-(1-acryloxyethyl)-ε-caprolactone were then copolymerized to introduce radical crosslinkable groups. The polymer was covalently zipped under dilute conditions and UV irradiation. A measured lower viscosity of the cyclic polymer, relative to its linear analog, confirmed its expected cyclic topology. Interestingly, cyclic tin alkoxide at the junction point remained intact after crosslinking; chain extension gave double tailed tadpole linear-cyclic copolymers. Because tin catalysts are compatible with various functional groups, this simple synthetic method further opens many possibilities for functional materials with advanced structures. For example, poly(ε-caprolactone-co-α-chloro-ε-caprolactone) were grafted from the cyclic poly(ε-caprolactone) using the tin catalyst located on the cyclic polymer backbone (*67*). Subsequent substitution with an azide gave CuAAC clickable tails and enabled PEGylation with alkyne terminated poly(ethylene glycol). The amphiphilicity of the resultant polymer was confirmed by the formation of micelles in water. The azide groups on the tails also allow efficient conjugation with other small molecules and polymers of interest, thus providing a series of novel materials with implications in self-assembly and drug delivery.

Finally, Fréchet, Szoka, and coworkers reported the preparation of cyclic poly(ε-caprolactone-co-α-chloro-ε-caprolactone) using ring-expansion copolymerization and photocrosslinking, providing a CuAAC clickable cyclic polymer template after azide substitution (*68*). PEG of various molecular weights, along with ^{125}I radiolabeled phenol, were grafted onto the polyester backbone. The pharmacokinetic studies showed that the cyclic polymers with molecular weight above the renal filtration threshold exhibited longer half-lives than their linear counterparts, addressing the impact of cyclic structures on retention time. The reduced renal clearance rate was attributed to the lack of end groups, and a higher translocation energy barrier of the cyclic polymer.

In summary, aliphatic polyesters, already an important class of synthetic degradable polymeric biomaterials, have acheived unprecedented levels of synthetic diversity and tailoring through the efforts of many research groups. Some of these have been described in this brief review, with a focus on pendent or graft functionality by polymerization of functionalized lactones, and post-polymerization modification. Future efforts in this area will connect these synthetic advances to specific applications, through the collaborative efforts

In Degradable Polymers and Materials: Principles and Practice (2nd Edition); Khemani, K., et al.;
ACS Symposium Series; American Chemical Society: Washington, DC, 2012.

of experts in the chemical, biological, and clinical use of synthetic polymer materials.

References

1. Ratner, B. D.; Hoffman, A. S.; Schoen, F. J.; Lemons, J. E. Biomaterials Science: A Multidisciplinary Endeavor. In *Biomaterials Science: An Introduction to Materials in Medicine*, 2nd ed.; Ratner, B. D., Hoffman, A. S., Schoen, F. J., Lemons, J. E., Eds.; Elsevier Academic Press: San Diego, CA, 2004; pp 1−9.
2. Albertsson, A. C.; Varma, I. K. *Biomacromolecules* **2003**, *4*, 1466–1486.
3. DeBakey, M. E.; Jordan, G. L.; Abbott, J. P.; Halput, B.; O'Neill, R. M. *Arch. Surg.* **1964**, *89*, 757–782.
4. Postlethwait, R. W.; Dillon, M. L.; Reeves, J. W. *Am. J. Surg.* **1961**, *102*, 706–709.
5. Nasongkla, N.; Shuai, X.; Ai, H.; Weinberg, B. D.; Pink, J.; Boothman, D. A.; Gao, J. *Angew. Chem., Int. Ed.* **2004**, *43*, 6323–6327.
6. Han, D. K.; Hubbell, J. A. *Macromolecules* **1996**, *29*, 5233–5235.
7. Orban, J. M.; Marra, K. G.; Hollinger, J. O. *Tissue Eng.* **2002**, *8*, 529–539.
8. Langer, R. *Acc. Chem. Res.* **2000**, *33*, 94–101.
9. Ihre, H. R.; Padilla De Jesús, O. L.; Szoka, F. C., Jr.; Fréchet, J. M. J. *Bioconjugate Chem.* **2002**, *13*, 443–452.
10. Carnahan, M. A.; Grinstaff, M. W. *Macromolecules* **2006**, *39*, 609–616.
11. Luman, N. R.; Smeds, K. A.; Grinstaff, M. W. *Chem. Eur. J.* **2003**, *9*, 561–5626.
12. Carnahan, M. A.; Middleton, C.; Kim, J.; Kim, T.; Grinstaff, M. W. *J. Am. Chem. Soc.* **2002**, *124*, 5291–5293.
13. Andersson, L.; Davies, J.; Duncan, R.; Ferruti, P.; Ford, J.; Kneller, S.; Mendichi, R.; Pasut, G.; Schiavon, O.; Summerford, C.; Tirk, A.; Veronese, F. M.; Vincenzi, V.; Wu, G. *Biomacromolecules* **2005**, *6*, 914–926.
14. Möller, M.; Kånge, R.; Hedrick, J. L. *J. Polym. Sci., Part A: Polym. Chem.* **2000**, *38*, 2067–2074.
15. Nyce, G. W.; Glauser, T.; Conner, E. F.; Möck, A.; Waymouth, R. M.; Hedrick, J. L. *J. Am. Chem. Soc.* **2003**, *125*, 3046–3056.
16. Savić, R.; Luo, L.; Eisenberg, A.; Maysinger, D. *Science* **2003**, *300*, 615–618.
17. Bogdanov, B.; Vidts, A.; Van Den Bulcke, A.; Verbeeck, R.; Schacht, E. *Polymer* **1998**, *39*, 1631–1636.
18. Mizutani, M.; Arnold, S. C.; Matsuda, T. *Biomacromolecules* **2002**, *3*, 668–675.
19. Nederberg, F.; Bowden, T.; Hilborn, J. *Macromolecules* **2004**, *37*, 954–965.
20. Padilla De Jesús, O. L.; Ihre, H. R.; Gagne, L.; Fréchet, J. M. J. *Bioconjugate Chem.* **2002**, *13*, 453–461.
21. Trollsås, M.; Löwenhielm, P.; Lee, V. Y.; Möller, M.; Miller, R. D.; Hedrick, J. L. *Macromolecules* **1999**, *32*, 9062–9066.
22. Liu, M.; Vladimirov, N.; Fréchet, J. M. J. *Macromolecules* **1999**, *32*, 6881–6884.

23. Rieger, J.; Bernaerts, K. V.; Du Prez, F. E.; Jérôme, R.; Jérôme, C. *Macromolecules* **2004**, *37*, 9738–9745.
24. Detrembleur, C.; Mazza, M.; Halleux, O.; Lecomte, P.; Mecerreyes, D.; Hedrick, J. L.; Jérôme, R. *Macromolecules* **2000**, *33*, 14–18.
25. Mecerreyes, D.; Miller, R. D.; Hedrick, J. L.; Detrembleur, C.; Jérôme, R. *J. Polym. Sci., Part A: Polym. Chem.* **2000**, *38*, 870–875.
26. Latere, J. -P.; Lecomte, P.; Dubois, P.; Jérôme, R. *Macromolecules* **2002**, *35*, 7857–7859.
27. Trollsås, M.; Lee, V. Y.; Mecerreyes, D.; Löwenhielm, P.; Möller, M.; Miller, R. D.; Hedrick, J. L. *Macromolecules* **2000**, *33*, 4619–4627.
28. Parrish, B.; Quansah, J. K.; Emrick, T. *J. Polym. Sci., Part A: Polym. Chem.* **2002**, *40*, 1983–1990.
29. Parrish, B.; Emrick, T. *Macromolecules* **2004**, *37*, 5863–5865.
30. Parrish, B.; Breitenkamp, R. B.; Emrick, T. *J. Am. Chem. Soc.* **2005**, *127*, 7404–7420.
31. Mecerreyes, D.; Humes, J.; Miller, R. D.; Hedrick, J. L.; Detrembleur, C.;
32. Mecerreyes, D.; Atthoff, B.; Boduch, K. A.; Trollsås, M.; Hedrick, J. L. *Macromolecules* **1999**, *32*, 5175–5182.
33. Taniguchi, I.; Mayes, A. M.; Chan, E. W. L.; Griffith, L. G. *Macromolecules* **2005**, *38*, 216–219.
34. Lee, C. C.; Grayson, S. M.; Fréchet, J. M. J. *J. Polym. Sci., Part A: Polym. Chem.* **2004**, *42*, 3563–3578.
35. Barrera, D. A.; Zylstra, E.; Lansbury, P. T.; Langer, R. *J. Am. Chem. Soc.* **1993**, *115*, 11010–11011.
36. Molander, G. A.; Harris, C. R. *J. Am. Chem. Soc.* **1995**, *117*, 3705–3716.
37. Darcos, V.; Habnouni, S. E.; Nottelet, B.; Ghzaoui, A. E.; Coudane, J. *Polym. Chem.* **2010**, *1*, 280–282.
38. Cooper, B. M.; Emrick, T. *J. Polym. Sci., Part A: Polym. Chem.* **2009**, *47*, 7054–7065.
39. Kolb, H. C.; Finn, M. G.; Sharpless, K. B. *Angew. Chem., Int. Ed.* **2001**, *40*, 2004–2021.
40. Wu, P.; Feldman, A. K.; Nugent, A. K.; Hawker, C. J.; Scheel, A.; Voit, B.; Pyun, J.; Fréchet, J. M. J.; Sharpless, K. B.; Fokin, V. V. *Angew. Chem., Int. Ed.* **2004**, *43*, 3928–3932.
41. Link, A. J.; Vink, M. K. S.; Tirrell, D. A. *J. Am. Chem. Soc.* **2004**, *126*, 10598–10602.
42. Cooper, B. M.; Chan-Seng, D.; Samanta, D.; Zhang, X.; Parelkar, S.; Emrick, T. *Chem. Commun.* **2009**, 815–817.
43. Parrish, B.; Emrick, T. *Bioconjugate Chem.* **2007**, *18*, 263–267.
44. Silvers, A. L.; Chang, C.-C.; Emrick, T. *J. Polym. Sci., Part A: Polym. Chem.* **2012**, in press.
45. Campos, L. M.; Killops, K. L.; Sakai, R.; Paulusse, J. M. J.; Damiron, D.; Drockenmuller, E; Messmore, B. W.; Hawker, C. J. *Macromolecules* **2008**, *41*, 7063–7070.
46. van der Ende, A. E.; Harrell, J.; Sathiyakumar, V.; Meschievitz, M.; Katz, J.; Adcock, K.; Harth, E. *Macromolecules* **2010**, *43*, 5665–5671.

47. Li, G. L.; Wan, D.; Neoh, K. G.; Kang, E. T. *Macromolecules* **2010**, *43*, 10275–10282.
48. Platel, R. H.; Hodgson, L. M.; Williams, C. K. *Polym. Rev.* **2008**, *48*, 11–63.
49. Kamber, N. E.; Jeong, W.; Waymouth, R. M. *Chem. Rev.* **2007**, *107*, 5813–5840.
50. Nederberg, F.; Connor, E. F.; Moller, M.; Glauser, T.; Hedrick, J. L. *Angew. Chem., Int. Ed.* **2001**, *40*, 2712–2715.
51. Myers, M.; Connor, E. F.; Glauser, T.; Mock, A.; Nyce, G. W.; Hedrick, J. L. *J. Polym. Sci., Polym. Chem.* **2002**, *40*, 844–851.
52. Beckerle, K.; Hultzsch, K. C.; Okuda, J. *Macromol. Chem. Phys.* **1999**, *200*, 1702–1707.
53. Dove, A. P.; Pratt, R. C.; Lohmeijer, B. G. G.; Waymouth, R. M.; Hedrick, J. L. *J. Am. Chem. Soc.* **2005**, *127*, 13798.
54. Lohmeijer, B. G. G.; Pratt, R. C.; Leibfarth, F.; Logan, J. W.; Long, D. A.; Dove, A. P.; Nederberg, F.; Choi, J.; Wade, C.; Waymouth, R. M.; Hedrick, J. L. *Macromolecules* **2006**, *39*, 8574–8583.
55. Pratt, R. C.; Lohmeijer, B. G. G.; Long, D. A.; Waymouth, R. M.; Hedrick, J. L. *J. Am. Chem. Soc.* **2006**, *128*, 4556–4557.
56. Pratt, R. C.; Lohmeijer, B. G.; Long, D. A.; Waymouth, R. M.; Hedrick, J. L. *J. Am. Chem. Soc.* **2006**, *128*, 4556.
57. Taylor, M. S.; Jacobsen, E. N. *Angew. Chem., Int. Ed.* **2006**, *45*, 1520.
58. Kaljurand, I.; Kutt, A.; Soovali, L.; Rodima, T.; Maemets, V.; Leito, I.; Koppel, I. A. *J. Org. Chem.* **2005**, *70*, 1019.
59. du Boullay, O. T.; Saffon, N.; Diehl, J.-P.; Martin-Vaca, B.; Didier Bourissou, D. *Biomacromolecules* **2010**, *11*, 1921–1929.
60. Jing, F.; Hillmyer, M. A. *J. Am. Chem. Soc.* **2008**, *130*, 13826.
61. Fiore, FG. L.; Jing, F.; Young, V. G., Jr.; Cramer, C. J.; Hillmyer, M. A. *Polym. Chem.* **2010**, *1*, 870–877.
62. Hoskins, J. N.; Grayson, S. M. *Macromolecules* **2009**, *42*, 6406–6413.
63. Stanford, M. J.; Pflughaupt, R. L.; Dove, A. P. *Macromolecules* **2010**, *43*, 6538–6541.
64. Kricheldorf, H. R.; Fechner, B. *Macromolecules* **2001**, *34*, 3517–3521.
65. Kricheldorf, H. R.; Lee, S.-R.; Schttenhelm, N. *Macromol. Chem. Phys.* **1998**, *199*, 273.
66. Li, H.; Debuigne, A.; Jerome, R.; Lecomte, P. *Angew. Chem., Int. Ed.* **2006**, *45*, 2264–2267.
67. Li, H.; Riva, R.; Jerome, R.; Lecomte, P. *Macromolecules* **2007**, *40*, 824–831.
68. Nasongkla, N.; Chen, B.; Macaraeg, N.; Fox, M. E.; Fréchet, J. M. J.; Szoka, F. C. *J. Am. Chem. Soc.* **2009**, *131*, 3842–3843.

Chapter 16

Degradable Poly(ethylene oxide)-*block*-polycaprolactone Worm-like Micelles: From Phase Transitions and Molecular Simulation to Persistent Circulation and Shrinking Tumors

Núria Sancho Oltra, Sharon M. Loverde, Takamasa Harada, Abdullah Mahmud, Karthikan Rajagopal, and Dennis E. Discher*

Department of Chemical and Biomolecular Engineering, University of Pennsylvania, Philadelphia, PA 19104-6391
***discher@seas.upenn.edu**

Novel giant and flexible worm-like micelles were self-assembled from degradable copolymer poly(ethylene oxide)-*block*-polycaprolactone (OCL). Such worm-like micelles spontaneously shorten to spherical micelles, triggered by hydrolytic degradation of polycaprolactone. Unique degradation mechanism and kinetics in OCL worm-like micelles were elucidated, and key activating conditions of temperature, pH, and polymer molecular weight were quantitatively assessed. We have also demonstrated that degradable OCL worm-like micelles possess great potential as novel controlled-release drug delivery vehicles: they are compatible with cultured cells and blood, they exhibit long circulation times in vivo, and are capable of loading a model hydrophobic anti-cancer drug (taxol). Moreover, the release of the drug is controlled by OCL worm-like micelle degradation rate. While molecular simulations capture many of these phenomena, in vivo experiments establish the effectiveness of worm-like micelles in the shrinkage of tumors.

In Degradable Polymers and Materials: Principles and Practice (2nd Edition); Khemani, K., et al.;
ACS Symposium Series; American Chemical Society: Washington, DC, 2012.

Introduction

Degradable polymers are crucial to a number of fields ranging from agricultural, environmental to biomedical applications (*1*). Degradable homopolymers and random copolymers have been widely used in bulk materials, micro/nano-particles, and films/monolayers; furthermore, a great deal of study has focused on their degradation mechanism and kinetics (*2–5*). In recent years, degradable self-assemblies of block copolymer amphiphiles are also emerging and have attracted considerable attention (*6–9*).

Self-assemblies of amphiphilic block copolymers with a hydrophilic block covalently connected to a hydrophobic block are a rapidly emerging subclass of colloids. Like conventional small-molecule surfactants (<<1kD), amphiphilic block copolymers self-assemble into spherical and cylindrical micelles, as well as bilayer vesicles, which are classic examples of thermodynamically stable self-assembly morphologies (*6*). While the self-assembly morphology is generally dictated by block proportions (*10*), desired physical-chemical-mechanical properties can be tuned through molecular weight (M_n), structure of each block, modification and crosslinking (*11–14*). Such flexibility in design of copolymer "macro"-surfactant offers clear material advantages over small surfactants. Moreover, copolymer assemblies are much more stable systems compared to small surfactants, since they generally have much lower critical micellar concentration (CMC) and slower dissociation rate (*6*). These features of diblock copolymers make them potentially useful in many applications, in particular drug delivery. The outer hydrophilic corona, generally poly(ethylene oxide) (PEO), maximizes biocompatibility and helps micelles escape the rapid reticuloendothelial system (RES) after intravenous administration and prolongs their circulation in blood. The hydrophobic micellar core can encapsulate drugs with poor water solubility (*15*). Compared to non-degradable polymers, using a degradable polymer as the hydrophobic block of the copolymers offers advantages of being able to degrade into non-toxic low-molecular weight molecules that can be either absorbed by the body or removed by metabolism and mediate the release of the encapsulated drug as it degrades.

Attention on self-assemblies of degradable copolymers has thus far been mostly limited to spherical micelles, typically from copolymers of hydrophobic polyesters such as polylactides and polycaprolactone connected with hydrophilic PEO (*7–9*). However, degradation has subtle if detectable effects on the spherical morphology, and degradation mechanisms and kinetics in spherical micelles have not been clearly distinguished in time scales or mechanisms from those in bulk or film (*7–9*). In this book chapter, we describe the different self-assembled morphologies of degradable poly(ethylene oxide)-*b*-poly(ε-caprolactone) copolymers (PEO-PCL, denoted OCL) paying particular attention to novel giant and flexible worm-like micelles. Such OCL worm-like micelles spontaneously shorten to generate spherical micelles due to polycaprolactone hydrolytic degradation. Its unique degradation mechanism, as well as the physical mechanism underlying micellar shape changes, corroborated by molecular simulations (*16*), and kinetics in OCL worm-like micelles are elucidated, and

In Degradable Polymers and Materials: Principles and Practice (2nd Edition); Khemani, K., et al.;
ACS Symposium Series; American Chemical Society: Washington, DC, 2012.

key activating conditions of temperature, pH, and polymer molecular weight are quantitatively assessed in this context of a microphase transition (*17*).

Up to date, drug delivery vehicles are overwhelmingly spherical in shape. Worm-like micelles have emerged as a novel system that provides larger core volume to load drugs and is able to flow readily through capillaries and pores, due to their cylindrical morphology and flexibility (*18*, *19*). In vivo injection of worm-like micelles into tail vein of rats has shown that they are able to circulate much longer than any spherical synthetics (*20*). One useful and novel strategy for drug delivery is to start as worm-like micelles with larger drug loading capacity and longer circulation time and later degrade into spherical micelles, which are already proven to be extremely useful for therapeutic applications (*21*). With clarified mechanism/kinetics, such degradability of worm-like micelles could also be exploited to control drug release. In this book chapter, we also describe the evaluation of degradable OCL worm-like micelles as drug delivery vehicles: their biocompatibility with cultured cells as well as blood, the loading of hydrophobic anti-cancer drug paclitaxel (henceforth referred to as TAX), and how degradation influences the release kinetics of TAX (*22*). Importantly, recent in vivo studies provide evidence of tumor shrinkage by TAX-loaded OCL worm-like micelles (*20*, *23*).

Experimental

Synthesis of PEO-*b*-PCL (OCL) and PEO-*b*-P(CL-*r*-*D,L*-LA) (OCLA) Diblock Copolymers

PEO-*b*-PCL block copolymers were generally synthesized by the ring-opening polymerization of ε-caprolactone using the required size of methoxy terminated poly(ethylene oxide) as macro initiator and stannous octoate as catalyst or were purchased from Polymer Source, Inc. (Dorval, Canada). Briefly, freshly distilled ε-caprolactone (2.5 g, 0.0219 mol), the required amount of methoxy-PEO (amount based on required MW of block copolymer), and stannous octoate (15 mg, 3.7 x 10^{-5} moles) were weighed out in a flamed and nitrogen-dried ampule. The ampule was sealed and placed in an oven pre-equilibrated to 140 °C and the polymerization reaction was allowed to proceed for 4 h. The reaction was terminated after cooling the ampule to room temperature. For the synthesis of OCLA(2, X, Y) copolymers, a mixture of ε-caprolactone and *D,L*-lactide were taken along with the required amount of poly(ethylene oxide) (2000 g/mol) and stannous octoate.

Preparation of OCL Worm-like Micelles

OCL worm-like micelles were prepared using either of the two following methods: thin film rehydration and solvent evaporation. For the thin film rehydration method, 100 μL of 10 mg/mL OCL stock solution in chloroform was added to a glass vial. Chloroform was removed under nitrogen. The remaining OCL film was then re-dissolved in 30 μL of chloroform, and 5 mL of water was added to the vial and stirred vigorously for 1-2 hours, yielding an opaque

In Degradable Polymers and Materials: Principles and Practice (2nd Edition); Khemani, K., et al.;
ACS Symposium Series; American Chemical Society: Washington, DC, 2012.

worm-like micelle dispersion (0.2 mg/mL). Chloroform (~ 0.5% of solution volume) was then slowly removed by evaporation at 4°C to minimize OCL worm-like micelle degradation. After 24 hours, the OCL worm-like micelle solution turned clear and did not contain detectable chloroform, confirmed by gas chromatography (GC) with the detection limit of 0.01% volume fraction of chloroform. The critical micelle concentration (CMC) of OCL copolymers is around 1.2 μg/ml (*24*); therefore, OCL copolymers are mainly in the form of micelles since their concentration exceeds the CMC by a factor of 100.

In the solvent evaporation method, a 1 mM stock of the polymer was first prepared in chloroform. Then 100 μL of this stock was added to 1 mL of DI water taken in a clean 2 mL glass vial. The contents of the vial were stirred gently (~ 200 rpm) on a magnetic stir plate using a microstirrer with the cap open at room temperature. Stirring was continued for 48 h or until no chloroform layer was observed.

Visualization of OCL Worm-like Micelles

Olympus IX71 inverted fluorescence microscope with a 60X objective and a Cascade CCD camera (Cascade 512, Roper Scientific) was used to visualize OCL worm-like micelles. A hydrophobic fluorophore dye (PKH 26, Sigma) was added to the OCL worm-like micelles, and 2 μL of sample was used in the glass slide-cover slip chamber. Approximately 20 pictures were taken per sample. Analysis details were described elsewhere (*25*). Cryo-TEM was also used to visualize the OCL worm-like micelle morphological change. Sample preparation and analysis has been described in detail elsewhere (*14*).

Measurement of Percentage of Rigid Worms

100 μL of 100 μM polymer solution was taken in an Eppendorf tube and equilibrated at the required temperature for a day. For imaging, 0.2 μL of 0.2 mM dye (PKH26, Sigma) was added and gently mixed. Then, 2 μL of this sample was spotted on a clear glass slide and a 18 mm coverslip was placed on top, pressed gently down and sealed with grease. Imaging was done on an Olympus IX71 microscope equipped with a Cascade 512B camera. For each sample, 200 worm-like micelles were randomly counted from 10 different fields of view, and the number of rigid worm-like micelles was recorded.

Circulation Studies

For circulation studies, previous polymer vesicle protocols were followed and performance was assessed in two rodent species for comparison with previous studies (*2*, *26–28*). Male Sprague–Dawley rats were injected with 0.5 mL of 5 $mg \cdot mL^{-1}$ copolymer in phosphate buffered saline (PBS); alternatively, equal numbers of male or female C57 mice (with similar results) were injected with 0.1 mL of the same. Orbital bleeds into heparin tubes were taken at various times during the study. The plasma (containing the worm-like micelles) was separated from the other blood components by centrifugation at 7,000 g for 10

In Degradable Polymers and Materials: Principles and Practice (2nd Edition); Khemani, K., et al.;
ACS Symposium Series; American Chemical Society: Washington, DC, 2012.

min to determine the number, N, and contour lengths of the worm-like micelles in circulation.

In Vitro Phagocytosis Assays

In vitro phagocytosis assays were performed on blood-drawn human neutrophils and also a human macrophage cell line, THP1 (ATCC). Worm-like micelle suspensions of 0.1 mg of copolymer (large excess for the number of cells) were incubated with the macrophage cell line for 24 h.

Gel Permeation Chromatography (GPC) Studies on OCL Worm-like Micelle Degradation

At different times, 1 mL of 0.2 mg/mL OCL worm-like micelle solution was lyophilized, re-dissolved in 150 μL of THF, passed through a 0.4 μm syringe filter and then analyzed by GPC. A Waters Breeze GPC equipped with Styragel HR2 and HR3 columns, connected with a refractive index detector was used. The mobile phase was THF and the flow rate was 1.0 mL/min. The copolymer peak was characterized by PEG standards. The predominant new peak generated with OCL worm-like micelle shortening was identified by "spiking" with standard monomer 6-hydroxycaproic acid (6-HPA) (Sigma-Aldrich: 6-HPA 80 wt%, mixed with other possible PCL hydrolysis products: dimer, trimer, tetramer and larger caprolactone oligomers). 6-HPA yield was estimated from its standard calibration curve that correlates peak area with amount.

^{1}H Nuclear Magnetic Resonance

^{1}H NMR was used to determine the loss of caprolactone units from OCL copolymer with worm-like micelle shortening. 20 mL of 0.2 mg/mL OCL worm-like micelle solution at different degradation time was lyophilized, after removing all possible degradation products by dialysis at 4 °C, and re-dissolved in chloroform (*d*) for ^{1}H NMR analysis on a Bruker 300 MHz spectrometer. At different degradation time, caprolactone units (PCL_t) remaining in the copolymer was estimated from comparing the summary of integral of PCL_t methylene peaks ($\delta \sim 4.0$ ppm **t**, 2.3 ppm **t**, 1.6 ppm **m**, 1.3 ppm **m**, total proton = 10 × $unit_{PCLt}$) to the integral of PEO methylene peak ($\delta \sim 3.6$ ppm **s**, total proton = 4 × $unit_{PEO}$), which is non-degradable and remains constant with OCL worm-like micelle shortening.

Cell Culture

Bovine aortic endothelial cells and vascular smooth muscle cells were purchased from ATCC (American Type Culture Collection). Cells were plated and allowed to attach for 12 h, after which a measured dose of OCL worm-like micelles in PBS was added to each plate. Cell viability after exposure to OCL worm-like micelles for up to 5 days was assayed by Trypan Blue exclusion.

In Degradable Polymers and Materials: Principles and Practice (2nd Edition); Khemani, K., et al.;
ACS Symposium Series; American Chemical Society: Washington, DC, 2012.

TAX Loading

Stock solutions of TAX in methanol (5 mg/mL) were added with a weight ratio of 0.2:1 to 1 mL of OCL worm-like micellar solutions at different concentrations and vortexed for 5 minutes. The small amount of methanol was removed by dialysis at 4 °C for 2 hours. Unloaded TAX precipitate was centrifuged at 3000 rpm for 5 min and further removed from the micelle supernatant by filtering with a 0.45 μm pore-sized syringe filter. The amount of TAX loaded into OCL worm-like micelles was then determined by HPLC. A Waters Breeze HPLC equipped with a diode array UV detector set at λ = 220 nm, connected with a Symmetry C-18 column, methanol as the mobile phase, and a flow rate of 0.8 mL/min was used. TAX is well resolved from OCL peak, and the amount of TAX was estimated from its calibration curve that correlates peak area with amount.

TAX loading into micelles for in vitro delivery to A549 lung carcinoma cells was done by addition of TAX 50 mg/mL in methanol into the micelle solutions to obtain desired spiked TAX/polymer ratios. The mixture was stirred at 25 °C for 20 min and transferred to dialysis cassettes (MWCO 10,000, Pierce, Rockford, IL). Dialysis was performed against DPBS (pH 7.4) for 2 h to remove methanol and small residues of dissolved TAX, and the obtained TAX-loaded micelles were separated from insoluble free TAX aggregates by extrusion through a 10 mL thermobarrel extruder (Northern Lipids, Vancouver, Canada) fitted with 0.65 mm filtering membranes (Millipore, Bedford, MA), and further purified by filtration through a 0.45 mm Fischerbrand MCE filter (Fisher Scientific).

Hemolysis Study

Fresh whole blood was pelleted by centrifugation and 100 μL of the collected red blood cell (RBC) suspension was added to 900 μL of 10 mg/mL OCL worm-like micelles in PBS (RBC: 10% hematocrit in PBS). The samples were incubated for 24 hours at 37 °C. The release of hemoglobin in the supernatant, collected by centrifugation, was measured by UV-Vis at 412 nm and compared to the complete hemolysis by 0.2% small surfactants Triton X-100.

TAX Release at Different pH

The release behavior of TAX from OCL worm-like micelles under different pH buffers (0.01 M PBS pH 7 and 0.01 M HEPES pH 5) was studied by dialysis at 37 °C. 10 mL of TAX-encapsulated 0.2 mg/mL OCL worm-like micelle in a dialysis tubing (MWCO: 1000) was placed in a l L beaker filled with buffer solutions. At specific time intervals, a 150 μL aliquot was removed from the dialysis bag, lyophilized and re-dissolved in $CHCl_3$. Buffer salt was centrifuged at 3000 rpm for 5 min and further removed from the micelle supernatant by filtering with a 0.45 μm pore-sized syringe filter. $CHCl_3$ was then evaporated under N_2 flow and the mixture of TAX and OCL polymer was redissolved in 150 μL of methanol and filtered through a 0.45 μm pore-sized syringe filter before injecting into HPLC. The amount of TAX remaining in the dialysis bag was thus estimated

In Degradable Polymers and Materials: Principles and Practice (2nd Edition); Khemani, K., et al.;
ACS Symposium Series; American Chemical Society: Washington, DC, 2012.

from its calibration curve and the percentage of released TAX was calculated as % Release = (total TAX – TAX remaining in dialysis bag)/total TAX × 100%.

TAX Delivery to A549 Lung Carcinoma Cells

Human lung-derived carcinoma cells A549 were grown in Ham's F12 media supplemented with 10% fetal bovine serum and 100 U/mL penicillin and 100 mg/mL streptamycin at 37 °C, 5% CO_2 to 60–70% confluence. A549 cells (50,000 cell/mL) were seeded in 96-well plates at 5,000 cells per well and cultured for 24 h to allow attachment. The medium was then exchanged and 100 μL of different tested formulations (free worm-like and spherical OCL3 micelles, Cremophor EL, free drug, TAX-loaded worm-like and spherical micelles, and Cremophor EL TAX) was added. As control, 100 μL of DPBS was added to cells not exposed to those formulations. After 37 °C, 5% CO_2 incubation for 72 h, the media were discarded, and 100 μL/well Ham's F12 medium and 11 μL/well of 5 mg/mL MTT solution in DPBS was added. The plates were incubated at 37 °C for 3 h and the media were removed again. The intracellular metabolized product MTT formazan was retrieved by addition of 100 μL/well DMSO and incubation at room temperature for 5 min. The plates were read at 550 nm, and the cell viability was calculated as (reading of wells with cells exposed to tested formulations - reading of blank wells)/(reading of wells with cells exposed to DPBS - reading of blank wells).

Tumor Shrinkage Studies

Human lung carcinoma cell line, A549, was injected subcutaneously onto the backs of nude mice and allowed to grow. After about 3 weeks, the tumor-bearing mice were injected with TAX-loaded OCL micelles at maximum tolerated doses (MTD) of the corresponding morphology, as well as free TAX at MTD (1 mg/kg) (*29*), PBS saline alone and/or worm-like micelle controls. Apoptosis was measured one week later by quantitative imaging of TUNEL-stained tumor section.

The same injections were repeated after 3, 7, 10, 14, 17, 21 days in the comparative study between worm-like and spherical micelles. Tumor area (A) was monitored 24 h after each injection by measuring two orthogonal dimensions as $A = [(L_1 \times L_2)/2]$ for each treatment group (*29*). The body weight of the mice was also monitored throughout the experiment.

Results and Discussion

Morphological Phase Behavior of OCL Assemblies

The preferred morphology of assemblies of OCL was studied for block copolymers containing different hydrophilic/hydrophobic ratios and mapped into a plot of core block hydrophobicity (M_{CH2}) versus hydrophilic mass fraction $f_{hydrophilic}$ (Figure 1) (*30*). The morphologies of the aggregates of OCL block copolymers appear to be dependent on the lengths of both blocks. This was previously observed by Fan and co-workers, who studied the effect of

In Degradable Polymers and Materials: Principles and Practice (2nd Edition); Khemani, K., et al.;
ACS Symposium Series; American Chemical Society: Washington, DC, 2012.

the microstructure of the block copolymers on the aggregate morphology by Transmission Electron Microscopy (TEM) (*31*).

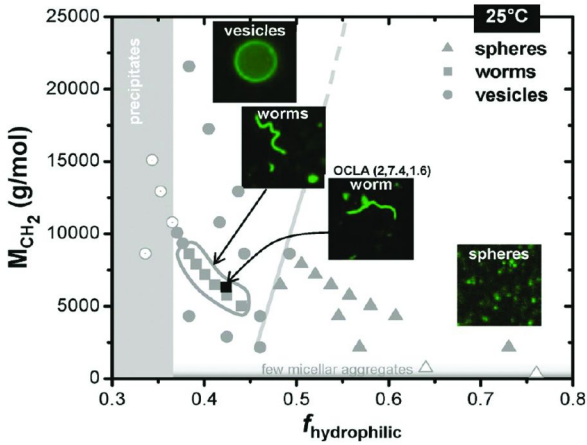

Figure 1. Morphological phase behavior of OCL assemblies in dilute solution prepared at 25 °C by chloroform evaporation method. Filled symbols in gray represent corresponding morphologies; triangles for spherical micelles, squares for worm-like micelles and circles for vesicles. Gray lines indicate the approximate phase boundaries. Worm-like micelles formed from poly(ethylene oxide)-b-poly(ε-caprolactone-r-D,L-lactide) (OCLA (2,7.4,1.6)) copolymer is indicated in the phase diagram with a filled black square. (Reprinted with permission from reference (30). Copyright 2010 American Chemical Society)

Aggregates were obtained at $f_{hydrophilic} > 0.36$. At lower $f_{hydrophilic}$ precipitation of the polymer occurred most probably because short PEO chains do not provide colloidal stability to the assemblies. The boundaries between the phases do not appear precisely defined with the coexistence of different morphologies in the transition regions. This has been previously observed for strongly segregating copolymers like OB (poly(ethylene oxide)-*b*-poly(1,2-butadiene) or PEO-*b*-PBD) (*10*). Interestingly, for OCL polymers the formation of worm-like micelles is only limited to a narrow morphological space that is buried within the vesicle region while for other copolymers, such as OB, worm-like micelles appear as a transition state between spherical micelles and vesicles (*10*). For lower $f_{hydrophilic} f_{CH2}$ the formation of vesicles is favored since this leads to a parallel alignment of polymer chains for cooperative crystallite growth. Frustration of crystallization occurs in high curvature structures leading to flexible worm-like micelles (*30*).

Aggregates of poly(ethylene oxide)-*b*-poly(ε-caprolactone-*r*-*D,L*-lactide) (OCLA) block copolymers showed likewise a worm-like micelle morphology that coincides in the worm-like micelle region of OCL.

In Degradable Polymers and Materials: Principles and Practice (2nd Edition); Khemani, K., et al.;
ACS Symposium Series; American Chemical Society: Washington, DC, 2012.

Controlling Rigidity of Worm-like Micelles

Fluorescence microscopy observation of OCL worm-like micelles shows persistent transverse fluctuations that are suggestive of a soft, fluid core. However, a small population of OCL(2,9) worm-like micelles exhibits inflexible and rigid body motion. This rigidity is dependent on the molecular weight of the hydrophobic block and is a consequence of the semi-crystalline nature of PCL (*30*). Close packing of PCL, which is viable for higher molecular weights of the hydrophobic block, results in crystallization of the core. For lower molecular weights, however, the core curvature 'frustrates' this crystallization process, resulting in flexible worm-like micelles (Figure 2a).

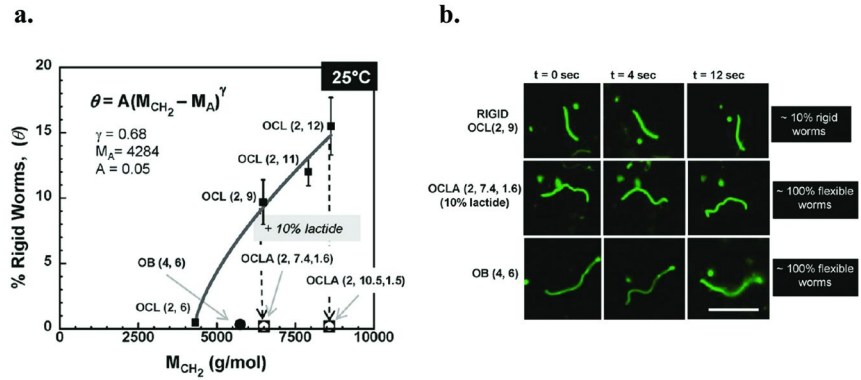

Figure 2. ***a.*** *Percentage of rigid OCL worm-like micelles (θ) as a function of the size of the hydrophobic block (M_{CH2}) is shown. The data is fit to a power law (R^2=0.985). The absence of rigid worm-like micelles in OB and OCLA samples is also indicated.* ***b.*** *Fluorescence microscopy snap shots representing worm-like micelle conformation at 4 s intervals is shown for a rigid OCL(2,9) worm-like micelle (top row), a flexible OCLA(2,7.4,1.6) worm-like micelle (middle row) and a flexible OB(4,6) worm-like micelle (bottom row). Approximately 10% of OCL(2,9) worm-like micelles exhibit rigid-body motion at room temperature while all of OCLA and OB worm-like micelles are completely flexible. Scale bar for all images is 10 μm. (Reprinted with permission from reference (30). Copyright 2010 American Chemical Society)*

The introduction of defects within the hydrophobic core can prevent core crystallization allowing for the formation of flexible worm-like micelles. By incorporating 10% of *D,L*-lactide (LA) within the PCL block of poly(ethylene oxide)-*b*-poly(ε-caprolactone-*r*-*D,L*-lactide) (OCLA) rigidity can be completely eliminated. Due to the bulkiness of the methyl groups on LA, core crystallization is suppressed and therefore, flexible worm-like micelles are obtained (Figure 2b). The physical state (crystalline vs amorphous) of the hydrophobic core not only influences the flexibility of the aggregates but also affects aggregate morphology (*32*).

In Degradable Polymers and Materials: Principles and Practice (2nd Edition); Khemani, K., et al.; ACS Symposium Series; American Chemical Society: Washington, DC, 2012.

Half-rigid worms of OCL were also observed (Figure 3) but were rare and decreased in number over days. Their existence is consistent with nucleation-growth of crystals that propagate within the core, along the worm contour.

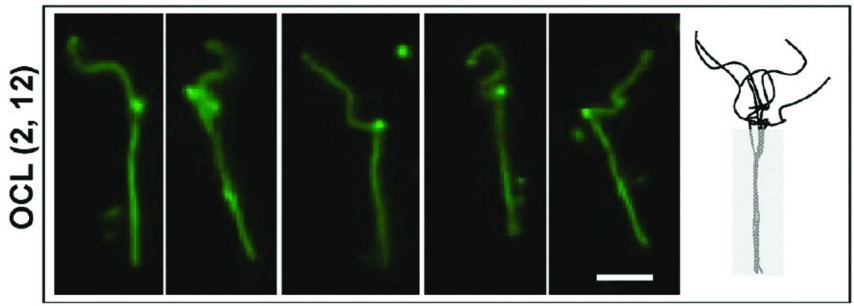

Figure 3. Visualization of partial rigidity in OCL worm-like micelles. Snapshots were taken every 30 s of OCL worms, and the contour was traced, rotated, and overlaid to highlight the rigid segment. Scale bar is 5 μm. (Reprinted with permission from reference (30). Copyright 2010 American Chemical Society)

In Vivo Circulation of OCL Worm-like Micelles

Fluorescent worm-like micelles or filomicelles from non-degradable (EO_{42}–EE_{35} (OE7')) and degradable/hydrolysable (EO_{44}–CL_{24} (OCL1) and EO_{110}–CL_{58} (OCL3)) diblock copolymers were injected into mice and rats and blood samples were analyzed by fluorescence microscopy. The images showed that a fraction of worm-like micelles circulate in vivo for up to one week (Figure 4a) (*23*). This persistent circulation is observed for inert (polyethylethylene) or degradable (OCL) worm-like micelles (Figure 4b and c) in contrast with published results for PEGylated 'stealth' vesicles and quasi-linear λ-phages viruses which were respectively cleared within two and one days (Figure 4b).

The fact that worm-like micelles remain longer in circulation compared to other aggregates makes them particularly interesting for drug delivery purposes. Longer circulation times result in more frequent passage through the tumor and thus more effective passive tumor delivery of aggregates via the enhanced permeability and retention (EPR) effect (*33*).

The circulation time of worm-like micelles was found to depend on their initial length. Worm-like micelles of different average initial lengths L_0 were prepared from OCL3 copolymer and injected into mice. The results obtained showed that for worm-like micelles of L_0 up to ~ 8 μm, longer worm-like micelles persist longest in the circulation (*23*). Interestingly, this length approximates the diameter of blood cells which are likewise flexible and have a circulation time of several weeks (*34*). Longer worm-like micelles undergo rapid fragmentation with a decrease in length over time consistent with progressive shortening by mechanical forces because the inert OE7' micelles showed the same trends. Moreover, the degradation rate depended on the initial length of the micelles with a slower shortening for the shortest micelles (< 4 μm) (Figure 4d).

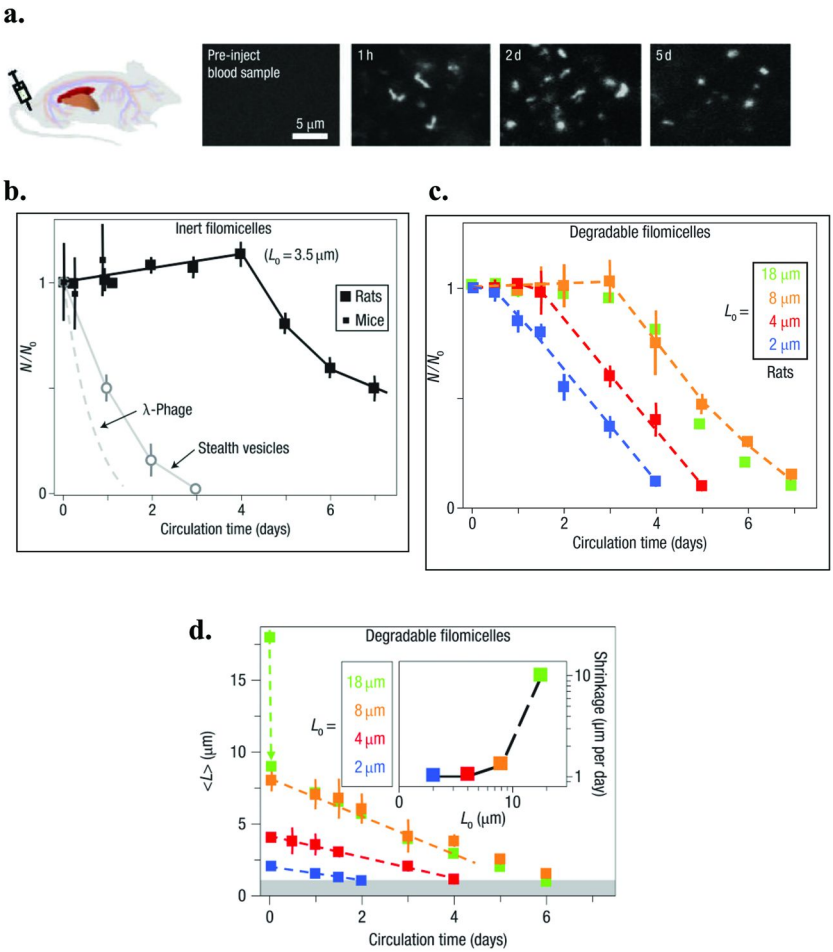

Figure 4. Filomicelles and their persistent circulation. ***a.*** *Injection of fluorescent filomicelles into rodents, followed by fluorescent imaging of blood samples showed that filomicelles circulated in vivo for up to one week.* ***b.*** *Relative numbers of filomicelles in the circulation show that inert filomicelles (of OE7') persist when compared with stealth polymersomes (26) and λ-phage (28).* ***c.*** *Degradable filomicelles (of OCL3) also persist, and filomicelles with longer initial lengths (L_0) circulate longer up to a limiting length. The error bars in b. and* ***c.*** *show the standard deviation for four or more animals.* ***d.*** *Kinetics of filomicelle length reduction in vivo. Degradable filomicelles (OCL3) shorten at a rate that depends on initial length. The inset plots the length-dependent shrinkage rate. (Reproduced with permission from reference (23). Copyright 2007 Nature Publishing Group) (See electronic version for proper color image)*

To further understand the persistence of filomicelles in the circulation, the interaction of worm-like micelles with phagocytic cells was investigated. Phagos means 'eating' and these cells are abundant in the spleen and liver where they have the principal job of ingesting particulates and cells that do not belong in the blood circulation; they constitute the 'active' filters for blood. Worm-like micelles of different lengths were incubated for a day with activated human-derived macrophages. Images obtained by fluorescence microscopy showed no detectable fluorescence in the macrophages for long worm-like micelles (≥ 3 μm) indicating that they were not internalized. On the contrary, when short worm-like micelles were studied a significant increase in fluorescence was observed (Figure 5).

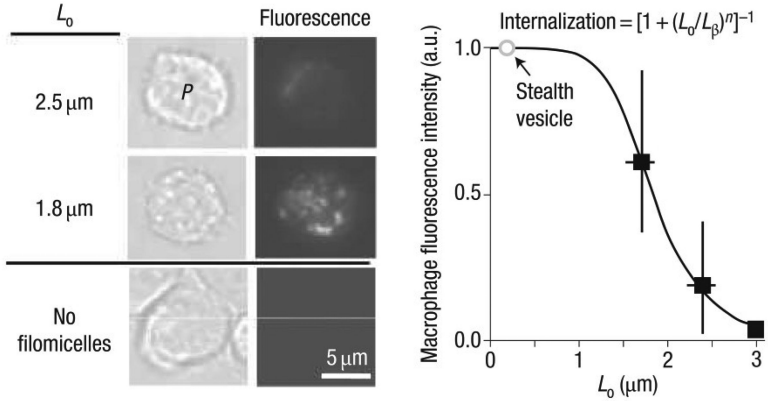

Figure 5. In vitro interactions between filomicelles and phagocytes (P). Fluorescent filomicelles of varying contour length were incubated with activated macrophages for 24 h in static culture. The fluorescence intensity of cells is proportional to the phagocytosis of filomicelles and proves to be a strong function of L_0. The Hill exponent, n = 6, suggests strongly cooperative binding along the length of the cylinder to the cell surface. L_β = 1.9 μm. The error bars in the plot show the standard deviation. (Reproduced with permission from reference (23). Copyright 2007 Nature Publishing Group)

Plotting phagocytosis efficiency versus micelle length fits a cooperative inhibition model with an effective Hill exponent of n = 6, suggesting that multisite attachment occurs between cell and micelle (Figure 5, plot).

A steady flow of cylindrical micelles and spherical vesicles was also studied in the presence of phagocytes to address the effect of the flow on internalization. Small particles were taken up by the phagocytes. In the case of the cylindrical micelles, however, the hydrodynamic shears induced alignment along stream lines, minimizing interactions with the phagocytes (Figure 6).

The in vitro results are in accordance with the in vivo studies in showing a clearance of submicron micelles and shorter worm-like micelles but not long worm-like micelles.

In Degradable Polymers and Materials: Principles and Practice (2nd Edition); Khemani, K., et al.;
ACS Symposium Series; American Chemical Society: Washington, DC, 2012.

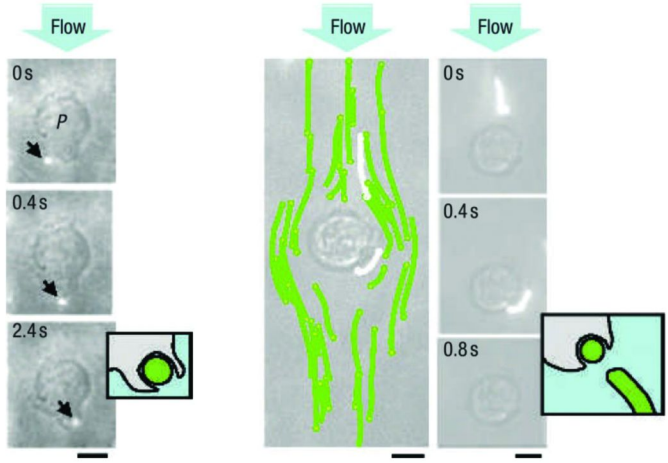

Figure 6. In a flow chamber with immobilized phagocytes, long filomicelles (right) flow past the cells, and occasionally leave a fragment, but smaller micelles and vesicles are captured (left, arrows point to small micelles and vesicles). Flow velocity is ~ 25 μm·s^{-1}, which is similar to that in the spleen. The scale bars represent 5 μm. (Reproduced with permission from reference (23). Copyright 2007 Nature Publishing Group)

Degradation Mechanism and Kinetics of OCL Worm-like Micelles

Giant and flexible worm-like micelles were self-assembled from degradable copolymer OCL (OCL1 M_n ~ 4700, OCL3 M_n ~ 11,000) with weight fraction of PEO, f_{EO} ~ 0.42, that favors worm-like micelle formation (*10*) (Figure 7a-0hr). The contour of the OCL worm is well resolved and considerably exceeds the optical resolution of the fluorescence microscope. Sequential snap-shots exhibiting thermal fluctuations of a single worm-like micelle (Figure 7b) demonstrate its flexibility. Overlays of skeletonized contours show that the distance R between worm ends fluctuates considerably, allowing evaluation of the thermal average $\langle R^2 \rangle = 2l_p^2[L/l_p - 1 + \exp(-L/l_p)]$ in terms of the measured contour length L of the worm and the flexibility as persistence length, l_p (*25*). From analysis of ~ 100 worm-like micelles, we determine an average l_p = 500 ± 200 nm for OCL1, and 5 ± 2 μm for OCL3 respectively. Both the persistence length l and diameter d of OCL worm-like micelles ($d \approx$ 11 nm for OCL1 and 29 nm for OCL3 as measured by TEM) are essentially the same as those of worm-like micelles made from non-degradable PEO-PBD with similar M_n and likewise fit well to the scaling relation $l_p \sim d^{2.8}$ that is indicative of a fluid rather than a glassy aggregate (*35*).

In Degradable Polymers and Materials: Principles and Practice (2nd Edition); Khemani, K., et al.;
ACS Symposium Series; American Chemical Society: Washington, DC, 2012.

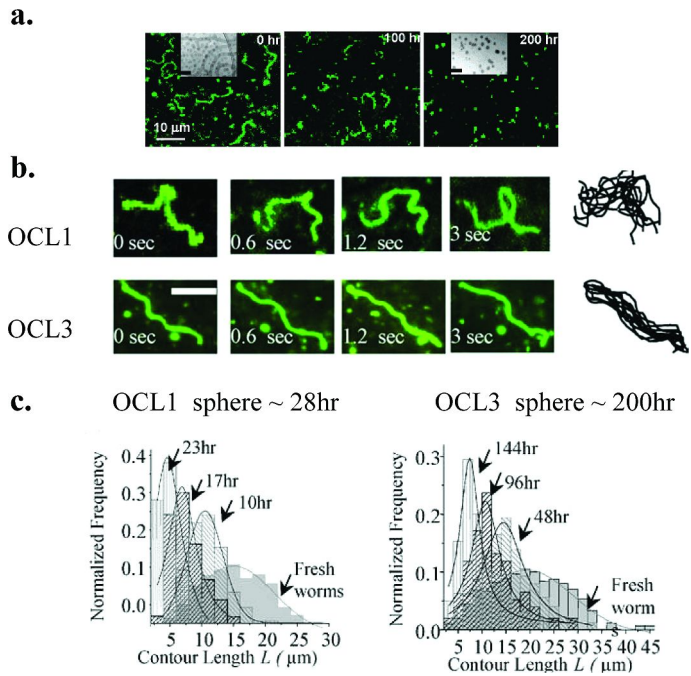

Figure 7. Self-assembled OCL worm-like micelles spontaneously shorten to spherical micelles. ***a.*** *Visualized by FM and cryo-TEM (inset, bar = 100 nm).* ***b.*** *Dynamic snapshots of single OCL worm-like micelle.* ***c.*** *Contour length distributions. (Reproduced from reference (17). Copyright 2005 American Chemical Society)*

Distribution of measurable contour lengths (> 1μm) of OCL worm-like micelles was plotted from ~ 200 worms measured by FM and fit with a Gaussian curve (Figure 7c at 0 hr). A mean contour length <*L*> ~ 15 μm for OCL1 and <L> ~ 18 μm for OCL3 is estimated from their distribution curves respectively.

On time scales of days, these giant OCL worm-like micelles spontaneously shorten to spherical micelles as observed by FM and Cryo-TEM (Figure 7a). The contour length shortening of OCL worm-like micelles can be quantitatively analyzed by tracing contour length distribution curves changing with time (Figure 7c). The mean contour length <*L*> clearly shrinks from the initial long worms towards spheres with time, while the distribution curve narrows as well. It takes ~ 28 hours for OCL1 and ~ 200 hours for OCL3 worm-like micelles to completely transit into spherical micelles at 37 °C in water.

As OCL worm-like micelles shorten to spherical micelles with time, the PCL hydrolysis monomer product, 6-hydroxycaproic acid (6-HPA), was found by GPC as the predominant new species generated (Figure 8).

In Degradable Polymers and Materials: Principles and Practice (2nd Edition); Khemani, K., et al.;
ACS Symposium Series; American Chemical Society: Washington, DC, 2012.

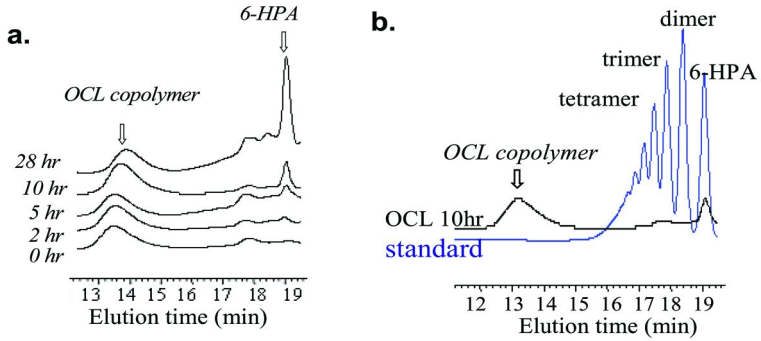

Figure 8. ***a.*** *GPC chromatograms of OCL1 worm-like micelle at different degradation times, at 37 °C.* ***b.*** *Identification of monomer 6-HPA with standards. (Reproduced from reference (17). Copyright 2005 American Chemical Society)*

The 6-HPA peak is well resolved from dimer, trimer, and larger caprolactone oligomers, and no other significant degradation products were detected (Figure 8b). The polydispersity of OCL copolymer remained essentially the same (Figure 8a), and the loss of caprolactone units from OCL copolymer was further confirmed by NMR (Figure 9).

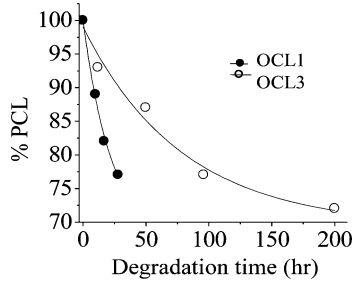

Figure 9. Percentage of caprolactone units remaining in OCL copolymer with degradation by ^{1}H NMR. (Reproduced from reference (17). Copyright 2005 American Chemical Society)

Quantitative accumulation of 6-HPA (Figure 10a), parallels both in form and time-scales of the decays in mean contour length of OCL worm-like micelles for both copolymers (Figure 10b). The analytical results thus demonstrate that PCL in these copolymers hydrolyzes from the end by "chain-end cleavage" rather than by "random-scission" that would yield various degradation products and broaden the polydispersity of the polymer far more than found here (*36*).

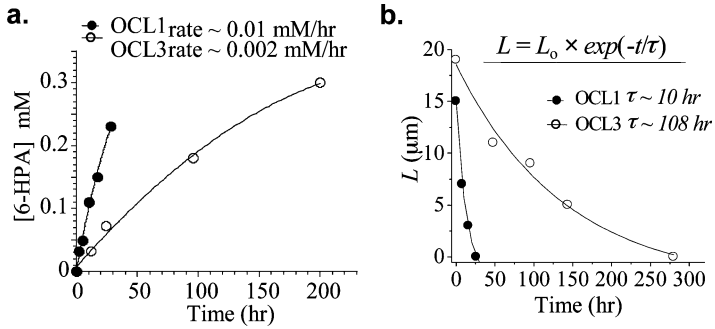

Figure 10. ***a.*** *Cumulative production of PCL hydrolysis monomer, 6-HPA with* ***b.*** *the decay of OCL worm-like micelle mean contour length L (37 °C, pH 5 buffer). (Reproduced from reference (17). Copyright 2005 American Chemical Society)*

End-hydrolysis of PCL increases f_{EO} and consequently shifts the preferred morphology towards a higher curvature structure (*10*). By the time worms have disappeared, PCL chains have on average lost ~ 30% of their length by hydrolysis (Figure 10A), which corresponds to increases in f_{EO} from 0.42 to 0.55. Such f_{EO} above 0.5 favors spherical micelle formation (*10*). This simple estimation highlights the reason why worm-like micelles are so susceptible to morphological transformation: only an extremely narrow range of f_{EO} favors the worm-like micelle structure, whereas spherical micelles are found with a much broader range of f_{EO} and are thus less sensitive to hydrolysis (*10*).

The worm-to-sphere transition occurs with bulb formation at the end of the worm, consistent with release of spherical micelles from the end (Figure 11) (*37*). This mechanism of micellar morphological change is confirmed by molecular simulations (*vide infra*).

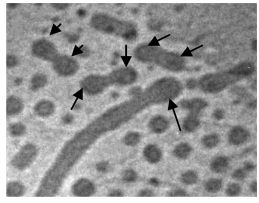

Figure 11. OCL worm-to-sphere transition occurs with bulb formation (arrow) at the end of the worm. (Reproduced from reference (17). Copyright 2005 American Chemical Society)

Conservation of mass allows one to show that the hydrolysis kinetics is the rate-limiting step in worm shortening kinetics. The amount of monomer generated initially from OCL1 and OCL3 worm-like micelles, ~ 0.01 and 0.002 mM/hr, respectively (Figure 10a), gives the volume of spherical micelles generated from the worm-like micelles, based on the above changes in f_{EO} and PCL's volume density. The estimations yield respective shortening rates of ~ 1.0 and 0.1 μm/hr

as observed in FM (Figure 10b). Such estimations apply equally well to the two copolymers that differ in M_n and thus differ in molecular mobility within worms by far more than two-fold (*13*). This suggests that the rate-limiting process is indeed hydrolysis rather than chain diffusion and segregation post-hydrolysis.

While the end-cleavage of PCL within worm-like micelles appears consistent with both the chemical and the nano-scale physical changes, it is also considerably faster than the slow hydrolysis reported for PCL homo/copolymer bulk, particle, or films, i.e. on the time scale of months-years under the same condition (*3–5*). The distinction arises with the specific effect of OCL worm-like micelles on PCL hydrolysis. As speculated from studies on spherical micelles (*38*), the terminal -OH of the hydrophobic PCL block is not strictly sequestered in the 'dry', hydrophobic core but tends to be drawn into the hydrated corona. A 'micellar catalysis' effect involving interfacial water (*39*) plus the likely participation of the terminal –OH (*40*) collectively foster the attack by H_2O of the end-ester group nearest the terminus -OH. Following this ester hydrolysis, a new -OH is generated to restart the process of PCL end-cleavage. To provide direct evidence for the crucial role of the terminal -OH, -OH was modified in OCL1 to an acetate group by esterification. Worm-like micelles still formed with OCL1-acetate, but they showed no significant morphological change after more than 24 hrs at 37 °C, by which time OCL1 worm-like micelles are completely degraded.

For both OCL1 and OCL3 worm-like micelles, shortening rate constants measured from FM increase exponentially with temperature, with minimal degradation at 4 °C but considerable hydrolysis at the physiological temperature of 37 °C. The temperature dependences fit classic Arrhenius behavior and yield activation energies E_a for the morphological transformations (Figure 12).

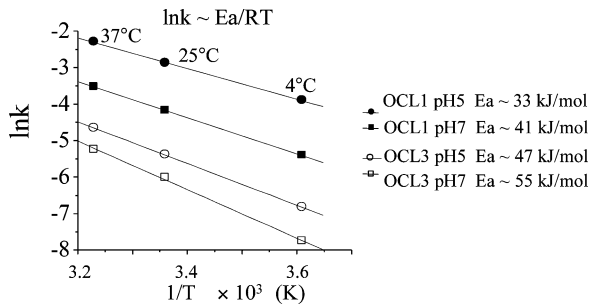

Figure 12. Arrhenius plots of OCL worm-like micelle shortening rate constants, k, with temperature. (Reproduced from reference (17). Copyright 2005 American Chemical Society)

Consistent with acid -catalyzed ester hydrolysis, acidic pH 5 (physiological HEPES buffer) enhances the shortening rate by 2-4 fold systematically and also lowers E_a by 7-8 kJ/mol, compared to neutral pH 7 (PBS buffer). At either pH, the higher M_n OCL3 decreases the shortening rate by 3-4 folds and raises E_a by 10 kJ/mol compared to OCL1. This higher E_a is consistent with a larger entropic penalty for an activated reptation (*13*), i.e. entanglement release, of the terminal hydroxyl group of the longer OCL3 chain to the micellar interface. Moreover,

In Degradable Polymers and Materials: Principles and Practice (2nd Edition); Khemani, K., et al.;
ACS Symposium Series; American Chemical Society: Washington, DC, 2012.

the values for E_a (33-55 kJ/mol) of OCL worm-like micelle shortening are in good agreement with E_a of homogeneous hydrolysis of water-soluble polyester oligomers reported in the literature (*41*). This adds to the proof that PCL hydrolysis is the driving force for worm-like micelle shortening and that such hydrolysis is surprisingly homogeneous rather than heterogeneous and limited – as seen in polyester degradation of bulk and particles – by the infiltration of water.

Molecular Simulation of the Degradation of Worm-like Micelles

Fragmentation of worm-like micelles into spherical micelles during the copolymer degradation process raises fundamental questions concerning the underlying physical mechanisms of this nonequilibrium transition. Mesoscopic simulation techniques, such as Dissipative Particle Dynamics (DPD), are attractive tools to study the molecular weight and copolymer dispersity contributions to the worm micellar stability and interfacial structure (*16*). DPD refers to the use of a momentum conserving Langevin thermostat, in combination with a soft, repulsive force interacting between the component beads and monomers; it has been used to study the properties and applications of a range of soft matter systems, including long chain polymers, surfactants, and biomembranes (*42*).

Utilizing DPD, the interfacial structure and stability effects of molecular weight and hydrophilic fraction, have been examined for worm-like micelles. The DPD models for hydrophilic PEO and hydrophobic poly(ethyl ethylene) (PEE) used here were previously developed using a density mapping approach (*43*). To begin with, holding constant the hydrophilic fraction, f_{eo}, of the chain, the radius of the core, d, is found to scale with the molecular weight of the hydrophobic tail, N, to the 0.59 power. Not only is this close to the experimentally found measurements of $d \sim N^{.61}$ (*16*), but is close to mean field results for the strong segregation limit (SSL), $d \sim N^{2/3}$. While the present DPD model is parameterized for PEO-PEE, where a strongly segregated interface would be expected due to the relatively high degree of immiscibility of the two components—for the case of PEO-PCL, as will be discussed in the section *Molecular Simulations of TAX Loading on OCL Worm-like Micelles*, a weakly segregated interface would be expected due to the comparably weaker degree of immiscibility between PEO and PCL. Increase in the hydrophilic fraction, f_{eo}, leads to an increase in fluctuations in the core and a strong probability of breakup for hydrophilic fractions, $f_{eo} > 0.72$. Stability typically initiates from a bulbous end of the worm, propagates as fluctuations in the core, and pinches off or buds after several μs into individual spherical micelles, as well as entangled spherical micelles, or 'dumbbells,' as shown in Figure 13.

Moreover, degradation of approximately 30% of the PCL has been estimated as a bulk average degradation that is necessary for budding and breakup of worms, thus motivating simulation studies of bidisperse mixtures of spherical- ($f_{eo} = 0.82$) and worm- ($f_{eo} = 0.50$) preferring copolymers. Including greater than 40 mol% spherical micelle preferring polymer induces radial undulations along the axis of the worm that grow with time until a spherical micelle eventually pinches off from the worm's end-cap in the μs timescales as shown in Figure 13. Analysis of the local mean concentration of the spherical and micelle preferring polymers indicate

In Degradable Polymers and Materials: Principles and Practice (2nd Edition); Khemani, K., et al.;
ACS Symposium Series; American Chemical Society: Washington, DC, 2012.

that the local interfacial concentration is in correlation with the mean curvature of the hydrophobic core along the axis of the worm, with the spherical micelle preferring polymer regions of higher mean curvature.

Here, mesoscale simulations accurately capture many processes and transformations across relevant scales, and so molecular dynamics seems to be a useful method for molecular scale investigations of the many PEG-based systems developed for a wide range of applications. In particular, in the section *Molecular Simulations of TAX Loading on OCL Worm-like Micelles* we will discuss the applications of coarse-grained simulations techniques to assess the solubility of hydrophobic drugs in worm-like and spherical micelles of PEO-PCL, in comparison with experimental results.

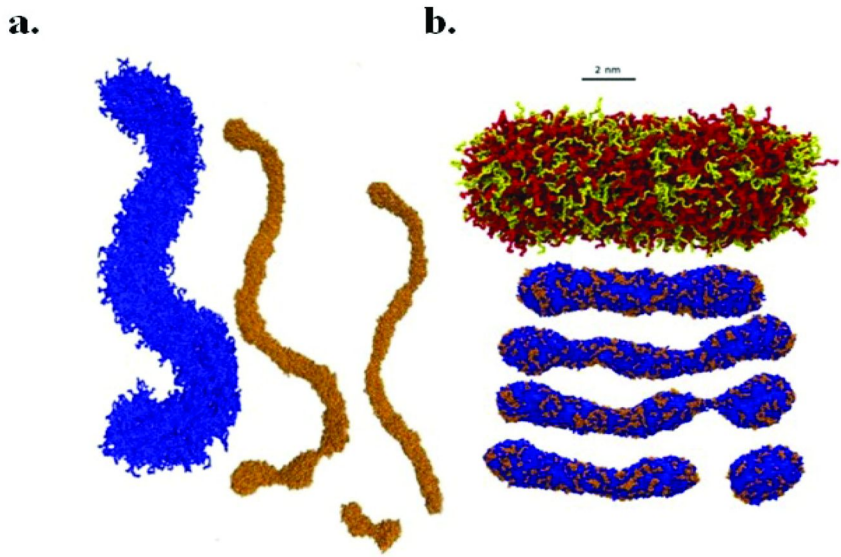

Figure 13. ***a.*** *The hydrophilic corona is represented in blue while the hydrophobic core is shown in gold. Instability propagates at hydrophilic fraction f_{eo} = 0.72 as fluctuations in the core thickness that initiate at the end of the worm, leading to bud formation at 2.4 μs and 'pinching' of a spherical micelle at 2.8 μs. Two interconnected spherical micelles give a 'dumbbell' micelle.* ***b.*** *Simulation results for a binary copolymer micelle, which details the transition dynamics. The random starting configuration of the corona or core with red and yellow or blue and gold respectively indicates polymers with two different length hydrophobic chains. Undulations develop with bud formation and pinch-off of a spherical micelle. (See electronic version for proper color image)*

Evaluation of Degradable OCL Worm-like Micelles for Drug Delivery

In Vitro Compatibility with Cultured Cells and Blood

Bovine aortic endothelial cells and vascular smooth muscle cells exposed to OCL worm-like micelles in PBS with a dose of 5 mg/mL showed no ill-effects for up to 5 days. OCL worm-like micelles and their degradation product, 6-hydroxycaproic acid, are non-toxic and compatible with cultured cells. Incubating OCL worm-like micelles with whole blood for two days at 37 °C shows that they do not stick to red blood cells (RBC) remaining suspended in plasma and they retain their flexibility. Also, a hemolysis study on OCL worm-like micelles (10 mg/mL) shows negligible hemolytic activity (< 1%) (*22*).

The current clinical formulation of anti-cancer drug TAX is in a 50:50 mixture of Cremophore EL and ethanol, which is physically incompatible with intravenous infusion system and causes serious side effects such as hypersensitivity and neurotoxicity (*44*). Here, degradable OCL worm-like micelles prove to be compatible with cultured cells and blood, offering great advantage over the conventionally surfactants as a potential alternative carrier for TAX.

TAX Loading into OCL Worm-like Micelles

Like spherical polymeric micelles (*7–9*), the hydrophobic core of OCL worm-like micelles solubilizes and encapsulates the hydrophobic solute molecules. TAX has very low water solubility of approximately 1 μg/mL (*45*), and is physically loaded into OCL worm-like micelles with a molar ratio of 1:7 for OCL1 and 1:2 for OCL3 respectively, determined by HPLC. The loading molar ratio does not change with OCL worm-like micelle concentrations. Such loading capability of OCL worm-like micelles significantly enhances the solubility of TAX in water, e.g. 10–15 wt% OCL worm-like micelles can dissolve 3-7.5 mg of TAX per mL, comparable to the maximum TAX solubility in Cremophore EL formulation (6 mg/mL) (*44*). Another advantage of using worm-like micelles as carrier for TAX is that each micron-long worm-like micelles provide much larger core volume compared to the same-diametered spherical micelles and thus can load much more drug per carrier. Moreover, loading TAX into the core does not significantly change the flexibility or degradation kinetics of the OCL worm-like micelles (studied by FM).

Molecular Simulations of TAX Loading in OCL Worm-like Micelles

It has been found that worm-like micelles of the same molecular weight of spherical micelles can load approximately twice as much hydrophobic drug (TAX) (*23*). While in the section *Molecular Simulation of the Degradation of Worm-like Micelles* we examined how mesoscopic models can be used to examine non-equilibrium properties of micelles such as the budding and break-up of worm-like micelles into spherical micelles and ‘dumbbells’, in this section we will discuss

In Degradable Polymers and Materials: Principles and Practice (2nd Edition); Khemani, K., et al.;
ACS Symposium Series; American Chemical Society: Washington, DC, 2012.

how rational coarse grain (CG) models can characterize TAX solubility in PEG-PCL micelles by utilizing free energy calculations (*46*). As shown in Figure 14a, based on all-atom computations, the diblock copolymer is modeled with one CG bead per ethylene glycol monomer and three CG beads per caprolactone monomer plus one interfacial CG bead between the two blocks. TAX's CG model maps 3-5 heavy atoms into each CG bead.

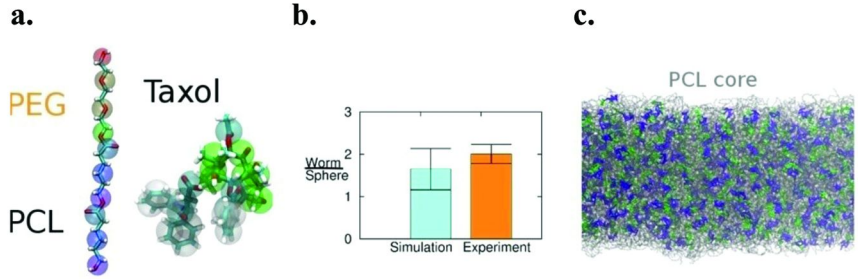

Figure 14. ***a.*** *Based on all-atom computations, the diblock copolymer is modeled with one CG bead per ethylene glycol monomer and three CG beads per caprolactone monomer plus one interfacial CG bead between the two blocks. TAX's CG model maps 3-5 heavy atoms into each CG bead.* ***b.*** *The partition coefficient for TAX transferred into water from each micelle is calculated, and the partition ratio (Worm/ Sphere) agrees with experiments.* ***c.*** *TAX dispersion at realistic drug concentrations within a worm-like micelle. CG TAX at 9 wt% in a PEG 2000 -PCL 5000 Worm-like micelle core, with TAX in purple and green and PCL chains as transparent grey (46). (Reproduced with permission from reference (46). Copyright 2011 John Wiley & Sons, Inc.)(See electronic version for proper color image)*

In order to ascertain if the PEG-PCL CG model possesses the correct hydrophobicity, we simulated seven PEG-PCL copolymers with a range of hydrophilic fractions (f_{EO}) and molecular weights and compared to the recent experimental phase diagram based on over 30 different PEG-PCL polymers (*30*). We performed coarse grain molecular dynamics simulations and found that the stable morphology in solution ranges from polymer vesicle bilayers to worm-like micelles to spherical micelles with transitions achieved primarily by increasing f_{eo}. Moreover, in the bilayer and worm-like micelle phase, we note weak interfacial segregation between the PEO and PCL, in contrast with strong segregation behavior observed in the section above *Molecular Simulation of the Degradation of Worm-like Micelles* of PEO and PEE. Next, we examine the behavior of CG TAX at the octanol water interface. We perform steered molecular dynamics of the drug across a CG octanol-water interface to find the transfer free energy of 1.9 kcal/mol, which is consistent with the experimentally known octanol/water TAX partition coefficient of 2.49-4.4 (*47*).

Following development of the TAX model, we examine the CG model behavior of the drug in OCL micelles. We begin by performing thermodynamic integration by constraining CG TAX at a radial position r from the center of mass

In Degradable Polymers and Materials: Principles and Practice (2nd Edition); Khemani, K., et al.;
ACS Symposium Series; American Chemical Society: Washington, DC, 2012.

of a micelle (spherical and worm-like) to find the change in free energy, ΔG (r), as a function of distance from the center of the core. From this, we can calculate the partition coefficient for TAX transfer across the interface to the minimum in the core, and the partition ratio (Worm/Sphere) agrees with experiments as shown in Figure 14b.

Finally, we examine the behavior of CG TAX in worm-like micelles at both 3 wt% and 9 wt% loading in a PEG 2000 -PCL 5000 worm-like micelle core as shown in Figure 14c. The radial distribution function of the TAX-TAX interactions indicate that the drug remains dispersed in the core after 0.5 μs simulation time. However, examination of the interfacial density profile indicates that the TAX density shifts towards the interface between the PEO-PCL. This behavior is consistent with the burst release phenomena of release of taxanes in polyesters, and more specifically as observed for TAX release by OCL worms (*23*).

In Vitro Release of TAX From OCL Worm-like Micelles

Release kinetics of TAX from OCL worm-like micelles was studied by dialysis method under "sink condition". Figure 15 shows the percentage of TAX released from OCL1 and OCL3 worm-like micelles versus time at 37 °C, under pH 5 (HEPES buffer) and pH 7 (PBS buffer) respectively. After an initial burst release, typical for polymeric micelle systems (*7*), a much slower and sustained release was observed till completion: TAX was released over 10 hours period at pH 5 and 36 hours at pH 7 for OCL1, and for OCL3, TAX was released over 3 days period at pH 5 and 8 days period at pH 7 respectively. The initial burst release is most likely due to the localization of some of the drug at the core-corona interface region, which does not have to diffuse through the large segments of the core to exit the micelle and thus exhibits rapid release (*7*).

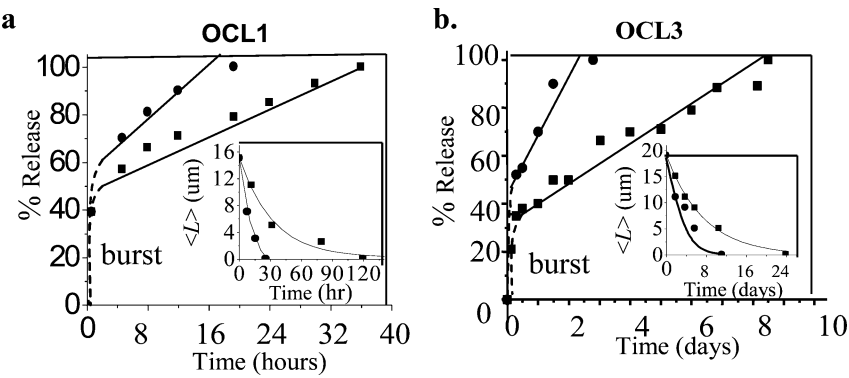

Figure 15. Release profiles of TAX from ***a.*** *OCL1 and* ***b.*** *OCL3 worm-like micelles in pH 5 Hepes (•) and pH 7 PBS buffers (■) at 37 °C. Insets are the corresponding degradation-induced OCL worm-like micelle contour length shortening with time.*

In Degradable Polymers and Materials: Principles and Practice (2nd Edition); Khemani, K., et al.;
ACS Symposium Series; American Chemical Society: Washington, DC, 2012.

For both copolymers OCL1 or OCL3, the gradual release after the initial burst release is 2-4 fold faster in acidic pH 5 than in pH 7 buffer at 37 °C (Figure 15). Similarly, for OCL vesicles, differences in drug release (doxorubicin) depending on the pH have also been reported (*48*). Control experiments of TAX release from OCL1 worm-like micelles at 4 °C, where degradation is negligible, show that the diffusion-controlled release kinetics are similar under two buffers, demonstrating that the faster release in acidic buffer is not due to diffusion but rather degradation (*22*). Further comparison of TAX release rate with the corresponding OCL worm-like micelle shortening/degradation rate at 37 °C (inset) demonstrates that TAX release is indeed dominated by degradation. TAX was released at a rate of ~ 3%/hour at pH 5, ~ 1.5%/hour at pH 7 for OCL1, and ~ 0.5%/hour at pH 5, ~ 0.3%/hour at pH 7 for OCL3 respectively. Whereas the corresponding degradation-induced decay of mean contour length of OCL worm-like micelles are initially linear and the shortening rates, expressed as percentage of length shortened compared to initial length per hour: 3.8%/hour at pH 5, 2%/hour at pH 7 for OCL1, and ~ 0.5%/hour at pH 5, ~ 0.3%/hour at pH 7 for OCL3, are essentially the same as the TAX release rate. This implies a tight coupling between degradation and release. Such degradation-dominant release behavior enables controlled drug release via tuning the degradation rate of OCL worm-like micelles. For example, low pH fosters degradation rate and release of the drug, which is especially interesting for the delivery of anti-cancer drugs to tumor tissues. While most of the drug remains encapsulated inside OCL worm-like micelles with relatively slow release rate during circulation in blood plasma (pH 7), much faster release occurs once the micelles reach the tumor site where pH is lower than that in the normal tissue (*49*). Furthermore, since polymeric micelles are usually internalized into the cells by endocytosis (*50*), the acidic environment of endosome/lysosome leads to accelerated drug release inside the cancer cells and faster therapeutic effect.

Further studies were carried out in the in vitro delivery of TAX by filomicelles to A549 lung carcinoma cells. Different samples containing unloaded worm-like and spherical OCL3 micelles, Cremophor EL, free drug, TAX-loaded worm-like and spherical micelles, and Cremophor EL TAX were added to cultured human lung-derived carcinoma cells A549. Cremophor EL is a solubilizer for hydrophobic drugs widely used in the clinic but it presents side-effects due to its intrinsic toxicity (*51*). The differences in cytotoxicity of the drug carriers without TAX (OCL3 spheres, worms, and Cremophor EL) on A5469 cancer cells can be seen in Figure 16. When compared to TAX-loaded carriers, a similar cytotoxicity can be observed for Chemophor EL. This indicates that the Cremophor EL excipient rather than TAX is clearly responsible for a significant fraction of the cytotoxicity. On the contrary, this effect was not observed in the case of OCL3 worm-like and spherical micelles. Therefore, the anticancer effects of TAX-loaded OCL3 micelles can be fully attributed to the drug instead to the toxicity of the carrier.

Results obtained using TAX-loaded OCL3 micelles showed 13-fold more potent cytotoxicity than free TAX and 5-fold more than Chremophor EL TAX (Figure 16c). Despite the fact that both OCL3 filomicelles and spherical micelles showed the same enhanced cytotoxicity, the use of filomicelles appears more

In Degradable Polymers and Materials: Principles and Practice (2nd Edition); Khemani, K., et al.;
ACS Symposium Series; American Chemical Society: Washington, DC, 2012.

attractive for drug delivery purposes since its loading capacity is considerably higher compared to spherical micelles (*52*).

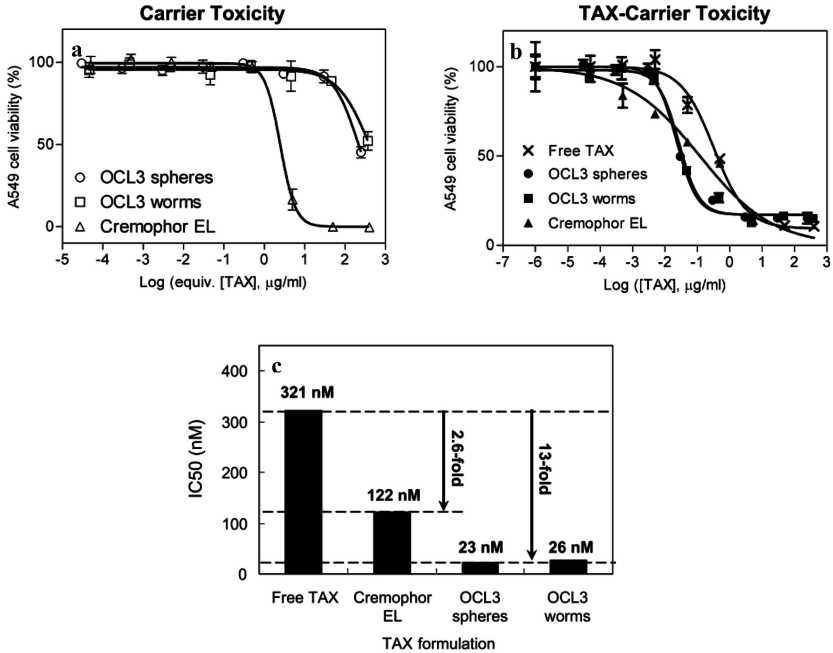

Figure 16. ***a.*** *Cytotoxicity of excipient only (OCL3 spheres, worms, and Cremophor EL) on A549 cell;* ***b.*** *cytotoxicity of different TAX formulations on A549 cells;****c.*** *comparison of IC50 of different TAX formulations. Sigmoid dose-responsive equation : Y = Bottom + (Top – Bottom)/(1 + 10^((LogIC$_{50}$ - X)* HillSlope)), where X is the logarithm of TAX concentration, Y is the response and starts at bottom and goes to top, and HillSlope is the slope for the linear dropping region in the sigmoid curve.*

In Vivo Tumor Shrinkage by TAX Loaded OCL Worm-like Micelles

Preliminary tests of OCL filomicelles as drug delivery systems were conducted by injection of worm-like micelles of PEO_{44}–PCL_{24} (OCL1) and PEO_{110}–PCL_{58} (OCL3) diblock copolymers loaded with the hydrophobic drug TAX to tumor-bearing nude mice. Results showed that an eightfold increase in filomicelle length for a 1 mg·kg^{-1} TAX dosage has about the same relative therapeutic effect as an eightfold increase in the TAX dosage (Figure 17) (*23*). An increase in filomicelle length and in TAX dosage resulted in a two-fold apoptosis and a relative decrease in tumor size. This represents a significant reduction of the TAX dosage compared to TAX-loaded spherical micelles of PEG-(polylactic acid) (*53*). Once again, this result confirms the importance of the morphology of the assemblies not only in transport and circulation but also for applications in drug delivery.

In Degradable Polymers and Materials: Principles and Practice (2nd Edition); Khemani, K., et al.;
ACS Symposium Series; American Chemical Society: Washington, DC, 2012.

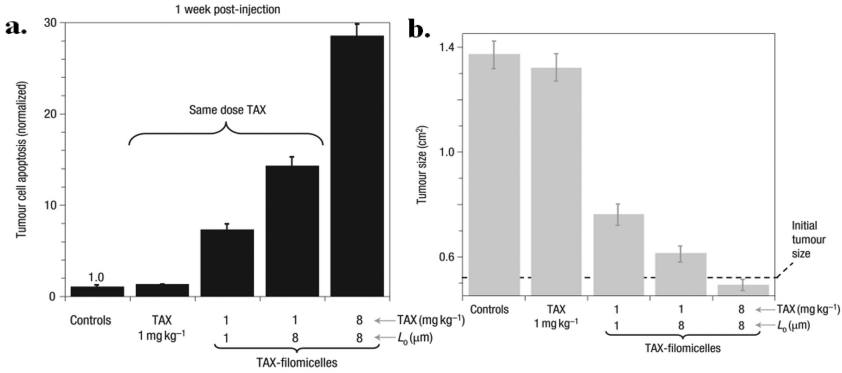

Figure 17. Filomicelles mediate TAX delivery to rapidly growing tumor xenografts on nude mice. Tumor-bearing mice were injected with either saline or OCL3 filomicelles as controls, TAX as free drug in ethanol (1 mg·kg^{-1} is its maximum tolerated dose), or TAX loaded at two doses into the hydrophobic cores of filomicelles of two lengths. ***a.*** *Apoptosis was measured one week later by quantitative imaging of TUNEL-stained tumor sections and shows little effect of free drug but increasing cell death with increasing L_0 and increasing TAX dose.* ***b.*** *Tumor size decreases with increasing apoptosis, with tumor shrinkage clear for the longest filomicelles at the highest TAX dose. All data shows the average from four mice. The error bars show the standard deviation. (Reproduced with permission from reference (23). Copyright 2007 Nature Publishing Group)*

In order to prove the advantageous features of worm-like micelles over spherical micelles, both of these aggregates, obtained from OCL3 diblock copolymer, were loaded with the hydrophobic drug TAX. Mice injected with TAX-loaded OCL3 filomicelles showed a higher maximum tolerated dose (MTD) ($MTD_{Fil} \approx 18$ mg·kg^{-1}) compared to mice injected with TAX-loaded OCL3 spherical micelles ($MTD_{Sph} \approx 10$ mg·kg^{-1}). This result demonstrates that higher dosage is possible when using filomicelles administrated into tumor-bearing mice.

Further studies were performed to clarify the degree of tumor shrinkage by injection of TAX-loaded filomicelles and spherical micelles into mice at TAX concentrations just below the MTD (Figure 18). Although in all cases where TAX was administrated significant tumor shrinkage was observed, there was a clear difference in tumor size between animals treated with free TAX, TAX-loaded spherical micelles or TAX-loaded filomicelles decreasing accordingly. Using worm-like micelles not only the tumor size of treated mice was the smallest but it also maintained its reduced size after 22-day treatment.

Additionally to this, filomicelles showed higher specificity of tumor cytotoxicity (*20*). Measurements of apoptosis within tumor and non-tumor organs showed greater apoptosis in the tumor without greatly increasing apoptosis in the non-tumor organs when using TAX-loaded micelles compared to free drug (Figure 19a). Moreover, the apoptosis in non-tumor organs was 15-30% *lower*

In Degradable Polymers and Materials: Principles and Practice (2nd Edition); Khemani, K., et al.;
ACS Symposium Series; American Chemical Society: Washington, DC, 2012.

with filomicelles than with spherical micelles indicating a shift in the effective activity and biodistribution of drug away from these major non-tumor organs (Figure 19b). The higher tumor accumulation of aggregates with filamentous compared to spherical morphologies has been also reported for other block copolymers (*54*).

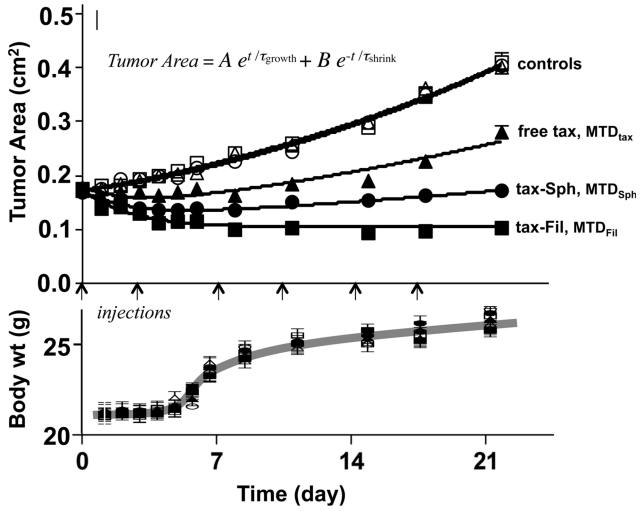

Figure 18. Measurements of A549 tumor shrinkage after TAX administration. Upper panel: Tumor inhibition studies over a 3-week period with multiple injections of different treatments including controls (PBS alone, empty OCL3 spherical micelles or filomicelles), free TAX in PBS, OCL3 spherical micelles loaded with TAX at MTD (~ 8 mg/kg) and OCL3 filomicelles loaded with TAX at MTD (~ 16 mg/kg). The tumor growth profile was determined by tumor area, which was monitored 24 h after each injection by measuring two orthogonal dimensions as [($L_1 \times L_2$)/2]. The tumor growth-inhibition curves were fitted by applying the exponential modeling equation: tumor area = $Ae^{t/\tau growth} + Be^{-t/\tau shrink}$, where t is the time (week), A and τ_{growth} are constants of the tumor growth phase, and B and τ_{shrink} are constants of the TAX-inhibition phase. Lower panel: The body weight changes measured at 24 h after each injection during the 3-week experiment process show the mice gained similar weight for all experimental groups. All data points in this figure show (av ± SD) for 4 mice. (Reprinted with permission from reference (20). Copyright 2009 American Chemical Society)

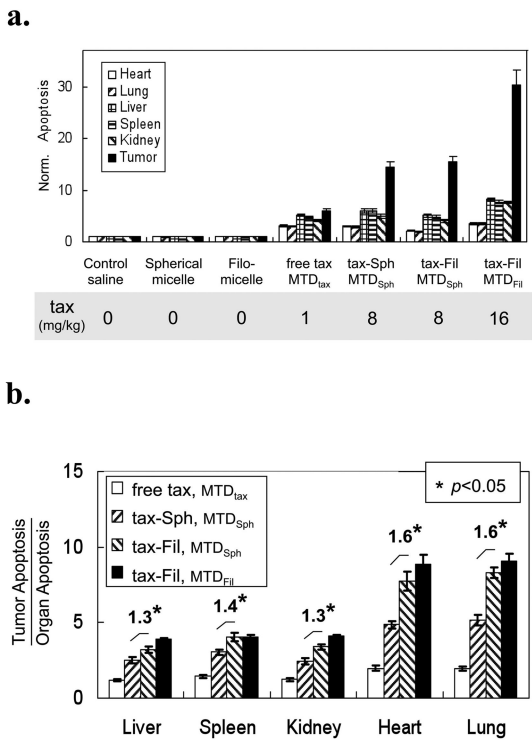

Figure 19. Measurement of cell apoptosis in tumor and non-tumor major organs. Measurements were made after the 22 day multiple injection experiment. ***a.*** *Cell apoptosis index measured by ELISA and calculated as: apoptosis index = enrichment factor of TAX treatment animal groups/enrichment factor of untreated animal groups.* ***b.*** *Cell apoptosis index ratio between tumors and other non-tumor organs ($p < 0.05$). All data points in this figure show (av ± SD) for 4 mice. (Reprinted with permission from reference (20). Copyright 2009 American Chemical Society)*

Compared to spherical micelles, filomicelles clearly increase the tumor-selective cytotoxicity of TAX by about 30-60% at a TAX dose of either 8 or 16 mg/kg.

In order to understand apoptosis in relation to injected drug, the distribution of TAX in vivo was measured. The biodistribution of TAX (as measured after extraction by HPLC) confirmed that TAX delivered by polymeric micelles accumulates in the tumors more than TAX injected as free drug (Figure 20). These results confirm the potential of OCL filomicelles not only as drug carriers but also as specific drug delivery systems.

In Degradable Polymers and Materials: Principles and Practice (2nd Edition); Khemani, K., et al.;
ACS Symposium Series; American Chemical Society: Washington, DC, 2012.

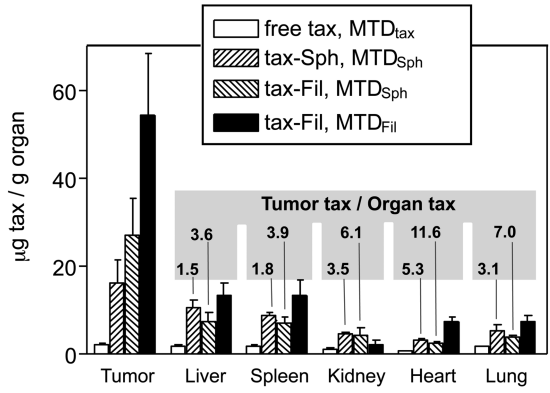

Figure 20. Measurement of TAX biodistribution 24 h after single injection. Biodistribution assay of TAX in different organs after 24 h of the single intravenous injection, using the RP-HPLC method. All data points in this figure show (av ± SD) for 4 mice. (Reprinted with permission from reference (20). Copyright 2009 American Chemical Society)

Conclusion

In summary, worm-like micelles formed via self-assembly of degradable PEO-*b*-PCL block copolymers spontaneously shorten to spherical micelles. Such a morphological transition is triggered by hydrolytic degradation of PCL, governed by an end-cleavage mechanism that is faster than in bulk/film. Degradation rate can be tuned by temperature, pH and M_n and quantitative assessment appears consistent with the molecular explanation whereby the hydroxyl end of the PCL chain localizes to the hydrated interface of the micelle. Degradable PEO-PCL worm-like micelles have been shown to possess longer circulation times in vivo than spherical assemblies, to be compatible with cultured cells and blood, and to be capable of loading a model anti-cancer drug TAX into the hydrophobic core as confirmed by detailed molecular simulations with a novel model of OCL. Subsequent release of TAX is dominated by OCL worm-like micelle degradation and in vivo studies have demonstrated its great potential as a novel controlled-release drug delivery vehicle.

Acknowledgments

Support of NIH-NIBIB, Penn's NSF MRSEC and NSEC is gratefully acknowledged. This chapter was extensively revised and updated based on an earlier version co-authored by Y. Geng and D.E. Discher.

References

1. Scott, G.; Gilead, D. *Degradable polymer*; Chapman & Hill: London, 1995.
2. Gref, R.; Minamitake, Y.; Peracchia, M. T.; Trubetskoy, V.; Torchilin, V.; Langer, R. *Science* **1994**, *263*, 1600–1603.
3. Li, S.; Garreau, H.; Vert, M.; Petrova, T.; Manolova, N.; Rashkov, I. *J. Appl. Polym. Sci.* **1998**, *68*, 989–998.
4. Lee, W.-K.; Gardella, J. A. *Langmuir* **2000**, *16*, 3401–3406.
5. Chen, D.; Chen, H.; Bei, J.; Wang, S. *Polym. Int.* **2000**, *49*, 269–276.
6. Alexandridis, P.; Lindman, B. *Amphiphilic Block Copolymers: Self Assembly and Applications*; Elsevier: New York , 2000.
7. Soo, P. L.; Luo, L.; Maysinger, D.; Eisenberg, A. *Langmuir* **2002**, *18*, 9996–10004.
8. Piskin, E.; Kaitan, X.; Denkbas, E. B.; Kucukyavuz, Z. *J. Biomater. Sci., Polym. Ed.* **1995**, *7*, 359–373.
9. Yokoyama, M.; Fukushima, S.; Uehara, R.; Okamoto, K.; Kataoka, K.; Sakurai, Y.; Okano, T. *J. Controlled Release* **1998**, *50*, 79–92.
10. Jain, S.; Bates, F. S. *Science* **2003**, *300*, 460–464.
11. Discher, B. M.; Won, Y.-Y.; Ege, D. S.; Lee, J. C.-M.; Bates, F. S.; Discher, D. E.; Hammer, D. A. *Science* **1999**, *284*, 1143–1146.
12. Discher, B. M.; Bermudez, H.; Hammer, D. A.; Discher, D. E. *J. Phys. Chem. B* **2002**, *106*, 2848–2854.
13. Lee, J. C.-M.; Santore, M.; Bates, F. S.; Discher, D. E. *Macromolecules* **2002**, *35*, 323–326.
14. Bermudez, H.; Brannan, A. K.; Hammer, D. A.; Bates, F. S.; Discher, D. E. *Macromolecules* **2002**, *35*, 8203–8208.
15. Discher, D. E.; Eisenberg, A. *Science* **2002**, *297*, 967–973.
16. Loverde, S. M.; Ortiz, V.; Kamien, R. D.; Klein, M. L.; Discher, D. E. *Soft Matter* **2010**, *6*, 1419–1425.
17. Geng, Y.; Discher, D. E. *J. Am. Chem. Soc.* **2005**, *127*, 12780–12781.
18. Dalhaimer, P.; Bates, F. S.; Discher, D. E. *Macromolecules* **2003**, *36*, 6873–6877.
19. Kim, Y.; Dalhaimer, P.; Christian, D. A.; Discher, D. E. *Nanotechnology* **2005**, *16*, S484–S491.
20. Christian, D. A.; Cai, S.; Garbuzenko, O. B.; Harada, T.; Zajac, A. L.; Minko, T.; Discher, D. E. *Mol. Pharmaceutics* **2009**, *6*, 1343–1352.
21. Kataoka, K.; Harada, A.; Nagasaki, Y. *Adv. Drug Delivery Rev.* **2001**, *47*, 113–131.
22. Geng, Y.; Discher, D. E. *Polymer* **2006**, *47*, 2519–2525.
23. Geng, Y.; Dalhaimer, P.; Cai, S.; Tsai, R.; Tewari, M.; Minko, T.; Discher, D. E. *Nat. Nanotechnol.* **2007**, *2*, 249–255.
24. Luo, L.; Tam, J.; Maysinger, D.; Eisenberg, A. *Bioconjugate Chem.* **2002**, *13*, 1259–1265.
25. Geng, Y.; Ahmed, F.; Bhasin, N.; Discher, D. E. *J. Phys. Chem. B* **2005**, *109*, 3772–3779.
26. Photos, P. J.; Bacakova, L.; Discher, B.; Bates, F. S.; Discher, D. E. *J. Controlled Release* **2003**, *90*, 323–334.

In Degradable Polymers and Materials: Principles and Practice (2nd Edition); Khemani, K., et al.; ACS Symposium Series; American Chemical Society: Washington, DC, 2012.

27. Oldenborg, P.-A.; Zheleznyak, A.; Fang, Y.-F.; Lagenaur, C. F.; Gresham, H. D.; Lindberg, F. P. *Science* **2000**, *288*, 2051–2054.
28. Merril, C. R.; Biswas, B.; Carlton, R.; Jensen, N. C.; Creed, G. J.; Zullo, S.; Adhya, S. *Proc. Natl. Acad. Sci. U.S.A.* **1996**, *93*, 3188–3192.
29. Ahmed, F.; Pakunlu, R. I.; Brannan, A.; Bates, F.; Minko, T.; Discher, D. E. *J. Controlled Release* **2006**, *116*, 150–158.
30. Rajagopal, K.; Mahmud, A.; Christian, D. A.; Pajerowski, J. D.; Brown, A. E. X.; Loverde, S. M.; Discher, D. E. *Macromolecules* **2010**, *43*, 9736–9746.
31. Du, Z.-X.; Xu, J.-T.; Fan, Z.-Q. *Macromolecules* **2007**, *40*, 7633–7637.
32. Zhang, J.; Wang, L.-Q.; Wang, H.; Tu, K. *Biomacromolecules* **2006**, *7*, 2492–2500.
33. Maeda, H.; Wu, J.; Sawa, T.; Matsumura, Y.; Hori, K. *J. Controlled Release* **2000**, *65*, 271–284.
34. Pierige, F.; Serafini, S.; Rossi, L.; Magnani, M. *Adv. Drug Delivery Rev.* **2008**, *60*, 286–295.
35. Dalhaimer, P.; Bermudez, H.; Discher, D. E. *J. Polym. Sci., Part B: Polym. Phys.* **2004**, *42*, 168–176.
36. Belbella, A.; Vauthier, C.; Fessi, H.; Devissaguet, J.-P.; Puisieux, F. *Int. J. Pharm.* **1996**, *129*, 95–102.
37. Burke, S. E.; Eisenberg, A. *Langmuir* **2001**, *17*, 6705–6714.
38. Nie, T.; Zhao, Y.; Xie, Z.; Wu, C. *Macromolecules* **2003**, *36*, 8825–8829.
39. Fendler, J. H.; Fendler, E. J. *Catalysis in Micellar and Macromolecular Systems*; Academic Press: New York, 1975.
40. de Jong, S. J.; Arias, E. R.; Rijkers, D. T. S.; van Nostrum, C. F.; Kettenes-van den Bosch, J. J.; Hennink, W. E. *Polymer* **2001**, *42*, 2795–2802.
41. Schliecker, G.; Schmidt, C.; Fuchs, S.; Kissel, T. *Biomaterials* **2003**, *24*, 3835–3844.
42. Groot, R. D. *Lect. Notes Phys.* **2004**, *640*, 5–38.
43. Ortiz, V.; Nielsen, S. O.; Discher, D. E.; Klein, M. L.; Lipowsky, R.; Shillcock, J. *J. Phys. Chem. B* **2005**, *109*, 17708–17714.
44. Gelderblom, H.; Verweij, J.; Nooter, K.; Sparreboom, A. *Eur. J. Cancer* **2001**, *37*, 1590–1598.
45. Liggins, R. T.; Hunter, W. L.; Burt, H. M. *J. Pharm. Sci.* **1997**, *86*, 1458–1463.
46. Loverde, S. M.; Klein, M. L.; Discher, D. E. *Adv. Mater.* **2011**, *24*, 3823–3830.
47. Forrest, M. L.; Yáñez, J. A.; Remsberg, C. M.; Ohgami, Y.; Kwon, G. S.; Davies, N. M. *Pharm. Res.* **2008**, *25*, 194–206.
48. Ghoroghchian, P. P.; Li, G.; Levine, D. H.; Davis, K. P.; Bates, F. S.; Hammer, D. A.; Therien, M. J. *Macromolecules* **2006**, *39*, 1673–1675.
49. Shuai, X.; Ai, H.; Nasongkla, N.; Kim, S.; Gao, J. *J. Controlled Release* **2004**, *98*, 415–426.
50. Kakizawa, Y.; Kataoka, K. *Adv. Drug Delivery Rev.* **2002**, *54*, 203–222.
51. Onetto, N; Canett, R.; Winograd, B.; Catane, R.; Dougan, M.; Grechko, J.; Burroughs, J.; Rozencweig, M. *J.Natl. Cancer Inst. Monogr.* **1993**, *15*, 131–139.

52. Cai, S.; Vijayan, K.; Cheng, D.; Lima, E. M.; Discher, D. E. *Pharm. Res.* **2007**, *24*, 2099–2109.
53. Kim, T.-Y.; Kim, D.-W.; Chung, J.-Y.; Shin, S. G.; Kim, S.-C.; Heo, D. S.; Kim, N. K.; Bang, Y.-J. *Clin. Cancer Res.* **2004**, *10*, 3708–3716.
54. Kim, T. H.; Mount, C. W.; Dulken, B. W.; Ramos, J.; Fu, C. J.; Khant, H. A.; Chiu, W.; Gombotz, W. R.; Pun, S. H. *Mol. Pharmaceutics* **2012**, *9*, 135–143.

Chapter 17

Thermo-Responsive Gels: Biodegradable Hydrogels from Enantiomeric Copolymers of Poly(lactide) and Poly(ethylene glycol)

Tomoko Fujiwara*

Department of Chemistry, The University of Memphis, 213 Smith Chemistry Bldg., Memphis, TN 38152
***tfjiwara@memphis.edu**

Hydrogels responding to temperature changes are used for injectable biomaterials with many potential applications. Specifically, biocompatible hydrogels that can be safely injected without surgery and sustained/disintegrated in a controlled manner are of interest. Poly(lactide), PLA, is the most studied and utilized bioresorbable polymer, and its block copolymers provide a great variety of structures and properties. Hydrogels utilizing stereocomplexation of the enantiomeric PLAs offer new polymer design and properties and expand their applications.

Introduction

Stimuli-sensitive hydrogels have the ability to respond to changes in the environment. Temperature is one of typical stimuli and can produce physically crosslinked gels. The physical gels are established by various interactions, such as van der Waals, hydrogen bonding, hydrophobic interaction, and molecular entanglement. Poly(N-isopropylacrylamide) (PNIPAM), which is the most widely known thermo-responsive physical gel, has a low critical solution temperature (LCST) around 32°C and forms a gel above the LCST as a result of dehydration of the hydrophobic isopropyl groups and hydrogen bonding to the carbonyl groups (*1–4*). Triblock copolymers of poly(ethylene oxide) and poly(propylene oxide) (PEO-PPO-PEO), are non-ionic surfactants known as Pluronic® and Poloxamer®, also exhibit sol-gel phase transition in water. The gelation mechanism (*5–9*) involves the formation and packing of micelles to induce sol-to-gel transition near

In Degradable Polymers and Materials: Principles and Practice (2nd Edition); Khemani, K., et al.;
ACS Symposium Series; American Chemical Society: Washington, DC, 2012.

LCST; the PEO corona blocks shrink to lead gel-to-sol transition at the higher temperature. In other mechanisms, helix formation is responsible for the gel formation in a cooled aqueous medium for gelatin and agarose (*10*), while simply the hydration of poly(oxyethylene) grafted onto a substrate forms a gel (*11*).

Polymer gels, applied as biomedical materials, have achieved remarkable advances in medical science and biotechnology (*12*). These applications include; cell culture, tissue engineering, drug delivery system (DDS) and medical sensing. The biocompatibility, biodegradability and safety of the gels are extremely important as well as the physicochemical properties for these applications. Hydrogel biodegradability, in particular, is essential for *in vivo* use; accordingly, they are prepared from degradable polymers with good biocompatibility. Polylactides (PLA) are among the commonly used biodegradable polymer that are of special interest not only as eco-plastic materials (*13*) but as biomedical materials as well (*14*). Since lactic acid, the original monomer for PLA, can be derived from renewable natural resources such as cornstarch, it is regarded as one of the sustainable materials. There is a great need for the polymer systems that can response to temperature changes and biodegrade safely in the body. Thermo-responsive biodegradable hydrogels have been actively studied for drug delivery systems and temporary implants (*15–18*).

Micelles and Hydrogels with Various Block, Graft, and Armed PLA Copolymers

One of the approaches to these hydrogels is to synthesize block copolymers that consist of segmented components; for example, PLA or poly(lactide-co-glycolide) (PLGA) hydrophobic "hard" A-blocks, and poly(ethylene glycol) (PEG) hydrophilic "soft" B-blocks. These copolymers form amphiphilic micelles in aqueous solution, which could transform into a hydrogel due to physical crosslinking influenced by swelling, hydration, and self-assembly of polymers responding to temperature. Typical chemical structures of ABA, BAB, and AB type block copolymers are shown in Figure 1. Since both PLA and PEG are biocompatible and bioresorbable, the PLA-PEG block copolymers have wide biomedical applications, such as temporary devices for clinical and pharmaceutical purposes.

The diblock copolymer, poly(DL-lactide)-block-poly(ethylene glycol) (PDLLA-PEG) was first used as a drug carrier in the early 1980's (*19*, *20*). The ABA triblock copolymer, PLA-PEG-PLA, was also prepared (*21–28*), and the properties were studied (*29*, *30*), such as degradability (*31–35*) and drug release (*36*, *37*). In the ABA gel system, PEG acts an intermolecular plasticizer for processing implant pastes, films, and scaffolds. These materials have been used for biomedical application since 1980's (*27*, *38–42*). Later, Vert et al. have reported the utilization of the hydrogels to protein release (*43*). Microspheres prepared from the ABA block copolymers by O/W or W/O/W emulsion technique (*44–46*) are used to encapsulate hydrophilic or hydrophobic drugs. PLA-PEG nanoparticles with much smaller diameters (10~500 nm) were studied as a drug delivery carrier (*47–50*).

In Degradable Polymers and Materials: Principles and Practice (2nd Edition); Khemani, K., et al.;
ACS Symposium Series; American Chemical Society: Washington, DC, 2012.

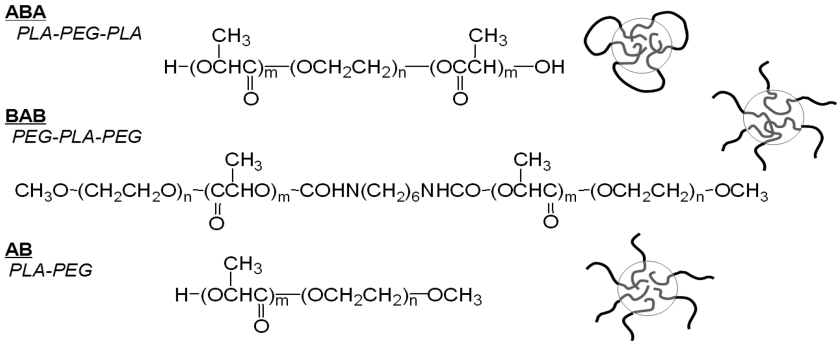

Figure 1. Polymer structures and schematics of the micelles in aqueous medium.

Injectable micro-particles for DDS were prepared from a BAB type triblock copolymer, PEG-PLLA-PEG (*51*, *52*). The aqueous micellar solution containing BAB copolymers exhibited a sol-to-gel phase transition with decreasing temperature from higher temperatures to the body temperature. The transition temperature is variable depending on the block lengths and polymer concentration. The mechanism of this hydrogel formation is considered to be a swelling and hydration of the PEG layers. As a family of this system, other BAB and ABA type thermo-sensitive hydrogels were made by incorporating poly(L-lactide-co-glycolide) (PLGA) as the A-block and PEG as the B-block; copolymer has a complicated phase diagram with both sol-to-gel and gel-to-sol transitions with increasing temperature, similar to PEO-PPO-PEO. From static (SLS) and dynamic light scattering (DLS) studies it appears that an increase in the aggregation number of the micelles causes the gelation (*53*, *54*). The in vitro drug release behavior of the PEG-PLGA-PEG hydrogels was evaluated by using the hydrophilic and hydrophobic model drugs (*55*, *56*). Also by other groups, ABA or BAB block copolymer gels based on PLGA and PEG have been studied (*57–63*). AB diblock copolymers have been used for many years to prepare micelles to encapsulate drugs and DNA (*45*, *64–66*). These AB diblock copolymers form hydrogels by temperature change similar to PEG-PLLA-PEG or other simple BAB triblock copolymers (*67*).

Sol-gel transition behavior and mechanical properties of hydrogels are particularly important for biomedical application. Block length, block sequence (*68*), and the crystallinity (*69*) of PLA-PEG copolymers were systematically studied by mixing ABA type and AB type copolymers or by mixing crystalline PLLA-PEG and amorphous PDLLA-PEG copolymer systems. The effect of the synthesis method on rheological properties is important (*70*) as well as polymer structural effects (*71*).

To improve the hydrogel properties, chemical crosslinking has been utilized for block copolymer systems. Several techniques are used for photo-crosslinking hydrogels of PLA-PEG block copolymer systems. As an example, methacrylate capped triblock copolymer MA-PLLA-PEG-PLLA-MA and its degradation properties were studied, and as reported the degradability of this high modulus gel

In Degradable Polymers and Materials: Principles and Practice (2nd Edition); Khemani, K., et al.;
ACS Symposium Series; American Chemical Society: Washington, DC, 2012.

can be controlled by tailoring the composition (*72*, *73*). Tissue-adhesive hydrogels were prepared using crosslinkable polymeric micelles of aldehyde-terminated PEG-*b*-PLA with a Schiff base polymer (*74*). When the polymeric micelle solution and a polyallylamine solution are mixed hydrogels are formed either in vivo or in vitro almost instantaneously.

Stereocomplexation of Enantiomeric PLAs and the Hydrogel Applications

PLAs consisting of enantiomeric L- and D-lactate units are generally differentiated as PLLA and PDLA, respectively. PLLA is produced by ring-opening polymerization of L-lactide that is made from L-lactic acid manufactured by large-scale fermentation. Enantiomeric PLLA and PDLA are both crystallizable in an orthorhombic or pseudo-orthorhombic unit cell with a 10_3 helical conformation (α-form). It is known that a racemic mixture forms the stereocomplex between the PLLA and PDLA by an alternate packing of β-form 3_1-helices of the opposite absolute configuration (left- and right-handed, respectively) side by side with van der Waals contact (Figure 2) (*75*, *76*). The stereocomplex crystal of a polymer blend of PLLA and PDLA has a melting temperature (T_m) at 230°C which is approximately 50°C higher than that of the single crystal of PLLA or PDLA due to the differences in crystal formation (*77–81*). Moreover, the stereocomplex crystal is insoluble for most of common organic solvents. Therefore, the improved mechanical properties are expected with the stereocomplexed PLA. Based on these backgrounds many attempts have been made to obtain polymer gels from PLA isomers.

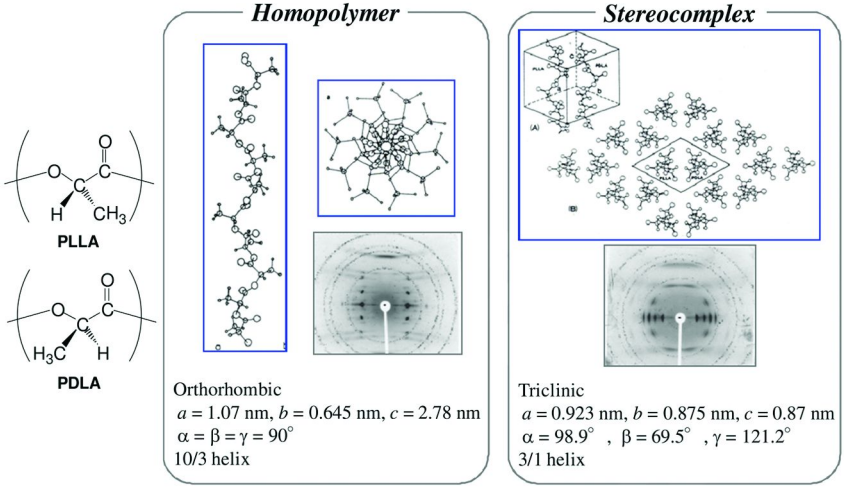

Figure 2. Stereochemistry of PLLA and PDLA, and crystal forms of the homopolymer and stereocomplex. Reproduced with permission from references (75, 76). Copyright 1990 and 1991 American Chemical Society.

In Degradable Polymers and Materials: Principles and Practice (2nd Edition); Khemani, K., et al.;
ACS Symposium Series; American Chemical Society: Washington, DC, 2012.

The use of stereocomplexation of PLLA and PDLA was first applied to form hydrogels in 2000 to form a P(HEMA)-graft-oligo(LA) system (*82*). In 2001 a dextran-graft-oligo(LA) system was prepared (*83–85*). Both systems involve stereocomplexation of the lactide oligomers that acts as crosslinkers between main hydrophilic polymers in the hydrogel. The hydrogels made with grafted oligo(LLA) and oligo(DLA) degraded more slowly than the gels made from the single P(HEMA)-graft-oligo(LA).

Biodegradable hydrogels based on block copolymer systems consisting of PLAs and poly(ethylene glycol) (PEG), as well as thermo-responsive gels that utilize stereocomplexation of enantiomeric PLAs are promising biomaterials. Fujiwara and Kimura reported the temperature-dependent, injectable hydrogels by stereocomplex formation of the enantiomeric micelle mixture of PLA-PEG-PLA triblock copolymers in 2001 (*86*). WAXS and rheological analyses monitored the increase of stereocomplex crystals and gelation process. The mechanism of this system was unique (vide infra) along with studies on BAB and AB block copolymers (*87*). Similar hydrogel formations from enantiomeric PLA-PEG di- and triblock copolymers were studied using Raman spectroscopy in addition to WAXS and rheology measurements to confirm the stereocomplex crystals (*88*).

Another in situ hydrogel system by stereocomplexation was developed from PEG-(PLLA)(8) and PEG-(PDLA)(8) star block copolymers (*89*). Relatively short chain PLA (9-17 lactate units per PLA block) was prepared by ring-opening polymerization of L- or D- lactide onto 8-arms PEG (MW: 22,000 and 44,000) as an initiator. Hydrogels were formed by mixing of solutions of L-star and D-star copolymers. With increasing PLA block length, water solubility and critical gel concentration (CGC) decreased. The protein delivery using these hydrogels was evaluated in vitro and in vivo (*90*). The relatively small protein lysozyme followed first order kinetics, wherein a high cumulative release of approximately 90% was obtained in 10 days. The larger protein IgG was released in vitro with nearly zero order kinetics for 16 days. The release of the therapeutic protein rhIL-2 followed almost zero order kinetics for 7 days, wherein up to 45% was released. To prepare robust hydrogels of stereocomplexed PLA copolymers, co-crosslinking systems by photo reactive groups are used by adding methacrylate groups on to star-block PLA-PEG chain ends (*91*). Stereocomplexation from the enantiomeric PLA still occurred. After UV-polymerization, the hydrogels showed significantly higher storage modulus and prolonged degradation times. Biodegradability of these stereocomplexed-photopolymerized hydrogels varied depends on the design and procedures.

In the late 90's, the authors discovered interesting band morphology formed from the micellar nanoparticles of PLLA-PEG diblock and PLLA-PEG-PLLA triblock copolymers that were placed on a flat substrate surface (*92–94*). The nanoparticles on the mica surface were self-organized into different structures by mild thermal treatment as seen in the atomic force microscopic (AFM) images (Figure 3a). It has been verified that the band morphology is directed by crystallization of the PLLA segments and that the PLLA chains take a doubly twisted structure in it with the ordinary 10/3 helical conformation preserved. Prior to this PLLA band formation, PEG blocks phase-separate and play an important role. The two-dimensional network formed by these copolymers on

In Degradable Polymers and Materials: Principles and Practice (2nd Edition); Khemani, K., et al.;
ACS Symposium Series; American Chemical Society: Washington, DC, 2012.

the surface well simulates the structure of the three-dimensional network systems observed in melt, concentrated solution, and hydrogel. These studies directed us to thermo-responsive hydrogel formation from PLA-PEG block copolymers.

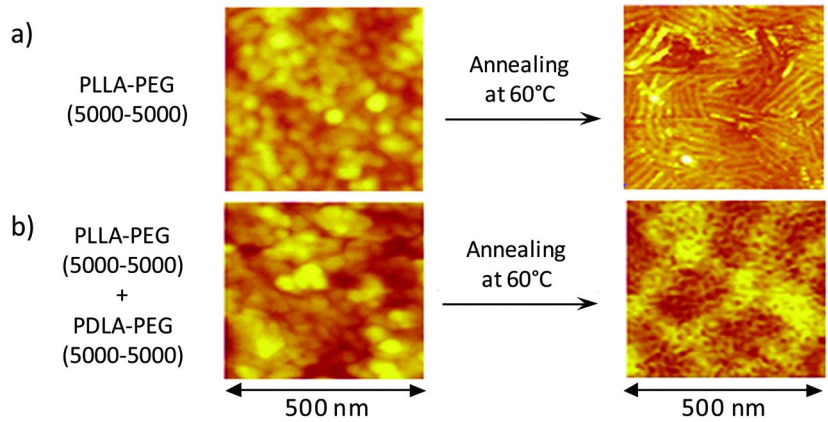

Figure 3. AFM height images of thermal reorganization of micelles from a) PLLA-PEG (5000-5000), and b) the mixture of PLLA-PEG (5000-5000) and PDLA-PEG (5000-5000) micellar solutions. (see color insert)

The bicontinuous network structure, in contrast, was formed from a mixture of PLLA-PEG (MW: 5000-5000) and PDLA-PEG (MW: 5000-5000) micellar solutions as shown in Figure 3b. Aqueous solutions (0.2 wt%) of both enantiomeric micelles were mixed at room temperature, cast on the mica surface, and then heated at 60°C for 1 hour. The gel-type network formation was clearly seen, which was totally different from the structure of a single polymer system of PLLA-PEG micelles (*93*). The enantiomeric micelle mixture was found to reorganize in different ways by thermal treatment, which inspired us to the temperature responsive network formation by PLA stereocomplexation.

Stereocomplaxed PLA Copolymer Gels

Copolymer Synthesis and Micelle Formation

A number of PLA-PEG block copolymers with various molecular weights (MWs) and block ratios have been synthesized. Summarized in Table I are typical copolymers of ABA, BAB, and AB types that induce thermo-sensitive gelation when L- and D-copolymer micelles are mixed. The ordinary ring-opening polymerization of L- or D-lactide, initiated with PEG and MePEG, generated the ABA and AB block copolymers, respectively, in high yields (*86*, *87*). The BAB triblock copolymers were obtained by the coupling the AB diblock copolymers with hexamethylene diisocyanate (HMDI) (Figure 1) (*51*). These copolymers readily formed the core-shell type amphiphilic micelles in water as illustrated in Figure 1. The average hydrodynamic diameters of the micelles measured

In Degradable Polymers and Materials: Principles and Practice (2nd Edition); Khemani, K., et al.;
ACS Symposium Series; American Chemical Society: Washington, DC, 2012.

by DLS for each copolymer with 1wt% concentration were in the range of 20-40 nm which is considered as a stable nanoparticle size in water. To obtain sol-to-gel or gel-to-sol transition, micellar solutions were prepared at various concentrations, and both solutions of L- and D-copolymers were mixed together at low temperature (typically at 4°C). Then the temperature was increased up to 75°C to observe the sol-gel behavior. All solutions were prepared in water.

Table I. Typical block copolymers and the molecular weights

types	*ID*	*Copolymers*	*Block MW (M_n)*	*MW (M_n)*
ABA	$L_{16}E_{104}L_{16}$	PLLA-PEG-PLLA	(1300-4600-1300)	7200
	$D_{16}E_{104}D_{16}$	PDLA-PEG-PDLA	(1100-4600-1100)	6800
BAB	$E_{45}L_{28}E_{45}$	PEG-PLLA-PEG	(2000-2000-2000)	6000
	$E_{45}D_{28}E_{45}$	PEG-PDLA-PEG	(2000-2000-2000)	6000
AB	$L_{28}E_{45}$	PLLA-PEG	(1100-2000)	3100
	$D_{28}E_{45}$	PDLA-PEG	(900-2000)	2900

The MWs of ABA, BAB and AB copolymers listed in Table I showed the best performance as a thermo-sensitive hydrogel. A variety of length and composition of copolymers for each block type were prepared and it was found that the PLA/PEG composition ratio and the thickness of appearance of PEG shell layer (since the PEG of ABA micelle makes a loop) were similar for three types of micelles rather than the MWs of PLA blocks.

Hydrogels from Micellar Solutions of ABA Triblock Copolymers

Spontaneous gel formation occurs when a micellar solution of the enantiomeric ABA triblock copolymers, PLLA-PEG-PLLA and PDLA-PEG-PDLA are mixed at specific conditions. This system is characterized by an interesting temperature-dependent sol-to-gel transition that is induced around 37°C by the stereocomplexation of the PLLA and PDLA block segments (*86*). As seen in Figure 4A, only enantiomeric mixture of micellar solutions formed hydrogels. With the 10 wt% enantiomeric mixture, the sol-to-gel transition was between room temperature (25°C) and the body temperature (37°C) as shown in Figure 4A(d,e). While the single micellar solution of PLLA-PEG-PLLA (control) turned white fluid after heating to 75°C (c) by the crystallization of homocrystals, the stereo-mixture became a white gel at 75°C (f). The sol-gel transition diagram of the mixed micellar solutions of PLLA-PEG-PLLA and PDLA-PEG-PDLA with respect to temperature and polymer concentration is shown in Figure 5. In contrast, the single PLLA-PEG-PLLA micellar solution had the only solution state at all temperatures and concentrations plotted in Figure 5 and all later phase diagrams.

In Degradable Polymers and Materials: Principles and Practice (2nd Edition); Khemani, K., et al.;
ACS Symposium Series; American Chemical Society: Washington, DC, 2012.

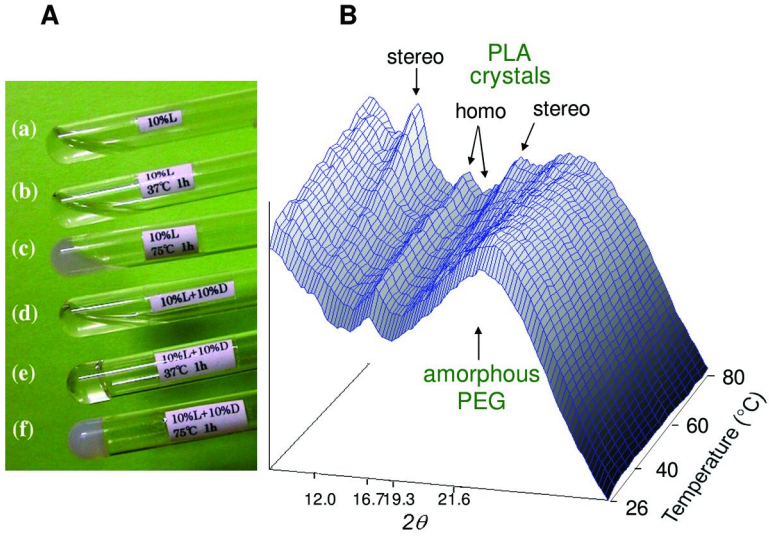

Figure 4. The appearances of 10wt% of ABA micellar solutions (A); PLLA-PEG-PLLA at room temperature(a), 37°C(b), 75°C(c), and PLA-PEG-PLA enantio-mixture at room temperature(d), 37°C (e), 75°C (f). The temperature-dependent WAXS measurement of the mixture at a heating rate 2°C/min (y-axis: intensity) (B). (A:Reproduced with permission from reference (86). Copyright 2001 Wiley-VCH.) (see color insert)

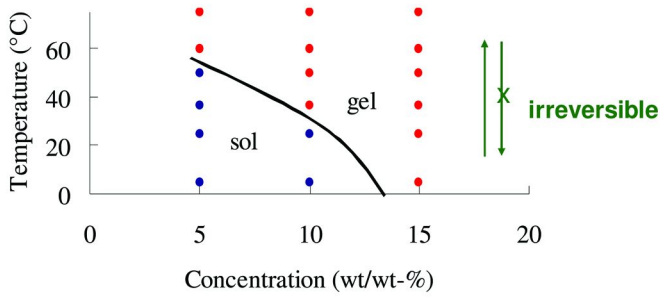

Figure 5. The phase diagram of mixed micellar solutions of PLLA-PEG-PLLA and PDLA-PEG-PDLA.

The responsibility for the stereocomplex formation of the enantiomeric polylactide blocks on the gelation was confirmed by synchrotron WAXS measurement. The temperature-dependent WAXS profiles for the mixed solution are shown in Figure 4B. The measurement was initiated immediately after the 10 wt% micellar solutions of PLLA-PEG-PLLA and PDLA-PEG-PDLA were mixed at room temperature, and the data was collected every half minute by in situ heating at a rate of 2°C/min. Small diffraction peaks are confirmed at 2θ = 16.8° and 19.4° in the starting mixture, which indicates that the small amount of

In Degradable Polymers and Materials: Principles and Practice (2nd Edition); Khemani, K., et al.;
ACS Symposium Series; American Chemical Society: Washington, DC, 2012.

hexagonal homocrystals of PLLA and PDLA exist in the core of the micelles at room temperature. These diffractions are attributed to the (200) or (110) plane and the (203) or (113) plane of the hexagonal crystal lattice comprising the PLLA or PDLA 10/3-helices (*95*). As increasing temperature, the WAXS profile displays two different reflections, at $2\theta = 12.1$ and 21.7°. These new peaks are reasonably ascribed to the crystals of the stereocomplex of PLLA and PDLA (*86*, *87*). Around 37°C, these reflections are still weak, indicating that both the PLLA and PDLA chains may be mixed into a complexation state prior to the crystallization. At 75°C, the significant crystal growth of the stereocomplex is clearly seen.

In the single PLLA-PEG-PLLA micellar solution (control experiment), the hexagonal crystal growth was also observed with increasing temperature despite its continuous sol nature. The total degree of crystallinity estimated from the WAXS was almost identical with that observed in the mixed solution at each temperature. Since the single and mixed solutions have same degree of crystallinity but have different major crystal forms which are hexagonal and stereocomplex, respectively, it is suggested that the gel formation in the mixed solution is closely related with the stereocomplexation of the enantiomeric PLA blocks.

In the micellar solutions of the enantiomeric ABA triblock copolymer, the hydrophobic PLLA or PDLA segments aggregate to form a core region, around which, the hydrophilic PEG segments settle to form a shell when the micelles are prepared separately. Consequently, the PLLA and PDLA segments can be isolated from each other when the micellar solutions of the enantiomeric block copolymers are mixed. Illustrate in Figure 6, is a schematic of an ABA system gelation. When heated, the aggregation of the PLLA and PDLA segments in the core/shell interface is weakened to allow the segments to mix outside of the original core. The shorter block length of PLLA and PDLA is favorable for this chain scrambling and mixing. As a result, the stereocomplexation starts as indicated by the WAXS data (Figure 4B), and the micelles are wholly crosslinked with each other at 37°C to form a gel. With increasing temperature, the crosslinking state is changed by reorganization of the hydrophobic cores and increased crystallization of the stereocomplex.

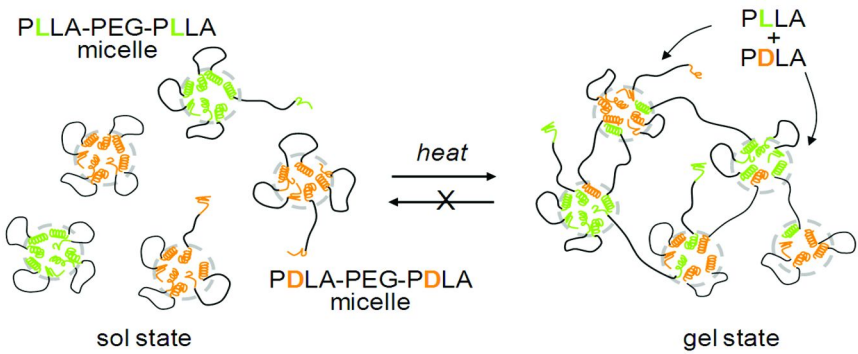

Figure 6. Proposed gelation mechanism of enantiomeric mixture of ABA triblock copolymers. (see color insert)

In Degradable Polymers and Materials: Principles and Practice (2nd Edition); Khemani, K., et al.;
ACS Symposium Series; American Chemical Society: Washington, DC, 2012.

This process was also supported by fluctuations in the storage modulus (G') curve in the rheology measurement (*87*). The temperature-dependent rheological changes with the gelation of the mixed dispersion of ABA-type block copolymers were monitored. A dramatic increase in storage modulus (G') was observed from 20 to 37°C. The crossing of the G' and loss modulus (G'') curves is detectable around 23°C. This change corresponds to the crosslinking reaction that leads to gel formation. Above 37°C, G' fluctuates around 10^3 Pa, which is an ordinary G' level for physically crosslinked gels. It starts to elevate again above 70°C, corresponding to the turbidity of the gel. Since this turbid gel regains its transparency to some degree when cooled, this turbidity change is mainly attributed to the clouding phenomenon resulting from the desolubilization of nonionic surfactants (such as PEG). This data supports the gel formation of the mixed dispersion at around 37°C. Because the stereocomplex formation depresses the mobility of the PLA chains and stabilizes the PEG crosslinkers, gel formation is only possible for the enantiomeric mixture. This sol-gel transition is irreversible though the crosslinking is performed by an ordinary physical mechanism.

Hydrogels from Hybrid Micelles of 'Pre-Mixed' ABA Triblock Copolymers

The PLA-PEG-PLA stereocomplex hydrogel described above, showed a relatively low storage modulus (ca. 1000 Pa), and thus was insufficient for many applications as an injectable implant material. There have been a few reports using similar materials for this hydrogel system. Vert et al. obtained hydrogels from increased MWs of PLA-PEG-PLA triblock copolymers but did not observe thermo-sensitive sol-to-gel transition (*88*). Furthermore, graft polymers (*96*) and star-block copolymers of enantiomeric PLAs, were synthesized (*97*, *98*), and used with other chemical crosslinking for the gelation process to obtain more robust gels (*89*, *91*). Despite many studies, there was no report for mechanically strong and controllable thermo-responsive hydrogels driven solely by stereocomplexation of PLAs. Hydrogels from stereo-mixture of enantiomeric PLA-b-PEG are promising safe biomaterials without the use of other materials or chemical crosslinking, therefore, an improvement of physical properties and deployable gelation behaviors is crucial.

Micelle formation mechanisms and the properties of hybrid micelles comprising more than two different block copolymers have been reported. As an example discussed by Munk, thermodynamic stability of hybrid micelles depends on many factors, such as core block sizes, total MW, medium, hydrophilic-lipophilic balance (HLB), and an interaction parameter of two blocks (*99*). Chaibundit studied a mixture of two different corona block sizes of Pluronic (PEG-PPG-PEG) to form co-micelles and then hydrogels (*100*). In achievement of novel properties and functions, designing hybrid micelles from multiple components is an attractive approach.

The hybrid micelles formed from two different sizes of 'pre-mixed' PLA-PEG-PLA triblock copolymers have been developed by the author, with the aim to obtain a tunable sol-to-gel transition at a wide range of temperatures and superior mechanical properties of injectable hydrogels for practical use (*101*). The structures and properties of the aqueous micelles consisting of longer and

In Degradable Polymers and Materials: Principles and Practice (2nd Edition); Khemani, K., et al.;
ACS Symposium Series; American Chemical Society: Washington, DC, 2012.

shorter PEG blocks in the corona with a constant size of PLA in the core have been studied.

On the basis of MW of previously reported triblock copolymers, PLA-PEG-PLA (e.g., 1100-4600-1100) (*86*), several groups examined a series of larger sized copolymers (*88*). We have also prepared larger triblock copolymers using PEG (MW: 10000) as an initiator, e.g., PLLA-PEG-PLLA and PDLA-PEG-PDLA (1300-10000-1300, 2500-10000-2500, etc). Similarly to other attempts, a "temperature-responsive hydrogel" by self-organized PLA stereocomplexation mechanism was not observed, although gels were formed more easily by using a mixture of enantiomeric copolymer micelles rather than from single homopolymer micelles at same concentration. As a next attempt, relatively low MW copolymers with both short PLA and PEG blocks were designed (*101*). The triblock copolymers were obtained by the ring-opening polymerization (ROP) of L- or D-lactide from PEG (MW: 2000 and 3350) macroinitiator at 120°C in the presence of $Sn(Oct)_2$. Table II summarizes the block copolymers used for this study; the number average (M_n) and weight average (M_w) molecular weights, and polydispersity index (PDI) were calculated from GPC (polystyrene conversion) and ^1H NMR. Narrow polydispersity was obtained for all block copolymers.

Table II. Molecular weights and polydispersity of PLA-PEG-PLA block copolymers

ID	*Block Copolymer*	*Theoretical (block MW)*	*M_n (NMR)*	*M_n (GPC)*	*PDI (GPC)*
$L_7E_{45}L_7$	PLLA-PEG-PLLA	(500-2000-500)	2870	2500	1.07
$D_7E_{45}D_7$	PDLA-PEG-PDLA	(500-2000-500)	2850	2470	1.08
$L_{11}E_{45}L_{11}$	PLLA-PEG-PLLA	(800-2000-800)	3610	3700	1.11
$D_{11}E_{45}D_{11}$	PDLA-PEG-PDLA	(800-2000-800)	3620	4020	1.15
$L_{11}E_{76}L_{11}$	PLLA-PEG-PLLA	(800-3350-800)	4960	5810	1.14
$D_{11}E_{76}D_{11}$	PDLA-PEG-PDLA	(800-3350-800)	4950	5880	1.11

Flower-type micelles with a spherical morphology are generally produced from PLA-PEG-PLA block copolymers. The hydrophobic PLA segments associate in the micelle core surrounded by the hydrophilic PEG segments in an aqueous medium. The three types of micelle structures specifically focused on for this hydrogel study are illustrated in Figure 7. Among copolymers with constant length of PLA blocks (800), the shorter PEG copolymer ($L_{11}E_{45}L_{11}$ or $D_{11}E_{45}D_{11}$) and the longer PEG copolymer ($L_{11}E_{76}L_{11}$ or $D_{11}E_{76}D_{11}$) form different micelles which are abbreviated as (M_{short}) and (M_{long}), respectively. The third micelle (M_{mix}) in Figure 7 was prepared by the pre-mixture of shorter and longer PEG copolymers (i.e., $L_{11}E_{45}L_{11}$+ $L_{11}E_{76}L_{11}$ or $D_{11}E_{45}D_{11}$+ $D_{11}E_{76}D_{11}$). As Figure 7 depicts, the 'pre-mixed copolymer micelle' (M_{mix}) is considered

In Degradable Polymers and Materials: Principles and Practice (2nd Edition); Khemani, K., et al.;
ACS Symposium Series; American Chemical Society: Washington, DC, 2012.

to be coassociated by both sizes of copolymers. Co-micellization of two block copolymers has been studied by several researchers (*99*, *100*, *102*). Munk discussed thermodynamic stability of hybrid micelles with di and triblock copolymers, which are dependent on various factors such as core block sizes, total MW, medium, HLB, interaction parameter of two block, and so on (*99*). Some combinations prevented hybridization, particularly at low core stability, whereas some formed uniform hybrid micelles. In such a situation, the solvent phase that is saturated by both unimers, may become supersaturated with respect to the hybrid micelles and their nucleation may possibly occur. Chang et al. used different corona blocks of copolymers with similar MW and block ratio on a silicon wafer. It is a clever experiment using AFM and pH change to demonstrate that hybrid micelles are formed by a pre-mixed copolymer method and post-mixed micelles consist of the mixture of two different micelles (*102*). For our (**M_{short}**) and (**M_{long}**) micelles, micelle size and stability are shown to be primarily influenced by the PEG block length. The hydrodynamic diameters of (**M_{short}-L)** and (**M_{long}-L)** by DLS gave 63 nm and 42 nm, respectively. The (**M_{short}-L)** micelle from PLLA-PEG-PLLA with the shorter PEG (800-2000-800) displayed a larger hydrodynamic size than the (**M_{long}-L)** micelle from the copolymer with the longer PEG (800-3350-800). The increase in PEG block length leads to a smaller micelle, which means that a fewer numbers of polymers associate in the micelle core due to the large corona volume. The hydrodynamic diameters of (M_{mix}) micelles with a varied copolymer ratio were measured by DLS. The sizes of 'pre-mixed copolymer micelles' were in the range of 50-80nm with some indication of aggregation (*101*).

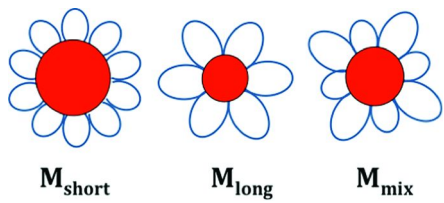

Figure 7. Proposed micelle structures influenced by PEG block length.

Hydrogels were prepared by mixing equal volumes of the enantiomeric micelle solutions at various polymer concentrations. The first set, the mixture of enantiomeric micelles composed of short PEG and PLA blocks, $\mathbf{L}_7E_{45}\mathbf{L}_7$ (MW: 500-2000-500) and $D_7E_{45}D_7$ (MW: 500-2000-500) in Table II, did not form a hydrogel at any given temperature or concentration. It is known that the PLA block length must be greater than 7 repeating monomer units for successful formation of stereocomplexation between PLLA and PDLA. The block copolymers with shorter PLA block have slightly below seven repeating lactate units; therefore, no gelation was observed. For the enantiomeric mixture of the micelle solutions from constant PLA size (MW: 800) polymers with different PEG sizes, (M_{short}-L + M_{short}-D) and (M_{long}-L + M_{long}-D), sol-to-gel transformation was induced (*101*). As the sol-gel transition temperature is reached, the micellar solution changes

In Degradable Polymers and Materials: Principles and Practice (2nd Edition); Khemani, K., et al.;
ACS Symposium Series; American Chemical Society: Washington, DC, 2012.

from a solution to a gel state. This phenomenon is easily witnessed by tilling the vial. Stereocomplexed PLA-PEG-PLA thermo-responsive hydrogels are considered to form by physical crosslinking induced by chain exchange between micelles, which is governed by temperature increase as illustrated in Figure 6 (*86*).

The stereo-mixture of the 'pre-mixed copolymer micelles' (M_{mix}-L and M_{mix}-D) exhibited distinguished sol-to-gel phase transition behaviors. The sol-to-gel phase diagram in Figure 8 shows a linear response in sol-gel transition temperature as a factor of short-PEG and long-PEG block copolymer ratio. The concentration of the micelles was kept at 10% for this series. Most interestingly, a sol-gel transition around body temperature can be achieved by simply adjusting the copolymer ratio. These mixed copolymer micelles have physiological relevant thermo-responsive properties and can be used as injectable thermo-sensitive hydrogels. Again, the mixed copolymer micelle solutions from single enantiomer, M_{mix}-L did not exhibit any hydrogel formation under the same given conditions.

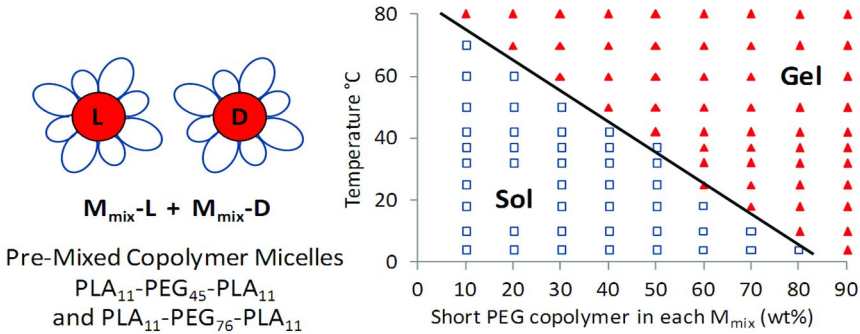

Figure 8. Sol-gel transition temperature of equimolar enantiomeric blends of the pre-mixed copolymer micelles (M_{mix}-L + M_{mix}-D). The x-axis shows the weight fraction of the short PEG copolymer (MW:800-2000-800) in the pre-mixed copolymer micelle (MW:800-2000-800 + 800-3350-800). The micelle solutions are maintained at 10% concentration. Plots represent solution state (open squares) and gel state (filled triangles). (Reproduced with permission from reference (101). Copyright 2012 American Chemical Society.)

As a contrast experiment, the enantiomeric mixture from the post-mixed micelles ((M_{short}+M_{long})-L and (M_{short}+M_{long})-D) was investigated using the same method. This stereo-mixture containing different types of micelles did not have any unique response at any given ratios, and behaved similarly to the single sized micelle of the major copolymer. The resulting hydrogels were apparently weaker than 'pre-mixed copolymer micelle' gels by tilt observation. Therefore the exceptional properties of the 'pre-mixed copolymer micelles' can be attributed to the unique micellar structures formed and not on the sole presence of both block copolymers.

The crystallization of PLLA and PDLA has been studied using wide-angle X-ray diffraction patterns. The hybrid "pre-mixed copolymer micelles" showed

In Degradable Polymers and Materials: Principles and Practice (2nd Edition); Khemani, K., et al.;
ACS Symposium Series; American Chemical Society: Washington, DC, 2012.

similar crystallization profiles as previously shown ABA-copolymer hydrogel system. It is proposed that the new micellar systems composed of mixed sized copolymers form hydrogels through the same stereocomplexation mechanism as described above. The stereocomplex peaks were shown to increase and the PLLA or PDLA homo-crystal peaks were shown to decrease as temperature rises (*101*). The chain exchange between the (M_{mix}-L) and (M_{mix}-D) micelle, followed by stereocomplexation, is a driving factor for cross-linking and hydrogel formation in the mixed copolymer systems.

Mechanical properties of these hydrogels were characterized by rheology. Figure 9 shows the storage modulus (G') and the loss modulus (G'') of the stereocomplexed hydrogels as a function of frequency (Hz) at 37°C. The racemic micelle mixture of the short PEG copolymers (M_{short}-L + M_{short}-D) has the lowest mechanical modulus (square). Both G' and G'' are less frequency dependant, which means this hydrogel is stable even though it is the weakest. It is reasonable that the short PEG micelles turn to gel immediately after mixing of L and D at any condition higher than 8% concentration. The micellar blend of the longer PEG copolymers (M_{long}-L + M_{long}-D) holds modest mechanical strength (triangle). Initial higher values of G'' explain the fluid-like characteristic of this hydrogel, however, upon further stereocomplexation, both moduli become stable. The racemic mixture of 'pre-mixed copolymer micelles' (M_{mix}-L + M_{mix}-D) exhibited the highest mechanical strength as the storage modulus immediately reached approximately 6000Pa (diamond). The higher value of G' indicates that this 'pre-mixed copolymer micelle' hydrogel possesses a more solid-like, rigid micro-structure. The loss modulus (G'') showed an unstable profile at relatively lower frequencies, which was reproducible for this particular hydrogel. This result indicates that chain exchange and structural reorganization occur in a different way from a single size copolymer hydrogel. The mechanical strength of this gel is a great improvement from the originally reported stereocomplexed PLA-PEG-PLA thermo-responsive hydrogel (ca. 1000Pa) (*86*).

The stress sweep of this 'pre-mixed copolymer micelle' gel (M_{mix}-L + M_{mix}-D) was examined at various temperatures to establish the linear viscoelastic region which is a characteristic of a gel material. The racemic mixture (50:50 wt%) of 'mixed copolymer micelle' solutions at concentration 20% turns to gel at a lower temperature than the 10% solution shown in the phase diagram in Figure 8. As seen in Figure 10, there was no stress-hardening or weakening observed for this hydrogel. It is observable that the complete destruction of the gel structure (cross-over of G' and G'' plots) occurred at oscillatory stress values of about 100 Pa at 37°C, and higher than 100 Pa at room temperature. The rheology results in this study support that the unique hybrid structure from 'pre-mixed copolymer micelles' offers additional factors on the gelation mechanism and the network structure towards a controlled thermo-responsive and robust hydrogel system.

In Degradable Polymers and Materials: Principles and Practice (2nd Edition); Khemani, K., et al.;
ACS Symposium Series; American Chemical Society: Washington, DC, 2012.

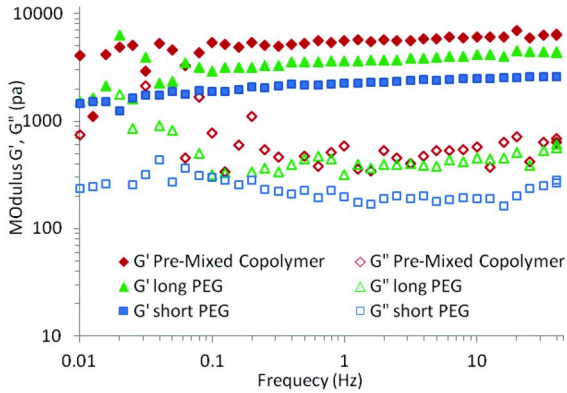

Figure 9. The plots of storage modulus (G') and loss modulus (G") as a function of frequency at 37°C for 1:1 stereo-mixture of micelle solutions: (closed diamond) G' of (M_{mix}-L + M_{mix}-D); (open diamond) G" of (M_{mix}-L + M_{mix}-D); (closed triangle) G' of (Mlong-L + Mlong-D); (open triangle) G" of (Mlong-L + Mlong-D); (closed square) G' of (Mshort-L + Mshort-D); (open square) G" of (Mshort-L + Mshort-D). Concentration of micelles; M_{mix}: 20%, Mlong: 20%, and Mshort: 15%. (Reproduced with permission from reference (101). Copyright 2012 American Chemical Society.)

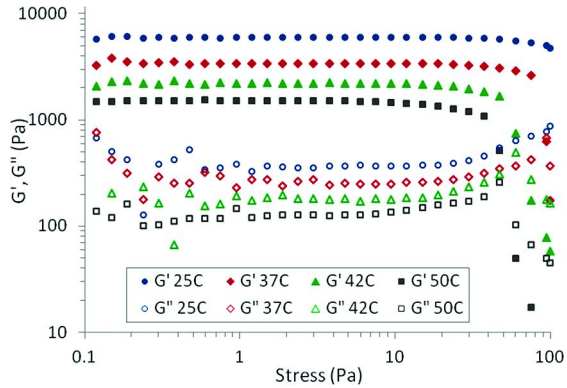

Figure 10. Stress sweep modulus profiles of the 'pre-mixed copolymer micelle' hydrogel (M_{mix}-L + M_{mix}-D, 50:50 wt%) with 20% concentration measured at 25°C, 37°C, 42°C, and 50°C. (Reproduced with permission from reference (101). Copyright 2012 American Chemical Society.)

Hydrogels from BAB Triblock and AB Diblock Copolymers

Another gel system consists of the enantiomeric BAB type triblock copolymers, PEG-PLLA-PEG and PEG-PDLA-PEG. The sol-gel transition of this system should be induced by the stereo interaction of L- and D-copolymers, which is different from the gel of the single BAB (PEG-PLLA-PEG) system that has previously been described to occur gelation by the hydrophobic/hydrophilic interaction (*51*).

The aqueous micellar solution of the single enantiomer, PEG-PLLA-PEG (2000-2000-2000) or PEG-PDLA-PEG (2000-2000-2000) remains a "sol" phase at all temperatures in the concentration range of 10-40 wt%. Shown in Figure 11 is a sol-gel transition diagram plotted for 1:1 (v/v) mixed micellar solutions of PEG-PLLA-PEG and PEG-PDLA-PEG with respect to temperature and polymer concentration. It is found that the gel state cannot be formed at concentrations lower than 30 wt% and that the gel state is preferentially kept below 75°C at concentrations higher than 40 wt%. The gel-to-sol transition temperature increases up to 75°C at higher concentrations. It should be noted here that in the present BAB system the gel and sol are formed, respectively, at low and high temperatures in a reversible manner. This is opposite to the above ABA system where gelation is induced with increasing temperature in an irreversible manner.

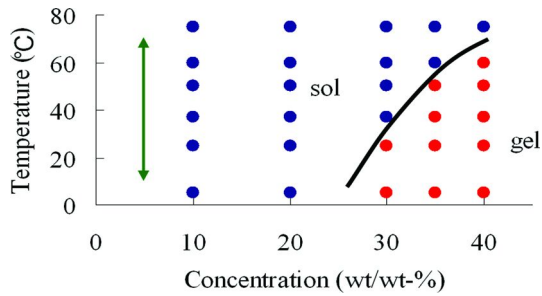

Figure 11. The phase diagram of mixed micellar solutions of PEG-PLLA-PEG and PEG-PDLA-PEG.

Shown in Figure 12A are the typical changes in the mixed solution at 35 wt% concentration before and after the heat treatment from 37°C (c) to 75°C (d). This gel is formed immediately after the L- and D- solutions are mixed at room temperature. It is observed that the mixed solution is in gel and sol states at 37 and 75°C, respectively, while the single solution remained fluid irrespective of the temperature (a,b). Since gel-to-sol transformation of the mixed solutions is reversible with the temperature change, sample (d) returns to gel after cooling to room temperature.

In Degradable Polymers and Materials: Principles and Practice (2nd Edition); Khemani, K., et al.;
ACS Symposium Series; American Chemical Society: Washington, DC, 2012.

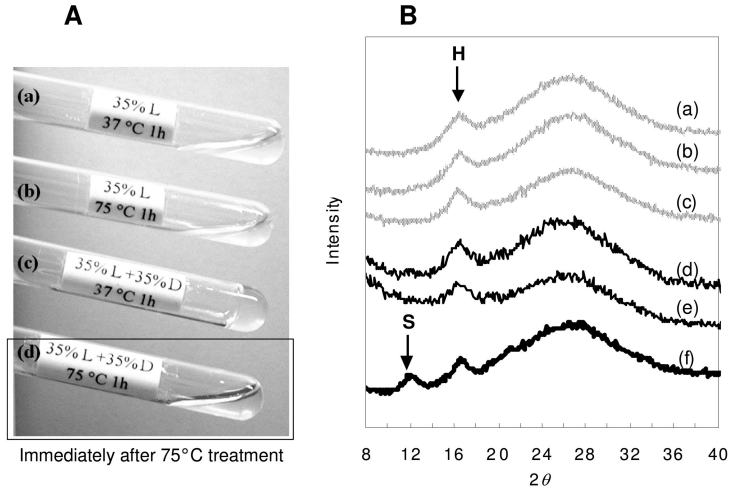

Figure 12. The appearance of 35wt% of BAB micellar solutions (A); PEG-PLLA-PEG at 37°C(a), 75°C(b), and enantio-mixture at 37°C(c), 75°C(d). The WAXS profiles of BAB micellar solutions (B); PEG-PLLA-PEG at room temperature(a), after 37°C(b), after 75°C(c), and enantio-mixture at room temperature(d), after 37°C(e), and after 75°C(f). (Reproduced with permission from reference (87). Copyright 2004 Wiley-VCH.)

The WAXS profiles of the single and mixed solutions at different temperatures are shown in Figure 12B. The mixed solution gave very small reflections at 2θ = 12.1 and 21.7° in addition to the reflections of the hexagonal crystals (2θ = 16.8°) of PLLA or PDLA only when heated at 75°C. This indicates that the stereocomplexation of the PLLA and PDLA blocks is induced even in the mixed solution heated at high temperatures where the sol state is achieved. When this BAB sol is cooled, the gelation is restored without significant change in the WAXS profile. Furthermore, the degree of crystallinity which was estimated by peak separation of each crystal and amorphous peaks does not increase by the heat treatment, being obviously different from the ABA gel system. It is, therefore, concluded that the stereocomplexation is not directly related with the gel formation mechanism for the BAB system.

The Mechanical properties of the hydrogels are examined. From the time-dependent rheological change of the mixed micellar solutions of ABA and BAB copolymers at 37°C, the mechanical properties of the BAB system are higher than those of the ABA system (*86*, *87*). For the BAB system, the storage modulus (*G′*) gradually rises up to reach 31 kPa after 60 min with the gelation occurring comparing to low *G′* of the ABA system, 400 Pa. This may be due to the increased polymer concentration in the micellar solution. The physical crosslinking though the PEG interaction can afford enough mechanical properties of the gel.

Mixed micellar solutions of enantiomeric ABA and BAB block copolymers exhibit very different gelation behavior and crystal structure. As a third system, the micellar solutions of AB block copolymers, PLLA-PEG and PDLA-PEG, were

In Degradable Polymers and Materials: Principles and Practice (2nd Edition); Khemani, K., et al.;
ACS Symposium Series; American Chemical Society: Washington, DC, 2012.

examined for the hydrogel formation. The AB system is similar to ABA in that the A-blocks associate in the core of the micelles, while being similar to BAB because the mobility of the corona B-blocks are comparable to each other.

A typical sol-gel phase diagram, plotted for the mixed solutions of the enantiomeric AB diblock copolymers, is illustrated in Figure 13. It resembles the BAB system diagram shown in Figure 11, where the gel-to-sol transition occurs with increasing temperature. The typical phase changes of a mixed solution of the PLLA-PEG and PDLA-PEG (total 30 wt%) are shown in Figure 14A at 37°C (c) and 75°C (d) as compared with those of the corresponding single micellar solution of PLLA-PEG (30 wt%) (a,b). Although the latter solution does not form a gel at any temperature, the mixed solution forms a gel on mixing at room temperature. The difference from the BAB system is that the sol formed at 75°C never returns to a gel again when cooled. This irreversible nature suggests that the interaction of the micelles formed in the hydrogel at lower temperature may be changed after turning to sol state by heating. Note that the normally synthesized AB diblock copolymer should involve a small amount of ABA triblock copolymer because MePEG is contaminated with dihydroxyterminated PEG (*103*, *104*). This impurity can be eliminated by high osmotic pressure chromatography; the same hydrogel formation for the pure enantiomeric AB system is also confirmed.

The WAXS profiles of the AB systems are shown in Figure 14B which are significantly different from those of the BAB system. The single micellar solution of PLLA-PEG shows an increase in the crystallinity (a,b) with increasing temperature, while that of PEG-PLLA-PEG does not have this behavior. In the mixed AB solution, the gel state formed at the lower temperature involves the hexagonal crystals, as shown by the reflection at 2θ = 16.8° (c); the sol state attained by heating at 75°C produces the stereocomplex crystals (2θ = 12.1 and 21.7°) with most of the hexagonal crystals being lost (d). This feature is similar to that of the ABA system rather than the BAB system.

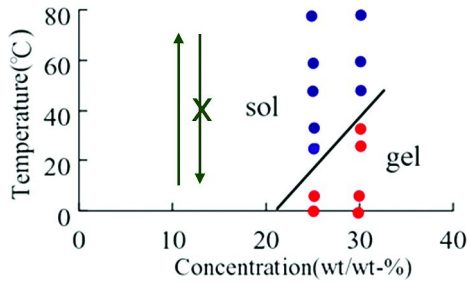

Figure 13. The phase diagram of mixed micelle solution of PLLA-PEG and PDLA-PEG.

In Degradable Polymers and Materials: Principles and Practice (2nd Edition); Khemani, K., et al.;
ACS Symposium Series; American Chemical Society: Washington, DC, 2012.

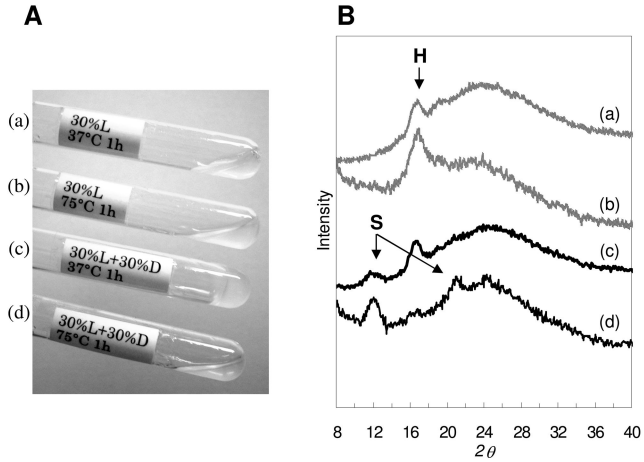

Figure 14. The appearance of 30wt% of AB micellar solutions (A); PLLA-PEG at 37°C(a), 75°C(b), and enantio-mixtur at 37°C(c), 75°C(d). The WAXS profiles of AB micellar solutions (B); PLLA-PEG after 37°C(a), after 75°C(b), and enantio-mixture after 37°C(c), and after 75°C(d). (Reproduced with permission from reference (87). Copyright 2004 Wiley-VCH.)

Gelation mechanism of the mixtures of enantiomeric BAB and AB block polymers may be much different from that of ABA system since the PEG blocks cannot act as direct crosslinkers between the micelles. The sol-gel transition diagrams and WAXS data suggest that the stereocomplexation between the PLLA and PDLA blocks is not directly correlated with the gelation of the mixed solution. Since, in the BAB triblock copolymers the hydrophobic PLLA and PDLA are confined in the core of the micelles and surrounded by the hydrophilic PEG shell, a sort of macromolecular reorganization is needed to grow the PLLA stereocomplexes and PDLA blocks in the micelles. Even when heated at high temperatures, the block chains are not easily exchanged among the micelles in the BAB system since PLLA and PDLA blocks are in the middle of copolymers (Figure 15A), so that the degree of stereocomplexation is limited. Even if the stereocomplex crystals could be formed, they are confined to the micelle core and cannot achieve an interaction between the particles strong enough as to induce gelation.

The WAXS data (Figure 12B) revealed that both PLLA and PDLA blocks of the BAB block copolymers form the hexagonal crystals in the micellar cores at room temperature. The IR spectra of the micellar solutions both in gel and sol states also have absorption bands at 921 and 1210 cm-1, supporting the presence of the 10/3 helical structure of the PLLA and PDLA blocks (*105*). One possible explanation of this gel-to-sol behavior is that PEG blocks between micelles act as crosslinkers at low temperature even though they are free to move. This helix formation of PLLA and PDLA blocks is possibly transmitted to the PEG chains through the block-linking bonds, because the PEG chain can readily take on a

In Degradable Polymers and Materials: Principles and Practice (2nd Edition); Khemani, K., et al.;
ACS Symposium Series; American Chemical Society: Washington, DC, 2012.

similar helical conformation. In fact, ordinary monoclinic crystals of PEG are known to consist of 7/2-helical chains. Since the helical senses of PLLA and PDLA are opposite to each other, the induced helices of the PEG chains should be right- and left-handed depending on the connecting PLA chains. Maybe, the helical chains of PEG, with opposite senses, aggregate through the chain interdigitation mechanism and change the hydrophilic/hydrophobic balance that leads to the inter-chain cohesion of the PEG blocks even in the aqueous environment. With the helical conformation, the hydrophilic ether linkages are surrounded by the hydrophobic alkylene chains to make the whole chain hydrophobic. With a single BAB copolymer, the helices have an identical sense, and the chain interdigitation to cause gelation is impossible. The interaction of the PEG chains in opposite helical senses was supported by the gelation behavior of the mixed micellar solution of the enantiomeric AB diblock copolymers (Figure 15B). In this case, the exchange of the core PLA blocks between micelles is much faster than that of the BAB system; in fact, the stereocomplex crystals grow with increasing temperatures of the mixture. At 75°C, most of the PLA crystals were replaced by the stereocomplex crystals. Therefore, most of the micelles comprise both PLLA and PDLA blocks in their core due to the exchange of PLA blocks at high temperature and inter-micelle interaction through the PEG is weakened even after cooling. The PEG interaction changed to intra-micellar instead of inter-micellar. This is why the AB system the gel is irreversible.

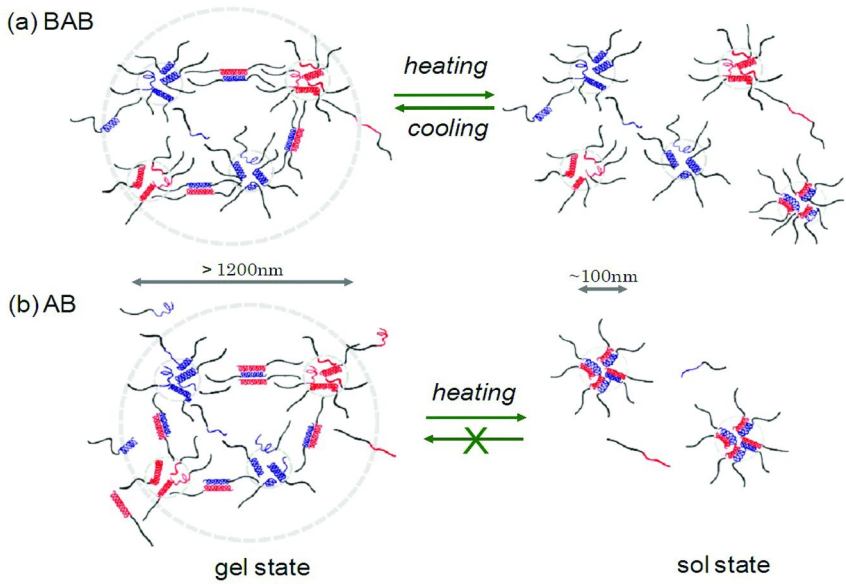

Figure 15. Proposed gelation mechanisms of enantiomeric mixture of BAB triblock (A) and AB diblock (B) copolymers. (see color insert)

In Degradable Polymers and Materials: Principles and Practice (2nd Edition); Khemani, K., et al.;
ACS Symposium Series; American Chemical Society: Washington, DC, 2012.

Another effect on these BAB and AB-type hydrogel formation is that micelles are aggregating into micro-gel size as depicted in Figure 15; a negligible amount of stereocomplex crystals of PLLA and PDLA blocks are still responsible for the gel formation. Dynamic light scattering revealed a bimodal size distribution of the AB-type gel of 120 and 1,200 nm. Upon heating, the microparticles at 1,200 nm disappear. The difference in reversibility for the BAB and AB gels is due to the rate of micelle reformation. If the core of all micelles become stereocomplexed PLA as seen in WAXS data of AB micelles (Figure 14B(d)), no more inter-micelle interaction occurs.

In addition to ABA-, BAB-, AB-micelles, and hybrid micelles of ABA copolymers described in this chapter, some mixed copolymer systems have been examined, such as comicellization of ABA and AB copolymers, and addition of fish collagen to ABA-micelles. These systems exhibited similar gelation by enantiomixtures with different so-gel phase diagrams. In summary, stereocomplexation of PLAs in PLA-PEG block copolymers provides a variety of hydrogels. Particularly, the hybrid micelles formed from two or more different copolymers are of interest for controllable robust hydrogels.

Conclusions

The combination of "thermo-responsive" and "biodegradable" properties is the grail being sought by scientists for biomedical use. Consequently, the hydrogel formation via block copolymer micelles consisting of enantiomeric PLA and PEG has an important role in many hydrogel bioapplications. The mixture of ABA-type block copolymers, PLLA-PEG-PLLA and PDLA-PEG-PDLA, with specific MW and block ratio exhibits attractive sol-to-gel transition between room and body temperature, can be used as an injectable biodegradable scaffold. Moreover, the comicellization of different sized ABA block copolymers have shown a controlled sol-to-gel transition behavior with temperature and improved properties. The reversible gel-sol transitions occur in the mixed micellar solution of the enantiomeric BAB triblock copolymers, PEG-PLLA-PEG and PEG-PDLA-PEG, depending on the polymer concentration and temperature. An understanding of the gelation mechanisms for ABA, BAB, and AB systems involving stereocomplex crystals is critical achieve their potential for bioapplications. There are many hydrogel formation theories and understanding gelation mechanisms will provide new prospective for biomaterial applications.

References

1. Ringsdorf, H.; Venzmer, J.; Winnik, F. M. *Macromolecules* **1991**, *24*, 1678–1686.
2. Takei, Y. G.; Aoki, T.; Sanui, K.; Ogata, N.; Sakurai, Y.; Okano, T. *Macromolecules* **1994**, *27*, 6163–6166.
3. Zareie, H. M.; Bulmus, E. V.; Gunning, A. P.; Hoffman, A. S.; Piskin, E.; Morris, V. J. *Polymer* **2000**, *41*, 6723–6727.
4. Maeda, Y.; Higuchi, T.; Ikeda, I. *Langmuir* **2000**, *16*, 7503–7509.

In Degradable Polymers and Materials: Principles and Practice (2nd Edition); Khemani, K., et al.;
ACS Symposium Series; American Chemical Society: Washington, DC, 2012.

5. Vadnere, M.; Amidon, G.; Lindenbaum, S.; Haslam, J. L. *Int. J. Pharm.* **1984**, *22*, 207–218.
6. Wanka, G.; Hoffmann, H.; Ulbricht, W. *Colloid. Polym. Sci.* **1990**, *268*, 101–117.
7. Jorgensen, E. B.; Hvidt, S.; Brown, W.; Schillen, K. *Macromolecules* **1997**, *30*, 2355–2364.
8. Deng, Y.; Yu, G. E.; Price, C.; Booth, C. *J. Chem. Soc., Faraday Trans.* **1992**, *88*, 1441–1446.
9. Alexandridis, P.; Holzwarth, J. F.; Hatton, T. A. *Macromolecules* **1994**, *27*, 2414–2425.
10. Rees, D. A. *J. Chem. Soc. B* **1969**, 217.
11. Hubbell, J. A.; West, J. L.; Chowdhury, S. M. In *Advanced Biomaterials in Biomedical Engineering and Drug Delivery Systems*; Springer: Tokyo, 1996; p 179.
12. Nagata, Y.; Kajiwara, K. *Gel Handbook*; NTS: Tokyo, 1997.
13. Steinbuechel, A. *Biopolymers*; Wiley-VCH: Weinheim, 2001; Vols. 3 and 4.
14. Tsuruta, T.; Hayashi, T.; Ishihara, K.; Kimura, Y. *Biomedical Applications of Polymeric Materials*; CRC Press: Boca Raton, 1993.
15. Lin, C. C.; Metters, A. T. *Adv. Drug Delivery Rev.* **2006**, *58*, 1379–1408.
16. Hoare, T. R.; Kohane, D. S. *Polymer* **2008**, *49*, 1993–2007.
17. Van Tomme, S. R.; Storm, G.; Hennink, W. E. *Int. J. Pharm.* **2008**, *355*, 1–18.
18. He, C. L.; Kim, S. W.; Lee, D. S. *J. Controlled Release* **2008**, *127*, 189–207.
19. Zhu, K. J.; Song, B. H.; Yang, S. L. *J. Polym. Sci., Part A: Polym. Chem.* **1989**, *27*, 2151–2159.
20. Zhu, K. J.; Lin, X. Z.; Yang, S. L. *J. Appl. Polym. Sci.* **1990**, *39*, 1–9.
21. Kricheldorf, H. R.; Boettcher, C. *Macromol. Symp.* **1993**, *73*, 47–64.
22. Kricheldorf, H. R.; Kreisersaunders, I.; Boettcher, C. *Polymer* **1995**, *36*, 1253–1259.
23. Kricheldorf, H. R.; Meierhaack, J. *Macromol. Chem. Phys.* **1993**, *194*, 715–725.
24. Cerrai, P.; Tricoli, M. *Macromol. Rapid Commun.* **1993**, *14*, 529–538.
25. Jedlinski, Z.; Kurcok, P.; Walach, W.; Janeczek, H.; Radecka, I. *Macromol. Chem. Phys.* **1993**, *194*, 1681–1689.
26. Xie, W. H.; Chen, D. P.; Fan, X. H.; Li, J.; Wang, P. G.; Cheng, H. N.; Nickol, R. G. *J. Polym. Sci., Part A: Polym. Chem.* **1999**, *37*, 3486–3491.
27. Li, S. M.; Rashkov, I.; Espartero, J. L.; Manolova, N.; Vert, M. *Macromolecules* **1996**, *29*, 57–62.
28. Goraltchouk, A.; Freier, T.; Shoichet, M. S. *Biomaterials* **2005**, *26*, 7555–7563.
29. Younes, H.; Cohn, D. *J. Biomed. Mater. Res. A* **1987**, *21*, 1301–1316.
30. Kubies, D.; Rypacek, F.; Kovarova, J.; Lednicky, F. *Biomaterials* **2000**, *21*, 529–536.
31. Li, Y. X.; Volland, C.; Kissel, T. *J. Controlled Release* **1994**, *32*, 121–128.
32. Rashkov, I.; Manolova, N.; Li, S. M.; Espartero, J. L.; Vert, M. *Macromolecules* **1996**, *29*, 50–56.

33. Shah, S. S.; Zhu, K. J.; Pitt, C. G. *J. Biomater. Sci., Polym. Ed.* **1994**, *5*, 421–431.
34. Li, S. M.; Garreau, H.; Vert, M. *J. Mater. Sci.: Mater. Med.* **1990**, *1*, 123–130.
35. Hu, D. S. G.; Liu, H. J. *Polym. Bull.* **1993**, *30*, 669–676.
36. Mason, M. N.; Metters, A. T.; Bowman, C. N.; Anseth, K. S. *Macromolecules* **2001**, *34*, 4630–4635.
37. Shah, N. M.; Pool, M. D.; Metters, A. T. *Biomacromolecules* **2006**, *7*, 3171–3177.
38. Graham, N. B.; McNeill, M. E. *Biomaterials* **1984**, *5*, 27–36.
39. Metters, A. T.; Anseth, K. S.; Bowman, C. N. *Polymer* **2000**, *41*, 3993–4004.
40. Metters, A. T.; Bowman, C. N.; Anseth, K. S. *J. Phys. Chem. B* **2000**, *104*, 7043–7049.
41. Metters, A. T.; Bowman, C. N.; Anseth, K. S. *AIChE J.* **2001**, *47*, 1432–1437.
42. Metters, A. T.; Anseth, K. S.; Bowman, C. N. *J. Phys. Chem. B* **2001**, *105*, 8069–8076.
43. Molina, I.; Li, S. M.; Martinez, M. B.; Vert, M. *Biomaterials* **2001**, *22*, 363–369.
44. Deng, X. M.; Li, X. H.; Yuan, M. L.; Xiong, C. D.; Huang, Z. T.; Jia, W. X.; Zhang, Y. H. *J. Controlled Release* **1999**, *58*, 123–131.
45. Perez, C.; Sanchez, A.; Putnam, D.; Ting, D.; Langer, R.; Alonso, M. J. *J. Controlled Release* **2001**, *75*, 211–224.
46. Beck, L. R.; Cowsar, D. R.; Lewis, D. H.; Gibson, J. W.; Flowers, C. E. *Am. J. Obstet. Gynecol.* **1979**, *135*, 419–426.
47. Gref, R.; Domb, A.; Quellec, P.; Blunk, T.; Muller, R. H.; Verbavatz, J. M.; Langer, R. *Adv. Drug Delivery Rev.* **1995**, *16*, 215–233.
48. Sakurai, K.; Nakada, Y.; Nakamura, T.; Tudomi, R.; Matumoto, J.; Takahashi, Y. *J. Macromol. Sci., Pure Appl. Chem.* **1999**, *36*, 1863–1877.
49. Matsumoto, J.; Nakada, Y.; Sakurai, K.; Nakamura, T.; Takahashi, Y. *Int. J. Pharm.* **1999**, *185*, 93–101.
50. De Jaeghere, F.; Allemann, E.; Feijen, J.; Kissel, T.; Doelker, E.; Gurny, R. *J. Drug Targeting* **2000**, *8*, 143–153.
51. Jeong, B.; Bae, Y. H.; Lee, D. S.; Kim, S. W. *Nature* **1997**, *388*, 860–862.
52. Jeong, B.; Kim, S. W.; Bae, Y. H. *Adv. Drug Delivery Rev.* **2002**, *54*, 37–51.
53. Jeong, B.; Bae, Y. H.; Kim, S. W. *Macromolecules* **1999**, *32*, 7064–7069.
54. Jeong, J. H.; Kim, S. W.; Park, T. G. *Pharm. Res.* **2004**, *21*, 50–54.
55. Jeong, B.; Bae, Y. H.; Kim, S. W. *J. Controlled Release* **2000**, *63*, 155–163.
56. Kim, Y. J.; Kim, S. W. *Polym. Gels: Fundam. Appl.* **2003**, *833*, 300–311.
57. Li, Z. H.; Ning, W.; Wang, J. M.; Choi, A.; Lee, P. Y.; Tyagi, P.; Huang, L. *Pharm. Res.* **2003**, *20*, 884–888.
58. Lee, P. Y.; Li, Z. H.; Huang, L. *Pharm. Res.* **2003**, *20*, 1995–2000.
59. Lee, P. Y.; Cobain, E.; Huard, J.; Huang, L. *Mol. Ther.* **2007**, *15*, 1189–1194.
60. Yu, L.; Chang, G. T.; Zhang, H.; Ding, J. D. *Int. J. Pharm.* **2008**, *348*, 95–106.
61. Qao, M. X.; Chen, D. W.; Hao, T. N.; Zhao, X. L.; Hu, H.; Ma, X. C. *Pharmazie* **2008**, *63*, 27–30.

62. Qiao, M. X.; Chen, D. W.; Ma, X. C.; Hu, H. Y. *Pharmazie* **2006**, *61*, 199–202.
63. Pratoomsoot, C.; Tanioka, H.; Hori, K.; Kawasaki, S.; Kinoshita, S.; Tighe, P. J.; Dua, H.; Shakesheff, K. M.; Rose, F. *Biomaterials* **2008**, *29*, 272–281.
64. Gref, R.; Minamitake, Y.; Peracchia, M. T.; Trubetskoy, V.; Torchilin, V.; Langer, R. *Science* **1994**, *263*, 1600–1603.
65. Miyamoto, S.; Takaoka, K.; Okada, T.; Yoshikawa, H.; Hashimoto, J.; Suzuki, S.; Ono, K. *Clin. Orthop. Relat. Res.* **1993**, 333–343.
66. Iijima, M.; Nagasaki, Y.; Okada, T.; Kato, M.; Kataoka, K. *Macromolecules* **1999**, *32*, 1140–1146.
67. Choi, S. W.; Choi, S. Y.; Jeong, B.; Kim, S. W.; Lee, D. S. *J. Polym. Sci., Part A: Polym. Chem.* **1999**, *37*, 2207–2218.
68. Aamer, K. A.; Sardinha, H.; Bhatia, S. R.; Tew, G. N. *Biomaterials* **2004**, *25*, 1087–1093.
69. Sanabria-DeLong, N.; Agrawal, S. K.; Bhatia, S. R.; Tew, G. N. *Macromolecules* **2006**, *39*, 1308–1310.
70. Sanabria-DeLong, N.; Agrawal, S. K.; Bhatia, S. R.; Tew, G. N. *Macromolecules* **2007**, *40*, 7864–7873.
71. Agrawal, S. K.; Sanabria-DeLong, N.; Tew, G. N.; Bhatia, S. R. *Macromolecules* **2008**, *41*, 1774–1784.
72. Bryant, S. J.; Bender, R. J.; Durand, K. L.; Anseth, K. S. *Biotechnol. Bioeng.* **2004**, *86*, 747–755.
73. Rice, M. A.; Anseth, K. S. *J. Biomed. Mater. Res., Part A* **2004**, *70A*, 560–568.
74. Murakami, Y.; Yokoyama, M.; Okano, T.; Nishida, H.; Tomizawa, Y.; Endo, M.; Kurosawa, H. *J. Biomed. Mater. Res., Part A* **2007**, *80A*, 421–427.
75. Hoogsteen, W.; Postema, A. R.; Pennings, A. J.; Tenbrinke, G.; Zugenmaier, P. *Macromolecules* **1990**, *23*, 634–642.
76. Okihara, T.; Tsuji, M.; Kawaguchi, A.; Katayama, K.; Tsuji, H.; Hyon, S. H.; Ikada, Y. *J. Macromol. Sci., Part B: Phys.* **1991**, *B30*, 119–140.
77. Ikada, Y.; Jamshidi, K.; Tsuji, H.; Hyon, S. H. *Macromolecules* **1987**, *20*, 904–6.
78. Tsuji, H.; Horii, F.; Hyon, S. H.; Ikada, Y. *Macromolecules* **1991**, *24*, 2719–24.
79. Tsuji, H. *Polymer* **2000**, *41*, 3621–3630.
80. Brochu, S.; Prudhomme, R. E.; Barakat, I.; Jerome, R. *Macromolecules* **1995**, *28*, 5230–5239.
81. Brizzolara, D.; Cantow, H. J.; Diederichs, K.; Keller, E.; Domb, A. J. *Macromolecules* **1996**, *29*, 191–197.
82. Lim, D. W.; Choi, S. H.; Park, T. G. *Macromol. Rapid Commun.* **2000**, *21*, 464–471.
83. de Jong, S. J.; De Smedt, S. C.; Wahls, M. W. C.; Demeester, J.; Kettenes-van den Bosch, J. J.; Hennink, W. E. *Macromolecules* **2000**, *33*, 3680–3686.
84. de Jong, S. J.; De Smedt, S. C.; Demeester, J.; van Nostrum, C. F.; Kettenes-van den Bosch, J. J.; Hennink, W. E. *J. Controlled Release* **2001**, *72*, 47–56.
85. de Jong, S. J.; van Eerdenbrugh, B.; van Nostrum, C. F.; Kettenes-van de Bosch, J. J.; Hennink, W. E. *J. Controlled Release* **2001**, *71*, 261–275.

86. Fujiwara, T.; Mukose, T.; Yamaoka, T.; Yamane, H.; Sakurai, S.; Kimura, Y. *Macromol. Biosci.* **2001**, *1*, 204–208.
87. Mukose, T.; Fujiwara, T.; Nakano, J.; Taniguchi, I.; Miyamoto, M.; Kimura, Y.; Teraoka, I.; Lee, C. W. *Macromol. Biosci.* **2004**, *4*, 361–367.
88. Li, S. M.; Vert, M. *Macromolecules* **2003**, *36*, 8008–8014.
89. Hiemstra, C.; Zhong, Z. Y.; Li, L. B.; Dijkstra, P. J.; Jan, F. J. *Biomacromolecules* **2006**, *7*, 2790–2795.
90. Hiemstra, C.; Zhong, Z.; Van Tomme, S. R.; van Steenbergen, M. J.; Jacobs, J. J. L.; Den Otter, W.; Hennink, W. E.; Feijen, J. *J. Controlled Release* **2007**, *119*, 320–327.
91. Hiemstra, C.; Zhou, W.; Zhong, Z. Y.; Wouters, M.; Feijen, J. *J. Am. Chem. Soc.* **2007**, *129*, 9918–9926.
92. Fujiwara, T.; Miyamoto, M.; Kimura, Y. *Macromolecules* **2000**, *33*, 2782–2785.
93. Fujiwara, T.; Miyamoto, M.; Kimura, Y.; Iwata, T.; Doi, Y. *Macromolecules* **2001**, *34*, 4043–4050.
94. Fujiwara, T.; Kimura, Y. *Macromol. Biosci.* **2002**, *2*, 11–23.
95. Fujiwara, T.; Miyamoto, M.; Kimura, Y.; Sakurai, S. *Polymer* **2001**, *42*, 1515–1523.
96. Takami, K.; Watanabe, J.; Takai, M.; Ishihara, K. *J. Biomater. Sci., Polym. Ed.* **2011**, *22*, 77–89.
97. Nagahama, K.; Nishimura, Y.; Ohya, Y.; Ouchi, T. *Polymer* **2007**, *48*, 2649–2658.
98. Nagahama, K.; Ouchi, T.; Ohya, Y. *Adv. Funct. Mater.* **2008**, *18*, 1220–1231.
99. Tian, M. M.; Qin, A. W.; Ramireddy, C.; Webber, S. E.; Munk, P.; Tuzar, Z.; Prochazka, K. *Langmuir* **1993**, *9*, 1741–1748.
100. Chaibundit, C.; Ricardo, G.; Costa, V.; Yeates, S. G.; Booth, C. *Langmuir* **2007**, *23*, 9229–9236.
101. Abebe, D. G.; Fujiwara, T. *Biomacromolecules* **2012**, *13*, 1828–1836.
102. Chung, B.; Choi, H.; Park, H. W.; Ree, M.; Jung, J. C.; Zin, W. C.; Chang, T. *Macromolecules* **2008**, *41*, 1760–1765.
103. Lee, D.; Teraoka, I. *Polymer* **2002**, *43*, 2691–2697.
104. Lee, D.; Teraoka, I. *Biomaterials* **2003**, *24*, 329–336.
105. Kister, G.; Cassanas, G.; Vert, M. *Polymer* **1998**, *39*, 267–273.

Chapter 18

PLA-PEO-PLA Hydrogels: Chemical Structure, Self-Assembly and Mechanical Properties

Surita R. Bhatia[1,*] and Gregory N. Tew[2,*]

[1]Department of Chemical Engineering, University of Massachusetts Amherst, Amherst, MA 01003
[2]Department of Polymer Science and Engineering, University of Massachusetts Amherst, Amherst, MA 01003
[*]Corresponding Authors. Email: sbhatia@ecs.umass.edu, tew@mail.pse.umass.edu

Poly(lactide) – *block* – poly(ethylene oxide) – *block* – poly(lactide) [PLA-PEO-PLA] triblock copolymers are known to form physical hydrogels in water. Their biodegradability makes them attractive for soft tissue scaffolds and drug delivery applications. In addition, they serve as an excellent model system for physical hydrogels or networks. Understanding their mechanical properties is an important objective. More recently, these non-covalent networks were converted to covalently cross-linked hydrogels that prevent the gel-to-sol transition upon exposure to infinite water. Specifically, this was accomplished by allowing the system to self-assemble followed by covalent capture of the self-assembled architecture.

Introduction

Polyesters remain an important class of materials for biomaterials applications from small area tissue repair to the growth of new organs (*1–4*). Their overwhelmingly attractive features are their biodegradability and ease of synthesis; however, with respect to the optimal requirements of a scaffold, these polymers are far from ideal because they are very hydrophobic. Although PLA-based materials are important technologically, they suffer from unwanted responses *in vivo* including foreign body response (*5*). At the same time, the

In Degradable Polymers and Materials: Principles and Practice (2nd Edition); Khemani, K., et al.; ACS Symposium Series; American Chemical Society: Washington, DC, 2012.

modulus of homopolyesters is quite far from many biological tissues. Although PLA and other synthetic polyesters, like poly(caprolactone), represent important materials for medical implants, they all suffer from a variety of critical limitations.

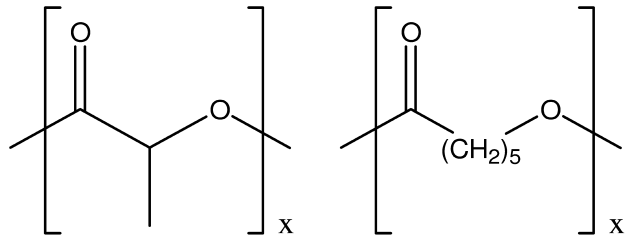

PLA PCL

One approach to enhancing the water-solubility of these polyesters is to make block copolymers containing a water soluble block such as polyethylene oxide (PEO) (*6*). Here the discussion is confined to copolymers composed of biodegradable hydrophobic poly(lactic acid) (PLA), including the two stereoisomers L and D, and biocompatible hydrophilic poly(ethylene oxide) (PEO). Both AB and ABA block copolymer architectures have been studied in some detail (*6–30*). These architectures can be used to create physically cross-linked hydrogels with transitions near body temperature.

Beyond the control of block lengths, the ability to control D,L stereochemistry directly impacts hydrogel modulus through crystallinity of the PLA blocks since pure L or D polymers are semi-crystalline but mixtures of D and L produce amorphous materials (*12*, *19*, *21*, *29*, *31*, *32*). It has been observed that gel-forming PLA-PEG diblock systems can be effectively modulated to vary a number of important physical properties including permeability and degradation rate. The structural properties of the gel matrix (micromorphology and pore size) are directly related to the mass transport of water into the gel and transport of drug out of the polymer. As a result, the chemical composition and microstructure design can produce tailor made polymer matrices.

As a class of materials, PLA-PEO-PLA materials are extremely versatile given their relatively simple chemical structures. They represent an important sub-division of the much broader area of hydrogels. Hydrogels remain of great interest in the area of biomaterials (*15*, *29*, *30*, *33–38*). There self-assembly is driven by the association of the hydrophobic endblocks into micelles, which are bridged by the water-soluble midblocks forming physically crosslinked networks. These physical hydrogels are attractive because no crosslinking agent is necessary and the gelation can be triggered by concentration, temperatue, pH, salt, etc. At the same time, the use of chemical cross-links have also been studied (*30*, *39–41*). Chemical crosslinking leads to a more permanent three-dimensional structure than the physically crosslinked counter-parts, but can still be degraded with time.

A variety of crosslinking techniques, polymer structures, and architectures have been used to synthesize biodegradable hydrogels; however, the corresponding mechanical properties are not as well characterized. Since the

In Degradable Polymers and Materials: Principles and Practice (2nd Edition); Khemani, K., et al.;
ACS Symposium Series; American Chemical Society: Washington, DC, 2012.

overall mechanical environment affects cell function, this is unfortunate (*33*, *42*, *43*). Cells typically bind to the extracellular matrix via surface receptors to generate traction forces. Cells can sense the restraining force of the substrate and respond by strengthening its cytoskeleton (*44*). Since the healthy survival of cells depends on the mechanical properties, it is important to consider these properties.

Mechanical properties impact all types of processes including cellular structure, metabolism, transcription/translation, and even viability (*44–50*). Pioneering work showed NIH3T3 fibroblasts underwent compliance dependent motility changes (*49*, *51*). Similar studies examined endothelial cells, myocytes, hepatocytes, neural/glial cells, and chondrocytes (*52–56*). Glial cells were unable to survive in soft materials, unlike neurons (*52*, *54*, *57*, *58*). The use of hydrogels has been proposed to limit scar tissue as a result of mismatch of mechanical properties at the wound site (*52*).

Motivated by these and other factors, we have studied PLA-PEO-PLA triblock copolymers over the last decade. Through these studies some insight into the structure-property relationships of PLA-PEO-PLA gels was obtained. Factors like dependency of gel strength on the molecular composition and polymer concentration, which directly impact gel structure, were investigated. This includes varying the stiffness by manipulating the length of the PLA endblocks (*6*), by changing the physical crosslinks from amorphous to crystalline (*32*), by varying the synthetic technique (*59*), by incorporating nanoparticles (*60*), and by covalently capturing the self-assembled structure (*26*). This last approach is particularly intriguing since it combines the advantages of self-assembly with the stability of covalent crosslinks. Coupling self-assembly to hydrogel mechanical properties in novel phase-separated systems has provided new insight and properties (*39*).

Materials and Methods

Materials

L-lactide, D-lactide, and *rac*-lactide (Aldrich) were purified by recrystallization in dry ethyl acetate and by sublimation prior to polymerization. The α,ω-dihydroxy polyethylene glycol macro initiator with molecular weight 8,900 (PEG 8KDa, Aldrich) was dried at room temperature under vacuum prior to polymerization. Stannous (II) 2-ethyl hexanoate (Alfa Aesar) was used without further purification.

Typical Synthesis of PLLA-PEO-PLLA Triblock Copolymer

PLLA-PEO-PLLA triblock copolymers were synthesized by bulk polymerization. PEG was introduced into a dried polymerization tube. The tube was purged with nitrogen, and placed in an oil bath at 150 °C. Stannous (II) 2-ethylhexanoate was introduced under nitrogen to the molten PEG and stirred for

In Degradable Polymers and Materials: Principles and Practice (2nd Edition); Khemani, K., et al.;
ACS Symposium Series; American Chemical Society: Washington, DC, 2012.

10 minutes followed by addition of L-lactide to the macroinitiator/catalyst melt. The polymerization was carried out at 150 °C for 24 h with stirring. after which it was quenched by methanol. The product was dissolved in tetrahydrofuran and precipitated in n-hexane. The process of dissolution/reprecipitation was carried out three more times. The copolymer was dried under vacuum at room temperature for two days.

Sample Preparation and Instrumentation

The copolymers polydispersity are measured versus polyethylene oxide standards using GPC (HP 1050 series, a HP 1047A differential refractometer, and three PLgel columns (5 μm 50Å, two 5 μm MIXED-D) in dimethylformamide as eluting solvent at a rate of 0.5 mL/min rate at room temperature. The copolymer compositions are determined by ^{1}H NMR (Bruker, DPX300, 300MHz spectrometer, d-chloroform).

Gels were prepared by slow addition of dried polymer sample to a fixed volume of DI water (15 mL) followed by stirring and heating. Gels were then transferred to a Bohlin CVO rheometer for oscillatory measurements. A cone-and-plate geometry with a 4° cone, 40 mm diameter plate, and 150 mm gap was used for all experiments on hydrogels. For liquid samples with a low viscosity, a couette geometry was used. Stress amplitude sweeps were performed to ensure that subsequent data was collected in the linear viscoelastic regime. Frequency sweeps were performed at a constant stress (0.1 - 2.0 Pa, depending on the sample) in the frequency range 0.01 - 100 Hz. At high frequencies, a resonant frequency of the rheometer motor was observed; thus, data are reported up to a frequency of approximately 10 Hz, again depending on the particular sample.

Crosslinking Chemistry

PLA-PEO-PLA triblock copolymer (10.0 g, 0.760 mmol, 1 equiv) was weighed into a dried round-bottom flask, dissolved in toluene, and attached to a Dean-Stark trap with a condenser. The system was evacuated and purged with nitrogen 3 times. The condenser was turned on and the solution was stirred and refluxed to azeotropically distill the solution. The distilled solution was cooled to room temperature and then placed in an ice bath. Triethylamine (1.06 mL, 7.60 mmol, 10 equiv) was added dropwise, followed by dropwise addition of acryloyl chloride (0.617 mL, 7.60 mmol, 10 equiv), and stirred overnight. Triethyl amine/hydrochloric acid salt was removed by filtration over filter paper, and the toluene was evaporated. The product was taken up in THF, passed through a plug of basic alumina, and precipitated in hexanes.

End-functionalized PLA-PEO-PLA (187 mg) was weighed into the wells of a 48-well cell culture plate. The plate was heated to 80°C in a vacuum oven for 1.5 hour to melt a polymer film. After heating, the plate was cooled to room temperature. A 0.05% w/v I2959 solution was prepared by weighing 26 mg I2959 in a vial, adding 52 mL of phosphate buffered solution, and heating and sonicating to dissolve. For a 25% w/v hydrogel, 0.745 mL of 0.05% w/v I2959 solution was added to each well plate and allowed to swell into a physical gel over 3 - 4 days.

In Degradable Polymers and Materials: Principles and Practice (2nd Edition); Khemani, K., et al.;
ACS Symposium Series; American Chemical Society: Washington, DC, 2012.

After full swelling of the physical hydrogel, the well plates were irradiated with long-wave UV radiation (~ 365 nm) for 5 minutes, flipped upside-down (hydrogel thickness is approximately 8 mm), and irradiated for 5 more minutes to initiate the photocrosslinking. The hydrogel concentration was varied (10, 15, 25, 35, and 45% w/v) by adjusting the amount of dry polymer added to the well, while maintaining a constant volume of added photoinitiator solution.

Results and Discussion

PLA-PEO-PLA Triblock Copolymers Synthesis

Lactide has two stereoisomers, D-lactide and L-lactide. The resulting polymers, poly(D-lactide) (PDLA) and poly(L-lactide) (PLLA), are isotactic and semicrystalline. In contrast, polymers formed by atactic poly(D,L-lactide), or racemic poly(R-lactide) (PRLA), are amorphous (*32*). In a unique, and perhaps the simplest system, this allowed direct control over the crystallinity of the self-assembled hydrophobic micelle formed by these copolymers. Generally, triblock copolymers synthesized through bulk-synthesis are more asymmetric, which reduced the mechanical stiffness of the gel phase. This had a larger impact on amorphous PRLA copolymers than their crystalline counterpart (*59*). Although a number of copolymers has been prepared, the PEO block length is held constant and the degree of polymerization (DP) for PLLA is varied (typically from ~52 to ~72) (*6*, *32*, *61–63*). In all cases, the polymerization was stopped before complete monomer consumption since this leads to broader molecular weight distributions (MWD).

Mechanical Properties of These Hydrogels

Mechanical properties of physically crosslinked hydrogels are typically characterized using shear rheometry, by exposing the material to an oscillatory shear stress at various frequencies. This leads to a determination of the storage modulus (G' and the loss modulus (G''), providing insight into the elastic and viscous responses of the material, respectively. Chemically crosslinked hydrogels are more typically characterized by measuring the stress in the material as strain is applied in compression. Implementing Hooke's Law ($\sigma = E\varepsilon$, where σ is stress, ε is strain, and E is the Young's or elastic modulus) to determine the slope of the stress-strain curve in the linear region at low strains yields the elastic modulus. However, Hooke's Law only applies to linearly elastic materials, while hydrogels typically have non-linear stress-strain responses in compression. Other models are available including the modified Neo-Hookean model (*64–66*) or a model defined by Mooney (*67*) and Rivlin (*68*). Regardless, many researchers only apply Hooke's Law despite the non-linear behavior of their materials.

In Degradable Polymers and Materials: Principles and Practice (2nd Edition); Khemani, K., et al.;
ACS Symposium Series; American Chemical Society: Washington, DC, 2012.

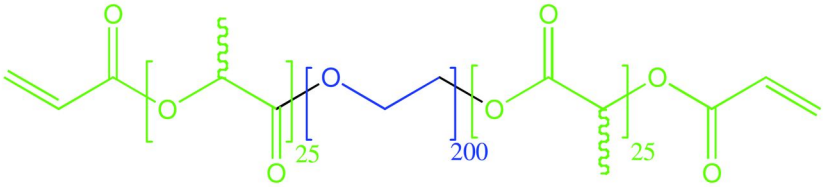

Figure 1. PLA-PEO-PLA was modified with acrylate end-endgroups. Hydrophobic PLA is illustrated in green; hydrophilic PEO is in blue. This triblock copolymer forms physical crosslinks which are captured covalently by photocrosslinking the junction points to make them permanent.

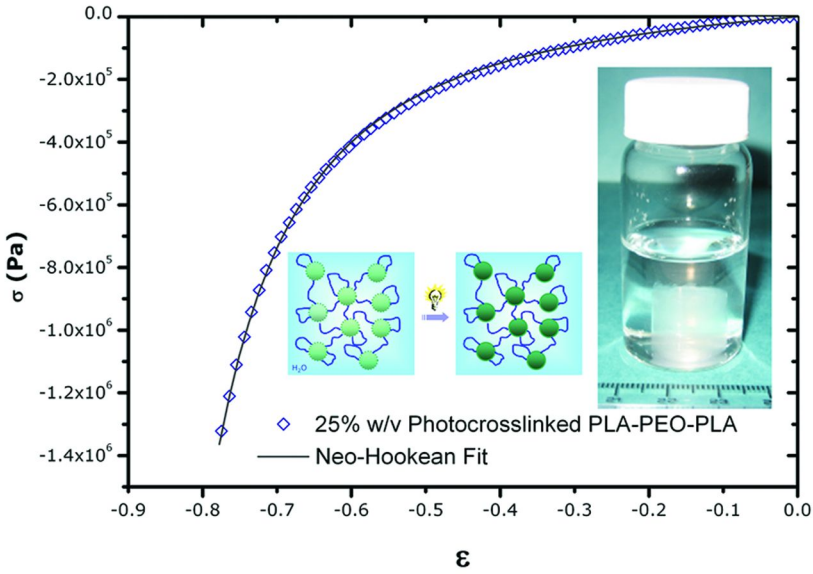

Figure 2. ***Typical Stress versus Strain Curve in Compression.*** *25% w/v photocrosslinked PLA-PEO-PLA before degradation. Stress curve is non-linear and typical of soft rubbery materials. (inset) Schematic representation of the self-assembly followed by the photochemical cross-linking reaction as well as a photograph of the slightly oqaque hydrogel in excess water. This demonstrates its lack of a gel-sol transition upon dissolution.*

Addition of water to these ABA triblock copolymers produces hard, physically associated gels typically above 16 wt%. The length of the PLA block directly impacts the wt% of this sol-gel transition. The longer the PLA block (up to a solubility limit), the lower the transition (*6*, *62*). To better quantify the mechanical properties of these hydrogels, dynamic mechanical shear rheology

was employed. A plot of G' vs. frequency for two polymers showed the gel with shorter PLA materials (52 PLA units, 20 wt %) forms a weaker gel than the one with the longer PLA blocks (72 PLA units,16 wt %). Stiffness increased by more than two decades, from ~100 Pa to 10,000 Pa, as the length of the hydrophobic block is increased by 20 units. Other PEO-containing systems with alkyl hydrophobe end-caps showed qualitatively similar trends (*24*). The elastic moduli of fluoroalkyl-capped PEO gels were insensitive to hydrophobe length at high frequency (*69*, *70*). The elastic modulus >10 kPa provides materials that are almost an order of magnitude stiffer than previously reported polymers composed of similar chemistry (*71*, *72*).

The self-assembled network structure of these ABA triblock copolymers is dynamic. As more water is added, the distance between micelles increases, lowering the density of junction points. However, by introducing a photocrosslinkable moiety (see Figure 1), the self-assembled structure can be covalently captured (*26*). This method allows the differences between chemical and physical crosslinking in the same polymer hydrogel system to be studied. It also represents a new strategy to form hydrogels and is likely to lead to novel properties since it has the advantages of self-assembly and covalent, permanent crosslinks.

In order to covalently capture the assembled hydrogel, the PLA-PEO-PLA triblock copolymer endgroups were functionalized with acrylates so that the self-assembled structure could be locked in by initiating photocrosslinking with ultra-violet radiation. The photocrosslinked PLA-PEO-PLA hydrogels remained intact when swollen in phosphate buffered saline solution (pH = 7.4) at body temperature (37 °C) for extended periods of time. This is in contrast to the physical hydrogels. Compression mechanical studies were performed to evaluate these photocrosslinked hydrogels. The Neo-Hookean constitutive relationship for rubbers was utilized to model the compression curves.

In this model, the specific form of the strain energy function (U) depends on the first invariant of the deformation tensor (I_1) by the constant, C_1:

$$U = C_1\left(I_1 - 3\right)$$
$$U = C_1\left(\lambda_1^2 + \lambda_2^2 + \lambda_3^2 - 3\right)$$

Where λ_i is equal to the extension ratio in the i-principal direction, or more specifically, the length in the i-direction over the initial (pre-stressed) length in the i-direction. The extension ratio is related to the strain, ε, by the following expression: $\lambda = \varepsilon + 1$. For the case of uniaxial compression and assuming the material to be incompressible:

$$\lambda_1^2 = \lambda^2,\ \lambda_2^2 = \lambda_3^2 = \lambda^{-1}$$
$$\lambda_1^2\lambda_2^2\lambda_3^2 = 1$$

In Degradable Polymers and Materials: Principles and Practice (2nd Edition); Khemani, K., et al.;
ACS Symposium Series; American Chemical Society: Washington, DC, 2012.

By substituting into the strain energy expression and differentiating with respect to the extension ratio, an expression for stress (σ) is derived:

$$U = C_1\left(\lambda^2 + \frac{2}{\lambda} - 3\right)$$

$$\sigma = \frac{\partial U}{\partial \lambda} = 2C_1\left(\lambda - \frac{1}{\lambda^2}\right) = 2C_1\left[(\varepsilon+1) - \frac{1}{(\varepsilon+1)^2}\right]$$

where the single parameter C_1 is defined as half of the shear modulus, G ($C_1 = G/2$). The same relationship can be derived using a statistical thermodynamic approach in which the distribution of end-to-end distances between crosslinks is assumed to be Gaussian (*64–66*).

A typical stress-strain curve is shown in Figure 2 along with its fit using this Neo-Hookean model. The fit agrees well with the data. It predicts the observed non-linear behavior, suggesting a Gaussian distribution of chains and few entanglements or looping chains. Initially, the 25% w/v hydrogels had a shear modulus of ~ 64 kPa. As they degraded, the shear modulus decreased exponentially to a value of ~ 7 kPa over 35 days. This agreed well with the swelling data.

Structural Properties of the Gel Phase

The structure of these hydrogels containing crystalline PLLA domains was investigated by WAXS, ultra small angle x-ray scattering (USAXS), ultra small angle neutron scattering (USANS) and confocal microscopy techniques (*6*, *31*, *60–63*). It was expected that the structure of a hydrogel would strongly influence its mechanical properties which are known to be dependent on both the nanoscale and microscale structure (*61*, *73*). All gel samples exhibited low q range scattering that followed power law behavior (*61*), indicating scattering from fractal structures (*74*, *75*). The power law exponents were found to be less than or equal to three, indicative of a mass fractal structure. Although more work is necessary to fully understand the subtleties of the PLLA-PEO-PLLA system, these differences might be related to the crystalline nature of the PLLA hydrophobic domains. WAXD studies (see Figure 3) on these gels show strong diffraction peaks at $2\theta = 17$ and 19 degrees corresponding to crystalline PLLA while the PRLA-based hydrogel showed no such peaks (*32*).

In Degradable Polymers and Materials: Principles and Practice (2nd Edition); Khemani, K., et al.;
ACS Symposium Series; American Chemical Society: Washington, DC, 2012.

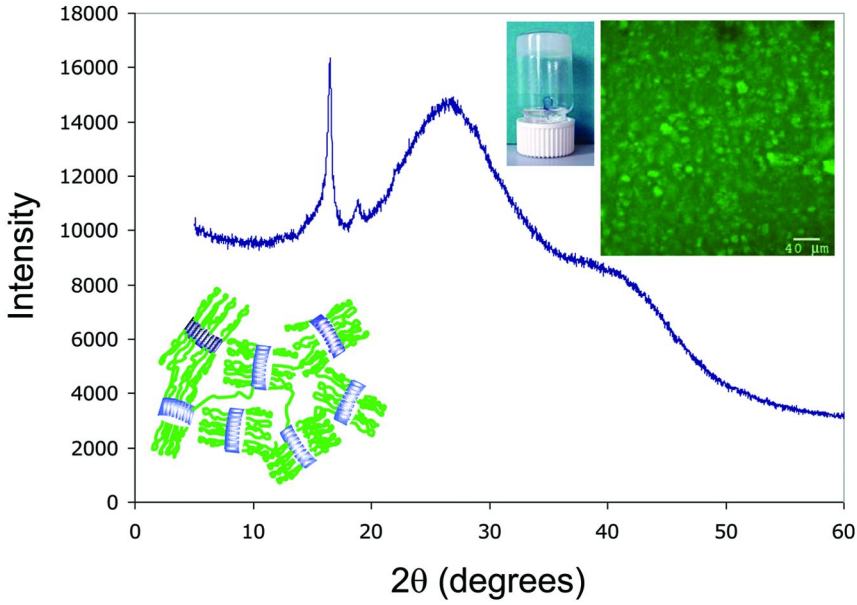

Figure 3. ***XRD showing crystalling PLLA in the hydrogel.*** *(insets) Schematic representation of the self-assembled crystalline network along with a photograph of the oqaque hydrogel and a confocal microscopy image.*

Conclusions

PLA-PEO-PLA triblock copolymers have been extensively studied over the years, and have found use in a wide variety of applications. Understanding this copolymer system at a more fundamental level has provided insight into the connection between the molecular structure, self-assembled network structure, and bulk properties. Further study is required before a full understanding is availabe and the ability to predict the material properties can be made. A number of ways to influence the mechanical properties of the resulting hydrogel have been demonstrated including: at the monomer level by alternating the stereo-center, and at the nanometer-scale by covalently capturing the self-assembled structure.

Acknowledgments

Data appearing in this review was supported by the central facilities of the NSF-funded Center for Hierarchical Manufacturing (CMMI-0531171) and the NSF-funded MRSEC on Polymers (DMR-0213695). We thank a number of agencies and companies for their support of the years including ARO, ONR, NSF, 3M, and DuPont.

References

1. Amass, W.; Amass, A.; Tighe, B. *Polym. Int.* **1998**, 89.
2. Marois, Y.; Zhang, Z.; Vert, M.; Deng, X.; Lenz, R. W.; Guidoin, R. In *Synthetic Bioabsorbably Polymers for Implants*; Agrawal, C. M., Parr, J. E., Lin, S. T., Eds.; ASTM: West Conshohocken, PA, 2000.
3. Stigers, D. J.; Tew, G. N. *Biomacromolecules* **2003**, *4*, 193.
4. Sudesh, K.; Doi, A. Y. *Prog. Polym. Sci.* **2000**, *25*, 1503.
5. Rotter, N.; F., U.; Roy, A. K.; Vacanti, M.; Eavey, R. D.; Vacanti, C. A.; Bonassar, L. J. *Tissue Eng.* **2005**, *11*, 192.
6. Aamer, K.; Sardina, H. A.; Bhatia, S.; Tew, G. N. *Biomaterials* **2004**, *25*, 1087.
7. Agrawal, S. K.; Sanabria-DeLong, N.; Coburn, J. M.; Tew, G. N.; Bhatia, S. R. *J. Controlled Release* **2006**, *112*, 64.
8. Bae, S. J.; Joo, M. K.; Jeong, Y.; Kim, S. W.; Lee, W.-K.; Sohn, Y. S.; Jeong, B. *Macromolecules* **2006**, *39*, 4873.
9. Bajpai, A. K.; Shukla, S. K.; Bhanu, S.; Kankane, S. *Prog. Polym. Sci.* **2008**, *33*, 1088.
10. Cerrai, P.; Tricoli, M.; Lelli, L.; Guerra, G. D.; Delguerra, R. S.; Cascone, M. G.; Giusti, P. *J. Mater. Sci., Mater. Med.* **1994**, *5*, 308.
11. Cohn, D.; Younes, H. *J. Biomed. Mater. Res.* **1988**, *22*, 993.
12. Fujiwara, T.; Mukose, T.; Yamaoka, T.; Yamane, H.; Sakurai, S.; Kimura, Y. *Macromol. Biosci.* **2001**, *1*, 204.
13. Kang, Y. M.; Lee, S. H.; Lee, J. Y.; Son, J. S.; Kim, B. S.; Lee, B.; Chun, H. J.; Min, B. H.; Kim, J. H.; Kim, M. S. *Biomaterials* **2010**, *31*, 2453.
14. Kim, M. S.; Hyun, H.; Khang, G.; Lee, H. B. *Macromolecules* **2006**, *39*, 3099.
15. Kissel, T.; Li, Y.; Unger, F. *Adv. Drug Delivery Rev.* **2002**, *54*, 99.
16. Kwon, K.-W.; Park, M. J.; Bae, Y. H.; Kim, H. D.; Char, K. *Polymer* **2002**, *43*, 3353.
17. Lassalle, V.; Ferreira, M. L. *Macromol. Biosci.* **2007**, *7*, 767.
18. Lee, D. S.; Shim, M. S.; Kim, S. W.; Lee, H.; Park, I.; Chang, T. *Macromol. Rapid Commun.* **2001**, *22*, 587.
19. Lee, H. T.; Lee, D. S. *Macromol. Res.* **2002**, *10*, 359.
20. Li, F.; Li, S. M.; Vert, M. *Macromol. Biosci.* **2005**, *5*, 1125.
21. Li, S.; Vert, M. *Macromolecules* **2003**, *36*, 8008.
22. Li, S. M.; Rashkov, I.; Espartero, J. L.; Manolova, N.; Vert, M. *Macromolecules* **1996**, *29*, 57.
23. Mai, S. M.; Abbot, A.; Norton, D.; McKean, R.; Ryan, A. J. *Macromol. Chem. Phys.* **2009**, *210*, 840.
24. Pham, Q. T.; Russel, W. B.; Thibeault, J. C.; Lau, W. *Macromolecules* **1999**, *32*, 5139.
25. Saffer, E. M.; Tew, G. N.; Bhatia, S. R. *Curr. Med. Chem.* **2011**, *18*, 5676.
26. Sanabria-DeLong, N.; Crosby, A. J.; Tew, G. N. *Biomacromolecules* **2008**, *9*, 2784.
27. Shin, D.; Shin, K.; Aamer, K. A.; Tew, G. N.; Russell, T. P.; Lee, J. H.; Jho, J. Y. *Macromolecules* **2005**, *38*, 104.

In Degradable Polymers and Materials: Principles and Practice (2nd Edition); Khemani, K., et al.; ACS Symposium Series; American Chemical Society: Washington, DC, 2012.

28. Tang, Y. Q.; Heaysman, C. L.; Willis, S.; Lewis, A. L. *Exp. Opin. Drug Delivery* **2011**, *8*, 1141.
29. Tew, G. N.; Sanabria-DeLong, N.; Agrawal, S. K.; Bhatia, S. R. *Soft Matter* **2005**, *1*, 253.
30. Tirelli, N.; Lutolf, M. P.; Napoli, A.; Hubbell, J. A. *Rev. Mol. Biotechnol.* **2002**, *90*, 3.
31. Agrawal, S. K.; Sanabria-DeLong, N.; Tew, G. N.; Bhatia, S. R. *Macromolecules* **2008**, *41*, 1774.
32. Sanabria-DeLong, N.; Agrawal, S. K.; Bhatia, S. R.; Tew, G. N. *Macromolecules* **2006**, *39*, 1308.
33. Brandl, F.; Sommer, F.; Goepferich, A. *Biomaterials* **2007**, *28*, 134.
34. Hoffman, A. S. *Adv. Drug Delivery Rev.* **2002**, *54*, 3.
35. Lee, K. Y.; Mooney, D. J. *Chem. Rev.* **2001**, *101*, 1869.
36. Li, Y. L.; Rodrigues, J.; Tomas, H. *Chem. Soc. Rev.* **2012**, *41*, 2193.
37. Yu, L.; Ding, J. D. *Chem. Soc. Rev.* **2008**, *37*, 1473.
38. Lutolf, M. P.; Hubbell, J. A. *Nat. Biotechnol.* **2005**, *23*, 47.
39. Cui, J.; Lackey, M. A.; Madkour, A. E.; Saffer, E. M.; Griffin, D. M.; Bhatia, S. R.; Crosby, A. J.; Tew, G. N. *Biomacromolecules* **2012**, *13*, 584.
40. Nuttelman, C. R.; Rice, M. A.; Rydholm, A. E.; Salinas, C. N.; Shah, D. N.; Anseth, K. S. *Prog. Polym. Sci.* **2008**, *33*, 167.
41. Elisseeff, J.; Anseth, K.; Sims, D.; McIntosh, W.; Randolph, M.; Langer, R. *Proc. Natl. Acad. Sci. U.S.A.* **1999**, *96*, 3104.
42. Huang, S.; Ingber, D. E. *Nat. Cell Biol.* **1999**, *1*, 131.
43. Georges, P. C.; Janmey, P. A. *J. Appl. Physiol.* **2005**, *98*, 1547.
44. Choquet, D.; Felsenfeld, D. P.; Sheetz, M. P. *Cell* **1997**, *88*, 39.
45. Huang, S.; Ingber, D. E. *Nat. Cell Biol.* **1999**, *1*, 131.
46. Lee, K. Y.; Peters, M. C.; Anderson, K. W.; Mooney, D. J. *Nature* **2000**, *408*, 998.
47. Chicurel, M. E.; Chen, C. S.; Ingber, D. E. *Curr. Opin. Cell Biol.* **1998**, *10*, 232.
48. Kim, B. S.; Nikolovski, J.; Bonadio, J.; Mooney, D. J. *Nat. Biotechnol.* **1999**, *17*, 979.
49. Pelham, R. J.; Wang, Y. L. *Proc. Natl. Acad. Sci. U.S.A.* **1997**, *94*, 13661.
50. Wang, H. B.; Dembo, M.; Wang, Y. L. *Am. J. Physiol.* **2000**, *279*, C1345.
51. Pelham, R. J.; Wang, Y. L. *Mol. Biol. Cell* **1999**, *10*, 935.
52. Georges, P. C.; Janmey, P. A. *J. Appl. Physiol.* **2005**, *98*, 1547.
53. Engler, A. J.; Griffin, M. A.; Sen, S.; Bonnetnann, C. G.; Sweeney, H. L.; Discher, D. E. *J. Cell Biol.* **2004**, *166*, 877.
54. Flanagan, L. A.; Ju, Y. E.; Marg, B.; Osterfield, M.; Janmey, P. A. *Neuroreport* **2002**, *13*, 2411.
55. Bryant, S. J.; Bender, R. J.; Durand, K. L.; Anseth, K. S. *Biotechnol. Bioeng.* **2004**, *86*, 747.
56. Moran, J. M.; Pazzano, D.; Bonassar, L. J. *Tissue Eng.* **2003**, *9*, 63.
57. Teng, Y. D.; Lavik, E. B.; Qu, X. L.; Park, K. I.; Ourednik, J.; Zurakowski, D.; Langer, R.; Snyder, E. Y. *Proc. Natl. Acad. Sci. U.S.A.* **2002**, *99*, 3024.
58. Woerly, S.; Doan, V. D.; Sosa, N.; de Vellis, J.; Espinosa-Jeffrey, A. *J. Neurosci. Res.* **2004**, *75*, 262.

59. Sanabria-DeLong, N.; Agrawal, S. K.; Bhatia, S. R.; Tew, G. N. *Macromolecules* **2007**, *40*, 7864.
60. Agrawal, S. K.; Sanabria-DeLong, N.; Bhatia, S. K.; Tew, G. N.; Bhatia, S. R. *Langmuir* **2010**, *26*, 17330.
61. Agrawal, S. K.; Sanabria-DeLong, N.; Jemian, P. R.; Tew, G. N.; Bhatia, S. R. *Langmuir* **2007**, *23*, 5039.
62. Agrawal, S. K.; Sanabria-DeLong, N.; Tew, G. N.; Bhatia, S. R. *J. Mater. Res.* **2006**, *21*, 2118.
63. Agrawal, S. K.; Sanabria-DeLong, N.; Tew, G. N.; Bhatia, S. R. *Langmuir* **2008**, *24*, 13148.
64. Wall, F. T. *J. Chem. Phys.* **1942**, *10*, 485.
65. Flory, P. J.; Rehner, J. *J. Chem. Phys.* **1943**, *11*, 512.
66. Treloar, L. R. G. *Trans. Faraday Soc.* **1943**, *39*, 241.
67. Mooney, M. *J. Appl. Phys.* **1940**, *11*, 582.
68. Rivlin, R. S. *Philos. Trans. R. Soc. London, Ser. A* **1948**, *241*, 379.
69. Tae, G.; Kornfield, J. A.; Hubbell, J. A.; Johannsmann, D.; Hogen-Esch, T. E. *Macromolecules* **2001**, *34*, 6409.
70. Tae, G.; Kornfield, J. A.; Hubbell, J. A.; Lai, J. *Macromolecules* **2002**, *5*, 4448.
71. Zhong, Z. Y.; Dijkstra, P. J.; Jan, F. J.; Kwon, Y. M.; Bae, Y. H.; Kim, S. W. *Macromol. Chem. Phys.* **2002**, *203*, 1797.
72. Fujiwara, T.; Mukose, T.; Yamaoka, T.; Yamane, H.; Sakurai, S.; Kimura, Y. *Macromol. Biosci.* **2001**, *1*, 204.
73. Sieminski, A. L.; Gooch, K. J. *Biomaterials* **2000**, *21*, 2233.
74. Crichton, M.; Bhatia, S. *J. Appl. Crystallogr.* **2003**, *36*, 652.
75. Schmidt, P. W. *J. Appl. Crystallogr.* **1991**, *24*, 414.

Chapter 19

Functional Degradable Polymeric Materials Prepared by Atom Transfer Radical Polymerization (ATRP)

Nicolay V. Tsarevsky,[1,*] Ke Min,[2] Nazeem M. Jahed,[3] Haifeng Gao,[2] and Krzysztof Matyjaszewski[4]

[1]Department of Chemistry, Southern Methodist University, 3215 Daniel Ave., Dallas, TX 75275
[2]Department of Chemistry and Biochemistry, University of Notre Dame, 365 Stepan Chemistry Hall, Notre Dame, IN 46556
[3]Department of Chemistry, University of the Western Cape, Private Bag X 17, Bellville 7530, Republic of South Africa
[4]Department of Chemistry, Carnegie Mellon University, 4400 Fifth Ave., Pittsburgh, PA 15213
[*]nvt@mail.smu.edu

ATRP was applied to synthesize well-defined halogen-functionalized linear polymers and gels with disulfide groups. The disulfide groups were introduced by using a disulfide-containing alkyl halide initiator or a dimethacrylate with internal disulfide link. The synthesized biocompatible linear disulfide-containing poly(2-hydroxyethyl methacrylate) degraded quickly upon reaction with tributylphosphine yielding lower molecular weight polymers. The gels with disulfide crosslinks prepared either by solution ATRP or by ATRP in miniemulsion also degraded in the presence of reducing agents leading to the formation of soluble polymers. The high degree of Br-functionalization of the gels was demonstrated by chain extension reactions with styrene and analysis of the degradation products by 2D chromatography. For the second edition of this book, the references to relevant work have been updated.

In Degradable Polymers and Materials: Principles and Practice (2nd Edition); Khemani, K., et al.;
ACS Symposium Series; American Chemical Society: Washington, DC, 2012.

Introduction

The past decade has witnessed the discovery of various strategies for the precise synthesis of novel, previously inaccessible, polymeric materials. Among the synthetic strategies, controlled/"living" radical polymerization (CRP) (*1–4*) and more specifically atom transfer radical polymerization (ATRP) (*5–8*) have found a wide application due to the easy experimental setup and tolerance towards functional groups, solvents and impurities. ATRP relies on the reversible reaction between a low oxidation state metal (often copper) complex and an alkyl halide (initiator) generating a high oxidation state metal complex with a coordinated halide ligand and radicals that can propagate in the presence of a monomer. An equilibrium between alkyl halide-type dormant polymeric species and active radicals is established which results in polymers of narrow molecular weight distribution and molecular weight or degree of polymerization (DP) predetermined by the ratio of the monomer to initiator. The polymers prepared by ATRP are halogen-capped which allows for further functionalization reactions (*9*). A number of nanostructured materials have been successfully prepared by ATRP using functional initiators or macroinitiators (*10*). The development of ATRP initiation techniques that employ very low (often of the order of ppm amounts) concentrations of catalyst has made the process very environmentally friendly and particularly suitable for the synthesis of polymers for biomedical applications. In one of these techniques, named ICAR (*initiators for continuous activator regeneration*), a radical initiator such as AIBN is used as the reducing agent (*11*). A drawback is the generation of more polymer chains than the amount of alkyl halide originally used due to some initiation by the radicals derived from the radical-based reducing agent, but the fraction of these chains is relatively small due to the relatively small amount of radical initiator used (typically, 10-15 mol % relative to the alkyl halide initiator). An alternative was also developed, ARGET (*activators regenerated by electron transfer*), in which the reducing agent (Sn^{II} compound, ascorbic acid, amines, etc.) is not able to initiate polymerization (*12*, *13*).

(Bio)degradable polymers are of significant interest in soil treatment, tissue engineering, and drug delivery, which has stimulated the development of novel methods for their synthesis (*14–16*). CRP methods have been successfully employed for the synthesis of a plethora of degradable and biodegradable polymers with various architectures, including linear, branched and hyperbranched, brush- or starlike, as well as crosslinked ones (*17*).

Disulfide is an example of a degradable group, which can be cleaved reversibly upon reduction to yield the corresponding thiols. The thiol-disulfide interconversion is widely utilized in nature, e.g., in the regulation of enzyme activity, in protein structure stabilization, and in various metabolic redox processes (*18*, *19*). Thiols (*20*), phosphines (*21*, *22*), metal hydrides, and various metal/acid combinations are often employed as reducing agents. Disulfide groups can be introduced in a polymer by using an appropriate sulfur-containing initiator or monomer. The preparation of polymeric materials with internal disulfide bonds including linear polystyrene (*23*), polymethacrylates (*24–26*), or polyacrylates (*27*) by ATRP has been reported. Among the first reported architectures were

In Degradable Polymers and Materials: Principles and Practice (2nd Edition); Khemani, K., et al.;
ACS Symposium Series; American Chemical Society: Washington, DC, 2012.

linear polymers, polymer gels (*26*) (including nanogels prepared in dispersed media (*28*, *29*)), and miktoarm star copolymers (*30*). The degradation of these materials in the presence of dithiothreitol or tributylphosphine (Bu_3P) was reported. The degradation products were thiol-containing polymers which could be oxidized quantitatively back to the corresponding disulfides (*23*).

Since the first edition of this chapter, several approaches to the synthesis of degradable hyperbranched polymers with disulfide groups have been reported. For instance, the utility was demonstrated of *"self-condensing vinyl polymerization"* (*31*, *32*), which employs compounds named *inimers* that contain both polymerizable and initiating groups. A unsymmetric disulfide with an ATRP initiating group and a polymerizable moiety, 2-bromoisobutyryloxyethyl 2′-methacryloyloxyethyl disulfide, was synthesized and homopolymerized or copolymerized with methyl methacrylate to yield degradable polymers with multiple peripheral bromine functionalities (*33*). The approach is useful but requires the multistep synthesis of asymmetric (bio)degradable inimer. A simpler route to disulfide-containing hyperbranched macromolecules is the copolymerization of divinyl monomers (crosslinkers) containing a disulfide group, in which gelation is delayed by limiting the molecular weight of the formed polymers by the addition of CBr_4 as an efficient chain transfer agent (*34*) or by conducting the synthesis under ATRP conditions (*35*). In both cases, peripherally brominated branched polymers were prepared. The multiple alkyl bromide end groups were used to prepare star-shaped polymers with hyperbranched degradable disulfide cores via chain extension under low-catalyst-concentration ATRP conditions (*34*).

Herein, we describe the ATRP of the biocompatible 2-hydroxyethyl methacrylate (HEMA) using a disulfide-containing alkyl halide initiator in protic media at near-ambient temperature. The reductive cleavage of this biocompatible polymer is studied as well. We also demonstrate that halogen-functionalized gels degradable in reducing environment can be prepared by ATRP in miniemulsion using a dimethacrylate with disulfide group as the crosslinker. This process is useful for the fabrication of fluid formulations containing gel nanoparticles that can release incorporated compounds (such as drugs or dyes) in a reducing environment.

Experimental

Materials

Prior to use, the neat monomer (methyl methacrylate (MMA), HEMA, or styrene (Sty)) was passed through a column filled with basic alumina to remove the polymerization inhibitor. CuBr (98%, Aldrich) was purified by washing with glacial acetic acid followed by 2-propanol. The conventional radical initiators V-70 and AIBN (Wako) were recrystallized from methanol. The disulfide-containing ATRP initiator bis(2-bromoisobutyryloxethyl) disulfide ($(BiBOE)_2S_2$) and the disulfide-containing crosslinker bis(methacryloyloxyethyl) disulfide ($(MAOE)_2S_2$) were synthesized using a literature procedure (*26*). The synthesis of bis(2-pyridylmethyl) octadecylamine (BPMODA) was

In Degradable Polymers and Materials: Principles and Practice (2nd Edition); Khemani, K., et al.;
ACS Symposium Series; American Chemical Society: Washington, DC, 2012.

described previously as well (*36*). All other reagents (2,2′-bipyridine (bpy), N,N,N′,N″,N″-pentamethyldiethylenetriamine (PMDETA), ethyl 2-bromoisobutyrate (EBiB), and Bu_3P) and the solvents were used as received. PMDETA and $(BiBOE)_2S_2$ were deoxygenated prior to the experiments by bubbling with nitrogen for 2-3 h.

ATRP of HEMA

HEMA (3 mL, 3.219 g, 27.4 mmol) and methanol (3 mL) were mixed in a Schlenk flask to which a stir bar had been added, and the mixture was deoxygenated by 5 freeze-pump-thaw cycles. The mixture was then frozen, the flask was filled with nitrogen, and the solid catalyst consisting of CuBr, $CuBr_2$, and bpy was added. The flask was quickly closed, and was then evacuated and back-filled with nitrogen several times. The reaction mixture was allowed to thaw, the reaction flask was immersed in a water bath thermostated at 30 °C, and the initiator $(BiBOE)_2S_2$ was injected. In all experiments, the molar ratio of bpy to total copper (CuBr + $CuBr_2$) was 2:1, and the ratio of total copper to initiator was 2:1 (i.e., the ratio of total copper to bromine groups from the initiator was 1:1). Two different monomer-to-initiator ratios, namely 300 and 150 were used. The amount of $CuBr_2$ in the catalyst varied from 20 to 80% of the total copper. Samples were periodically withdrawn with a nitrogen-purged syringe and analyzed.

Preparation of Degradable Gels with Disulfide Groups (26)

MMA (5 mL, 0.0467 mol) and $(MAOE)_2S_2$ (0.15 mL, 0.57 mmol) were dissolved in 2 mL of acetone and the mixture was degassed as described above. The catalyst consisted of 0.0334 g (0.233 mmol) CuBr and 0.0727 g (0.4667 mmol) bpy. The reaction mixture was heated to 50 °C and deoxygenated $(BiBOE)_2S_2$ (150 μL, 0.491 mmol, 1/95 vs. MMA) was added. Gelation was observed in ca. 150 minutes (93 % monomer conversion determined by gravimetry). The obtained gel was washed repeatedly with acetone (4-5 times with 500-mL portions, keeping the gel in the solvent for ca. 12 h) to remove any free polymer. Gels with disulfide crosslinks were also synthesized from MMA and $(MAOE)_2S_2$ using conventional radical initiators such as V-70.

Chain Extension of the Disulfide-Containing polyMMA-Based "Supermacroinitiator" Gel with Sty (26)

0.3 g of the dried gel described above was mixed with 8 mL of Sty and the mixture was kept in a refrigerator overnight and then at room temperature for 2

In Degradable Polymers and Materials: Principles and Practice (2nd Edition); Khemani, K., et al.;
ACS Symposium Series; American Chemical Society: Washington, DC, 2012.

hours to allow the gel to swell. The mixture was degassed as described above and 0.0286 g (0.20 mmol) of CuBr was added, followed by injection of 42 μL (0.20 mmol) of PMDETA. The reaction was carried out for 2.5 h at 90 °C. The product was washed repeatedly with THF to remove any free polymer that was not chemically attached to the gel.

Preparation of Latexes Degradable in Reducing Environment by ATRP

Simultaneous Reverse and Normally Initiated ATRP (*37*, *38*) was applied in miniemulsion to synthesize degradable latex particles. $CuBr_2$ (0.0044 g, 0.020 mmol), BPMODA (0.0090 g, 0.020 mmol), MMA (2g, 20.0 mmol), EBiB (14.6 μL, 0.1 mmol), the degradable crosslinker ($(MAOE)_2S_2$, 0.1 g) and hexadecane (used as co-stabilizer, 0.10 mL) were added to a round-bottom flask, and heated upon stirring at 60 °C. After the formation of stable Cu^{II} complex, the mixture was cooled to room temperature, and AIBN (0.0020 g, 0.0125 mmol) was added. After the addition of the aqueous solution of surfactant Brij 98 (5 mM of polyoxyethylene(20) oleyl ether, 20 mL), the oil/water mixture was ultrasonificated (Heat Systems Ultrasonics W-385 sonicator; output control set at 8 and duty cycle at 70% for 1 min) in an ice bath to prevent a significant temperature rise. The resulting miniemulsion exhibited good shelf life stability at room temperature, as evidenced by a lack of visible creaming or phase separation over 1 day of aging. After homogenization and transfer to a 25 mL Schlenk flask, nitrogen was bubbled through the miniemulsion for 30 min at room temperature. The flask was then immersed in an oil bath thermostated at 80 °C, corresponding to time zero of the polymerization. After 4 h, the reaction was stopped by exposing the reaction mixture to air; the monomer conversion was 80%. The final miniemulsion was dried overnight.

Reductive Degradation of the Disulfide-Containing Linear Polymers and Gels

0.01 g of the linear polymer was dissolved in 1 mL 50 mM solution of LiBr in DMF (same solution as the eluent for SEC) containing Ph_2O (SEC standard), and Bu_3P (10 μL) was added. The reaction mixture was analyzed by SEC after 30 min. The gels were degraded in a similar fashion: 0.02 g of the dry gel was kept in 3 mL of THF containing 0.05 mL of Ph_2O for 1 h to let it swell, and Bu_3P (50 μL) was added. The degradation was accompanied by complete dissolution and took several hours to days depending on the crosslink density. The disulfide-containing gel nanoparticles prepared by ATRP in miniemulsion were swelled (after removal of the surfactant) for 24 h in THF (12.3 g/L) and Bu_3P was added. The change of particle size was tracked by Dynamic Light Scattering (DLS) on High Performance Particle Sizer, Model HP5001 from Malvern Instruments, Ltd. The measurement took ca. 5 min. The particle size reported in this work is the one obtained at the end of each measurement.

In Degradable Polymers and Materials: Principles and Practice (2nd Edition); Khemani, K., et al.;
ACS Symposium Series; American Chemical Society: Washington, DC, 2012.

2-Dimensional Chromatographic Analysis

After reductive degradation, the gels were analyzed by liquid chromatography under critical conditions (LCCC) for polyMMA. The chromatograph was equipped with a Waters 600 controller and pump. The mobile phase was a mixture of butanone and cyclohexane (74:26 by volume). The column used for separation was Macherey & Nagel, Nucleosil silica gel (particle size 5 μm, pore size 300 Å and column dimensions 250 × 4 mm i.d.). The column oven temperature was set at 32 °C. The mobile phase flow rate was 0.5 mL/min. An evaporative light scattering detector (ELSD, Polymer Laboratories, PL-ELS 1000, nitrogen flow 1.2 L/min, evaporator temperature 90 °C) was used. Dilute polymer solutions were prepared from 5 mg of degraded by reduction with Bu_3P gel (washed with methanol) in 1 mL mixture of butanone and cyclohexane (3:1 by volume). Each time a 5 μL sample was used for analysis. Data acquisition was accomplished with PSS-WINGPC 7 from Polymer Standards Service (PSS; Mainz, Germany). Following the LCCC analysis, the samples were analyzed by 2D liquid chromatography. For the first dimension (HPLC), the conditions were the same as for the LCCC, except that the flow rate was set to 0.08 mL/min. Sample fractions from the first dimension were transferred to the second dimension (SEC) via an eight-port valve system (VICI Valco EHC8W), which consisted of two 200-μL loops. The second dimension (SEC) consisted of a Waters 515 pump delivering THF at a flow rate of 5 mL/min. The column used was a PSS SDV linear M, high-speed column (pore size 5 μm, dimensions 50 × 20 mm i.d.). The same ELS detector was used as in HPLC analysis, and the second dimension was calibrated using polyMMA homopolymer standards. Data acquisition and processing were automatically performed by the WINGPC 7 and PSS-2D-GPC software, respectively.

Results and Discussion

Synthesis of Degradable Linear polyHEMA

PolyHEMA is a polymer that has attracted significant attention due to its biocompatibility; applications include hydrogels and contact lenses (*39*). Well-defined polyHEMA with internal disulfide group was synthesized using $(BiBOE)_2S_2$ as the ATRP initiator as shown in Figure 1. The polymerizations were carried out in methanol at 30 °C and were relatively fast (high conversion was reached in 2-5 h depending on the conditions) similar to other ATRP reactions in protic media (*40*). In all cases, the first order kinetic plots were linear or showed insignificant curvature (Figure 2a) indicating a constant number of active species throughout the reaction. It was recently shown (*40*) that in order to achieve satisfactory polymerization control in ATRP in protic media, a relatively large initial amount of deactivator ($CuBr_2$ / bpy) should be added to the reaction mixture. This is necessary because the Cu^{II} halide complexes are relatively unstable in protic solvents such as alcohols and water. Thus, a significant part of the deactivator may be lost, leading to inefficient deactivation and therefore to

In Degradable Polymers and Materials: Principles and Practice (2nd Edition); Khemani, K., et al.;
ACS Symposium Series; American Chemical Society: Washington, DC, 2012.

poor polymerization control. This process is especially pronounced in solutions dilute with respect to Cu^{II} and halide ions. Indeed, Figure 2b shows that although the polymer molecular weights increased linearly with conversion, the dispersities (M_w/M_n) of the polymers isolated from a reaction mixture containing only 20% (with respect to the total copper) of initially added deactivator in the case of low total catalyst concentration (i.e., targeted DP of 300) were relatively large. The control over polymerization was largely improved when the amount of deactivator was increased to 40%. When the targeted DP was decreased twofold, the polymerization control was better due to the higher total concentration of catalyst and therefore of deactivator.

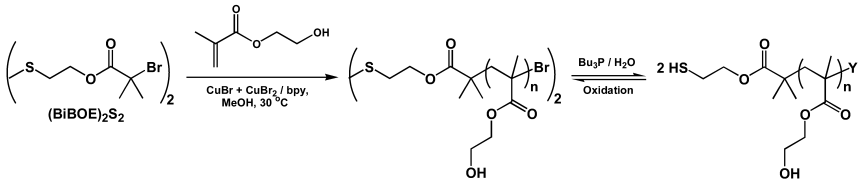

Figure 1. Preparation of degradable polyHEMA by ATRP.

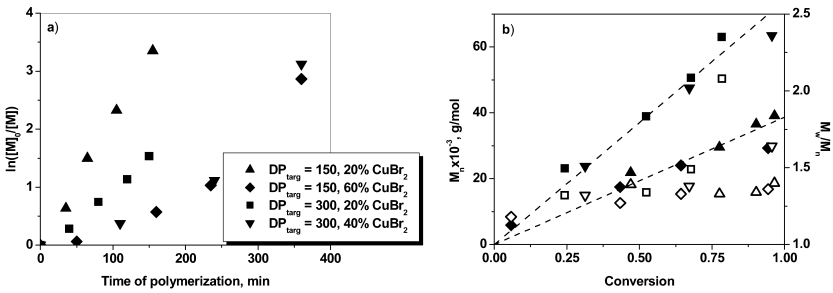

Figure 2. ATRP of HEMA using $(BiBOE)_2S_2$ as the initiator: a) kinetics and b) evolution of molecular weights (filled symbols with same shape as in graph a)) and polydispersity indices (open symbols) with monomer conversion.

The degradation of polyHEMA in DMF was rather efficient and fast when Bu_3P was used as the reducing agent. Figure 3 shows the SEC traces of polymers obtained at two different monomer conversions before and after reductive degradation for 30 min at room temperature.

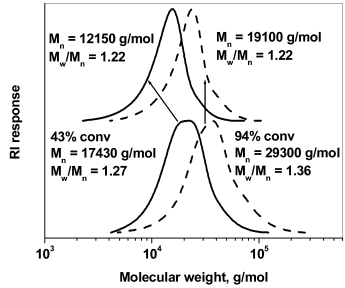

Figure 3. SEC traces of polyHEMA obtained at 43% and 94% monomer conversion using [HEMA]:[(BiBOE)$_2$S$_2$]:[CuBr]:[CuBr$_2$]:[bpy] = 150:1:0.8:1.2:4 before (bottom) and after (top) reductive degradation in the presence of Bu$_3$P (30 min).

Preparation and Degradation of Functional polyMMA-Based Gels

The radical polymerization of a mixture of MMA and a difunctional monomer containing a disulfide bond, (MAOE)$_2$S$_2$, leads to the formation of a gel that can degrade in reducing environment yielding soluble linear polyMMA with thiol side groups. The polymerization was carried out in acetone at 50 °C using V-70 as the radical initiator in the presence of a dye, methyl violet. The gel with incorporated dye thus obtained was swollen in toluene and Bu$_3$P was added. Gradually, the disulfide links originating from the dimethacrylate crosslinker were cleaved and the gel degraded releasing the dye which precipitated in the solvent used (Figure 4).

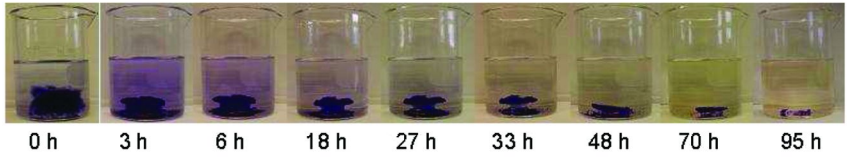

Figure 4. Degradation of polyMMA-based gel with disulfide groups in the presence of Bu$_3$P in toluene at room temperature producing soluble polyMMA. During the degradation, the incorporated dye (methyl violet) was released from the gel. (Synthesis: MMA (10 mL), (MAOE)$_2$S$_2$ (0.05 mL), acetone (4 mL), methyl violet (0.01 g), and V-70 (0.05 g), nitrogen atmosphere, 50 °C, 1.5 h.).

The degradation rate can be adjusted by varying the crosslink density (i.e., by using various amounts of the dimethacrylate crosslinker). It also depends on the nature of the reaction medium. For instance, it is well documented that the redox potentials (and therefore the degradation efficiency) of disulfides depend significantly upon pH, solvent polarity and the presence of various reagents forming complexes with the free thiols or thiolate ions produced in the reduction (*41*). The disulfide-based gels prepared by ATRP can be designed to degrade

In Degradable Polymers and Materials: Principles and Practice (2nd Edition); Khemani, K., et al.;
ACS Symposium Series; American Chemical Society: Washington, DC, 2012.

only in an environment with certain redox potential by changing the substituents at the disulfide group in the initiator and/or monomer. Gels with the potential to release incorporated compounds upon reduction are of significant interest for the biomedical sciences and engineering. Cancer tissues are hypoxic and the degradation of a gel accompanied with the release of a drug in such reducing environment is promising in cancer treatment (*42*, *43*).

Once it was demonstrated that degradable crosslinked materials could be formed using the radical polymerization of $(MAOE)_2S_2$, the ATRP of MMA in the presence of this disulfide was studied. The reaction was initiated by the disulfide initiator $(BiBOE)_2S_2$ and yielded functional degradable gels (see the left-hand side of Figure 5). Both the initiator and the difunctional monomer served as sources of degradable disulfide groups in the gels. The high degree of chain end functionalization was demonstrated by a chain extension with a second monomer, Sty (Figure 5, right hand-side). This reaction was recently described in detail (*26*).

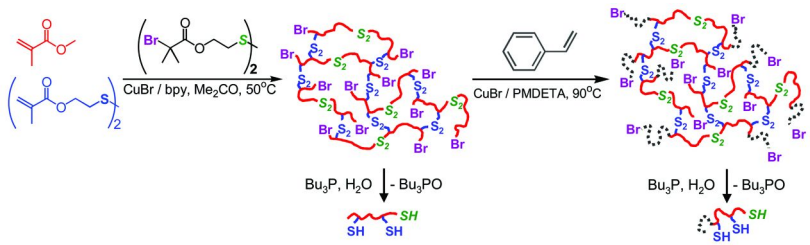

Figure 5. Preparation of degradable polyMMA-based gels by ATRP and their use as "supermacroinitiators". The disulfide and thiol groups originating from the functional initiator are shown in italics and the ones from the functional monomer in regular font. PolyMMA and polySty chains are represented with solid and dotted lines, respectively. (Reproduced from reference (26). Copyright 2005 American Chemical Society.)

In this work, we present further evidence that the bromide end groups in the gel remained intact during the synthesis and purification of the gel. The polyMMA-based gels were successfully degraded in THF using Bu_3P as the disulfide reducing agent, forming linear soluble polyMMA chains containing at least one thiol end-group originating from the disulfide initiator, and potentially one or more attached to the backbone originating from the disulfide-containing crosslinker $(MAOE)_2S_2$ (Figure 5). The soluble polymers formed by the reduction were analyzed by SEC. After the chain extension, the gel with pendant polySty chains was washed repeatedly with THF to remove any free polySty, generated by thermal initiation, and degraded using Bu_3P. The formed block copolymer was analyzed by SEC. The molecular weights of the products of reductive degradation of the gels demonstrate the efficient initiation from the polyMMA-based "supermacroinitiators". This is further verified from the symmetrical shift observed in the SEC traces of the soluble linear polymers formed after the reduction of the gels (Figure 6). No significant amount of homopolymer of MMA was observed in the products of degradation of the gels with segmented structures, indicating the high degree of functionalization of the gel prepared by ATRP.

In Degradable Polymers and Materials: Principles and Practice (2nd Edition); Khemani, K., et al.;
ACS Symposium Series; American Chemical Society: Washington, DC, 2012.

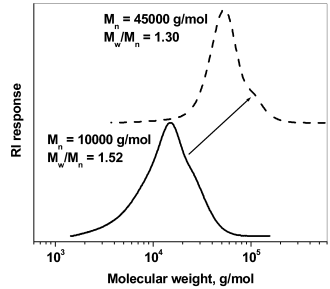

Figure 6. SEC traces of the products of reductive degradation of a disulfide-containing "supermacroinitiator" gel (bottom) and the gel prepared therefrom by chain extension with Sty (top).

The products of reductive degradation of polyMMA gel and the gel with "blocky" structure prepared from it were also analyzed by 2D chromatography. The analysis at the HPLC dimension was carried out at critical conditions for polyMMA. The position of the peak on the y-axis of the 2D plot (Figure 7) depends on the composition of the polymer. The second dimension (x-axis of the 2D plot) corresponds to SEC where the separation depends upon the molecular weight. The spot of the "supermacroinitiator" decomposition product (Figure 7a) is situated at molecular weight about 10^4 g/mol, which is in good agreement with the SEC trace from Figure 6. Some spreading is observed on the HPLC axis, most likely due to the variable number of thiol groups per polymer chain. The average number, based on monomer feed composition was 2.2 (one thiol group originating from the disulfide initiator and an average of 1.2 originating from the disulfide dimethacrylate). The gel with "blocky" structure degraded in the presence of Bu_3P (Figure 7b) forming a MMA-Sty block copolymer of molecular weight of about 5×10^4 g/mol (again, in good agreement with the data from Figure 6), which did not contain any detectable amount of free polyMMA (which would originate from chains in the "supermacroinitiator" which were not chain extended with Sty). This result clearly demonstrates the high degree of bromine-functionalization of the parent polyMMA-based "supermacroinitiator".

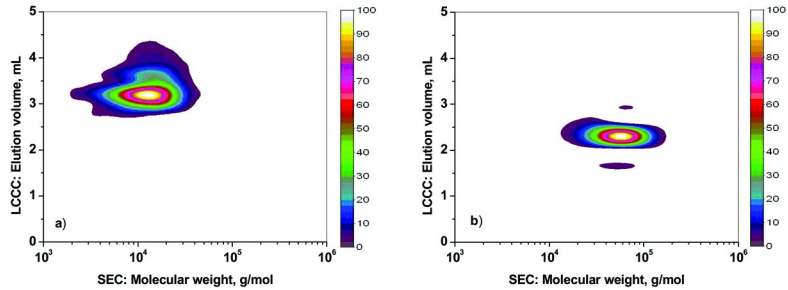

Figure 7. 2D chromatography plots of the products of reductive degradation of a) polyMMA-based "supermacroinitiator" gel and b) polyMMA-block-polySty-based gel.

In Degradable Polymers and Materials: Principles and Practice (2nd Edition); Khemani, K., et al.;
ACS Symposium Series; American Chemical Society: Washington, DC, 2012.

Synthesis of Functional Degradable polyMMA-Based Gels by ATRP in Miniemulsion

ATRP of various monomers can be successfully carried out in aqueous dispersed media yielding well-defined functional latexes (*44–47*). Miniemulsion polymerization, including CRP in miniemulsion, is widely used for the preparation of latexes with particle sizes of the order of 100-500 nm. If the proper surfactant is used, the miniemulsions are stable for prolonged periods.

A degradable functional latex was prepared by the atom transfer copolymerization of MMA and $(MAOE)_2S_2$ in miniemulsion. The latex particles thus obtained, when swollen in THF, had a diameter of about 220 nm. The latex could be rapidly (20-30 min) degraded by Bu_3P. For the two experiments shown in Figure 8, 12 μL and 20 μL of Bu_3P was added to 2 mL of the particle suspension (12.3 g/L), respectively, to study the effect of the reducing agent amount on the degradation rate. As the reaction time progressed, the particle size increased due to the increasing amount of reductively cleaved disulfide crosslinks. The formed loosely crosslinked gel particles had higher swelling ratios than the starting material. At a certain moment which depended upon the amount of added reducing agent the gel degraded completely forming soluble linear polymer chains which was accompanied by a sharp decrease in the measured hydrodynamic volume.

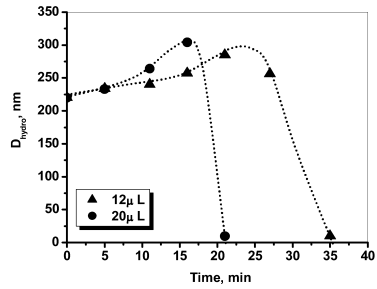

Figure 8. Reductive degradation of polyMMA-based latex crosslinked with $(MAOE)_2S_2$ in the presence of various amounts of Bu_3P in THF at ambient temperature.

In the future, surface modification of the degradable latex particles will be studied. Also, the possibility to incorporate various compounds in the degradable "nanocages" prepared by the atom transfer radical copolymerization of a disulfide-containing crosslinker and other monomers in miniemulsions, as well as the release of those compounds will be explored.

Conclusions

Bis[2-(2-bromoisobutyryloxy)ethyl] disulfide was employed as an initiator for the ATRP of 2-hydroxyethyl methacrylate (HEMA) in methanol using CuBr + $CuBr_2$ / 2,2′-bipyridine as the catalyst to yield linear biocompatible polymers

In Degradable Polymers and Materials: Principles and Practice (2nd Edition); Khemani, K., et al.;
ACS Symposium Series; American Chemical Society: Washington, DC, 2012.

with internal disulfide bond. Sufficient deactivation rate and therefore satisfactory polymerization control in the protic reaction medium was observed only when the catalyst contained relatively large initial amount of deactivator (higher than 20% of the total catalyst). The reductive cleavage of the disulfide-containing polyHEMA with tributylphosphine in DMF at room temperature was complete in 30 min and produced polymers of lower molecular weight than the starting materials.

Mixtures of methyl methacrylate (MMA) and a difunctional methacrylate monomer with internal disulfide bond were copolymerized by ATRP both in an acetone solution and in an aqueous dispersed (miniemulsion) system to form functional degradable gels. The high degree of Br-functionalization of the gels was demonstrated by a chain extension reaction with styrene followed by reductive degradation and 2D chromatographic analysis of the degradation products which showed no significant amount of unextended polyMMA chains. The degradation of the degradable, disulfide-crosslinked, functional latex particles prepared by miniemulsion ATRP was monitored by DLS. At the early stages of degradation the particles showed increased swellability due to the decreasing crosslink density. Eventually, the particles degraded completely forming linear, soluble polyMMA chains with free thiol groups.

References

1. Matyjaszewski, K., Davis, T. P., Eds. *Handbook of Radical Polymerization*; Wiley: Hoboken, 2002.
2. Braunecker, W. A.; Matyjaszewski, K. *Prog. Polym. Sci.* **2007**, *32*, 93.
3. Matyjaszewski, K., Sumerlin, B. S., Tsarevsky, N. V., Eds. *Progress in Controlled Radical Polymerization: Mechanisms and Techniques*; ACS Symposium Series 1100; American Chemical Society: Washington, DC, 2012.
4. Matyjaszewski, K., Sumerlin, B. S., Tsarevsky, N. V., Eds. *Progress in Controlled Radical Polymerization: Materials and Applications*; ACS Symposium Series 1101; American Chemical Society: Washington, DC, 2012.
5. Matyjaszewski, K.; Xia, J. *Chem. Rev.* **2001**, *101*, 2921.
6. Kamigaito, M.; Ando, T.; Sawamoto, M. *Chem. Rev.* **2001**, *101*, 3689.
7. Tsarevsky, N. V.; Matyjaszewski, K. *Chem. Rev.* **2007**, *107*, 2270.
8. Ouchi, M.; Terashima, T.; Sawamoto, M. *Chem. Rev.* **2009**, *109*, 4963.
9. Coessens, V.; Pintauer, T.; Matyjaszewski, K. *Prog. Polym. Sci.* **2001**, *26*, 337.
10. Matyjaszewski, K.; Tsarevsky, N. V. *Nature Chem.* **2009**, *1*, 276.
11. Matyjaszewski, K.; Jakubowski, W.; Min, K.; Tang, W.; Huang, J.; Braunecker, W. A.; Tsarevsky, N. V. *Proc. Natl. Acad. Sci. U.S.A.* **2006**, *103*, 15309.
12. Jakubowski, W.; Min, K.; Matyjaszewski, K. *Macromolecules* **2006**, *39*, 39.
13. Jakubowski, W.; Matyjaszewski, K. *Angew. Chem., Int. Ed.* **2006**, *45*, 4482.
14. Schnabel, W. *Polymer Degradation: Principles and Practical Applications*; Hanser International: Munich, 1981.

15. Hamid, S. H., Ed. *Handbook of Polymer Degradation*; Marcel Dekker: New York, 2000.
16. Edlund, U.; Albertsson, A.-C. *Adv. Polym. Sci.* **2002**, *157*, 67.
17. Tsarevsky, N. V. In *Green Polymerization Methods: Renewable Starting Materials, Catalysis and Waste Reduction*; Mathers, R. T., Meier, M. A. R., Eds.; Wiley-VCH: Weinheim, 2011; pp 235−261.
18. Singh, R.; Whitesides, G. M. In *Supplement S: The Chemistry of Sulphur-Containing Functional Groups*; Patai, S., Rappoport, Z., Eds.; Wiley: Chichester, 1993; pp 633−658.
19. Gilbert, H. F. In *Bioelectrochemistry: Principles and Practice*; Lenaz, G., Milazzo, G., Eds.; Birkhaeuser: Basel, 1997; Vol. 5: Bioelectrochemistry of Biomacromolecules, pp 256−324.
20. Singh, R.; Lamoureux, G. V.; Lees, W. J.; Whitesides, G. M. *Methods Enzymol.* **1995**, *251*, 167.
21. Humphrey, R. E.; Hawkins, J. M. *Anal. Chem.* **1964**, *36*, 1812.
22. Humphrey, R. E.; Potter, J. L. *Anal. Chem.* **1965**, *37*, 164.
23. Tsarevsky, N. V.; Matyjaszewski, K. *Macromolecules* **2002**, *35*, 9009.
24. Shah, R. R.; Merreceyes, D.; Husseman, M.; Rees, I.; Abbott, N. L.; Hawker, C. J.; Hedrick, J. L. *Macromolecules* **2000**, *33*, 597.
25. Bontempo, D.; Heredia, K. L.; Fish, B. A.; Maynard, H. D. *J. Am. Chem. Soc.* **2004**, *126*, 15372.
26. Tsarevsky, N. V.; Matyjaszewski, K. *Macromolecules* **2005**, *38*, 3087.
27. Van Camp, W.; Du Prez, F. E.; Alem, H.; Demoustier-Champagne, S.; Willet, N.; Grancharov, G.; Duwez, A.-S. *Eur. Polym. J.* **2010**, *46*, 195.
28. Oh, J. K.; Tang, C.; Gao, H.; Tsarevsky, N. V.; Matyjaszewski, K. *J. Am. Chem. Soc.* **2006**, *128*, 5578.
29. Oh, J. K.; Siegwart, D. J.; Matyjaszewski, K. *Biomacromolecules* **2007**, *8*, 3326.
30. Gao, H.; Tsarevsky, N. V.; Matyjaszewski, K. *Macromolecules* **2005**, *38*, 5995.
31. Frechet, J. M. J.; Henmi, M.; Gitsov, I.; Aoshima, S.; Leduc, M. R.; Grubbs, R. B. *Science* **1995**, *269*, 1080.
32. Hawker, C. J.; Frechet, J. M. J.; Grubbs, R. B.; Dao, J. *J. Am. Chem. Soc.* **1995**, *117*, 10763.
33. Tsarevsky, N. V.; Huang, J.; Matyjaszewski, K. *J. Polym. Sci., Part A: Polym. Chem.* **2009**, *47*, 6839.
34. Popescu, D.-L.; Tsarevsky, N. V. *Aust. J. Chem.* **2012**, *65*, 28.
35. Li, Y.; Armes, S. P. *Macromolecules* **2005**, *38*, 8155.
36. Xia, J.; Matyjaszewski, K. *Macromolecules* **1999**, *32*, 2434.
37. Gromada, J.; Matyjaszewski, K. *Macromolecules* **2001**, *34*, 7664.
38. Li, M.; Min, K.; Matyjaszewski, K. *Macromolecules* **2004**, *37*, 2106.
39. Montheard, J.-P.; Chatzopoulos, M.; Chappard, D. *J. Macromol. Sci., Rev. Macromol. Chem. Phys.* **1992**, *C32*, 1.
40. Tsarevsky, N. V.; Pintauer, T.; Matyjaszewski, K. *Macromolecules* **2004**, *37*, 9768.
41. Gilbert, H. F. *Methods Enzymol.* **1984**, *107*, 330.
42. Harris, A. L. *Nature Rev. Cancer* **2002**, *2*, 38.

In Degradable Polymers and Materials: Principles and Practice (2nd Edition); Khemani, K., et al.;
ACS Symposium Series; American Chemical Society: Washington, DC, 2012.

43. Brown, J. M.; Wilson, W. R. *Nature Rev. Cancer* **2004**, *4*, 437.
44. Qiu, J.; Charleux, B.; Matyjaszewski, K. *Prog. Polym. Sci.* **2001**, *26*, 2083.
45. Cunningham, M. F. *Prog. Polym. Sci.* **2002**, *27*, 1039.
46. Cunningham, M. F. *Prog. Polym. Sci.* **2008**, *33*, 365.
47. Zetterlund, P. B.; Kagawa, Y.; Okubo, M. *Chem. Rev.* **2008**, *108*, 3747.

Subject Index

In Degradable Polymers and Materials: Principles and Practice (2nd Edition); Khemani, K., et al.; ACS Symposium Series; American Chemical Society: Washington, DC, 2012.

C

D

E

F

In Degradable Polymers and Materials: Principles and Practice (2nd Edition); Khemani, K., et al.; ACS Symposium Series; American Chemical Society: Washington, DC, 2012.

G

H

J

L

M

N

O

In Degradable Polymers and Materials: Principles and Practice (2nd Edition); Khemani, K., et al.;
ACS Symposium Series; American Chemical Society: Washington, DC, 2012.

P

In Degradable Polymers and Materials: Principles and Practice (2nd Edition); Khemani, K., et al.;
ACS Symposium Series; American Chemical Society: Washington, DC, 2012.

R

S

In Degradable Polymers and Materials: Principles and Practice (2nd Edition); Khemani, K., et al.; ACS Symposium Series; American Chemical Society: Washington, DC, 2012.

T

W

In Degradable Polymers and Materials: Principles and Practice (2nd Edition); Khemani, K., et al.;
ACS Symposium Series; American Chemical Society: Washington, DC, 2012.